SLAC-179
Volume I
(T/E)
UC-34d

PROCEEDINGS OF SUMMER INSTITUTE
ON PARTICLE PHYSICS

(In Two Volumes)

July 29-August 10, 1974

VOLUME I
THE STRONG INTERACTIONS

Program Directors

D.W.G.S. Leith
R. Blankenbecler

Ed. by Martha C. Zipf

Sponsored by Stanford University, National Science Foundation,
and Stanford Linear Accelerator Center under contract with the
U. S. Atomic Energy Commission
Contract AT(04-3)-515

November 1974

Printed in the United States of America. Available from National Technical Information Service, U. S. Department of Commerce, 5285 Port Royal Road, Springfield, VA 22161.
Price: Printed Copy $10.60; Microfiche $1.45.

PREFACE

SLAC's second Summer Institute on Particle Physics was held at Stanford on July 29-August 10, 1974. This year the meeting was jointly sponsored by Stanford University, the Atomic Energy Commission, and the National Science Foundation. The motivation for the meetings derives from the need for continuing education of young people who are working in the field and the desire of the SLAC faculty to contribute to this post-graduate educational process. Because of the rapid progress in the field and its concentration at fewer and fewer research centers, it is important to offer the opportunities both for initial review of recent major progress and for the continuing education of the post Ph.D. research community.

Two hundred and twenty participants, drawn from all corners of the world, joined in a program combining summer school and topical conference formats. A ten-day school of a highly pedagogic nature was followed by an intense three-day topical conference in which experts in the field described their current work. The topic for this year's Institute was "The Strong Interactions" which, together with last year's coverage of the weak and electromagnetic interactions, provides a broad overview of the entire field of high energy physics.

The success of this year's Institute was again due, in large part, to the careful and thoughtful organization by the coordinator, Martha C. Zipf with the assistance of Sharon Traweek. Ms. Zipf also collected and edited these proceedings of the 1974 Institute.

We would like to thank Rosemarie Stampfel for typing the manuscripts and for her assistance and advice in the preparation of the finished copy.

David W.G.S. Leith and Richard Blankenbecler

Program Directors

TABLE OF CONTENTS

DIFFRACTIVE PROCESSES

David W.G.S. Leith

Stanford Linear Accelerator Center,
Stanford University, Stanford, California 94305

Lecture notes for the 1974 SLAC Summer Institute
in Particle Physics

OUTLINE

I. INTRODUCTION

1. General

These lectures are intended to review what we know of diffractive processes--to summarize the available data and what it teaches us about the structure of the proton and the dynamics of high energy scattering.

Despite the large volume of data presented in these notes, there are some topics which I know (and probably many more that I am not so aware of), that have not been discussed--I apologize for the omissions.

Finally, I list a set of review papers[1-20] that I have found invaluable in preparing my lectures--I recommend them to you for further study.

Diffraction is an important phenomenon in high energy physics, accounting for ~ 30% of the total cross-section. Our motivations for studying these processes range through the following viewpoints:

- That the diffractive processes are not the most fundamental or interesting processes in themselves, but that they cover up,[†] or conceal, the remaining two-thirds of the cross-section which is accounted for by a variety of processes which exhibit a great deal of exciting structure, and from which one is going to learn about the dynamics of two body scattering, particle production and perhaps, the internal structure of the nucleon. In other words, one has to understand the one before proceeding to the other;
- That diffraction is simply related to geometry, optics and absorption, and also represents the single largest cross-section we deal with in particle physics--therefore we should try to understand it before moving on to the more complex, smaller cross-section processes;
- or perhaps we feel that because diffraction is basically the reflection of all the absorptive processes, that through its study we might find other insights into the regularities of the inelastic scattering, or into the structure of the proton itself;

[†]Apologies to R.M.N., Rodino, Ervin et al.

Whatever our motivation, we are going to spend the next four lectures thinking about these diffractive processes.

2. Models

Diffraction scattering can be discussed in terms of two pictures--the t-channel or the s-channel pictures. In the t-channel, or exchange picture the scattering is thought to proceed through the exchange of a singularity called the Pomeron. The language of this picture is that of Regge exchange models, and we will discuss below the properties of the Pomeron trajectory and how we use this picture to learn more of the Pomeron. The s-channel picture or direct channel, is seen in geometric or optical terms--here diffraction is generated by the absorption due to the competition among the many inelastic channels. The target proton is talked of in terms of an absorbing disc of a given size and with a given opacity, and sometimes with some edge structure.

The experience has been that both the s-, and t-channel points of view seem to be important for the description of the various systematic features of elastic and inelastic amplitudes. In general, the t-channel picture has been more successful in explaining the energy dependence of hadronic amplitudes, while the s-channel picture has been very useful in understanding the structure of amplitudes as a function of momentum transfer. In discussing the Pomeron, or the diffractive mechanism, we will be using both points of view.

A. The t-channel view

In Regge theory the scattering amplitude is given by

$$F(s,t) = \beta(t)\,\frac{[1 + \tau\, e^{-i\pi\alpha(t)}]}{\sin \pi\alpha(t)} \cdot \left(\frac{s}{s_0}\right)^{\alpha(t)} ,$$

where $\tau = \pm 1$ for even or odd signature trajectories, and where the trajectory of the exchange system is

$$\alpha(t) = \alpha_0 + \alpha' \cdot t \ .$$

In general, the physical interpretation of this amplitude is that the crossed channel Regge pole represents the collective amplitude due to single exchanges of all the particles that lie on the trajectory.

Within this model, the energy dependence of the cross-section is controlled by the trajectory properties of the exchanged particle--

$$\sigma(s) \propto s^{\alpha(0)-1}$$

Also the behaviour of the differential cross-section is given by

$$\frac{d\sigma}{dt}(s,t) \propto s^{2\alpha(t)-2}$$

So, studies of the s-, and t-dependence of the cross-sections of diffractive processes will teach us about the Pomeron trajectory.

The assumption that the asymptotic behaviour of total cross-sections would be a constant required that the leading trajectory have $\alpha(0) = 1$ and $\tau = +1$.

In fact Khuri[21] has shown that in any unitary theory satisfying the two conditions--

- that an exclusive cross-section for producing n particles does not outgrow the total elastic cross-section by a power of the energy,
- that the multiplicity of secondaries must grow slower than a power of the energy

then $\alpha(0) = 1$. The data from high energy interactions suggest that these conditions are easily fulfilled.

The Pomeron has quite an unusual role in particle physics, in that--

- no other pole has a trajectory with $\alpha(0) = 1.0$;
- there is no known particle to be associated with this trajectory-- i.e. unusual behaviour of the trajectory in $t > 0$ region
- the behaviour of the trajectory for $t < 0$, as seen in the shrinkage of the differential cross-section, is quite different from other trajectories. The Pomeron trajectory is observed to have a rather flat t-dependence, with

  $$\alpha_P(t) = 1 + \alpha' \cdot t \quad \text{and} \quad 0 < \alpha' < 0.3 \ ,$$

  while most Regge trajectories for meson exchanges behave like

  $$\alpha_R(t) = 0.5 + 1.0 \cdot t \quad \text{i.e.} \quad \alpha' \sim 1.0 \ .$$

- the Pomeron behaves in scattering processes as though it carried the quantum numbers of the vacuum, whereas it behaves with respect to the energy dependence of cross-sections, as though it carries spin 1.

In all of these properties the Pomeron is quite different from the other known Regge trajectories. Further, we have no idea about the physical origin of this singularity.

B. The s-channel view

The geometrical model describes scattering in terms of the size and opacity of the object from which scattering.

$$\frac{d\sigma}{dt} = \pi |F(s,t)|^2$$

where

$$F(s,t) = \frac{1}{\pi} \int d^2b \; e^{iq\cdot b} f(s,b)$$

and

$$q = \sqrt{-t}$$

$$b = \text{impact parameter}$$

and $f(s,b)$ is the partial wave amplitude corresponding to angular momentum $\ell \sim bk$.

In the eikonal form,

$$f(s,b) = \frac{i}{2}\,[1 - e^{2i\delta(s,b)}]$$

where $\delta(s,b) = \delta_R(s,b) + i\delta_I(s,b)$.

For diffraction scattering, we assume the scattering is due to the absorption of the incoming wave caused by the many open inelastic channels. For this case $\delta_R \sim 0$.

$$\text{Im } f(s,b) = \frac{1}{2}\left(1 - e^{-2\delta_I(s,b)}\right)$$

If we define $\Omega(b) = 2\delta_I$ as the opaqueness of the target, we have

$$\sigma_T = 4\pi \int_0^\infty (1 - e^{-\Omega(b)})b\,db$$

$$\sigma_{el} = 2\pi \int (1 - e^{-\Omega(b)})^2 b\,db$$

$$\sigma_{in} = 2\pi \int (1 - e^{-2\Omega(b)})b\,db\ .$$

The differential cross-section is a measure of the size of the scattering object, and of its opacity. The determination of $\Omega(b)$ allows a mapping of the blackness, and size, of the scatterer.

The transformation from t-space to impact parameter space is given by (for given s),

$$F(t) \sim \int_0^\infty b\,db\,J_0(b\sqrt{-t})\cdot f(b)$$

For a peripheral collision, the t-dependence is then a J_0 Bessel function giving a peak at small t; a central collision will result in either a J_1 Bessel function, or an exponential, t-dependence depending on how sharp the edge is in $f(b)$. Various examples are given in Fig. 1. It is interesting to see how deformations of $f(b)$ from a gaussian distribution in b affect the distribution of $f(t)$ and hence the elastic differential cross-section. If one adds some large partial wave contributions to $f(b)$, they result in an increase of the slope of $F(t)$ near $t = 0$. (See Fig. 2.) If one absorbs out some low partial waves from $f(b)$, then this produces large t structure in the exponential $F(t)$, producing a dip followed by a secondary maximum. (Again see Fig. 2.)

It is therefore of interest to study the s-, and t-dependence of the diffractive cross-sections to determine $f(s,b)$ or $\Omega(s,b)$, within the direct channel picture and through them learn of the proton's structure.

C. s-channel unitarity and the overlap function

One can extend these simple geometrical ideas by formally applying the idea that diffraction scattering is the shadow of absorption, which in turn is due to the many open inelastic channels.

One may write (following Van Hove[22] and others),

$$\text{Im } T_{fi} = \sum_{el} T^*_{el,f}\cdot T_{el,i} + \sum_{in} T^*_{in,f}\cdot T_{in,i}$$

where the T's represent the initial and final states in inelastic (in) and elastic scattering (el). This may be illustrated as shown in Fig. 3. Usually the two terms on the left-hand side above are written as $G_{el} + G_{in}$, the elastic and inelastic overlap functions.

So we see that the imaginary part of the elastic amplitude is built up by two parts--the shadow of the inelastic channels and the elastic scattering itself. The strong lesson from these studies is that not only are the magnitudes of the inelastic amplitudes important in making up G_{in}, but also the phases of all the open channels.

It is interesting to transform this relationship into impact parameter space--there the s-channel unitarity relation becomes

$$\text{Im } a(s,b) = |a(s,b)|^2 + a_{in}(s,b)$$

where a_{in} is the inelastic overlap function. Notice that this equation connects the inelastic and total overlap functions at the same impact parameter! This makes the impact parameter representation very convenient to study unitarity effects.

For a purely imaginary high energy amplitude we have the above relation rewritten

$$a_{tot}(s,b) = a_{el}(s,b) + a_{in}(s,b)$$

and

$$a_T^2 = a_{el}$$

therefore

$$a_{tot} = \frac{1}{2}\left[1 - \sqrt{1 - 4a_{in}}\right] .$$

The relationship of the various overlap functions, as a function of the inelasticity are shown in Fig. 4. Notice that $[0 \leq a_{in} \leq 1/4]$.

Here we see the rapid variation of the elastic amplitude with inelasticity; for full absorption, $a_{in} = 1/4$ and $\sigma_{el}/\sigma_{tot} = 1/2$. But as the scatterer becomes just slightly less than black, the elastic contributions fall quickly and σ_{el}/σ_{tot} falls rapidly from $1/2$. For $a_{in} \sim 75\%$, the ratio is about 25%.

So, once more, for small inelasticity the imaginary part of the elastic amplitude is given by the inelastic contribution--as the inelastic cross-section grows, the elastic part increases.

This picture of the impact structure of high energy collisions is very useful, and we will return to it in trying to interpret the structure of the proton from high energy proton-proton scattering and diffraction inelastic scattering.

3. The Data

Now, having discussed the viewpoints from which we may analyze the diffraction scattering, let us consider the processes that we may study.

- $A + B \rightarrow A + B$

  Elastic scattering, and through the optical theorem, the total cross-section, allows study of the Pomeron, or the absorption profile. These data are reviewed in Chapter II.

- $A + B \rightarrow A^* + B$

  $\quad\quad A + B^*.$

  Inelastic exclusive diffraction scattering. This process was discussed by Good and Walker[23] in analogy to optical diffraction by an opaque disc. They predicted that such processes would occur, that they would proceed coherently in nuclei, and that the scattering properties would be very similar to those of elastic reaction. This data is reviewed in Chapters III and IV.

  $A + B \rightarrow A + X$

  $\quad\quad \rightarrow X + B.$

  Leading particle inclusive scattering. This process becomes of considerable interest at high energies. These data are reviewed in Chapters VI and VII.

4. The Rules

Unfortunately beyond the two pictures discussed above, we have no good theoretical description of the dynamics of diffractive processes, or no basic understanding of what the Pomeron singularity is--we rather have a set of phenomenological rules which allow us to identify what we mean by diffraction--

These rules are listed below.[12]

--energy independent cross sections (to factors of $\log s$)

--sharp forward peak in $d\sigma/dt$

--particle cross sections equal to antiparticle cross sections

--factorization

--mainly imaginary amplitude

--exchange processes characterized by the quantum numbers of the vacuum in the t-channel (i.e. $I = 0$, $C = +1$). Also, the change in parity in the scattering process follows the natural spin-parity series $(-1)^J$ or $P_f = P_i \cdot (-1)^{\Delta J}$, where ΔJ is spin change.

--the spin structure in the scattering is s-channel helicity conserving (SCHC).

These rules and how well the diffractive processes obey them, are discussed in Chapter V.

II. TOTAL CROSS-SECTIONS AND THE ELASTIC SCATTERING REACTION

1. Total Cross-Sections

The most classical of particle experiments is the measurement of the total cross-section. Interest in these measurements stems from the insight into the behaviour of the elastic scattering amplitude obtained through the optical theorem:

$$\sigma_T(s) \propto \operatorname{Im} f_{el} \qquad (s,\ t = 0)$$

where f_{el} is the forward spin-averaged elastic scattering amplitude. The linear relationship between σ_T and $\operatorname{Im} f_{el}$ allows a study of the different contributions to the elastic amplitude and their separate energy dependence, without the difficulty of unscrambling the information from expressions involving the absolute squares of amplitudes, as determined in studies of the elastic scattering reaction itself.

From the optical theorem, the s-dependence of σ_T is fixed when the behaviour of the elastic scattering amplitude is defined. This is usually done through Regge pole fits, since this theory has done a fair job of describing two-body peripheral processes. In these fits two components are postulated--

- an energy independent term due to the exchange of the Pomeron, with trajectory $\alpha(t) = 1$,
- an energy dependent term due to the exchange of ρ, ω, f, A_2 trajectories, which are usually assumed to have the same form--

$$\alpha(t) = \frac{1}{2} + t$$

This formalism leads to the simple parametrization--

$$\sigma_T(AB) = a(AB) + b(AB)\ p^{-1/2}$$

$$\sigma_T(\bar{A}B) = a(\bar{A}B) + b(\bar{A}B)\ p^{-1/2}$$

The terms $a(AB)$, $b(AB)$ represent the two terms described above, and p is the laboratory momentum of the particles.[24]

The Pomeranchuck theorem which states that at infinite energy, particle cross-sections will be equal to antiparticle cross-sections, is taken care of in this model with $a(AB) = a(\bar{A}B)$.

The data up to 30 GeV (i.e. in pre-Serpukov days) for all hadron and photon cross-sections were well fit by this description--that is, the data fell on straight lines when plotted against $p^{-1/2}$, and particle and anti-particle data converged to a common asymptotic limit (or at least everything was consistent with such a picture).

Representative fits are shown in Figs. 5 and 6, and the parameters for these fits given in Table I.[25]

Data from the Serpukov accelerator, extending these measurements up to 65 GeV/c dispelled this simple picture of the elastic amplitude. Data for $\pi^\pm p$, $K^\pm p$, $p^\pm p$ total cross-sections are shown in Fig. 7, and may be summarized as follows--

- $\pi^\pm p$, $K^- p$, $K^- n$, pp, pn total cross-sections seem to have reached a plateau with little or no energy dependence;
- $\bar{p}p$, $\bar{p}n$ total cross-sections are decreasing;
- K^+p, K^+n total cross-sections are increasing with energy through the region (20-60) GeV/c;
- the difference between particle and antiparticle cross-sections, $\Delta\sigma = \sigma(\bar{x}p) - \sigma(xp)$ is decreasing with energy, and fits $\Delta\sigma \propto Ap^{-n}$.

The values of the exponent for π, K, p are given in Table II.[26]

This data indicated that probably at just slightly higher energies, the Okun-Pomeranchuck theorem (which states that the cross-sections for particles belonging to the same isospin multiplet should become equal asymptotically), and the Pomeranchuck theorem would be satisfied.

Other measurements became available around this time, which generally confirmed the above trends.

a) The Λp and Λn total cross sections were measured at CERN[27] with a wire chamber spectrometer set up to study K^0 decays. The results are shown in Fig. 8, together with the cross-section for $\Sigma^- p$ measured at 19 GeV/c in the hyperon beam at CERN.[28]

The additive quark model gives relationships between ΛN, pN, KN, πN cross sections--

$$\sigma_T(\Lambda p) = \sigma_T(pp) + \sigma_T(K^- n) - \sigma_T(\pi^+ p)$$

which seem to be reasonably satisfied (see Fig. 8).

b) The total cross-section for γp and γn have been measured up to 30 GeV at Serpukov (extending the old SLAC, DESY and DARESBURY measurements).[29] The data is shown in Fig. 9. The s-dependence of these data is fit to

$$\begin{aligned}\sigma_T(\gamma p) &= A + Bp^{-1/2} \\ &= (97.4 \pm 1.9) + (55 \pm 5)^{I=0}\, E^{-1/2} + (12 \pm 2.5)^{I=1}\, E^{-1/2}\ .\end{aligned}$$

The photon data up through 30 GeV behave very much like the $\pi^\pm N$ cross-sections (only 1/200 smaller).

When the ISR--the proton-proton storage rings at CERN--started doing experiments, there were almost immediately rumors of large p-p absorption cross-sections. Last year these preliminary reports settled down, and the picture of the elastic amplitude has again been shattered--the pp total cross-section rises ~ 4mb through the ISR energy region (~ 200 - 1500 GeV/c equivalent momentum range). It is now clear that statements on σ_T becoming constant must be modified--it may become constant asymptotically or it may not. The simple picture in which there are just two contributions--an energy independent one, due to Pomeron exchange, and a decreasing contribution as energy increases due to Regge exchange, is not a good model. It is now clear that the region which gave credibility to the idea of constant asymptotic cross-section is actually only a local minimum, where the s-dependence of the various contributions cancel. Whether eventually σ_T does approach a constant (this time from below), or continues to rise indefinitely, remains for some experimenters of the future. (See Fig. 10.)

Let us now review these exciting new measurements in more detail. The data (when finally the ISR was running reliably enough to make precision cross-section measurements) came from two groups using two quite different methods--

1) CERN-Rome:[30] They measure the forward scattering angular distribution $d\sigma/dt$, with a scintillation counter telescope and extrapolate to find the the forward cross-section, $d\sigma/dt\big|_{t=0}$. They also measure the real part of the forward scattering amplitude in this energy range and find it small and essentially negligible. From the optical theorem, they can then determine the total cross-section

$$\sigma_T^2 = 16\pi \left.\frac{d\sigma}{dt}\right|_{t=0} .$$

This experiment normalizes their total cross-section measurement two ways--(a) internally, by measuring the elastic scattering into small enough angles to observe the Coulomb scattering, which can be absolutely calculated, and (b) externally, by using the Van der Meer luminosity measurement of the circulating proton beams. Both methods agree well.

2) Pisa-Stony Brook.[31] They measure the reaction rate in pp collisions with an almost 4π counter hodoscope. This experiment is normalized using two external methods--the Van der Meer beam displacement measurement, and actual measurement of the individual beam profiles by scattering in gas. Again, both these methods of normalizing agree well. This group has made the highest energy measurement, when the stored 25 GeV/c proton beams were accelerated in the storage ring to 31.4 GeV/c in each beam.

The results of these experiments are shown in Fig. 11, and summarized in Table III.

Good agreement is obtained between these two groups in the cross-section rise. It is interesting to note that they depend quite differently on the luminosity measurement--

CERN-Rome $\qquad \sigma_T \propto \sqrt{\left.\frac{d\sigma}{dt}\right|_{t=0} \cdot \frac{1}{L}}$

Pisa-Stony Brook $\qquad \sigma_T \propto \frac{\text{Rate}}{L}$

So if there were systematic problems with the measurement of the ISR luminosity, it would affect the total cross-sections of these two experiments in a markedly different way. The agreement is evidence that they indeed do measure L reliably.

A further interesting comment should be made on the independence of the rise in $\sigma_T(pp)$ on the luminosity measurement. It is clear from the above discussion that the ratio of the measured quantity in these two experiments is a measure of the total cross-section, completely independently of measurements of L.

$$\left[\left.\frac{d\sigma}{dt}\right|_{t=0} \Big/ \text{Rate}\right] \propto \frac{\sigma_T^2 \cdot L}{\sigma_T \cdot L} = \sigma_T$$

If the proton beam phase space and luminosity does not vary around the ring, then the data from the two groups taken simultaneously (a small fraction of their total running) could be used to perform this check. It is interesting that the results confirm the measured rise in $\sigma_T(pp)$, but with poorer error since one has to add the errors of the two measurements and only a small fraction of the data satisfied conditions of simultaneous running, and well steered beams. The cross-sections are given in Table IV.[2]

To summarize, the luminosity measurements seem to be well understood and in good agreement, and the 4 mb rise in the pp total cross-section through the ISR energy range, an established fact.

This rise in $\sigma_T(pp)$ was also indicated in an analysis of very high energy proton flux at an atmospheric depth of 550 gm/cm^2 on a mountain top in Bolivia, compared to the flux at the top of the atmosphere. This analysis (by Yodh, Pal and Trefil)[32] indicated that the nucleon-nucleon cross-section increased with energy significantly at laboratory energies about 500 GeV. The lower bound for the energy dependence, from their analysis, agrees well with the measured increase through the ISR--and is indicated in Fig. 12 by the dashed line.

One amusing thought, while still considering this rising cross-section: for many years we have been concerned about how fast the $\bar{p}p$ cross-section is falling as the energy increased, and wondering when it would finally fall sufficiently to reach the pp cross-section to fulfill the Pomeranchuck theorem. Now the pp cross-section has risen so high that we now have the situation that the $\bar{p}p$ total cross-section will have to turn around and <u>increase</u> with energy to catch up with the pp cross-section.

Kycia[33] will report on the new precision measurements for $\pi^{\pm}N$, $K^{\pm}N$, $p^{\pm}N$ at NAL at the Topical Conference.

The energy dependence of the $\sigma_T(pp)$ have been shown to be compatible with both a $\ln s$ and $\ln^2 s$ growth with energy.

2. <u>Elastic Cross-Section</u>

We first review the p-p scattering data through the ISR energy region, and then follow other particle scattering up through Serpukov energies.

At the ISR the CERN-Rome[34] and ACGHT[36] groups measured the elastic scattering distribution (described in the next section), and by integration obtain the elastic cross-section. This data, together with measurements from the NAL bubble chambers[36] is summarized in Fig. 13, and Table V. The elastic cross-section increases by ~ 10% through the ISR region--the same fraction as σ_T.

The 205 GeV/c NAL-LBL-Berkeley HBC π^-p experiment[37] has measured the π^-p elastic cross-section as (3.03 ± 0.3)mb. This result is plotted with other π^-p data in Fig. 14. Also shown are the energy dependencies for K^-p and $\bar{p}p$ elastic scattering. The π^-p data shows evidence of flattening out, similar to the p-p data. (The extrapolated value of the 205 GeV/c cross-section if the lower energy s-dependence had continued would have given $\sigma_{el} \sim 2.3$ mb.)

New measurements of the high energy elastic cross-section are summarized in Table VI, and the fitted energy dependencies of the cross-sections given in Table VII. (Remember that this slow falling of the cross-section eventually flattens out as shown for π^-p and pp in Figs. 13 and 14--and that the σ_{el} at sufficiently high energy starts to rise with σ_T, as shown in Fig. 13 for pp.)

The new elastic scattering experiments at NAL will be reviewed by Ritson at the Topical Conference.[38]

Before finishing our examination of the elastic scattering data, I would like to consider two interesting ratios: a) (σ_{el}/σ_T), and b) $[\sigma(AB \to AB)/\sigma(\bar{A}B \to \bar{A}B)]$.

a) In asymptotic geometrical models, where the proton is seen as a completely absorbing black disc of radius R, the ratio of the elastic to the total cross-section is 0.5. However, for a gaussian distributed absorption, 100% at $R = 0$ the ratio is ~ 0.15-0.20, being 0.185 for $R = 1f$. The ratio is plotted in Figs. 15 and 16 for p-p and π^-p interactions, respectively. The rather sparse data for other processes is given in Table VIII. Clearly, the ratio is far from 0.5, and, moreover, for the $\pi^- p$ and p-p reactions (where there is data at high energy), has reached a plateau value which is independent of energy.

b) Martin[39] has proved (for quite general assumptions on the analyticity of the elastic scattering amplitude) that one should expect the elastic (diffractive) cross-section for particle processes to equal the antiparticle elastic cross-section at asymptotic energies. This work has been generalized to include inelastic quasi-two-body cross-sections too.[40] Table IX summarizes some data on the ratios of particle to antiparticle elastic cross-sections. It is surprising the extent to which the equality seems to be preserved, even at energies where one knows that Regge exchange processes contribute substantially, and therefore, the scattering cannot be all due to Pomeron exchange.

3. Elastic Differential Cross-Sections.

In this section we review the data on $d\sigma/dt$ for elastic processes, first the p-p scattering at ISR and NAL and then working down in energy, for both baryon-baryon and baryon-meson scattering.

A. Baryon-baryon scattering

The forward angular distribution in pp elastic scattering is sharply peaked, as expected in a diffractive process. However, recently, very accurate measurements at the ISR have shown the presence of some interesting structure around $t \sim 0.15$ GeV^2. (This possibility had been pointed out many years earlier by Carrigan,[41] who noted that at (10-30) GeV energies the value of the slope in pp scattering differed experiment to experiment. He suggested the changes were due to the different t ranges being studied. However, no sufficiently systematic and accurate experiments had been done before the ISR studies brought the feature to clear light.)

The small t-region ($t < .15$ GeV^2) has been studied by CERN-Rome[42] and ACGHT[43] at the ISR, and by US-USSR group[44] at NAL. Lower energy measurements are also available from Serpukov.

The large t-region of the forward scattering ($.2 < t < .5$ GeV^2) has been studied by the ACGHT group at ISR.[43] The same group has also measured large t-scattering out to t values of ~ 5 GeV^2.[45]

We first consider the systematics of the forward region. The general conclusion is that the region with $t < .15$ GeV^2 has a steep slope (≈ 12 GeV^{-2}), which shrinks as energy increases. The region with ($.2 < t < .5$ GeV^2) has a somewhat flatter angular distribution (about 2 units smaller slope value), and exhibits essentially no energy dependence.

Typical data is shown in Fig. 17, where (a) shows data from the highest energy ISR studies of the ACGHT group--the two regions of the scattering distribution are clearly visible; (b) shows data from the US-USSR collaboration at one of the energies in this NAL experiment--this experiment measures entirely in the "small t-region" discussed above. Notice in the very forward direction the observation of p-p Coulomb scattering.

There has been much discussion as to whether there really are two distinct regions or whether the slope smoothly decreases as the scattering angle increases. New data from CERN-Rome[42] at $\sqrt{s} = 53$ GeV show that the slope is not continuously changing through the "small t region," but that one value of the slope parameter describes all of the data. If the cross-section within this "small t" interval is fit with $\frac{d\sigma}{dt} = \left.\frac{d\sigma}{dt}\right)_0 \cdot e^{-bt}$, then for

$$0.01 < t < 0.06 \text{ GeV}^2 \quad \text{they find} \quad b = 13.1 \pm 0.3 \text{ GeV}^{-2}$$
$$0.04 < t < 0.16 \text{ GeV}^2 \quad \text{they find} \quad b = 13.0 \pm 0.3 \text{ GeV}^{-2}$$

Further confirmation of this effect can be seen in Table X, where all of the ISR forward slope measurements are gathered.[3]

The slope of the larger t region is also quite stable with t interval used. The results of the fitting in this region are also given in Table X.[3]

The situation on the s-dependence of the slope prior to the NAL experiment is shown in Fig. 18. The data were fit to an exponential in the two ranges, $t < 0.1$ GeV^2 and $0.15 < t < 0.5$ GeV^2, from 1 GeV/c beam momentum through the ISR energy (~ 2000 GeV/c equivalent momentum). The Serpukov data were lowered by $\Delta b \sim 0.4$ GeV^{-2}, which is within their quoted systematic error. The data show b increasing with increasing energy, but the rate of change becoming relatively constant above 30 GeV/c. The data above 30 GeV/c were fit to

$$b(s,t) = b_0(t) + 2\alpha'(t) \ln \frac{s}{s_0} .$$

The fits are quite good and result in the following parameters

(low t region):	$b_0 = (7.0 \pm 1.2)$,	$\alpha' = (0.37 \pm 0.08)$
(larger t region):	$b_0 = (9.2 \pm 0.94)$,	$\alpha' = (0.10 \pm 0.06)$

In other words, the cross-section is made up of a forward region which exhibits substantial shrinkage, and a larger t region which is essentially constant in t.

The US-USSR group[44] at NAL have studied small t pp elastic scattering, detecting the recoil proton from 'beam-hydrogen gas jet' collisions in an array of solid state counters. A typical $d\sigma/dt$ was shown in Fig. 17. This group found their data consistent with a logarithmic growth of the slope with energy, and fitting their data above $s \sim 100$ GeV^2 to

$$b(s) = b_0 + 2\alpha' \ln s$$

yielded

$$\left.\begin{aligned} b_0 &= 8.23 \pm 0.27 \text{ GeV}^{-2} \\ \alpha' &= 0.278 \pm 0.024 \text{ GeV}^{-2} \end{aligned}\right\} \quad \text{for} \quad t < 0.15 \text{ GeV}^2$$

The most complete analysis of all of the data is shown in Fig. 19 (from Amaldi '73), where the dashed line corresponds to the parameters

$$\left.\begin{aligned} b_0 &= 8.32 \text{ GeV}^{-2} \\ \alpha' &= 0.275 \pm 0.02 \text{ GeV}^{-2} \end{aligned}\right\} \quad \text{for} \quad t < 0.12 \text{ GeV}^2$$

The ACGHT group[45] have extended their studies of elastic pp scattering out to larger momentum transfers by using a double arm wire chamber spectrometer with momentum analysis in both arms. This set-up provides enough discrimination against the inelastic background that they can follow the cross-section down seven orders of magnitude. The scattering distributions are shown in Fig. 20 for four energies at the ISR. The break in the pp scattering cross-section for $t \sim 1.2$ GeV^2 observed at lower energies now becomes a sharp dip, with a secondary peak. The position of the dip, and the height of the secondary peak are essentially independent of energy.

[At London, apparently the CHVO group reported preliminary results on a second generation study of large angle pp elastic scattering. This new data is claimed to show the position of the dip moving in (i.e. to smaller t-values) as the energy increased, and the height of the secondary maximum also increasing.]

The break in the pp scattering distribution at low energies is shown in Fig. 21 and again in Fig. 22 where the measured cross-section has been divided by $G^4(t)$, where $G(t)$ is the electromagnetic form factor $G(t) = [(1 + t/\mu^2)^2]^{-1}$, and $\mu^2 = 0.71$ GeV^2. (This is the optical model of Chou-Yang, where the matter density is assumed to have the same distribution as the charge density. The shape of this curve is shown in Fig. 21.) Not too much energy dependence is apparent.

The ACGHT group report the t-value of the dip, as a function of energy:

$\sqrt{s}$ (GeV)	t_{dip} (GeV^2)
23.5	--
30.7	1.45 ± .1
44.9	1.38 ± .04
53.0	1.37 ± .04

The $G(t)^4$ description clearly does not fit the data, but the model has been extended by Durand and Lipes (and others) to give a good representation of the scattering of ISR energies. These fits will be discussed later.

The data on np elastic scattering shows very much the same structure as the pp data discussed above. Two experiments--one at CERN studying $np \to np$ up to 24 GeV/c[46] and the other at Serpukov[47] measuring up to 65 GeV/c --are reviewed. The $d\sigma/dt$ of the CERN experiment are presented in Fig. 23 and clearly show the development of the large t-dip. Figure 24 compares the n-p scattering distribution with the data of Allaby et al. at 19.2 GeV/c--the agreement is very good.

The shape of the angular distribution has been analyzed in terms of the exponential slope, b. The results below 30 GeV/c are shown in Fig. 25, where the p-p and n-p data have been fit for $t < 0.3$ GeV^2. The higher energy data has been obtained in a gas jet target experiment at Serpukov, and measures only the small t-region. The value of the slope for $t < 0.05$ GeV^2, for np scattering data between (10-65) GeV/c is given in Fig. 26, where it is compared to the dashed line--which represents the fit to the small t pp data discussed above. For both experiments the agreement between the np and p-p data is good.

It is interesting to notice that the small t slope for np is 1-2 units in b larger than the slope measured for data with $.07 < t < .3$ GeV^2, in keeping with the effect observed for pp scattering (i.e. 2 region in $d\sigma/dt$).

As a final comment on baryon-baryon scattering, the hyperon beam group at BNL (the Yale-NAL group)[48] have studied the slope of $\pi^- p$ and $\Sigma^- p$ elastic scattering at 23.3 GeV/c, while setting up to study the Σ-decays. Figure 27 shows the two differential cross-sections. The data are well represented by $d\sigma/dt = Ae^{-bt}$; with

$$\left.\begin{aligned} b_\pi &= 7.99 \pm 0.22 \text{ GeV}^{-2} \\ b_\Sigma &= 8.97 \pm 0.26 \text{ GeV}^{-2} \end{aligned}\right\} \quad (0.07 < t < 0.21 \text{ GeV}^2)$$

The slope parameter for Σp is, not surprisingly, very similar to the slope in p-p scattering at the same energy. (The p-p data in Fig. 25 are taken over a similar t-range, and indicate a value of the slope ~ 8.8 GeV^{-2}.)

B. Meson-baryon scattering

We now move on to consider meson-baryon scattering data.

Some recent data on $\pi^- p$ elastic scattering is summarized in Table XI. Three experiments, covering similar t ranges analyzed the cross-section in terms of $d\sigma/dt = Ae^{-bt}$, and the slope values are given in the top part of the table. Weak evidence of shrinkage is observed. However, it is clear from the high statistics studies at 14,[49] 25, 40[50] GeV/c that there is curvature in the cross-section, and that if one attempts to fit the data out to large t, a quadratic term is required--see Figs. 28 and 29. The slope b from this analysis is given in the bottom part of Table XI, and displayed in Fig. 30. Very clear evidence of shrinkage is observed.

Figure 29 also shows the differential cross-section for $K^- p$ and $\bar{p}p$ elastic scattering at 25, 40 GeV/c from Serpukov.[50] The slope parameters are summarized in Table XII.

The CERN-Serpukov group[50] studied the shrinkage of the forward peak by fitting all the available data for $10 < s < 70$ GeV^2, at $t = 0.2$ GeV^2 with the slope parametrized as

$$b = b_0 + 2\alpha' \ln s \ .$$

They found quite small shrinkage for the $\pi^- p$, $K^- p$ scattering, and very substantial antishrinkage for $\bar{p}p$.

$$\left.\begin{aligned} \alpha'(\pi^-) &= 0.18 \pm .04 \\ \alpha'(K^-) &= 0.19 \pm .04 \\ \alpha'(\bar{p}) &= -0.5 \pm .05 \end{aligned}\right\} \quad \text{at } t \sim 0.2 \text{ GeV}^2$$

However, they also observed a rather strong t-dependence to the shrinkage. This effect is shown in Table XIII where $2\alpha'$ is listed as a function of the t-value at which it was evaluated. The $\pi^- p$ and $K^- p$ scattering is seen to have very substantial shrinkage for $t \lesssim 0.1$ GeV^2 with $\alpha \sim (0.26\text{-}0.36)$ GeV^{-2}, while for t larger then 0.2 GeV^2 the shrinkage is quite small with $\alpha' \sim 0.1$ GeV^{-2}.

<u>This is very reminiscent of what we have learned of the pp system above</u>.

Another experiment commenting on the curvature of the differential cross-section is reported by 10 GeV/c $K^- p$ CERN-HBC collaboration.[51] They report a slope of 9.8 ± 0.5 GeV^{-2} for the elastic $K^- p$ peak for $t < 0.1$ GeV^2, and a slope of $7.1 \pm .2$ GeV^{-2} when $.12 < t < .4$ GeV^2.

A word of caution is in order here. The curvature of the differential cross-section in processes like $\pi^{\pm} p$, $K^- p$ and $\bar{p}p$ elastic scattering at low (or even moderate) energies should not be taken as indicative of diffractive behavior. It <u>may</u> be associated with the behavior of p-p scattering at the ISR (and hence the "Pomeron"), but it may very well not--since we do have an alternative explanation.

We know that there is substantial Regge exchange contribution to the $\pi^{\pm} p$, $K^- p$ elastic amplitudes in the (5-40) GeV/c range--if from nothing else, the $\pi^- p \to \pi^0 n$, $K^- p \to \bar{K}^0 n$ cross-sections or from the energy dependence of the difference in total cross-sections discussed in II.1 above. We believe these Regge components to be peripheral, and so contribute a term like $J_0(R\sqrt{-t})$ to the differential cross-section. The diffractive contribution we believe is central in impact parameter space, and behaves like an exponential, e^{-bt}. Therefore, the $d\sigma/dt$ for these processes is the sum of the Bessel function and the exponential, which certainly shows curavture or may even look like two exponentials. (See Fig. 31.) A good example of such behaviour is shown in Fig. 32 where $K^+ p$ and $K^- p$ elastic $d\sigma/dt$ at 5 GeV/c is shown. The $K^+ p$ process is believed to be mainly diffractive (with very little Regge), while the $K^- p$ is believed to have quite substantial peripheral Regge amplitude in addition to the diffractive contribution. The $K^- p$ cross-section is seen to start higher than the $K^+ p$ forward cross-section, fall faster and then oscillate about the essentially exponential $K^+ p$ data. This is just the behavior one would expect from the above model.

We should therefore be skeptical of assuming the $d\sigma/dt$ behaviour of the $\pi^{\pm} p$, $K^- p$ is the same phenomenon observed in p-p. It will be interesting to see the results of high statistics studies of $K^+ p$ scattering in the (5-20) GeV/c region, and the behaviour of all of these processes at NAL. If the NAL experiments find the small t steepening of the cross section, and it proves to be s-independent, then we will be forced to associate this behaviour with that observed in pp scattering at ISR, and of course, with the Pomeron. It will be especially interesting to see the results of the NAL $K^+ p$ experiments and the very high statistics $K^+ p$ scattering at SLAC--here the Regge contributions are known to be small.

If the experimental evidence supports that indeed the small t steepening is due to the Pomeron, the same two component mechanism discussed above may be at work (i.e. a $J_0(R\sqrt{-t})$ term adding to a central, e^{-bt}, term)--where now the peripheral contribution may be associated with the Pomeron, an additional piece coming from the grey ring around the edge of the proton. We discuss such a model[52] for the Pomeron later.

C. Meson-meson scattering

There is very little systematic data on π-π, K-π scattering in the diffraction-dominated region, although there are several good experiments studying the resonance region. The difficulties in these studies are 1) having high energy so that the diffraction region is accessible in the meson-meson scattering, 2) the event rate is small since the meson cloud presents a low luminosity target for the scattering, and 3) finding a reliable analysis technique to separate meson diffraction from resonance production at the other vertex. Below we report briefly on some π-π, K-π scattering data to give a flavor of what is known.

Walker et al.[54] have studied

$$\pi^- p \to \pi^+\pi^- n \qquad \text{at } 25 \text{ GeV/c}$$

$$\pi^- p \to \pi^-\pi^-\Delta \qquad \text{for } (5\text{-}25) \text{ GeV/c}$$

The production angular distributions are shown in Fig. 35. They find the forward peak is well fit to

$$\frac{d\sigma}{dt} \propto e^{-bt}$$

$$b(\pi^+\pi^-) = 5.9 \pm 0.54 \text{ GeV}^{-2}$$

$$b(\pi^-\pi^-) = 6.1 \pm 0.51 \text{ GeV}^{-2}$$

The integrated data yields $\sigma_{el}(\pi^+\pi^-) \sim \sigma_{el}(\pi^-\pi^-) \sim 1.5$ mb and the total cross-sections are $\sigma_T(\pi^+\pi^-) \sim \sigma_T(\pi^-\pi^-) \sim 15$ mb. (See Fig. 36.) This analysis compared all data[54,55] to isolate the 3 isospin cross-section in π-π scattering and found (as expected for diffractive processes) that they were all equal

$$\sigma_0 \sim \sigma_1 \sim \sigma_2 = (15\text{-}20) \text{ mb} .$$

(Again, there is rumor from the London Conference that the Carnegie-Mellon-BNL group presented an analysis of 8, 16 GeV/c $\pi^- p$, $K^- p$ elastic scattering data and report a break in the $d\sigma/dt$ at $t \sim 0.2$ GeV^2. I do not know if the data demands a break or is merely consistent with curvature as in the data discussed above.)

A summary of the s-dependence of the slope for elastic scattering as measured at $t \sim 0.2$ GeV^2, is shown in Fig. 33. The slopes for particle and for antiparticle scattering seem to become equal at high energies, with asymptotic slopes of ~ 8 GeV^{-2} for πN, ~ 7.5 GeV^{-2} for KN and ~ 11 GeV^{-2} for NN. The $\pi^- p$ and $K^- p$ data show almost no shrinkage (i.e. no s-dependence of the slope), while the $\bar{p}p$ data shows considerable antishrinkage up through the Serpukov energy region. The $K^+ p$ and pp data show considerable shrinkage, while the $\pi^+ p$ data also shows shrinkage, but much less. Ritson will present the preliminary results on the NAL elastic scattering slopes at the Topical Conference.[38]

Why do the $\pi^\pm p$ angular distributions show so little energy dependence compared to $K^+ p$ and pp, if they are all diffraction dominated? This question was answered in a very nice analysis by Davier,[53] applying the Dual Absorption Model to the combination of the $\pi^+ p$ and $\pi^- p$ that isolates isoscalar exchange, and assuming only the Pomeron and f-meson contribute to the exchange amplitude. The Pomeron was parametrized as a central collision process while the f^0 was given a Regge energy dependence and assumed to be peripheral. The data were well fit with this composite amplitude and the resulting Pomeron contribution showed substantial shrinkage, in good agreement with the $K^+ p$ data. Figure 34 shows the $K^+ p$ slope as a function of energy as the shaded band, and the data points are the Pomeron contribution to the $\pi^\pm p$ scattering from Davier's analysis. The agreement is good. It is interesting to see that small admixtures of a non-diffractive amplitude may markedly change the energy dependence of the differential cross-section, and, further, that the Pomeron derived from this analysis agrees so well with the classic "$K^+ p$ Pomeron".

In addition, some data is available from 8 GeV/c π^+p and 12 GeV/c K^+p experiments at LBL.[56] The diffractive scattering is isolated by choosing small t for the meson-scattering, selecting $M(p\pi^+) > 1400$ MeV to remove the strong pion exchange reaction, and requiring $M(\pi\pi)$ or $M(K\pi)$ to be greater than 1600 MeV to isolate the diffractive scattering from the "s-channel" resonance formation processes.

For $t < 0.3$ GeV^2 they find

$$b(\pi\pi) = 4.14 \pm .22 \text{ GeV}^{-2}$$

$$b(K\pi) = 4.10 \pm .25 \text{ GeV}^{-2}$$

D. Cross-over phenomenon

The differential cross-section for the elastic scattering reaction $\bar{X}p \to \bar{X}p$ is known to have a steeper slope and a larger forward intercept than the reaction $Xp \to Xp$. This leads to the well-known cross-over effect in which the differential cross-sections cross at a t-value of ~ 0.2 GeV^2. The difference in these cross-sections is due to the imaginary part of the non-flip odd C amplitude in the t-channel. This phenomenon is understood in terms of the Dual Absorption Model in which the K^+p and pp reactions (being exotic in the s-channel) have dominant contribution from the Pomeron, while $\pi^\pm p$, K^-p and $\bar{p}p$ all have a mixture of Pomeron and Regge terms. The KN and NN data show clear cross-overs (since the Regge contribution appears only in one term), while the $\pi^\pm p$ differential cross-sections have very similar slopes and magnitudes, since both terms (Regge and Pomeron) contribute to both cross-sections.

A beautiful experiment[57] at Argonne has studied these phenomena in the (3-6) GeV/c region--the data is displayed in Figs. 37-40 and summarized in Table XIV. The cross-over in particle antiparticle cross-section were found to be quite energy independent

$$\pi : t_c = 0.14 \pm .03 \text{ GeV}^2$$

$$K : t_c = 0.19 \pm .006 \text{ GeV}^2$$

$$p : t_c = 0.16 \pm .004 \text{ GeV}^2$$

At SLAC a high statistics wire chamber experiment[58] is in progress studying $K^\pm p$ scattering at 6, 10, 14 GeV/c, and $\pi^\pm p$ and $p^\pm p$ scattering at 10 GeV/c. A preliminary measurement was performed at 13 GeV/c for $K^\pm p$ (see Fig. 41), and indicated $t_c = 0.21 \pm .03$ GeV^2. Final results on the SLAC systematic study should be available shortly. (Representative cross-sections are shown in Fig. 42.)

The s-independence of t_c indicates that the effective radius of the peripheral amplitude (the odd C Regge exchange term) is constant and not expanding as the energy increases.

E. Real parts of forward scattering amplitude

Typical differential cross-sections are shown in Figs. 43 and 44 for the NAL experiment[59] and the CERN-Rome ISR epxeriment,[60] respectively.

This quantity is becoming very interesting, given the observation of rising total cross-sections. Dispersion relations provide a connection between the behavior of the ratio of the real to imaginary parts of the forward scattering amplitude, ρ, and the energy dependence of the pp and $\bar{p}p$ total cross-sections. This integral relation is such that ρ measured at energy E is sensitive to the behavior of $\sigma_T(pp)$ and $\sigma_T(\bar{p}p)$ for energies larger than E.

Khuri and Kinoshita[61] have shown that total cross-sections, rising indefinitely as a power of the logarithm of the energy, imply ρ approaching zero from above. The argument goes as follows:

> An amplitude that corresponds to $\sigma_T \propto (\ln s)^\nu$ at high energies is $F^+(s) = i|\gamma^+|s\,(\log s)^{\nu^+}$.

However, this amplitude does not satisfy the requirements of analyticity and crossing in the complex energy plane. Such an amplitude can, instead, be written as

$$F^+(s) = i|\gamma^+| s \left(\log s - i\frac{\pi}{2}\right)^{\nu^+}$$

$$\sim i|\gamma^+| s (\log s)^{\nu^+} + \frac{\pi\nu^+}{2}\gamma^+ s (\log s)^{\nu-1^+}$$

Thus

$$\rho = \frac{\mathrm{Re}\, F^+(s)}{\mathrm{Im}\, F^+(s)} = + \frac{\pi\nu}{2} \cdot \frac{1}{\log s}$$

The derivation is for the sum of the pp and $\bar{p}p$ amplitudes (i.e. the even signature amplitude), but for no pathological behaviour of $\bar{p}p$ it may be assumed to apply to the pp data alone.

Then, for the total cross-section approach a constant from above, the ρ goes to zero from below, but for a rising cross-section, the ρ must be positive (and if the $d(\sigma_T)/ds$ stops, ρ approaches zero from above).

Therefore, one may use careful measurements of ρ to try to gain insight on the s-dependence of σ_T at still higher energies. How sensitive is it? Bartels and Diddens[62] have investigated this sensitivity by calculating $\rho(s)$ for σ_T becoming constant at various energies. The results are shown in Fig. 45. Clearly, precision measurements through the ISR region would allow useful limits to be placed on the high energy behavior of $\sigma_T(pp)$.

The measurements for pp are shown in Fig. 46 up through 400 GeV/c,[59] while new data on the real part for np scattering at Serpukov[47] is shown in Fig. 47. It is interesting to see the agreement between this data and the p-p data discussed above.

Finally, Fig. 48 shows the real part measured in $\pi^- p$ scattering through Serpukov energies.[63] It will be interesting to see what is measured at NAL, both in terms of the $\sigma_T(\pi^\pm p)$ and their real parts.

F. Some theoretical comments

I. Asymptotic Bounds

At asymptotic energies, the bound of Lugunov and Van Hieu (Topical Conference on H.E. Collisions, Vol. II, p. 74, 1968) may be written

$$\sigma_{el} \gtrsim \frac{\sigma_T^2}{(\ln s)^2}$$

but we know

$$\sigma_{el} \leq \sigma_T$$

Then, if $\sigma_T \propto (\ln s)^\alpha$,

for $\alpha = 1$, $\quad$ constant $\leq \sigma_{el} \leq \ln s$

and $\alpha = 2$, $\quad$ $\sigma_{el} \propto \ln^2 s$

Further, if $d\sigma/dt = \sigma_T^2 \cdot e^{-bt}$, then

$$b = \frac{\sigma_T^2}{\sigma_{el}}$$

and

for $\alpha = 1$, $\quad$ $\ln^2 s \geq b \geq \ln s$

and $\alpha = 2$, $\quad$ $b \propto \ln^2 s$

One interesting point of these bounds is that if the σ_T ever saturates the Froissart bound and increases like $\ln^2 s$, then the energy dependence of b must change from the present ln s behaviour.

II. Fits to High Energy p-p Scattering

There are two main types of models for the Pomeron in pp elastic scattering:

(a) the two component models typical of the work of Cheng-Walker-Wu,[64] Kane,[8,9,10] Barger-Geer-Phillips,[65] Allcock-Cottingham-Michael,[66] which are summarized in Fig. 49.

The main contribution to the Pomeron is from the central collisions giving rise to the exponential,(or $e^{at} J_1(R\sqrt{-t})$, t-dependence arising from absorption from a disc of radius of about 0.6 f. The e^{at} modifier accounts for the smoothing of the edge of the disc. The dip at $t \sim 1.4$ GeV^2 is the diffraction zero from the disc.

In addition to this central piece there is a peripheral contribution from the edge of the proton. Constructive interference between these two terms produces the upward curvature in $d\sigma/dt$ for small t.

There are differences in the details of the models, but the essential two components are as described.

Allcock et al.[66] make the point that the edge component may be due to 2π exchange. Their calculation indicates that in shape and in magnitude the 2π exchange term fits the extra high partial wave tail that is the characteristic of the second component.

Henyey et al.[10] describe this component as due to dissociation of the incoming particle; Cheng-Walker-Wu[64] ascribe Diffraction Dissociation to the ring component.

(b) The pole and cut models, typical of the work of Durand-Lipes,[67] Chou-Yang,[68] Frautschi-Margolis,[69] etc. These models are described in Fig. 50. The dip at large t is generated by the destructive interference of a structureless pole term, with a cut of opposite sign.

The small t structure has to be explained by introducing modifications to the pole term (e.g. the 2π contribution discussed in the above models could be used to modify the pole term).

A typical fit to the scattering data at the ISR is shown in Fig. 51. The height of the secondary maximum is related to the total cross-section used in the optical model calculation (40 mb in this case), so a more realistic σ_T would allow for better fit in this t range.

4. Summary

- $\sigma_T(pp)$ increases for (200-1500) GeV/c by $(10 \pm 2)\%$,

  $\sigma_{el}(pp)$ increases for (200-1500) GeV/c by $(12 \pm 4)\%$,

  $\rho \sim 0$ for 300 GeV/c

  slope, b, increases for (200-1500) GeV/c by $(11 \pm 3)\%$

  $\sigma_{inel}(pp)$ increases for (200-1500) GeV/c by $(10 \pm 2)\%$.

This data is consistent with an optical model picture of a gray absorbing disc of constant opacity, (σ_{el}/σ_T flat), and with the radius increasing with energy.

Since, in this picture σ_T, b, σ_{el}, σ_{inel} are all proportional to R^2 --the radius of the proton--then R should have increased by ~ 5%. If we interpret the deep dip in pp scattering as a diffraction minimum, then this is a measure of the radius of the scatterer: the dip should move in t-value--it seems that it probably does.

If one looks at the rate of change of R with energy--the σ_T, b are consistent with (ln s) growth in R^2, while the diffraction minimum seems consistent with moving to smaller t-values like $\sqrt{\ln s}$--again things make a consistent picture.

If one looks more carefully, this picture requires more fine structure. The small t p-p scattering implies that the proton has an outer edge or "ring," and that this is expanding quite rapidly with energy, ~ ln s. The large t scattering gives us information on the "core" of the proton, which even at ISR energies is not black but ~ 92% of its unitary value, and quite constant with energy.

- The real part crossing zero and going positive for momentum ~ 300 GeV/c is consistent with the measured rise in σ_T up through 2000 GeV/c. Careful measurements of the real part in pp scattering up through 2000 GeV/c would give useful constraints on the behaviour of $\sigma_T(pp)$ up to $(10^4 - 10^5)$ GeV.

• The elastic scattering data shows that diffractive scattering is sharply peaked and well parametrized as $as(d\sigma/dt) \sim Ae^{-bt}$ for small t. Good indications for steepening of the $d\sigma/dt$ as a function of t are observed for $\pi^{\pm}p$ and K^-p in the (5-40) GeV/c energy region, which is parametrized as two exponentials or one exponential with quadratic t dependence. A straightforward explanation for the steepening of $d\sigma/dt$ for these processes is found in a peripheral Regge exchange contribution to the t-channel amplitude. However, similar behaviour is observed in p-p scattering at 2000 GeV/c where Regge is not expected to play a great role. This may imply a peripheral piece to the Pomeron.

The slope parameter, b, is steeper in $\bar{X}p$ scattering than for Xp scattering. This fact, together with the observed equality of the integrated cross-sections (i.e. $\sigma_{el}(\bar{X}p) = \sigma_{el}(Xp)$), implies a cross-over of the differential cross-sections. This cross-over phenomena has been studied for $p <$ 15 GeV/c and no s-dependence found. It will be interesting to follow these studies at NAL.

The slopes of the scattering distribution are observed to change with energy--the K^+p and pp systems exhibiting strong shrinkage, the $\pi^{\pm}p$ and K^-p slopes being essentially flat, and the $\bar{p}p$ scattering showing an anti-shrinkage behaviour. This shrinkage phenomena observed in K^+p and pp scattering, is normally understood as being due to the slope of the Pomeron trajectory--the effect is masked by Regge effects in the other elastic reactions.

• Pomeranchuck theorem predicts asymptotically $\sigma_T(AB) = \sigma_T(\bar{A}B)$, while Martin has shown that $\sigma_{el}(AB)$ should equal $\sigma_{el}(\bar{A}B)$, and the slope, $b(AB)=b(\bar{A}B)$.

The data is consistent with these predictions; the differences in particle and antiparticle total cross-section are falling like $s^{-0.5}$, while elastic cross-sections are equal even at low energy. The slopes of the differential cross-section seem consistent with an asymptotic common value for particle and antiparticle scattering.

III. PHOTOPRODUCTION OF VECTOR MESONS

In this section we review data on the photoproduction of vector mesons, (ρ, ω, ϕ).[19] Within the spirit of the Vector Dominance Model, (VDM), these processes should be more properly considered with the elastic scattering reactions (see Fig. 52), than considered together with the other exclusive inelastic diffraction processes. The early experimental results on rho production with polarized photons strongly supported that picture.[70] (See Fig. 53 where the $\rho \to 2\pi$ decay distributions show that the ρ has fully taken over the polarization of the photon, and that no longitudinal ρ decays are observed.) We shall summarize the data on cross-sections and angular distributions.

1. Cross-Sections

The cross-section for $\gamma p \to \rho^0 p$ is shown in Fig. 54, for photon energies between (1-15) GeV/c. The cross-section falls rapidly as the energy increases up to ~ 5 GeV, above which it has a rather slow energy dependence. For comparison the energy dependence of the πN elastic cross-section is shown; it exhibits an s-dependence very similar to $\gamma p \to \rho p$.

The ω photoproduction cross-section is shown in Fig. 55 from threshold to 9 GeV. Again one sees a very rapid fall-off of the cross-section at low energies, flattening out around 5 GeV. The SLAC-Berkeley-Tufts experiment[71] using a polarized photon beam (obtained by backscattering a laser beam on the primary SLAC electron beam) is able to separate the cross-section into the natural parity and unnatural parity t-channel contributions at 2.8, 4.7 and 9.3 GeV.† The unnatural parity cross-section falls very rapidly, in good agreement with the one-pion exchange model, and is essentially zero by 9 GeV. The natural parity exchange cross-section, which one would hope to be diffraction dominated, falls off like the ρ photoproduction data shown above, and hence like the πN elastic data.

†For natural parity exchange the pions from ρ decay, emerge preferentially in the plane of the photon polarization, while for unnatural parity exchange they emerge perpendicular to it.

The ϕ photoproduction cross-section is plotted in Fig. 56. The energy dependence for this process is either flat or rising very slowly--however, it is a small cross-section reaction and not very well measured.

2. Differential Cross-Sections

The differential cross-section for $\gamma p \to \rho^0 p$ is shown in Figs. 57 and 58, for two representative experiments. In Fig. 57, the $d\sigma/dt$ is displayed for a hydrogen bubble chamber experiment at 9.3 GeV,[71] while Fig. 58 shows the cross-section from (9-16) GeV from a wire spark chamber experiment.[72]

The differential cross-section have been fit to the form

$$\frac{d\sigma}{dt} = \left.\frac{d\sigma}{dt}\right|_{t=0} \cdot e^{-bt}$$

and the resulting slopes plotted as a function of photon energy, in Fig. 59 (from an analysis by Moffeit[19] of all the $\gamma p \to \rho^0 p$ data that could be analyzed in a standard way). Note the different t-ranges used in obtaining these slopes--especially remembering what we learned of the t-dependent shrinkage behaviour in elastic scattering in Chapter II. Figure 60 shows $d\sigma/dt$ (from the SBT bubble chamber, and from the SLAC wire chamber) for the small t region, where the two experiments overlap--the agreement is good. However, the slopes obtained from the two experiments are different by ~ 2.5 units when the full t-range of the HBC data is used--perhaps an indication of the same steepening of the $d\sigma/dt$ slope as t becomes smaller, that we observed for πN scattering in the (5-40) GeV/c energy region. The slopes show very little energy variation (at most 1 - 1/2 units for 3-16 GeV), and are consistent with the s-dependence of the average of the $\pi^{\pm} p$ elastic scattering slopes in the region $0.1 < + < .4$ GeV^2, shown as a dashed line in Fig. 59.

We might ask again, why a diffractive process should show so little shrinkage. Chadwick et al.[73] have performed an analysis on the energy dependence of the slope for $\gamma p \to \rho^0 p$, similar to that of Davier[53] described in the πN elastic section in Chapter II. They assume a central Pomeron and a peripheral f^0-meson exchange dominate the reaction, à la Davier, and hence uncover shrinkage in the Pomeron contribution to $\gamma p \to \rho^0 p$, which behaves just like the "$K^+ p$ Pomeron" and the "Davier πN Pomeron." Their fits to the data, and the results of the Pomeron and f^0 slopes as a function of energy are shown in Fig. 61.

The ω differential cross-sections, from the S-B-T collaboration,[71] are given in Fig. 62. The slope of the cross-section is reported as ~ 7 GeV^{-2} and quite independent of energy. (An analysis of the natural parity contribution results in the same conclusion, but with somewhat larger errors.)

The study of the photoproduction of the ϕ meson has been an interesting area. Since the ϕ meson decouples from other mesons we do not expect any strong t-channel amplitudes other than the Pomeron. Thus, the study of ϕ photoproduction should be an ideal laboratory to learn of the Pomeron's properties--much better in principle than the study of $K^+ p$ or pp where the Pomeron dominance depends on cancellations of Regge amplitudes through exchange degeneracy.

The ϕ is observed to be strongly produced coherently from complex nuclear targets, and the t-channel amplitude in $\gamma p \to \phi p$ is essentially purely natural parity (from asymmetry studies with polarized photons). These observations support the Pomeron exchange dominance hypothesis.[74]

The data on the differential cross-section is rather sparse and quite inconclusive as to whether there is any shrinkage of the forward slope, never mind any quantitative measure of how much it shrinks! Figure 63 shows the S-B-T bubble chamber data for (2.8 + 4.7) GeV and 9.3 GeV, respectively, and compared to neighboring energy data from other groups, there is clearly very little energy dependence at large t, and unfortunately, essentially no data in the small t region, where we have seen from elastic scattering the strongest s-dependence may be expected. Figure 64 shows another summary of the data on $d\sigma/dt$ ($\gamma p \to \phi p$), displaying new data from a Bonn group measuring at 2 GeV. A summary[12,19] of the slopes from these experiments is given in Fig. 65.

A recent SLAC experiment[75] measures the s-dependence of the ϕ cross-section at a fixed $t = 0.6$ GeV^2. Their data, together with the 2 GeV Bonn point[76] are shown in Fig. 66. Clearly the data support the "no shrinkage" conclusion, and more quantitatively, when fit to a slope with the usual energy dependence

$$b = b_0 + 2\alpha' \ln s$$

find $\alpha' = 0.14 \pm 0.09$ GeV^{-2}. This is in strong contrast to the strong energy dependence found in p-p scattering at the same energies--see Fig. 67.

It is interesting to note that the analysis of $\pi^- p$ and $K^- p$ elastic scattering reported in Chapter II and summarized in Table XIII, gave $\alpha'_\pi = 0.04 \pm 0.03$ GeV^{-2} and $\alpha'_K = 0.00 \pm 0.04$ GeV^{-2} for t-values around 0.4 GeV^2. Further, at high energies the pp scattering distributions for approximately the same t-values show no energy dependence. The fits to the ISR p-p scattering data in this t range yield $\alpha' = 0.10 \pm 0.06$. These results are remarkably in agreement with the ϕ photoproduction data. This prompts the question of whether the s-dependence observed in p-p scattering in the (5-20) GeV/c region (see Fig. 67) is due to Regge, or other non-diffractive effects and that the bare Pomeron properties are seen in the very high energy scattering. Then $\gamma \to \phi$ may indeed be exhibiting Pomeron like behaviour at low energies, as expected.

An interesting explanation of the lack of shrinkage is offered in the two component model of the Pomeron described by Kane. He introduces a central contribution (the conventional Pomeron) and an additional peripheral piece which accounts for the small t shrinkage observed in high energy p-p scattering. These two contributions would then lead to the picture shown in Fig. 68.

The central contribution has a slow (or zero) energy dependence while the peripheral contribution shrinks quite rapidly (like $\ln s$). The peripheral contribution behaves in t-space like a Bessel function and has its first zero around $t \sim 0.2$ GeV^2. As s increases there is a region in t around ~ 0.5 GeV^2 where the peripheral contributions cross for different s values, and which therefore displays no (or very weak) energy dependence. This model allows an explanation of the small t shrinkage, and the lack of it in the large (~ 0.4-0.8 GeV^2) region.

It would be nice to have some good data at small t, to see if the $\gamma \to \phi$ cross-section does indeed shrink for small t.

IV. DIFFRACTION DISSOCIATION (EXCLUSIVE INELASTIC DIFFRACTION)

1. Introduction

By Diffraction Dissociation we mean the non-elastic processes in which either the incident particle or the target particle is excited to a low mass system. These excitations seems to be strongest near to quasi-two-body thresholds and it is far from clear whether they are due to resonant behavior or to some kinematic effect which enhances the scattering cross-section. There is a growing amount of evidence that at least the dominant effect is due to kinematices. For the moment we will not try to answer the question of whether these inelastic processes are kinematic in origin or are caused by resonance production, but merely observe that production of "the A region" by π's, or "the Q region" by K's, or "excited N^*'s" by N's are well defined, clearly indentifiable reactions characterized by natural parity exchange in the t-channel and dominated by a single well defined spin-parity state in the meson decay system. The cross-sections for these processes are slowly varying in energy, and the differential cross-sections are sharply forward peaked. The general trends of these data are very similar to the elastic scattering and photoproduction of vector meson processes reviewed in Chapters II and III.

2. Baryons

A. $N \to N\pi$ Dissociation

We first examine the process $N \to N\pi$, from studies of

$$\pi N \to \pi\pi N \tag{IV.1}$$

$$NN \to NN\pi \tag{IV.2}$$

The cross-section for reaction (IV.1) is shown in Fig. 69. The data are consistent with a fall-off of $p^{-1.6}$, which is typical of meson exchange processes. A CERN bubble chamber collaboration[77] studied the charge related reactions

$$\begin{aligned}\pi^+p &\to \pi^+p\pi^0\\ &\ \pi^+\pi^+n\end{aligned}$$

at 4, 5, 8, and 16 GeV/c, and were able to isolate the isospin of the $(N\pi)$ system. The cross-sections for the separate isospin states are shown in Fig. 70, where the $I = 1/2$ cross-section falls slowly like $p^{-.6}$ while the $I = 3/2$ part falls like meson exchange, $p^{-1.6}$. The mass spectra for the separate I-spin states are shown in Fig. 71, for the 8 and 16 GeV/c data. The $I = 3/2$ plots show strong production of Δ, and the relative cross-section at the two energies reflects the steep energy dependence of this amplitude. The $I = 1/2$ mass spectrum shows a smooth low mass enhancement, extending from below 1300 MeV to about 1700 MeV, but exhibiting no structure at the masses of known nuclear isobars. The cross-section for this low mass bump changes very little between 8 and 16 GeV/c (at 16 GeV/c it is ~ 1/2 of the $\pi\pi N$ cross-section).

The same group[77] studied both $\pi^+p \to \pi\pi N$ and $\pi^-p \to \pi\pi N$ at 16 GeV/c and were able to isolate the isospin exchanged in the scattering process (i.e. find I_t). The various matrix elements are shown in Fig. 72--where all moments are seen to be small except the $M_1^{3/2}$ and $M_0^{1/2}$ (i.e. isovector production of the $I = 3/2$ πN system, and isoscalar exchange leading to the $I = 1/2$ πN system).

A similar analysis has been performed in the reaction (IV.2) by another bubble chamber collaboration (Bonn-Hamburg-Munich),[78] working at 12 and 24 GeV/c. The two cross-sections are shown in Fig. 73, and the $M^{1/2}_{0,1}$ and $M^{3/2}_{1}$ mass spectra are shown in Fig. 74 and 75 respectively. The same features of smooth, energy independent, low mass enhancement for the diffraction process, and the fast falling Δ production for the exchange process.

This feature of low mass enhancement is confirmed in studies of $n \to p\pi^-$; Fig. 76 shows the results of an experiment using a deuteron beam at 25 GeV/c to study "stripped" neutron interactions in a hydrogen bubble chamber,[74] especially the reaction--

$$np \to p\pi^- p \quad \text{at} \quad 12.5 \text{ GeV/c};$$

Fig. 77 shows the $p\pi^-$ mass plot for the reaction

$$K^+d \to K^+p\pi^-(p_s) \quad \text{at} \quad 12 \text{ GeV/c}.^{80}$$

The differential cross-section for $n \to p\pi^-$ in this latter experiment is shown in Fig. 78 for three mass cuts. The cross-section has a very steep slope for the lowest masses, flattening out as the mass of $(p\pi^-)$ increases. The values of the slopes found are:--

$$1.1 < M(p\pi) < 1.3\,, \qquad b = 14 \quad \text{GeV}^{-2}$$
$$1.3 < M(p\pi) < 1.5\,, \qquad b = 8 \quad \text{GeV}^{-2}$$
$$1.5 < M(p\pi) < 1.7\,, \qquad b = 3.5 \quad \text{GeV}^{-2}$$

Similiar behaviour is observed in the other studies. This variation of the slope of the differential cross-section with the mass of the produced system is displayed in Fig. 79 (for the "deuteron stripping" experiment[79]) and summarized in Table XV (from the Bonn-Hamburg-Munich experiment[78]). One sees for the diffractive channel (or rather, the $I_t = 0$, $I_{p\pi} = 1/2$ channel), that the slope at threshold is very high ($\sim 2 \times$ elastic slope, $b \sim 15$ GeV^{-2}), and falls very fast with increasing mass up to $M^2 \sim 2$ GeV^2, at which point the slope is ~ 4-5 GeV^{-2} and remains rather constant for further increases in mass. The $I_t = 3/2$ slopes are not very dependent on mass, and both $I_t = 1/2$, $3/2$ slopes do not change much with energy.

Fig. 80 shows the mass plot of $(p\pi^-)$ system produced by a high energy neutron beam from the AGS (mean momentum ~ 23 GeV/c) on complex nuclear targets.[81] The same smooth low mass enhancement is observed, produced with a characteristically coherent differential cross-section from the various nuclear targets.

The decay angular distribution of the $p\pi^-$ system has been studied in each of these experiments. Typical results are shown in Fig. 81, where the Jackson angular distribution is shown for various t and M cuts. The data indicate that for small mass and small t, the angular distributions are rather isotropic, but as mass or t increase, the distributions become more complex, reflecting an increasing complexity of the spin structure in the $(p\pi^-)$ system.

As one selects larger t, the mass distributions begin to reflect the presence of the well-known isobars--$D_{13}(1520)$, $F_{15}(1688)$--and the angular distributions may be well explained in terms of the known angular momentum of the expected resonances. However, the increased complexity in the small t data does not accompany any clear mass structure--the mass distributions remain smooth, just moving to larger mean masses as the t-cut is increased.

To summarize the data on $N \to N\pi$:

- a large cross-section for producing $I = 1/2$ $(N\pi)$ state is observed,
- the process involves $I = 0$ exchange,
- has a very slow energy dependence of the cross-section,
- has a very steep $d\sigma/dt$ for low masses; the slope decreases as the mass increases,
- no resonance structure is observed for the small t, steep $d\sigma/dt$, low mass component; as one looks at larger and larger t's, the expected resonances are observed,
- this low mass process is observed to proceed coherently on nucleii.

B. $N \to N\pi\pi$ dissociation

Another strong diffractive channel for nucleons is observed to be $N \to (N\pi\pi)$. Typical mass plots are shown in Figs. 82 and 83, where a large low mass enhancement is seen, with some structure at ~ 1450 MeV and 1700 MeV. These are associated with the production of resonances, but only represent a fraction of the total low mass system.

The cross-section for the production of this $N\pi\pi$ system is observed to be almost flat as a function of energy, falling like $p^{-0.4}$.

The differential cross-section is strongly peaked, and displays the same feature discussed above in $N\pi$--i.e. as the mass of the $(N\pi\pi)$ system increases from threshold the $d\sigma/dt$ become flatter. This is summarized in Table XVI. It is interesting to note that the $(N\pi\pi)$ and $(N\pi)$ slopes seem to agree well, for a given mass of the baryon system. These studies also show that if the mass spectrum is examined for larger t values (e.g. $t > 0.1$ GeV^2), the resonance signals become much clearer (just as discussed above for the $N\pi$ system).

Finally, there is strong evidence for the coherent production of this low mass $(N\pi\pi)$ system. We will be hearing more of this in Gobbi's talk[82] at the Conference.

In summary, the $N \to N\pi$, $N\pi\pi$ reactions display the same properties.

C. Nucleon dissociation at high energies

Having reviewed the data on diffraction dissociation of the nucleon at (5-30) GeV/c energies, let us look at a few results from NAL. Several experiments have found evidence for the reaction

$$pp \to pN^*$$

at high energies, where N^* refers to the phenomena we have been discussing above.

First, the NAL US-USSR collaboration[83] using the solid state detectors to identify the recoil proton from 'beam-hydrogen gas jet' collisions to study elastic scattering, have also measured the missing mass spectrum. This belongs more properly in the chapter on Inclusive Diffraction, but it is interesting to refer to it here, since it measures in the low mass region and ties on nicely to what we have been discussing with respect to $d\sigma/dt$, and s-dependence of the cross-sections. (We will discuss this experiment again in the inclusive section, to review some recent results on $dp \to dX$ at 100-400 GeV/c.)

The missing mass spectrum is shown in Fig. 84. The resolution in missing mass is dominated by the angular resolution of the detectors and is typically $\pm$ 100 MeV in the resonance region. The four histograms are the MM^2 distributions measured by four different counters placed at different angles (near 90°) to the incident proton beam, for an incident beam momentum of 200 GeV/c. Data were taken at 175, 200 and 400 GeV/c. The arrows mark the positions of known isobars which could be diffractively excited N(1450), N(1560), N(1688), ... A preliminary analysis of the data indicate the cross section in the resonance region is independent of energy. In particular, the cross-section in the 1400 MeV region exhibits a very steep t dependence, e^{-15t}, and that the NAL cross-section is the same to within 20% as that measured at 20 GeV/c.

Further, the $\pi^- p$[84] and pp[85] bubble chamber experiments at 205 GeV/c have both studied the exclusive four body reactions--

$$\pi^- p \to \pi^- \pi^- \pi^+ p$$

$$pp \to p\pi^+\pi^- p$$

and have isolated fairly clean samples. The mass distribution of the $(p\pi^+\pi^-)$ system is shown in Figs. 85 and 86 for these two processes, and clearly shows the low mass enhancement, with some evidence of N(1450) and N(1700) structure. The proton experiment also shows the strong $\Delta\pi$ component of this low mass region, just as is observed at low energies.

Figure 87 shows the topological cross-section for inelastic 2 prong reactions, from pp interactions from (12-300) GeV/c. The cross-section is falling with increasing energy. Also shown as a shaded band, is the estimate of the diffractive component in the two prong topology from model fits to the high energy multiplicity distributions and topological cross-sections (Miettinen,[86] Harari[87]). The isospin analysis from the Bonn-Hamburg-Munich group provides the cross-section for the $(I_t = 0, I(N\pi) = 1/2)$ process up through 24 GeV/c, at which point the 2-body diffractive cross-section is about equal to the predicted total 2 prong cross-section. However, if the $N \to N\pi$ cross-section keeps falling like $p^{-0.5}$--which it does up to 24 GeV/c--then would predict ~ 0.9 mb at 200 GeB/c, or about half the total topological limit.

(Another rumor from London-SFM group studied $pp \to p\pi\pi^+$ at $\sqrt{s} = 53$ GeV, and see cross-section falling off like $p^{-0.5}$ up to 1500 GeV/c. They also see many of the same features discussed in this section for $N \to N\pi$ diffraction--

- slow σ variation (mentioned already),
- sharp $d\sigma/dt$, being very steep for small mass, and flattening out as $M(n\pi^+)$ increases,
- $\cos\theta_J^{pn} > 0$--smooth structureless low mass bump, where θ_J is the Jackson polar angle,
- $\cos\theta_J^{pn} < 0$--begin to see resonance structure in the mass plot.)

D. Hyperon dissociation

Before leaving the baryon system, we report the observation of a threshold enhancement in the reaction

$$\Sigma^- + Z \to \Lambda\pi^- + Z$$

at 24.6 GeV/c from the NAL-Yale hyperon beam group at BNL.[88] The mass spectrum for the $\Lambda\pi^-$ system is shown in Fig. 88--it is interesting to see the same smooth, structureless, low-mass enhancement in this process as we have been discussing for nucleon diffraction.

3. Meson Dissociation

A. Cross-sections

For meson diffraction dissociation we have two basic processes to be studied

$$\pi N \to (3\pi)N \qquad (IV.3)$$

$$KN \to (K\pi\pi)N \qquad (IV.4)$$

The cross-section for reaction (IV.3) is displayed in Fig. 89 from 2 GeV/c up through 205 GeV/c. The energy dependence of this data is very mild above 5 GeV/c, with a distinct flattening off at high energy. The high energy data is dominated by the $N \to (N\pi\pi)$ diffraction discussed above in Chapter IV.2 and the meson dissociation $\pi \to 3\pi$. Typical mass distributions for the 3π system are shown in Fig. 82 for $\pi^\pm p$ at 16 GeV/c[77] (from a bubble chamber study), Fig. 90 for $\pi^- p$ at 40 GeV/c (from a spark chamber spectrometer experiment at Serpukov),[89] and in Fig. 91 for $\pi^- p$ at 205 GeV/c (from a HBC experiment at NAL).[84] All spectra show a rapid rise of the cross-section to form a broad peak called the A_1, followed by a shoulder at around 1700 MeV called the A_3. For data cut on larger t values (e.g. $t > 0.2$ GeV^2), another structure becomes very prominent--the A_2 meson. The A_1 and A_2 regions are observed to decay into $\rho\pi$, while the A_3 region is associated with the $f\pi$ system. (There is evidence from the Washington-Berkeley $\pi^- d$ HBC experiment[90] at 15 GeV/c of a $g\pi$ enhancement around 1900 MeV, which they name the A_4.)

The s- and t-dependencies of the reaction (IV.3) have been studied as a function of (3π) mass, and the results are summarized in Table XVII. The energy dependence of the cross-section as a function of mass, evaluated above 11 GeV/c, are given in the last column of the table, and indicate rather flat energy dependence--being very similar to the elastic cross-section energy dependence for small 3π masses, $(\sigma \propto p^{-.3})$ and falling just slightly faster for masses in the neighborhood of 2000 MeV, $(\sigma \propto p^{-.5})$.

The energy dependence of the three enhancement regions--the A_1, A_2 and A_3 regions--is given in Figs. 92, 93 and 94 from (5-40) GeV/c. Fitting the cross-section to $\sigma \propto p^{-n}$ they find

$$n(A_1) = 0.40 \pm 0.06$$

$$n(A_2)^{\text{natural}} = 0.51 \pm 0.05$$

$$n(A_2)^{\text{unnatural}} = 2.1 \pm 0.2$$

$$n(A_3) = 0.57 \pm 0.2$$

It is interesting that the A_2 cross-section (supposedly mainly vector and tensor exchange) has such a similar energy dependence to the A_1 and A_3 regions (which are thought to be produced by Pomeron exchange).

The fact that the A_1 energy dependence in Table XVII, and in the above fit are somewhat different implies that the $\sigma(A_1)$ flattens out at higher energies. This is confirmed by the 205 GeV/c $\pi^- p$ experiment, which reports a cross-section for $0.8 < M(3\pi) < 1.2$ GeV as 160 ± 40 μb. At the foot of Table XVII this is compared to the 25 and 40 GeV/c cross-sections.

The energy dependence of reaction IV.4 is shown in Fig. 95 for $K^0 p \to Q^0 p$.† The cross-section for Q^0 production is quite flat from 5 GeV/c-12 GeV/c,[91] having a momentum dependence of $p^{-.59\pm.16}$. Complementary data on Q^+ production is shown in Fig. 96 from the "world K^+ collaboration."[92] The energy dependence from (2.5-12.7) GeV/c is studied as a function of the $(K\pi\pi)$ mass, in 40 MeV steps from 1200-1500 MeV. All six mass intervals exhibit the same behaviour, with an average momentum dependence of $p^{-.60\pm.05}$. The $K^- \to Q^-$ data (for $M_Q < 1.5$ GeV), show a somewhat flatter dependence, with $\sigma \propto p^{-.3\pm.09}$.

†The $K_S^0\pi^+\pi^- p$ reaction cross-section rises rapidly from threshold, and then falls off as $p_{\text{lab}}^{-1.2}$. This is somewhat more rapid than the equivalent reactions for K^+p and K^-p, and is presumably due to the fact that the $K^\pm p$ reactions have substantial contributions from proton diffraction, $(p \to p\pi\pi)$, at the nucleon vertex, while such a process is forbidden in the K_L^0 experiment due to the change of C at the $K_L^0 \to K_S^0$ vertex.

A CERN bubble chamber collaboration (CERN-Brussels-Krakow)[93] have performed an isospin decomposition for the diffractive processes $K \to K\pi\pi$, $N \to N\pi\pi$ at 5.0 and 8.2 GeV/c. The various charge states for $(K^*\pi)$ and $(\Delta\pi)$ were selected from the following reactions--

$$K^+p \to K^+\pi^-\pi^+p$$

$$K^0\pi^+\pi^0p$$

$$K^0\pi^+\pi^+n \; .$$

They find that the $K\pi\pi$ system is dominated by the $I = 1/2$ amplitude, which is constant in magnitude between 5 and 8.2 GeV/c, as one would expect for a diffractive process. The mass distributions for the $I = 1/2$ and $3/2$ amplitudes are shown in Fig. 97. The low mass $K\pi\pi$ enhancement--the Q region--is clearly seen in the $I = 1/2$ data, and quite absent for the $I = 3/2$ data.

So we see that the cross-sections for these diffractive processes are quite flat as a function of energy, and that they fall off only slightly faster than the elastic scattering cross-sections themselves. The data exhibit another feature of the elastic cross-sections discussed in Chapter II--namely, the equality of particle and antiparticle cross-sections. Cornille and Martin[40] predicted that asymptotically this ratio should be 1, even for inelastic diffractive two body processes.

In Fig. 98 the ratio of the cross-section for $K^0p \to Q^0p$ and $\bar{K}^0p \to \bar{Q}^0p$ is shown as a function of momentum from (2-12) GeV/c. The equal components of K^0 and $\bar{K}^0$ in the K_L^0 beam, for this experiment, allow a comparison of these cross-sections to be made over the entire energy region free from problems of relative normalization between the strangeness states. The ratio is consistent with a constant value of 0.99 ± 0.08 over the entire energy region. Similar studies have been performed around 16 GeV/c for $\pi^\pm \to (3\pi)^\pm$ in HBC[94] and wire spark chamber[95] experiments, with the result,

$$R = \frac{\pi^-p \to (3\pi)^-p}{\pi^+p \to (3\pi)\,p} = 1.00 \pm 0.07,\; 0.94 \pm 0.12 \; .$$

B. Differential cross-sections

The (3π) data angular distributions have been analyzed to determine the spin-parity amplitudes involved in the reaction. These analyses are summarized below.

The A_1 region--(the 1100 MeV enhancement)--is associated with $J^P = 1^+$, s-wave $\rho\pi$ decay. (See the amplitudes in Fig. 99.) The phase of this wave shows very little energy dependence with respect to any of the background waves, and gives no indication of behaving like a Breit-Wigner resonance amplitude--see Fig. 99. The differential cross-section for this region (selected in mass and only taking the 1^+ s-wave part of the data), is plotted in Fig. 100--where the slope is shown as $e^{-(6.7\pm.8)t}$.

The A_2 region is identified as $J^P = 2^+$, with a d-wave $\rho\pi$ decay mode. The amplitude and phase of this wave is shown in Fig. 101, where the 2^+ phase with respect to background is seen to move rapidly through the resonance mass, as would be expected from a Breit-Wigner amplitude. The mass and width is found to be $M = (1315 \pm 5)$ MeV, and $\Gamma = (115 \pm 15)$ MeV. The differential cross-section, for the 2^+ amplitude in the A_2 region, is shown in Fig. 102, and exhibits a dip in the forward direction. The data are fit with $d\sigma/dt \propto |t|\, e^{-bt}$ with $b = (8.6 \pm 1.2)$ GeV^{-2}.

A similar analysis in the A_3 region is shown in Fig. 103, where the enhancement is assigned $J^P = 2^-$, and associated with an s-wave $f\pi$ system. The mass and width are found to be $M = (1650 \pm 30)$ MeV, and $\Gamma = (300 \pm 50)$ MeV. Again the phase shows no mass dependence, like the $A_1(1^+)$ wave, and not like the resonant 2^+ A_2 wave. (Purdue[97] has reported finding a phase variation in $\pi^+p \to (3\pi)^+p$ in contradiction to the above result from CERN-IHEP (Ascoli) analysis[96] of $\pi^-p \to (3\pi)^-p$; however, Morrison[18] has reported that his CERN HBC collaboration in analysing both $\pi^\pm p \to (3\pi)^\pm p$ at 16 GeV/c see no phase movement for the 2^-A_3 phase; same for LBL.[98]) The production distribution for the 2^- events in the A_3 region, and the background events, are shown in Fig. 104, where the enhancement data is shown to be more peripheral ($b = 9.9 \pm 1.2$ GeV^{-2}) than the background $b = (6.4 \pm 0.6$ GeV^{-2}).

The slope of the differential cross-sections, and the dependence on $M(3\pi)$ has been mentioned above (Table XVII). Further data on this effect are given in Table XVIII for both π^+p and π^-p at 16 GeV/c. It is interesting to note that there is not much sign of shrinkage for these slopes--see Table XIX --the small t, small (3π) mass slope being the same at 16 GeV/c and at 40 GeV/c.

Similar analysis of the decay distribution have been performed for the $(K\pi\pi)$ system--a typical set of amplitudes is shown in Fig. 105, where the dominant wave for the Q region is seen to be the $J^P = 1^+$, and where the phase of this wave moves only slowly with energy--like the A_1.

Clear evidence for the low mass diffractive enhancement in $K \to K\pi\pi$ is given in Fig. 106 from a 14.3 GeV/c K^-p bubble chamber experiment.[99] The mass of $(K^*\pi)$ is plotted against the mass of $K\pi$ system. Two points are of interest--a) the $K\pi\pi$ system couples strongly to $K^*(890)\pi$ and $K^*(1420)\pi$, b) the low mass enhancement is quite absent in the charge exchange reaction $K^- \to (\bar{K}^0\pi^+\pi^-)$, where only the 3-body decay of the K^*_{1420} is observed. (The $K^*(1420)$ is the SU(3) partner of the A_2 resonance discussed above in the 3π data.)

The differential cross-section from this same data is shown in Fig. 107 where the distinct difference in slopes between the diffractive Q-region and the Regge exchange $K^*(1400)$ region is demonstrated.

The dependence of the slope of the differential cross-section on the mass of the $(K\pi\pi)$ system is shown in Fig. 108 for $K^0 \to Q^0$ and $\bar{K}^0 \to \bar{Q}^0$, and in Fig. 109 for $K^- \to Q^-$. The slope values for the $S = -1$ data are in good agreement. This effect is very similar to that observed in the $\pi \to 3\pi$ and $N \to N\pi$, $N\pi\pi$ data discussed above.

Finally, the inelastic diffractive reactions exhibit the cross-over phenomenon in the differential cross-sections. We discussed this effect in Chapter II--it is caused by a C odd Regge exchange contribution to the process in addition to the dominant Pomeron exchange. This additional contribution gives rise to different slopes in the differential cross-section for particle and for antiparticle scattering. An example of this phenomenon is shown in Fig. 110 where 13 GeV/c K^+p and K^-p elastic scattering data from the SLAC wire spark chamber spectrometer experiment are displayed.[58] A clear cross-over of the two cross-sections is seen for momentum transfers, $t \sim 0.2$ GeV^2. Similar behaviour is observed for $\pi^{\pm}p \to (3\pi)^{\pm}p$ around 16 GeV/c from the SLAC wire chamber experiment[95] and from the CERN 16 GeV/c $\pi^{\pm}p$ HBC experiment[94] --see Fig. 111. Again, for KN reactions we show the cross-over for K^0 in Fig. 112, and for $K^{\pm}p$ in Fig. 113. The diffraction dissociation data is much less precise than the elastic data, but the positions of the cross-overs are consistent with the corresponding elastic reaction cross-over. Also, the change in slope between the particle and the antiparticle process is similar in elastic and in the inelastic reactions--see Table XX.

4. Summary

- In summary, we have seen that $N \to N\pi$, $N\pi\pi$; $\pi \to 3\pi$; $K \to K\pi\pi$ reactions exhibit large low mass enhancements. The cross-sections for the various processes are listed in Table XXI and compared to the elastic reactions. The inelastic processes seem to fall off a little faster than the corresponding elastic reaction. It is not clear whether this difference is important (or real), or just due to the technical difficulty of determining an "A" cross-section above background (or even knowing what an A cross-section really means!). However, it is clear that these inelastic diffractive processes are much more like the elastic reactions than the typical Regge exchange processes where cross-sections fall off like $p^{-1.5}$ or faster.
- The angular distributions for these inelastic diffractive processes are sharply peaked with slopes about twice the slope for elastic scattering for threshold mass of the diffracted system, and flattening out to a slope value of about half the elastic scattering slope for masses about 1000 MeV above threshold. The slopes for some specific mass states are summarized in Table XXII. It appears that the same regularities found among the elastic slopes are to be seen in the inelastic slopes.
- These reactions all exhibit the cross-over phenomenon in $d\sigma/dt$ very similar to the elastic reactions and also have $\sigma(Ap) = \sigma(\bar{A}p)$.

It is interesting to see how similar the elastic and inelastic diffractive processes are with respect to total cross-section and differential cross-section behavior.

5. Final Comment on Exclusive Diffraction Dissociation

I have isolated this section from the general conclusions since it is a mixture of personal opinion and a summary of known facts. However, it may be helpful, if only to stimulate argument and catalyze you to forming your own "picture."

We know that the pion, kaon and proton all produce low mass enhancements which have the following features:

- mainly $I = 1/2$;
- mainly $I = 0$ in t-channel;
- smooth, featureless bump, rising quickly from threshold;
- cross-section only weakly s-dependent;
- can be produced coherently on nuclear targets;
- no sign of well-knwon resonance structure;
- sharp $d\sigma/dt$ with slope about twice the elastic slope at threshold, falling as the mass of the produced system increases, until about 1 GeV above threshold it is rather flat, with slope about half the elastic slope;

- we also know that for larger momentum transfers, one sees signs of resonance structure in the mass distribution, and in the decay angular distributions. The πd, Kd experiments see clear signs of $D_{13}(1500)$, $F_{15}(1700)$ when making larger t cuts--they also see zero phase difference between these two production amplitudes, as would be expected from diffraction production;
- there is also good evidence that for the small t smooth enhancement, the angular momentum in the decay is simplest (i.e. s-wave) for threshold masses and becomes more complex as the mass increases;
- if cuts are made on the decay angle of the $N\pi$ decay system for $N \to N\pi$, for $\cos\theta_J^{NN} > 0$, see only the smooth bump, but for $\cos\theta_J^{NN} < 0$, begin to see the usual resonances being produced;
- we have neglected the process $\gamma p \to \pi^+\pi^- p$ in our discussion of inelastic diffraction, because $\gamma \to \rho$ was dealt with separately. However, here we have a reaction in which accidentally the "elastic" processes take place above the threshold for inelastic diffraction. However, there is a well-known diffractive non-resonant background below the rho meson, well described by the Drell diagram. It displays all the features we have learned of the other low mass diffractive processes. (An example of the dependence of slope on mass is shown in Fig. 114.)

So we suggest that we have the following situation--there are two components in diffractive reactions: 1) a dissociation of the incoming beam, and 2) diffractive production of resonances. The cross-section for dissociation starts at quasi-two-body threshold and rises rapidly followed by a long tail as a function of mass. (See Fig. 115.)

Following Lubbatti and Moriyasu[100] we may think of the dissociation as the coupling of the incident (or target) particle to a whole string of virtual states

$$\pi \to \pi\rho,\quad \pi f,\ --$$

$$N \to N\pi,\quad \Delta\pi,\ --$$

and in the collision, it picks up some longitudinal momentum to make up the change in mass.

With these excited states populated, the particle has an effective size larger than its "ground state" size. As the mass of the excited state increases, the momentum distribution associated with the excited state increases and there will be a reciprocal decrease in the size of the hadron (from the uncertainty principle). A reasonable measure of the mean square momentum might be $(M^2 - M_i^2)$ where M is the mass of the excited state and M_i is the mass of the constituents. Then $R^2 \sim (M^2 - M_i^2)^{-1}$.

Lubbatti and Moriyasu have plotted the known slopes we have discussed above in this form--see Fig. 116--and find that the data seem to fall on universal curves.

There are deviations at the known resonances, and we might think of their being different anyway--that is, as having a size of their own.

With respect to the second component--we know in $N \to N\pi$, $\Delta\pi$ where we have a solid knowledge of the N^* spectrum from s-channel studies, that there are resonances produced diffractively. Given the success of the whole structure of SU(3) and quark model classification schemes, it seems highly probable that A_1 and Q mesons do exist. The problem of experimentally isolating this signal from the dissociation background is very difficult (like sorting out ρ photoproduction from Drell background if the non-resonant $\pi\pi$ background was the dominant amplitude).

Perhaps with Omega, MPS and LASS systems coming into operation,[101] we will be able to see independent signs of these states from analysis of reactions like

$$\pi p \to Q\Lambda$$

$$Kp \to A_1\Lambda$$

or as SPEAR II, DORIS and PEP come along, in production experiments like

$$e^+e^- \to \pi A_1$$
$$\bar{K}Q \; .$$

Perhaps one of the more direct ways we will find out what is going on in diffractive processes will be from analysis of the Caltech-LBL-SLAC $\pi^\pm p$ experiment[102] with a hybrid spark chamber--bubble chamber set-up. They are studying the baryon break-up for processes where a fast beam-like pion leaves the bubble chamber and triggers the downstream system--in particular they will have good information on $p \to p\pi\pi$. See Fig. 117. An analysis of the $N\pi\pi$ amplitudes obtained from this t-channel experiment and their comparison with the detailed amplitudes for the same state obtained in the SLAC-LBL s-channel phase shift analysis[103] should allow great insight into diffraction processes and perhaps throw some light on this two component hypothesis.

We will return to a discussion of the dynamics of diffraction at the end of the section on Inclusive Scattering.

V. RULES OF DIFFRACTION

1. Introduction

As we discussed in the Introduction we have very little theoretical understanding of the diffractive process, and our main guide as to whether a process is diffractive or not, is often how well it obeys our list of phenomenological "rules."[12]

These rules are listed below.

a) energy independent cross sections (to factors of $\ln s$)

b) sharp forward peak in $d\sigma/dt$

c) particle cross sections equal to antiparticle cross sections

d) factorization

e) mainly imaginary amplitude

f) exchange processes characterized by the quantum numbers of the vacuum in the t-channel (i.e. $I = 0$, $C = +1$). Also, the change in parity in the scattering process follows the natural spin-parity series $(-1)^J$ or $P_f = P_i \cdot (-1)^{\Delta J}$, where ΔJ is spin change.

g) the spin structure in the scattering is s-channel helicity conserving (SCHC).

In Chapters II, III and IV we have seen points (a), (b), (c), (e) all borne out by the data. We now examine the other points.

2. Quantum Numbers in Pomeron Exchange (point f) above):

The "rules" for diffractive processes said that, from a t-channel point of view, the Pomeron would carry the quantum numbers of the vacuum (i.e. $C = +1$, $I = 0$ exchange). How well does the data support this assertion?

(a) I = 0 character:

We know from amplitude analysis of elastic scattering[104] (which we suppose to be mainly diffractive) that the dominant amplitude is the non-flip isoscalar t-channel amplitude. We also know that processes involving a change of charge in the scattering (and hence $I \neq 0$ in the t-channel) have cross sections which fall quite rapidly with energy and do not have the character of diffractive reactions.

Below we consider two examples of $I = 0$ character of diffractive processes from inelastic scattering:

The reactions $\pi^- p \to N\pi\pi$ were studied at 16 GeV/c by the ABBCCHW collaboration[105] and the $N\pi$ mass spectra are shown for the various possible charge combinations (see Fig. 119). The $(N\pi)^+$ combinations (i.e., $p\pi^0$, $n\pi^+$) which can be produced with no charge exchange and hence accessible from $I = 0$ exchange in the t-channel, exhibit a large low mass enhancement in the (1400-1700) MeV range. This enhancement has an almost energy-independent cross section and is related to the diffractive excitation of N^*'s. The $(N\pi)^-$ combinations (i.e. $p\pi^-$, and $n\pi^-$ respectively), which cannot be reached with $I = 0$ exchange, have no low mass diffractive enhancement.

A similar example[105] is shown in Fig. 120 where 10 GeV/c $K^- p \to \bar{K}(N\pi\pi)$ reactions have been studied. Again the $(N\pi\pi)^+$ mass spectrum shows a low mass enhancement associated with the diffractive production of excited N^*, while the $(N\pi\pi)^0$ spectrum shows no such structure.

Thus we see quite clearly that the observation of diffractive phenomena is closely connected with $I = 0$ in the t-channel.

(b) C = +1 character:

To examine this property we compare the $K^- p \to K^-(p\pi\pi)$ data already displayed in Fig. 120 above, to data on $K_L^0 p \to K_S^0(p\pi\pi)$ of approximately the same energy, from the SLAC bubble chamber experiment.[91] The data is selected to isolate out the peripheral $p \to p\pi\pi$ reaction mechanism and the resulting $(p\pi\pi)$ mass spectrum is shown in Fig. 121. The low mass diffractive enhancement in the K^- reaction is not observed in the K_L^0 data, although these two reactions are so very similar. The difference lies in that the K_L^0 and K_S^0 are eigenstates of C with opposite sign and therefore the t-channel exchange in the K_L^0 reaction must carry $C = -1$. This may be viewed as evidence of the $C = +1$ character of diffractive processes.

(c) Spin-parity changes:

As per our "rules" we expect that diffraction will proceed most simply with no change of spin or parity for either the target or projectile particles, but that if there is a change it will follow the natural spin-parity sequence, viz.

$$P_f = P_i(-1)^{\Delta J}$$

This may be thought of as picking up angular momentum in the "Pomeron-diffracting-particle" scattering.

This is a phenomenological rule,[106] whose main claim to correctness is that there are no known diffractive processes which violate it. There exists rigorous proof for the spin zero case, but there is no general theorem for the more interesting spin situations.

The main evidence for justification for this "rule" is negative in nature (as mentioned above); however, one recent confirmation of the rule comes from a bubble chamber experiment on $\pi^- n \to \pi^- \pi^- p$ at 11.7 GeV/c by the Riverside group.[107] They observe diffractive production of N^*'s decaying into $p\pi^-$ final state. The analysis is free from complications of π-π resonance effects and deals with the well understood two-body elastic decay of the N^*; (i.e. it avoids, the complication of previous studies which have observed diffractive production of $N^* \to N\pi\pi$, and then applied assumptions about two-body decays into $\Delta\pi$ final states). The Riverside results show production of P_{11}, D_{13}, F_{15} N^*'s (i.e. the correct parity sequence for the "rule") and no sign of the D_{15} state. Further, the production phase between the D_{13} and

F_{15} processes was found to be 0^0, in agreement with the hypothesis of diffractive production.

On the negative side, three threats to the rule existed over the last few years--vector K^* production by K's, tensor A_2 production by π's and axial vector B production by γ's. Each of these processes violates the natural spin-parity sequence, but claims of "diffraction-like" properties had been made. We discuss them at more length below:

(i) $K^*(890)$ production:

At the Oxford conference[108] data on $K^-p \to K^{*-}_{890}p$ was reported implying that the cross section, which had been falling like p_{lab}^{-2} up to 8 GeV/c actually flattened out to an almost constant value for higher energies. This was taken as evidence of Pomeron contribution to K^* production.

However, new data up to 16 GeV/c is now available,[109] and the cross section seems to fall like p_{lab}^{-1} beyond 8 GeV/c and the production and decay characteristics are in good agreement with isoscalar, natural spin parity exchange. Presumably ω^0 exchange takes over from π exchange at the higher energies, and this "threat" to the parity rule has disappeared.

(ii) A_2 production:

There have been suggestions for some time that perhaps the A_2 meson is produced via Pomeron exchange, thus violating our simple rule of natural spin-parity excitation in diffraction processes. Kruse et al.[96] have submitted an analysis of A_2 production in bubble chamber data in the energy range from (5-25) GeV/c. There is also a paper from Ascoli et al.[96] on A_1, A_2, and A_3 production at 40 GeV/c. The facts are summarized below:

i. The A_2 cross-section falls off as $p^{-0.8\pm0.08}$ in the (5-25) GeV/c range;
ii. The relative energy dependence of A_1, A_2, and A_3 between 25 GeV/c and 40 GeV/c are essentially the same;
iii. The natural parity exchange contribution to A_2 production falls off as $p^{-0.57\pm0.09}$;
iv. The t-channel exchange in A_2 production is mainly isoscalar;
v. The s-dependence of the cross section implies an effective intercept, $\alpha_{eff}(0) \sim 0.7$;
vi. An analysis of the shrinkage of the $J^P = 2^+ A_2$ differential cross-section yields an $\alpha_{eff}(0) \sim 0.8$.

The energy dependence and α_{eff} values quoted above are more in agreement with a strong Pomeron contribution to A_2 production than the vector, and tensor meson contributions one expected. However, we must understand at least one other fact before throwing away our current picture of Pomeron processes--the energy dependence for the A_2 cross section as measured in the $K\bar{K}$ decay mode seems to be faster than $p_{lab}^{-1.0}$. This is a clean reaction in which to study A_2 production with very little background, and the observed momentum dependence is very much in agreement with that expected for meson exchange in the t-channel. Several experiments should be reporting new cross-sections for $A_2 \to K\bar{K}$ within the near future, and we wait impatiently for their results. Another indication that A_2 is not diffractively produced comes from the differential cross-section shown in Chapter IV--it was well fit with $d\sigma/dt \propto |t|e^{-bt}$, with a forward turnover.

(iii) Photoproduction of the B-Meson:

Finally, in this section on "bogey-men," we deal with the photoproduction of the B-meson.[110] The reaction $\gamma p \to Bp$ violates the natural spin-parity series expected in diffractive processes, yet the B signal is observed with the same strength at 2.8, 4.7, and 9.3 GeV. The energy independent cross-section has encouraged speculation as to the validity of the simple rules on spin couplings for the Pomeron.

However, the statistics on these observations are rather limited, each energy point having a cross section of (1.0 ± 0.4) μb. One could accommodate quite a variety of energy dependences within these measurements. It is an important reaction and to be followed with interest, but the present results are not strong enough to call our ideas on Pomeron coupling to question--at least not yet. (This effect is most probably the diffractive production of a ρ' meson (coupling strongly to $\pi\omega$), with a mass close to the B-meson.

For the moment the rule seems to be obeyed.

(d) G-parity:

It is interesting to observe that G-parity is strongly recognized in diffractive processes. For π reactions, one sees strong diffractive cross-section for 3π, 5π but not 4π final states. This observation is confirmed in coherent processes with π on nuclear targets.

Perhaps an even more interesting example is the relative coherent production of A_1 and B systems in π^- experiment at 11.7 GeV/c in a heavy liquid bubble chamber.[111] These two systems have the same $J^P = 1^+$, but A_1 has $G = -1$ like the π, while the B Has $G = +1$. The experiment observes strong coherent A_1 production, with a cross-section of $\approx$ 2mb/nucleon, while there is no evidence of B- production with an upper limit of < 30 μb/nucleon.

The Pomeron seems to care about G-parity.

3. Spin Structure in Diffractive Processes (point g) above):

Our "rules" assert that diffractive processes are s-channel helicity conserving (SCHC). This hypothesis derives from the early experimental work of the SLAC-Berkeley-Tufts group[112] on their study of ρ^0-meson photoproduction with the polarized photon beam, at 4.7 GeV. They found that the diffractively produced ρ^0-meson maintained the photon helicity in the s-channel. Gilman and co-workers[113] then hypothesized that all diffractive processes conserved s-channel helicity and showed that the understanding of the πN scattering amplitudes at that time was consistent with that assumption.

New data on $\gamma p \to \rho^0 p$ at 9 GeV from the SBT group,[71] and measurements of the R, A parameters in πN and NN scattering by a Saclay group[114] confirm, in the main, the early conclusions. The new experiments are discussed in more detail below.

It is interesting to note that if s-channel helicity conservation really holds, then the old "lore" that the Pomeron behaves in the energy dependence of cross-sections like a particle of spin 1, but has the couplings of a particle of spin 0, cannot be true. SCHC requires quite specific couplings in the t-channel--in general helicities will flip and there must be quite specific relations between the t-channel spin flip and non-flip couplings.

The density matrix elements from the new SBT experiment at 9.3 GeV[71] are shown in Fig. 122. They confirm the dominant behaviour as being SCHC and show that it holds out to larger t than previously observed. However, the ρ_{10} element (i.e. SCH flip) is quite definitely non-zero as is shown more clearly in Fig. 123. It was confirmed that the effect was real and not due to a scanning bias, by rotating the plane of polarization of the incident photons with respect to the bubble chamber camera axis; no change in the result was found. Further, they find when isolating the separate exchange amplitudes that the effect belongs to the natural-parity exchange amplitude. It is also found that the magnitude of the effect does not change rapidly with energy. All these factors imply that there is a small helicity flip amplitude, of about 15% the SCHC amplitude, which may be associated with Pomeron exchange. Results of their analysis of the helicity flip contribution are given in Table XXIII.

The Saclay experiment[114] studied $\pi^\pm p$ scattering at 6, 16 GeV/c from a polarized proton target. The recoil proton was detected in a spark chamber polarimeter. The spin rotation parameters R and A were measured. Actually good measurements of R were obtained and A found from the relation $P^2 + A^2 + R^2 = 1$, using the existing precision measurements of the polarization (P), in p-p scattering. Rough measurements of A were taken to resolve the quadratic ambiguity in the above equation. They find A to be close to +1 as expected from SCHC.

At 6 GeV/c, an amplitude analysis[104] was performed using all the available data on total and elastic πN cross sections, differential cross-sections, charge exchange cross sections, polarization for elastic and charge exchange reactions and their own new R and A parameters. Results for the isoscalar flip and non-flip amplitudes are shown in Fig. 124. The flip amplitudes has a kinematic zero in the forward direction but is certainly nonzero at larger t. For the region of $t > 0.2$ GeV^2, they find the ratio of flip to non-flip amplitude to be 0.17 ± 0.2 at 6 GeV/c.

There is not sufficient πN scattering data to perform a complete amplitude analysis at 16 GeV/c but a reasonable choice of solutions gives the flip to non-flip ratio, at 16 GeV/c, to be 0.14 ± 0.03. That is, the πN data shows that SCHC is the dominant amplitude but that again a small (~ 15%) helicity flip amplitude is present and that it is isoscalar and weakly s-dependent--presumably associated with the Pomeron. It is important to remember that although the $\gamma \to \rho$ experiment and this πN experiment are both measuring 15% helicity flip amplitudes which are isoscalar and weakly energy dependent, they are not measuring the same thing; the photon experiment measures the spin structure at the meson vertex while the πN experiment measures the spin structure at the nucleon vertex.

The Saclay group also measured R, A parameters for p-p scattering at 6, 16 GeV/c,[114] and found the parameters consistent with dominance of SCHC. There is not sufficient data to perform an amplitude analysis for p-p scattering, but it is clear that this data would be consistent with a small helicity flip amplitude.

Finally, we must consider the spin structure for inelastic processes. Table XXIV summarizes recent work on this question.[12,14] It shows that the vector meson photoproduction behaves very much like elastic scattering--SCHC in the main, but with a small helicity violating amplitude. The various diffraction dissociation processes do not conserve s-channel helicity. Most of them are much more close to t-channel helicity conservation, but in general do not conserve that either. Thus, although their inelastic processes looked very much like elastic reactions from the point of view of cross section and differential cross sections, they have bery different spin structure. This difference may be due to the fact that these processes are perhaps not really particle production, but kinematic enhancements, or alternatively, may be due to the spin change that occurs in these inelastic processes and the complex t-channel spin structure of the Pomeron.

4. Factorization

If we really believed that diffraction reactions are dominated by the exchange of a simple Pomeron, we should be able to factorize, or separate, the different vertices appearing in these processes. It is interesting to test how well the cross-section data supports the factorization hypothesis. Below we examine several tests:

(1) A simple factorization test involving the isospin of the breakup of the low mass $N\pi$ enhancement may be performed, checking whether $\frac{\sigma(pp \to p(n\pi^+))}{\sigma(pp \to p(p\pi^0))}$ is actually 2. Studies on 19 GeV/c pp interaction report[115] this ratio as 1.9 ± 0.2.

(2) Another test is found in the three sets of reactions, shown in Fig. 125, involving the excitation of the proton to $N^*(1688)$ in π^-, K^- or $\bar{p}$ interactions. These cross-sections should have the same ratio with respect to elastic scattering, independent of the nature of the incident particle. The results of the test are shown in Fig. 126 where the ratio $\left[\frac{Ap \to AN^*(1688)}{Ap \to Ap}\right]$ is plotted against momentum transfer, for two energies--8 and 16 GeV/c. Factorization is observed to hold within 20% and even works well as a function of momentum transfer at least out to $t \sim 0.2$ GeV^2.[105]

(3) Consider the processes illustrated in Fig. 127, with elastic pion

and proton scattering at the upper vertex, and proton diffraction into proton plus zero, one, two or three pions at the bottom vertex. The ratio between cross-sections for reactions involving the upper two vertex processes should be the same, independent of which of the four bottom vertices they interact. That is, $R_1 = \sigma(\pi p \to \pi p)/\sigma(pp \to pp)$ should equal $R_2 = \sigma(\pi p \to \pi(p\pi^0))/\sigma(pp \to p(p\pi^0))$ etc.

The cross-section for each of the bottom vertices was isolated in 16 GeV/c $\pi^- p$ and 19 GeV/c pp bubble chamber experiments,[116] using the Van Hove Longitudinal Phase Space analysis[117] to isolate the diffractive components. The results are given in Table XXV. Good agreement is observed.

(4) Another interesting test of factorization in diffractive processes is shown schematically in Fig. 128. If the Pomeron contribution were well behaved and factorizable, we would expect the ratio of cross-sections for each of the upper vertex processes--$\gamma \to \rho^0$, $\pi \to \pi$, $p \to p$--being joined in turn to both of the bottom vertex process--$p \to p$, $p \to (p\pi^+\pi^-)$--to be equal. That is, we would expect to find

$$R_1 = \frac{\sigma(\gamma p \to \rho p)}{\sigma(\gamma p \to \rho p\pi\pi)}, \qquad R_2 = \frac{\sigma(pp \to pp)}{\sigma(pp \to pp\pi\pi)}, \qquad R_3 = \frac{\sigma(\pi p \to \pi p)}{\sigma(\pi p \to \pi p\pi\pi)}$$

The diffractive component for these reactions was again isolated using the LPS analysis.

The experimental values[118] for R_1, R_2 and R_3 are given in Table XXVI for three different energy regions. The agreement is surprisingly good.

(5) We may use the results of the various isospin amplitude studies discussed in Chapter IV to further test factorization. The integral over t of the isoscalar t-channel amplitude leading to the $I = 1/2$ final state $(N\pi)$ system is calculated for incident π, K and proton collision, $(\int |M_0^{1/2}|^2 \, dt)$. The ratio $R(H) = [\sigma(Hp \to H(N\pi))/\sigma(Hp \to Hp)]$, where $H = \pi, K, p$. We expect $R(\pi) = R(K) = R(p)$ if the factorization holds. The results are given in Table XXVII, where again quite remarkable agreement is found.[119] (The agreement is even better when one notes that the 24 GeV/c pp point includes some $I = 1$ t-channel exchange contribution since no pn data were available to do the t-channel I-spin decomposition.)

(6) An interesting factorization test has been made possible by the study of the four body exclusive reaction in pp and $\pi^- p$ collisions at 205 GeV/c.[120] The diffraction of the target proton into a $(p\pi^+\pi^-)$ system has been isolated in each experiment--see Fig. 129.

The cross-section for $\pi p \to \pi(p\pi\pi)$, $\sigma_1 = (180 \pm 36)\ \mu b$

The cross-section for $pp \to p(p\pi\pi)$, $\sigma_2 = (370 \pm {}^{40}_{140})\ \mu b$

The cross-section for $\pi^- p$ reaction is $\alpha g^2_{\pi\pi P} * g^2_{pN^*P}$

The cross-section for the pp reaction is $\alpha g^2_{ppP} \times g^2_{pN^*P}$

Now

$$\begin{aligned} \frac{\sigma_1}{\sigma_2} &= g^2_{\pi\pi P} \cdot g^2_{pN^*P} / g^2_{ppP} \cdot g^2_{pN^*P} \\ &= g^2_{\pi\pi P}/g^2_{ppP} \\ &= \frac{\sigma(\pi p \to \pi p)}{\sigma(pp \to pp)}, \text{ or } \frac{\sigma_{el}(\pi p)}{\sigma_{el}(pp)} \\ &= \frac{3.0 \pm 0.3}{6.8 \pm 0.2} \\ &= 0.44 \pm 0.05 \end{aligned}$$

while σ_1/σ_2 are measured to be ~ 0.5.

(7) A final example comes from a study of inclusive scattering at 25 and 40 GeV/c at Serpukov. The CERN-IHEP collaboration[89] measured

$$\pi^- p \to X^- p$$

$$K^- p \to X^- p$$

with their missing mass spectrometer. The cross-sections $(d^2\sigma/dt\,dx)$ are shown in Fig. 130 where the dashed line represents the pion data, and the circles represent the kaon cross-sections. If factorization holds, we expect

$$\left[\frac{\frac{d\sigma}{dx}(\pi^- p)}{\frac{d\sigma}{dx}(K^- p)}\right] = \left[\frac{\sigma_T^{inel}(\pi^- p)}{\sigma_T^{inel}(K^- p)}\right] .$$

Integrating over t, they find the left-hand side of this equation to be 1.20 ± 0.09, while the right-hand side is 1.18 ± 0.04.

To summarize, we have learned that factorization in diffractive processes--elastic, diffraction dissociation and leading particle inclusive reactions--is surprisingly good, holding to ~ 20%.

It would be interesting to have data on an even wider variety of processes, and more importantly, with rather better accuracy. At intermediate energies, we know that non-leading effects such as cuts, are quite important and at high energies the observations of rising cross sections have killed any idea of simple single pole dominance of the interactions--thus, we expect breaking of factorization to occur, maybe even at the 10% level. It would be very interesting to have experiments of sufficient accuracy to observe this breaking, and perhaps even see some s-dependence to the breaking of factorization.

VI. INCLUSIVE SCATTERING

1. High Energy Inclusive pp Scattering

A. Missing mass distribution

It has been known for some time that inclusive pp scattering at high energy is characterized by a large quasi-elastic peak which is associated with the diffractive production of high mass states[121] (see Fig. 131). It is interesting to study the energy, mass and momentum transfer dependencies of this process to learn more of the dynamics of diffraction. A considerable amount of new data on this topic has become available recently.

In Fig. 132 the missing mass plots from the NAL bubble chamber experiments [122] are given. The HBC pictures are scanned for slow protons which can be identified by their ionization; for those events so identified the missing mass is then calculated. The lowest masses are seen to be produced with almost constant cross-section between 100 and 400 GeV/c.[123] For larger masses the cross-section is falling almost linearly with energy. An alternative display is in terms of the Feynman x variable, the fractional longitudinal momentum, p_L/p_{max} or $x = (1 - M^2/s)$. The 100 and 400 GeV/c data are shown, plotted as a function of x, in Fig. 133.[124] From this plot, we see the cross-section for $x \approx 1$ increasing with energy, as it must if the cross section at small masses is constant in energy. This region is presumably the classical diffraction dissociation region. For $x \sim .6$ to $.8$ region the cross-section scales in x. The intermediate region of $x \sim .95$ seems to show some energy dependence indicating that the quasi-elastic peak does not quite scale in x at these energies.

The 200 GeV/c missing mass data[125] is shown again in Fig. 134 and broken down in the various topological contributions in Fig. 135. The cross-section in the small mass region (up to masses of 4 GeV), is seen to fall off like M^{-2} and the diffraction peak is developed by peaks in each of the lower topological cross-sections. It also appears that the mean mass of the diffractive peak increases as the topology or multiplicity, n, increases. The total cross-section of this low mass diffraction peak is estimated at ~ 6 mb, independent of energy.

The same behavior is observed at ISR energies where the CHLM[122,126] and ACGHT[127] groups have demonstrated the existence of the low mass diffractive enhancement. In Fig. 136 the missing mass distribution from the two arm spectrometer ACGHT experiment, is shown. They are able to make a rough multiplicity assignment, using a scintillation counter hodoscope round the aperture of each spectrometer. There is clear evidence for the increase of mean mass in the diffractive peak as the multiplicity increases.

It is interesting to note that the term "low mass" peak is purely relative and that these diffractive peaks include masses up to 7 GeV.

Figure 13 shows the missing mass spectrum from the Columbia-Stony Brook experiment at NAL.[128] This experiment uses polyethelene and carbon targets and detects the recoil proton in an array of solid state counters. The normalization is effected by counting the d, T, He^3 and He^4 production in both the polyethelene and carbon targets simultaneously with the protons, thus allowing for a very accurate subtraction and hence reliable proton cross-sections.[129] The resolution in missing mass squared is very good, being of order of 1 GeV^2 near $x \sim 1$, whereas the CHLM group has $\delta M^2 \sim 9$ GeV^2 and the ACGHT group has $\delta M^2 \sim 20$ GeV^2. Their missing mass plot shows a very sharp peak with some structure around 3-4 GeV^2 and becoming essentially flat for masses above 16 GeV^2.

This missing mass distribution is quite different from the ISR data. Part of this difference is due to the missing mass resolution of the different experiments, but part is also due to the fact the measurements have been made at different t values; the ISR experiment has typically $t \sim 0.8$ GeV^2, while the NAL experiment had $t \sim 0.06$ GeV^2. We will come back to this point later.

B. Energy dependence, or scaling

The energy dependence of the quasi-elastic pp scattering has been studied at NAL from (50-400) GeV/c by Rutgers-Imperial College group.[139] The recoil proton is detected and identified in a scintillation counter telescope with a total absorption counter. The momentum of the proton is determined from time of flight measurements over 186 cm flight path.

The invariant cross-section, for four different t values, is given in Fig. 138 for five energies between 50 and 400 GeV. For x values close to 0.8 there is very little energy dependence, while for x values around 0.9, close to the quasi-elastic peak, quite considerable variation is observed through this energy region. In Fig. 139 the invariant cross-section is plotted against $s^{-1/2}$ for the four t ranges measured, for x values of 0.83 and 0.91. Again substantial s-dependence is clearly visible.

They fit the data to the form

$$s \frac{d^2\sigma}{dt\, dM^2} = A(x)\, e^{b(x)t} [1 + B(X)\, s^{-1/2}] \; .$$

This form represents the data well, with b being essentially independent of x and having a value of ~ 6 GeV^{-2}. The best fit to the data gave

x = 0.83	A = 71 ± 7 mb/GeV^2	B = 1.9 ± .7 GeV
x = 0.91	A = 66 ± 3 mb/GeV^2	B = 4.3 ± .4 GeV

Through the NAL energy range, there is ~ 20% change in the cross-section for x values near unity, and the fits to the data imply that the variation remaining in the cross-section through the ISR energy range will be less than 10%.

The fall-off in the cross-section for $x \sim .95$ as measured in the four NAL HBC experiments and discussed above in Fig. 133 is also compatible with this s-dependence.

The experimental results from the CHLM group[126] at the ISR are given in Fig. 140 and show that in this region the cross-section is observed to scale to within 10%. Note that both the ISR and NAL experiments are performed at intermediate t values.

In summary then, the invariant cross-section $s(d^2\sigma/dt\, dM^2)$ is observed to be almost energy independent for x values of order 0.8 from 50 GeV/c through 2500 GeV/c; for $x \sim 0.9$ the cross-section is observed to have a component with $s^{-1/2}$ dependence which amounts to a 20% effect through the NAL energy region ((50-400) GeV/c), but which is < 10% effect through the ISR range (200-2500 GeV/c).

C. Momentum transfer dependence

The momentum transfer dependence of the production of the diffraction peak has been studied at NAL by the bubble chamber experiments[122] and the Columbia-Stony Brook experiment[128] and at the ISR by the CHLM[126] and ACGHT[127] groups.

The t-dependence as a function of the missing mass squared, $(x = 1 - M^2/s)$, is shown in Fig. 141 from the 200 GeV/c HBC experiment.[125] For small masses, the slope of the inelastic diffractive scattering is close to, but a little less than, the elastic scattering slope. As the masses increase, the slope decreases, until one reaches masses corresponding to an x value of ~ 0.9. For masses beyond that there seems to be only a weak M dependence left.

In Fig. 142 the t-dependence of the diffraction peak is shown, from experiments at NAL and the ISR. The cross-section is exponential but with at least two slopes. The dashed line shows a fit which behaves like e^{-7t} at small t and e^{-4t} at large t.

D. Aside on the missing mass distribution

From the above discussion it seems plausible that the differential cross-section, $d\sigma/dt$, is mass dependent. The diffraction peak studied in Fig. 142 contains a wide range of masses (up to $M^2 \sim 50$ GeV^2) and the two exponential shape of that $d\sigma/dt$ may be just a reflection of this mass dependence. Such a dependence would imply that the shape of the missing mass distribution would change for different t values, and perhaps account for some of the difference between the ISR[126,127] and NAL (Columbia-Stony Brook)[128] mass plots (Fig. 137). Indeed, if one assigns an e^{-7t} dependence to the peak masses, and an e^{-4t} dependence to the large mass region $(M^2 \sim 20$ GeV$^2)$ then quantitative agreement between the measured missing mass distributions results.

Further, if such a dependence exists then the peak to shoulder ratio (low mass to high mass ratio) should be seen to change for measurements at different t. In Figs. 143, 144 the missing mass squared distribution as measured by the CHLM group[126] at the ISR, for four different t ranges is shown. Clear evidence of this effect is observed.

Thus it seems that in fact the different missing mass distributions are in good agreement--there exist three separate regions in the mass plot:

1. The threshold region $(x \approx 1.0)$ where the cross-section, $d^2\sigma/dt\, dx$, is growing linearly with s (i.e., scaling in M^2) and has a steep t dependence;

2. The diffraction peak $(1.0 > x > .9)$ where the cross-section is nearly constant in s--some 20% variation in the NAL region (50-400) GeV/c and less than 10% variation at the ISR (200-2500) GeV/c, and with a $d\sigma/dt$ that depends on M^2, becoming flatter as M^2 increases.

3. Multiparticle production region $(.8 < x < .2)$, where the cross-section seems essentially independent of s and where $d\sigma/dt$ is rather flat $(\sim e^{-4t})$ and varying slowly with s and M^2.

The mass dependence in the diffraction peak appears to be compatible with a $1/M^2$ fall off:

1. The 200 GeV/c HBC expt. (Ref. 125)(see Fig. 134).
2. ACGHT group[127] at ISR find $d\sigma/dM^2 \propto (M^{-2})^{1.15\pm.1}$.
3. CHLM group[126] at ISR find $d\sigma/dM^2 \propto (M^{-2})^{0.98\pm.1}$.
4. Columbia-Stony Brook[128] at NAL find $d\sigma/dM^2$ compatible with M^{-2}.

E. Back to momentum transfer studies

Above we had shown that there was evidence that the slope of the differential cross-section for the diffraction peak became flatter as the diffracted mass increased, and that the $d\sigma/dt$ for the whole peak (averaging over all masses) was exponential but with at least two slopes.

In Fig. 145 the s-dependence of the $d\sigma/dt$ is studied. The data comes from the Rutgers-Imperial College group[130] at NAL. For $x = 0.87$ the differential cross-section, $d\sigma/dt$, is shown for $s = 108$ and $752\ GeV^2$. Essentially no energy dependence is observed, at these x values.

The $d\sigma/dt$ as measured by the Columbia-Stony Brook group[128] at NAL, for missing mass squared around $40\ GeV^2$ is shown in Fig. 146, together with data from Rutgers-Imperial College[130] and from the CHLM[126] group at ISR. Good agreement is observed between the measurements. A flattening of the cross-section is observed for small t values ($t < .2\ GeV^2$). For smaller masses, this effect becomes a turnover in the very forward direction, with a maximum to the cross-section at $t \sim 0.1\ GeV^2$, as shown in Fig. 147. Again the data comes from the Columbia-Stony Brook experiment.[128] Corrected data from a previous run by the same group at 200 GeV/c is also shown.[131]

Similar behaviour is observed in some preliminary data from the (100 + 400) GeV/c HBC experiments at NAL.[132] In Figs. 148 and 149 the p_T^2 distribution is shown for small masses and large masses respectively. The low mass spectrum shows the same tendency to a forward turnover as the NAL counter experiment, whereas the distribution for large missing masses seems to be quite linear.

2. Pion Diffraction Scattering

The first systematic study of high energy pion-proton collisions has been reported by the Berkeley-NAL collaboration working on a 205 GeV/c $\pi^- p$ exposure of the 30 NAL HBC.[133,134] Their results are briefly outlined below.

They have analyzed the exclusive process

$$\pi^- p \rightarrow \pi^- \pi^- \pi^+ p$$

and claim to have an event sample with less than 25% background. They see strong evidence of the pion diffracting into 3π, and the target proton diffracting into a $(p\pi^+\pi^-)$ system, Figs. 150 and 151. The cross-section for both these processes is estimated to be 1.5 mb.

In addition, the diffraction of a $\pi \rightarrow \pi^*$, shown schematically in Fig. 152, has been studied using the same technique as in the p-p HBC experiments. The pictures were scanned for events in which a slow recoil proton could be identified by ionization. This selection works well for proton momenta up to 1.5 GeV/c. The missing mass distribution obtained from these events is shown in Fig. 153. A low mass peak is observed, extending out to $M^2 \sim 20\ GeV^2$, associated with the diffractive excitation of the incoming pion.

The mass dependence is shown in Fig. 154, where over a substantial range of masses, the data are consistent with a $1/M^2$ fall-off.

In Fig. 155, the composition of this low mass diffractive peak by topology is presented and as in the p-p studies, one remarks that only the lowest multiplicities contribute to the peak. Again, the central value moves to larger masses as the multiplicity increases. The mean multiplicity in the diffraction peak is about half that of the overall multiplicity ($\langle n_d\rangle^{charged} \sim 4$, $\langle n_{all}\rangle^{charged} \sim 8$) and increases with M^2.

The differential cross-section, $d\sigma/dt$, is shown by topology in Fig. 156 and for two different mass regions in Fig. 157. No turnover in the forward direction is observed, nor any sizable mass dependence of the slope.

In all these features the pion diffraction data show the same trends as the proton diffraction. Below, the invariant cross sections for $\pi^- p \to X^- p$ and $pp \to pX^+$ are shown with a relative normalization set to compare the x distributions. (See Fig. 158.) Again good agreement is observed.

3. Multiplicity in Inclusive Collisions

As we noted earlier when discussing the structure of the low mass diffractive peak, these events are characterized by a smaller multiplicity, n, than the average. The NAL HBC experiments[122] report that the mean diffractive multiplicity, $\langle n_d \rangle$ is about half the total mean multiplicity, i.e.

$$\langle n_d \rangle \sim \frac{1}{2} \langle n_{all} \rangle .$$

A similar study in the $\pi^- p$ 205 GeV/c bubble chamber experiment[84] finds the diffractive multiplicity, $\langle n_d \rangle = 3.8 \pm 0.2$ while the total multiplicity, $\langle n_{all} \rangle = 8.02 \pm 0.12$. The frequency distribution is given in Fig. 159. At higher energies, the CHLM group[126] at the ISR report that the mean charged multiplicity $\langle n \rangle$ is 2.8 ± 0.5 for $x > 0.99$, while for $x \sim 0.8$ it is measured as $\langle n \rangle \sim 6.7 \pm 1.0$, in good agreement with the NAL bubble chamber conclusions.

Both the p-p and $\pi^- p$ HBC groups at NAL have found an interesting correlation of multiplicity with energy available in the collision. They plot the multiplicity for diffractive reactions as a function of the mass squared of the excited system.

They then plot the mean charged multiplicity of the entire reaction as a function of available energy in the center of mass, and find both sets of data fall on the same curve. The results of the pion experiments are shown below in Fig. 161, but the proton experiments at 100, 200 and 300 GeV/c exhibit the same behaviour.

The implication is that the final multiplicity depends on the available energy but not on whether the initial state consisted of a pion and a proton or of a Pomeron and a proton.

While discussing the multiplicity distributions it is interesting to ask what we can learn of diffraction from their frequency distributions and their correlations.

For diffractive processes, we expect to find a large rapidity gap between the leading particle and the fragments of the excited system. (Rapidity is defined as $y = \frac{1}{2} \ln[(E + p_L)/(E - p_L)]$, where p_L is the longitudinal momentum of a particle and E is its energy. A useful variable which approximates y for high energy particles is $\eta = \ln \tan(\theta/2)$.) We would therefore expect to find a "typical diffraction event" to look like Fig. 162 in rapidity space. Other inelastic processes are expected to be characterized by rather uniform distributions in rapidity space, on average. (See Fig. 163.)

The Pisa-Stony Brook collaboration[135] at the ISR have studied the multiplicity distribution in high energy p-p collisions, measuring the angles of each charged particle in a large counter hodoscope system. They group their events according to the total multiplicity, and characterize each event by two numbers--they throw away the largest and smallest rapidities and then calculate a mean rapidity and a dispersion, for what is left. The two variables are defined

$$\bar{\eta} = \Sigma(\eta_i/n-2)$$

$$\delta(\bar{\eta}) = \sqrt{\frac{\Sigma(\eta_i - \bar{\eta})^2}{n-3}}$$

We may now expect diffractive events to show large values of $\bar{\eta}$ and a small dispersion about this $\bar{\eta}$, while the other inelastic events should be centered at $\bar{\eta} = 0$, and with a broad dispersion.

A three-dimensional presentation of the same plot for two energies--the lowest and highest available at the ISR, $\sqrt{s} = 23.6$ and 62.8 GeV--is shown in Fig. 165. Again, for low multiplicities the diffractive component ($\bar{\eta}$

large and sharp), is seen to dominate over the non-diffractive component. As the multiplicity increases their roles reverse. As one goes to larger energies the diffractive component contributes to larger and larger multiplicities. These correlations plots are a nice independent verification of the presence of the diffractive component and a confirmation of several of the properties derived from the magnetic spectrometer studies.

4. Single Particle Inclusive Studies at Low Energy (i.e. $p < 50$ GeV/c)

The high energy single particle inclusive experiments from NAL and the ISR have shown the existence of a large energy independent cross-section for the production of a low mass peak. This process is assumed to be diffractive excitation of the target or projectile and has a cross-section almost equal to the elastic scattering cross-section (i.e. $\sigma_{diff} \sim 6$ mb). At the highest energies this low mass peak in fact includes rather large masses--up to 7 GeV. The low mass peak is made up mainly from low multiplicity channels and the mean charged multiplicity is about half the total charge multiplicity for all processes. The multiplicity increases with increasing mass. For recent review see Ref. (13).

It is interesting to see what can be learned in similar processes at lower energies. Two groups have presented such data in the last year--the CERN-Serpukov collaboration[89] on the missing mass studies at 25 and 40 GeV/c for π^- and K^- beams, and a CERN bubble chamber experiment[136] on $\pi^+p \rightarrow$ anything at 8, 16 and 23 GeV/c.

The x distribution (where $x = p_{11}/p_{11}^{max}$) for the π^+ at all three energies from the CERN HBC experiment[136] are shown in Figs. 167, 168 and 169. One can clearly observe the build up of the diffractive $x \approx 1$ peak as the energy increases, but it is interesting to notice that the peak is fed only by the 2 prong and the 4 prong topologies. They show that indeed only three exclusive reactions make up ~ 80% of the forward peak cross sections--

$$\pi^+p \rightarrow n\pi^+\pi^+$$
$$\pi^+p \rightarrow p\pi^+\pi^0$$
$$\pi^+p \rightarrow \pi^+\pi^+\pi^-p \ .$$

The x-distributions for these processes are shown in Figs. 170 and 171 where events were selected to emphasize the diffractive phenomena, by choosing only those in which the π^+ is the only particle going forward in the c.m.s. and all other particles are going backwards. These contributions are shown as the heavy lines in Figs. 170 and 171. The shaded area in Fig. 171 represents events in which the proton is the only particle going backwards in the c.m.; these events correspond to dissociation of the incoming pion.

The sum of the contributions from the proton diffraction dissociation in the three exclusive reactions studied above, is compared to the diffractive peak obtained in the ISR p-p scattering experiments in Fig. 172. The ISR data were extrapolated to low transverse momenta (where the HBC data exists) under the assumption that

$$E\,\frac{d^3\sigma}{dp^3} = A(x)\ e^{-B(x)p_\perp^2}$$

and then integrated over the entire $p_\perp$ range. (The ISR data was taken for $0.7 < p_\perp < 1.2$ GeV/c.) They further assumed factorization of the diffraction dissociation process and scaled down the p-p cross-sections by

$$\left(\frac{\sigma^T_{pp}}{\sigma^T_{\pi^+p}}\right)^2 = 3.08$$

to compare to the π^+p cross-sections.

The errors associated with these extrapolations are large and indicated on Fig. 172 as the hatched band. The data indicate that within 20-30% one can observe scaling of the forward peak in energy range, $s = 31$ to 2000 GeV^2.

This scaling conclusion is also verified by the CERN-Serpukov experiment.[89] The missing mass spectrum for π^-p collisions is shown in Fig. 173. Production of peaks in the A_1, A_2 and A_3 regions are observed but no further narrow high mass structure is seen. The invariant cross-sections $d^2\sigma/dt\,dx$ and $d\sigma/dx$ are compared in Fig. 174. The cross-sections scale (i.e. are seen to be independent of s for a given x) and the ratio

$$\frac{\frac{d\sigma}{dx}(25\text{ GeV/c})}{\frac{d\sigma}{dx}(40\text{ GeV/c})} \quad \text{for} \quad -0.90 < x < -0.75$$

is given as 1.01 ± 0.03. Also the slope of the cross-section in t is observed to be independent of energy--see Fig. 175.

The same apparatus was used in the study of the reaction $K^- p \to X^- p$ at 25 and 40 GeV/c. The missing mass distribution is shown in Fig. 176. The Q region is the only structure observed. The shape of the cross-section in t is observed to be energy independent and very similar to the $\pi^- p$ distribution (the dashed line)--see Fig. 177. The question of scaling was also addressed for the K^- experiment and the invariant cross-sections are shown in Fig. 178 as a function of x. The scaling hypothesis holds well for this reaction, too. The dashed line represents the invariant cross-section for the pion data and lies somewhat about the K^- cross-section. However, if factorization is assumed then the π and K data are observed to be in good agreement--

$$\frac{\frac{d\sigma}{dx}(\pi^- p)}{\frac{d\sigma}{dx}(K^- p)} = \frac{\sigma^T_{incl}(\pi^- p)}{\sigma^T_{incl}(K^- p)}$$

$$1.20 \pm 0.07 \quad 1.18 \pm 0.04$$

Another interesting measurement from Serpukov has been done by Derevshchikov et al.[137] who have studied the proton diffraction region from high energy pions--

$$\pi^- p \to \pi^- X \quad \text{for} \quad 0.9 < x < 1.0 ,$$

and for pion momenta of 42 GeV/c and 51 GeV/c. The invariant cross-sections are shown in Fig. 166 where the sharp diffractive peak at $x \sim 1.0$ is seen. The data exhibit the same general behavior as pp scattering. It will be interesting to see higher energy data from NAL, to see if the s-dependence matches that of pp scattering.

5. Conclusions

In conclusion, the single particle inclusive studies have shown the existence of a large energy independent cross-section for the production of a low mass peak. The process is assumed to be diffraction excitation of the target or projectile and has a cross-section almost equal to the elastic scattering cross-section (i.e. $\sigma_D \sim 6$ mb). The peak extends up to quite large masses (for example, at ISR energies, it extends up to 7 GeV), and seems to have a M^{-2} fall off. This diffractive peak is made up mainly from low multiplicity events, the mean multiplicity in the peak being about half the mean multiplicity for all events. The multiplicity increases with the mass of the diffracted system. The s-dependence of the cross-section for the peak is very slow, exhibiting a small component with $s^{-1/2}$ behavior, which causes ~ 20% fall in cross-section through NAL (50-400 GeV/c), but which is less than a 10% through the ISR range (200-2500 GeV/c). The momentum transfer behaviour of the diffraction peak is consistent with an exponential fall off, in which the slope decreases as the mass of the diffracting system increases. (This behaviour is very reminiscent of the exclusive diffraction reactions.) Very similar properties are observed for the diffraction of pions and for protons.

Finally, the reports from London bring results from Cool et al.'s[138] measurements on $pd \to Xd$ through the energy range of NAL. By observing the recoil deutron from a deuterium gas jet target, they assure $I = 0$ exchange in the proton excitation. They study the diffraction scattering region for $x > 0.93$.

As in the $pp \to px$ experiment, discussed in Chapter IV above, they observe structure at small missing mass, but for $M \sim 2$ GeV they find the spectrum falling off like M^{-2}. They also find the cross-section independent of energy, namely,

$$M^2 \frac{d\sigma}{dM\,dt} \quad \begin{cases} \text{flat in } s \\ \text{flat in } M \end{cases} \qquad (\text{for } M > 2 \text{ GeV}).$$

The region below 2 GeV they estimate has a total cross-section at 300 GeV of around 0.75 mb, compared to ~ 1 mb at 20 GeV. This resonance diffraction region exhibits the flat energy dependence we expect.

For the data above 2 GeV, integration over t gives a cross-section, $\sigma \sim (0.7\ \text{mb}/M^2)$, and now integrating over M, they find $\sigma \sim \ln s$, with the single diffraction cross-section at 305 GeV, $\sigma_{SD} \sim 3$ mb.

If they subtract off from the inelastic cross-section, the diffractive component indicated here, the resulting non-diffractive inelastic cross-section is flat through the NAL-ISR range, i.e. $\sigma_{inel} - 2\sigma_{SD} - \sigma_{DD}$ = constant as function of s. So in addition to the other properties defined above, this new NAL experiment gives more weight to the suggestion that the rise in the total cross-section observed in the ISR region is due to the expanding phase space of the diffraction process, and the constancy of the cross-section at each individual mass.

VII. TRIPLE REGGE PHENOMENOLOGY

1. Which Terms are Important?

Analysis of the single particle distributions at high energies may be done through the application of triple-Regge theory. One wants to calculate the cross-section for processes of the type (a) in Fig. 179. Applying an equivalent of the optical theorem in $2 \to 2$ body scattering, the total cross-section is then given by the square of the forward scattering amplitude--so for processes of the type (a) we square the forward amplitude by multiplying by itself, shown diagrammatically in Fig. 179(b). This is then approximated by the triple-Regge diagram--Fig. 179(c).

The cross-section obtained from this exercise is then written as

$$s\,\frac{d^2\sigma}{dt\,dM^2} = \sum_{1,2,3} \frac{R_{123}(t)}{s} \left(\frac{s}{M^2}\right)^{\alpha_1(t)+\alpha_2(t)} M^{2\alpha_3(0)}$$

$$= \sum_{1,2,3} \left(\frac{1}{s}\right)^{1-\alpha_3(0)} R_{123}(t) \left(\frac{s}{M^2}\right)^{\alpha_1(t)+\alpha_2(t)-\alpha_3(0)}$$

It is supposed that such a description should be valid for (s/M^2) and M^2 large.

One then tries to fit the data as a function of s, M^2 and t with an appropriate selection of the trajectories α_1, α_2 and α_3 (see Fig. 179). For Pomeron exchanges, P, $\alpha(0)$ is taken to be 1, and for Regge terms, R, $\alpha(0)$ is taken to be 1/2. Excluding interference terms, there are four leading terms to be used in fitting the data--PPP, PPR, RRP, and RRR. The s-dependence for fixed x and M^2-dependence of each is summarized in Table XVIII and in Fig. 180.

If the PPP contribution is not zero,[139] it is expected to dominate at large s and large M^2. Fits to the ISR data[140] show that the data is compatible with substantial PPP coupling, but important contributions from the other trajectories are also required and the fits are by no means unique.

The most systematic attempts to study the triple-Regge question have been performed by the Rutgers-Imperial College Group at NAL,[130,141] and the CHLM group at the ISR.[140,20] Fox[5] has recently given a critical review of this field (recommended reading). In the meantime, we will follow the work of these two experimental groups with the single "Fox caution" kept in mind--it is probably not a good approximation only to keep the four leading terms--appreciable interference effects should be expected.

The Rutgers-Imperial College data spans a large range in the important variables:

$$100 \leq s \leq 750 \text{ GeV}^2$$
$$0.14 \leq t \leq 0.38 \text{ GeV}^2$$
$$5 \leq s/M^2 \leq 12.5$$

and has already been discussed (in Chapter VI) with respect to the scaling behaviour of the cross-section. The wide energy range available in this experiment allows a clean separation of the energy dependent terms, PPR and RRR, from the energy independent terms, PPP and RRP.

The data was divided into four t intervals--$0.14 < t < 0.18$, $0.18 < t < 0.22$, $0.22 < t < 0.28$, $0.28 < t < 0.38$ GeV^2, and fit to the triple-Regge cross-section formula given above, with the couplings being left free in each t interval.

Five fits were attempted: (1) in which the four leading triple-Regge terms were used with $\alpha_P = 1 + 0.25\,t$ and $\alpha_R = 0.5 + t$. This fit was quite poor, not reproducing the dip structure for $x \sim 0.88$. It is interesting to note that the PPP term exhibits a dip in the forward direction with a maximum at $t \sim 0.2$ GeV^2--see Fig. 181; (2) which uses the same trajectories as in fit (1) but only fits the data for $x > 0.84$. This fit is much better but still not very good. The PPP term still shows the forward turnover; (3) in which the trajectory of the RRP terms is taken to be $\alpha = 0.2 + t$ (after Miettinen and Roberts)[142] to allow for the effects of lower lying trajectories. This provides a much better fit to the data, but now the PPP term has no forward turnover--see Fig. 181; (4) is very similar to fit (3) but an explicit parametrization is used for a $\pi\pi P$ term (due to Bishari)[143], together with the four leading triple Regge terms with conventional trajectories. This gives a rather good fit to the data, and no forward structure to the PPP term; (5) in which the RRP term is replaced by an exponential e^{-cx}, as suggested by Capella et al.[144] This provides the steeper x-dependence required by the data and indeed this parametrization gives the best fit. Again, the PPP term shows no forward turnover--see Fig. 181.

It is interesting to note that despite the uncertainty and variation in the PPP term between the several fits tried, the energy dependent term--PPR--seems very stable, quite model independent and rather well determined.

In summary, a clear separation between the s-dependent and s-independent terms has been observed. For the s-dependent terms the RRR contribution is small and negligible, while the PPR contribution is well determined. The energy independent part requires both the PPP and RRP terms, and no unambiguous isolation if the PPP coupling seems possible at this time. Fits with conventional trajectories yielded a PPP coupling which peaked for $t \sim 0.2$ GeV^2 and turned over in the forward direction, while better fits to the data (with modified trajectories) had a quite structureless PPP t-dependence. Therefore not much light can be shed on the question of whether g_{PPP} vanishes at $t = 0$. To make more progress in studying the triple-Regge phenomenology and in particular to identify unambiguously the PPP contribution new data extending further into the diffraction peak, to x values nearer 1, are urgently required.

Sens[20] fits the CGHL group data, which is characterized by:

$s = 1995$ GeV^2	$0.5 < x < 0.82$	$0.7 < P_T < 1.2$ GeV/c
$= 551$ GeV^2	$5 < M^2 < 30$ GeV^2	$.15 < P_T < 1.25$ GeV/c
$= 930$ GeV^2	$7 < M^2 < 50$ GeV^2	$.45 < P_T < 1.65$ GeV/c

The medium x data at $s = 1995\ GeV^2$ were fit assuming that by this high an energy RRR components had died out, and only one term is dominating the cross-section, namely, the RRP contribution. This may be justified by inspection of Fig. 182, which shows s-independence in the medium x region (0.5-0.7), from $\sqrt{s} = 23$ GeV to $\sqrt{s} = 53$ GeV. Terms like RRR, or interference terms may be expected to be small, or at least to contribute less than 20%, to the cross-section.

For this one term we may rewrite the triple Regge relationship:

$$E \cdot \frac{d^3\sigma}{dp^3} = \frac{M_0^2}{16\pi^2 s} \cdot G_{ffp}(t) \left(\frac{s}{M^2}\right)^{2\alpha_f(t)} \cdot \left(\frac{M^2}{M_0^2}\right)^{\alpha_p(0)}$$

where f is the effective meson trajectory in the RRP term.

Taking $M_0^2 = 1$ and $\alpha_p(0) = 1.0$, this reduces to

$$E\, \frac{d^3\sigma}{dp^3} = \frac{G_{ffp}(t)}{16\pi^2} \cdot \left(\frac{M^2}{s}\right)^{1-2\alpha_f(t)}$$

The data at $s = 1995\ GeV^2$, when fitted to this form, give

$$\alpha_f(t) = 0.45 + 0.75\ t,$$

and the results are plotted in Fig. 183. The dashed line gives the sensitivity of the data to the more usual unit slope of the meson trajectory.

At high x, the data is a mixture of diffraction dissociation and high momentum fragments from the pion production region. This is especially true in a poor resolution situation. Sens subtracts out the high momentum fragments assuming they are well explained by the RRP term just determined above.

The M^2-distribution is shown in Fig. 184 and the extrapolated fragmentation component under the diffraction peak is shown as the "background" curve.

The mass spectrum falling like M^{-2} (see Fig. 184), and the s-independence of the cross-section for $x \sim 1.0$ shown in Fig. 185, suggests that the peak may be dominated by the PPP term. See Table XXVIII for M^2, x and s-dependence of the different terms.

Sens then assumes only the PPP term, which gives

$$E \cdot \frac{d^3\sigma}{dp^3} = \frac{G_{PPP}(t)}{16\pi^2} \cdot \left(\frac{M^2}{s}\right)^{1-2\alpha_p(t)}$$

Fitting the data near $x = 1$, and making sure to remove the elastic scattering contamination of the data, allowing for the momentum resolution of the spectrometer and subtracting the high momentum fragmentation "background" using the RRP term, finally yields the Pomeron trajectory

$$\alpha_p(t) = 1 + 0.2t$$

shown in Fig. 186.

This trajectory was compared to that derived from a study of elastic scattering assuming Pomeron dominance of the two-body reaction--

$$\frac{d\sigma}{dt} = f(t)\cdot s^{2\alpha_p(t)-2}$$

Using elastic scattering data at $s = 551{,}930\ GeV^2$ they find good agreement with this Pomeron trajectory (shown as crosses, (x), on Fig. 186). This is also in good agreement with the best overall fit to all elastic pp scattering above $s = 100\ GeV^2$, which gave $\alpha' \sim 0.275\ GeV^{-2}$. (See Chapter II.)

This analysis shows that the triple Regge framework allows a consistent description of the data, but as Fox[5] points out, there are are so many parameters and the correlations in the data are so strong that it is difficult to learn anything at present.

2. Decoupling of the Triple Pomeron Term as $t \to 0$.

The question of the vanishing of the triple Pomeron coupling as $t \to 0$ is always of interest, and should be addressed before leaving the triple Regge chapter.

Abarbanel et al.[139] have shown that the triple Pomeron coupling $g_p(t)$ is given by

$$g_p(t) = \frac{(16\pi)^{1/2} \cdot G_p(t)}{\sqrt{\sigma_T} \cdot \sqrt{d\sigma/dt_{el}}}$$

where

$$E \cdot \frac{d}{dp^3}\,(\text{diffractive}) = \frac{1}{\pi} \cdot G_p(t) \cdot \frac{s}{M^2}$$

and

$$\frac{d\sigma}{dt\,dx} = G_p(t) \cdot \frac{1}{s} \cdot \left(\frac{s}{M^2}\right)^{2\alpha_p(t)} \cdot (M^2)^{\alpha_p(0)}$$

and where σ_T, $d\sigma/dt|_{el}$ are the asymptotic values of the cross-sections. (This is strictly only true for $\alpha_p(0) = 1$.)

This may be rewritten in the following way

$$\frac{1}{16\pi} \cdot \frac{1}{2\alpha_p'(0)} \cdot g_p^2(0) \leq 1 - \alpha_p(0) .$$

The Abarbanel et al. paper points out that if the Pomeron is a factorizable simple pole, that the above triple Pomeron relation cannot be self consistent unless $\alpha_p(0) < 1$ or $G_p(0) = 0$.

Hence the interest in the question of whether PPP vanishes at $t = 0$.

The data of Columbia-Stony Brook[128,129] discussed in Chapter VI, and shown again below as Fig. 187, show a dip at small t for $8 < M^2 < 14$ GeV^2. This dip is not present for larger $(20 < M^2 < 60$ MeV$^2)$ or smaller masses. The interpretation of this turnover as a zero in g_{ppp} may be justified by--

- $8 < M^2 < 14$ GeV^2 region is roughly optimal for seeing the triple Pomeron term at this energy. At lower masses the PPR term is domiant, while at larger masses the RRP term is important,
- the value of $(d\sigma/dtdM^2)$ is non-zero for $t = 0$, but is in agreement with many of the fits for PPR and RRP contributions. (See Fox's review of all these fits.) However, away from $t = 0$ there seems to be a need for an extra contribution to the (PPR and RRP) to fit the data--is this an indication of the presence of the PPP term?

Before accepting that $g_{ppp} \to 0$ as $t \to 0$ as fact, we should notice several other points:

- First, if we use the extrapolated value of the PPP term (going to $t = 0$ with an exponential) from the Sens analysis,[20] and put $G_p(0)$ into the formula derived above, we find

$$1 - \alpha_p(0) \geq \frac{10^{-3}}{2\alpha_p'(0)}$$

which implies for $0.05 < \alpha' < 0.5$, the Pomeron intercept must lie in the range

$$0.99 < \alpha_p(0) < 0.999$$

Clearly this is not too serious a departure from $\alpha(0) = 1$.

This means that the self-consistency equations do not demand that the triple Pomeron coupling have a sharp turnover as $t \to 0$.

If fact, if we write

$$\alpha_p(t) = 1 - \epsilon + \alpha_p(0) \cdot t$$

then for $\alpha' = 0.25$ GeV^{-2}, $\epsilon \geq 2.10^{-3}$. This changes the definition of the cross-section

$$\frac{d\sigma}{dt\,dx} = s^{-\epsilon} \cdot G_p(t) \cdot \left(\frac{s}{M^2}\right)^{1+2\alpha_p'(t)-\epsilon}$$

For small values of ϵ, as those indicated, the scale breaking is very small. For $\epsilon < 10^{-2}$ the cross-section is still well approximated by a logarithmic growth. Indeed the $s^{-\epsilon}$ factor contributes only a 2% correction between $s = 200$ and 3000 GeV^2. Therefore, the cross-section increases with s in this energy range.

- We may also take the PPP term obtained in the Sens fit,[20] and extrapolate to the t-range measured by the Columbia-Stony Brook experiment at NAL.[129] Sens has attempted this comparison, adding to the PPP terms his RRP term (to account for high momentum fragmentation protons). The result is shown in Fig. 188.

  For $5 < M^2 < 30$ GeV^2--the region of Sens high energy fit--the agreement may be interpreted as confirmation that down to $t \sim 0.056$ GeV^2 there is no sign of $G_{PPP}(t)$ turnover.

- Finally, what do the bubble chamber experiments say on the question of the forward dip? (This question was reviewed in Chapter VI in discussing the t-dependence of the inclusive scattering.)

The 200 GeV/c $\pi^- p$ and pp experiments looking at $d\sigma/dtdM$ see no sign of a forward turnover for small masses--(i.e. the $8 < M^2 < 14$ GeV^2 region studied in the Columbia-Stony Brook experiment). The data are repeated below in Figs. 189 and 190. The pp experiment does observe some flattening of the t-distribution for M^2 above 25 GeV^2.

Vander Velde,[145] in a summary of all four pp experiments (102, 205, 303, 405 GeV/c) reports that for the broad hump region (i.e. $0.9 > x > 0.5$), the $d\sigma/dt$ is exponential with a slope of $\exp(-8.5P_T^2)$, and the region of large mass in the diffraction peak ($x > .9$ but $M^2 > 10$GeV^2) is also quite exponential with slope $\exp(-7P_T^2)$. However, in studying the four prong data they do observe a dip in the forward direction for $P_T^2 \leq 0.4$ GeV^2 for $M^2 < 10$ GeV^2. Beyond $P_T^2 \sim 0.05$ GeV^2 the data are exponential with a slope of $\exp(-10P_T^2)$. See Fig. 191.

The bubble chamber data do not help to clarify this question. It is important to establish the existence of the dip firmly, and then by studies of its s- and M^2-dependence attempt to associate it with one of the triple Regge terms contributing to the process. In this way, we may see some progress on the question of whether the triple Pomeron coupling vanishes as $t \to 0$. As mentioned before, unambiguous determination of the triple Pomeron term needs experiments measuring s-, t- and M^2-dependences well inside the diffraction peak for x nearer 1.0.

VIII. IMPACT PARAMETER ANALYSIS OF HIGH ENERGY SCATTERING

1. Summary of Data

a) σ_T increases by ($10 \pm 2\%$) in NAL-ISR energy range.

σ_{el} increases by $\sim 10\%$ in NAL-ISR energy range.

σ_{inel} is responsible for most of rise in σ_T, it grows by $\Delta\sigma \sim 3.3$ mb ($\sigma_{inel} = 32.3 \pm .4$ mb at $\sqrt{s} = 23.4$ GeV and $35.6 \pm .5$ mb at 53 GeV).

b) Real part of elastic scattering amplitude at $t = 0$ changes sign around $p \sim 300$ GeV/c crossing from negative to positive values.

c) Small t slope of $d\sigma/dt$ (i.e. $|t| < 0.15$ GeV^2), is steep ~ 12 GeV^{-2}, and grows like $\ln s$. Parametrizing this shrinkage in terms of a Pomeron trajectory yields $\alpha' = (0.27 \pm 0.05)$GeV^{-2}.

d) The slope of $d\sigma/dt$ changes rapidly by $\Delta b \sim 2$ GeV^{-2} around $t \sim 0.15$ GeV^2. The cross-section for larger t values shows weak energy dependence.

e) The break in $d\sigma/dt$ observed in the 10-30 GeV/c energy region for $t \sim 1.3$ GeV^2 develops into a beautiful diffraction minimum, at high energy.

f) Production of a low mass peak in inelastic scattering with an s-independent cross-section; the peak extends up to masses of about 7 GeV at ISR energies and seems to behave like M^{-2}.

g) The cross-section for the inelastic diffractive process is found to grow like $\ln s$, and to account for a substantial part of the rise in the total cross-section; (one experiment indicates that the inelastic cross-section minus the single and double diffractive contributions is a constant from NAL through ISR).

h) The multiplicity in diffraction scattering is lower than for other processes--typically the mean diffractive multiplicity is about half the total mean multiplicity. This multiplicity increases with the mass of the diffraction excited system.

i) The differential cross-section, $d^2\sigma/dM^2dt$, is peaked and consistent with an exponential behaviour where the slope is a function of the mass of the diffracted system, $d^2\sigma/dM^2dt \propto \exp(-b(M^2)\cdot t)$. The slope, $b(M^2)$, falls from a value close to twice the elastic value for low masses, to ~ 4 GeV^{-2} for the high mass tail.

j) The properties of pion diffraction, ($\pi \to \pi^*$), and proton diffraction, ($p \to p^*$), are observed to be very similar.

2. Elastic Scattering Analysis

In Chapter I we discussed diffraction scattering as the shadow of inelastic processes and through s-channel unitarity arrived at the relation--

$$\mathrm{Im}\, T_{fi} = G_{el} + G_{inel}$$

where T_{fi} is the elastic amplitude and G_{el}, G_{inel} the elastic and inelastic overlap functions.

From the measured data on $d\sigma/dt$ for pp elastic scattering one can *determine* $\mathrm{Im}\, b_{el}(s,t)$ and $\mathrm{Re}\, b_{el}(s,t)$. Most simply one can assume pure imaginary, non-flip for the elastic amplitude and solve for $\mathrm{Im}\, b_{el}(t)$ directly from the data. The next stage in sophistication is to attempt to find $\mathrm{Re}\, b_{el}(t)$. The real part is known only at $t = 0$, but a reasonable estimate of the phase is obtained by assuming that the imaginary part of the scattering amplitude vanishes for $t \sim 1.3$ GeV^2 dip, and the measured cross-section gives the real part at that t-value. Using smoothness to connect, one may estimate $\mathrm{Re}\, b_{el}(t)$. *(It turns out not to be at all sensitive to the phase assumed.)*

Given the elastic amplitude, one may use the s-channel unitarity equation to find $G_{inel}(t)$--see Fig. 192.

Here we see the inelastic overlap function changing sign as a function of t, for $t \sim 0.6\ GeV^2$, and a second zero for $t \sim 2.2\ GeV^2$. The change of sign shows how important are the phases of the many open channels, in making up the inelastic overlap function.

Perhaps one sees more clearly what is going on, if we Fourier-Bessel transform the $\mathrm{Im}\ b_{el}(s,t)$ and $\mathrm{Re}\ b_{el}(s,t)$ into b-space (i.e. impact parameter space). We may then find $G_{inel}(s,b)$ from the relation

$$\mathrm{Im}\ b_{el}(s,b) = \frac{1}{4}\,|b_{el}(s,b)|^2 + G_{inel}(s,b)\ .$$

Figure 193 shows the result for the total, elastic and inelastic overlap functions using the ISR pp scattering at $\sqrt{s} = 53$ GeV. (This is from the analysis of Pirila and Miettinen,[16,17] but all of the analyses are in fairly good agreement.) The "blackness" of the proton is observed to be ~ 94% of the unitarity black disc limit, and the inelastic overlap looks like a gaussian with average radius a little less than 1 fermi. On closer inspection, G_{inel} flattens out near $b = 0$, and has a long tail.

This long tail of the $G_{inel}(b)$, (or $\mathrm{Im}\ b_{el}(b)$--as for large b they are the same), is directly related to the sharp break in $d\sigma/dt$ at $t = 0.15\ GeV^2$. There is much discussion as to the origin of this tail--2π contributions, dissociation, etc.

The dip at $t \sim 1.3\ GeV^2$ is related to the flattening of G_{inel} as $b \to 0$, but the corresponding effect in the elastic amplitude is very difficult to see. (Remember, the cross-section at the dip is between six and seven decades down from $d\sigma/dt|_0$, so it does not take a big change in the elastic amplitude). It is also interesting to note that if $G_{inel}(s,b)$ did not level off near $b \sim 0$, it would violate unitarity. This suggests that absorptive effects are at least partially responsible for the small b flattening.

It is of interest to study the s-dependence of the overlap function--the same analysis was performed for $\sqrt{s} = 21$, 30, 44 and 53 GeV. The results are shown in Fig. 194, where we see that the radius grows ~ 5% through this energy range, but that the absorption at $b = 0$ stays constant at 94% of its unitary value. So the protons are getting bigger not blacker.

In addition, if we look at where G_{inel} changes between 53 and 31 GeV, we find that the increase in the inelastic cross-section comes from a narrow region, a ring around 1 fermi. Perhaps it is not so surprising if we remember that the increase in the elastic cross-section comes mainly from the small t region--i.e. for large impact parameters. (See Fig. 194.)

3. Inelastic Diffractive Scattering: Impact Parameter Analysis

The measurements of the inclusive proton spectra at NAL and the ISR show that at high energies inelastic diffractive scattering and non-diffractive scattering populate different regions of phase space. This suggested that it may be useful to consider their contributions to the elastic scattering separately. Hence the inelastic overlap may be split into two parts--

$$G_{inel}(t) = G_{prod}(t) + G_D(t)$$

Rewriting the s-channel unitarity relation, we have--

$$\mathrm{Im}\ T_{fi}(t) = G_{el}(t) + G_D(t) + G_{prod}(t)\ ,$$

where $G_{prod}(t)$ is the shadow of the non-diffractive particle production processes and G_D the same for the diffractive part.

The analysis closely parallels the elastic study above, except now have to take into account spin and helicities in the inelastic scattering while "non-flip only" was taken in the elastic case. Sakai and White[146] have done a careful analysis of this case--they assume that as the mass of the excited system grows, the spins involved grow quite rapidly.

They also assume that the diffraction scattering conserves helicity in the t-channel. (The data discussed in Chapter V showed that the data favour TCHC over SCHC, but still shows some violation. However, Miettinen points out that the impact analysis is not crucially dependent on rigourous TCHC, but merely demand substantial SCH flip--which the data certainly confirms.)

Sakai and White fit the $(d^2\sigma/dM^2dt)$ for the single particle spectra and find that the diffractive shadow $G_D(s,b)$ has a peripheral profile, and that diffraction occurs at the edge of the absorption region around $b \sim 1$ fermi. See Fig. 195. (Note that if SCHC had been assumed, the impact profile for diffraction would have been central. Further note that the large b tail is ascribed to central inelastic amplitude in this model. G_{in} dominates for $b < 1f$ and for $b > 1f$.)

4. Slope-Mass Correlation

This association of the diffractive production with peripheral impact parameters allows a very natural explanation of the observed correlation of the slope of the diffraction peak with the mass of the system. The production from a ring at large impact parameters will contribute a term $(e^{at} J_{\Delta\lambda}(R\sqrt{-t}))$ to the differential cross-section, $d^2\sigma/dM^2dt$, where $\Delta\lambda$ is the helicity flip involved in the scattering and where the exponential accounts for the smearing of the edge of the ring.

When the mass is close to threshold, the spin (J) is low and the contribution of helicity flip amplitudes are small. For this situation the shape of the amplitude is given by $J_0(R\sqrt{-t})$, which for $R \sim 1$ fermi gives a zero at $t - 0.2$ GeV^2. This would mean that the very steep slope for the low mass diffraction is caused by a zero at small t values in the dominant helicity amplitude, and not by a large value of the exponential slope, a.

As the mass of the system increases, this zero becomes washed out by contributions of the flip amplitude, and/or real parts--as the mass increases the spin increase and the helicity flip amplitudes grow--flattening out the cross section, $d\sigma/dt$. See Fig. 196.

It will be interesting to see inelastic diffraction data from NAL at small mass and over large enough a t region to convincingly see this structure. At these energies the real parts should be small enough that if this is really what is going on, we should see the characteristic J_0 structure in the $d\sigma/dt$.

There is some confirmation of this suggestion,from two bubble chamber experiments--one on $pp \to pn\pi^+$ at 19 GeV/c[147]--see Fig. 197--and the other on $np \to p\pi^- p$ at 12.5 GeV/c[79]--see Fig. 198. For small masses of the diffractively excited $(N\pi)$ system there are signs of small t structure.

However, for the moment only a hint.

5. Rise of σ_T

In the summary of the data, we found that the rise in σ_T comes from σ_{inel} mainly, and that it originates for large impact parameters--from a narrow ring around $b \sim 1$ fermi.

We have also argued that the inelastic diffraction is peripheral and comes from a narrow ring around $b \sim 1$ fermi.

Further we have several experiments which indicate that the diffractive cross-section increases like $\ln s$, and could account for the increase in the total cross-section.

It is very tempting to tie all of these points together; to be sure we would like to have $G_D(s,b)$ at several energies to find where the increase in diffraction comes from. This is a necessary precaution, because one can imagine a situation where the increase is due to a central contribution but which produces a peripheral increment to the total amplitude.

Consider the case of σ_{inel} being constant, but the elastic differential cross-section shrinks. This causes G_{inel} to fall at $b = 0$ and go up for large b. If, as the energy increases, we add a new central contribution then the new total G_{inel} at the higher energy could be compensated such that G_{inel} has not changed at $b = 0$, and the difference of the two G_{inel} would peak at ~ 1 fermi (i.e. have produced a peripheral increase in G_{inel} from a new central piece, plus a shrinking elastic amplitude). See Fig. 199.

6. Conclusion

Finding the reason for this phenomenon of rising total cross-section is one of the most interesting questions in particle physics. It is clear that the rise is not due to the saturation of unitarity (Froissart, Chen-Wu), but which of the several other possible mechanisms nature is using is far from clear Is it due to an expanding core?, or to an expanding ring around the edge of the absorption region?, or to an increasing blackness of this outer ring? (or something else?). Defining the specific amplitude and mechanism for the growing cross-section is a very tantalizing and fundamental question!

IX. CONCLUSIONS

Having completed a review of the data on diffractive processes, we now collect together some of the questions raised in the preceding chapters.

1. Total Cross-sections--what is the asymptotic behaviour? Do they continue to rise with increasing energy or do they approach a constant value at high energy? See Fig. 200.

   Some useful insight on this matter will come from:

   -study of the "early rising" K^+p cross-sections through the NAL energy range;

   -good measurements of the magnitude of the real part of the forward scattering amplitude in p-p scattering at highest energies of the ISR;

   -watching for changes in the s-dependence of σ_{el}, σ_{el}/σ_{tot}, b (the slope of the forward cross-section) for all processes through the NAL energy range;

   -watching the energy dependence of the difference in total cross-section for particle and antiparticle processes through the NAL range, to see if (and when), the Pomeranchuk theorem will be satisfied.

2. Elastic Cross-section--are there really two components to the Pomeron? There are three interesting areas to watch here:

   -study of the s-dependence of the small t cross-section, especially for the K^+p system, though NAL energies. (Do we find diffractive amplitudes with upward curvature at small t?)

   -study of the s-dependence of the larger t cross-section and of the diffractive dips, to provide more imformation on the "central collisions." (Do K^+p, $\gamma \to \Phi$, $\pi^{\pm}p$ reactions show deep diffraction dips? If so at what t-values and how do they move with energy?)

   -the determination of the real part of the elastic scattering amplitude at all t values--see Davier's lectures.[104]

3. Inelastic Diffraction Scattering--here we have quite a long list of interesting questions:

-understand the two components of exclusive diffraction (the threshold kinematic amplitude and the diffractive production of resonant states), and their relationship to each other;

-from studies at NAL energies of low mass exclusive diffraction, determine whether the slope-mass correlation is caused by a zero in the amplitude at small t (which gets filled in as the mass grows and spin structure gets more complicated), or is due to a real shrinkage of an exponential cross-section as masses go to threshold.

-understand the anomalous nuclear absorption in diffractively produced systems, wherein the absorption cross-section for (3π) and (5π) states is the same as a single pion, $(K\pi\pi)$ like the K and $(N\pi\pi)$ like the nucleon. (See the lecture of B. Gobbi.[82])

-where are the meson resonances, which correspond to the diffractive N^* production? Hoepfully, with new tools becoming available[101] we will be able to study A_1 and Q production in non-diffractive channels--

$$K^-p \rightarrow A_1\Lambda,\ Q^-\Delta^+$$

$$\pi p \rightarrow Q\,\Lambda,\ A_1\Lambda$$

$$e^+e^- \rightarrow \pi A_1,\ \bar{K}Q\ .$$

-is the inclusive diffractive amplitude peripheral? Is the increase in this amplitude, with increasing energy, peripheral or central? Does the increase in the diffractive cross-section account for the observed rising total cross-section?

-if we think of the proton as an almost black disc with an edge contribution, are the disc and the edge both growing with energy? If so, how fast? Does the edge get blacker?

-for a better understanding of the triple Regge picture experiments covering a large s- and t-range and measuring x-values from $x \sim 0.8$ right up to almost 1.0 are required. Such studies should also allow a better discussion of the question of the decoupling of the triple Pomeron coupling at small t values.

4. Factorization--we know from studies of two-body processes around 10 GeV/c that secondary processes (cuts, absorption, double exchanges, etc.) are important, and further the rising total cross-sections observed at high energies exclude a simple pole description. These observations lead us to expect a breakdown of factorization. It would be interesting to have good experiments, with a few percent accuracy, to observe this breakdown and attempt to follow any s-dependence of the violation.

5. Comment on the s-Dependence of the Impact Structure of Pomeron

Since s-channel unitarity relates elastic and inelastic behaviour at a given impact paramter through the equation:

$$\mathrm{Im}\ f_{el}(s,b) = f_{el}(s,b) + f_{inel}(s,b)$$

we have to be prepared for the impact structure of Pomeron to change with energy, despite our prejudice as to its constancy.

We know that the total inelastic cross-section is flat (slowly rising--but maybe if take out the diffraction dissociation contribution, then it would be flat). But we also know that there are different reaction channels contributing at any two energies s_1 and s_2, being driven by quite different mechanisms. For example, at 10 GeV/c we have mainly quasi-two-body processes, which are very peripheral, while at 1000 GeV/c it is not mainly quasi-two body and I do not think peripheral--i.e. although the total inelastic cross-section is flat, the distribution in b-space will probably change--therefore the diffractive b structure must change (since one is the shadow of the other).

Perhaps there is a neat collaboration in the turning-on of the diffractive dissociation piece, which is peripheral and inelastic, and which feeds the Pomeron such that it picks up what is disappearing as the Regge two-body processes die out with increasing energy. (I think this is unlikely given the respective energy dependencies.)

At any rate, a study of the change of the impact parameter structure of the Pomeron, and of the inelastic processes which are coming in or dying out, may allow a deeper understanding of what diffraction is and how the proton is built up.

TABLE I

"OLD" REGGE POLE PARAMETRIZATION

$$\sigma_t(\pi^- p) = 21.3 + 17.6\ p^{-1/2}\ \text{mb}$$
$$\sigma_t(\pi^+ p) = 21.3 + 11.2\ p^{-1/2}$$
$$\sigma_t(K^- p) = 17.1 + 17.1\ p^{-1/2}$$
$$\sigma_t(K^- n) = 17.1 + 11.45\ p^{-1/2}$$
$$\sigma_t(K^+ p) = 17.1$$
$$\sigma_t(K^+ n) = 17.1$$
$$\sigma_t(\bar{p}p) = 37.4 + 50.7\ p^{-1/2}$$
$$\sigma_t(pp) = 37.4 + 7.4\ p^{-1/2}$$
$$\sigma_t(\gamma p) = 94.1 + 79.9\ p^{-1/2}\ \mu\text{b}$$
$$\sigma_t(\gamma n) = 94.1 + 53.6\ p^{-1/2}$$

TABLE II

THE VALUES OF THE PARAMETERS A AND n RESULTING FROM THE FITTING OF THE TOTAL CROSS-SECTION DIFFERENCES ABOVE 3 GeV/c TO THE FORMULA

$$\Delta\sigma = Ap_{lab}^{-n} .$$

(The errors shown in the table have been evaluated taking into account statistical and systematic errors.)

Cross-section differences	A (mb)	n
$\Delta(\pi^{\mp} p)$	4.0 ± 0.3	0.32 ± 0.02
$\Delta(K^{\mp} p)$	18.1 ± 0.3	0.54 ± 0.02
$\Delta(K^{\mp} n)$	13 0 ± 0.4	0.67 ± 0.02
$\Delta(p^{\mp} p)$	63 ± 2	0.64 ± 0.02
$\Delta(p^{\mp} n)$	49 ± 7	0.61 ± 0.05

TABLE III

ELASTIC DIFFERENTIAL AND TOTAL CROSS-SECTIONS MEASURED BY THE CERN-ROMA COLLABORATION

$\sqrt{s}$ (GeV)	$\|t\|$ (GeV^2) $\times 10^{-3}$	$(d\sigma/dt)_t$ (mb/GeV^2)	$b^{a)}$ (GeV^{-2})	$\epsilon = e^{b\|t\|}$ Extrapolation factor$^{b)}$	$(d\sigma/dt)_{t=0}$ (mb/GeV^2)	σ_t (mb)	σ_{el} $^{c)}$ (mb)	σ_{in} (mb)
23.4	8.1	71.0 ± 1.5	11.8	1.10 ± 0.004	78.1 ± 1.7	39.1 ± 0.4	6.8 ± 0.2	32.3 ± 0.4
30.5	13.5	71.0 ± 1.6	12.3	1.18 ± 0.007	83.8 ± 1.9	40.5 ± 0.5	7.0 ± 0.2	33.5 ± 0.4
44.8	17.5	73.8 ± 1.7	12.8	1.25 ± 0.010	92.3 ± 2.2	42.5 ± 0.5	7.5 ± 0.3	35.0 ± 0.5
52.8	23.0	70.6 ± 1.8	13.1	1.35 ± 0.014	95.4 ± 2.6	43.2 ± 0.6	7.6 ± 0.3	35.6 ± 0.5

a) The values of the forward slope b are obtained by fitting the Serpukhov and the ISR results on the hypothesis that $b \propto \ln s$.

b) The extrapolation factor ϵ increases with energy because the elastic scattering events are measured at a fixed angle, and thus at a momentum transfer $|t|$ which increases by a factor of about three when the energy is increased. The error on ϵ is obtained by assuming a very generous error $\Delta b = \pm 0.5$ GeV^{-2} on the interpolated values of b. The fitted errors are half of the error chosen.

c) The elastic cross-section σ_{el} is obtained from the quoted values of $(d\sigma/dt)_{t=0}$ and the shape of the differential cross-section as measured by the CERN-Roma and the Aachen-CERN-Genova-Harvard-Torino collaborations.

TOTAL CROSS-SECTIONS MEASURED BY THE PISA-STONY BROOK COLLABORATION

$\sqrt{s}$ (GeV)	Detected cross-section	Increment for elastic losses (mb)	Increment for inelastic losses (mb)	η	σ_t (mb)
23.4	38.66 ± 0.79	0.54 ± 0.10	0.10 ± 0.02	1.017 ± 0.003	39.30 ± 0.79
30.5	39.93 ± 0.81	0.75 ± 0.10	0.17 ± 0.04	1.023 ± 0.004	40.85 ± 0.82
44.8	40.69 ± 0.84	1.54 ± 0.15	0.34 ± 0.10	1.047 ± 0.006	42.57 ± 0.86
52.8	40.53 ± 0.83	1.95 ± 0.20	0.50 ± 0.12	1.060 ± 0.008	42.98 ± 0.84
62.8					44.0 ± 0.8

TABLE IV

LUMINOSITY INDEPENDENT MEASUREMENT OF $\sigma_T(pp)$ AT THE ISR

p (GeV/c)	σ_T (mb)
11.8	40.5 ± 1.0
15.4	40.3 ± 1.0
22.6	42.6 ± 1.1
26.6	43.1 ± 1.2

TABLE V

RESULTS ON PROTON-PROTON TOTAL CROSS-SECTIONS, ELASTIC CROSS-SECTIONS AND ρ

P_1 (lab) (GeV/c)	$P_1 + P_2$ (GeV/c)	$\sqrt{s}$ (GeV)	σ_{tot} (mb)	σ_{el} (mb)	ρ
102		13.9	39.7 ± 1.5	6.9 ± 1.0	
200		19.4	39.5 ± 1.1	6.92 ± 0.4	
303		23.9	39.0 ± 1.0	7.2 ± 0.4	
	15.4 + 15.4	30.6	40.3 ± 2.0	6.8 ± 0.6	
	11.8 + 11.8	23.5	38.9 ± 0.7	6.7 ± 0.3	+0.02 ± 0.05
	15.4 + 1 .4	30.6	40.2 ± 0.8	6.9 ± 0.4	+0.03 ± 0.06
	11.8 + 11.8	23.5	39.3 ± 0.8		
	15.4 + 15.4	30.6	40.9 ± 0.8		
	22.6 + 22.6	44.9	42.6 ± 0.9		
	26.6 + 26.6	52.8	43.0 ± 0.8		
	11.8 + 11.8	23.5	39.1 ± 0.4	6.8 ± 0.2	
	15.4 + 15.4	30.6	40.5 ± 0.5	7.0 ± 0.2	
	22.6 + 22.6	44.9	42.5 ± 0.5	7.5 ± 0.3	
	26.6 + 26.6	52.8	43.2 ± 0.6	7.6 ± 0.3	

TABLE VI

NEW ELASTIC CROSS-SECTIONS

p (GeV/c)	Group	σ_{el} (mb)	
25	CERN-IHEP	3.35 ± .06	π^-p
32.8	IHEP	3.91 ± .22	π^-p
35.4	IHEP	3.48 ± .36	π^-p
40.0	CERN-IHEP	3.32 ± .06	π^-p
42.0	IHEP	3.23 ± .10	π^-p
45.3	IHEP	3.44 ± .19	π^-p
48.6	IHEP	3.22 ± .12	π^-p
54.7	IHEP	3.35 ± .17	π^-p
205.0	NAL-LBL-Berkeley	3.03 ± .30	
25.0	CERN-IHEP	2.46 ± 03	K^-p
40.0	CERN-IHEP	2.33 ± .03	K^-p
25.0	CERN-IHEP	8.7 ± .2	$\bar{p}p$
40.0	CERN-IHEP	7.2 ± .3	$\bar{p}p$

TABLE VII

ENERGY DEPENDENCE OF ELASTIC CROSS SECTION

$\sigma \propto p^{-n}$

Particle	Exponent, n	Range of Fit
π^-	-0.25 ± .02	(5-40) GeV/c
π^+	-0.28 ± .06	(5-40) GeV/c
K^-	-0.26 ± .03	(5-40) GeV/c
K^+	-0.09 ± .03	(4-15) GeV/c
$\bar{p}$	-0.42 ± .03	(5-40) GeV/c
p	-0.26 ± .02	(5-30) GeV/c

TABLE VIII

RATIO OF ELASTIC TO TOTAL CROSS-SECTION, $(\sigma_{el}/\sigma_{tot})$

	p_{lab} (GeV/c)	Ratio
π^-	5.5	.188 ± .005
	55.0	.138 ± .007
π^+	7.0	.192 ± .004
	16.0	.170 ± .006
K^-	10	.140 ± .003
	40	.126 ± .014
K^+	5	.225 ± .024
	15	.196 ± .017
p	6	.294 ± .006
	60	.187 ± .008
	200	.174 ± .005
	1000	.176 ± .007
$\bar{p}$	8.0	.225 ± .012
	16.0	.185 ± .010
	40.0	.178 ± .018

TABLE IX

RATIO OF $\dfrac{\sigma(Xp \to Xp)}{\sigma(\bar{X}p \to \bar{X}p)}$

Ratio \ Momentum (GeV/c)	5	10	40
$R(\pi^-/\pi^+)$	1.01 ± .06	1.00 ± .02	1.03 ± .02
$R(K^-/K^+)$	1.09 ± .06	0.94 ± .09	1.01 ± .03
$R(\bar{p}/p)$	1.26 ± .06	1.19 ± .04	1.05 ± .11

TABLE X

RESULTS ON THE EXPONENTIAL SLOPE b IN ELASTIC PROTON-PROTON SCATTERING AT THE CERN ISR. THE ERRORS INCLUDE AN ESTIMATE OF THE SYSTEMATIC CONTRIBUTIONS TO THE ERROR

		$\|t\| \leq 0.15$ GeV^2		$\|t\| \geq 0.15$ GeV^2	
$P_1 + P_2$ (GeV/c)	$\sqrt{s}$ (GeV)	t-range (GeV^2)	slope b (GeV^{-2})	t-range (GeV^2)	slope b (GeV^{-2})
10.8 + 10.8	21.5	0.05 -0.09	11.6 + 0.3	0.14-0.24	10.4 ± 0.2
15.5 + 15.5	30.6	0.05 -0.09 0.015-0.06	11.9 ± 0.3 13.0 ± 0.7	0.14-0.24	10.9 ± 0.2
22.5 + 22.5	44.9	0.05 -0.09 0.03 -0.12 0.01 -0.05	12.9 ± 0.2 12.9 ± 0.4 12.6 ± 0.4	0.14-0.24	10.8 ± 0.2
26.5 + 26.5	52.8	0.06 -0.11 0.04 -0.16 0.01 -0.06	12.4 ± 0.3 13.0 ± 0.3 13.1 ± 0.3	0.17-0.31	10.8 ± 0.2
31.4 + 31.4	62.6	0.01 -0.06	13.1 ± 1.0		

TABLE XI

$\pi^- p$ ELASTIC SLOPES

p (GeV/c)	t-Range (GeV^2)	Slope, b (GeV^{-2})
	$\left[\frac{d\sigma}{dt} \propto e^{-bt}\right]$	
14	.05 < t < .78	7.7 ± .03
55	.05 < t < .53	8.8 ± .2
205	.03 < t < .60	9.0 ± .7
	$\left[\frac{d\sigma}{dt} \propto e^{-bt-ct^2}\right]$	
3.0	.05 < t < .44	7.61 ± .11
3.7	.05 < t < .44	7.60 ± .12
5.0	.05 < t < .44	7.66 ± .09
6.0	.05 < t < .44	7.70 ± .08
14.0	.05 < t < .78	8.26 ± .10
25	.1 < t < .6	9.07 ± .32
40	.1 < t < .6	9.63 ± .31

TABLE XII

PARAMETERS OF ELASTIC SCATTERING (25 AND 40 GeV/c) - $\left(\frac{d\sigma}{dt} = \left.\frac{d\sigma}{dt}\right)_0 e^{bt+ct^2}\right)$

	P_{inc}	Events	b	c	χ^2/pts	$(d\sigma/dt)_{t=0}$	OTP	σ_{el}
π^-	25	8600	9.07 ± 0.32	2.4 ± 0.6	34/38	28.6 ± 2.6	31.6 ± 0.3	3.35 ± 0.06
	40	9300	9.63 ± 0.31	2.9 ± 0.5	38/38	29.8 ± 2.6	30.1 ± 0.3	3.32 ± 0.06
K^-	25	12400	8.71 ± 0.21	2.4 ± 0.4	34/38	19.9 ± 1.6	22.1 ± 0.2	2.46 ± 0.03
	40	15400	8.90 ± 0.23	2.8 ± 0.4	36/38	19.0 ± 1.5	21.2 ± 0.2	2.33 ± 0.03
$\bar{p}$	25	12000	12.8 ± 0.4	2.3 ± 0.8	25/33	108 ± 9	112 ± 1	8.7 ± 0.2
	40	4400	12.2 ± 0.7	2.0 ± 1.4	28/33	85 ± 9	101 ± 1	7.2 ± 0.3

TABLE XIII

t-DEPENDENCE OF SHRINKAGE IN ELASTIC $\pi^- p$, $K^- p$, and $\bar{p}p$ SCATTERING

($2\alpha'$ GeV^{-2})

	t = 0	-0.1	-0.2	-0.3	-0.4 (GeV^2)
π^-	0.72 ± 0.18	0.52 ± 0.12	0.35 ± 0.08	0.23 ± 0.05	-0.08 ± 0.06
K^-	0.73 ± 0.16	0.54 ± 0.12	0.38 ± 0.08	0.20 ± 0.06	0.00 ± 0.08
$\bar{p}$	-0.8 ± 0.2	-1.1 ± 0.1	-1.0 ± 0.1	-1.4 ± 0.2	-2.0 ± 0.2

TABLE XIV

RESULTS OF FITTING THE CROSS SECTIONS. FITS OF THE TYPE $A\ \exp(Bt)$ WERE MADE TO THE $\pi^{\pm}$ AND $K^{\pm}$ CROSS SECTIONS FOR THE RANGE $0.05 \leq -t \leq 0.44\ GeV^2$; THE FORM $A\ \exp(Bt + Ct^2)$ WAS USED FOR p AND FOR $\bar{p}$ DATA OVER THE INTERVALS 0.05 to 1.0 GeV^2 AND 0.05 TO 0.44 GeV^2, RESPECTIVELY. THE SUPERSCRIPTS $\pm$ REFER TO THE CHARGE OF THE INCIDENT PARTICLE. ERRORS SHOWN INCLUDE STATISTICAL ERRORS AND UNCERTAINTY IN THE CORRECTIONS FOR SINGLE COULOMB SCATTERING.

Beam	p_{beam} (GeV/c)	A^+ mb/GeV^2	B^+ GeV^{-2}	GeV^{-4}	χ^2 per degree of freedom	A^- mb/GeV^2	B^- GeV^{-2}	C^- GeV^{-4}	χ^2 per degree of freedom
	3	52.7 ± 1.2	7.03 ± .12		17/19	55.6 ± 1.1	7.61 ± .11		24/19
	3.65	44.8 ± 1.0	6.75 ± .12		20/19	51.5 ± 1.2	7.60 ± .12		14/19
π	5	39.4 ± 0.7	6.94 ± .09		24/19	44.1 ± 0.7	7.66 ± .09		32/19
	6	37.1 ± 0.7	7.08 ± .10		14/19	40.2 ± 0.6	7.70 ± .08		33/19
	3	17.5 ± 0.4	3.64 ± .11		24/19	38.7 ± 0.9	7.96 ± .13		16/19
K	3.65	17.1 ± 0.5	4.12 ± .12		29/19	33.9 ± 0.8	7.57 ± .13		22/19
	5	16.2 ± 0.4	4.62 ± .10		23/19	28.9 ± 0.6	7.65 ± .10		24/19
	6	15.7 ± 0.4	4.87 ± .11		12/19	27.0 ± 0.7	7.57 ± .13		18/19
	3	117.0 ± 2.3	7.80 ± .15	2.66 ± .20	19/26	299 ± 19	12.2 ± .8	-5.7 ± 2.4	28/18
p	3.65	110.1 ± 2.4	8.29 ± .16	3.06 ± .22	23/26	264 ± 20	12.1 ± 1.0	-7.6 ± 3.0	12/18
	5	97.3 ± 2.0	8.46 ± .16	2.66 ± .22	22/26	194 ± 14	11.4 ± 1.0	-5.9 ± 2.9	15/18
	6	91.2 ± 1.9	8.63 ± .16	2.50 ± .23	31/26	198 ± 22	12.4 ± 1.5	-2.5 ± 4.0	19/18

TABLE XV

SLOPE PARAMETER $b[GeV^{-2}]$ OF THE SQUARE ISOSPIN AMPLITUDES

AT 12 AND 24 GeV/c IN $pp \rightarrow (N\pi)p$

$(N\pi)$ Mass interval [GeV]	$I = \frac{1}{2}$ $(N\pi)$-state 12 GeV/c	$I = \frac{1}{2}$ $(N\pi)$-state 24 GeV/c	$I = \frac{3}{2}$ $(N\pi)$-state 12 GeV/c	$I = \frac{3}{2}$ $(N\pi)$-state 24 GeV/c
1.08-1.32	11.7 ± 0.6	9.6 ± 0.6	10.1 ± 0.6	9.1 ± 1.2
1.32-1.44	8.4 ± 0.5	8.8 ± 0.6	8.7 ± 1.1	9.7 ± 1.5
1.44-1.56	6.1 ± 0.5	6.4 ± 0.6	8.2 ± 1.6	
1.56-1.80	4.4 ± 0.4	3.8 ± 0.4	8.3 ± 1.2	11.2 ± 1.3
1.80-2.28	4.4 ± 0.4	3.7 ± 0.7	10.1 ± 1.2	

TABLE XVI

CROSS SECTION $(d\sigma/dt')_{t'=0}$ AND SLOPE PARAMETER b, FOR THE REACTIONS

$\pi^{\pm}p \rightarrow (\pi^{\pm}\pi^{+}\pi^{-})p$ and $\pi^{\pm}p \rightarrow \pi^{\pm}(p\pi^{\pm}\pi^{-})$ at 16 GeV/c,

AS A FUNCTION OF (3π) AND $(p\pi\pi)$ MASS

Mass, GeV	$\pi^-p \rightarrow \pi_f^-(\pi_s^-\pi^+p)$: $(\frac{d\sigma}{dt'})_0 \cdot \frac{mb}{GeV^2}$	$\pi^-p \rightarrow \pi_f^-(\pi_s^-\pi^+p)$: b, GeV^{-2}	$\pi^+p \rightarrow \pi_f^+(\pi^+\pi^-p)$: $(\frac{d\sigma}{dt'})_0 \cdot \frac{mb}{GeV^2}$	$\pi^+p \rightarrow \pi_f^+(\pi^+\pi^-p)$: b, GeV^{-2}
All	1.4 ± 0.2	5.9 ± 0.4	1.6 ± 0.2	6.5 ± 0.5
1.2 -1.52	0.63 ± 0.08	11.7 ± 1.2	0.65 ± 0.08	11.8 ± 1.2
1.52-1.64	0.26 ± 0.03	7.5 ± 0.6	0.35 ± 0.05	8.3 ± 0.9
1.64-1.80	0.30 ± 0.03	4.7 ± 0.3	0.29 ± 0.04	4.6 ± 0.7
1.80-2.08	0.17 ± 0.03	2.5 ± 0.9	0.26 ± 0.04	5.3 ± 0.8
2.08-3.20	0.18 ± 0.03	4.0 ± 0.8	0.17 ± 0.03	3.7 ± 0.7

TABLE XVII

SLOPE b OF DIFFERENTIAL CROSS-SECTION $d\sigma/dt$, INTEGRATED CROSS-SECTION σ AND EXPONENT n OF THE ENERGY DEPENDENCE FOR THE REACTION $\pi^- p \to \pi^-\pi^-\pi^+ p$ versus 3π MASS. THE SYSTEMATIC ERRORS ARE GIVEN IN PARENTHESES

$m_{3\pi}$ [GeV]	25 GeV/c b [GeV/c^{-2}]	25 GeV/c σ [μb]	40 GeV/c b [GeV/c^{-2}]	40 GeV/c σ [μb]	11-40 GeV/c n [$\sigma \propto p_{inc}^n$]
0.8-1.0	14.3 ± 0.8	36.6 ± 3.3 (3.7)	14.9 ± 0.6	37.3 ± 2.2 (3.7)	-0.31 ± 0.11
1.0-1.1	11.7 ± 0.5	51.6 ± 3.6 (5.2)	12.6 ± 0.5	50.9 ± 2.3 (5.2)	-0.29 ± 0.10
1.1-1.2	10.0 ± 0.4	68.4 ± 3.4 (7.0)	10.7 ± 0.4	64.5 ± 2.2 (6.5)	
1.2-1.3	8.3 ± 0.4	71.7 ± 3.1 (7.6)	8.5 ± 0.4	63.5 ± 2.1 (6.4)	-0.29 ± 0.10
1.3-1.4	7.3 ± 0.4	56.5 ± 2.6 (7.0)	6.1 ± 0.4	53.9 ± 2.1 (5.5)	
1.4-1.5	7.2 ± 0.6	35.6 ± 2.3 (5.0)	7.2 ± 0.5	30.6 ± 1.5 (3.1)	-0.42 ± 0.11
1.5-1.6	6.2 ± 0.6	35.3 ± 2.1 (5.2)	7.2 ± 0.5	33.2 ± 1.5 (3.4)	
1.6-1.8	6.6 ± 0.5	80.9 ± 3.8 (11.0)	7.2 ± 0.3	72.5 ± 2.1 (7.4)	-0.50 ± 0.11
1.8-2.0	5.1 ± 0.6	48.5 ± 3.2 (7.0)	5.6 ± 0.6	44.0 ± 2.1 (4.6)	
	25 GeV/c		40 GeV/c		205 GeV/c
[0.8-1.2]	(157 ± 6) μb		(153 ± 5) μb		(160 ± 40) μb

TABLE XVIII

CROSS SECTION $(d\sigma/dt')_{t'=0}$ AND SLOPE PARAMETER b, FOR THE REACTIONS $\pi^\pm p \to (\pi^\pm\pi^+\pi^-)p$ AND $\pi^\pm p \to \pi^\pm(p\pi^+\pi^-)$ AT 16 GeV/c, AS A FUNCTION OF (3π) AND $(p\pi\pi)$ MASS

Mass, GeV	$\pi^- p \to (\pi_f^-\pi_s^-\pi^+)p$ $(\frac{d\sigma}{dt'})_0 \cdot \frac{mb}{GeV^2}$	$\pi^- p \to (\pi_f^-\pi_s^-\pi^+)p$ b, GeV^{-2}	$\pi^+ p \to (\pi_f^+\pi_s^-\pi^+)p$ $(\frac{d\sigma}{dt'})_0 \cdot \frac{mb}{GeV^2}$	$\pi^+ p \to (\pi_f^+\pi_s^-\pi^+)p$ b, GeV^{-2}
All	4.9 ± 0.4	9.1 ± 0.3	3.7 ± 0.3	7.2 ± 0.3
0.6 -1.0	1.0 ± 0.1	14.6 ± 1.8	0.58 ± 0.05	11.3 ± 0.5
1.0 -1.12	1.2 ± 0.1	11.5 ± 0.8	0.8 ± 0.1	9.6 ± 0.7
1.12-1.28	1.2 ± 0.1	9.8 ± 0.7	1.0 ± 0.1	7.6 ± 0.6
1.28-1.40	0.57 ± 0.06	7.1 ± 0.5	0.40 ± 0.06	5.0 ± 0.6
1.40-3.00	1.3 ± 0.2	7.2 ± 0.7	1.0 ± 0.1	5.7 ± 0.3

TABLE XIX

SLOPE PARAMETER FOR $\pi \to (3\pi)$ AT 16 AND 40 GeV/c

Mass (3π) (GeV)	16 GeV/c (ABBCCH Collab[12])	40 GeV/c (Antipov et al.[24])
(1.0 -1.2)	(10.6 ± 0.9) GeV^{-2}	(11.2 ± 0.9) GeV^{-2}
(1.25-1.45)	(7.1 ± 0.5) GeV^{-2}	(6.7 ± 0.9) GeV^{-2}
	$(0.02 < t < 0.4\ GeV^2)$	$(0.04 < t < 0.33\ GeV^2)$

TABLE XX

THE DIFFERENCE IN SLOPE FOR $K^-p \to Q^-p$, $K^+p \to Q^+p$

Mom. (GeV/c)	Elastic Scattering Slope Diff. (GeV^{-2})	Q, Slope Diff. (GeV^{-2})
8	2.70 $\pm$ .16	1 $\pm$ 1
10	2.05 $\pm$ .13	1.8 $\pm$ 1.2
(12-14)	1.60 $\pm$ .10	1.7 $\pm$ 0.4
13		1.1 $\pm$ 0.4
		A, Slope Diff.
15	1.5 $\pm$ 0.8	2.0 $\pm$ .9
		1.1 $\pm$ .8

TABLE XXI

ENERGY DEPENDENCE OF DIFFRACTION PROCESSES,

$\sigma \propto p^{-n}$; (5-20 GeV/c)

Process	Exponent, n
$K^0 \to Q^0$	0.59 $\pm$ .16
$K^+ \to Q^+$	0.60 $\pm$ .05
$K^- \to Q^-$	0.30 $\pm$ .10
$\pi^- \to A_1^-$	0.41 $\pm$ .11
$\pi^- \to A_3^-$	0.57 $\pm$ .2
$N \to N\pi$	0.5 $\pm$ .1
$N \to N\pi\pi$	0.4 $\pm$ .06
For Comparison, the Elastic Scattering Energy Dependence is:	
K^+p	~ 0.1
K^-p	~ 0.4
πN	~ 0.2
NN	~ 0.2

TABLE XXII

SLOPE OF DIFFERENTIAL CROSS-SECTIONS

Process	Slope (GeV^{-2})
$\gamma \to \rho$	~ 6-8
$\pi \to A_1$	~ 9-11
$\pi \to A_3$	~ 9
$K \to Q$	~ 5-7
$\bar{K} \to \bar{Q}$	~ 8-10
$N \to (N\pi\pi)_{1400}$	~ 10-11
$N \to (N\pi\pi)_{1700}$	~ 5

For comparison, the elastic slopes are ~

Process	Slope (GeV^{-2})
γN	~ 6
πN	~ 7-9
KN	~ 5-6
$\bar{K}N$	~ 7-8
NN	~ 9-10

TABLE XXIII

s-CHANNEL HELICITY-FLIP AMPLITUDE RATIOS IN THIS EXPERIMENT

AND IN πN SCATTERING FOR $.18 < |t| < .80\ GeV^2$

	Experimental Values of Density Matrix Elements			
Amplitude Ratios*	2.8 GeV	4.7 GeV	9.3 GeV	Average
Photoproduction				
$\|T_{01}\|^2/\|T_{11}\|^2 \simeq \rho^0_{00}$	$-.01 \pm .03$	$.07 \pm .02$	$-.01 \pm .02$	$.018 \pm .012$
$\|T_{-11}\|^2/\|T_{11}\|^2 \simeq \rho^1_{1-1} + \mathrm{Im}\ \rho^2_{1-1}$	$.04 \pm .05$	$.11 \pm .05$	$-.02 \pm .05$	$.04 \pm .03$
$\mathrm{Im}\ T_{01}/\|T_{11}\| \simeq 2\ \mathrm{Re}\ \rho^0_{10}$	$.16 \pm .03$	$.12 \pm .03$	$.14 \pm .02$	$.14 \pm .016$
$\mathrm{Im}\ T_{-11}/\|T_{11}\| \simeq \rho^0_{1-1}$	$-.06 \pm .03$	$-.05 \pm .03$	$-.10 \pm .02$	$-.08 \pm .02$
πN Scattering				
$\|F^0_{+-}\|/\|F^0_{++}\|$ Isospin 0 Exchange		6 GeV/c		$.15 \pm .02$

*The nucleon helicities in the photoproduction amplitudes listed are $\frac{1}{2}\ \frac{1}{2}$ (or $-\frac{1}{2}\ -\frac{1}{2}$).

TABLE XXIV

Reaction		p_{lab}(GeV/c)	Group	Analyzer	SCHC	TCHC
$\gamma \to \rho^0$		2.8,4.7,9.3	Ballam et al.	Azimuthal and polar angle of π.	Yes (They report a possible 2% flip contribution.)	No
		(2.7-4.0)	Gladding et al.	Same	Yes ($t < .5$ GeV)	No
		(4-6)	Struczinski et al.	Same	Yes	No
		(9-16)	Bulos et al.	Same	Yes	No
$\gamma \to \omega$		2.8,4.7,7.3	Ballam et al.	Same	Yes	No
$\gamma \to \phi$		2.8,4.7,7.3	Ballam et al.	Same	Consistent	No
	$\pm$	8.16	ABBCH	LPS selection, and polar angle of π	No	No
	$\pm$	16	ABBCCHLVW	Azimuthal study, normal to 3π and polar angle of π	No	No
$\pi \to A_1$	-	5-40	Kruse et al.		No	Slight violation
	-	40	Antipov et al.		No	Slight Violation
	-	4.5	Beketov et al.	Normal to 3π plane	No	Yes
$\pi^- \to A_3^-$		(5-2.5)	Ascoli et al.	π^+ polar angle	No	Yes (but not very strong)
	-	10	ABBCCHLVW	Azimuthal study, and normal to plane and π polar angles	No	No
$K \to Q$	-	14.3	Barloutaud et al.	Normal to $K\pi\pi$ plane, and polar angles of π	No	No
	0	(4-12)	Brandenburg et al.	Normal to $K\pi\pi$ plane	No	Yes (but not very strong)

TABLE XXIV Cont.

Reaction		p_{lab}(GeV/c)	Group	Analyzer	SCHC	TCHC
	1400	10,16	ABBCCHLVW	Azimuthal study, and normal, and polar	Data Insensitive	
	1700	10,16	ABBCCHLVW	Same	No	Yes
$p \to p\pi\pi$	All	8,16	ABBCH	LPS and polar angles of π	No	Yes
	All	25	Chapman et al.	Azimuthal	No	No
	1700	11.6	Oh et al.		No	Yes
	1500		Lamsa et al.	Azimuthal	No	Yes
	1700		Lamsa et al.	Azimuthal	No	Yes
$p \to n\pi$	All	11.0	Evans et al.	Azimuthal	No	No
$\pi \to 3\pi$	All $\pm$	11.0	Evans et al.	Azimuthal	No	No

TABLE XXV

FACTORIZATION TEST IN πN AND pp REACTIONS

$$R_1 = \frac{\sigma(\pi^- p \to \pi^- p)}{\sigma(pp \to pp)} = 0.43$$

$$R_2 = \frac{\sigma(\pi p \to \pi(p\pi^0))}{\sigma(pp \to p(p\pi^0))} = 0.46 \pm .15$$

$$R_3 = \frac{\sigma(\pi p \to \sigma(p\pi^+\pi^-))}{\sigma(pp \to \delta(p\pi^+\pi^-))} = 0.35 \pm .18$$

$$R_4 = \frac{\sigma(\pi p \to \pi(p\pi\pi\pi))}{\sigma(pp \to \delta(p\pi\pi\pi))} = 0.45 \pm .15$$

TABLE XXVI

A FACTORIZATION TEST FOR γp, πp, and pp REACTIONS

	Momentum (GeV/c)		
	(6-10)	(10-14)	(14-18)
$R_1 = \frac{\sigma(\gamma p \to \rho^0 p)}{\sigma(\gamma p \to \rho^0 p\pi^+\pi^-)}$	0.053 ± 0.014	0.035 ± 0.014	0.055 ± 0.024
$R_2 = \frac{\sigma(pp \to pp)}{\sigma(pp \to pp\ \pi^+\pi^-)}$	0.064 ± 0.07	$0.061 \pm .008$	0.060 ± 0.009
$R_3^+ = \frac{\sigma(\pi^+ p \to \pi^+ p)}{\sigma(\pi^= p \to \pi^+ p\pi^+\pi^-)}$		$0.061 \pm .006$	0.063 ± 0.003
$R_3^- = \frac{\sigma(\pi^- p \to \pi^- p)}{\sigma(\pi^- p \to \pi^- p\pi^+\pi^-)}$		0.052 ± 0.005	0.059 ± 0.003

TABLE XXVII

VALUES OF THE PARAMETERS R(H)

$R(H) = \frac{\sigma[Hp \to H(N\pi)]}{\sigma[Hp \to Hp]}$	p_{lab} [GeV/c]
$R(\pi^+) = 0.11 \pm 0.02$	8
$R(\pi^\pm) = 0.11 \pm 0.02$	16
$R(K^-) = 0.10 \pm 0.02$	10
$R(p) = 0.11 \pm 0.02$	12
$R(p) = 0.14 \pm 0.02$	24

TABLE XXVIII

ENERGY AND M^2-DEPENDENCE OF THE VARIOUS TRIPLE COUPLINGS

Triple Regge Term	s-dependence (fixed x)	M^2-dependence, (fixed s, t)	(x-dependence)
PPP	constant	$1/M^2$,	$1/(1-x)$
PPR	$1/\sqrt{s}$	$1/M^3$,	$1/(1-x)^{3/2}$
RRP	constant	constant,	(constant)
RRR	$1/\sqrt{s}$	$1/M$,	$(1/(1-x)^{1/2})$
		$M^2 = (1-x)s$	

References and Footnotes

1. U. Amaldi, Rapporteur's talk at IInd Aix-en-Provence Conference on High Energy Physics, p. 241, 1973.
2. U. Amaldi, "Elastic and Inelastic Processes at the ISR" CERN Report NP-73-19 (unpublished).
3. A. Diddens, "Very High Energy Hadron Experiments" CERN Report 1973 (unpublished).
4. L. Foa, Rapporteur's talk at IInd Aix-en-Provence Conference on High Energy Physics, p. 317, 1973.
5. G. Fox, "Inclusive Structure of Diffraction Scattering," California Institute of Technology Report, CATL-68-413, 1973.
6. F. Halzen, "Model Independent Features of Diffraction," Lectures, 1973.
7. J.D. Jackson, "Lectures on Hadronic Interactions at High Energies," LBL-2079, 1973.
8. G. Kane, "Phenomenology of Diffractive Reactions," Rutherford Laboratory report, PR-20, 1972.
9. G. Kane, "Implications of Experimental Data for Our View of the Pomeron," Michigan report UM-73-10, 1973.
10. G. Kane and J. Hartley, "Towards a General Description of Two-Body Hadron Reactions," Nuclear Physics, B57, 157 (1973).
11. D.W.G.S. Leith, SLAC preprint, SLAC-PUB-1141, invited talk at XVIth International Meeting on High Energy Physics, Batavia, Sept. 1972.
12. D.W.G.S. Leith, SLAC preprint, SLAC-PUB-1263, invited talk at the 8th Rencontre de Moriond, France, March 1973.
13. D.W.G.S. Leith, SLAC preprint, SLAC-PUB-1330, invited talk at Meeting of APS Division of Particles and Fields, Berkeley, August, 1973.
14. D.W.G.S. Leith, SLAC preprint, Supplement to SLAC-PUB-1330.
15. H. Lubatti, Washington University Preprint, VTL-PUB-9.
16. H. Miettinen and E.H. Groot, Talk presented at the VIIIth Rencontre de Moriond, Méribel Les Allues, 1973.
17. H. Miettinen, Invited talk at the IXth Rencontre de Moriond, Méribel Les Allues, 1974, and CERN Preprint, CERN-TH-1864.
18. D.R.O. Morrison, Lectures given at the Vth Hawaii Topical Conference in Particle Physics, 1973, and CERN Preprint, CERN-D.P.II-73-46.
19. K. Moffeit, "Diffractive Processes," SLAC-PUB 1314 (1973), invited talk at the International Symposium on Electron and Photon Physics, Bonn, 1973.
20. J.C. Sens, "Topics in Particle Physics at ISR," Lectures, 1973.
21. N.N. Khuri, Physical Review Letters 30, 1094, 1973.
22. L. Van Hove, Nuovo Cimento 28, 798, 1963 and Review Modern Physics 36, 655, 1964.
23. M.L. Good and W.D. Walker, Physical Review 120, 1854 (1960).
24. In a process $a + b \to a + b$ the square of the total centre of mass energy, s, is given by $s = M_a^2 + M_b^2 + 2M_b E_a^{lab}$, where M is the mass of the particle and E the laboratory energy. For collision on a proton target at energies about 5 GeV, this reduces to $s \sim 2p_{lab}$ where p_{lab} is the laboratory momentum of the incident particle.
25. V. Barger and R.J.N. Phillips, Nuclear Physics B32, 93 (1971).
26. G. Giacomelli, Rapporteur's talk at XVIth International Conference on High Energy Physics, Chicago, 1972.
27. S. Gjesdal et al. See referenece 26.
28. J. Badier et al. See reference 26.
29. A.S. Belousov et al. See reference 26.
    D.O. Caldwell et al. See reference 26.
    T.A. Armstrong et al. See reference 26.
    J. Ballam et al. See reference 26.
30. U. Amaldi et al. Physics Letters 44B, 112 (1973).
31. S.R. Amendolia et al. Physics Letters 44B, 119 (1973).
32. G.B. Yodh, T. Pal and J.S. Trefil, Physical Review Letters 28, 1005 (1972).

33. T. Kycia, Paper presented at the 1974 SLAC Summer Institute Topical Conference--see these proceedings.

34. U. Amaldi et al. See reference 30.

35. G. Barbiellini et al. Physics Letters B39, 663 (1972) and Physics Letters B35, 355 (1971).

36. J. Chapman et al. Physical Review Letters 29, 1686 (1972).
G. Charlton et al. Physical Review Letters 29, 515 (1972).
T. Dao et al. Physical Review Letters 29, 1627 (1972).

37. D. Bogert et al. NAL Preprint 73/57 (1973).

38. D. Ritson, Talk presented at the SLAC Summer Institute, 1974--see these proceedings.

39. A. Martin, Physical Review 129, 1432 (1963) and Nuovo Cimento 42, 930 (1966).

40. H. Cornille and A. Martin, Physics Letters 40B, 671 (1972).

41. R.A. Carrigan, Physical Review Letters 24, 168 (1970).

42. U. Amaldi et al. Paper presented to the APS Division of Particle and Fields Meeting, Berkeley, August 1973.

43. G. Barbiellini et al. Physics Letters B39, 663 (1972); Physics Letters B35, 355 (1972).

44. V. Bartenev et al. NAL PUB 73/54.

45. A. Böhm et al. Physics Letters B49, 491 (1974).

46. J. Engler et al. CERN Preprint, 1973.

47. G. Beznogikh et al. Nuclear Physics B54, 97 (1973) and JINR preprint.

48. V. Hungerbuehler et al. Paper presented to the Berkeley APS Meeting of the Division of Particles and Fields, August 1973.

49. A.R. Dzierba et al. Physical Review D7, 725 (1973).

50. Yu. M. Antipov et al. Paper presented to the IInd Aix-en-Provence Conference on High Energy Physics, Sept. 1973.

51. R. Campbell et al. Nuclear Physics B64, 1 (1973).

52. See G. Kane's work in references 8, 9, 10.

53. M. Davier, Physics Letters B40, 369 (1972).

54. W.D. Walker et al. Physical Review 7, 2554 (1973).

55. P. Caso et al. Paper submitted to the XIV International Conference on High Energy Physics, Vienna (1968).
N.N. Biswas et al. Physical Review Letters 18, 273 (1967).

56. L. Barbaro-Galtieri, Private communication.

57. I. Ambats et al. Argonne preprint ANL/HEP-7329.

58. G. Brandenburg et al. Private communication.

59. V. Bartenev et al. NAL preprint NAL-73/73.

60. U. Amaldi et al. Physics Letters 43B, 231 (1973).

61. N.N. Khuri and T. Kinoshita, Physical Review 137B,, 720 (1965).

62. W. Bartel and A.N. Diddens, CERN Internal Report NP 73-4 (1973).

63. V.D. Apokin et al. IHEP preprint.

64. H. Cheng, J.K. Walker and T.T. Wu, Physics Letters B44, 283 (1973).

65. V. Barger, K. Geer, R.J.N. Phillips, Nuclear Physics B47, 29 (1972).

66. J.W. Allcock, N. Cottingham and C. Michael, CERN preprint TH-1765 (1973).

67. L. Durand and R. Lipes, Physical Review Letters 20, 637 (1968).

68. T.T. Chou and C.N. Yang, Physical Review Letters 20, 1213 (1968).

69. S. Frautschi and B. Margolis, Nuovo Cimento 56A, 1153 (1968).

70. J. Ballam et al. Physical Review Letters 24, 960, 1970.

71. J. Ballam et al. SLAC preprint SLAC-PUB-1092.

72. F. Bulos et al. Paper presented to XVIth International Meeting on High Energy Physics, Chicago (1972), and R. Giese, Ph.D. Thesis, Stanford University (1973).

73. G. Chadwick et al. SLAC preprint SLAC-PUB-1093.

74. For a discussion of these experiments see reference 12.

75. R. Anderson et al. SLAC preprint SLAC-PUB-1086.

76. H.J. Besch et al. Paper presented to the International Symposium on Electron and Photon Interactions at High Energies, Bonn, August 1973.

77. P. Bosetti et al. Nuclear Physics B62, 1 (1973).

78. K. Böckmann et al. Bonn University preprint, PIB-3-27 and paper presented to the IInd Aix-en-Provence Conference on Elementary Particle Physics, September 1973.

79. J.W. Cooper et al. Michigan preprint, UMBC 74-1.

80. D. Lissauer et al. Physical Review D6, 1852 (1972).

81. M. Longo et al. Physics Letters 36B, 560 (1971).
J.C. Vander Velde et al. Nuclear Physics B45, 1 (1972).

82. B. Gobbi, Invited talk at the 1974 SLAC Summer Institute Topical Conference --these proceedings.

83. V. Bartenev et al. "Diffraction Excitation of Nucleon Resonances in pp Collisions at Incident Proton Energies from (174-400) GeV/c," paper submitted to the APS Division of Particles and Fields Meeting, Berkeley, August 1973, and NAL preprint.

84. G.S. Abrams et al. Berkeley preprint LBL-2112.

85. M. Derrick et al. Argonne preprint, ANL/HEP-7332.

86. M. Miettinen et al. Physics Letters B43, 61 (1973).

87. H. Harari et al. Physics Letters B43, 49 (1973).

88. V. Hungerbuehler et al. Yale University preprint, and paper presented to the IInd Aix-en-Provence Conference on Elementary Particles, September 1973.

89. Yu. M. Antipov et al., Series of papers summarized by W. Kienzle in a paper presented to Joint CERN-IHEP Scientific Council, IHEP, Protrino, May 1973.

90. H.H. Bingham et al. Washington University preprint, VTL-PUB-16.

91. G. Brandenburg et al. SLAC PUB 1038 and Nuclear Physics B.

92. H.H. Bingham et al. Paper presented to the XVIth International Meeting on High Energy Physics, Batavia, September 1972.

93. CERN-Brussels-Krakow Collaboration. Paper presented to the XVIth International Meeting on High Energy Physics, Batavia, September 1972.

94. ABBCH Collaboration, Paper presented to the XVIth International Conference on High Energy Physics, Chicago, September 1972.
J. Ballan et al. SLAC preprint, SLAC-PUB-900.

95. P. Baillon et al. Paper presented to the XVIth International Conference on High Energy Physics, Chicago, September 1972.

96. G. Ascoli et al. Physics Review B7, 669 (1973).
U. Kruse et al.. Paper submitted to the XVIth International Conference on High Energy Physics, Chicago, September 1972.
Yu. M. Antipov et al. Nuclear Physics B63, 153 (1973).

97. G. Thompson et al. Physics Review Letters 32, 331 (1974).

98. M. Tabak et al. Berkeley preprint LBL-3010.

99. R. Barloutand et al. Saclay preprint, D.PhPE 73-01.

100. H.J. Lubatti and K. Moriyasu, Washington preprint, VTL-PUB-18.

101. D.W.G.S. Leith, Invited talk at the IVth International Conference on Experimental Meson Spectroscopy, Boston, April 1974 and SLAC-PUB-1440.

102. C. Peck et al. Caltech-SLAC Collaboration, private communication.

103. D.J. Herndon et al. LBL-1065 (Rev)/SLAC PUB 1108 (Rev), and A.H. Rosenfeld et al. LBL 2633/SLAC-PUB-1386, and R.J. Cashmore et al. LBL 2634/SLAC-PUB-1387.

104. See lectures by M. Davier in these proceedings.

105. D.R.O. Morrison, Rapporteur's talk, Kiev Conference and CERN/D.Ph.II/Phy 71-10 and 70-6.

106. D.R.O. Morrison, Physical Review 165, 1699 (1968).

107. Y. Oh et al. Paper submitted to XVI International Conference on High Energy Physics, Batavia, 1972.

108. See R. Barloutaud, Rapporteur's talk at Oxford Meeting on High Energy Physics, 1971.

109. Y. Goldschmidt—Cleremont, Review talk at the XVIth International Conference on High Energy Physics, Batavia, 1972.

110. J. Ballam et al. Paper presented to the Cornell International Conference on Electrons and Photons.

111. R. Arnold et al. Paper presented to the XVIth International Conference on High Energy Physics, Batavia, September 1972.

112. J. Ballam et al. Physical Review Letters 24, 960, 1970.

113. F. Gilman et al. Physics Letters 31B, 387, 1970.

114. A. de Lesquer et al. Physics Letters 40B, 277 (1972).
G. Cozzika et al. Physics Letters 40B, 281 (1972).
J. Deregel et al. Paper submitted to XVIth International Conference on High Energy Physics, Batavia, 1972.

115. O. Danielson et al. University of Stockholm preprint, 1971.

116. S. Ljung et al. Paper submitted to XVIth International Conference on High Energy Physics, Batavia, 1972.

117. W. Kittle, S. Ratti and L. Van Hove, Nuclear Physics B30, 333, 1971.

118. F. Liu et al. SLAC preprint, SLAC-PUB-1047.

119. H. Lubatti, Mini-review talk presented at IInd Aix-en-Provence Conference on Elementary Particle Physics, September 1973.

120. F. Winkelman, Physics Letters 48B, 273 (1974).

121. M.G. Albrow et al. CERN preprint, and paper submitted to the XVIth International Conference on High Energy Physics, Batavia, September 1972.

122. There are four HBC pp experiments at NAL: (a) 102 GeV/c--Michigan-Rochester collaboration; (b) 205 GeV/c--ANL-NAL collaboration; (c) 303 GeV/c--NAL-UCLA collaboration; (d) 405 GeV/c--Michigan-Rochester collaboration.

123. From a compilation by J. Whitmore (private communication).

124. J. Vander Velde (private communication).

125. S.J. Barish et al. ANL/HEP 7338 and paper presented to the APS Division of Particles and Fields Meeting, Berkeley, August, 1972.

126. M.G. Albrow, et al. CERN preprint, December 1972.

127. Aachen-CERN-Harvard-Genoa-Torino report, communicated by G. Goldhaber.

128. R. Schamberger et al. Paper submitted to the APS Division of Particles and Fields Meeting, Berkeley, August 1973.

129. S. Childress, et al. Paper submitted to the APS Division of Particles and Fields Meeting, Berkeley, August 1973.

130. K. Abe et al. "Measurement of $pp \to pX$ between 50 and 400 GeV/c," paper submitted to the APS Division of Particles and Fields Meeting, Berkeley, August 1973.

131. This data was originally presented in preliminary form at the Vanderbilt Conference on Inclusive Processes at High Energy, 1973. Corrections for instrumented failure have changed the cross-sections in the forward direction.

132. J. Vander Velde (private communication).

133. G.S. Abrams et al. LBL-2112 and paper submitted to the APS Division of Particles and Fields Meeting, Berkeley, August 1973.

134. F.C. Winkelmann et al. LBL-2113 and paper submitted to the APS Division of Particles and Fields Meeting, Berkeley, August 1973.

135. J. Bellettini et al. Paper presented to the IInd Aix-en-Provence Meeting on Elementary Particle Physics, September 1973.

136. R. Stroynowski, CERN/D.PhII/PHY-73-13.

137. Derevshchikov et al. See reference 4.

138. R. Cool et al. Paper presented at the XVIIth International Conference on High Energy Physics, London, July, 1974.

139. Abarbanel et al. Phys. Rev. Letters 26, 937 (1971); Ellis et al. Phys. Rev. D6, 1347 (1972).

140. CERN-Holland-Lancaster-Manchester Group, M.G. Albrow et al. CERN preprint; A. Capella et al. SLAC report no. SLAC-PUB-1252. References to earlier work may be found in this paper.

141. K. Abe et al. "Determination of Triple-Regge Coupling from a Study of Reaction $pp \to pX$ between 50 and 400 GeV/c," paper submitted to the IInd Aix-en-Provence International Conference on Elementary Particles, September 1973.

142. H.I. Miettinen and R.G. Roberts, Rutherford Lab Preprint RPP/T/40 (1973).

143. M. Bishari, Phys. Letters 38B, 510 (1972).

144. A. Capella et al. Orsay Preprint 72/73.

145. J. Vander Velde. Invited talk presented at the Vth International Conference on High Energy Collisions, Stony Brook, 1973.

146. N. Sakai and J.N.J. White, Nuclear Physics B59, 511 (1972) and Max-Plank Institute Preprint, June 1973.

147. Scandinavian Collaboration--unpublished data. Reviewed by H. Miettinen in references 16, 17.

Figure Captions

Fig. 18. Energy dependence of the slope of the elastic p-p differential cross-section for two regions of momentum transfer--(a) $|t| < 0.1$ GeV^2, (b) $0.15 \leq |t| \leq 0.5$ GeV^2.

Fig. 19. Compilation of the s-dependence of the slope of the pp scattering cross-section for small momentum transfers (i.e. $|t| < 0.12$ GeV^2).

Fig. 20. The differential cross-section, $d\sigma/dt$, in pp elastic scattering out to very large t, as measured by the ACGHT group at the ISR.

Fig. 21. The differential cross-section for pp elastic scattering from (3-1500) GeV/c. The dashed curve represents the fourth power of the electromagnetic form factor, $G(t) = 1/(1 - t/\mu^2)^2$, with $\mu^2 = 0.71$ GeV^2.

Fig. 22. Normalized differential cross-sections for pp elastic scattering, $(d\sigma/dt)/(d\sigma/dt)_0$, divided by $G^4(t)$ where $G(t)$ is the electromagnetic form factor.

Fig. 23. Differential cross-section for np elastic scattering from (13-21) GeV/c.

Fig. 24. Comparison of pp and np elastic scattering cross-sections at 19 GeV/c.

Fig. 25. Energy dependence of the slope for pp and np elastic scattering from (2-30) GeV/c.

Fig. 26. Slope of the forward neutron-proton elastic scattering cross-section, as a function of energy. The dashed line represents the behaviour of pp scattering in the same t-range.

Fig. 27. Production angular distribution for elastic π^-p and Σ^-p scattering at 23 GeV/c.

Fig. 28. The differential cross-section for π^-p elastic scattering at 14 GeV/c. (Also shown for comparison, are the results of previous measurements at 15 and 16 GeV/c.)

Fig. 29. Differential cross-section for elastic π^-p, K^-p and $\bar{p}p$ scattering at 25 and 40 GeV/c.

Fig. 30. Shrinkage of the differential cross-section for π^-p elastic scattering.

Fig. 31. Two components of the forward elastic cross-section--an exponential part usually associated with the Pomeron contribution, and a "J_0" Bessel function piece which may be associated with the peripheral Regge contribution or with an additional peripheral part of the Pomeron. This second contribution causes an upward curvature in the cross-section at small t.

Fig. 32. The differential cross-section for K^+p and K^-p elastic scattering at 5 GeV/c.

Fig. 33. The energy dependence of the slope of the cross-section (evaluated at $t = .2$ GeV^2) for elastic $\pi^\pm$, $K^\pm$ and $p^\pm$ scattering in hydrogen.

Fig. 34. The energy dependence of the slope parameter of the Pomeron contribution in K^+p scattering (shown as the shaded region) and $\pi^\pm p$ scattering (shown as the circles).

Fig. 35. π-π scattering angle distributions in the dipion rest system (θ) and invariant four-momentum transfer squared in π-π scattering for the reactions $\pi^-+p \to \pi^-\pi^+ + n$ and $\pi^-p \to \pi^- + \pi^- + \Delta^{++}$. Note that the scales for the sections of $M(\pi\pi)$ are nonlinear.

Fig. 36. Elastic and total cross-section determinations for $\pi^- - \pi^+$ and $\pi^- - \pi^-$ scattering as a function of the dipion invariant mass.

Fig. 37. Differential cross-section for scattering of $\pi^\pm$, $K^\pm$, $p^\pm$ on protons at 3 GeV/c.

Fig. 38. Differential cross-section for scattering of $\pi^\pm$, $K^\pm$, $p^\pm$ on protons at 3.65 GeV/c.

Fig. 39. Differential cross-section for scattering of $\pi^\pm$, $K^\pm$, $p^\pm$ on protons at 5 GeV/c.

Fig. 40. Differential cross-section for scattering of $\pi^\pm$, $K^\pm$, $p^\pm$ on protons at 6 GeV/c.

Fig. 41. Preliminary production angular distribution for 13 GeV/c K^+p and K^-p elastic scattering.

Fig. 42. a. Production angular distribution for $p^{\pm}p$ elastic scattering at 10.4 GeV/c.

b. Production angular distribution for $K^{\pm}p$ elastic scattering at 10.4 GeV/c.

Fig. 43. Differential cross-section for pp elastic scattering at 50 and 400 GeV, in the very forward direction, showing the Coulomb scattering contribution.

Fig. 44. Differential cross-section for pp elastic scattering at two energies of the CERN ISR in the very forward direction, showing the Coulomb scattering contribution.

Fig. 45. Calculated energy dependence of the ratio of the real to imaginary parts of the forward scattering amplitude in pp elastic scattering, assuming the total cross-section stops rising at 100, 1000, 10,000 and 100,000 GeV, respectively.

Fig. 46. The measured energy dependence of the ratio of the real to imaginary parts of the forward pp scattering amplitude.

Fig. 47. The measured energy dependence of the ratio of the real to imaginary parts of the forward np scattering amplitude.

Fig. 48. The measured energy dependence of the ratio of the real to imaginary parts of the forward $\pi^- p$ scattering amplitude.

Fig. 49. Two-component amplitudes from the model of Cheng-Walker-Wu,[64] Kane,[8,9,10] Barger-Geer-Phillips,[65] Allcock-Cottingham-Michael.[66] The two contributions are associated with a central process and a peripheral process respectively.

Fig. 50. Two-component amplitudes from the models of Durand-Lipes,[67] Chou-Yang,[68] Frautschi-Margolis.[69] The two components are associated with a pole term and a cut term respectively. The observed structure in the angular distribution comes from the interference of these two contributions.

Fig. 51. Fit to the ISR pp elastic scattering cross-section using the optical model approach of Durand and Lipes.[67]

Fig. 52. Schematic for the vector dominance model description of rho meson photoproduction.

Fig. 53. The decay correlations for $\gamma p \to \rho^0 p$ at 9.3 GeV, in the SLAC-Berkeley experiment using polarized photons.

Fig. 54. The energy dependence of the cross-section for $\gamma p \to \rho^0 p$.

Fig. 55. The cross section for $\gamma p \to \omega p$ as a function of energy, also showing the natural parity (σ^N) and unnatural parity (σ^U) contributions at 2.8, 4.7 and 9.3 GeV.

Fig. 56. The cross-section for the reaction $\gamma p \to \phi p$ as a function of energy.

Fig. 57. The differential cross-section for $\gamma p \to \rho^0 p$ at 9.3 GeV.

Fig. 58. The differential cross-section for $\gamma p \to \rho^0 p$ at energies from 9 to 16 GeV.

Fig. 59. The energy dependence of the slope of the differential cross-section for $\gamma p \to \rho^0 p$.

Fig. 60. Comparison of the data on the forward cross-section for $\gamma p \to \rho^0 p$ at 9 GeV.

Fig. 61. (a) Fits of $d\sigma/dt$ of ρ^0 photoproduction to sum of P and f exchange, utilizing Dual Absorption Model. (b) P and f exchange amplitude slopes as obtained from fits of $d\sigma/dt$. The errors in $\gamma p \to \rho^0 p$ are statistical only. The systematic uncertainties are estimated to be $\pm$ 10%.

Fig. 62. The differential cross section for the reaction $\gamma p \to \omega p$ at 2.8, 4.7 and 9.3 GeV(ϕ) and the natural parity contribution to the differential cross-section (-+-).

Fig. 63. Reaction $\gamma p \to p\phi$ at 2.8, 4.7 and 9.3 GeV. Differential cross section: (a) 2.8 and 4.7 GeV data combined: (b) 9.3 GeV: (c) shows the experimental values for $d\sigma/dt$ for ϕ photoproduction at 12 GeV as a function of $-t$ from 0.2 to 1.0 $(\mathrm{GeV}/c)^2$.

Fig. 64. The differential cross-section for $\gamma p \to \phi p$ for energies between (2-12) GeV.

Fig. 65. The slope of the differential cross-section for $\gamma p \to \phi p$ as a function of energy.

Fig. 66. The energy dependence of the cross-section for $\gamma p \to \phi p$ at $t = 0.6$ GeV^2.

Fig. 67. The elastic pp differential cross-section for momenta between 3 and 16 GeV/c.

Fig. 68. Schematic representation of the amplitudes in the two-component Pomeron model.

Fig. 69. The energy dependence of the cross-section for $\pi N \to \pi\pi N$.

Fig. 70. The energy dependence of $\pi N \to \pi(\pi N)$ where the $I = 3/2$ and $1/2$ πN contributions are displayed separately.

Fig. 71. The separate mass spectra for the $I = 1/2$ and $3/2$ contributions to the reactions $\pi^+ p \to \pi^+(N\pi)^+$ at 8 and 16 GeV/c.

Fig. 72. The mass spectra for the various exchange isospin and (πN) decay isospin amplitudes in the reactions $\pi^\pm p \to (N\pi)\pi$ at 8 and 16 GeV/c.

Fig. 73. The cross-sections for $pp \to N(N\pi)$ as a function of energy. The contributions for $(N\pi)$ with isospin 3/2 and 1/2 are shown separately.

Fig. 74. The mass spectra in the reaction $pp \to N(N\pi)$, for $I = 0, 1$ in the t-channel, and $(N\pi)$ with isospin 1/2, are shown for incident proton momentum of 12 and 24 GeV/c.

Fig. 75. The mass spectra in the reaction $pp \to N(N\pi)$ for $I = 1$ in the t-channel and $(N\pi)$ with isospin 3/2, are shown for incident proton momentum of 12 and 24 GeV/c.

Fig. 76. (a) Invariant mass of the $p_p\pi^-$ system in the reaction $np \to p_n\pi^- p_p$ at 12.5 GeV/c. The shaded histogram is for events with $M(p_p\pi^-) < M(p_n\pi^-)$.

(b) Invariant mass of the $p_n\pi^-$ system. The shaded histogram is for events with $M(p_n\pi^-) < M(p_p\pi^-)$.

Fig. 77. Mass of the $p\pi^-$ system for $K^+n \to K^+\pi^- p$ at 12 GeV/c.

Fig. 78. The differential cross-section, $d\sigma/dt$, for three ranges of $M(p\pi^-)$, (a) $1.1 < M(p\pi^-) < 1.3$ GeV, (b) $1.3 < M(p\pi^-) < 1.5$ GeV, (c) $1.5 < M(p\pi^-) < 1.7$ GeV. The curves correspond to exponential fits with slopes equal to 14, 8 and 3.5 GeV^{-2}, respectively.

Fig. 79. Slope-mass correlation for $np \to (p_n\pi^-)p_p$. The slope b is determined by fitting the differential cross-section, $d\sigma/dt'$, to $Ae^{bt'}$ in each mass bin, for t intervals ranging from $0.02 < t' < 0.3$ GeV^2 near threshold to $0.05 < t' < 0.6$ GeV^2 in the higher mass bins.

Fig. 80. Mass distributions (events per 10 MeV) for the $p\pi^-$ system observed with carbon, copper, and lead targets. The efficiency of the apparatus vs. mass, shown by the dashed curve in (a), has not been unfolded.

Fig. 81. Distributions in $\cos\theta_J$ and ϕ_J for the proton (p_n) in $np \to p_p(p_n\pi^-)$. The distributions are of the Gottfried-Jackson frame. (a) $-t' < 0.1$ GeV^2 and $M(p_n\pi)) < 1.4$ GeV; (b) $-t' > 0.1$ GeV^2 and $M(p_n\pi^-) < 1.4$ GeV; (c) $-t' < 0.1$ GeV^2 and $1.4 < M(p_n\pi^-) < 1.8$ GeV; (d) $-t' < 0.1$ GeV^2 and $1.4 < M(p_n\pi^-) < 1.8$ GeV.

Fig. 82. The mass distribution for $(\pi^\pm\pi^\pm\pi^-)$ and $(p\pi^+\pi^-)$ from the reactions $\pi^\pm p \to \pi^\pm\pi^+\pi^- p$ at 16 GeV/c. Below the ratio of the mass distributions for the π^+p and π^-p reactions are also shown.

Fig. 83. Mass distribution for $(N\pi\pi)$ for π and K induced reactions. The $(N\pi\pi)$ shows familiar resonance structure at low masses.

Fig. 84. Missing mass distribution in $pp \to pN^*$ for an incident proton energy of 260 GeV/c.

Fig. 85. The effective mass distribution for $(p\pi^+\pi^-)$ from 200 GeV/c $\pi^- p \to p\pi^+\pi^-\pi^-$.

Fig. 86. (a) The effective mass distribution for $(p\pi^+\pi^-)$ from 200 GeV/c $pp \to pp\pi^+\pi^-$. (b) and (c) show the mass spectra for the $p\pi^+$ and $p\pi^-$ subsystems.

Fig. 87. The cross-sections for the inelastic two prong events and for the separated isoscalar t-channel, $I = (N\pi)/2$ amplitude, as a function of beam momentum.

Fig. 88. The mass spectrum for $M(\Lambda\pi^-)$ from the reaction $\Sigma^- p \to \Lambda\pi^- p$ at 24.6 GeV/c. The curve is a Monte Carlo calculation of the Deck diagram in the figure.

Fig. 89. The cross-section for $\pi^- p \to \pi^-\pi^-\pi^+ p$ as a function of energy.

Fig. 90. The (3π) and (2π) effective mass distributions from the CERN IHEP experiment on $\pi^- p \to \pi^-\pi^+\pi^- p$ at 40 GeV/c.

Fig. 91. The effective mass distribution of $(\pi^+\pi^-\pi^-)$ from 200 GeV/c $\pi^- p \to \pi^+\pi^-\pi^- p$.

Fig. 92. The energy dependence of the cross-section for $\pi^- p \to A_1 p$ where A_1 is defined as $1000 < M(3\pi) < 1200$ MeV. $\hookrightarrow \rho\pi$

Fig. 93. The energy dependence of the cross-section for $\pi^- p \to A_2 p$ where A_2 is defined as $1200 < M(3\pi) < 1400$ MeV. $\hookrightarrow \rho\pi$

Fig. 94. The energy dependence of the cross-section for $\pi^- p \to A_3 p$ where A_3 is defined as $1500 < M(3\pi) < 1800$ MeV. $\hookrightarrow f\pi$

Fig. 95. The cross sections for the process $K^0_L p \to K^0_S \pi^+\pi^- p$, and the subprocess $K^0_L p \to Q^0 p$ as a function of energy.

Fig. 96. The cross section for $K^+ p \to Q^+ p$ as a function of energy for six regions of $(K\pi\pi)$ mass from (1200-1500) MeV.

Fig. 97. The mass distribution for the $K^*\pi$ system from the reaction $K^+ p \to K^*(890)\pi N$ at 5 GeV/c and 8.2 GeV/c for I = 1/2 and I = 3/2 amplitudes separately.

Fig. 98. The ratio of the cross sections $K^0 p \to Q^0 p$ and $\bar{K}^0 p \to \bar{Q}^0 p$ as a function of momentum.

Fig. 99. The energy dependence of the 3π amplitudes in the A_1 region.

Fig. 100. The differential cross section for $\pi^- p \to A^- p$ at 40 GeV/c. The A_1 region is here defined as the 1^+ spin parity amplitude for $1.215 \leq M(3\pi) \leq 1.415$ GeV.

Fig. 101. The energy dependence of the 3π amplitudes in the A_2 region.

Fig. 102. The differential cross-section for $\pi^- p \to A_2 p$ $(A_2 \to \rho\pi)$ at 25 and 40 GeV/c.

Fig. 103. The energy dependence of the 3π amplitudes in the A_3 region.

Fig. 104. The differential cross-section for $\pi^- p \to A_3 p$ $(A_3 \to f\pi)$ at 40 GeV/c.

Fig. 105. The energy dependence of the $K\pi\pi$ amplitudes in the Q and L regions.

Fig. 106. Scatter plot of $M(K\pi)$ against $M(K\pi\pi)$ for $K^- p \to K^- p\pi^+\pi^-$, $\bar{K}^0 p\pi^-\pi^0$ and $\bar{K}^0 n\pi^+\pi^-$ at 14 GeV/c.

Fig. 107. The production angular distribution for low mass $(K\pi\pi)$ in $K^- p \to K^- p\pi^+\pi^-$, $\bar{K}^0 p\pi^-\pi^0$ and $\bar{K}^0 n\pi^+\pi^-$ at 14 GeV/c.

Fig. 108. Exponential slope parameter, b, averaged over the interval $4 < P_{beam} < 12$ GeV/c and plotted versus the mass of the $K^*(890)^+\pi^-$ (squares) and the mass of the $K^*(890)^-\pi^+$ (circles).

Fig. 109. The mass dependence of the slope of the differential cross-section in $K^- p \to Q^- p$ at 14 GeV/c.

Fig. 110. The differential cross-section for $K^+ p$ and $K^- p$ elastic scattering at 13 GeV/c.

Fig. 111. The four-momentum transfer distribution, $d\sigma/dt'$, for the reaction $\pi^\pm p \to (\pi^\pm\pi^\pm\pi^-)p$ in the pion-dissociation sector.

Fig. 112. Differential cross sections for $K^0 p \to Q^0 p$ (squares) and $\bar{K}^0 p \to \bar{Q}^0 p$ (circles) over the momentum range 4 to 12 GeV/c. The scale of the ordinate is determined for neutral Q mesons decaying into $K^0_S \pi^+\pi^-$. The curves result from the following exponential fits:

$$\frac{d\sigma}{dt'}(Q^0 p) = 0.83 \exp(5.9t') \text{ mb/GeV}^2,$$

$$\frac{d\sigma}{dt'}(\bar{Q}^0 p) = 1.36 \exp(9.7t') \text{ mb/GeV}^2.$$

Fig. 113. The differential cross-section for $K^\pm p \to Q^\pm p$ at energies around 14.GeV/c.

Fig. 114. Reaction $\gamma p \to p\pi^+\pi^-$ at 9.3 GeV. Results of fits of the form

$$d\sigma^2/dtdM_{\pi\pi} = \left(d\sigma^2/dtdM_{\pi\pi}\right)_{t=0} \cdot e^{At}$$

in the interval $0.02 \leq t \leq 0.5$ GeV^2. The curve is from the Söding model.

Fig. 115. Mass spectra showing the elastic peak and the threshold enhancement for inelastic diffraction, for π, K, N and γ reactions.

Fig. 116. Plot of the slope of the differential cross-section, b, versus $1/(M^2 - m_i^2)$, where M is the mass of the 3π, $K\pi\pi$ or $N\pi$ diffractively produced systems, and M_i is the sum of the constituent masses.

Fig. 117. Schematic diagram for the peripheral production of $p\pi^+\pi^-$ system.

Fig. 118. Diagrams for the s-channel and t-channel production of $(N\pi\pi)$ systems.

Fig. 119. Mass spectrum for $(N\pi)$ in $\pi N \to \pi\pi N$ at 16 GeV/c.

Fig. 120. Mass spectrum for $(N\pi\pi)$ in $\bar{K}N \to \bar{K}(N\pi\pi)$ at 10 GeV/c.

Fig. 121. Mass spectrum for $(N\pi\pi)$ in $\bar{K}(N\pi\pi)$ collisions; 10 GeV/c K^- and (6-12) GeV/c K_L^0.

Fig. 122. Density matrix elements for ρ^0 photoproduction by polarized photons at 9.3 GeV.

Fig. 123. The momentum transfer dependence of the matrix element, ρ_{10}, for $\gamma p \to \rho^0 p$ at 2.8, 4.7 and 9.3 GeV. This matrix element indicates the presence of a spin flip amplitude.

Fig. 124. The momentum transfer dependence of the flip and non-flip isoscalar πN scattering amplitudes at 6 GeV/c.

Fig. 125. Schematic diagrams for elastic π^-, K^- and $\bar{p}$ scattering and diffractive production of $N^*(1690)$.

Fig. 126. The ratio of the elastic cross-section to the $N^*(1690)$ production cross-section for incident π^-, K^- and $\bar{p}$ at 8, 16 GeV/c, as a function of momentum transfer.

Fig. 127. A schematic of diffractive reactions studied in a test of factorization. The ratios R_1-R_4 refer to the ratio of the cross-section for the reactions when the top two vertices (pion and proton elastic scattering) are joined successively to the bottom four vertices representing proton diffraction into a proton plus zero, one, two or three pions respectively, e.g.

$$R_1 = \frac{\sigma(\pi p \to \pi p)}{\sigma(pp \to pp)} \quad , \quad R_2 = \frac{\sigma(\pi p \to \pi p\pi)}{\sigma(pp \to pp\pi)} \text{ , etc.}$$

Fig. 128. A schematic of diffractive reactions studied in a test of factorization. The ratios R_1, R_2, R_3 refers to the ratio of the cross-sections when each of the upper vertices ($\gamma \to \rho$, $p \to p$, $\pi \to \pi$) is connected with the two lower vertices representing proton diffraction into a proton or a $(p\pi\pi)$ system, respectively.

Fig. 129. Schematic diagrams for the diffractive production of $(p\pi^+\pi^-)$ systems in $\pi p \to (p\pi\pi)\pi$ and $pp \to (p\pi\pi)p$ reactions.

Fig. 130. The invariant cross-section for the process $K^-p \to pX^-$ at 25 and 40 GeV/c as a function of x.

Fig. 131. (a) The invariant cross-section $d^2\sigma/dt\,dx$, as a function of x, for the process $pp \to pX$. The cross-section exhibits a large hump for $0.2 < x < .8$ which is characteristic of the multiparticle production region, then a minimum for $0.8 < x < .9$, followed by a sharp peak for $0.9 < x < 1.0$ which is characteristic of diffractive quasi-elastic scattering shown diagrammatically in (b).

Fig. 132. The missing mass distribution in $pp \to pX$ at 100, 200, 300 and 400 GeV/c, as measured in the NAL HBC experiments.

Fig. 133. The invariant cross-section for $pp \to pX$ as a function of x for the 100 and 400 GeV/c NAL HBC experiments.

Fig. 134. The missing mass distribution in $pp \to pX$ at 200 GeV/c as measured in the NAL HBC experiment.

Fig. 135. The missing mass distribution in $pp \to pX$ at 200 GeV/c for each topology as measured in the 200 GeV/c NAL HBC experiment.

Fig. 136. The missing mass distribution in $pp \to pX$ at the ISR, as measured by the ACGHT group.

Fig. 137. The missing mass distribution in $pp \to pX$ at 300 GeV/c as measured by the Columbia-Stony Brook collaboration.

Fig. 138. The invariant cross-section for $pp \to pX$ as a function of x, for $100 \leq x \leq 750$ GeV^2, as measured by the Rutgers-Imperial College group. Data is presented in four t intervals.

Fig. 139. The invariant cross-section for $pp \to pX$ as a function of $s^{-1/2}$ for x = 0.83 and 0.91.

Fig. 140. The invariant cross-section for $pp \to pX$ as a function of x, for a fixed $P_T = 0.8$ GeV^2. Data comes from the CHLM group at the ISR, for $\sqrt{s} = 22$, 31 and 45 GeV.

Fig. 141. The differential cross-section, $d\sigma/dt$, for $pp \to pX$, as a function of the missing mass. Data comes from the 200 GeV/c NAL HBC experiment.

Fig. 142. The t-dependence for the production of the diffraction peak in $pp \to pX$ at high energies.

Fig. 143. Missing mass spectra for $pp \to pX$ as measured by the CHLM group at the ISR at $s = 930$ GeV^2 and for $t = 0.35$, 0.55, 1.05 and 1.75 GeV^2.

Fig. 144. Missing mass distribution at fixed t for $\sqrt{s} = 53$ GeV, as measured by the CHLM group at the ISR. Data is presented for $t = 1.2$ and 1.4 GeV^2.

Fig. 145. Differential cross-section for $pp \to pX$ for $x = 0.87$ and for $s = 108$ and 752 GeV^2.

Fig. 146. Differential cross-section for $pp \to pX$ for missing mass squared ~ 40 GeV^2.

Fig. 147. Differential cross-section for $pp \to pX$ for $8 \leq M^2 \leq 14$ GeV^2.

Fig. 148. P_T^2 distributions for small missing masses in $pp \to pX$. Preliminary data from the 100, 400 GeV/c NAL HBC experiments.

Fig. 149. (a,b) P_T^2 distribution for large missing masses in $pp \to pX$. Preliminary data from the 100, 400 GeV/c NAL HBC experiments.

Fig. 150. The effective mass distribution of $(\pi^+\pi^-\pi^-)$ from 200 GeV/c $\pi^-p \to \pi^-\pi^-\pi^+p$.

Fig. 151. The effective mass distribution for $(p\pi^+\pi^-)$ from 200 GeV/c $\pi^-p \to p\pi^+\pi^-\pi^-$.

Fig. 152. Schematic diagram for the pion dissociation process.

Fig. 153. The missing mass squared distribution for $\pi^-p \to pX$ at 200 GeV/c.

Fig. 154. The missing mass squared distribution for $\pi^-p \to pX$ at 200 GeV/c.

Fig. 155. The missing mass squared distribution, topology by topology, for $\pi^-p \to pX$ at 200 GeV/c.

Fig. 156. The momentum transfer distribution, topology by topology, for $\pi^-p \to pX$ at 200 GeV/c.

Fig. 157. The momentum transfer distribution for $\pi^-p \to pX$ at 200 GeV/c for $M^2 \leq 10$ GeV^2 and $10 < M^2 < 40$ GeV^2.

Fig. 158. Comparison between x dependences for p inclusive invariant cross sections in pp interactions and π^-p interactions. The relative normalization is arbitrary, o:$s = 551$ GeV^2, $p_\perp \sim .15$ GeV/c (CHLM); ■:$s = 380$ GeV^2, integrated over $p_\perp$ (Berkeley NAL).

Fig. 159. The charged particle multiplicity distribution for $\pi^-p \to$ anything (solid curve), and for pion diffraction (dashed curve).

Fig. 160. Schematic diagram for the diffractive dissociation of an incident particle with a system of charged multiplicity, n, and mass M.

Fig. 161. The mean charged multiplicity for all events, $\pi^-p \to$ anything, is plotted against the square of the available center of mass energy, while the multiplicity of the diffractive system in $\pi^-p \to Xp$, is plotted against the square of the mass of the diffractive system.

Fig. 162. The rapidity spectrum of a "typical" diffractive event.

Fig. 163. The rapidity spectrum of a "typical" non-diffractive event.

Fig. 164. Behaviour of the density of events as a function of $\bar{\eta}$ and $\delta(\bar{\eta})$ (see text) for various charged multiplicities at C.M. energy $\sqrt{s} = 62.8$ GeV. The curves are polynomial interpolation of the points of equal density.

Fig. 165. (a,b) Three dimensional representation of the density of events as a function of $\bar{\eta}$ and $\delta(\bar{\eta})$ for various charged multiplicities at the two extreme ISR energies.

Fig. 166. Derevshchikov et al. data on x dependence of the π^-p interactions of two incident momenta and two p intervals. X:$p_{inc} = 42$ GeV/c, o:$p_{inc} = 51$ GeV/c.

Fig. 167. The x-distribution for the fast forward π^+ in $\pi^+p \to \pi^+ +$ (anything) at 8 GeV/c. The distribution is broken down topology by topology.

Fig. 168. The x-distribution for the fast forward π^+ in $\pi^+ p \to \pi^+$ + (anything) at 16 GeV/c. The distribution is broken down topology by topology.

Fig. 169. The x-distribution for the fast forward π^+ in $\pi^+ p \to \pi^+$ + (anything) at 23 GeV/c. The distribution is broken down topology by topology.

Fig. 170. The x-distribution for the forward π^+ in the reactions $\pi^+ p \to p\pi^+\pi^0$, $n\pi^+\pi^+$ at 8, 16 and 23 GeV/c.

Fig. 171. The x-distribution for the forward π^+ and backward proton in the reaction $\pi^+ p \to \pi^+\pi^-\pi^+ p$ at 8, 16 and 23 GeV/c.

Fig. 172. The invariant cross-section, $d\sigma/dt$, for the proton dissociation in $\pi^+ p \to \pi^+$ + (anything) at 8, 16 and 23 GeV/c. The ISR pp data are also shown, after being extrapolated to small $p_\perp$ and adjusted for the difference in $\pi^+ p$ and pp total cross-sections (see text for details).

Fig. 173. The missing mass distribution in $\pi^- p \to pX^-$ at 25 and 40 GeV/c.

Fig. 174. The invariant cross-section as a function of x for $\pi^- p \to pX^-$ at 25 and and 40 GeV/c.

Fig. 175. The slope of the differential cross-section for $\pi^- p \to pX^-$ at 25 and 40 GeV/c as a function of x.

Fig. 176. The missing mass distribution in $K^- p \to pX^-$ at 25 and 40 GeV/c.

Fig. 177. The slope of the production angular distribution in $K^- p \to pX^-$ at 25 and 40 GeV/c as a function of x.

Fig. 178. The invariant cross-section for the process $K^- p \to pX^-$ at 25 and 40 GeV/c as a function of x.

Fig. 179. The triple Regge calculation of the single particle inclusive cross-section. (a) is the forward scattering amplitude for the single particle inclusive process, and (b) represents diagrammatically the square of that amplitude, (c) is the triple Regge generalization of diagram (b).

Fig. 180. A qualitative map of the M^2 and x dependence of the triple Regge terms for inclusive proton scattering.

Fig. 181. Plot of G_{PPP} and G_{PPR} versus t for the five fits discussed in the text. For all fits $G_{PPR}(t)$ lies within the shaded band. The shape and magnitude of $G_{PPP}(t)$ depends on the fit assumption.

Fig. 182. Inclusive proton spectra at various ISR energies at fixed p_T versus x.

Fig. 183. The effective meson trajectory obtained in a triple Regge analysis of the data on $pp \to pX$ at s = 1995 GeV^2.

Fig. 184. The mass dependence of the forward scattering peak in $pp \to pX$ showing the decomposition into contributions arising from leading protons and from fragmentation protons.

Fig. 185. Inelastic proton spectra at various ISR energies and fixed p_T at high x.

Fig. 186. The effective Pomeron trajectory obtained by fitting the PPP triple Regge term to the $pp \to pX$ data at s = 551 and 930 GeV^2 (after correction for elastic contamination, resolution and the contribution of fragmentation protons). The crosses (x), indicate the Pomeron trajectory obtained from an analysis of elastic pp scattering at the same energies.

Fig. 187. The differential cross-section for $pp \to pX$ for $8 \leq M^2 \leq 14$ GeV^2.

Fig. 188. The PPP cross-section obtained from ISR data at $0.15 < t < 1.25$ GeV^2, extrapolated down to $t \sim 0.056$ GeV^2 and compared to the NAL inelastic pp scattering data. The PPP term was obtained in the mass interval $5 < M^2 < 30$ GeV^2.

Fig. 189. The momentum transfer distribution for $\pi^- p \to pX$ at 200 GeV/c for $M^2 < 10$ GeV^2 and $10 < M^2 < 40$ GeV^2.

Fig. 190. The differential cross-section, $d\sigma/dt$, for $pp \to pX$, as a function of the missing mass. Data comes from the 200 GeV/c NAL HBC experiment.

Fig. 191. The P_T^2 dependence of protons from the NAL HBC experiments. 0, 102, 405 GeV/c for four prong or higher multiplicities and with $0.9 < x < 0.6$; • 102, 205, 303, 405 GeV/c for four prong events with $M^2 < 10$ GeV^2.

Fig. 192. The inelastic overlap function calculated from the 1500 GeV/c proton-proton data.

Fig. 193. The impact structure of proton-proton scattering at $\sqrt{s} = 53$ GeV. Shown are Im $h_{el}(s,b)$ and the inelastic and elastic overlap functions extracted from the experimental data. The "black disc limit" indicates the maximum value of the inelastic overlap function allowed by unitarity (i.e., 100% absorption).

Fig. 194. a) Inelastic overlap functions calculated from the $\sqrt{s} = 21, 31, 44$, and 53 GeV ISR data.
b) Difference of the $\sqrt{s} = 53$ and 31 GeV inelastic overlap functions, $\Delta G_{inel}(s,b)$, showing that the cross-section increase comes from a rather narrow region around 1 fermi.

Fig. 195. The decomposition of the imaginary part of the elastic scattering amplitude into its components assuming t-channel helicity conservation in inelastic diffraction.

Fig. 196. Schematic illustration of the origin of the mass slope correlation in the peripheral model of inelastic diffraction.
a) M^2 small. The non-flip amplitude dominates, faking a steep exponential t-dependence in the small t region.
b) M^2 large. Several helicity amplitudes contribute appreciably. The differential cross-section is much flatter than in the case a).

Fig. 197. Differential cross-section for the process $pp \to pn\pi^+$ at 19 GeV/c for $(n\pi^+)$ masses in the interval (1200-1300) MeV. The curves illustrate the possible peripheral diffraction mechanism: -·-·- is the contribution of the imaginary part of the non-flip amplitude given by $Ae^{at}\,|J_0(R\sqrt{-t})|^2$; ---- is the smooth background (Be^{bt}) which includes real contributions.

Fig. 198. a) The differential cross-section, $d\sigma/dt'$, for $np \to (p\pi^-)p$ at 12.5 GeV/c for $m(p\pi^-)$ less than 1200 MeV.
b) The differential cross-section, $d\sigma/dt'$, for $np \to (p\pi^-)p$ at 12.5 GeV/c for four ranges of $(p\pi^-)$ mass--(a) $M(p\pi^-) < 1300$ Mev, (b) $1300 < M(p\pi^-) < 1450$ MeV, (c) $1450 < M(p\pi^-) < 1600$ MeV, (d) $1600 < M(p\pi^-) < 1800$ MeV.

Fig. 199. Illustrations of how central channels opening up may generate a peripheral $\Delta G_{inel}(s,b)$. (a) The inelastic cross-section stays constant but the elastic differential cross-section shrinks. $G_{inel}(s,b)$ decreases at $b = 0$ and increases at $b > 1$ fermi.
(b) Same as for (a) but some new channels open up causing the inelastic cross-section to rise. The new processes are central, and they compensate the decrease of $G_{inel}(s, b = 0)$ due to shrinkage. As a result the cross-section increase appears peripheral. (c) The difference of the two overlap functions of (b).

Fig. 200. The energy dependence of the total cross-section at high energy--which way will it go?

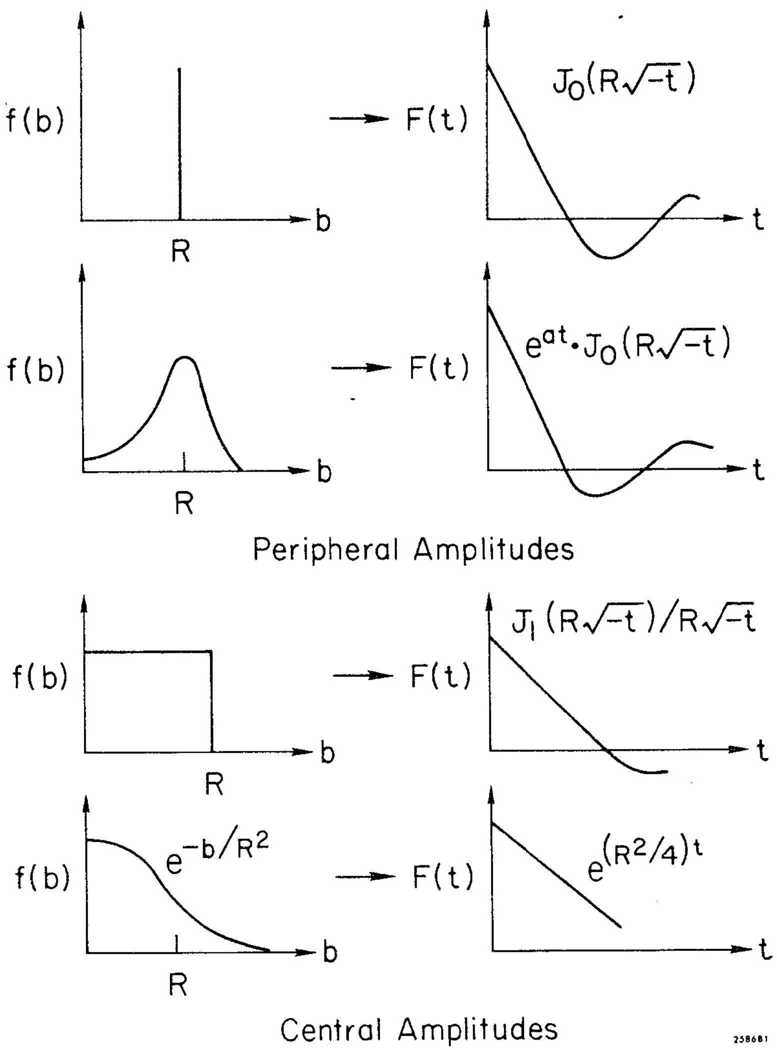

Figure 1

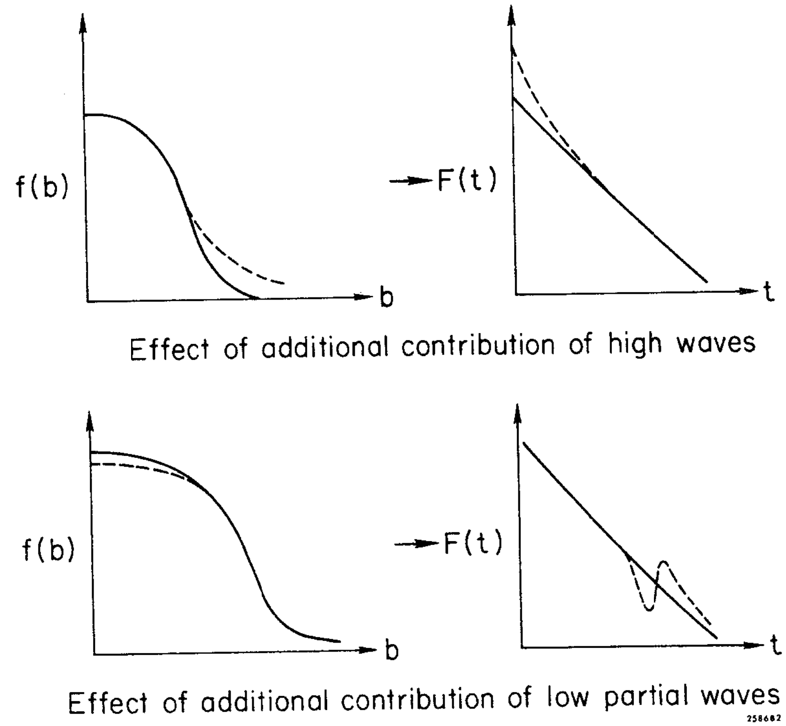

Figure 2

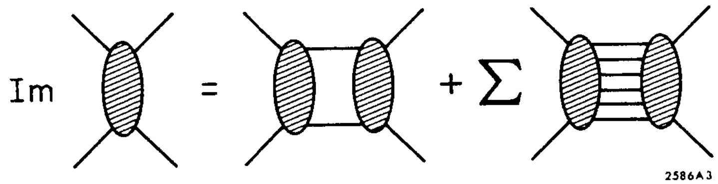

Figure 3

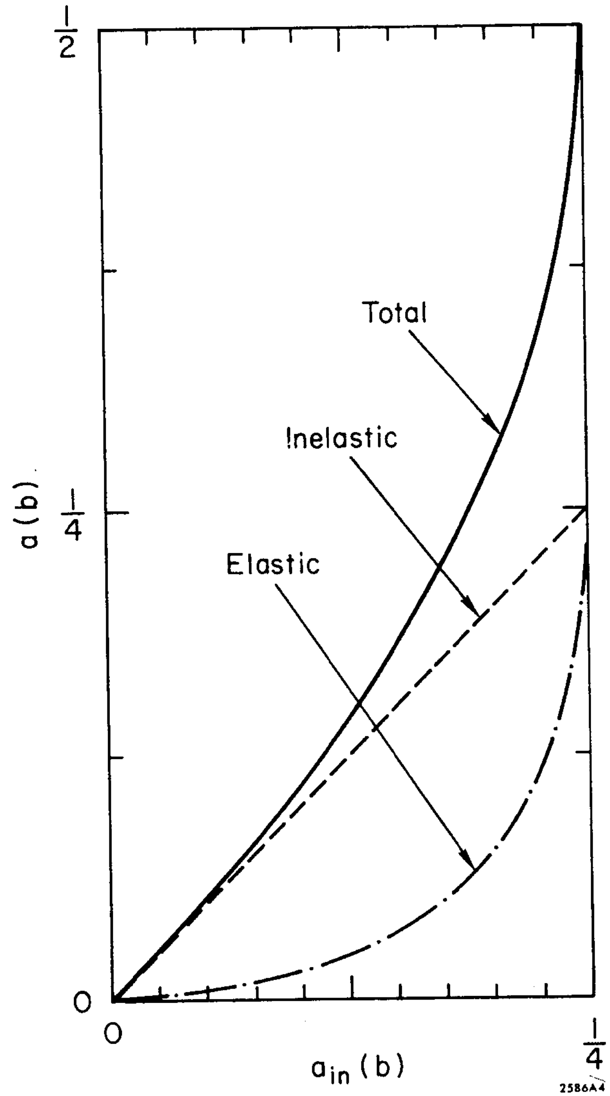

Figure 4

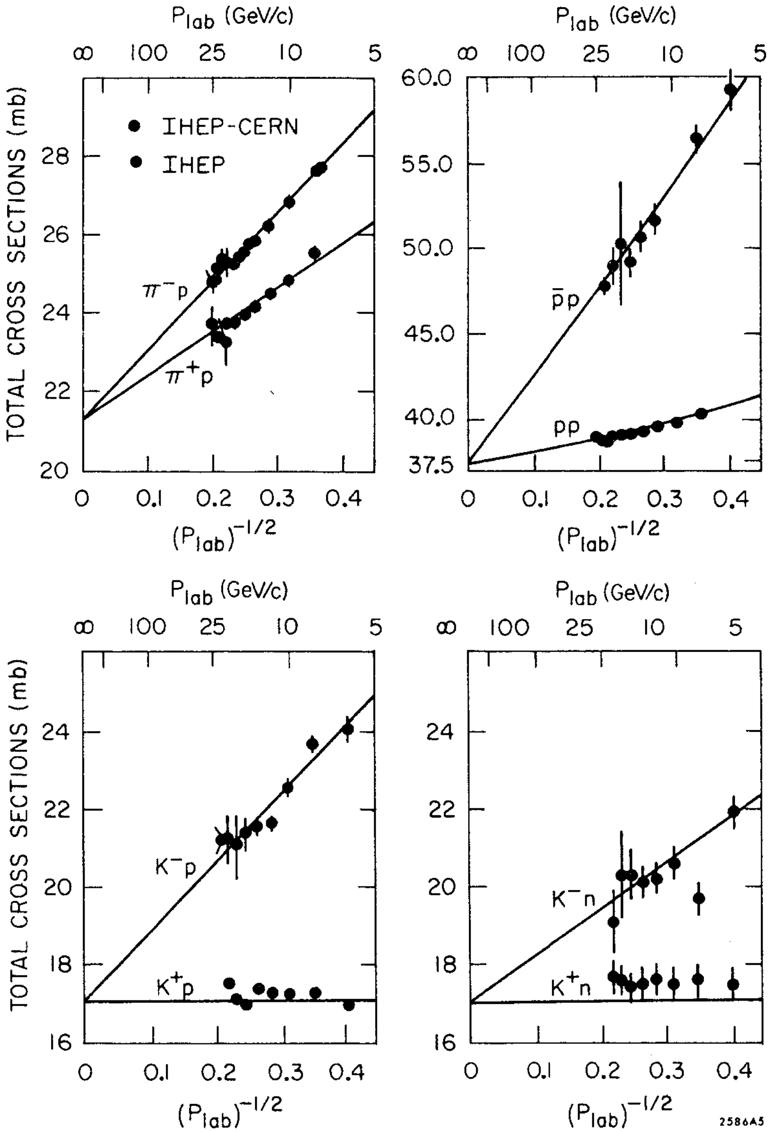

Figure 5

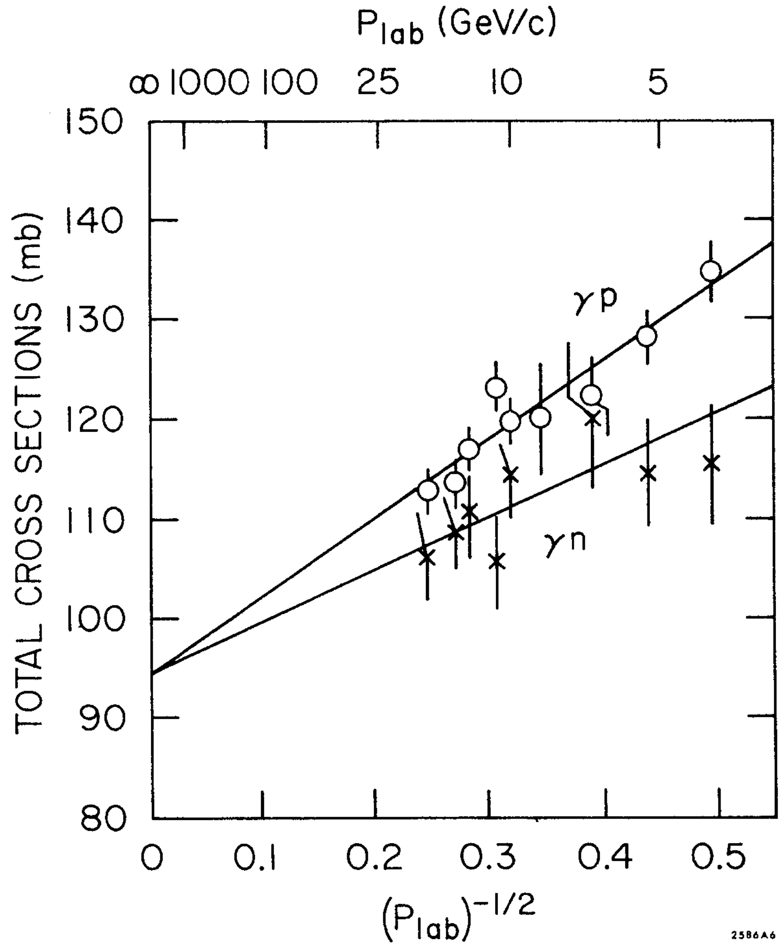

Figure 6

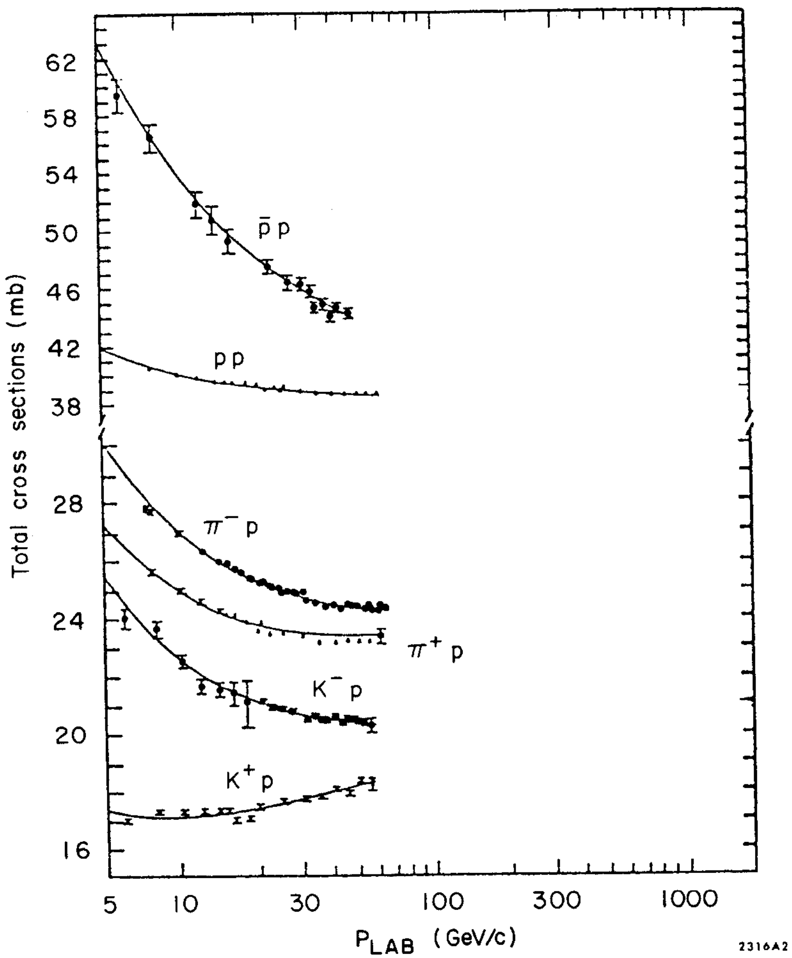

Figure 7

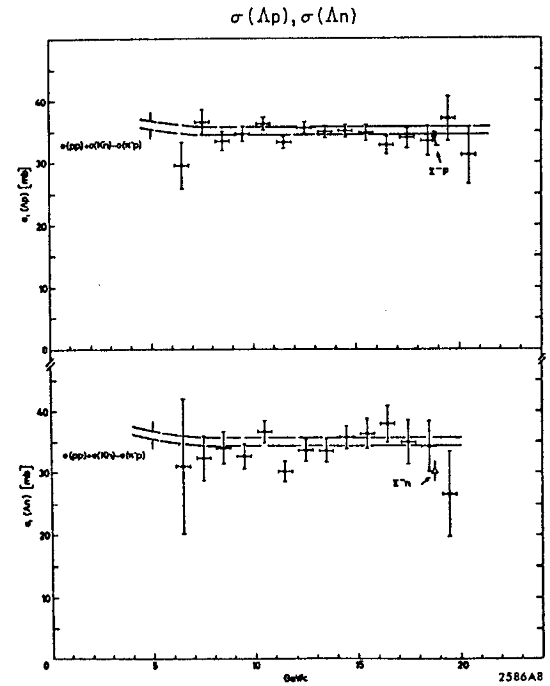

Figure 8

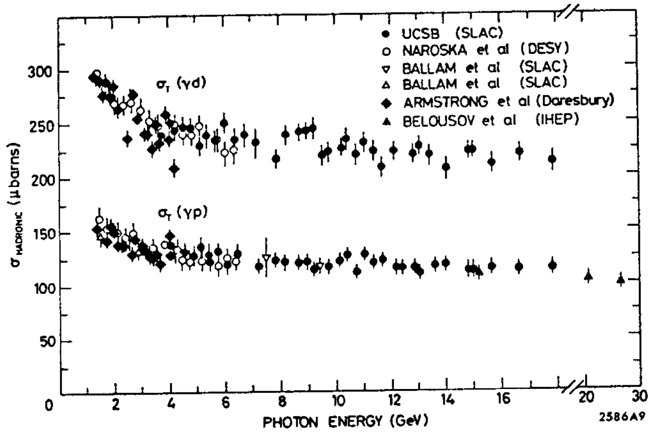

Figure 9

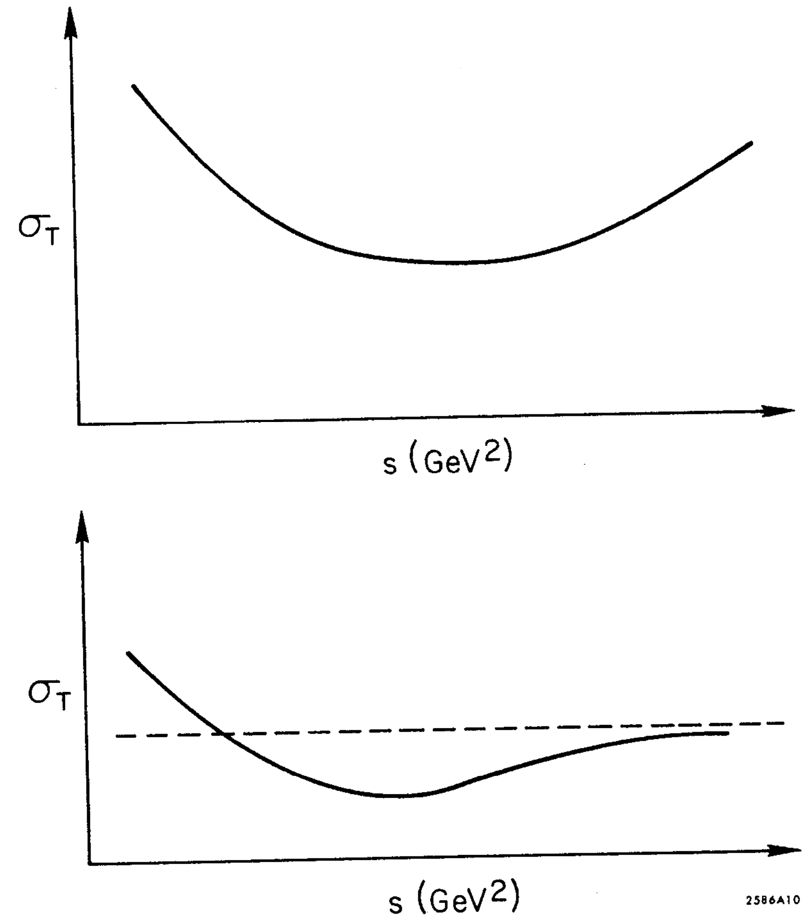

Figure 10

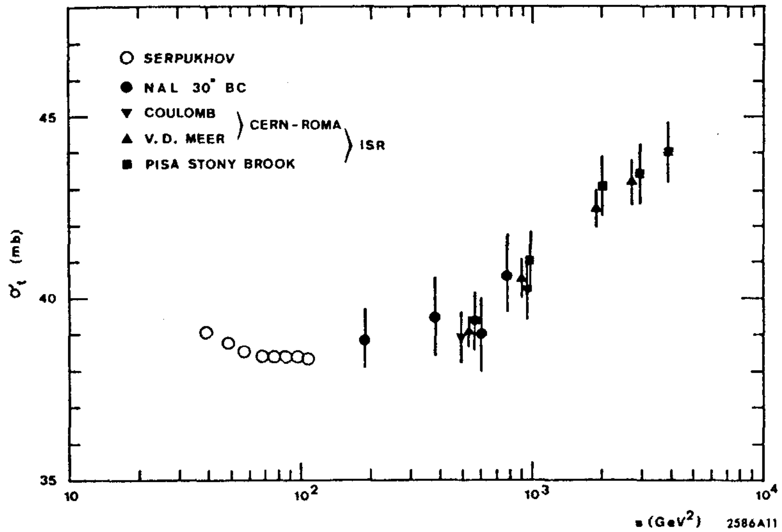

Figure 11

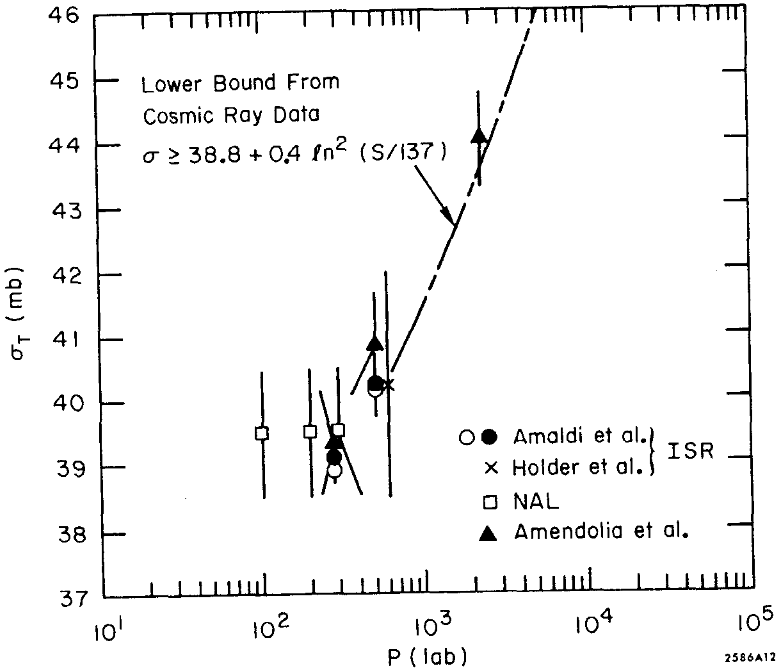

Figure 12

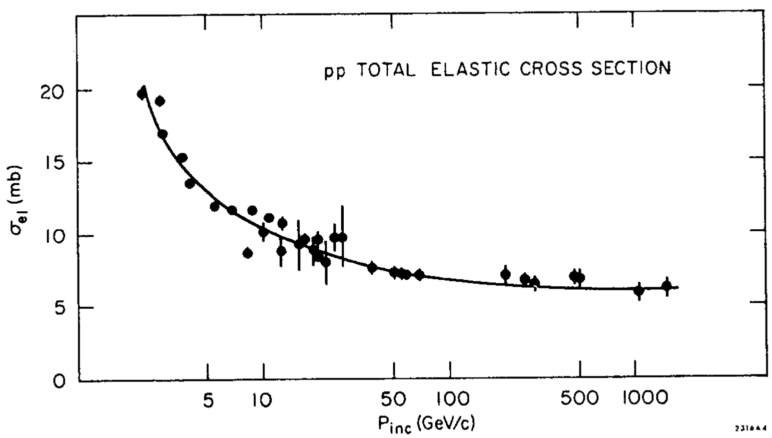

Figure 13

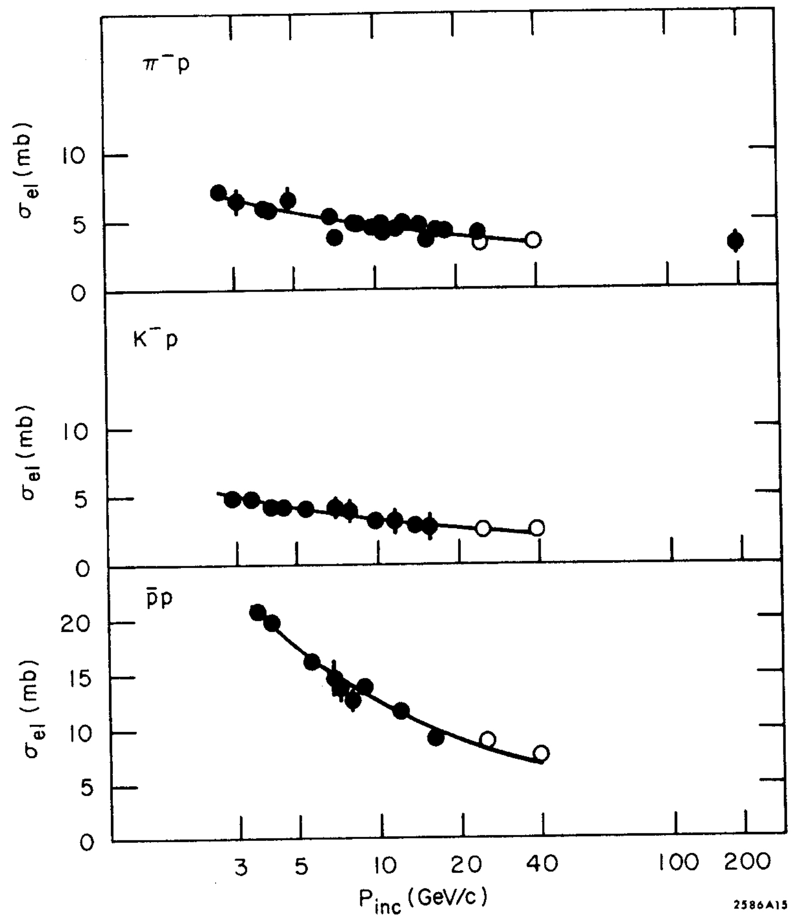

Figure 14

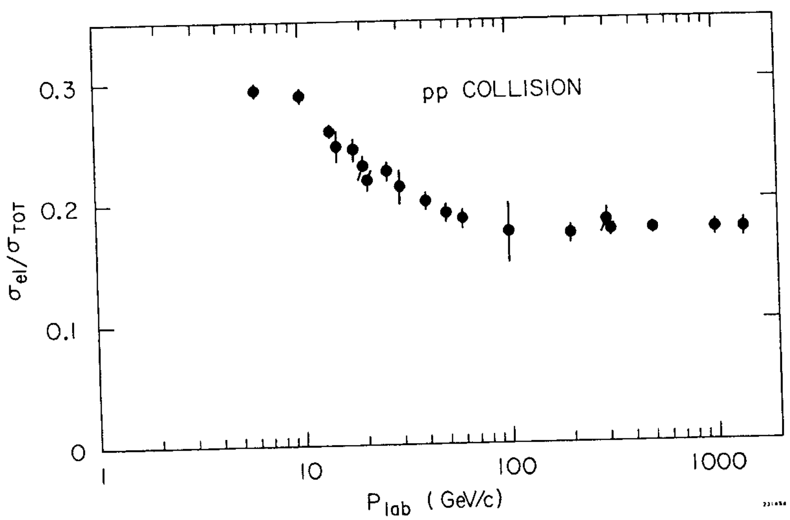

Figure 15

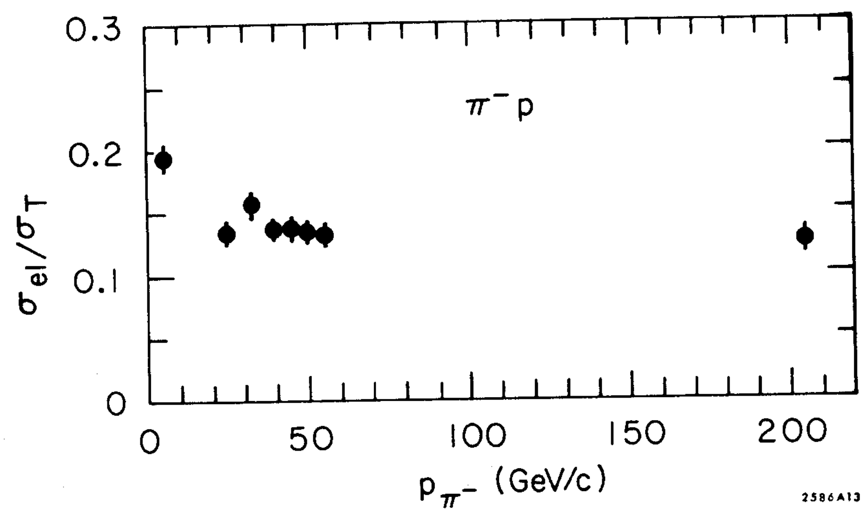

Figure 16

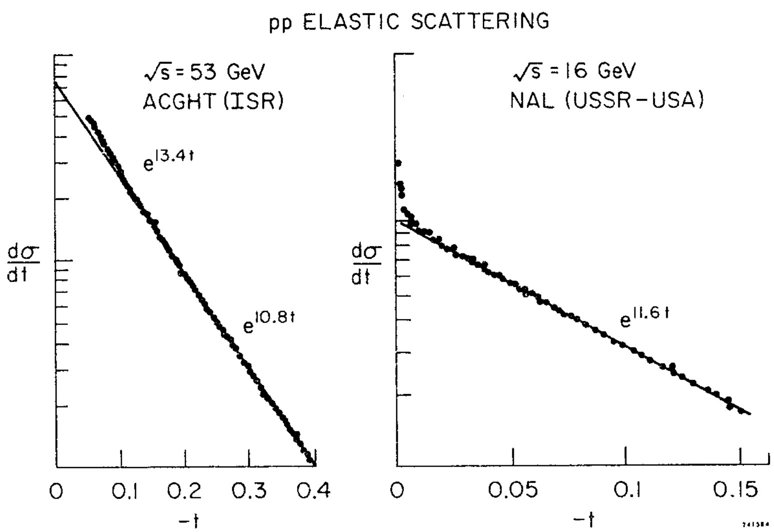

Figure 17

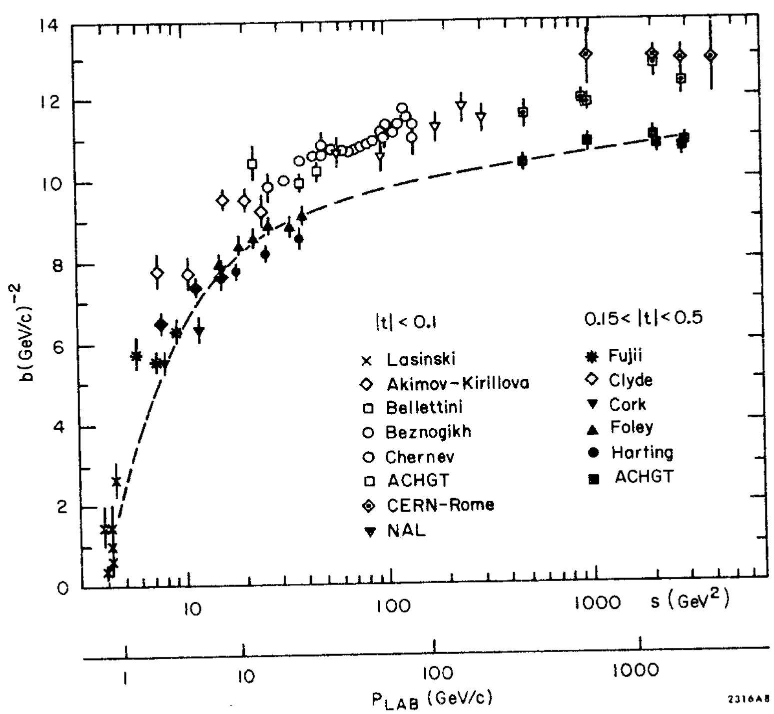

Figure 18

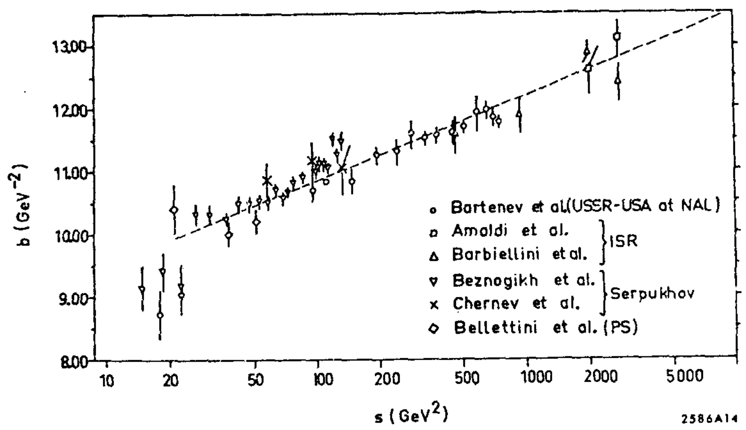

Figure 19

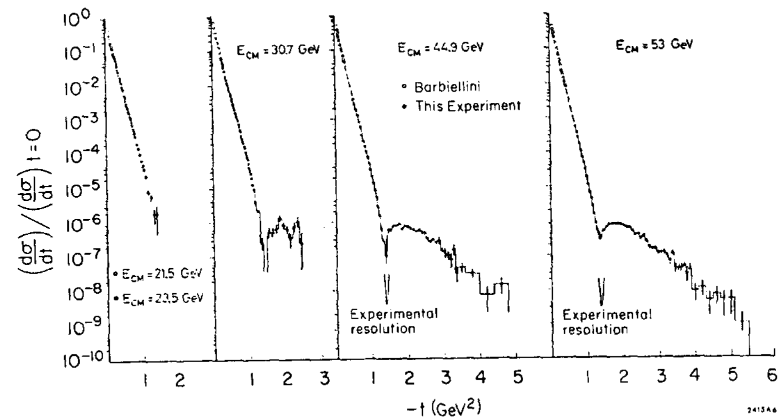

Figure 20

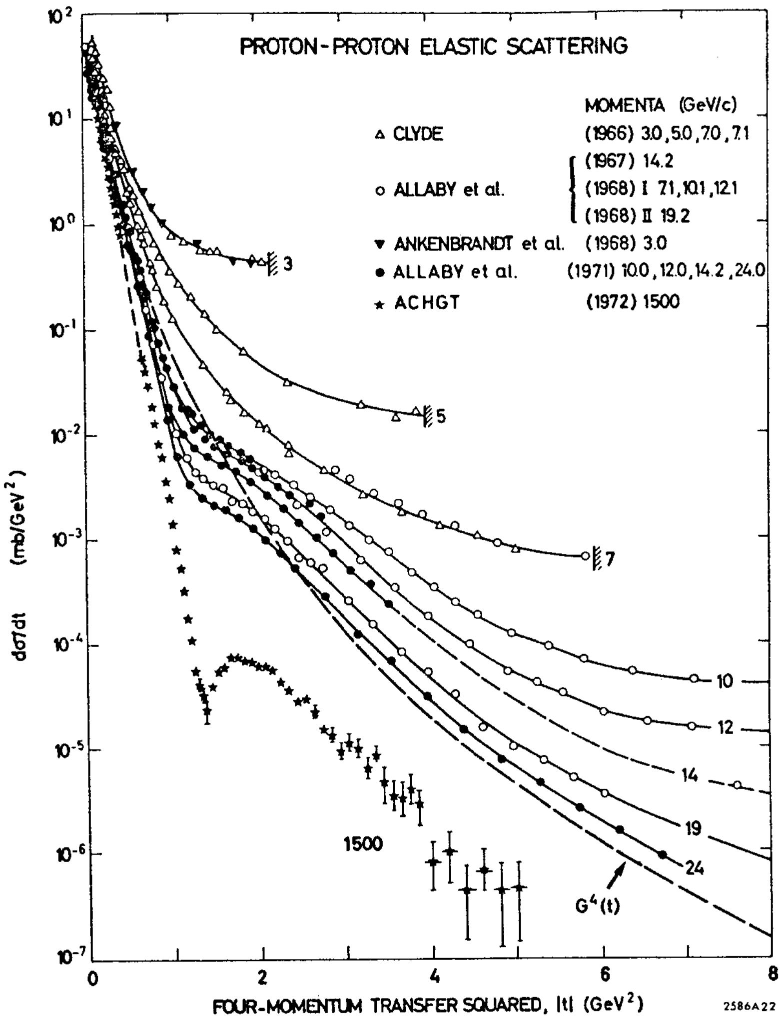

Figure 21

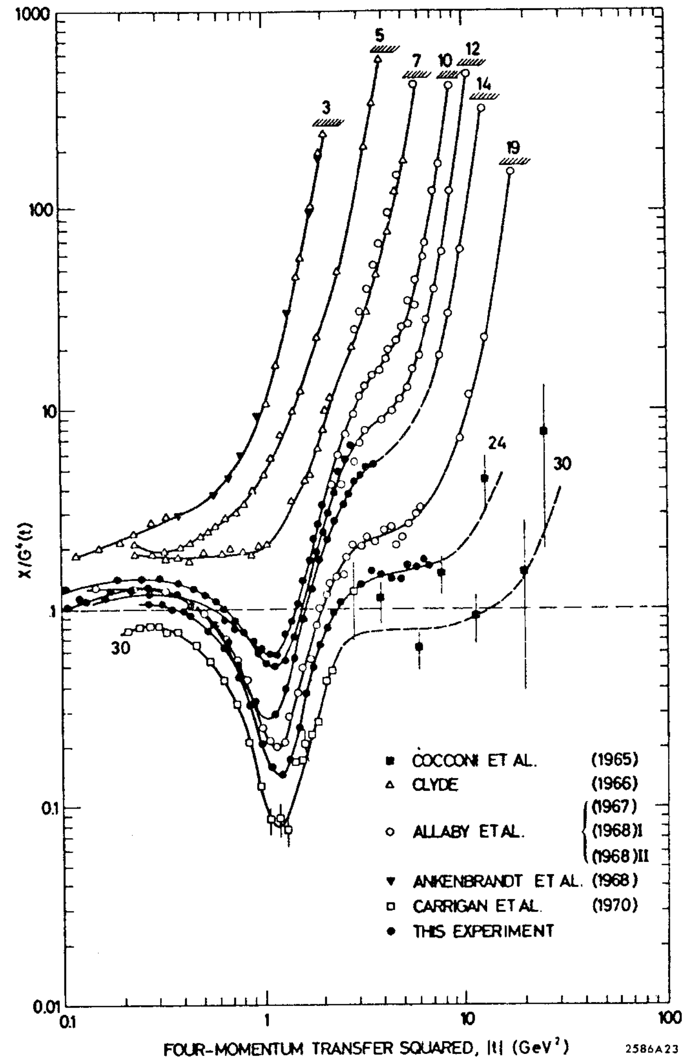

Figure 22

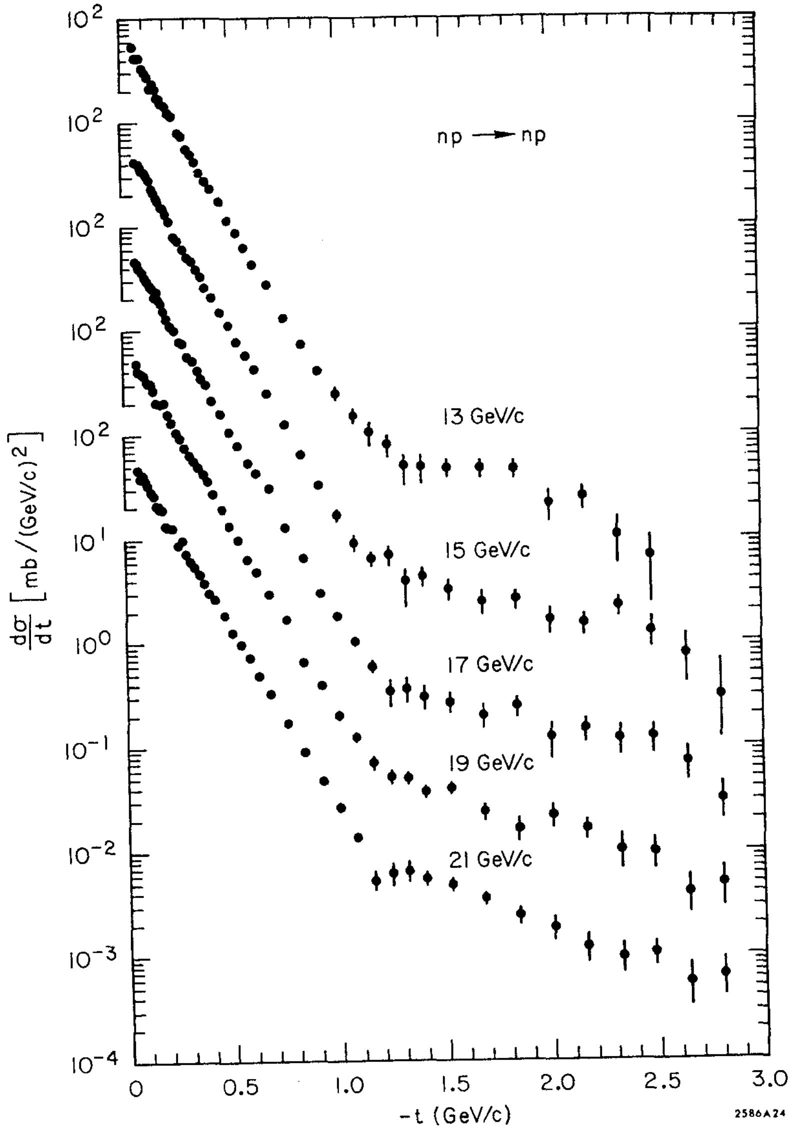

Figure 23

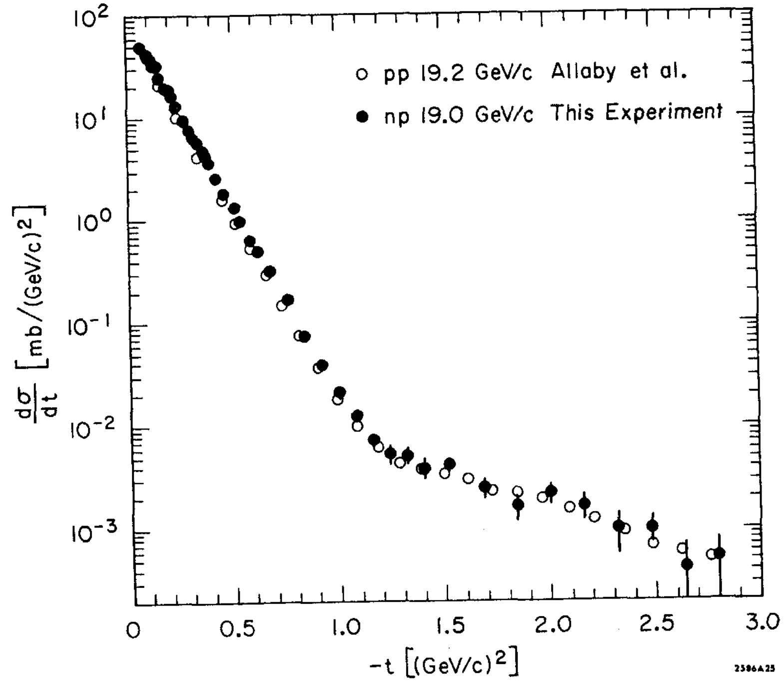

Figure 24

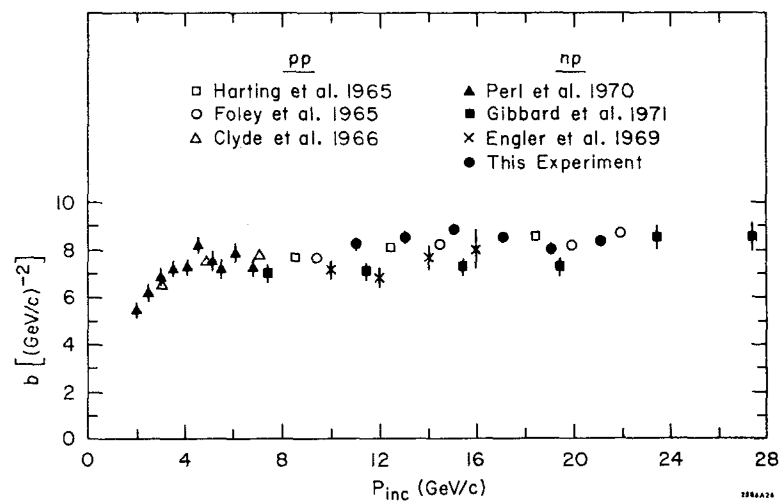

Figure 25

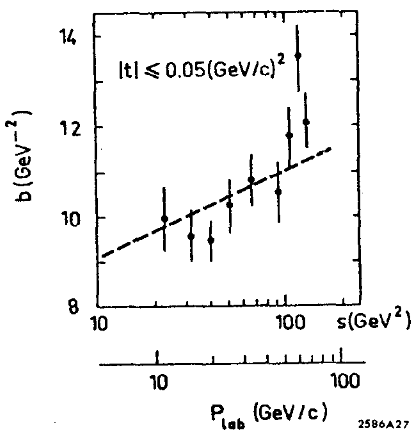

Figure 26

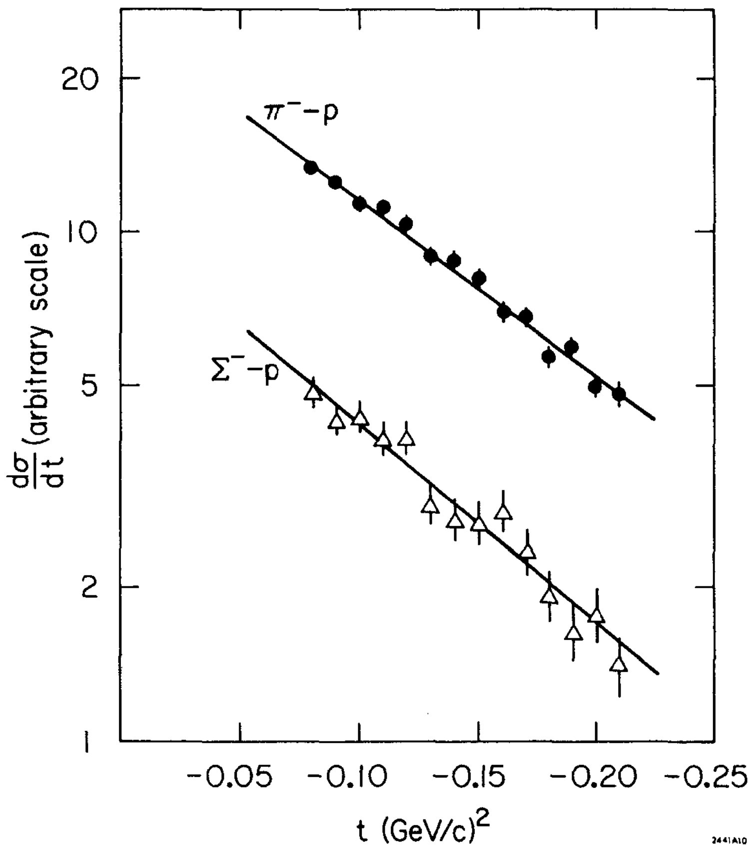

Figure 27

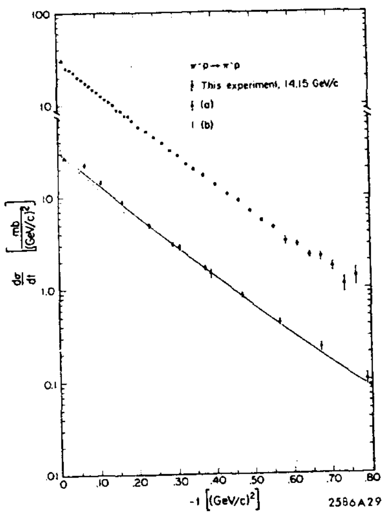

Figure 28

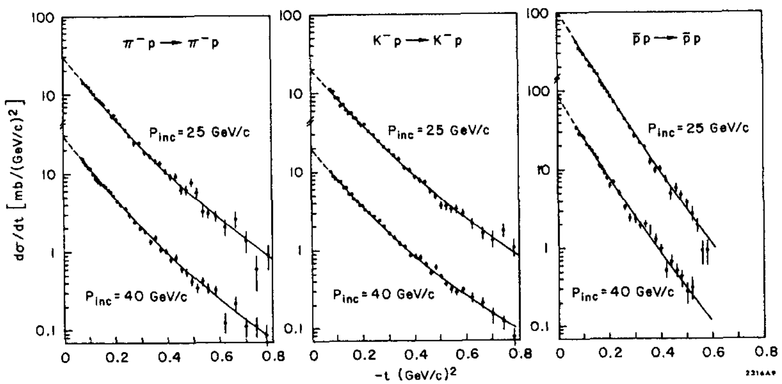

Figure 29

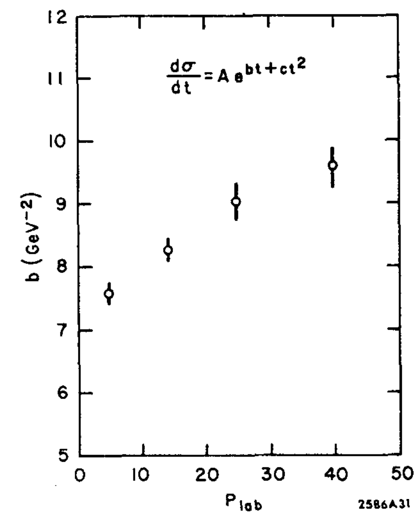

Figure 30

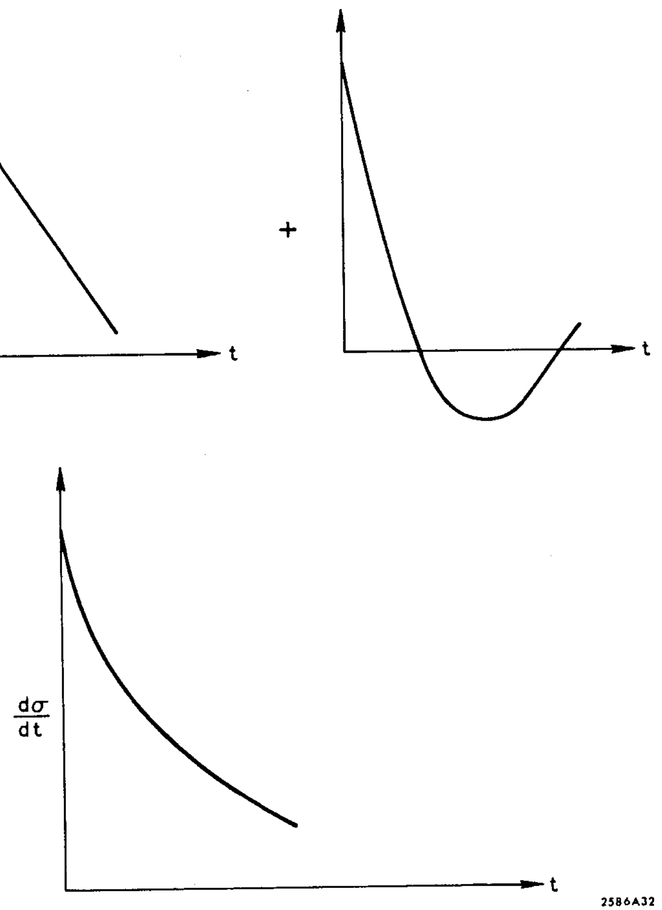

Figure 31

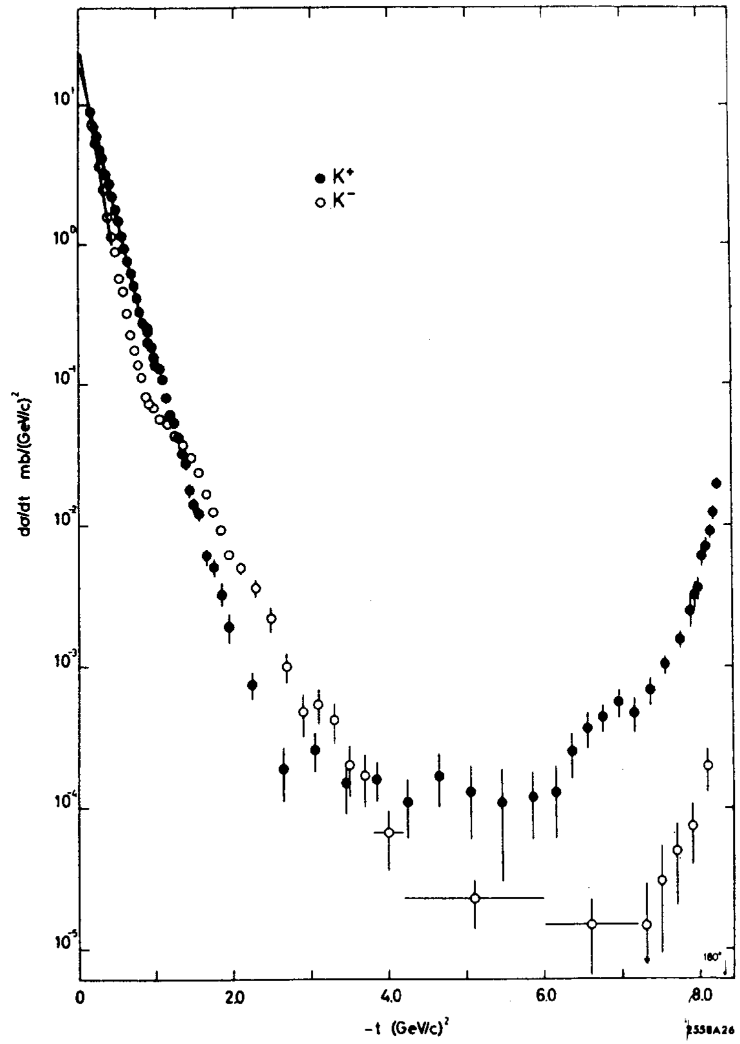

Figure 32

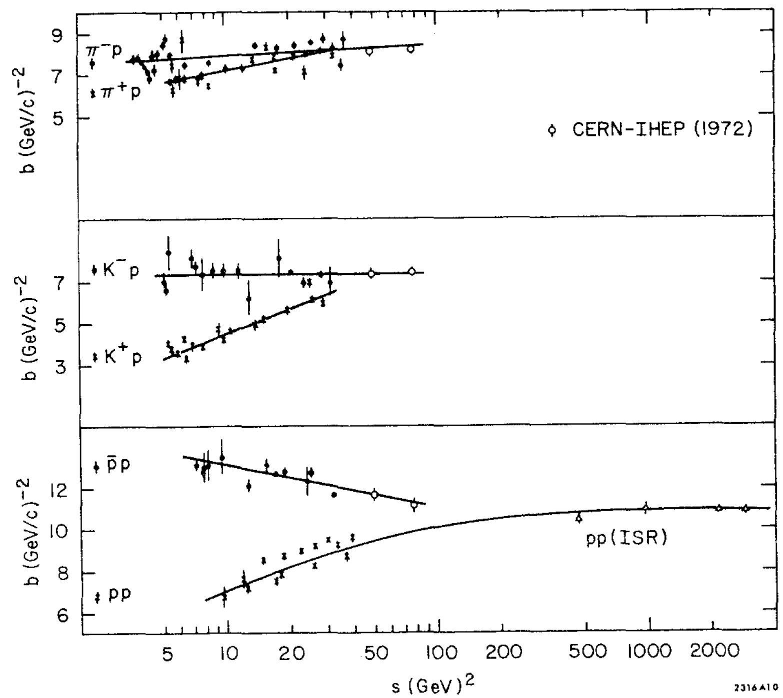

Figure 33

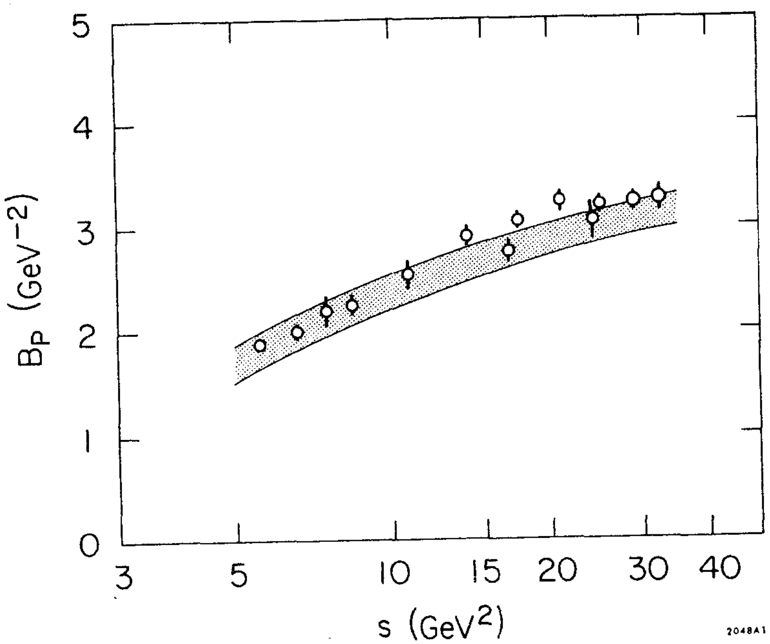

Figure 34

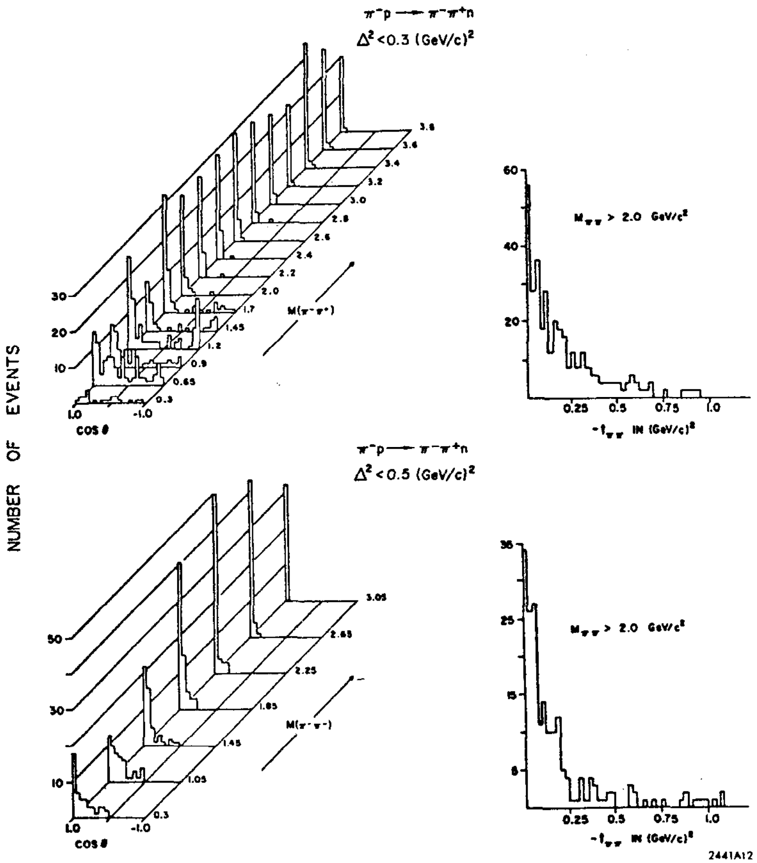

Figure 35

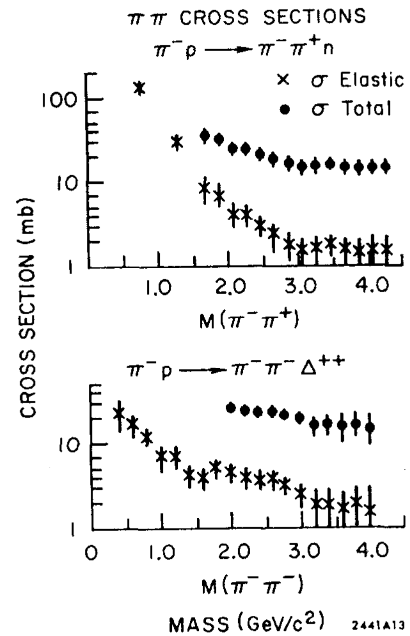

Figure 36

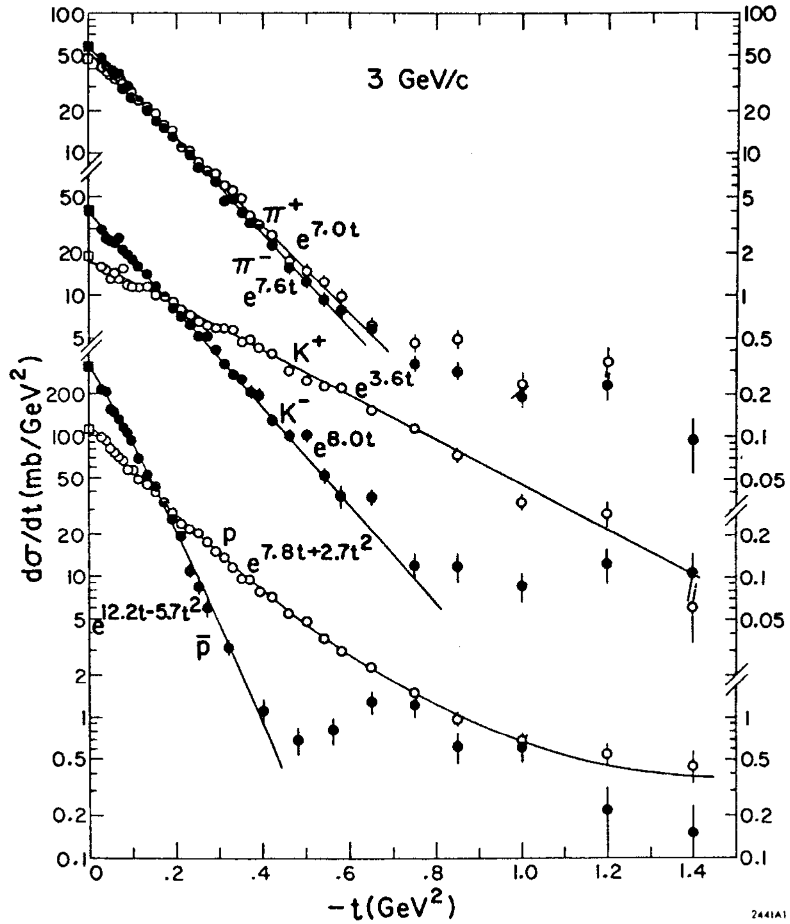

Figure 37

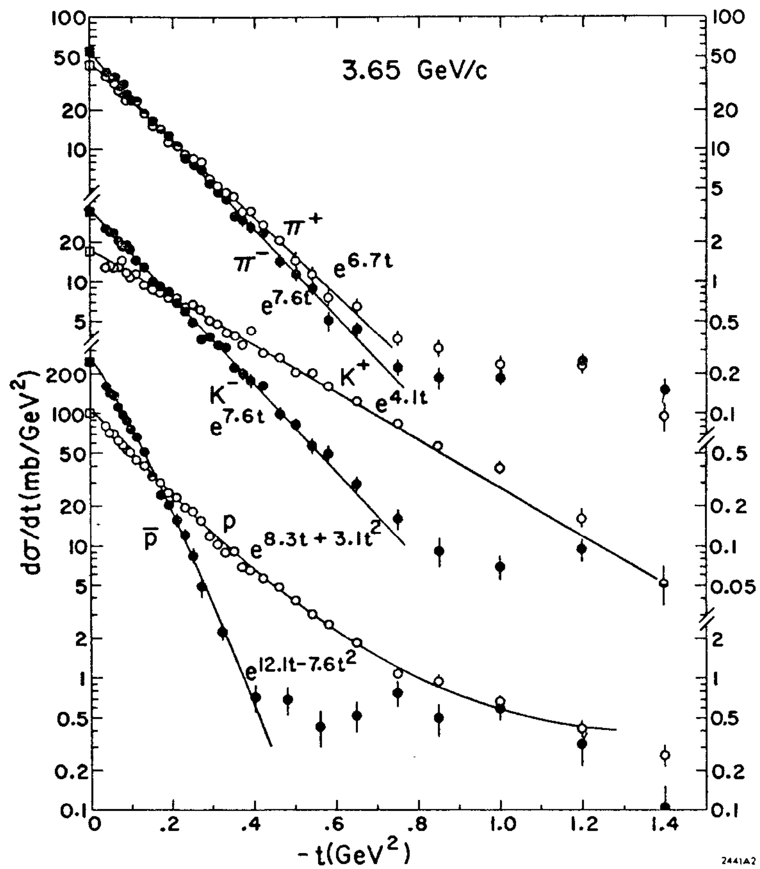

Figure 38

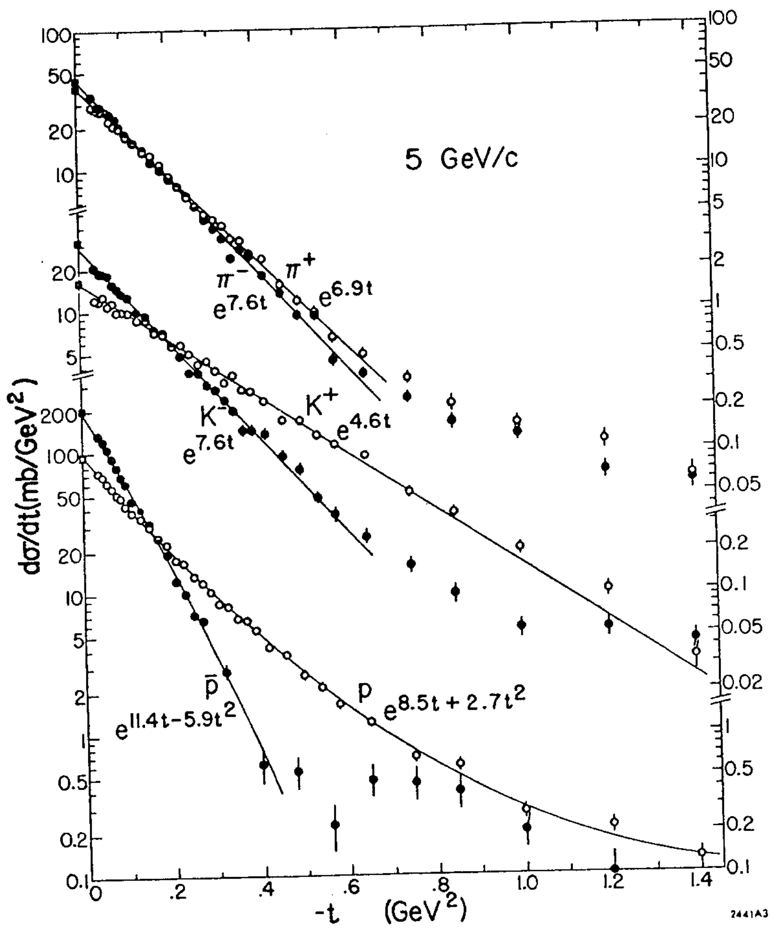

Figure 39

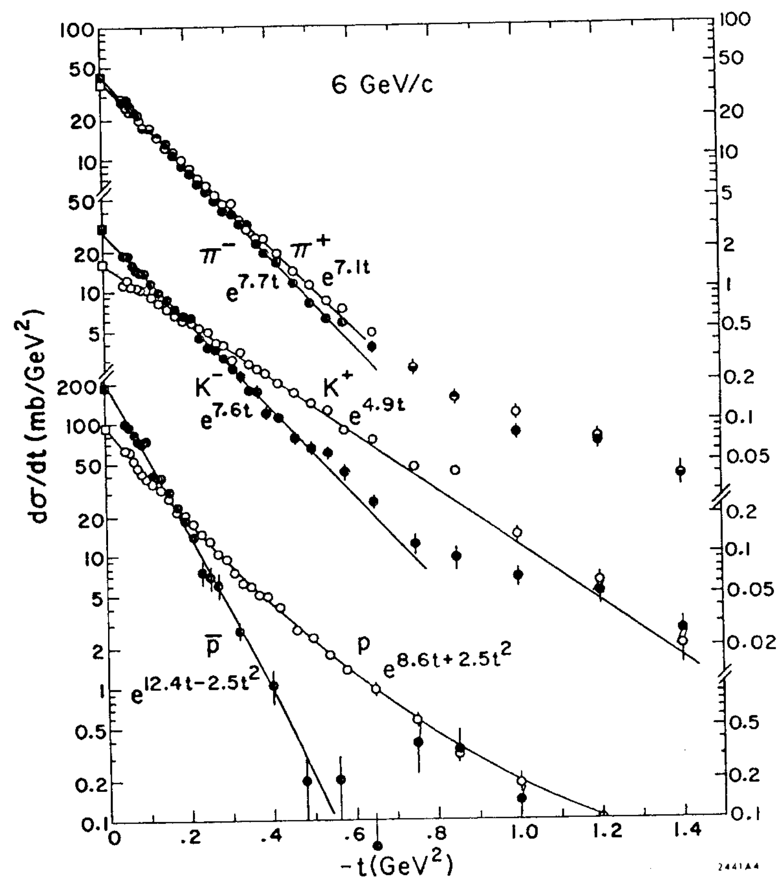

Figure 40

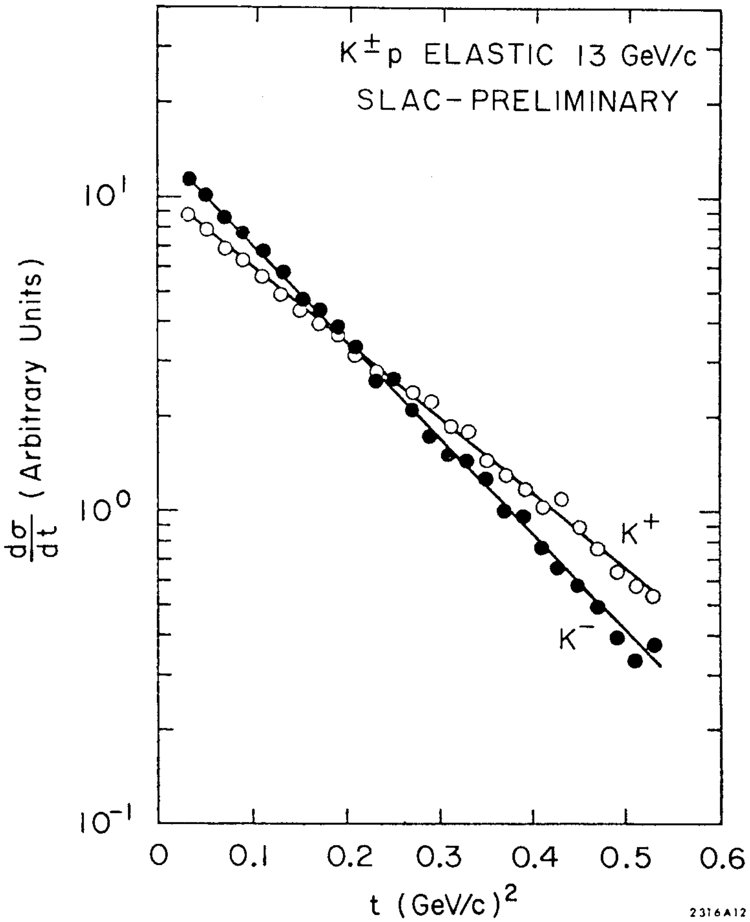

Figure 41

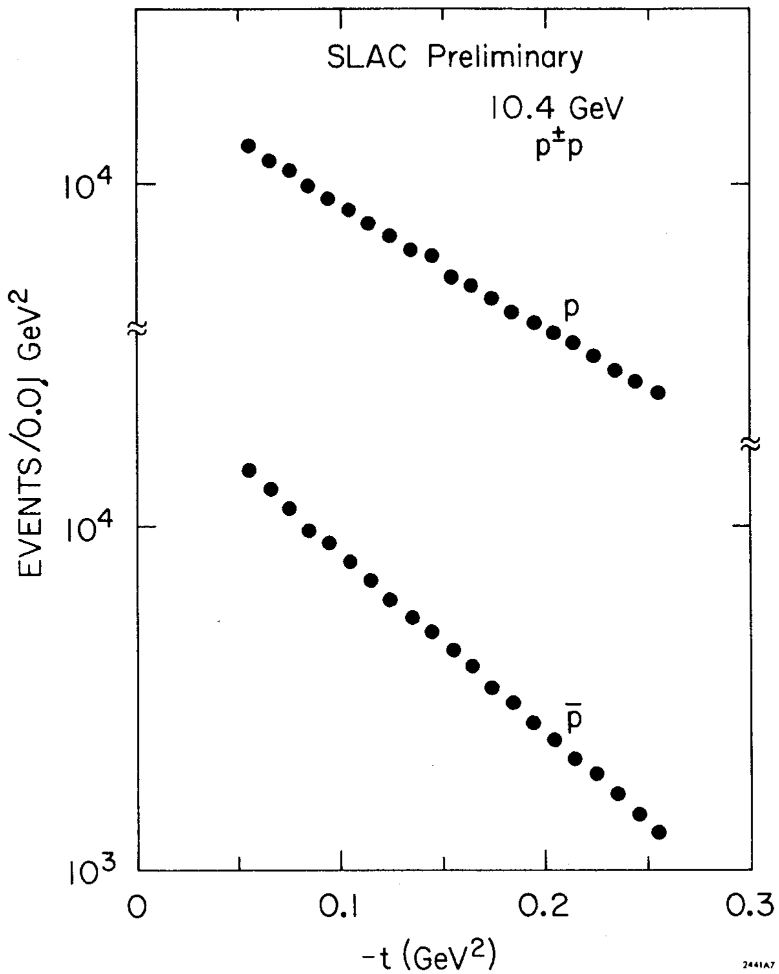

Figure 42a

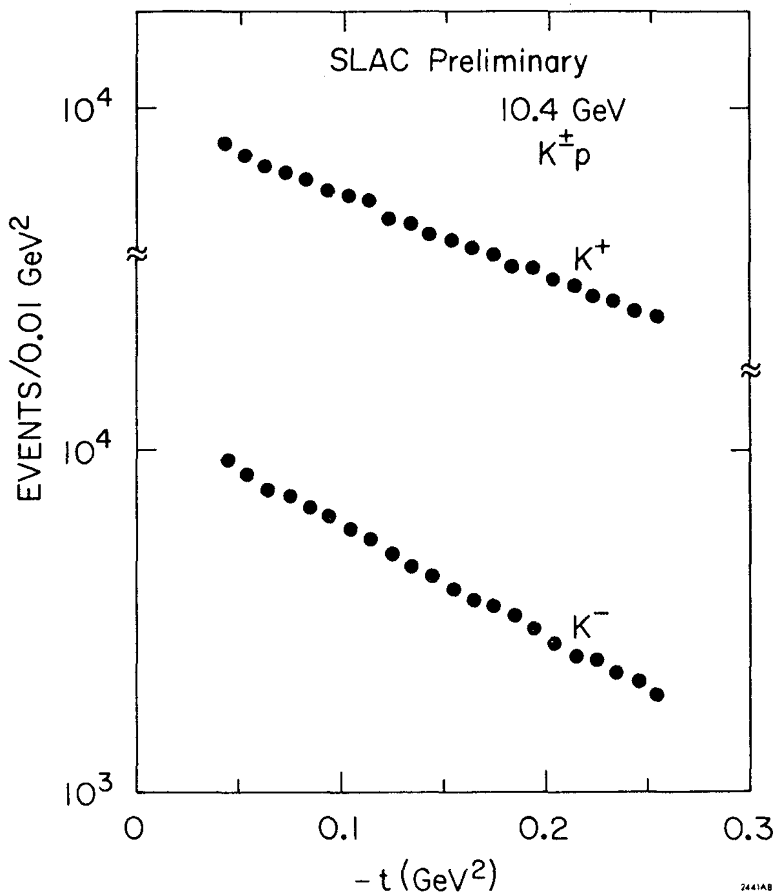

Figure 42b

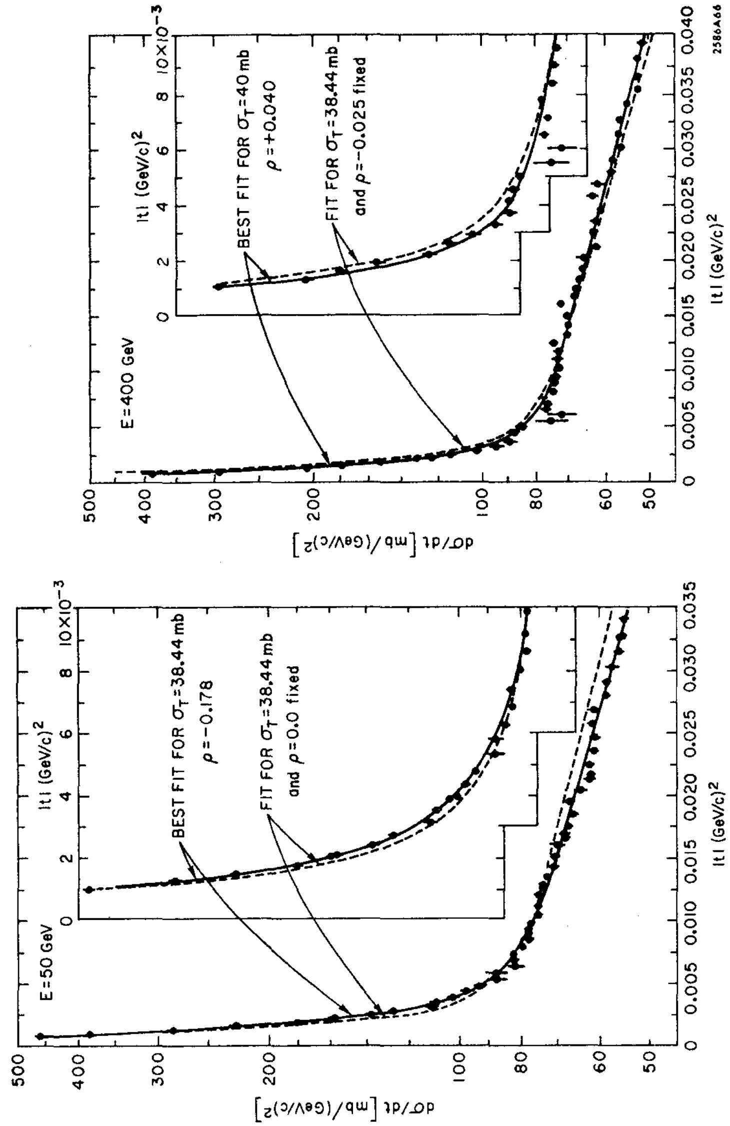

Figure 43

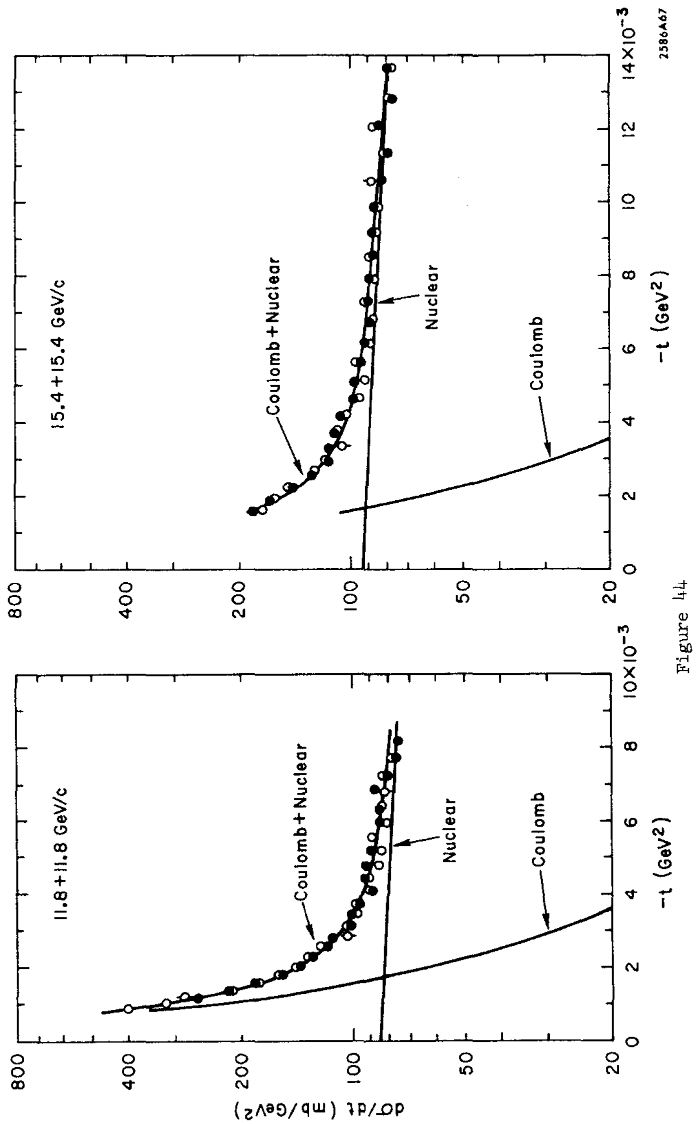

Figure 44

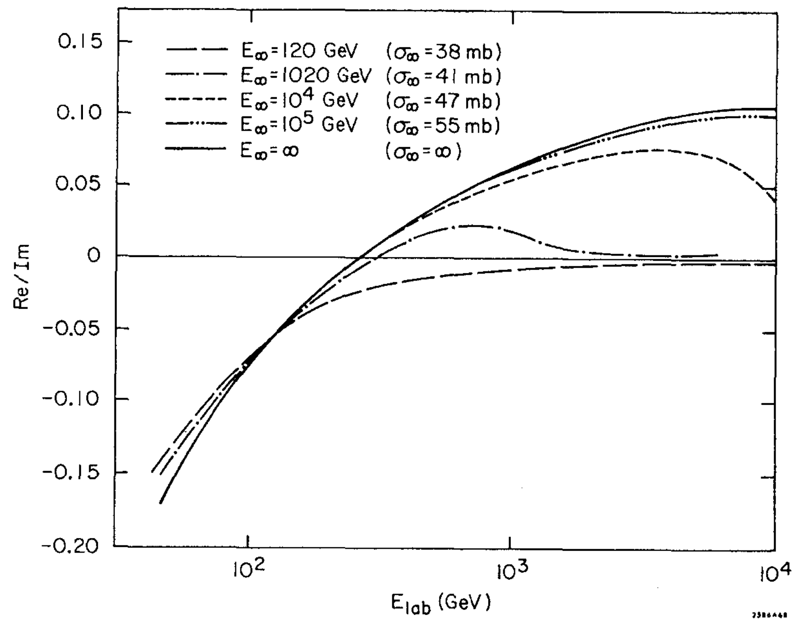

Figure 45

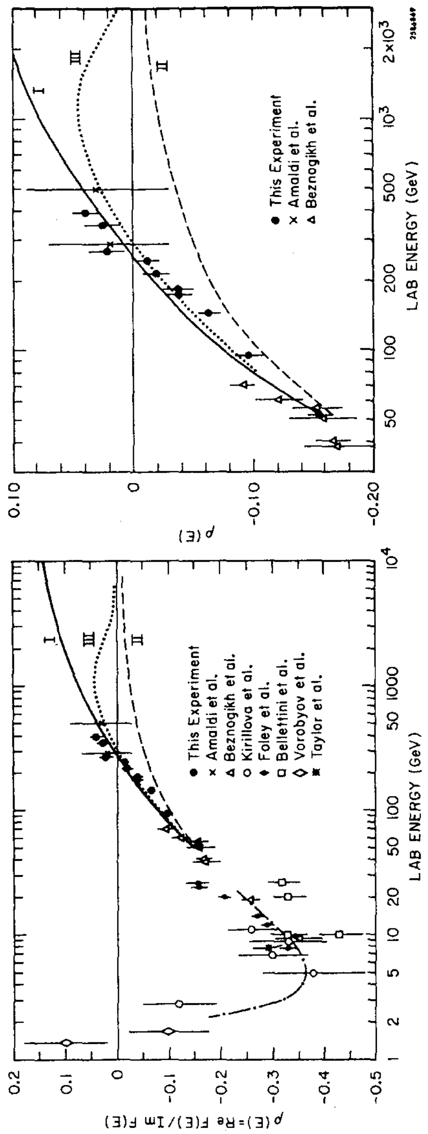

Figure 46

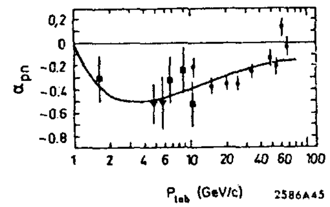

Figure 47

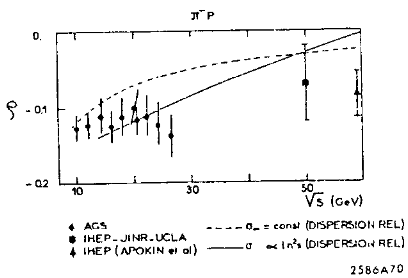

Figure 48

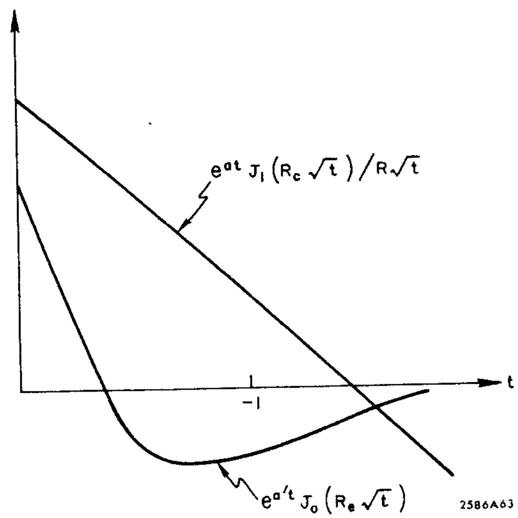

Figure 49

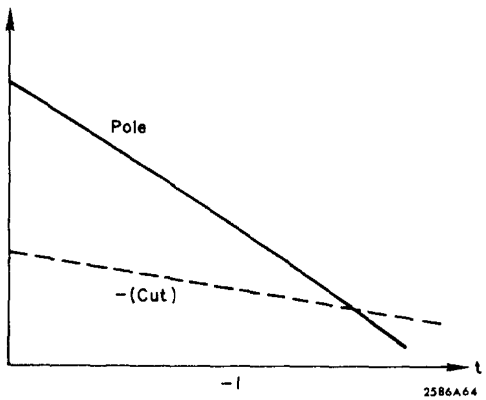

Figure 50

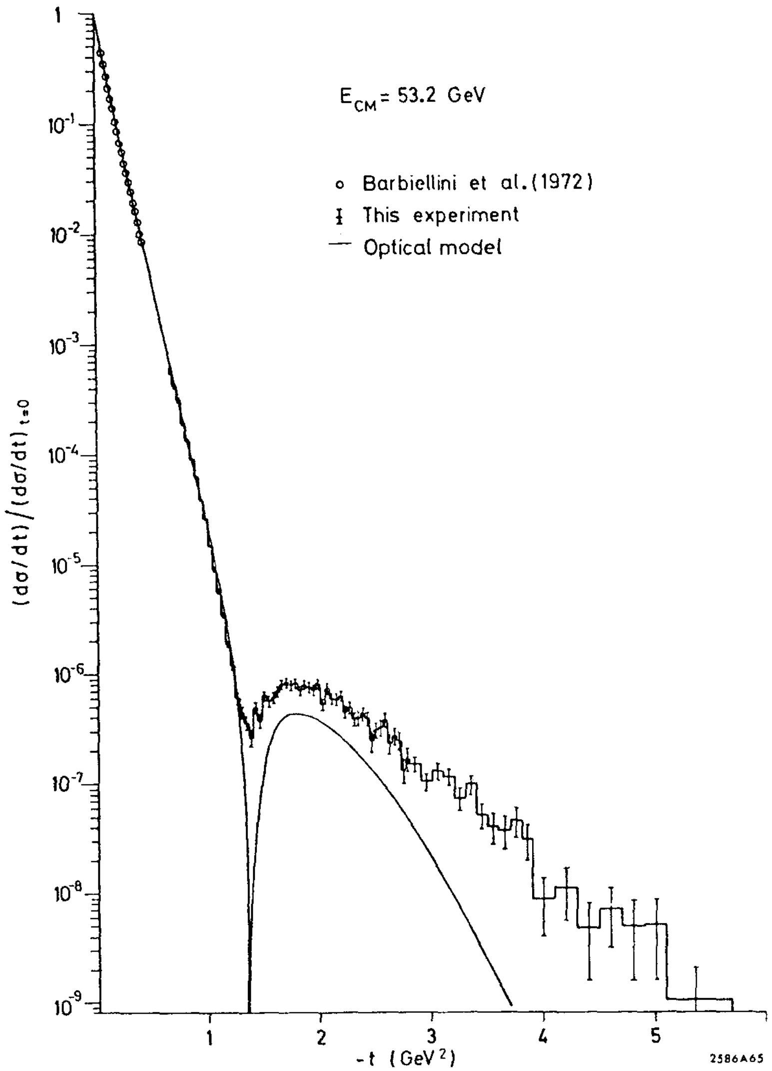

Figure 51

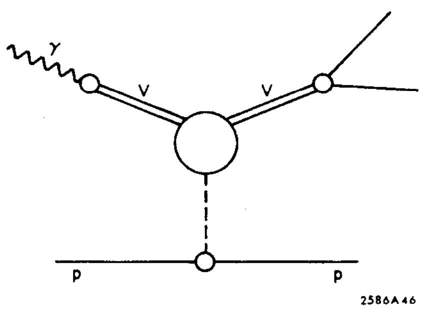

Figure 52

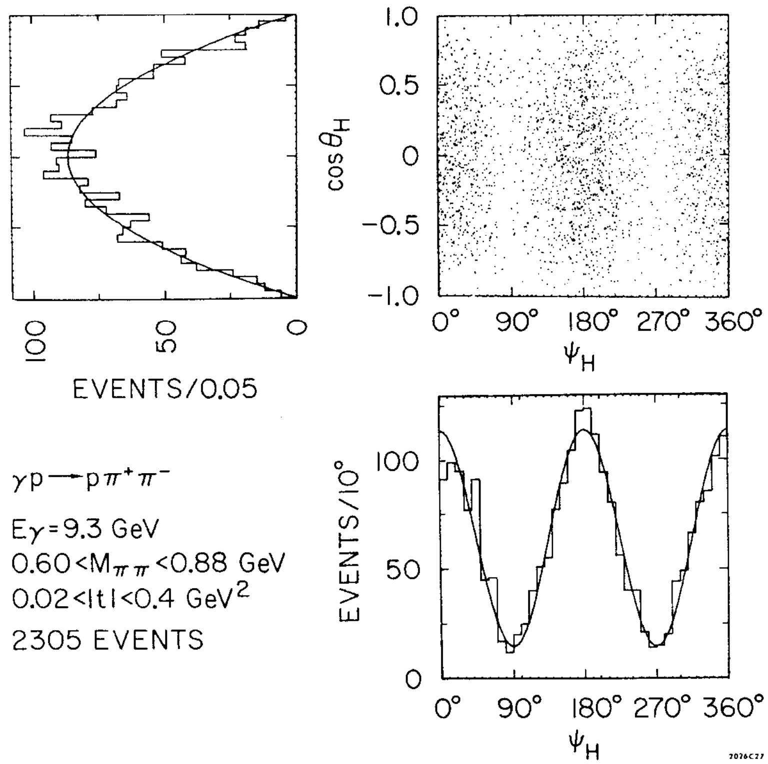

Figure 53

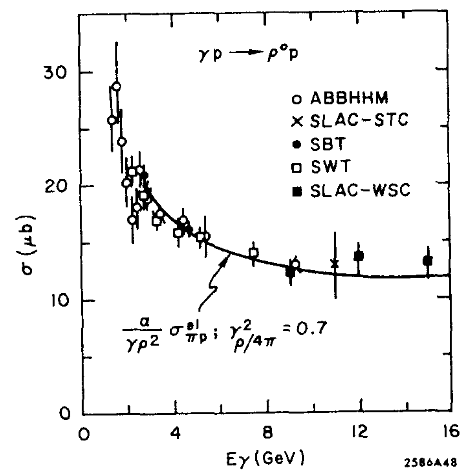

Figure 54

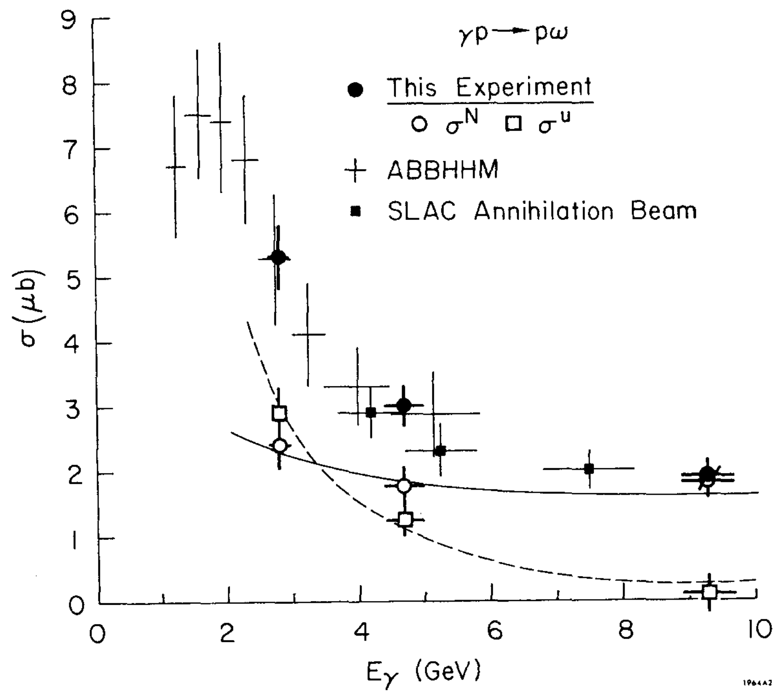

Figure 55

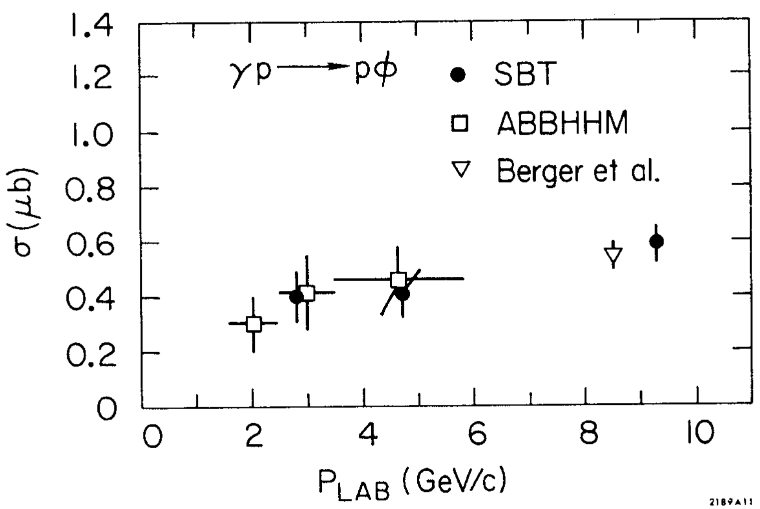

Figure 56

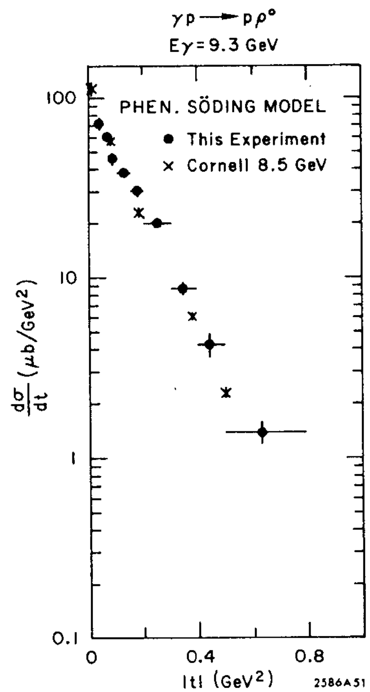

Figure 57

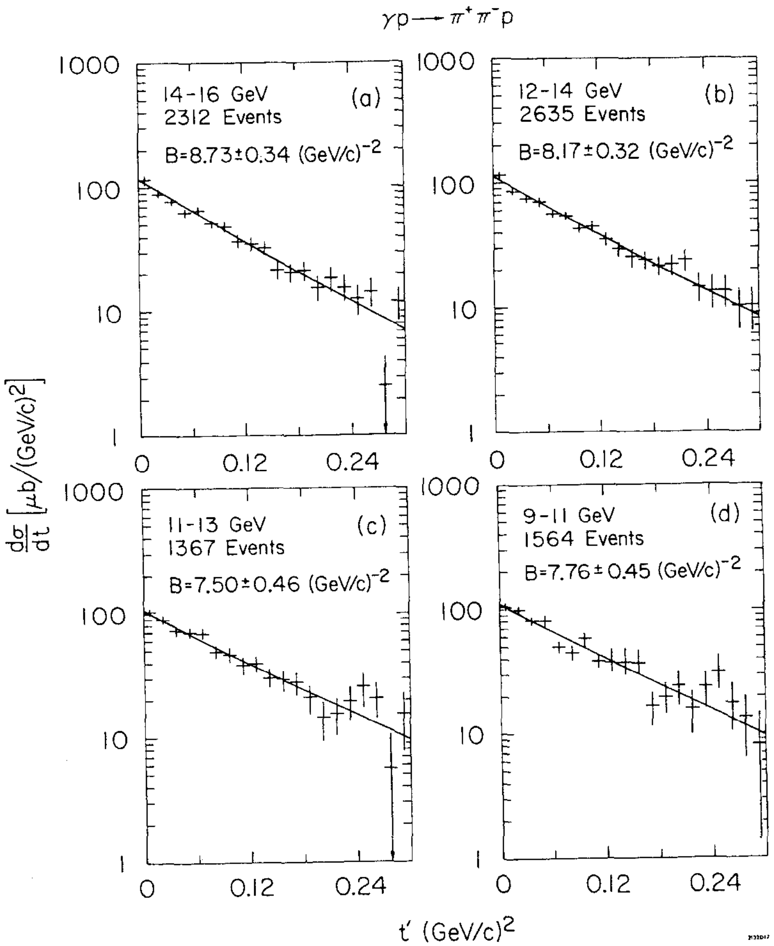

Figure 58

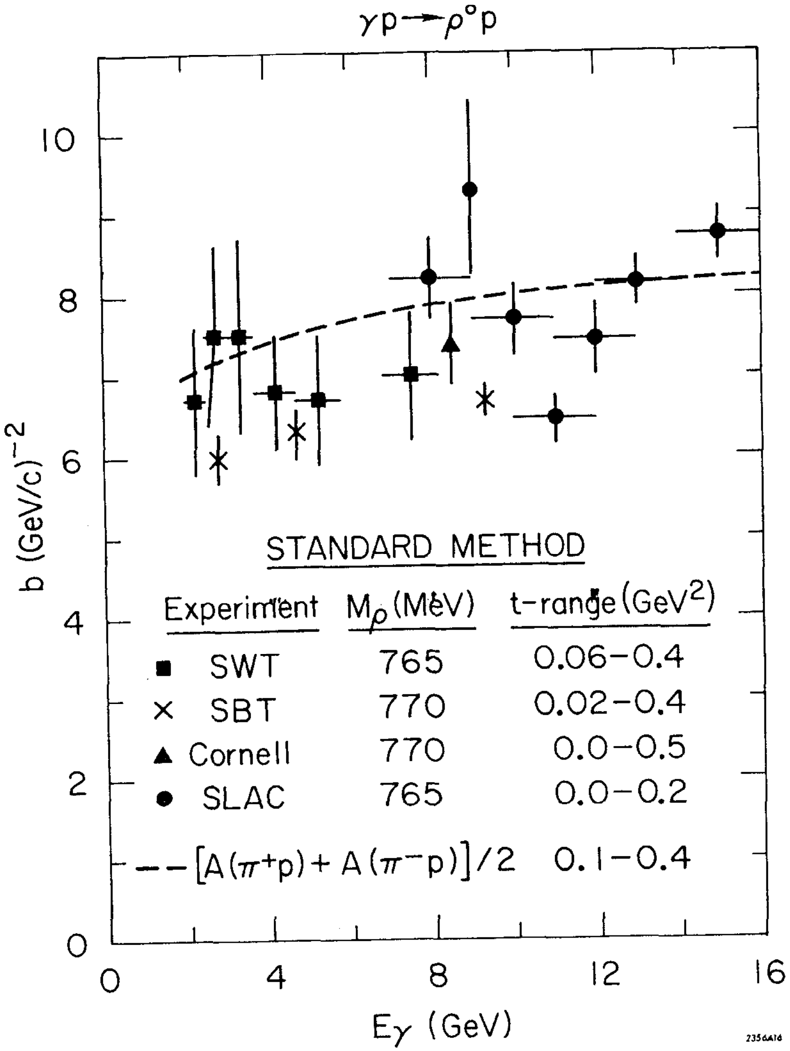

Figure 59

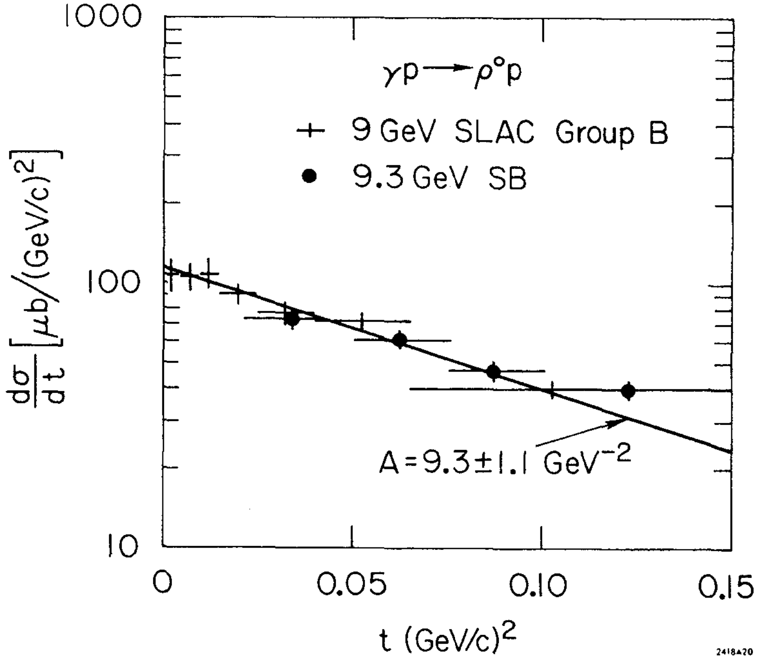

Figure 60

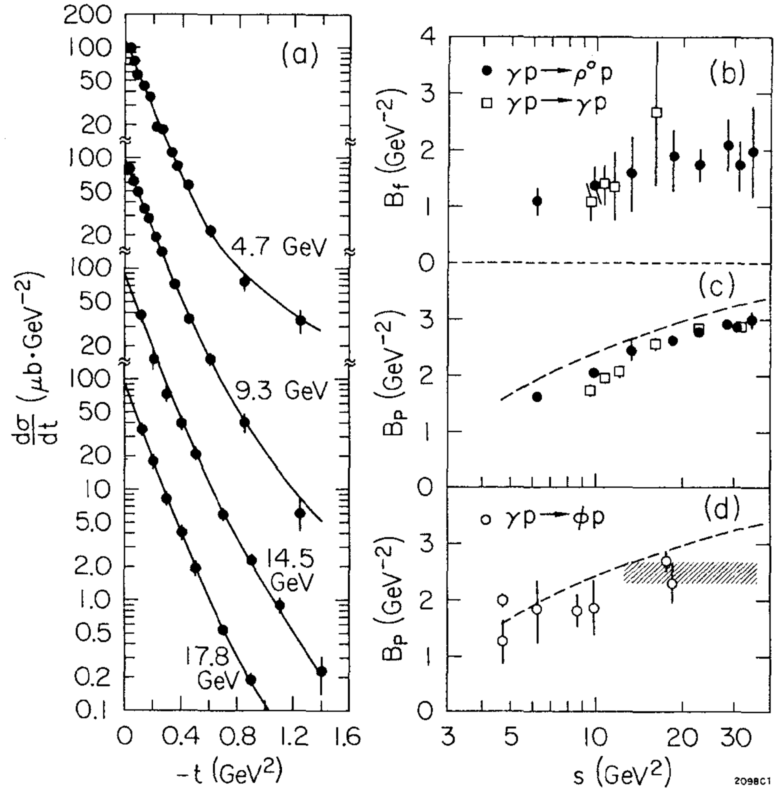

Figure 61

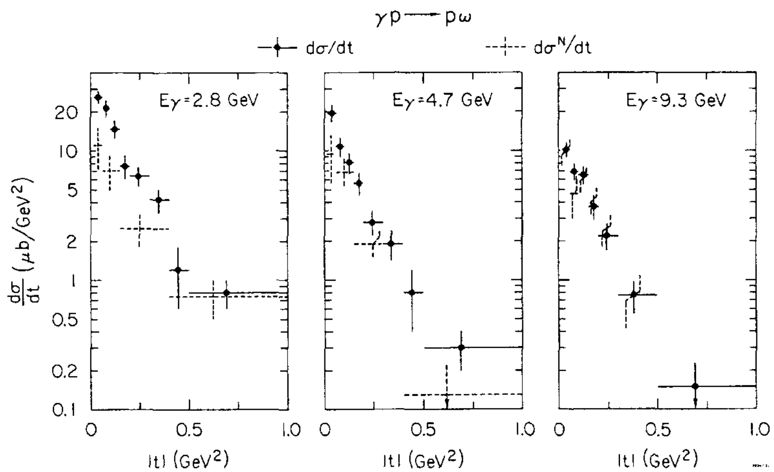

Figure 62

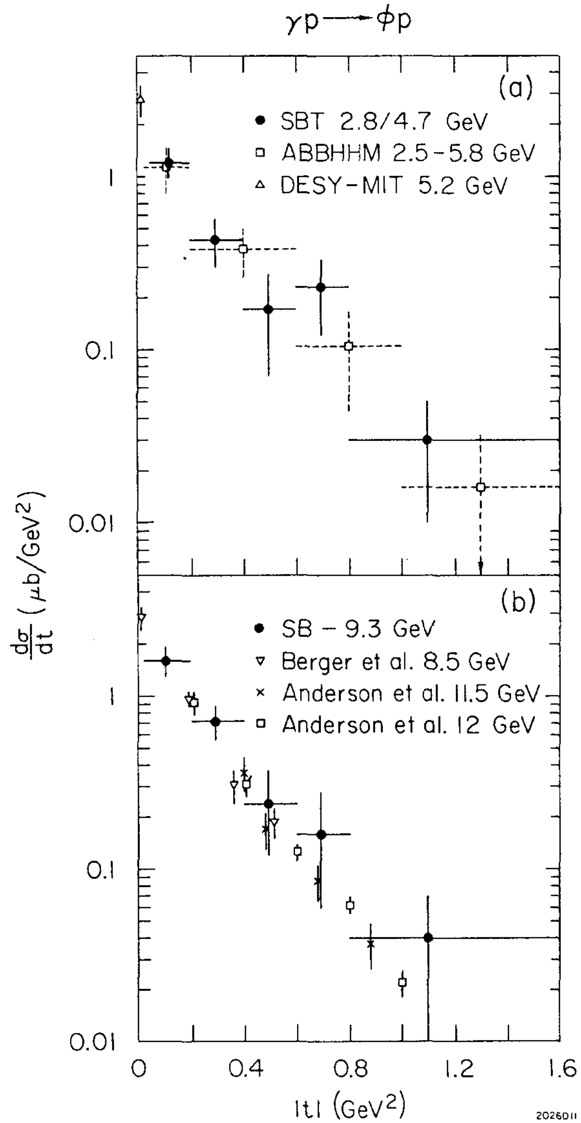

Figure 63

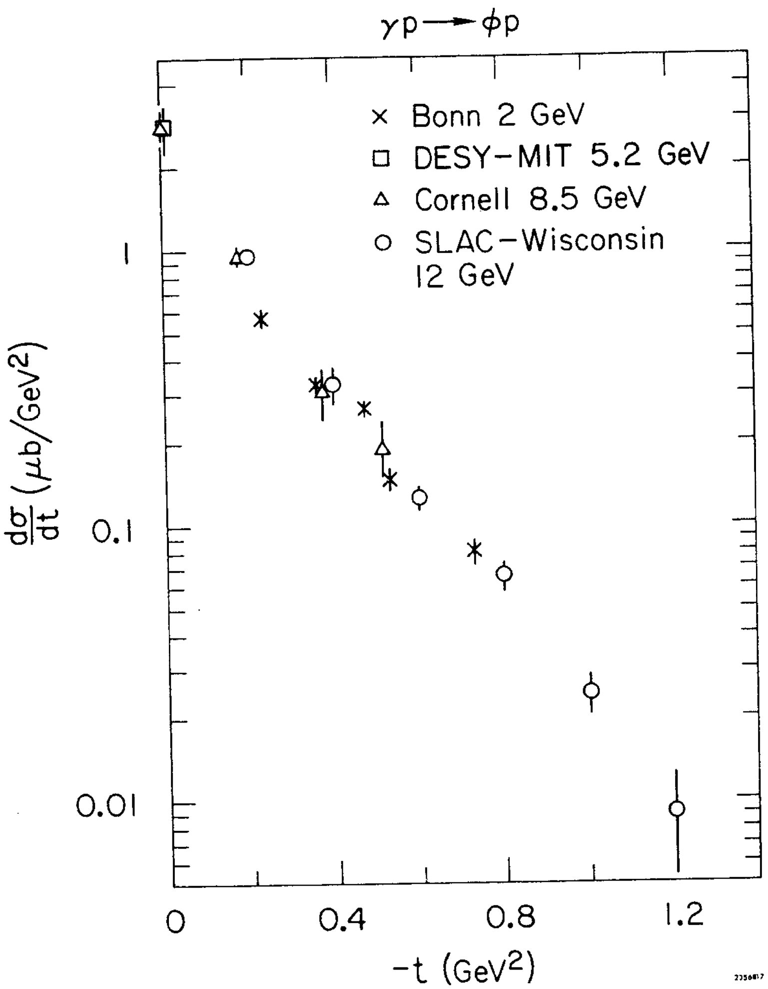

Figure 64

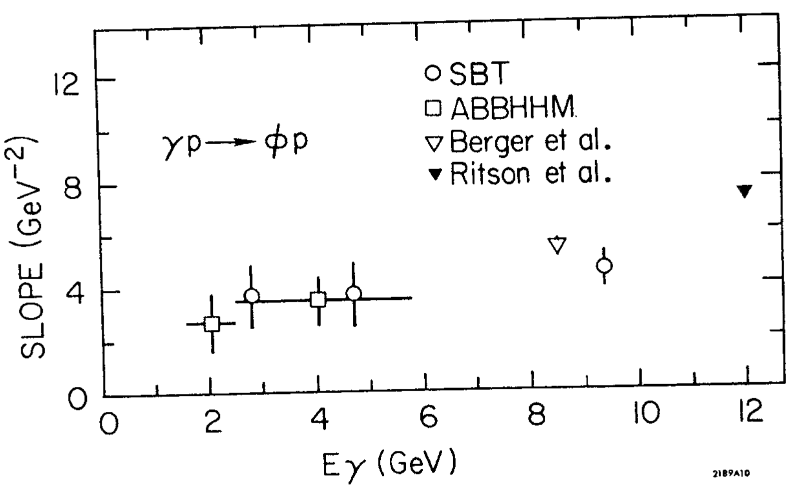

Figure 65

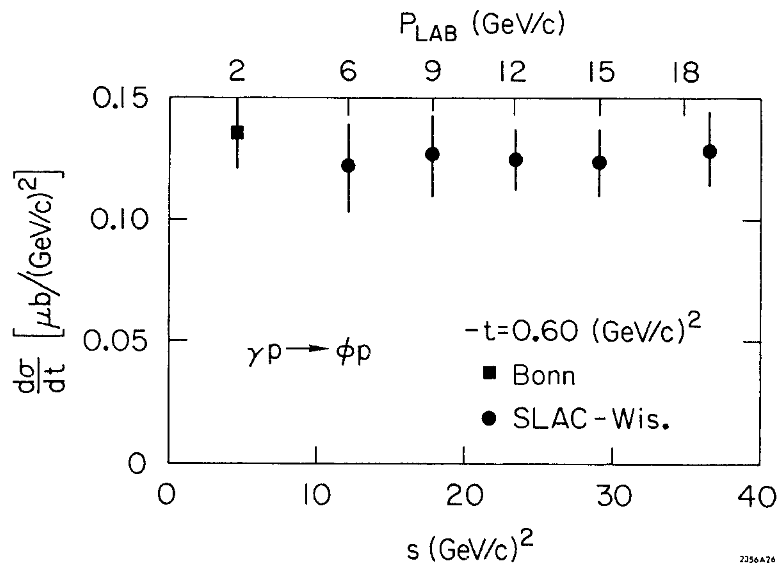

Figure 66

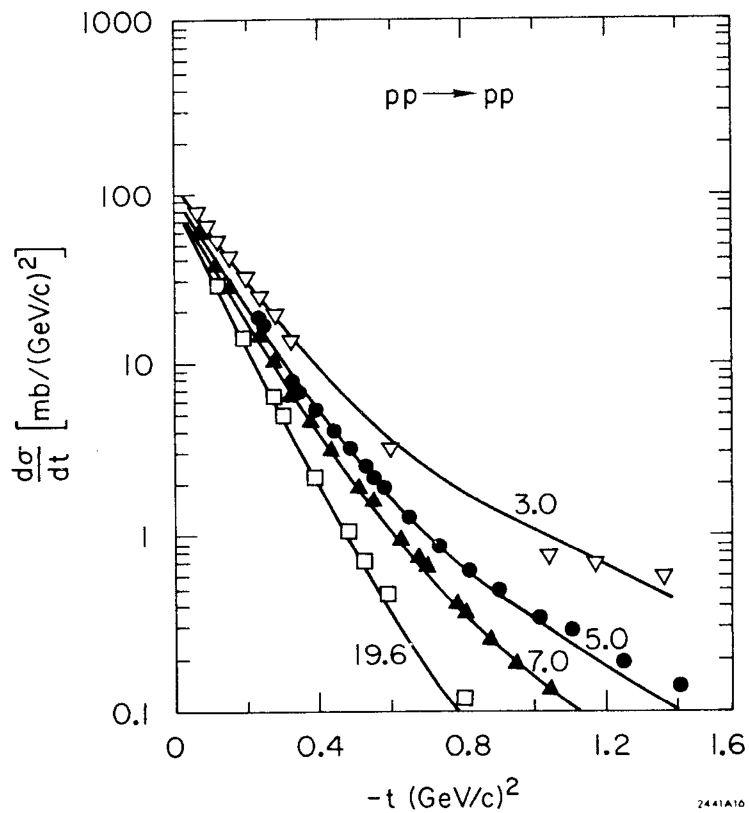

Figure 67

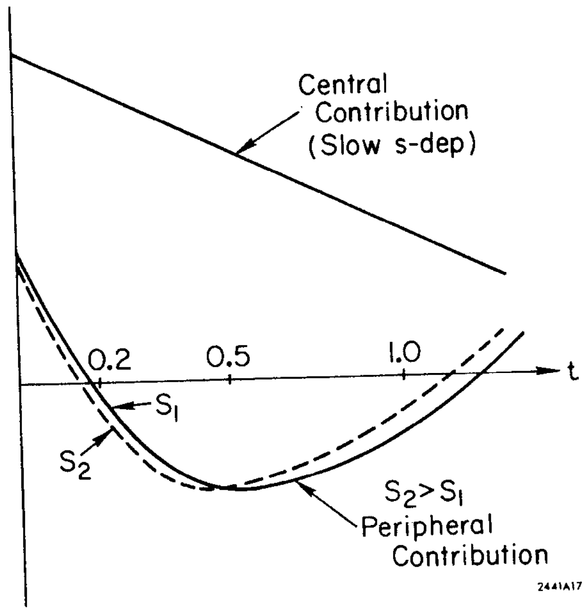

Figure 68

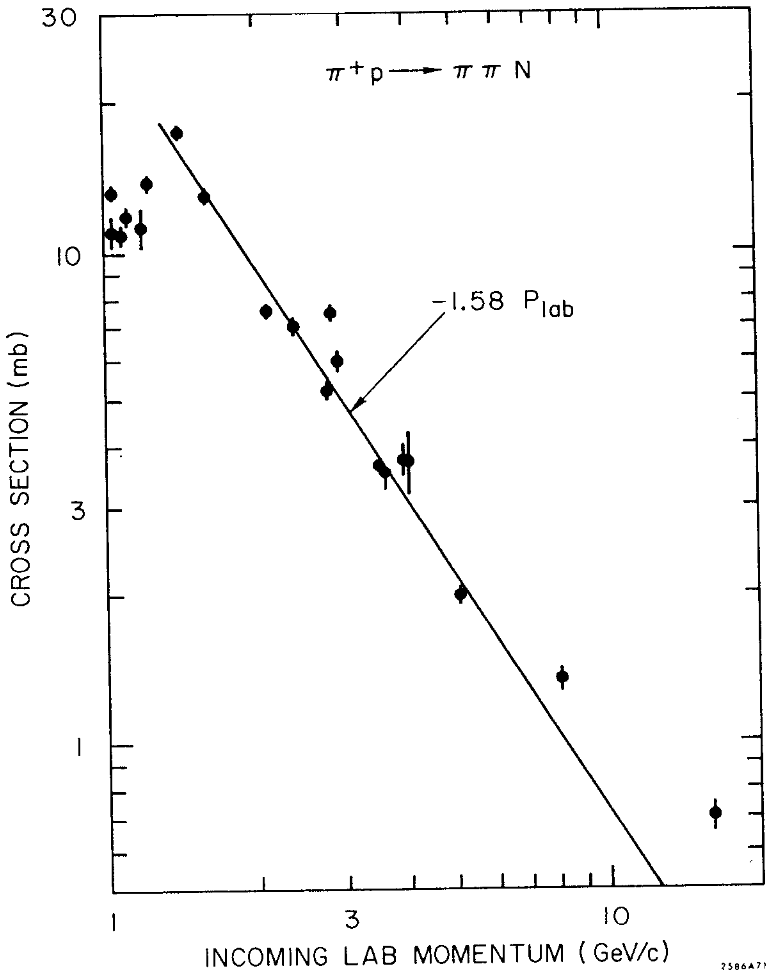

Figure 69

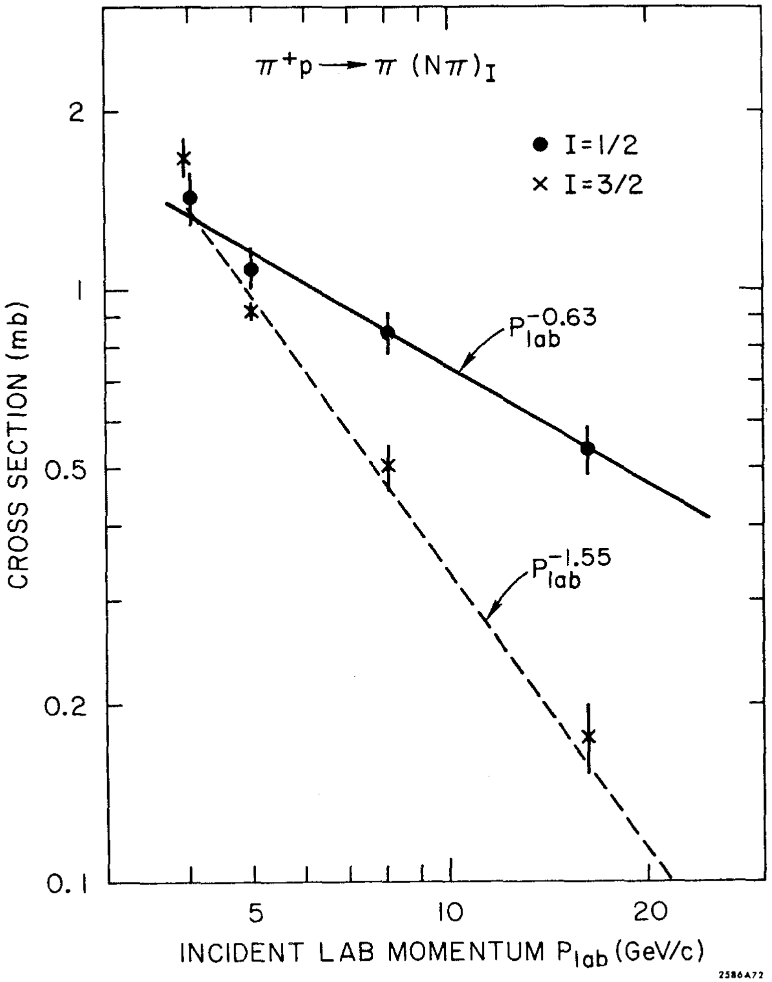

Figure 70

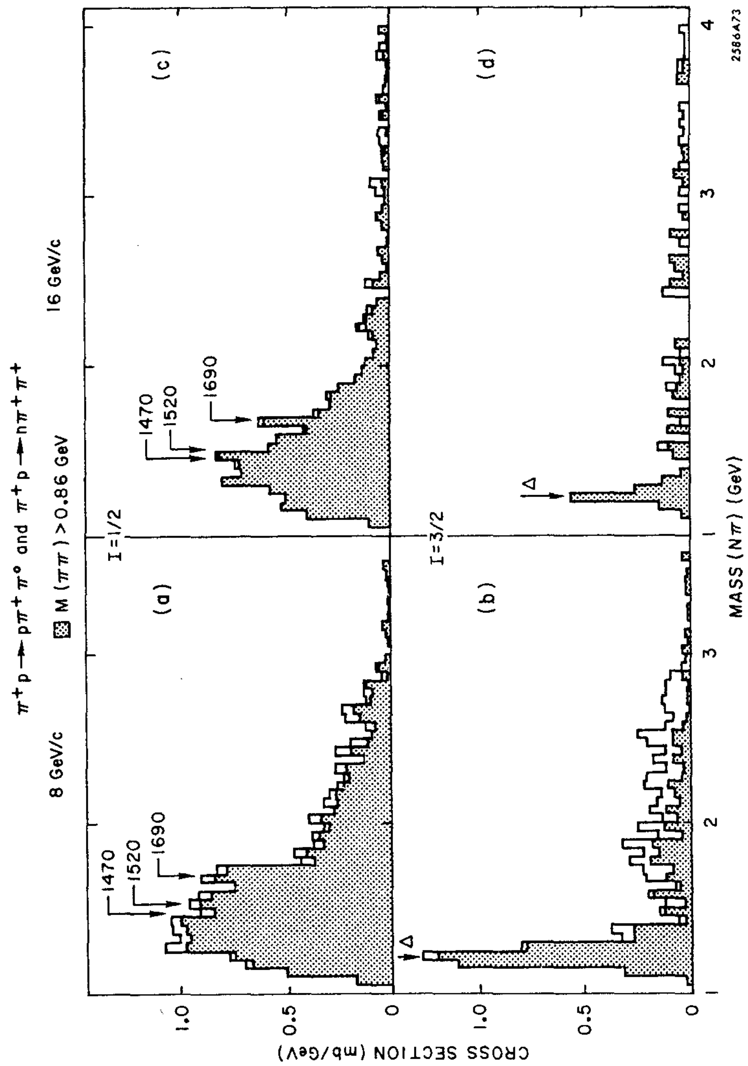

Figure 71

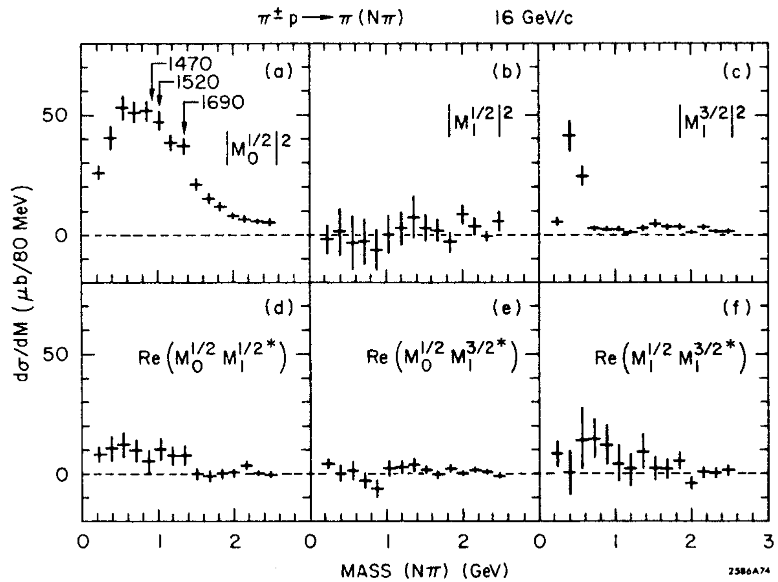

Figure 72

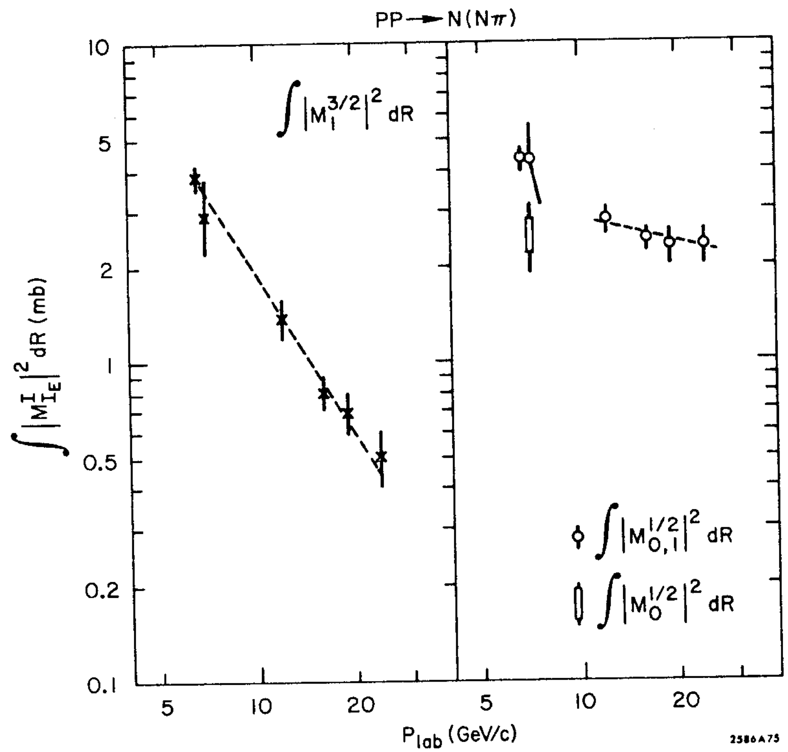

Figure 73

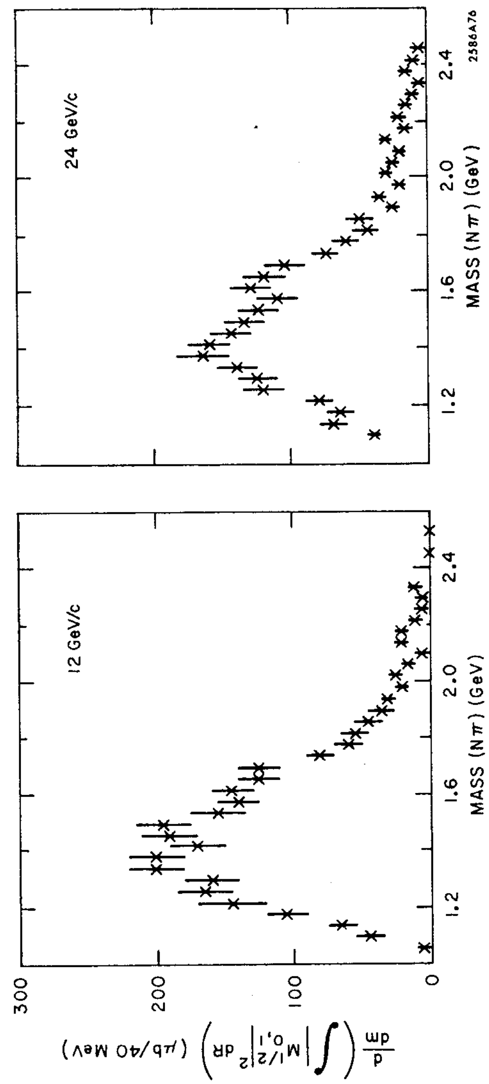

Figure 74

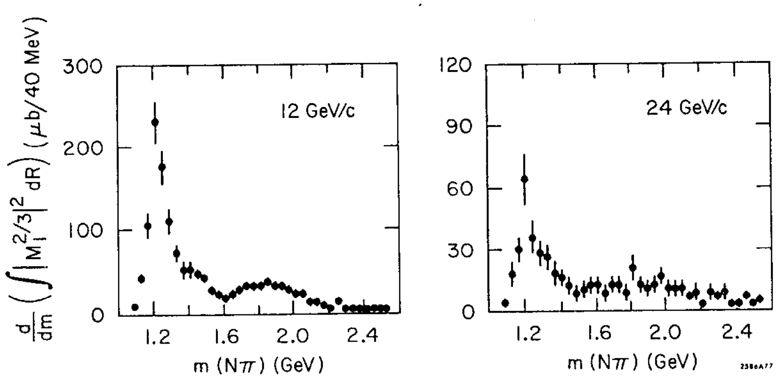

Figure 75

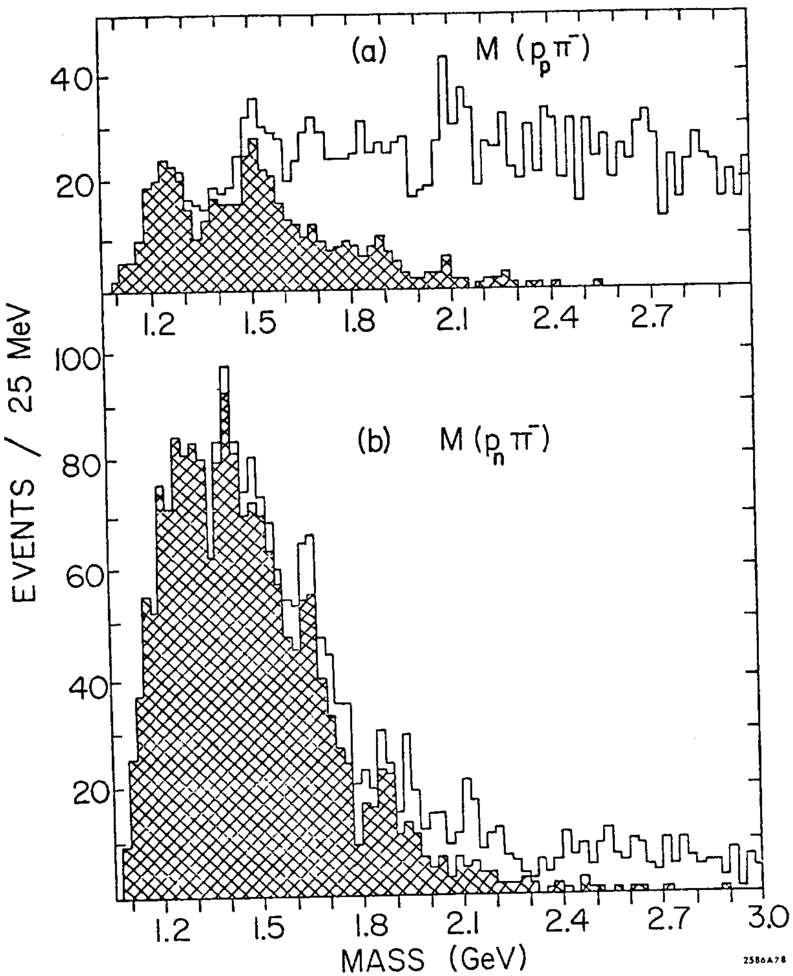

Figure 76

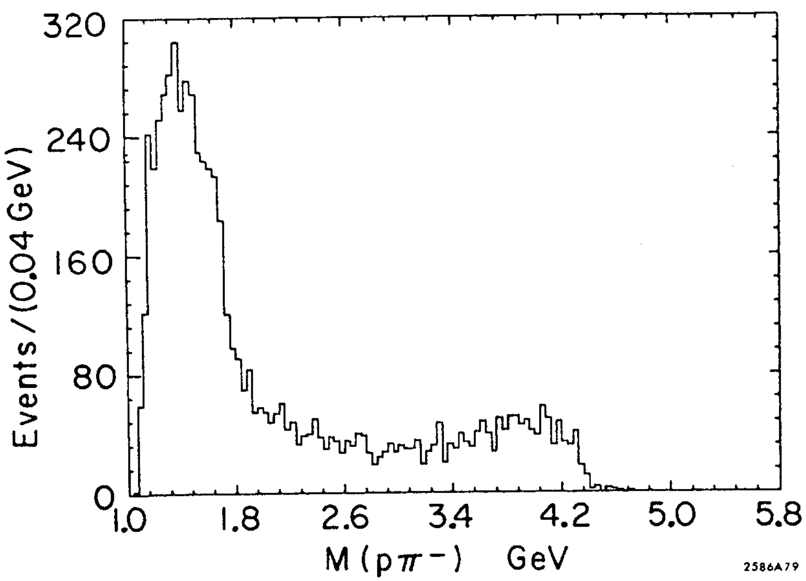

Figure 77

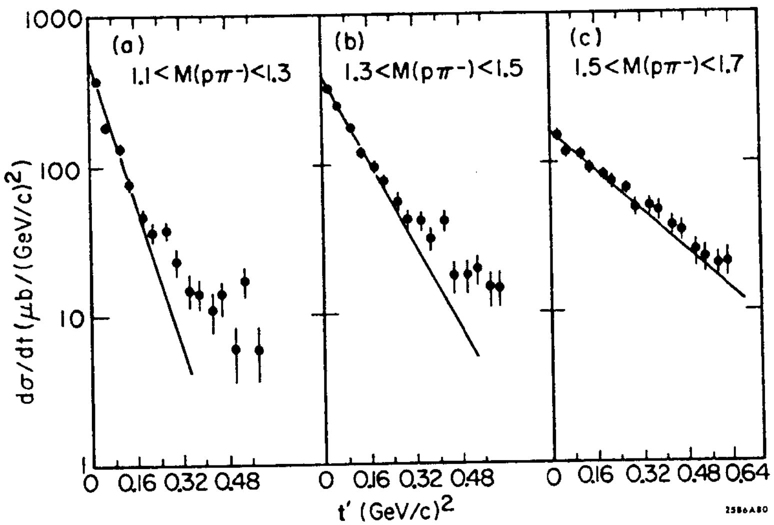

Figure 78

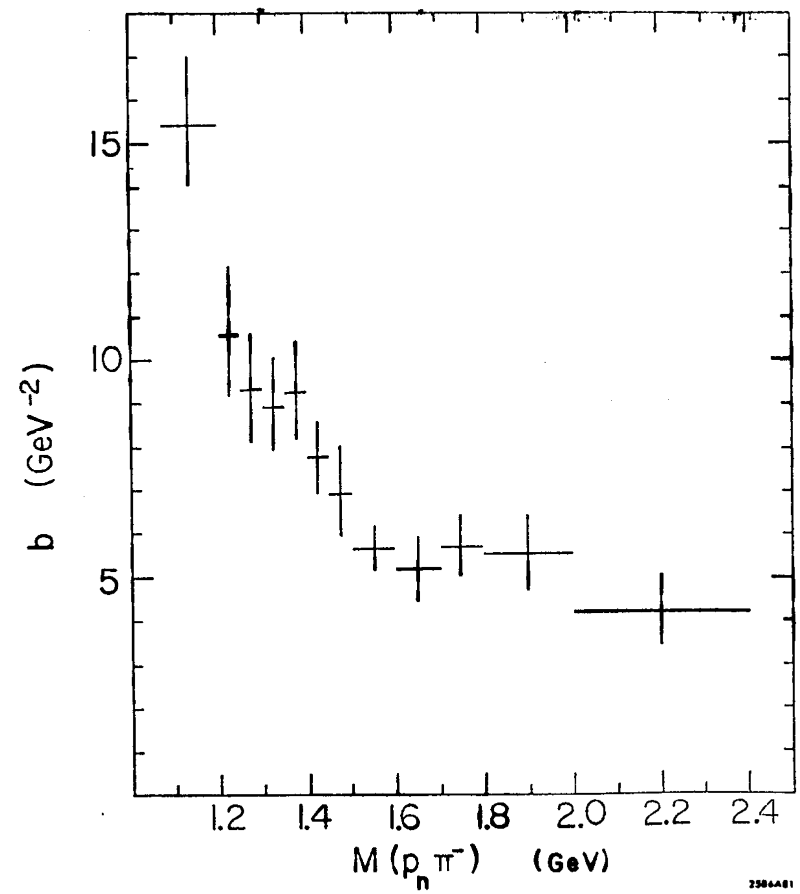

Figure 79

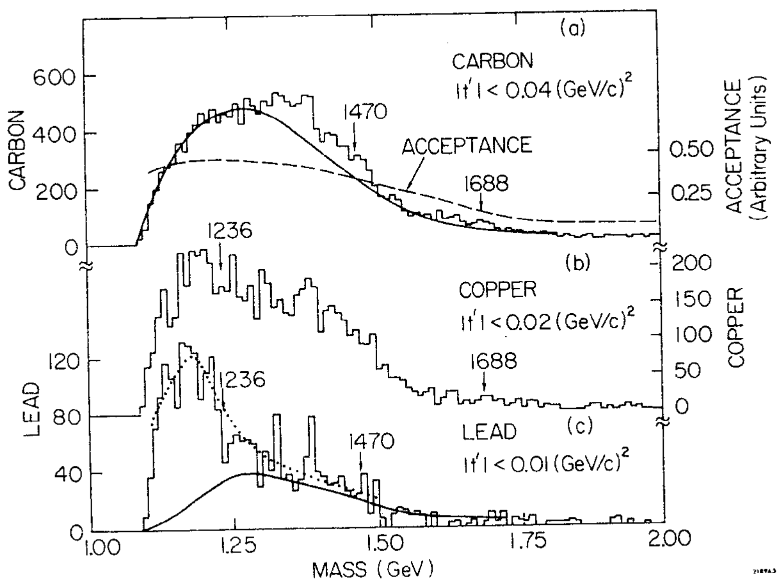

Figure 80

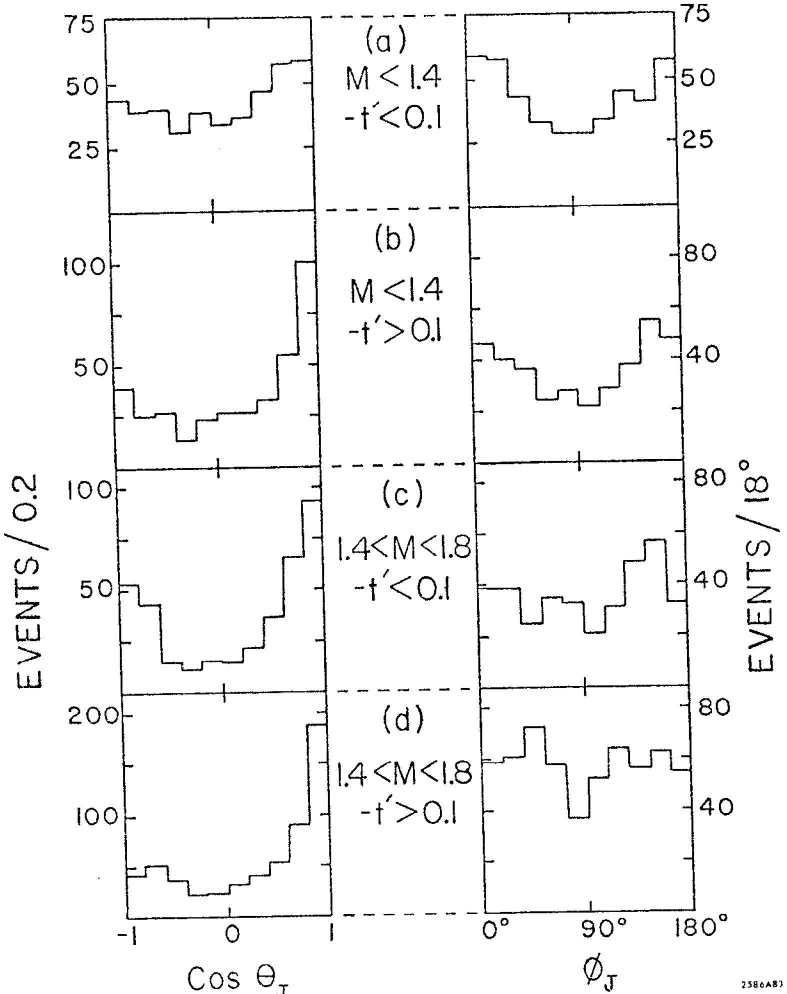

Figure 81

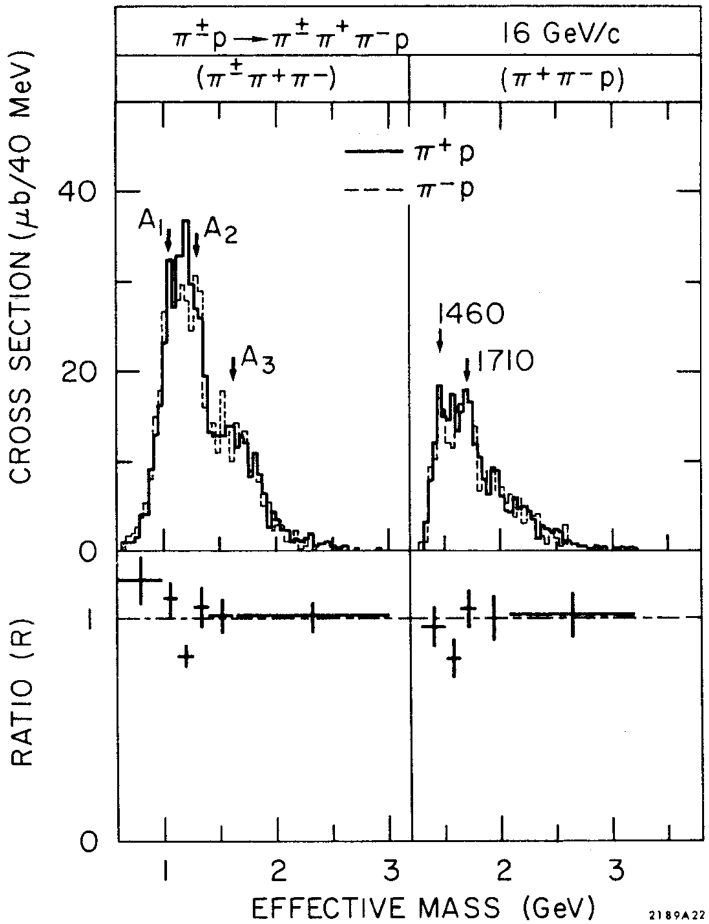

Figure 82

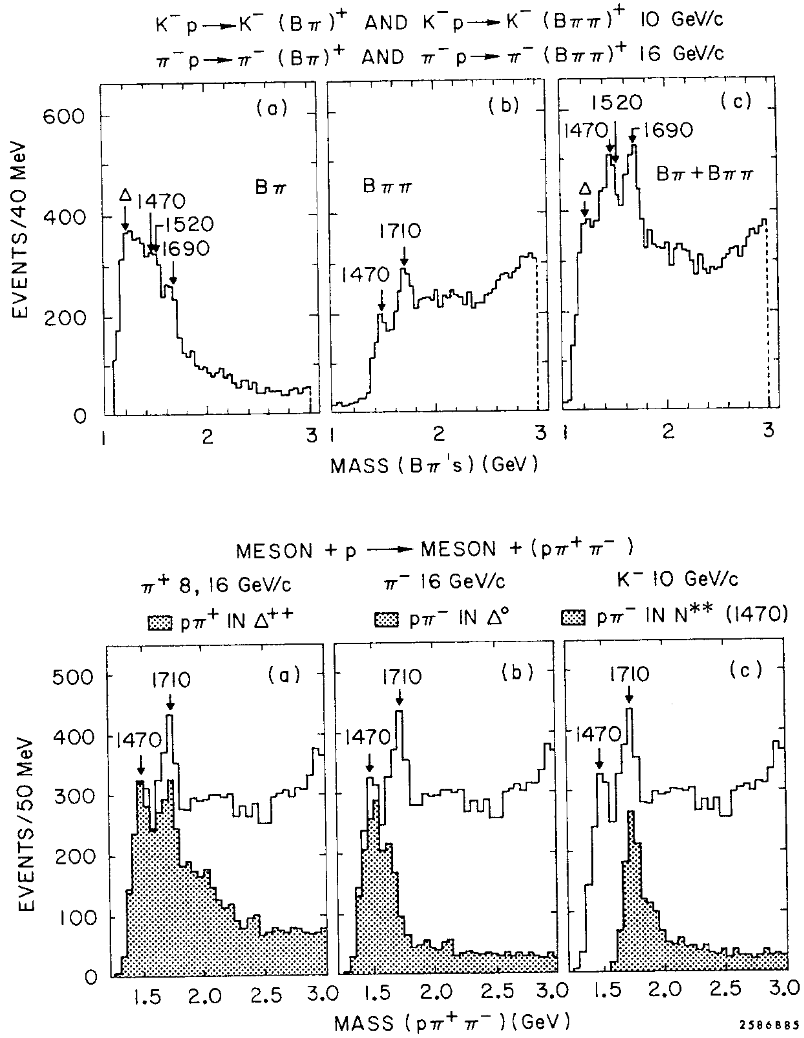

Figure 83

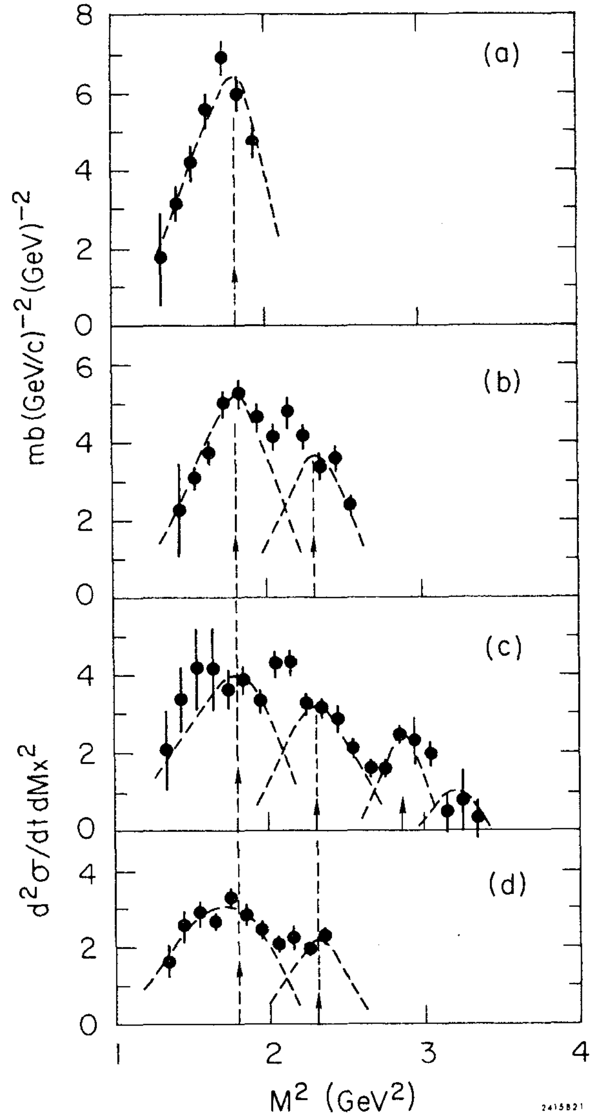

Figure 84

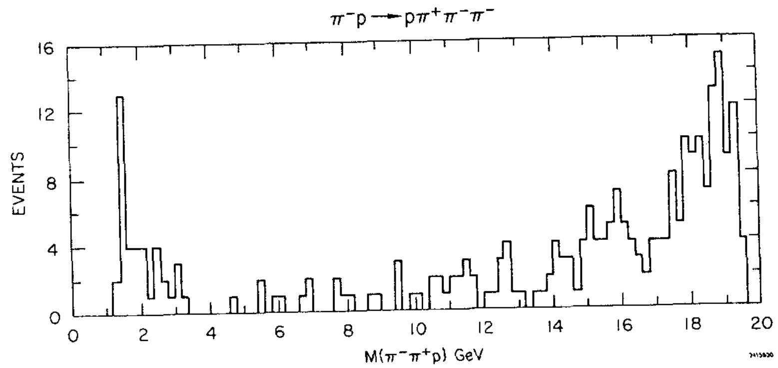

Figure 85

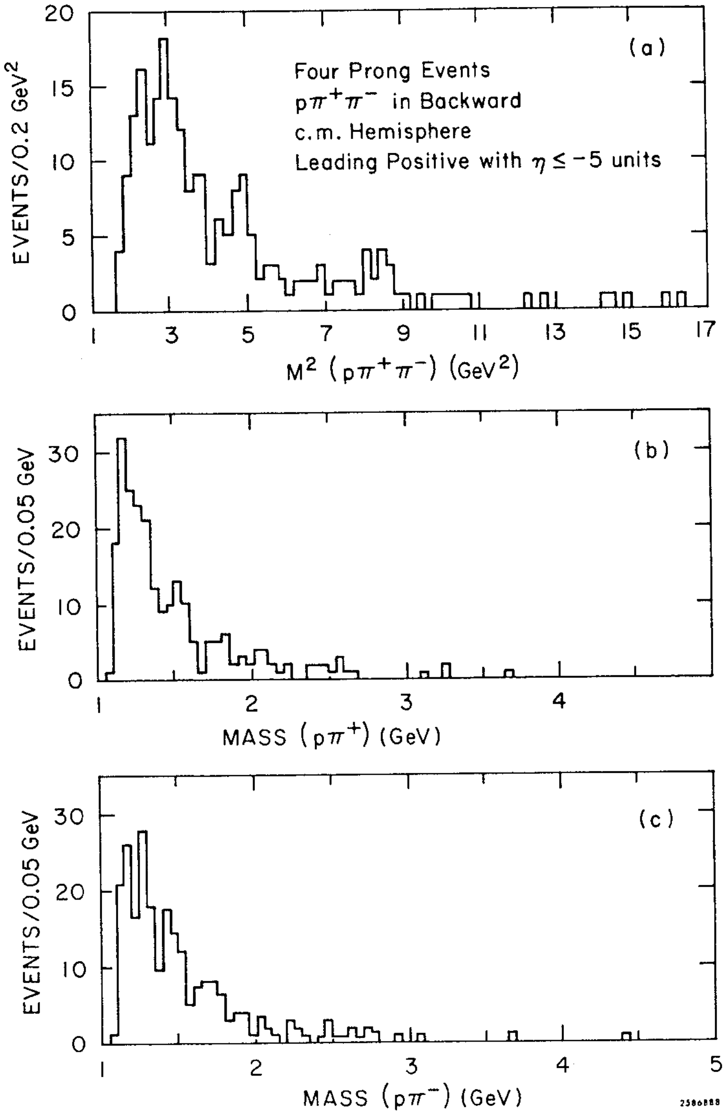

Figure 86

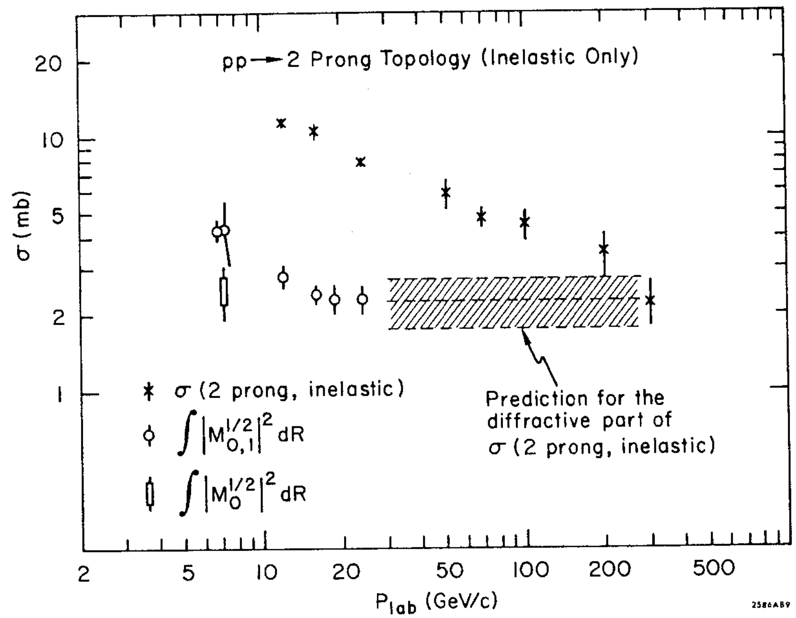

Figure 87

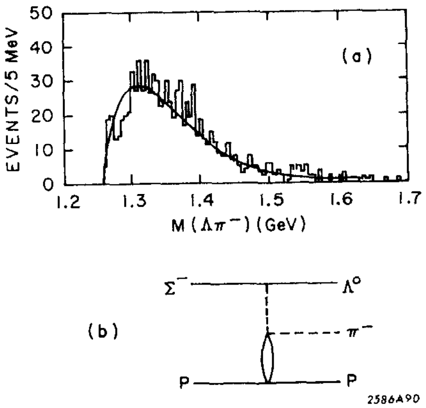

Figure 88

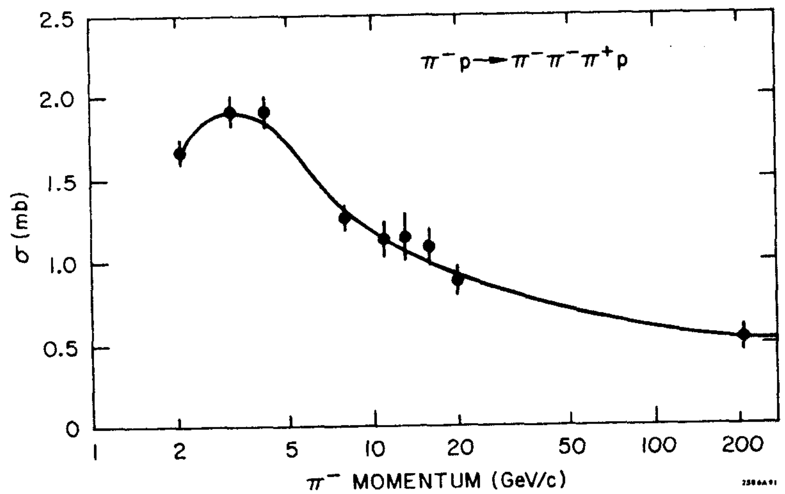

Figure 89

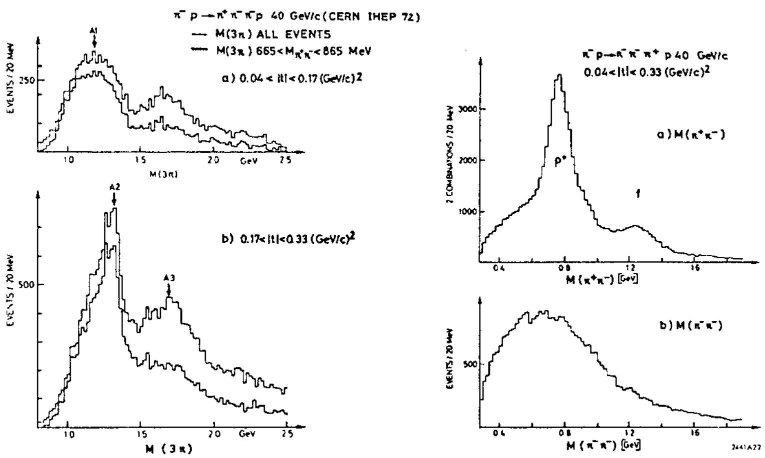

Figure 90

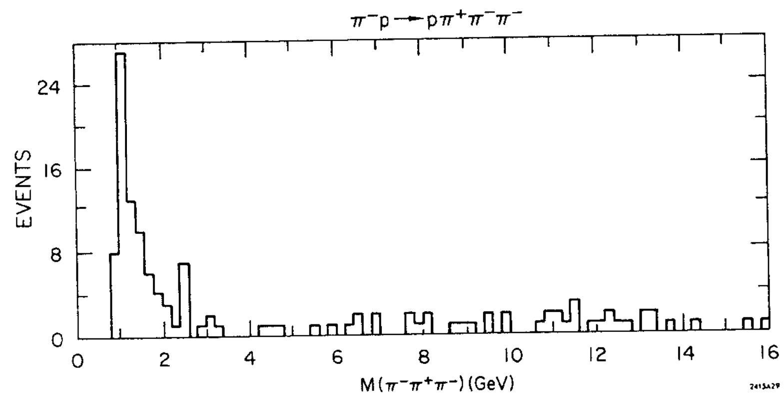

Figure 91

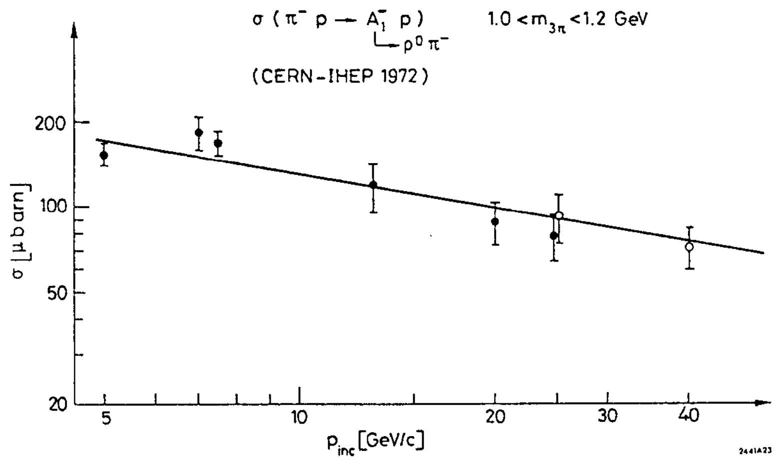

Figure 92

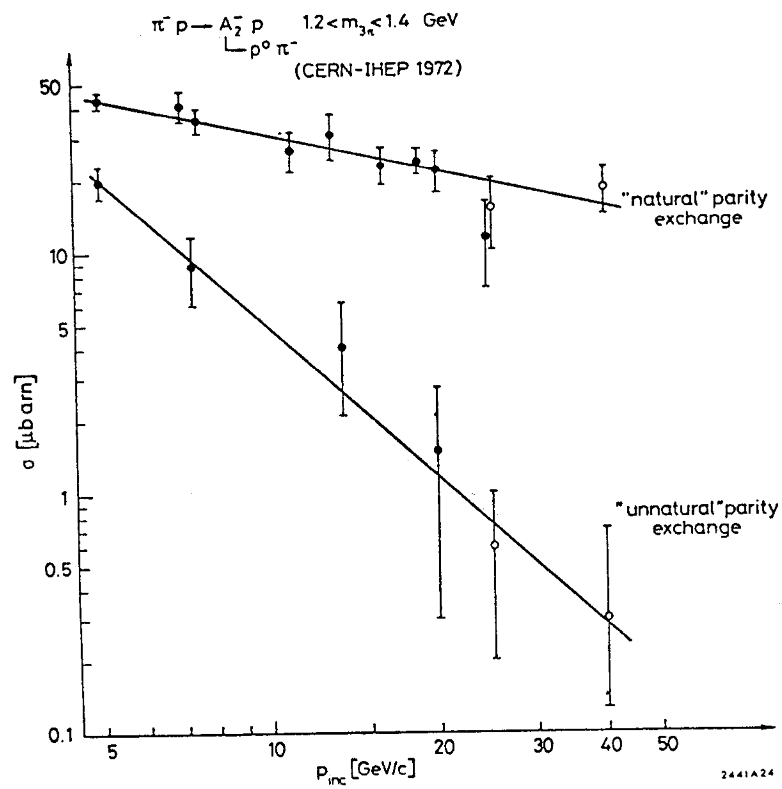

Figure 93

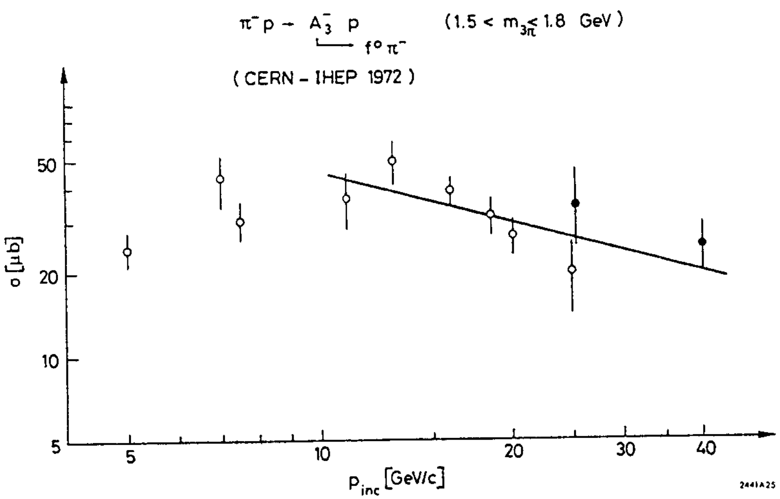

Figure 94

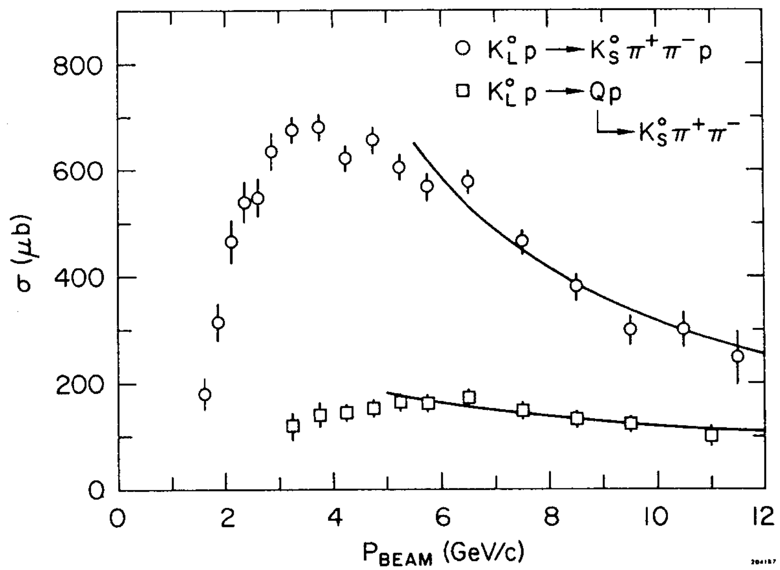

Figure 95

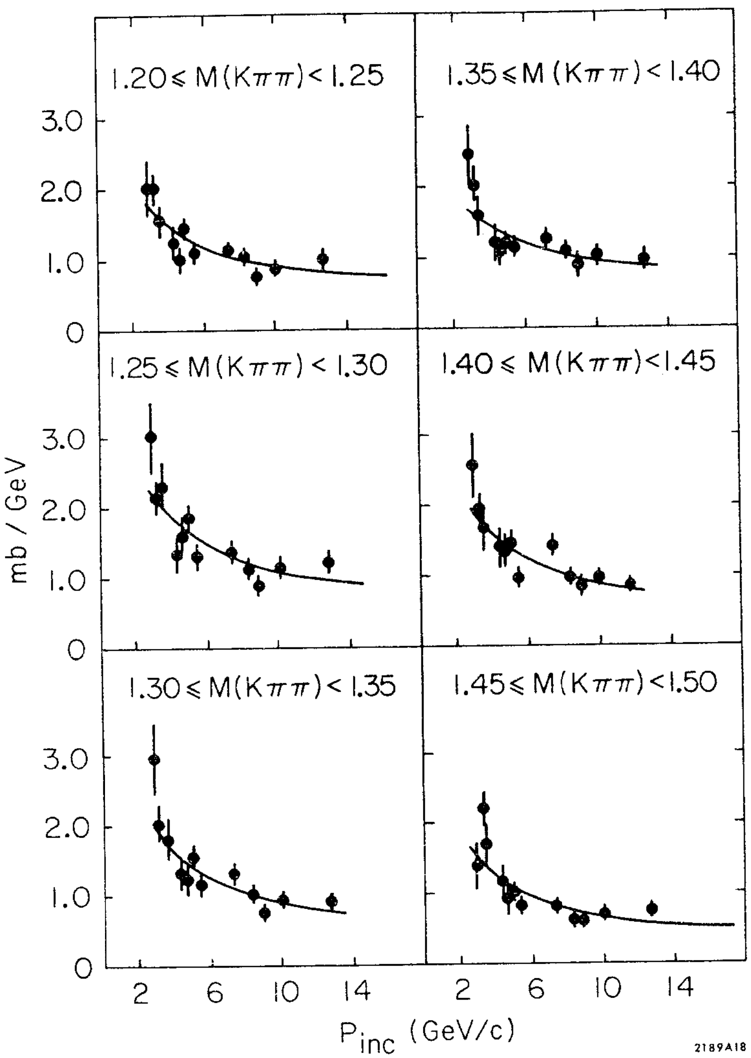

Figure 96

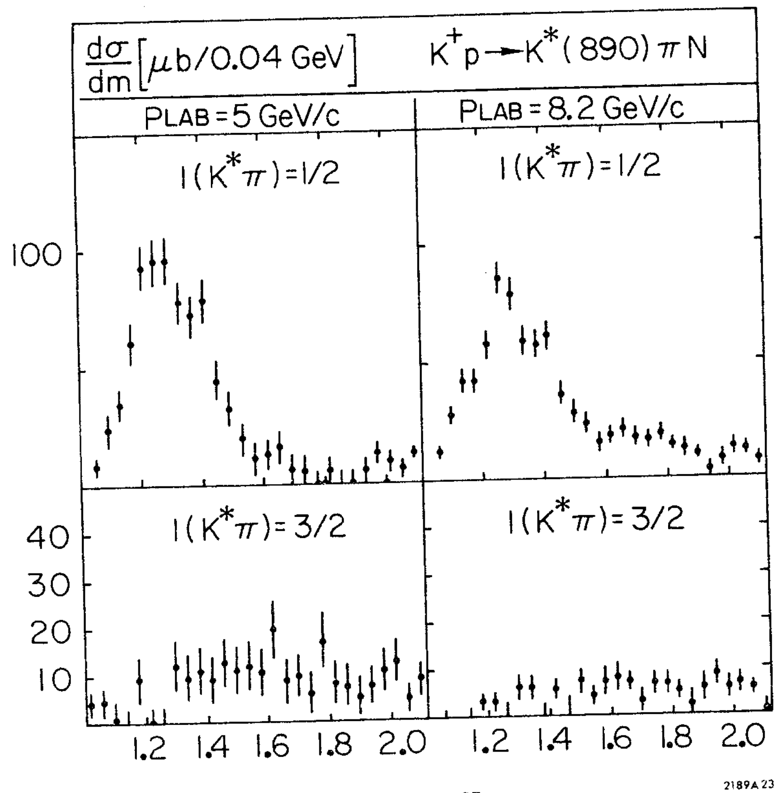

Figure 97

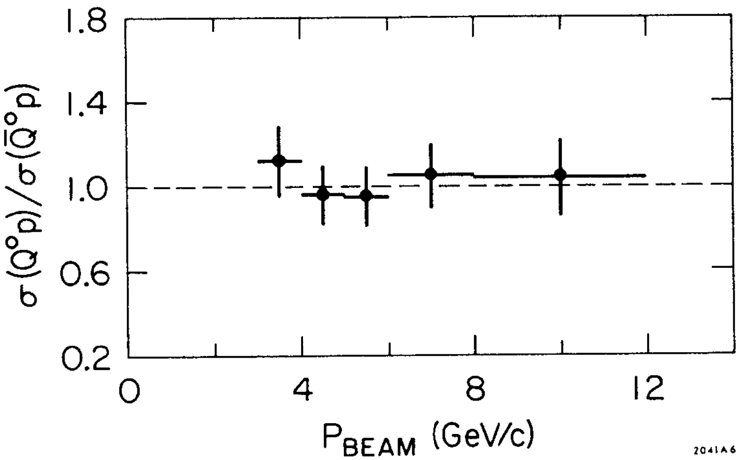

Figure 98

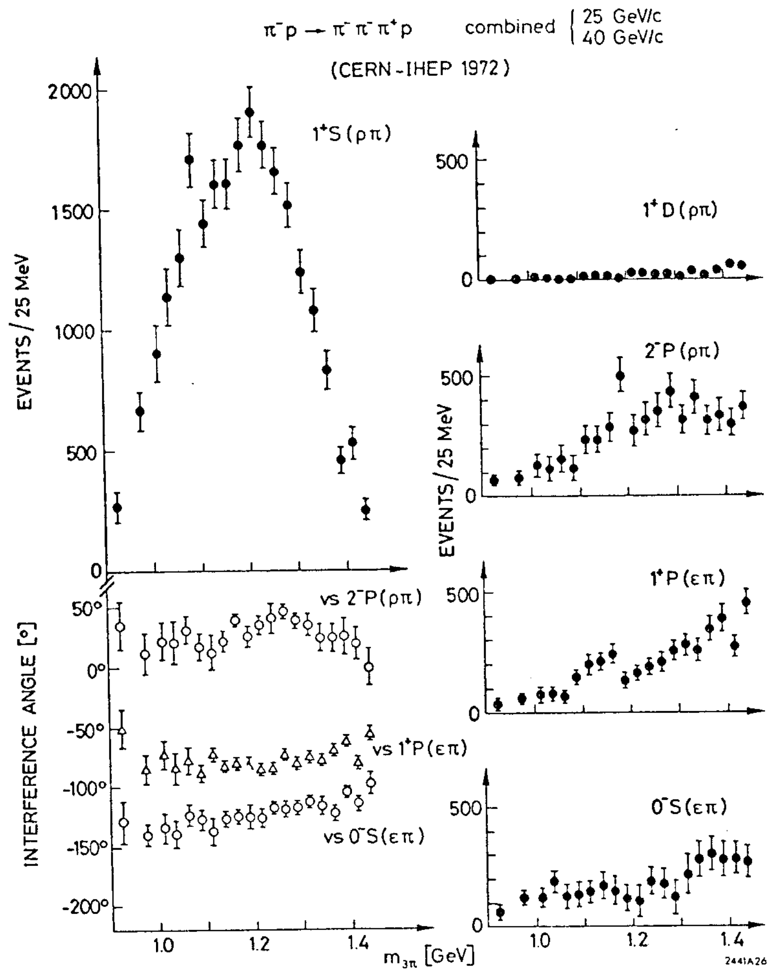

Figure 99

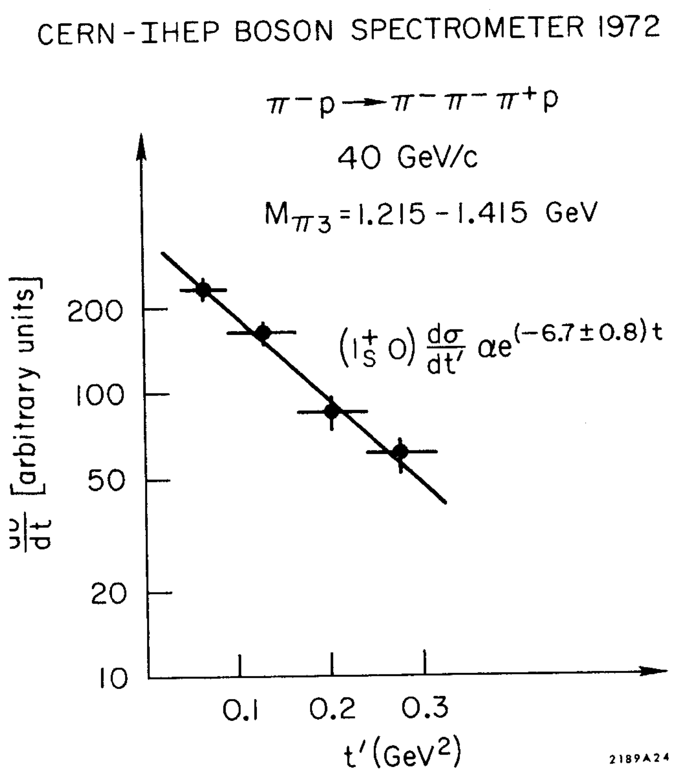

Figure 100

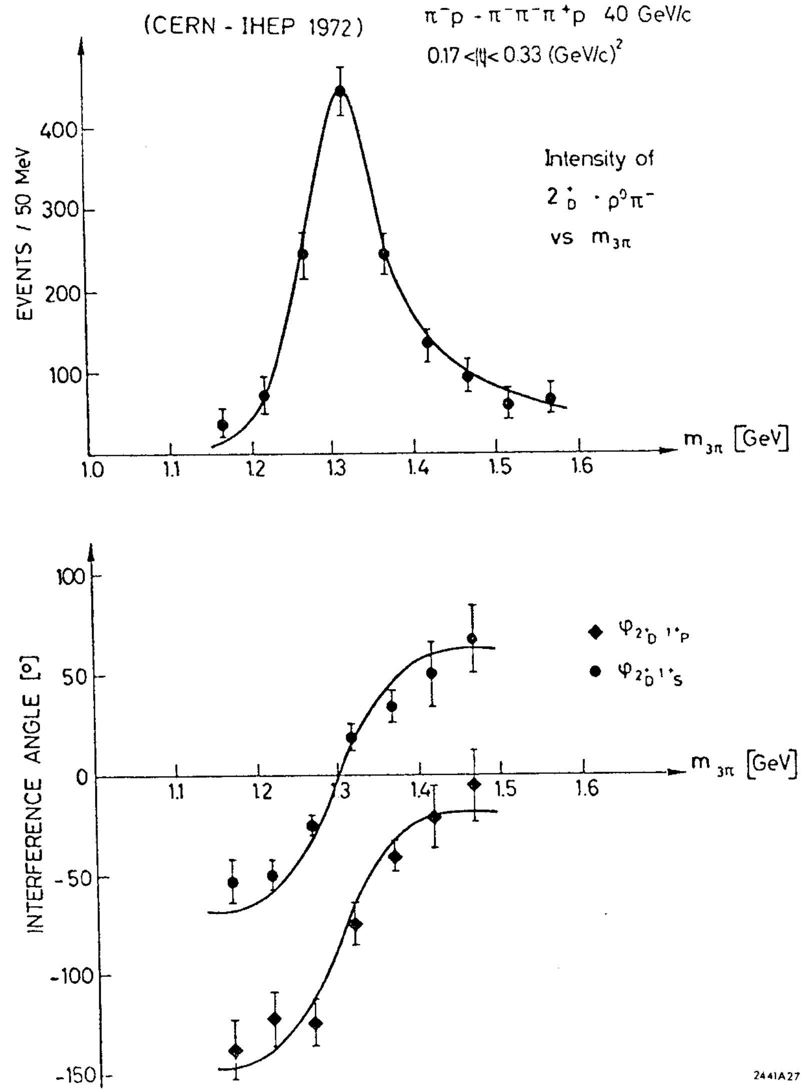

Figure 101

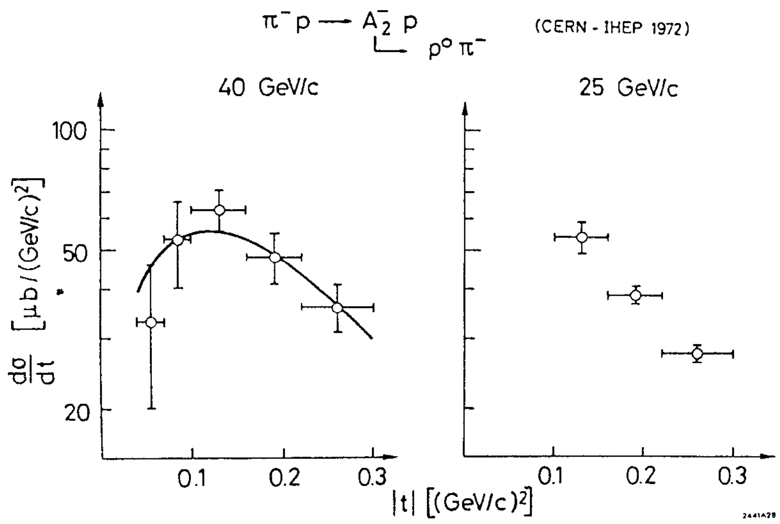

Figure 102

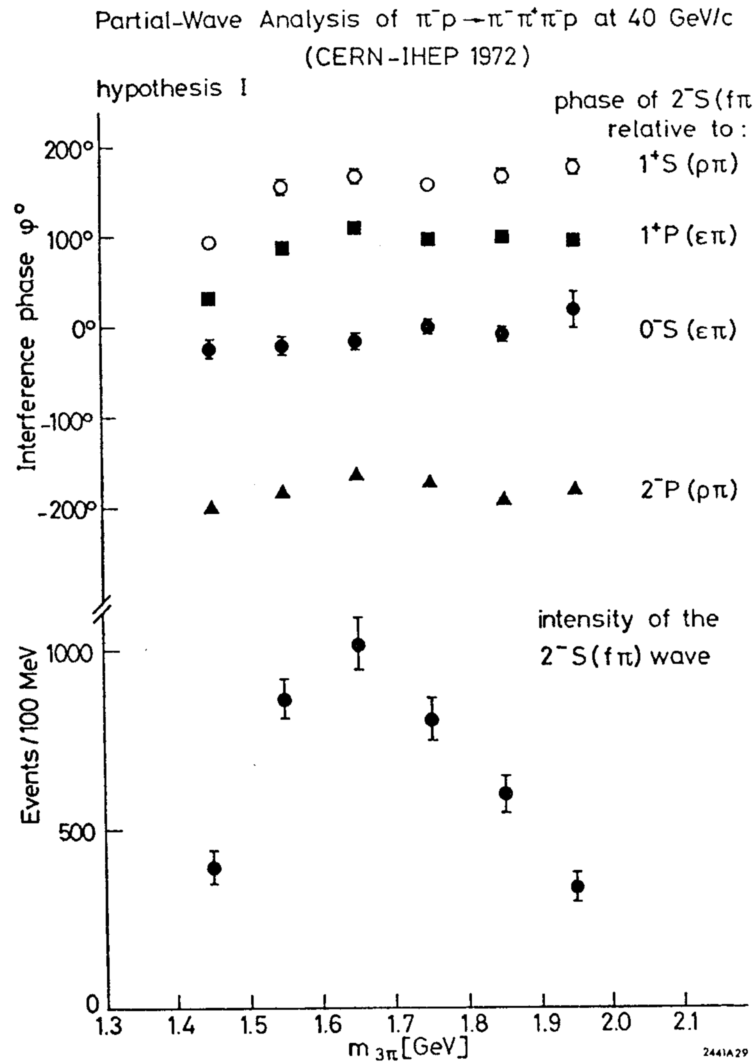

Figure 103

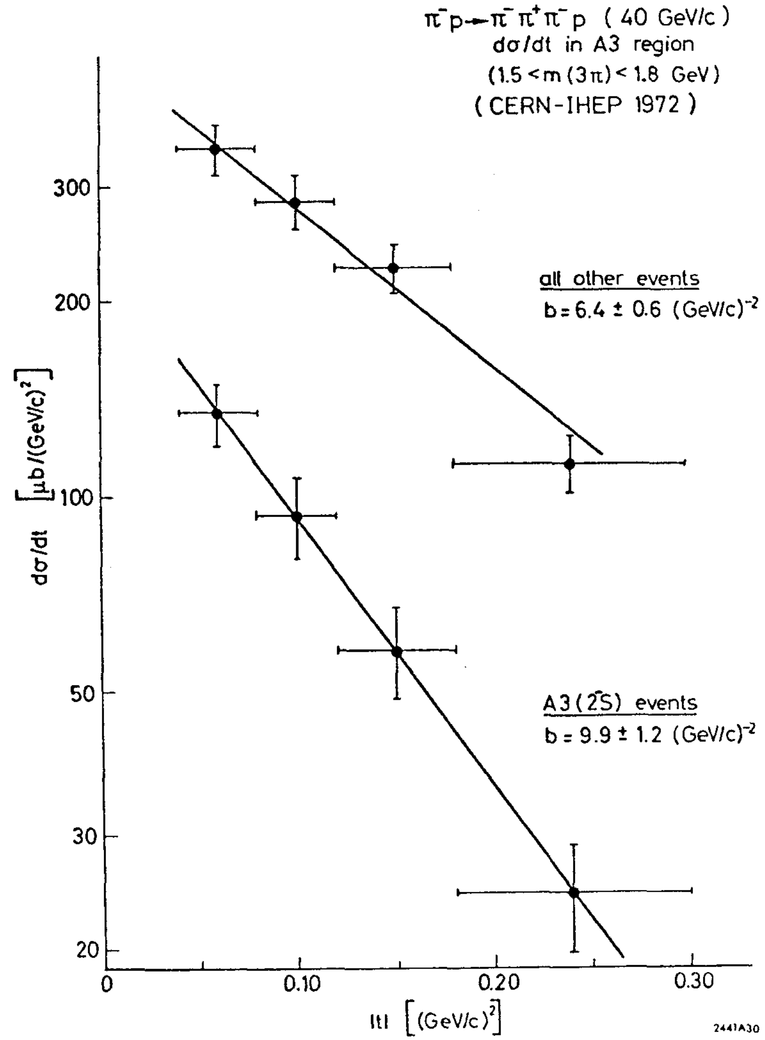

Figure 104

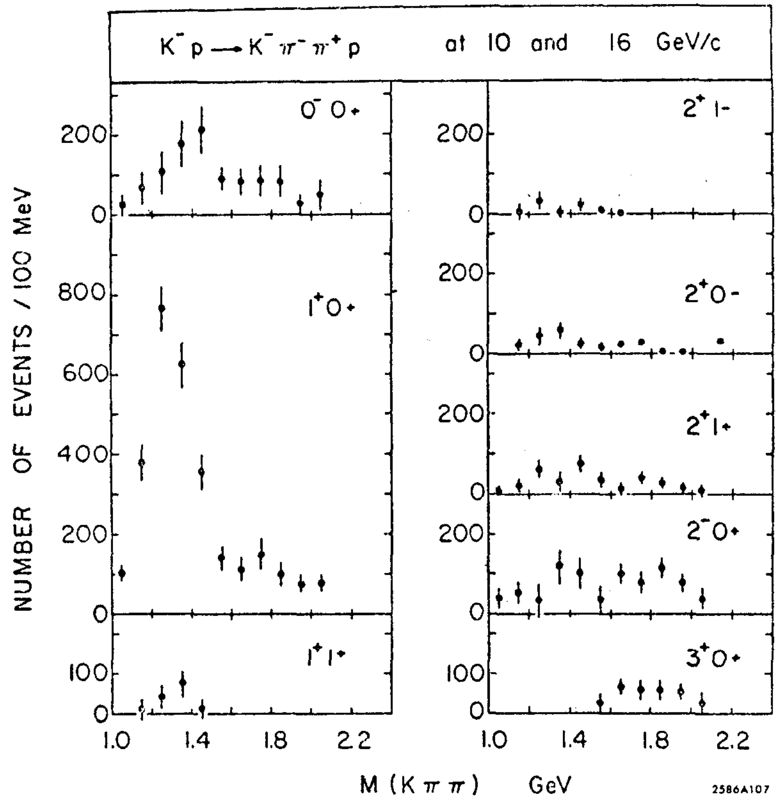

Figure 105

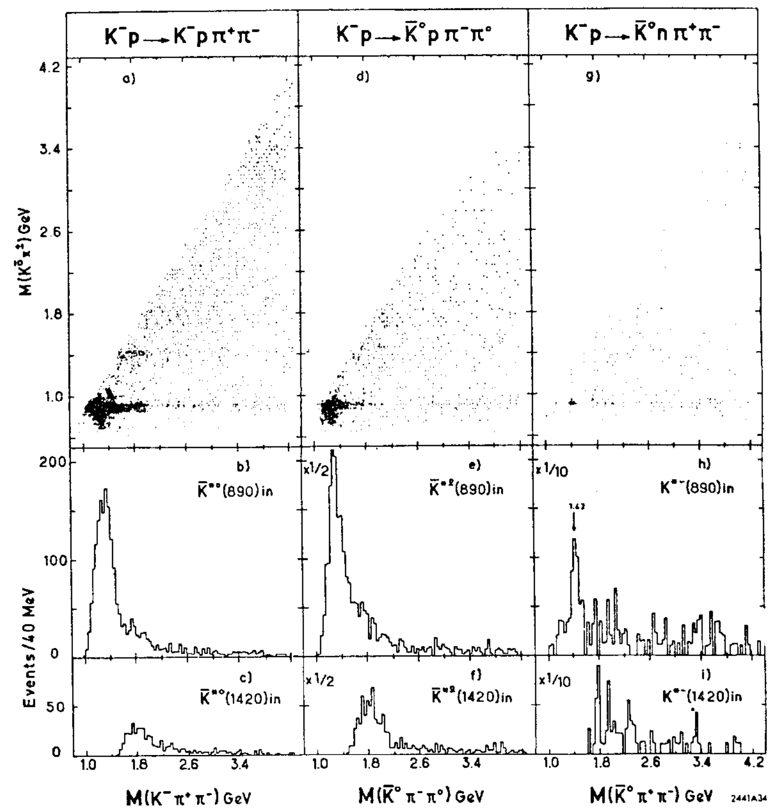

Figure 106

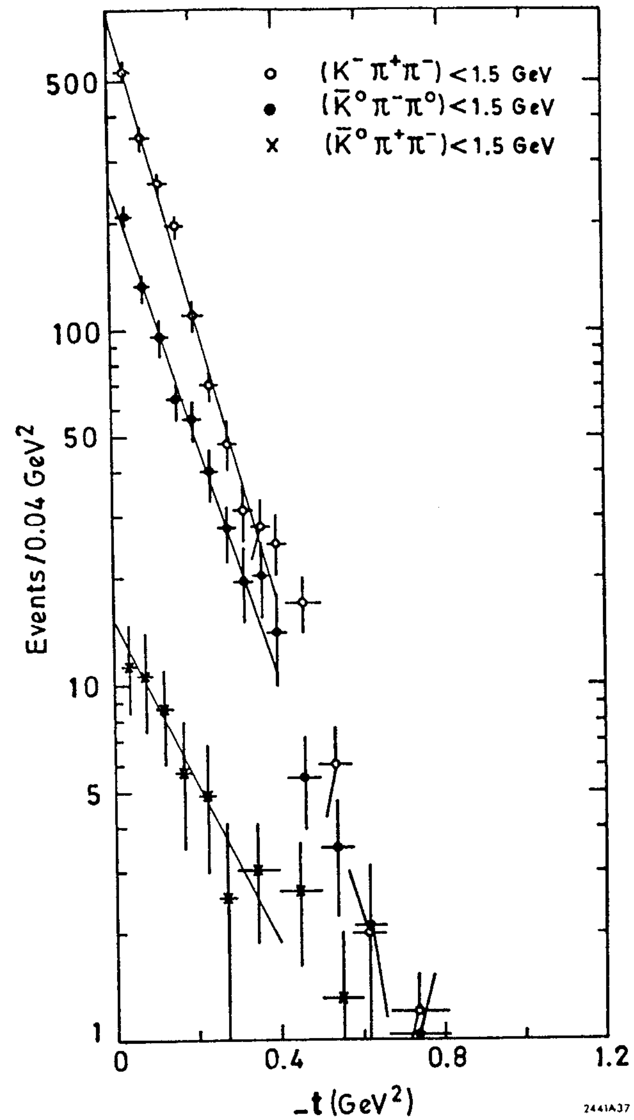

Figure 107

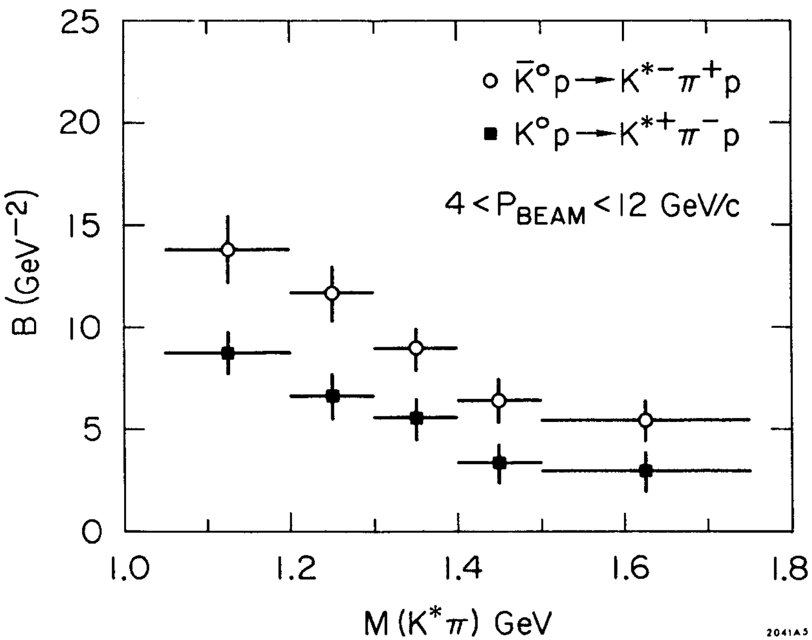

Figure 108

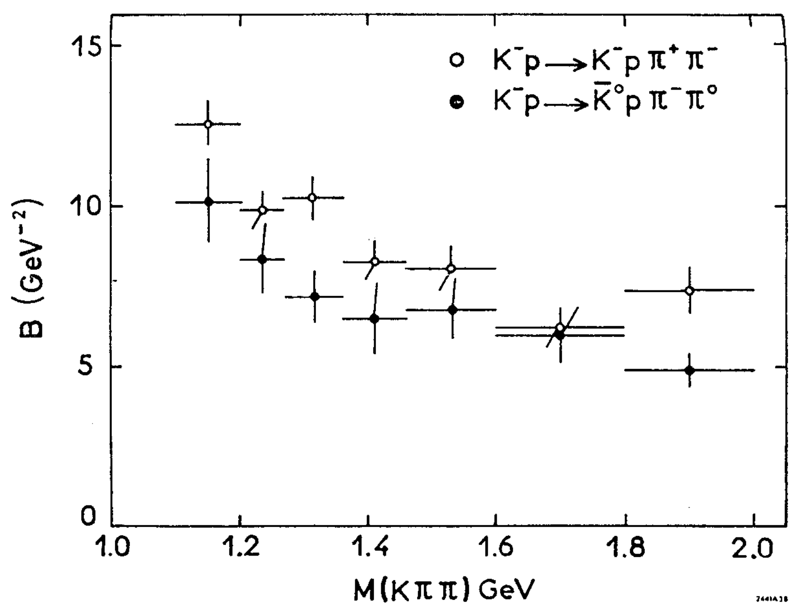

Figure 109

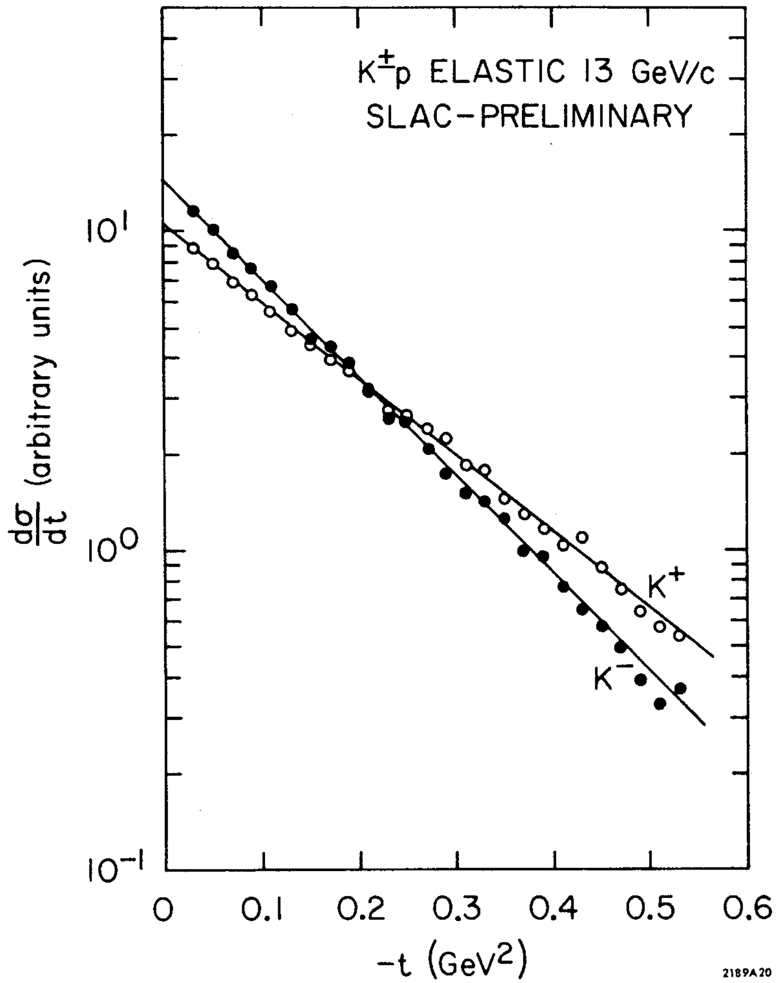

Figure 110

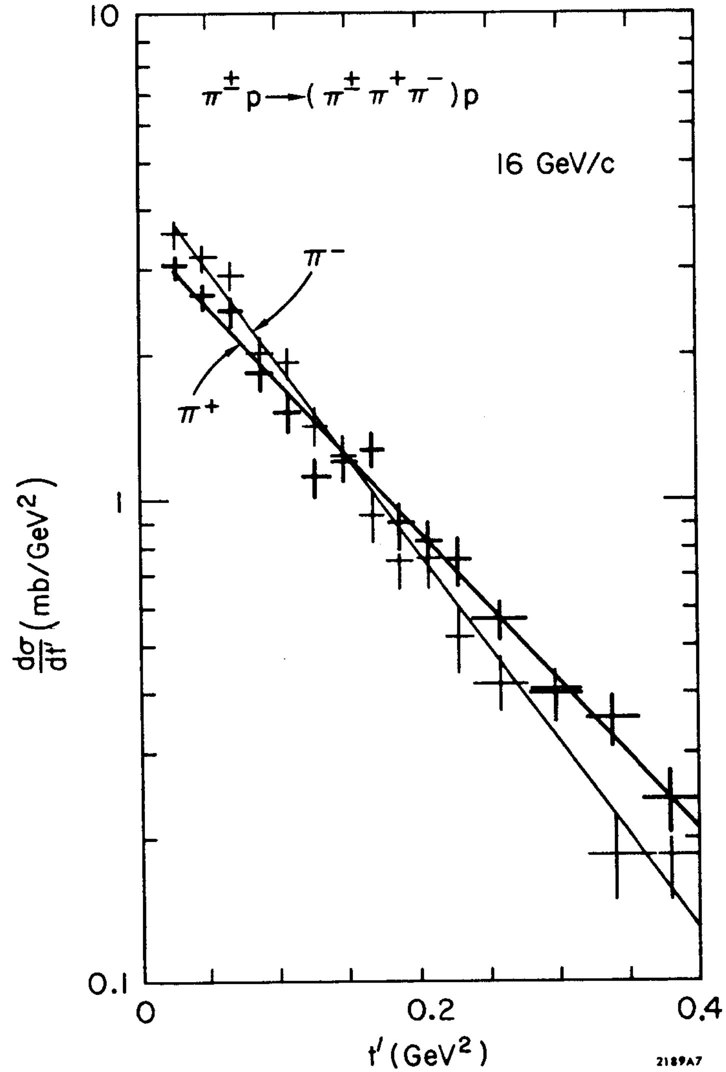

Figure 111

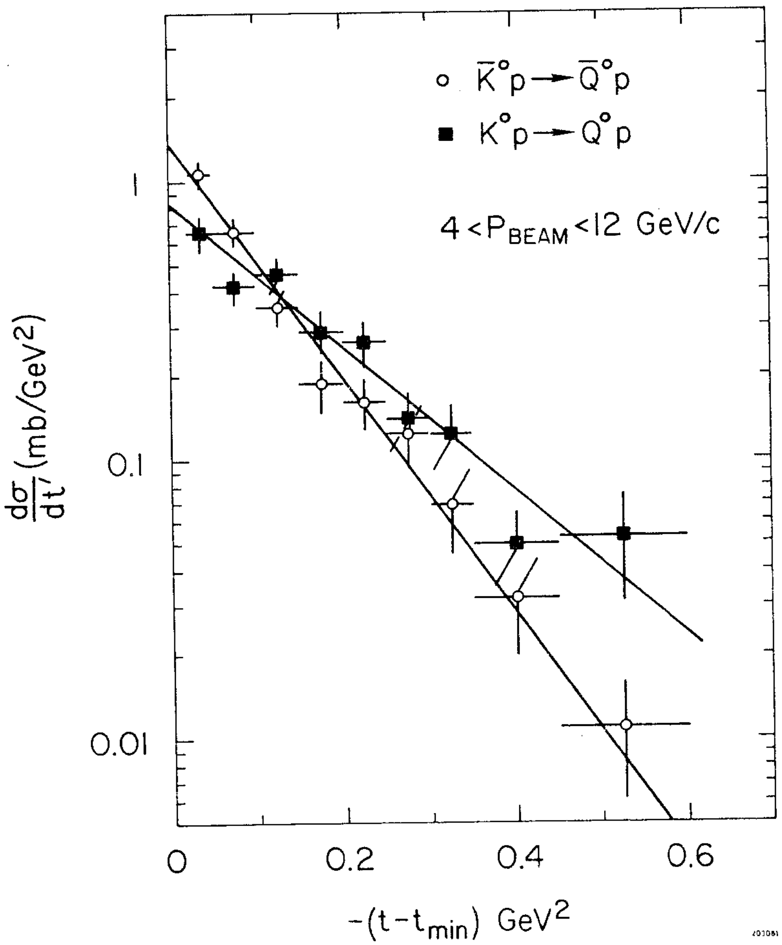

Figure 112

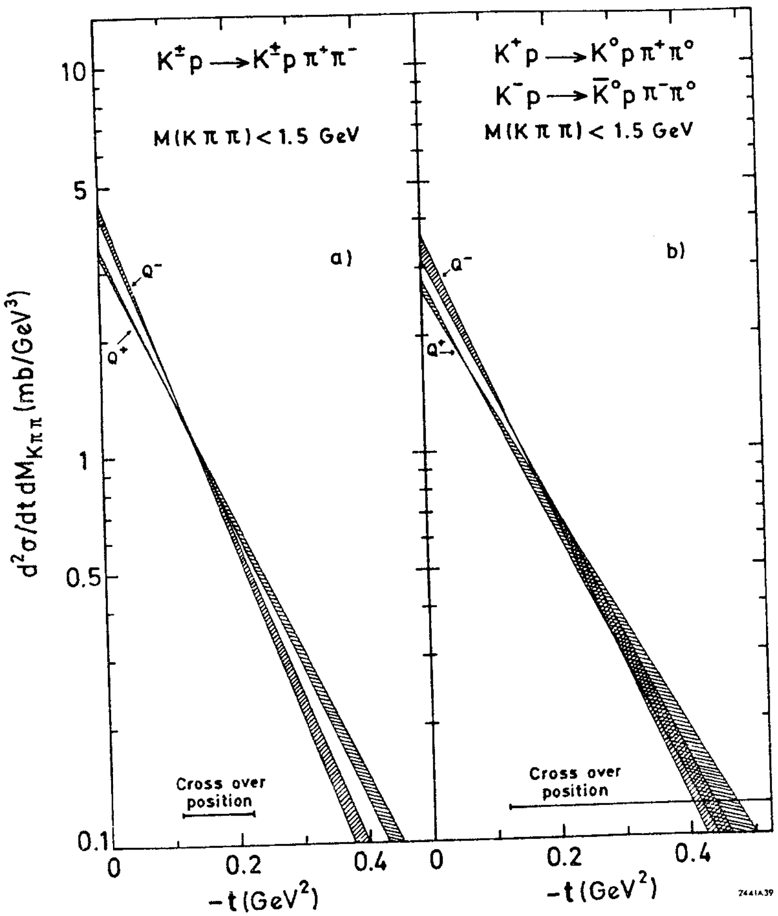

Figure 113

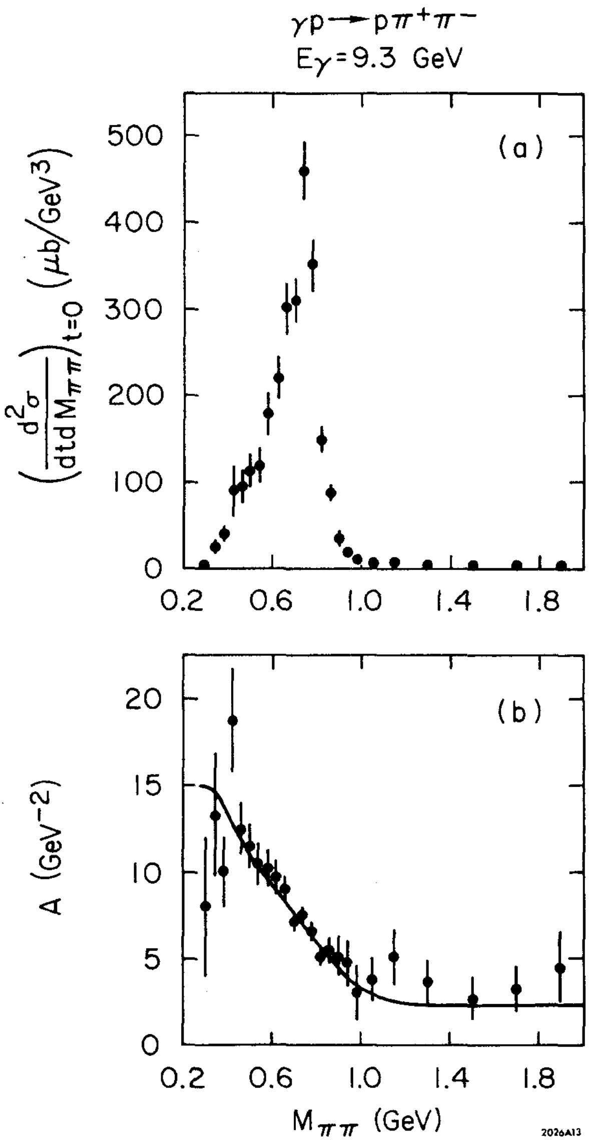

Figure 114

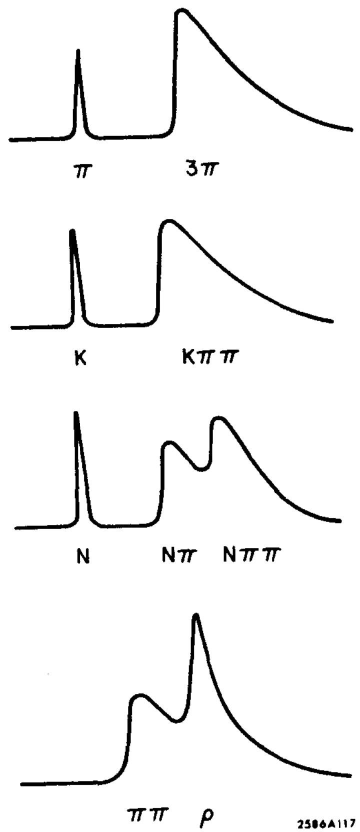

Figure 115

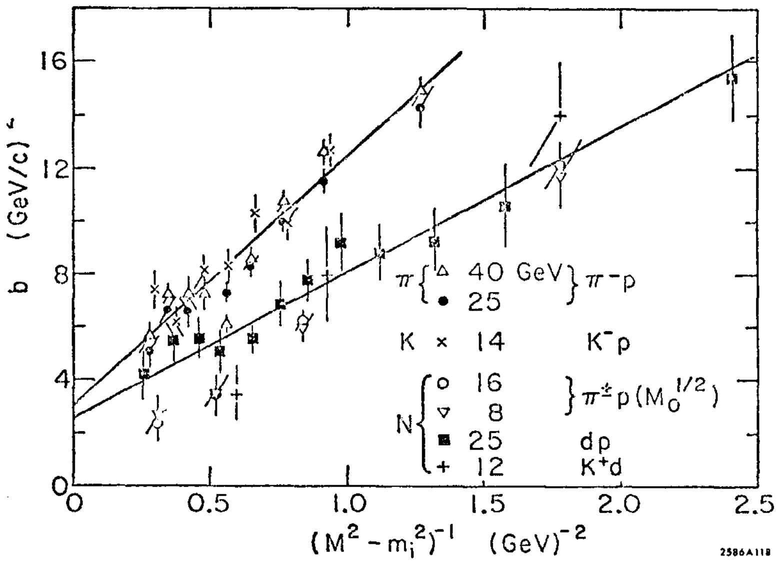

Figure 116

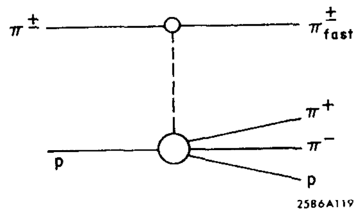

Figure 117

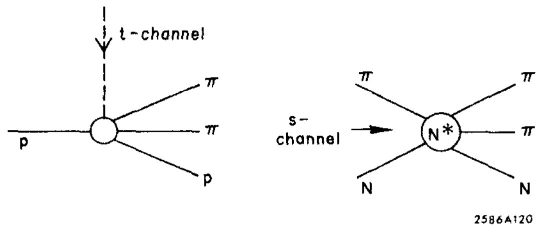

Figure 118

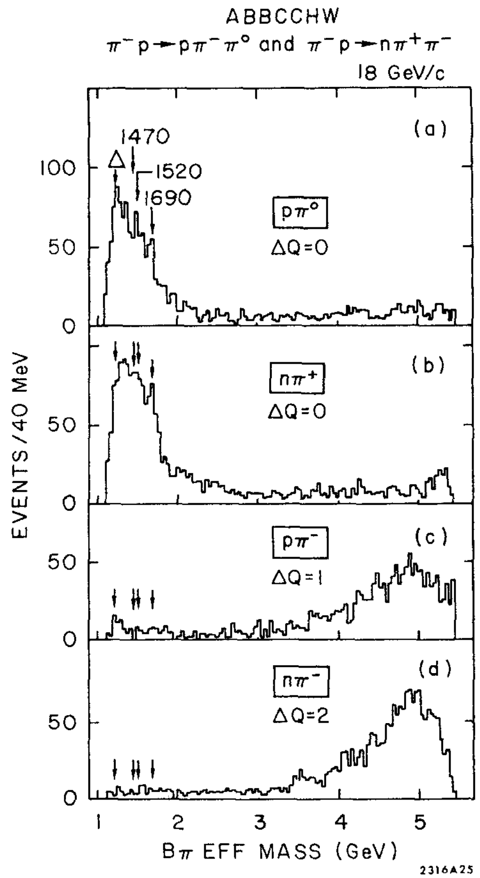

Figure 119

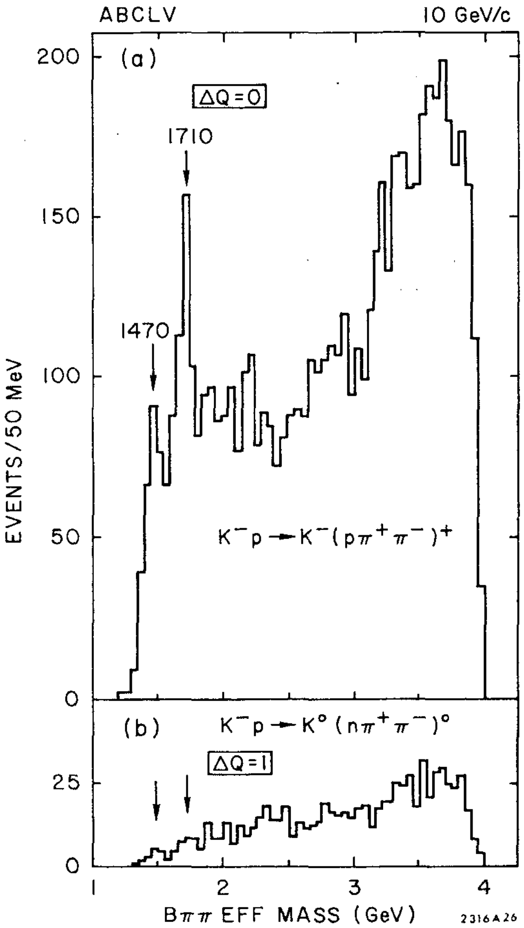

Figure 120

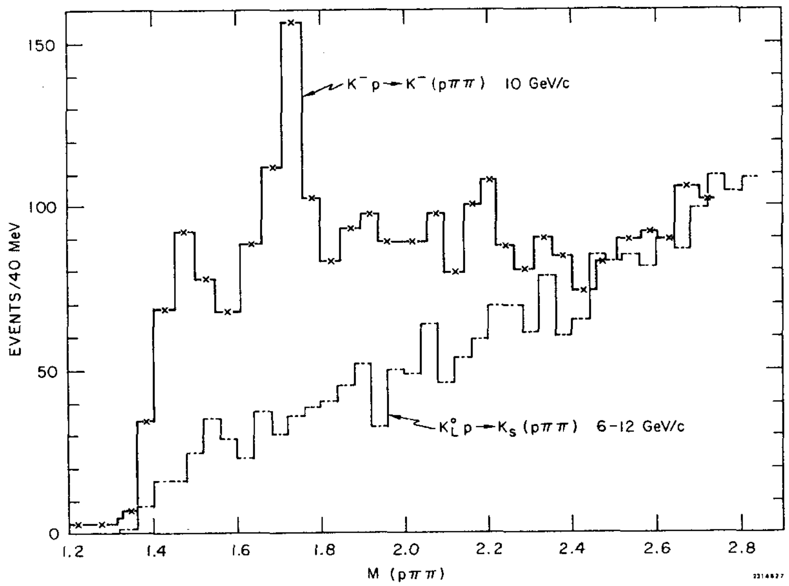

Figure 121

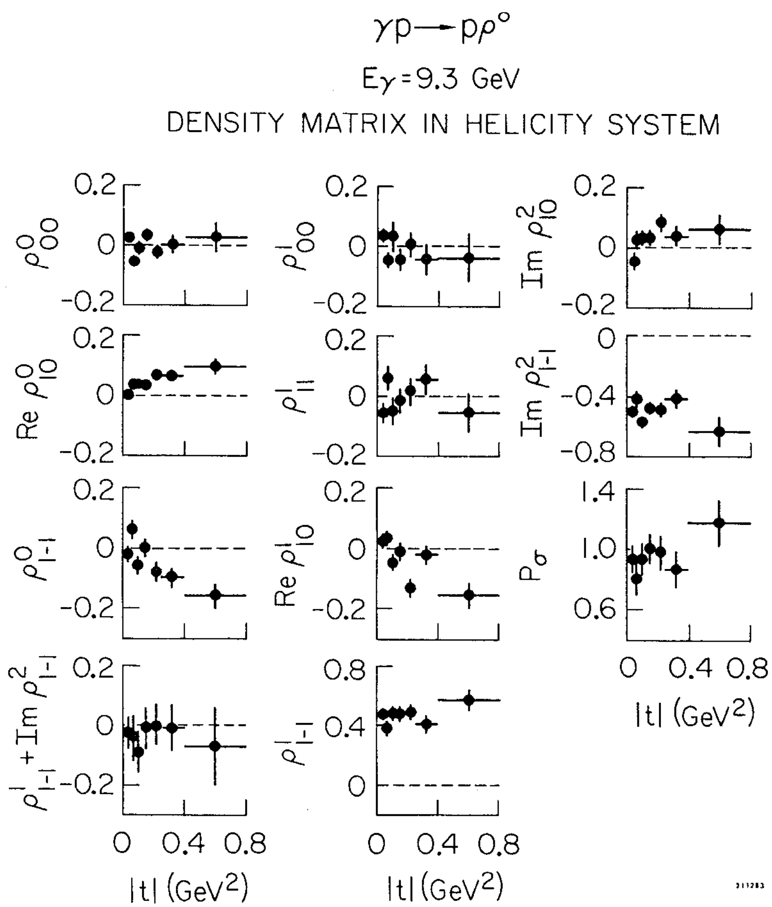

Figure 122

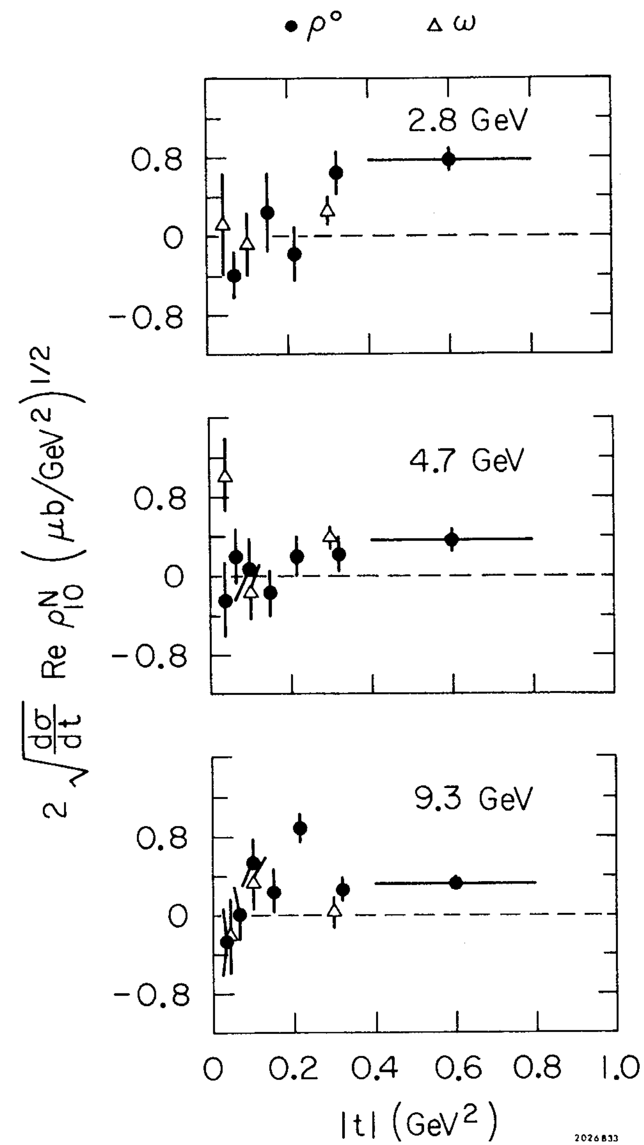

Figure 123

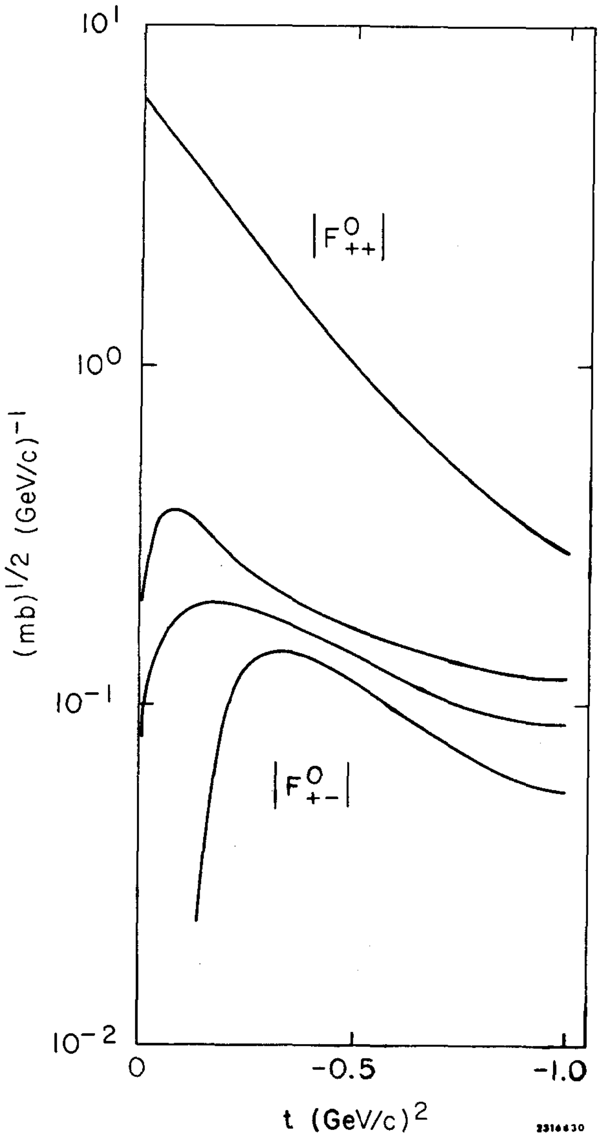

Figure 124

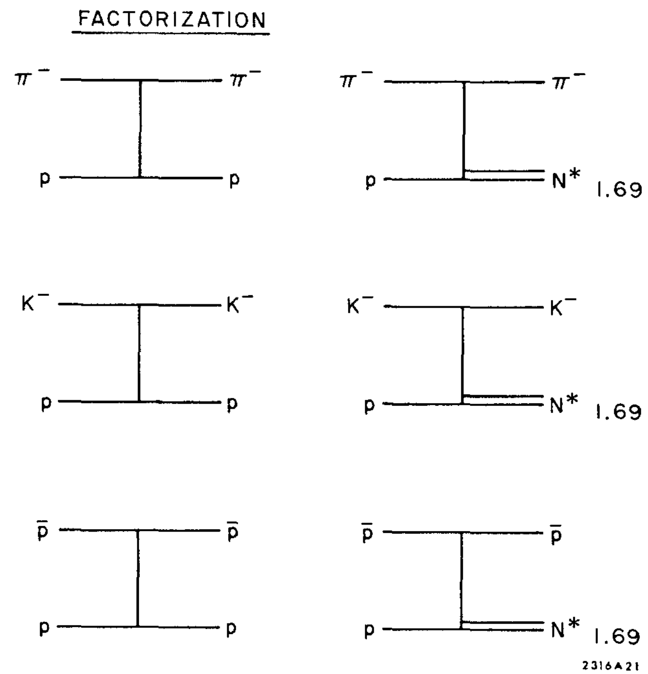

Figure 125

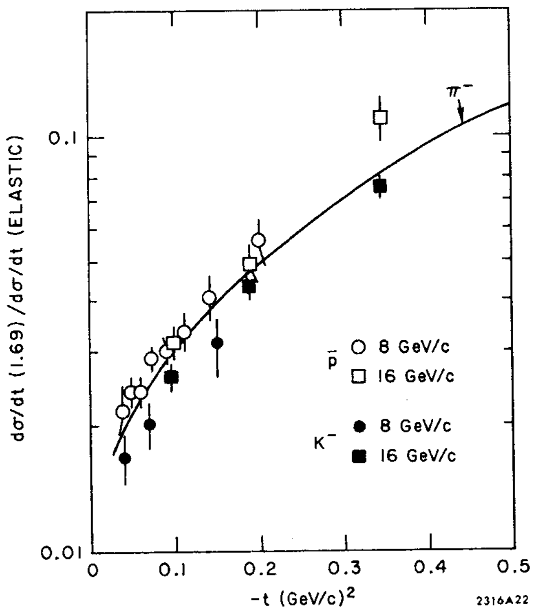

Figure 126

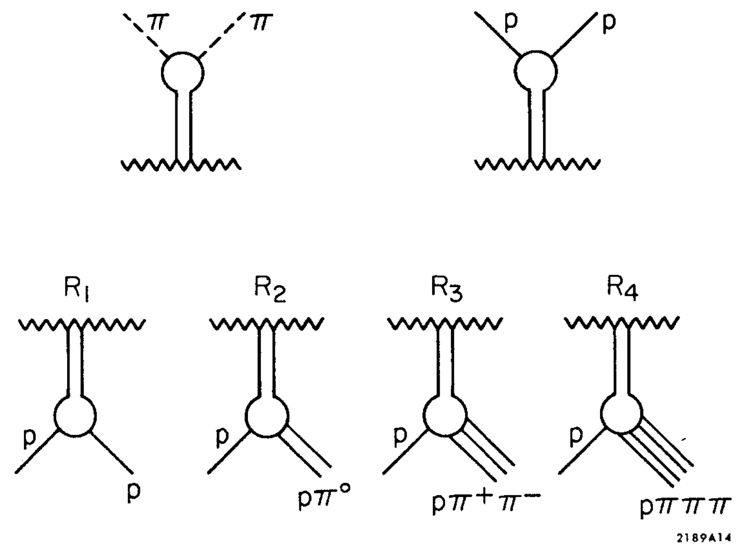

Figure 127

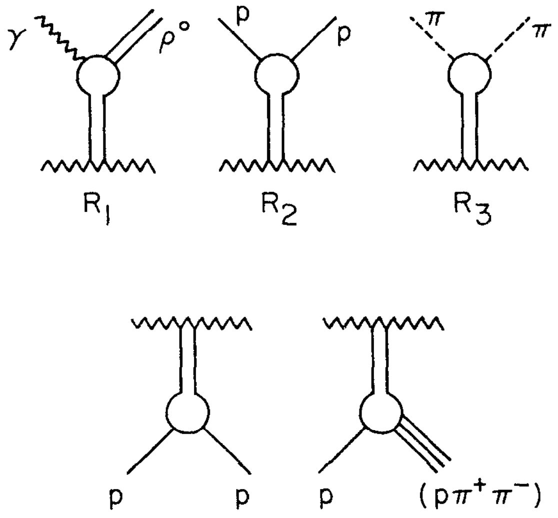

Figure 128

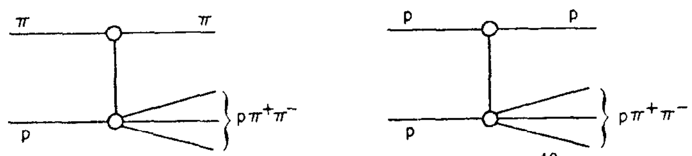

$\sigma_1 = 180 \pm 36\ \mu b$

$\sigma_1 \sim g^2_{\pi\pi \mathbb{P}*}\, g^2_{pp*\mathbb{P}}$

$\sigma_2 = 370 \pm {}^{40}_{140}\ \mu b$

$\sigma_2 \sim g^2_{pp\mathbb{P}*}\, g^2_{pp*\mathbb{P}}$

$$\frac{\sigma_1}{\sigma_2} = \frac{g^2_{\pi\pi\mathbb{P}}}{g^2_{pp\mathbb{P}}} = \frac{\sigma^{\text{elastic}}_{\pi p}}{\sigma^{\text{elastic}}_{pp}} = \frac{3.0 \pm 0.3}{6.8 \pm 0.2} = 0.44 \pm 0.05$$

$= 0.5.$

2586A131

Figure 129

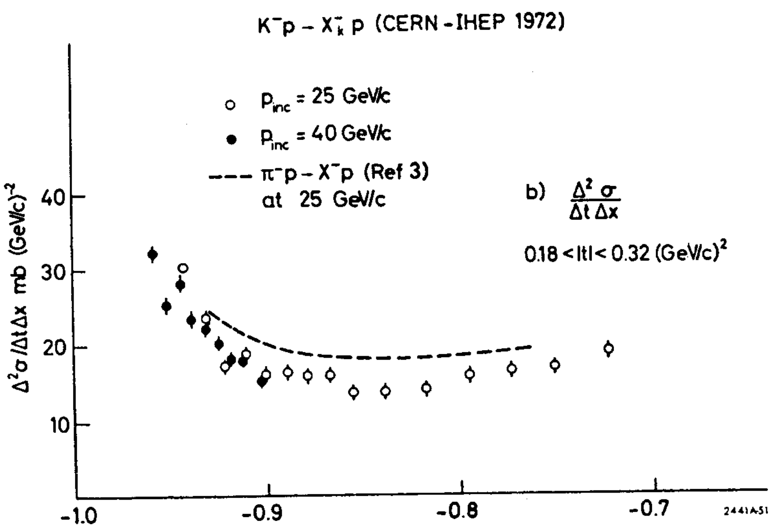

Figure 130

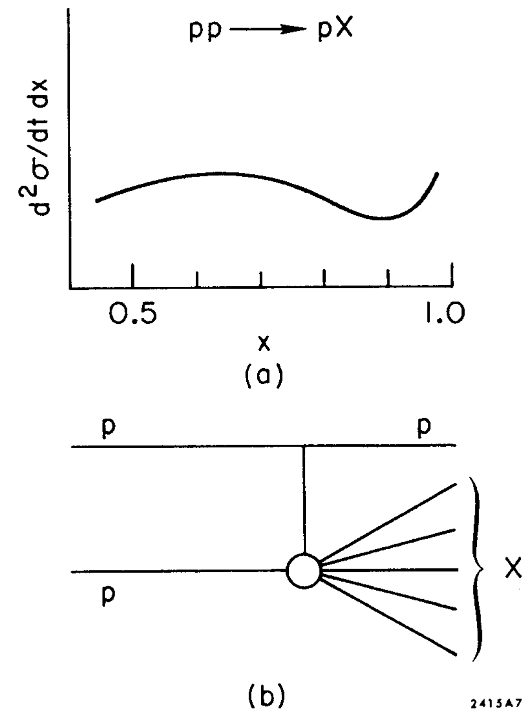

Figure 131

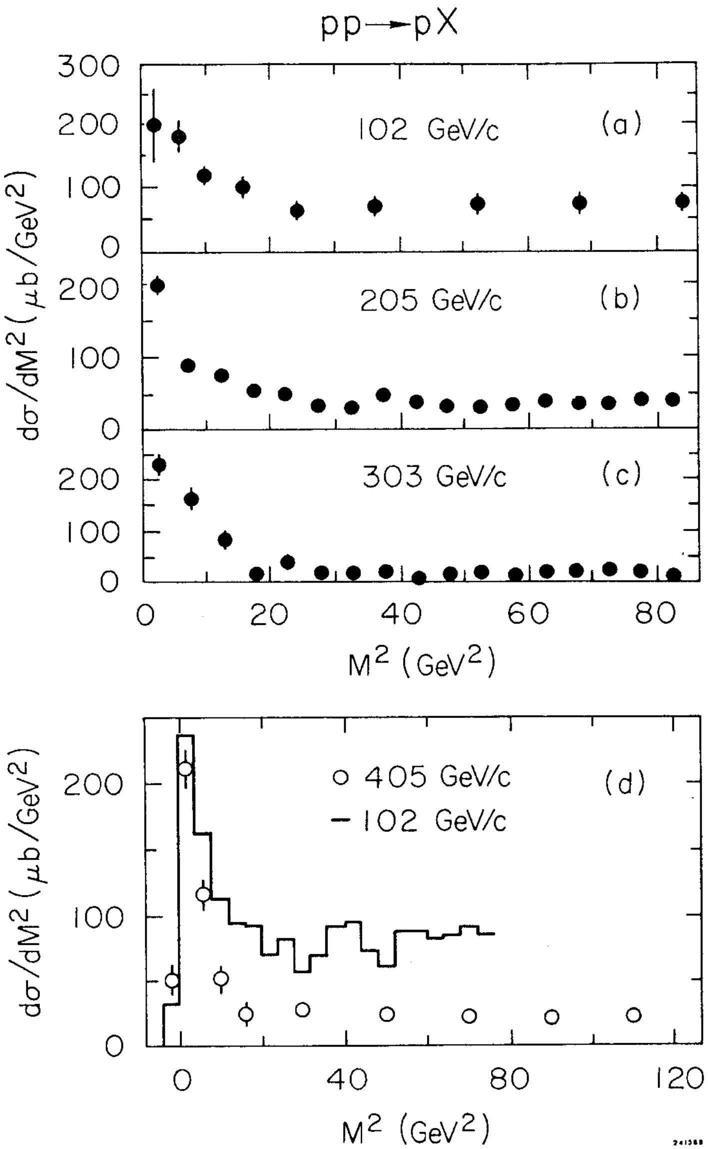

Figure 132

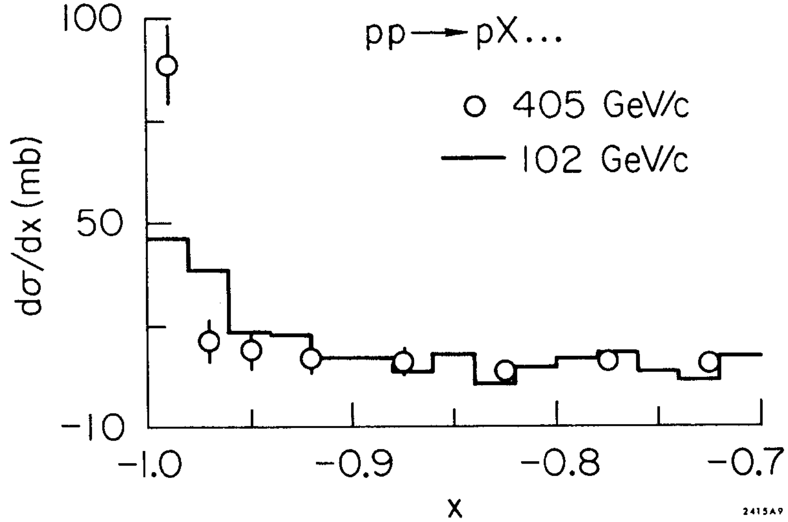

Figure 133

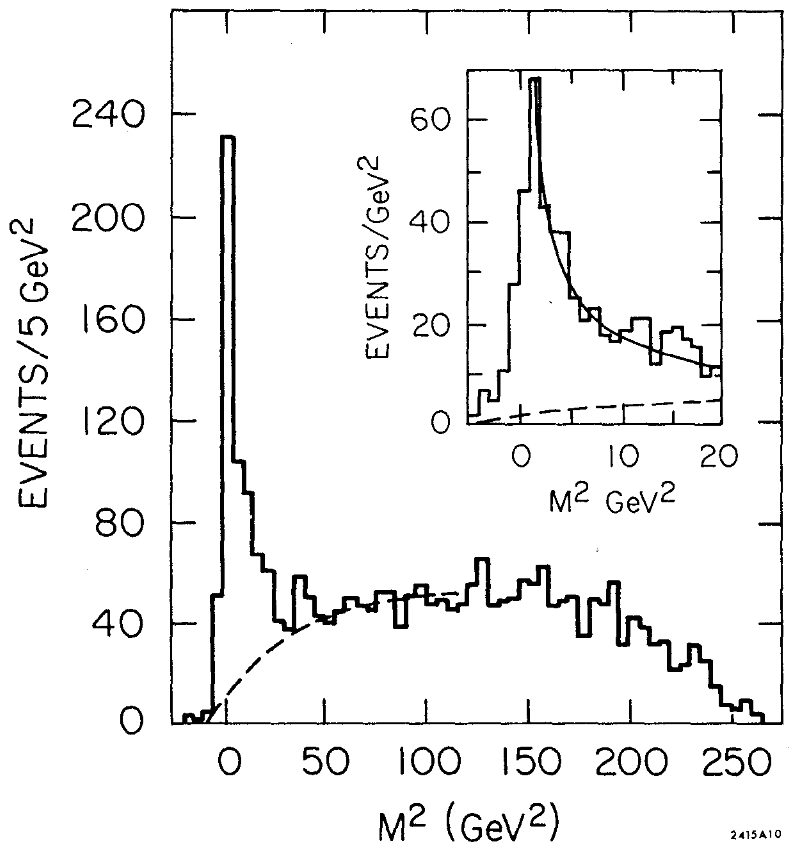

Figure 134

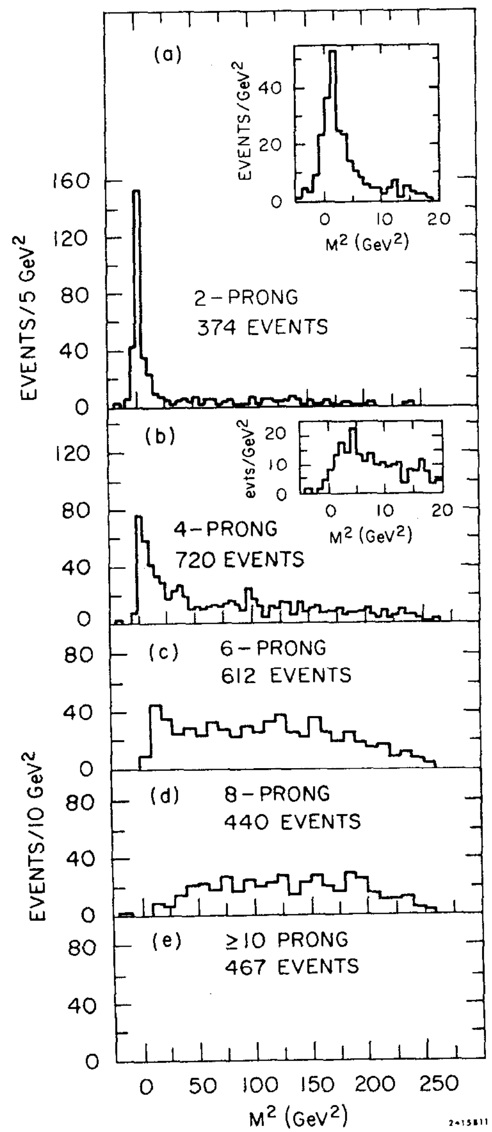

Figure 135

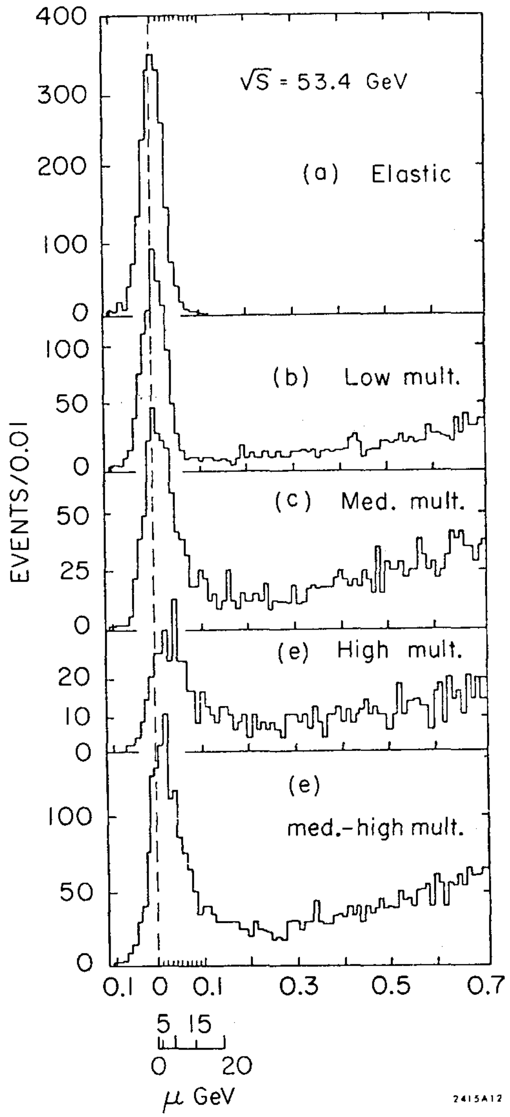

Figure 136

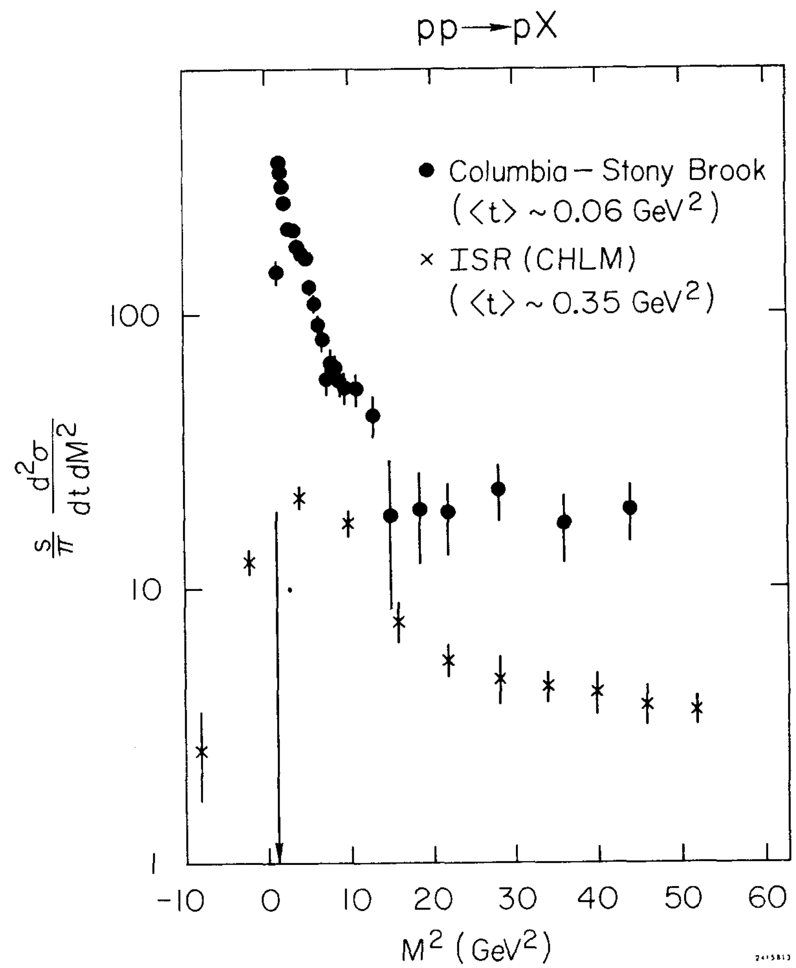

Figure 137

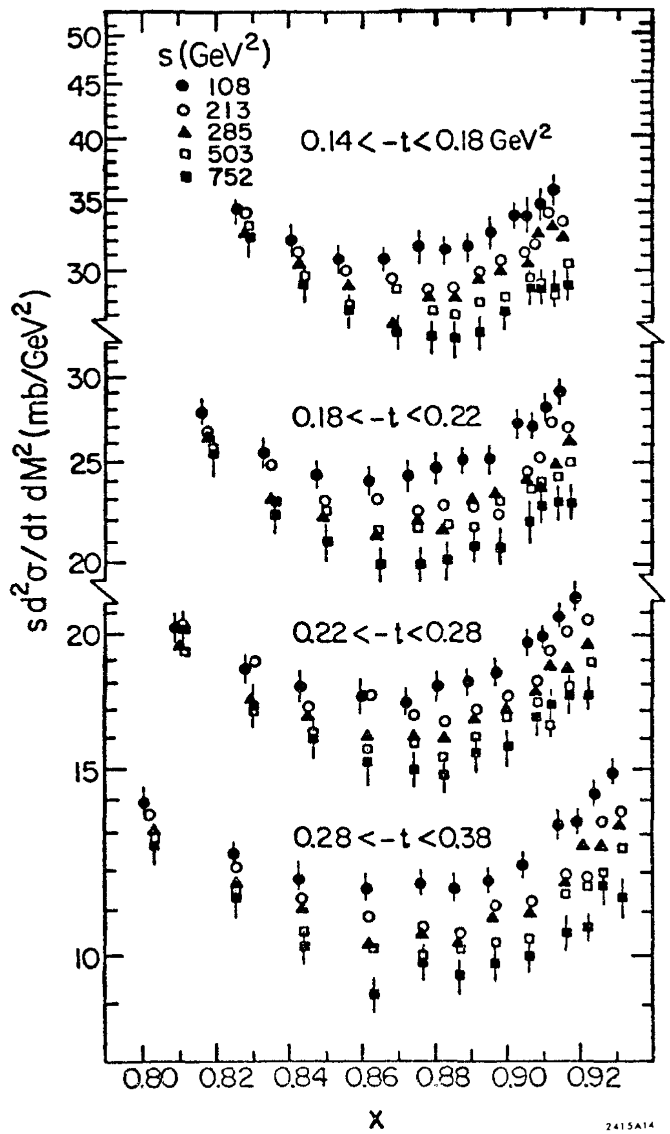

Figure 138

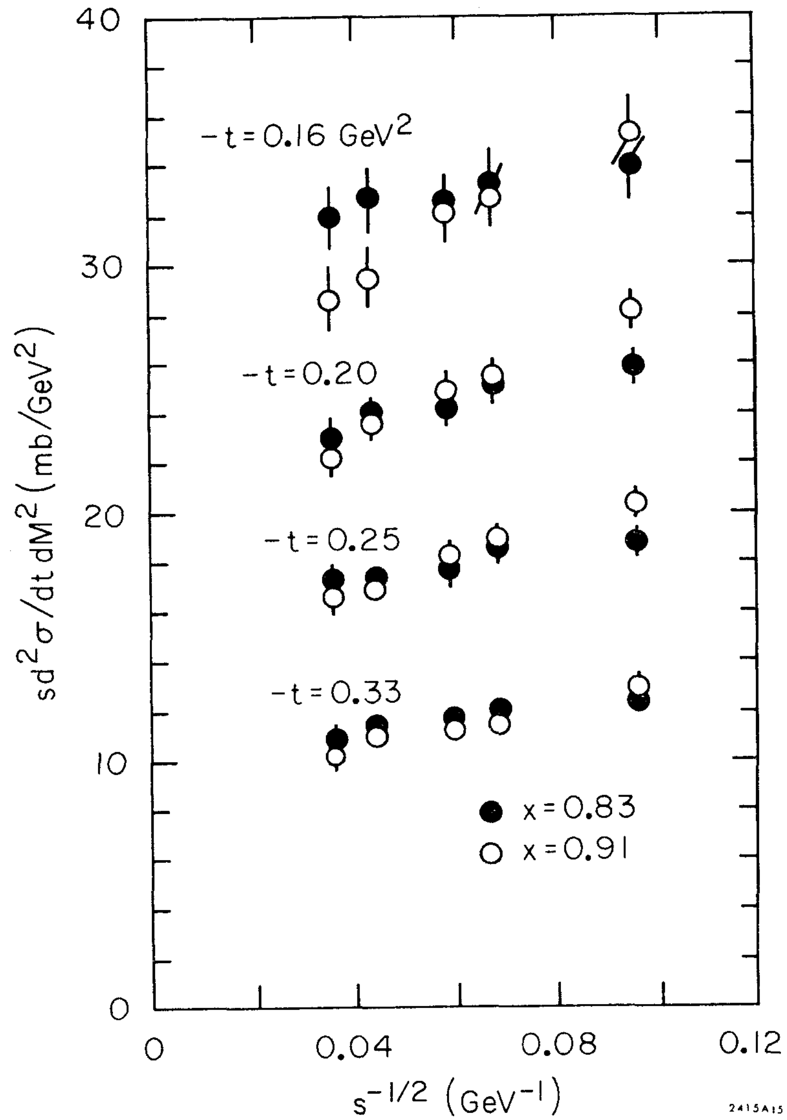

Figure 139

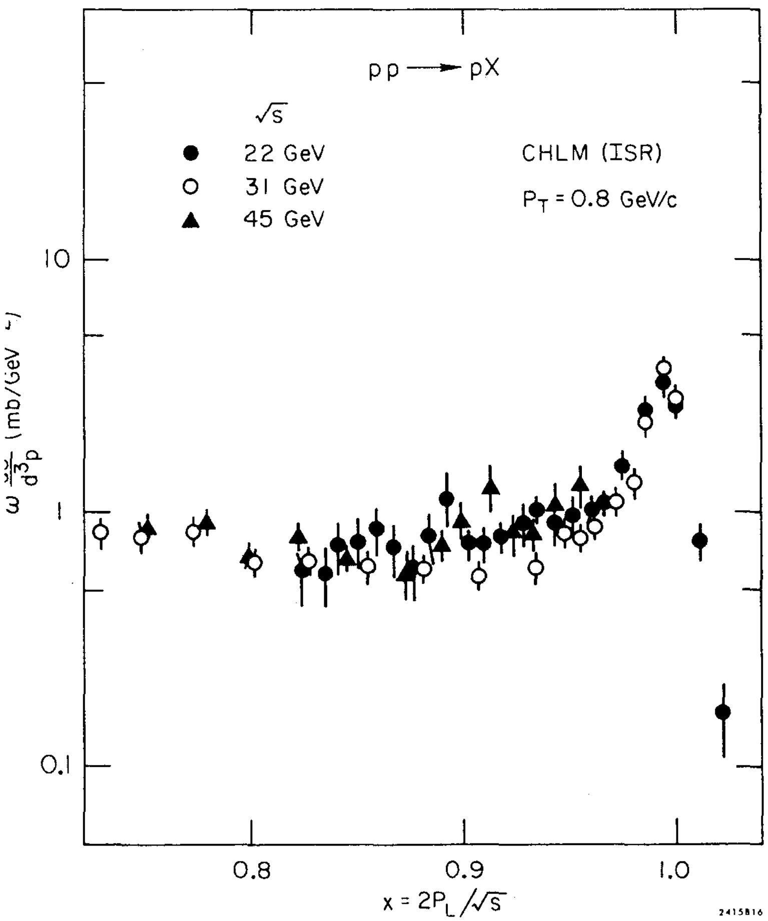

Figure 140

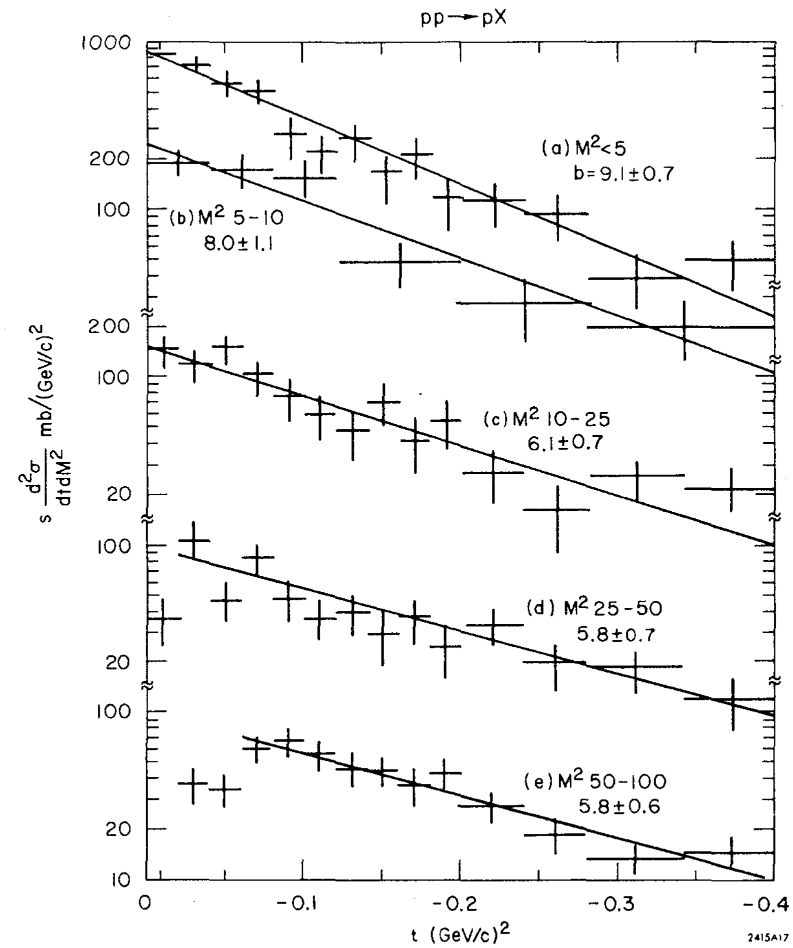

Figure 141

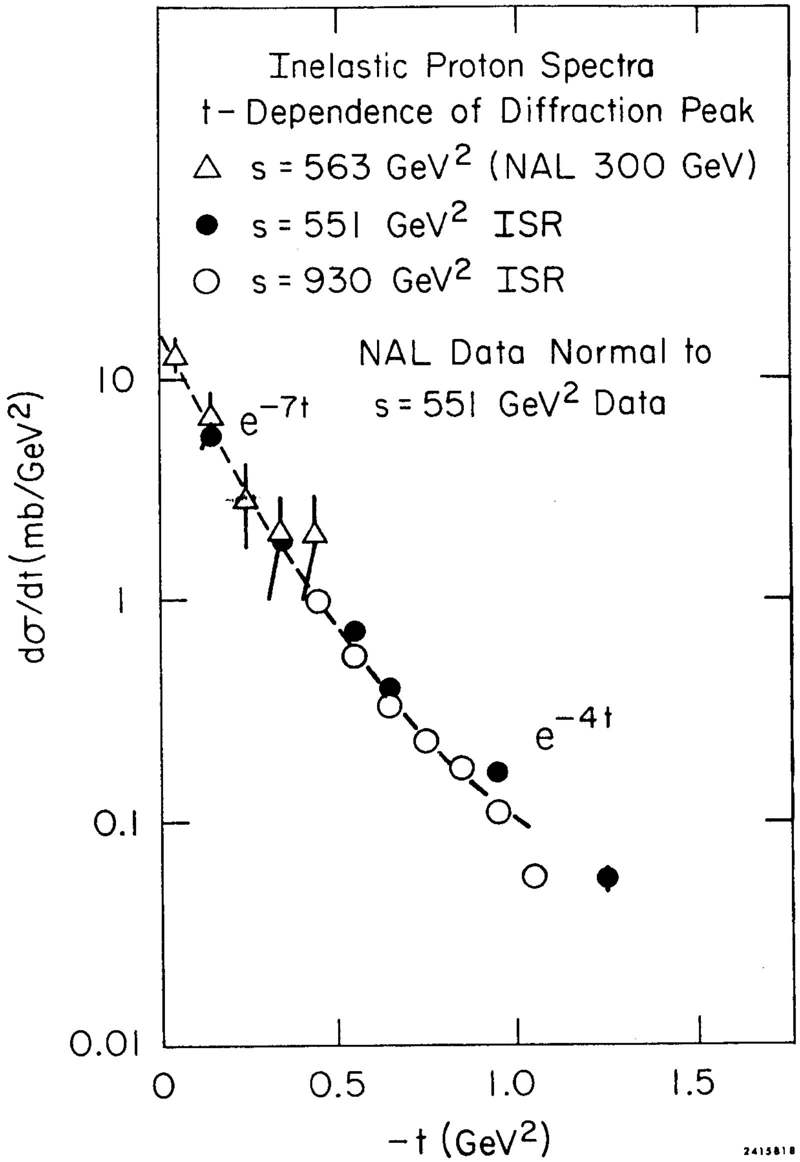

Figure 142

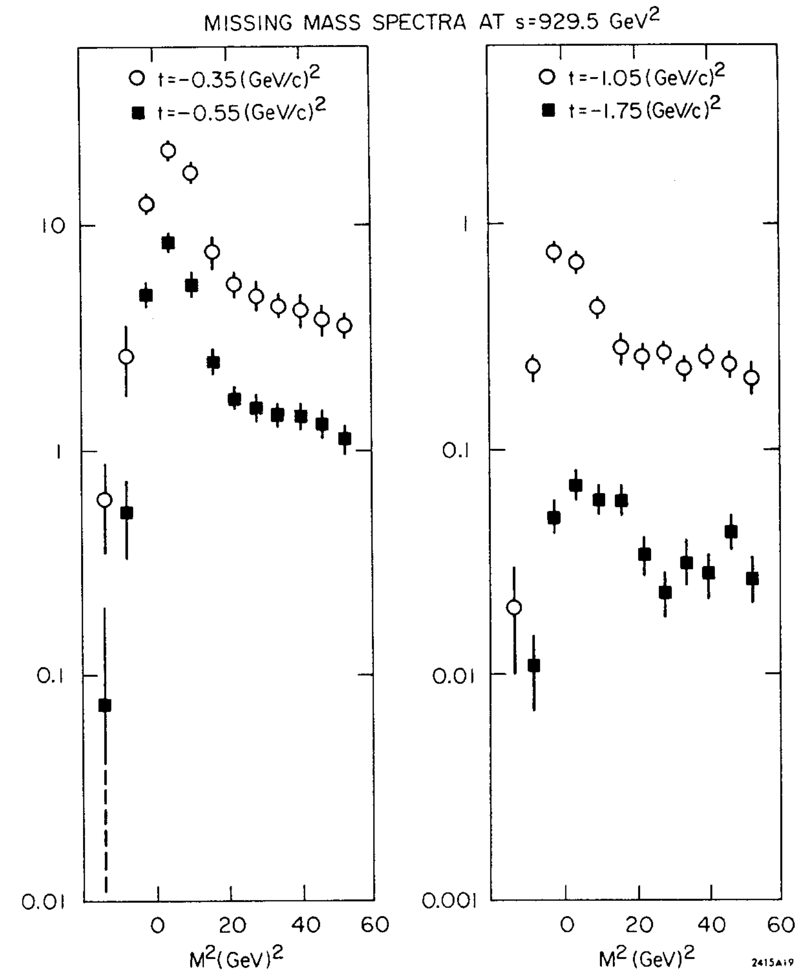

Figure 143

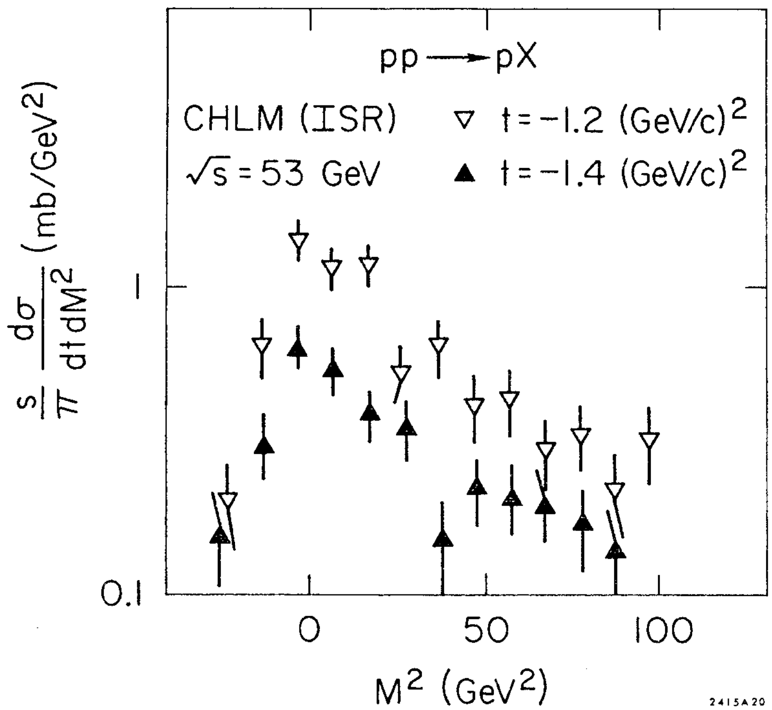

Figure 144

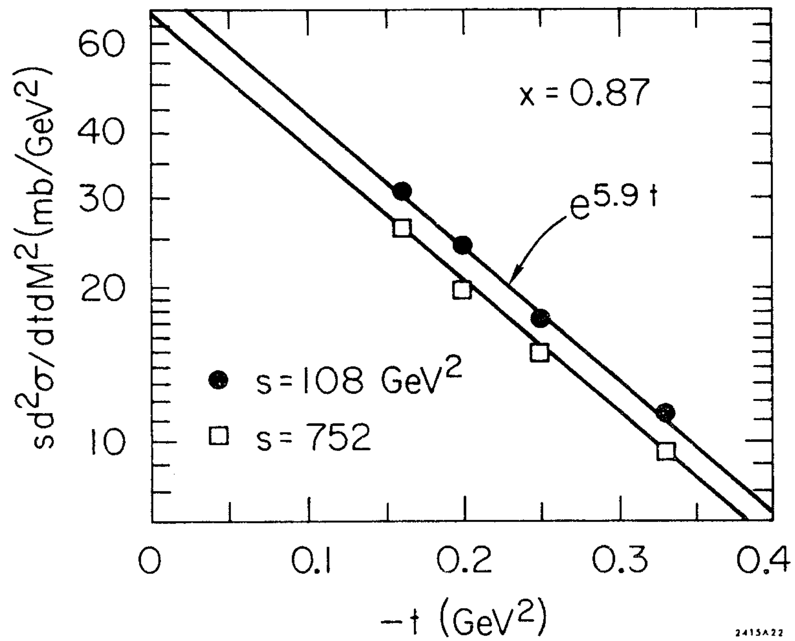

Figure 145

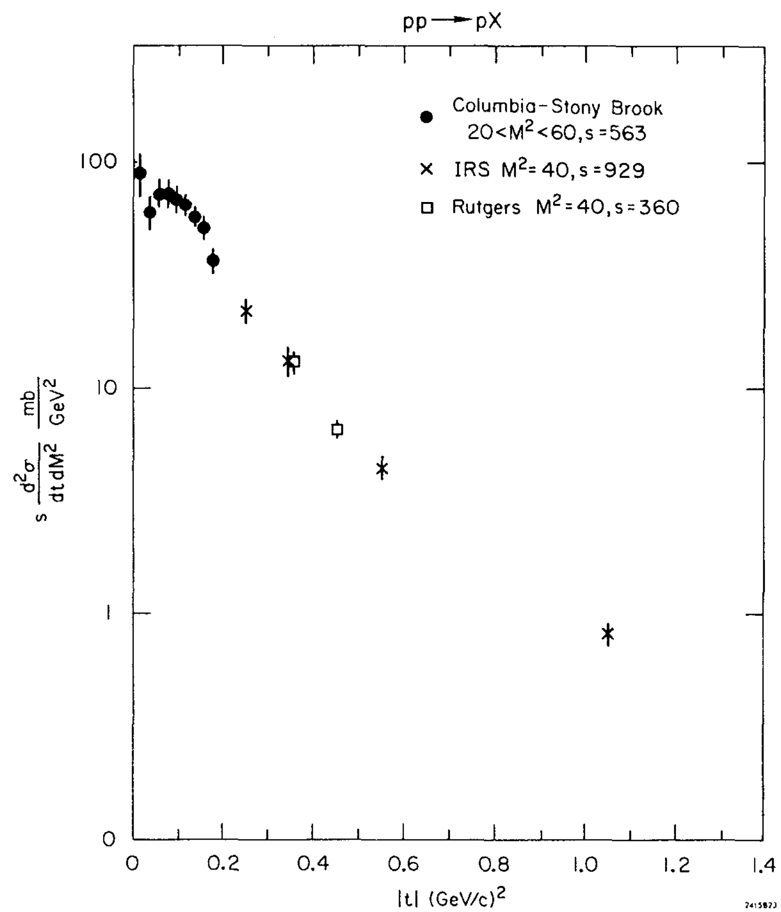

Figure 146

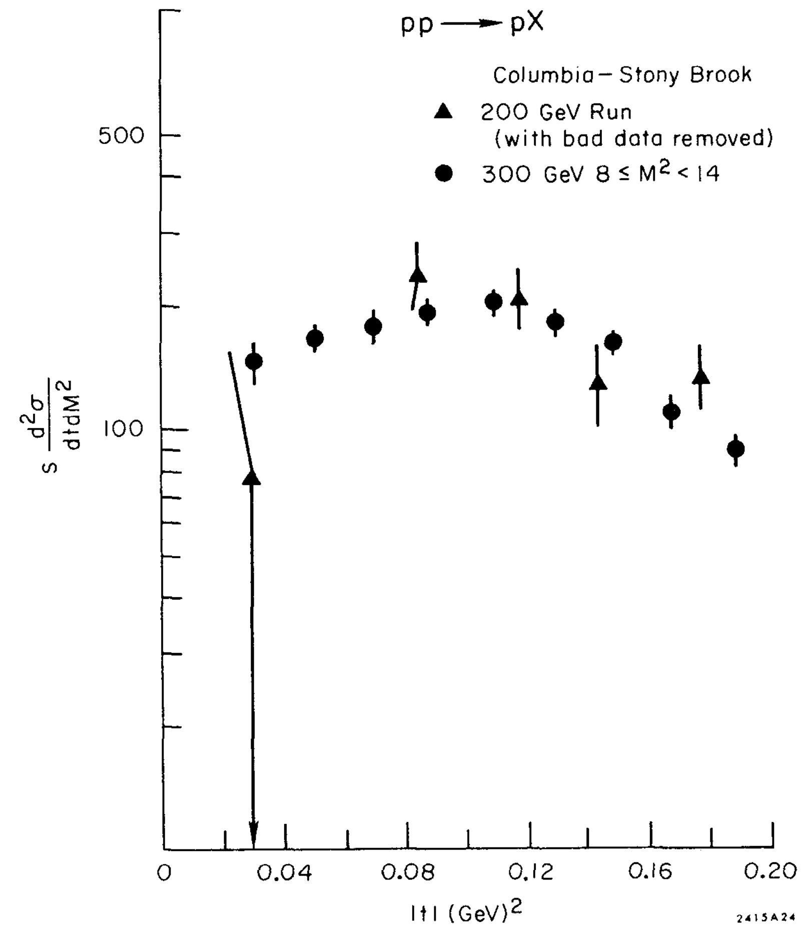

Figure 147

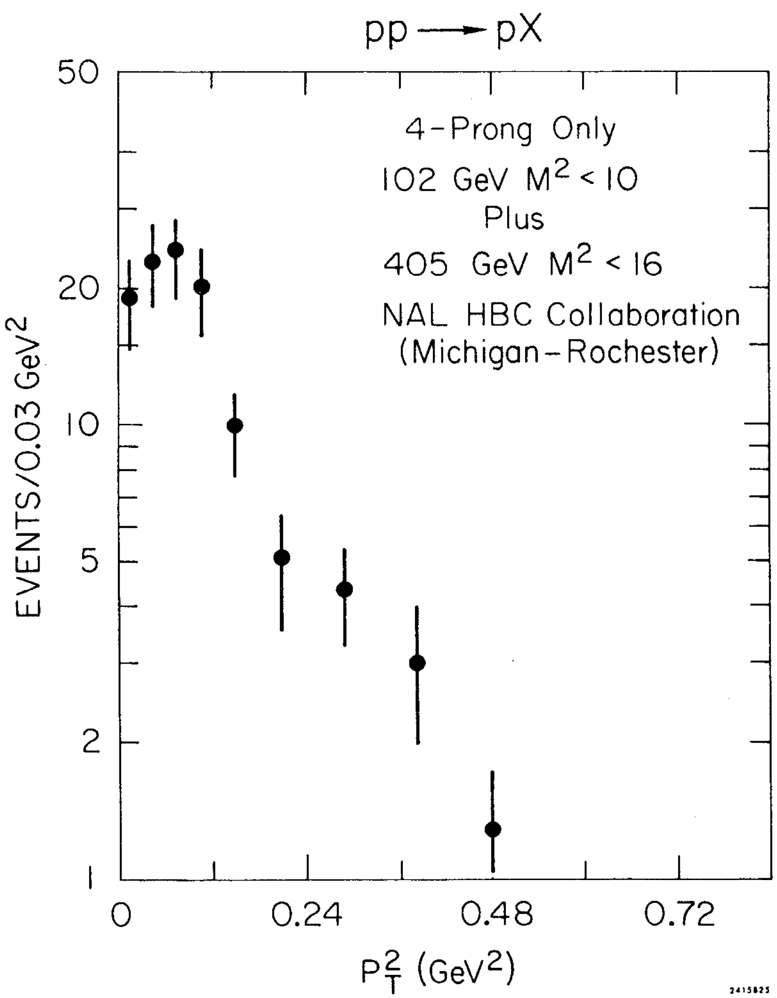

Figure 148

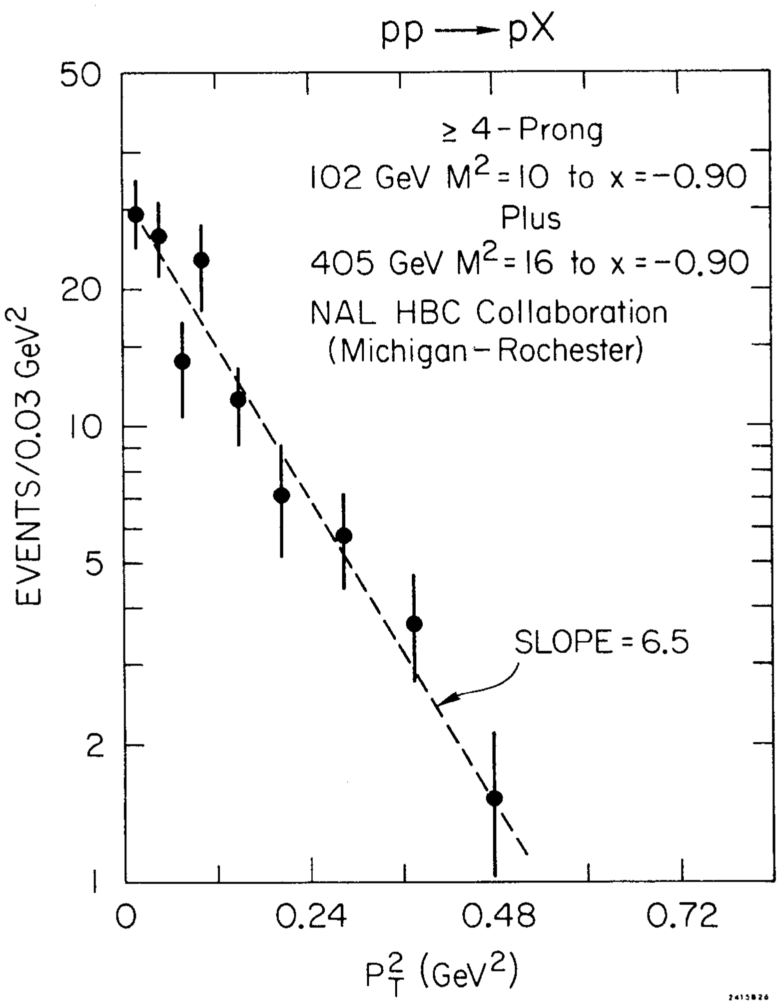

Figure 149a

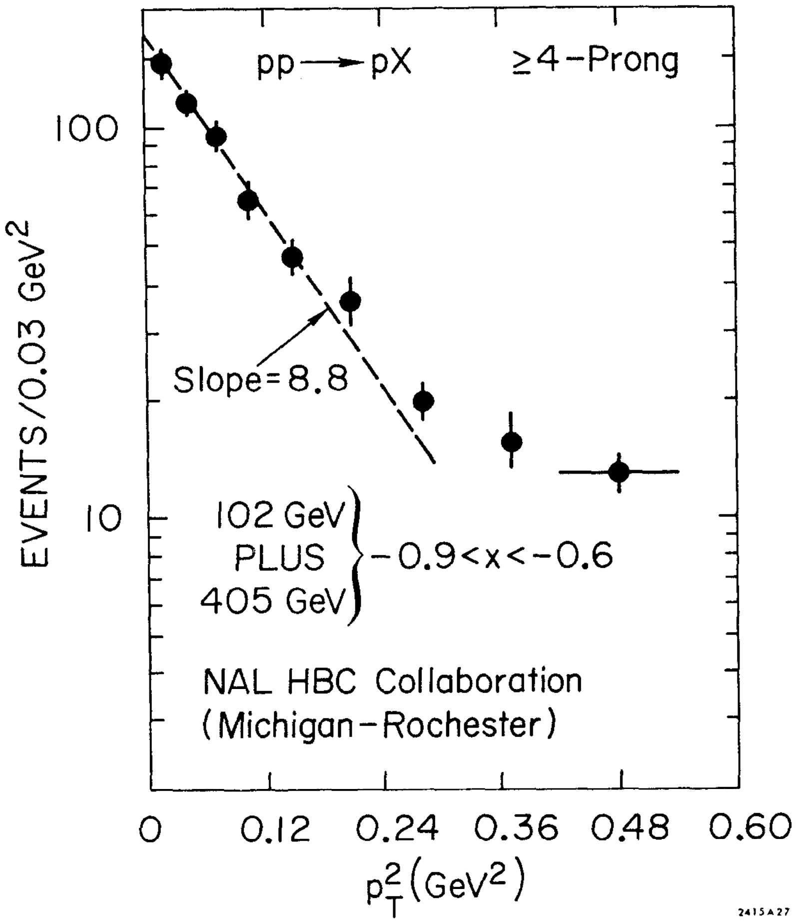

Figure 149b

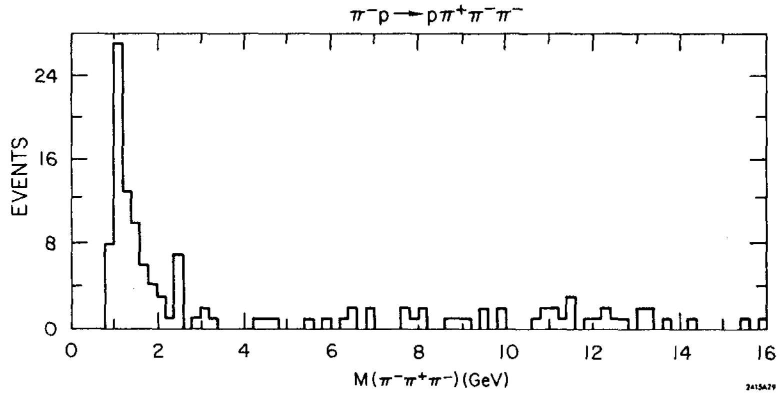

Figure 150

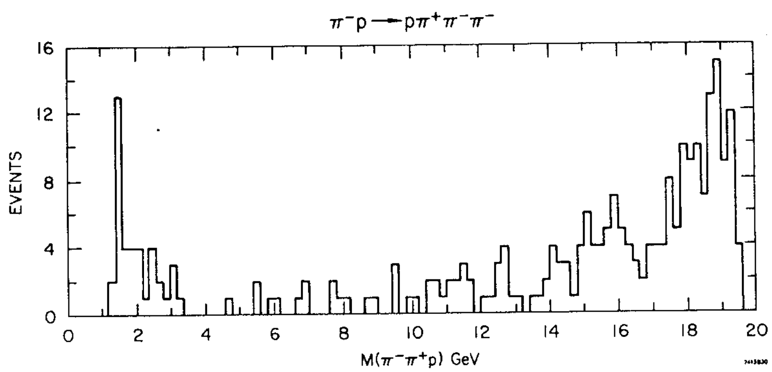

Figure 151

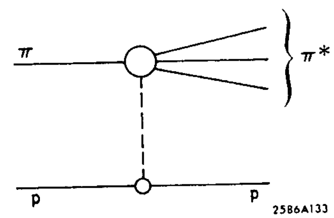

Figure 152

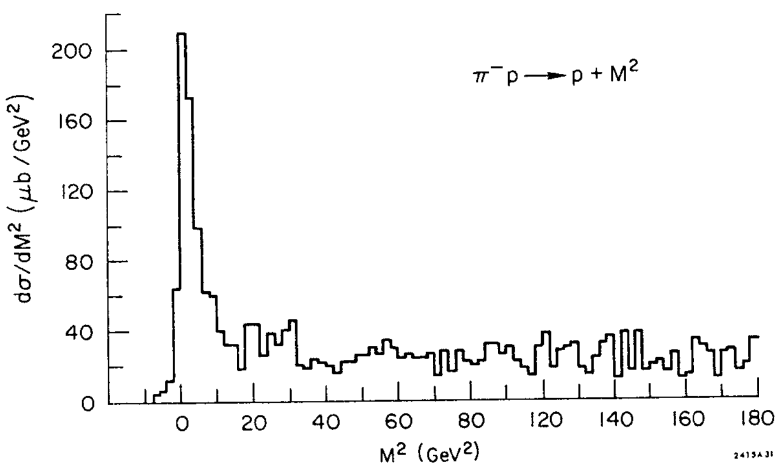

Figure 153

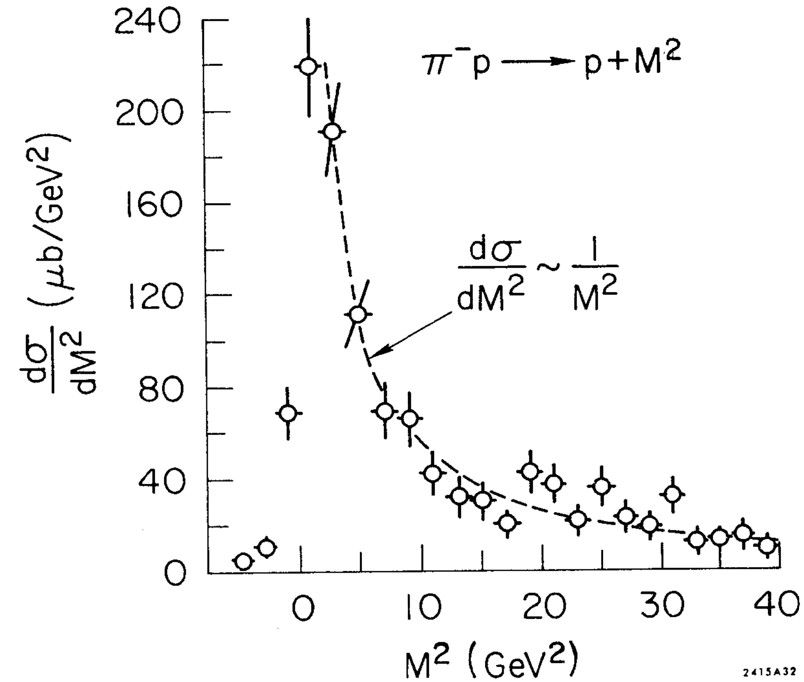

Figure 154

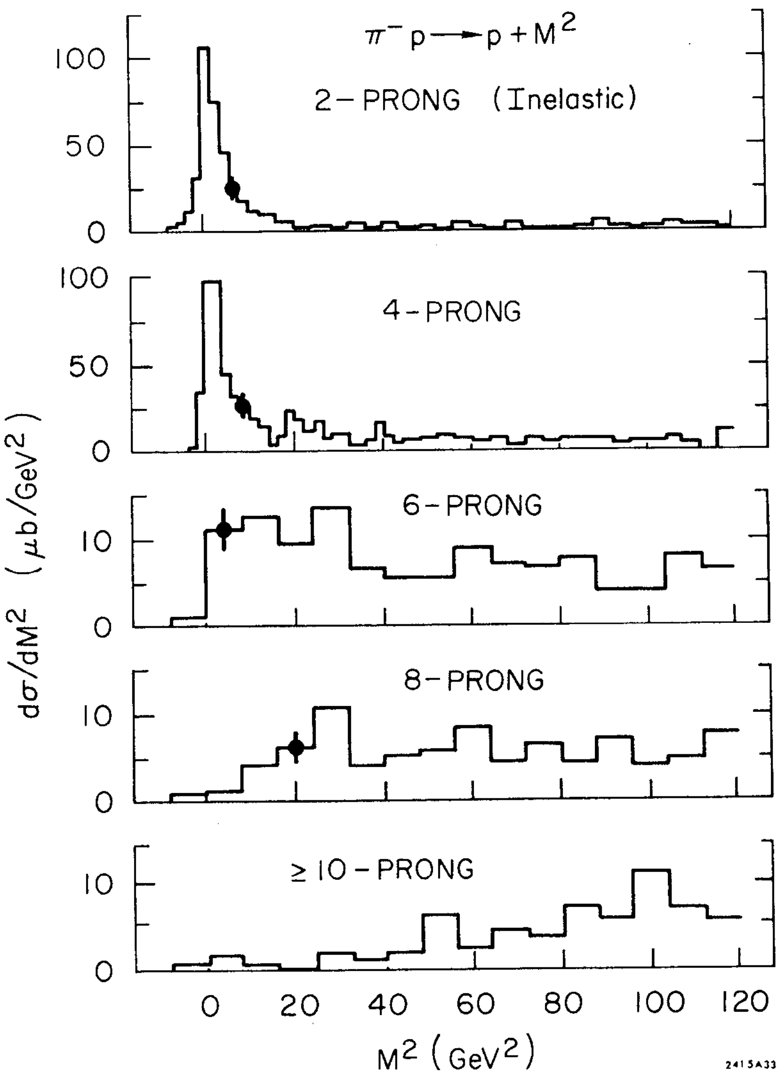

Figure 155

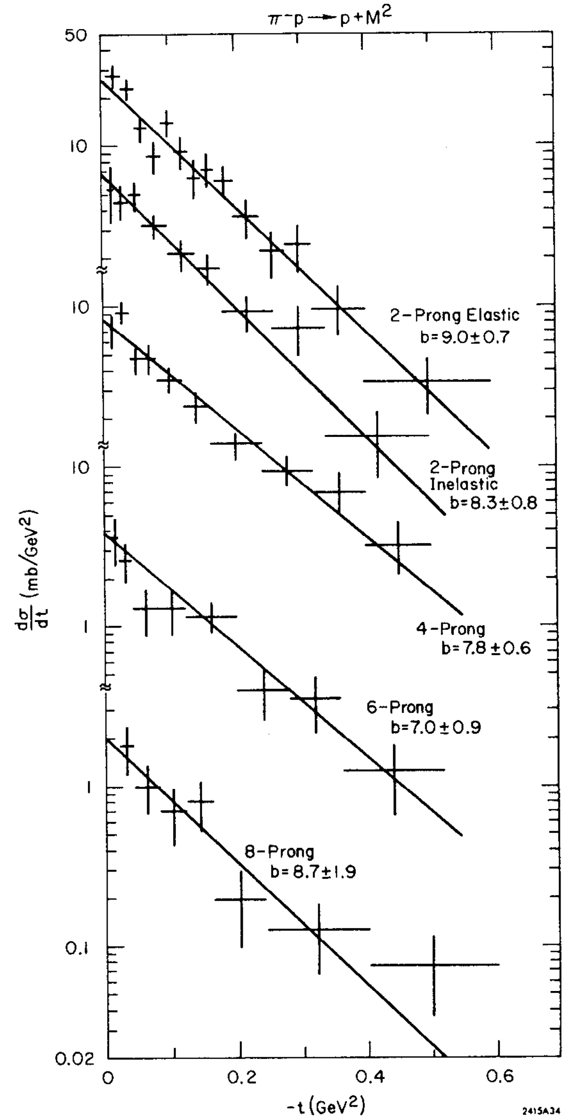

Figure 156

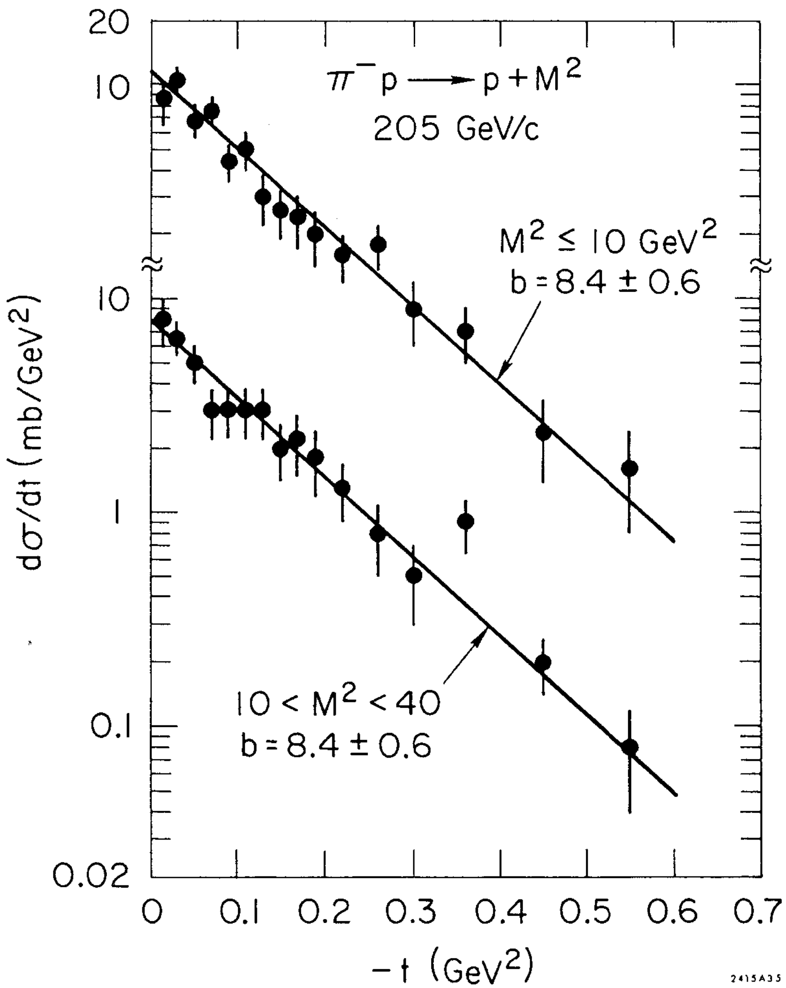

Figure 157

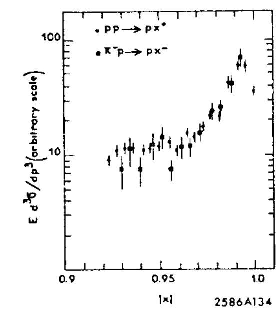

Figure 158

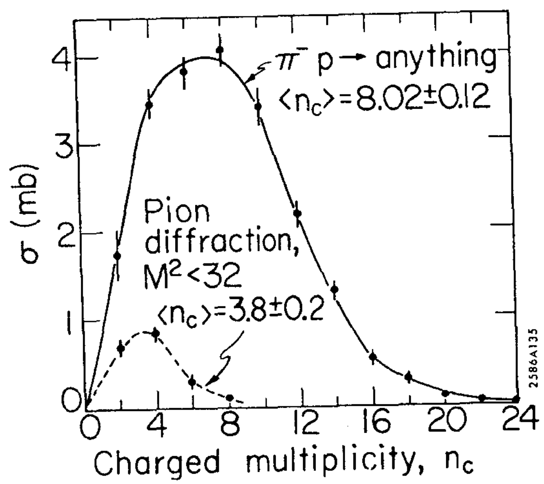

Figure 159

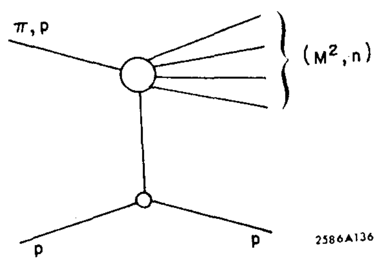

Figure 160

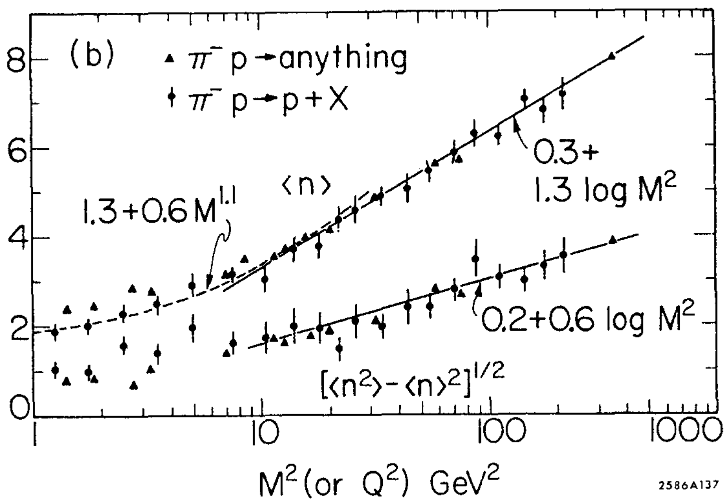

Figure 161

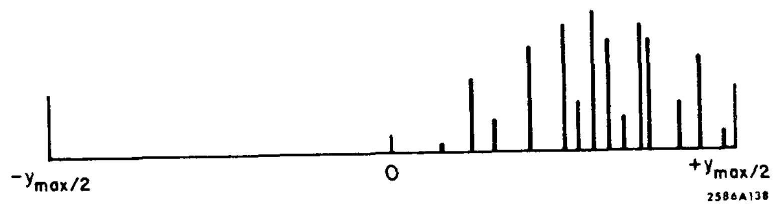

Figure 162

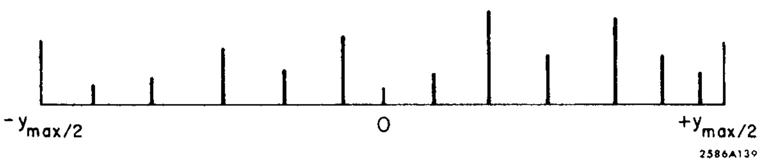

Figure 163

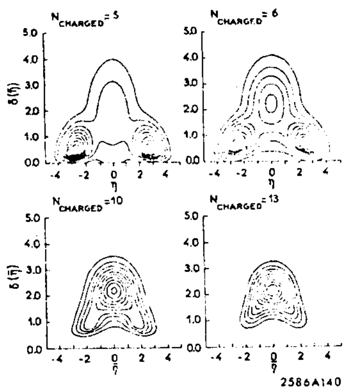

Figure 164

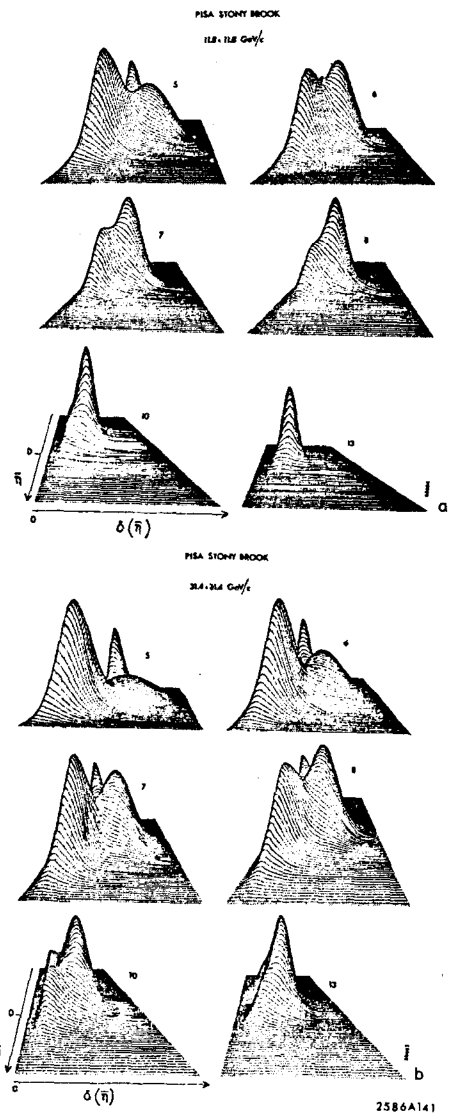

Figure 165

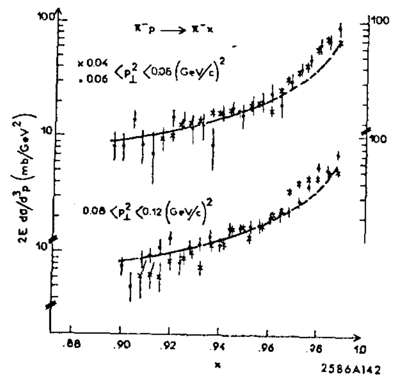

Figure 166

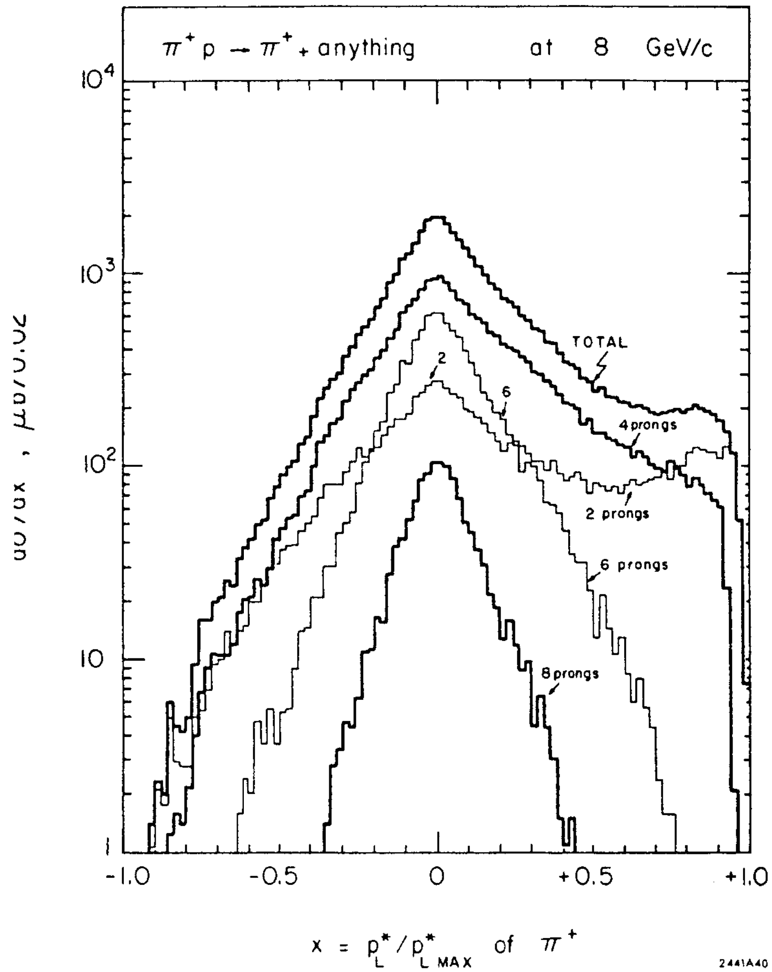

Figure 167

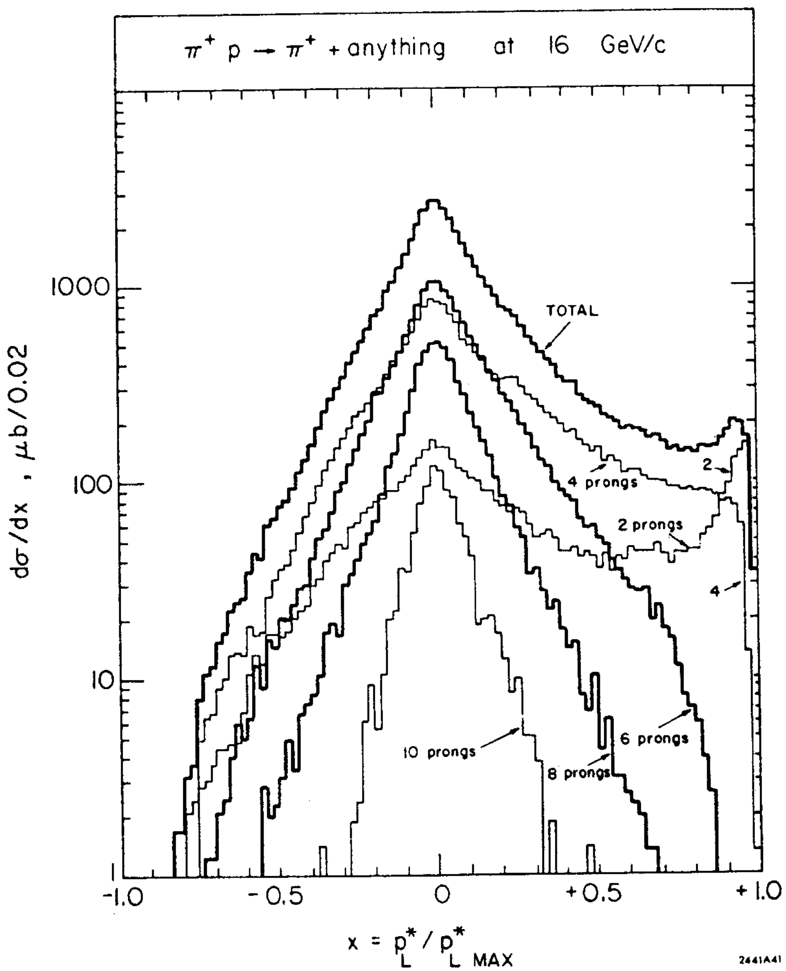

Figure 168

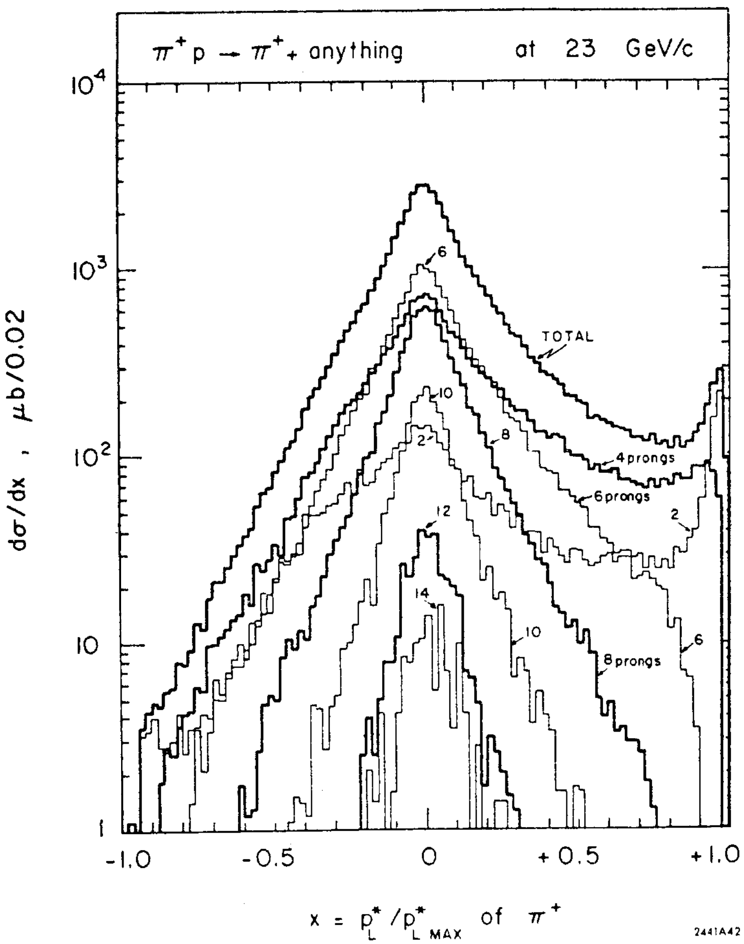

Figure 169

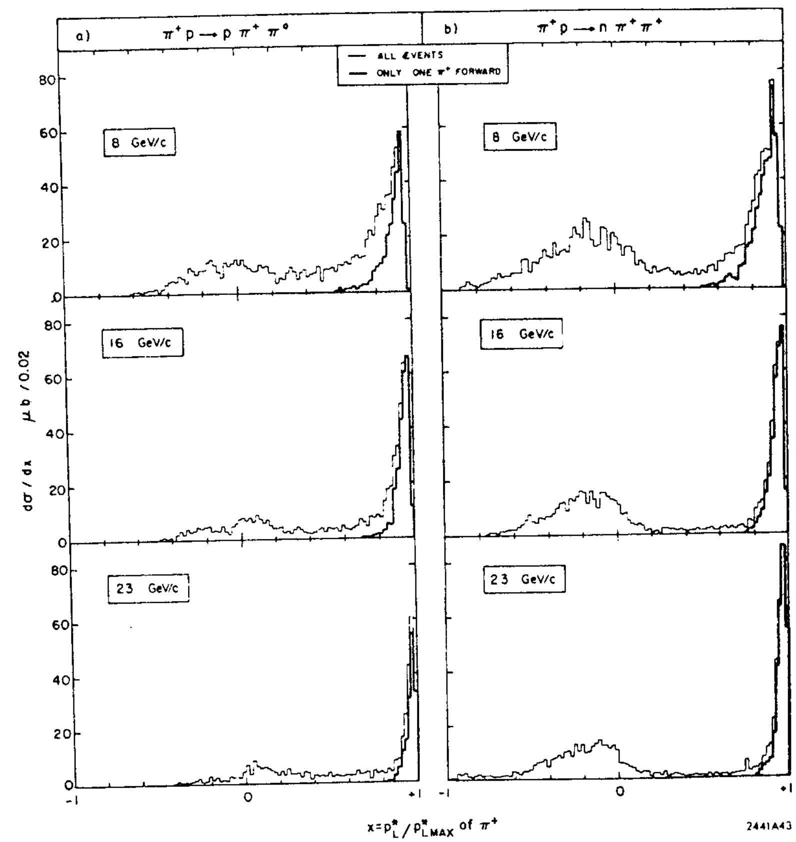

Figure 170

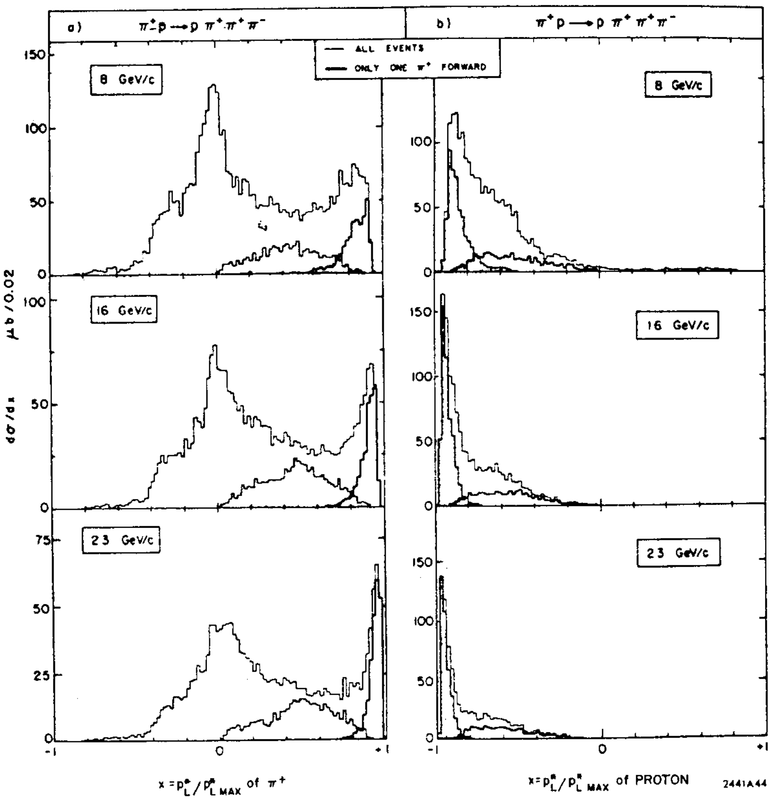

Figure 171

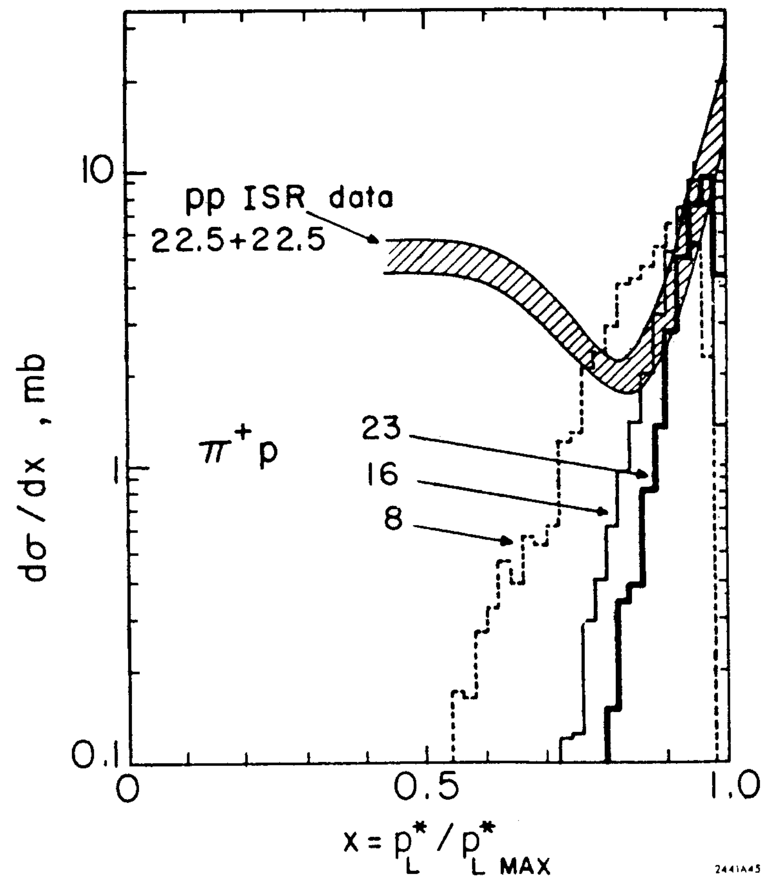

Figure 172

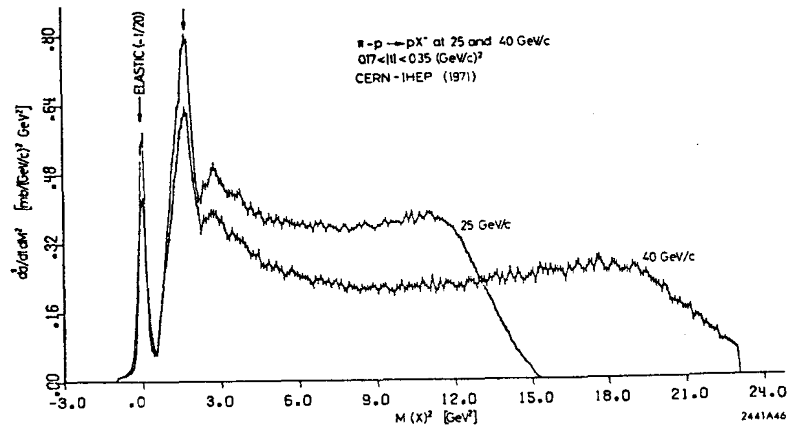

Figure 173

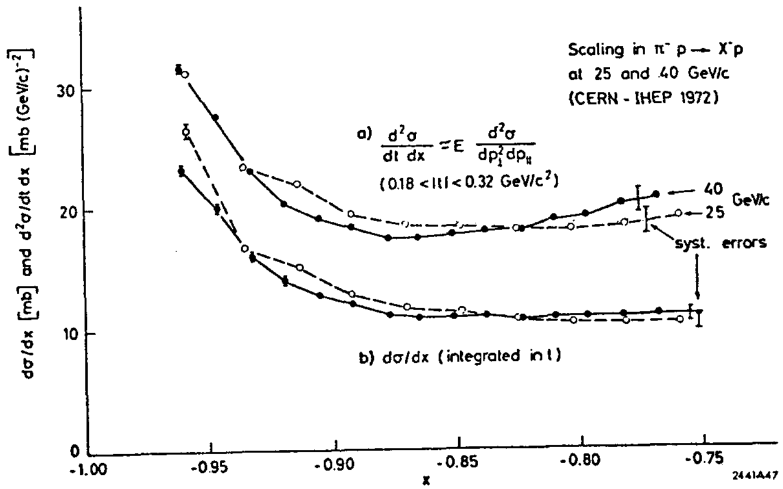

Figure 174

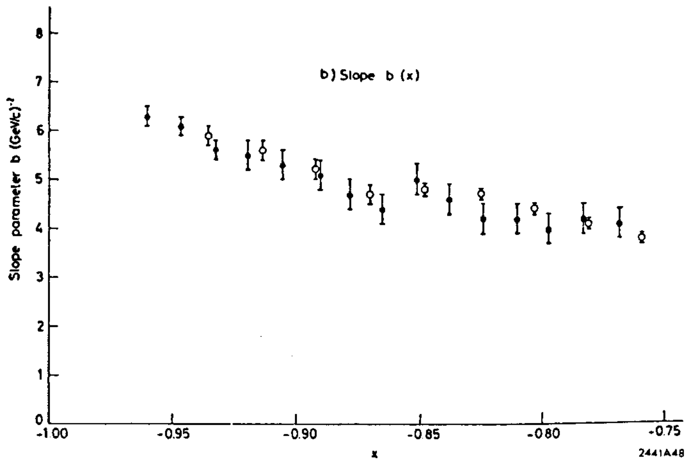

Figure 175

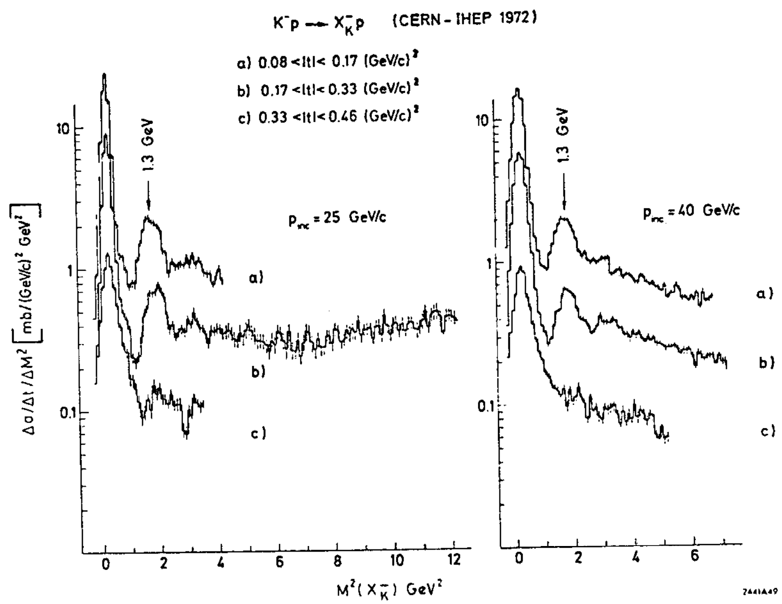

Figure 176

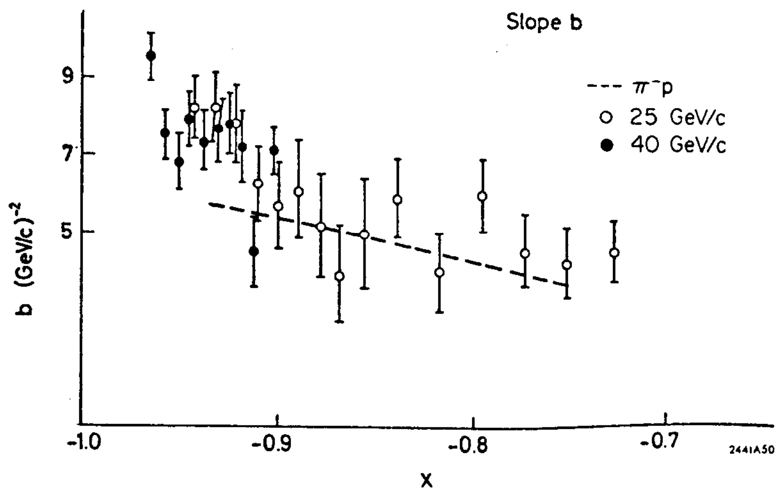

Figure 177

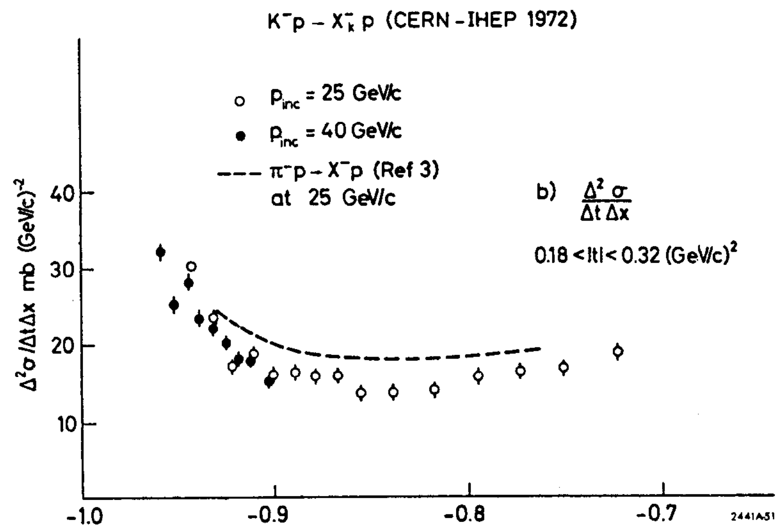

Figure 178

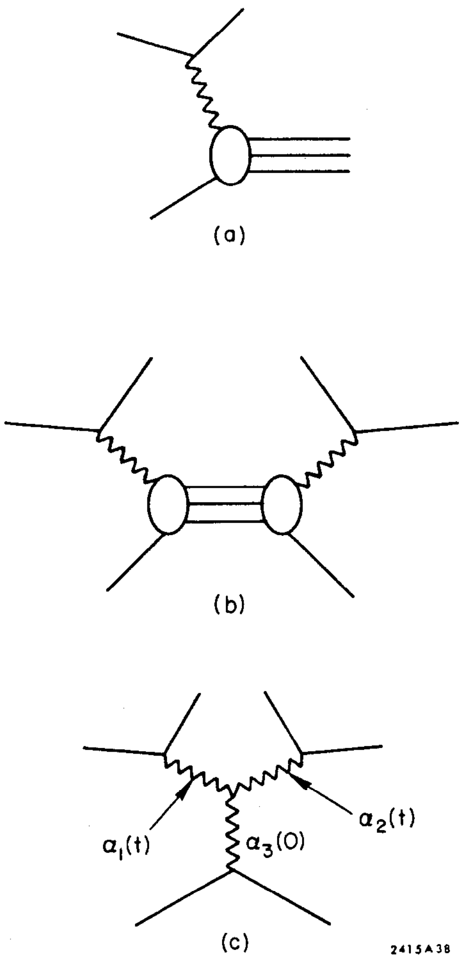

Figure 179

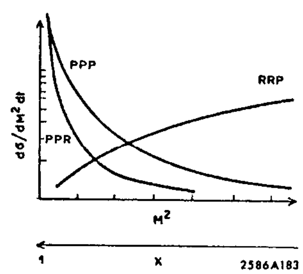

Figure 180

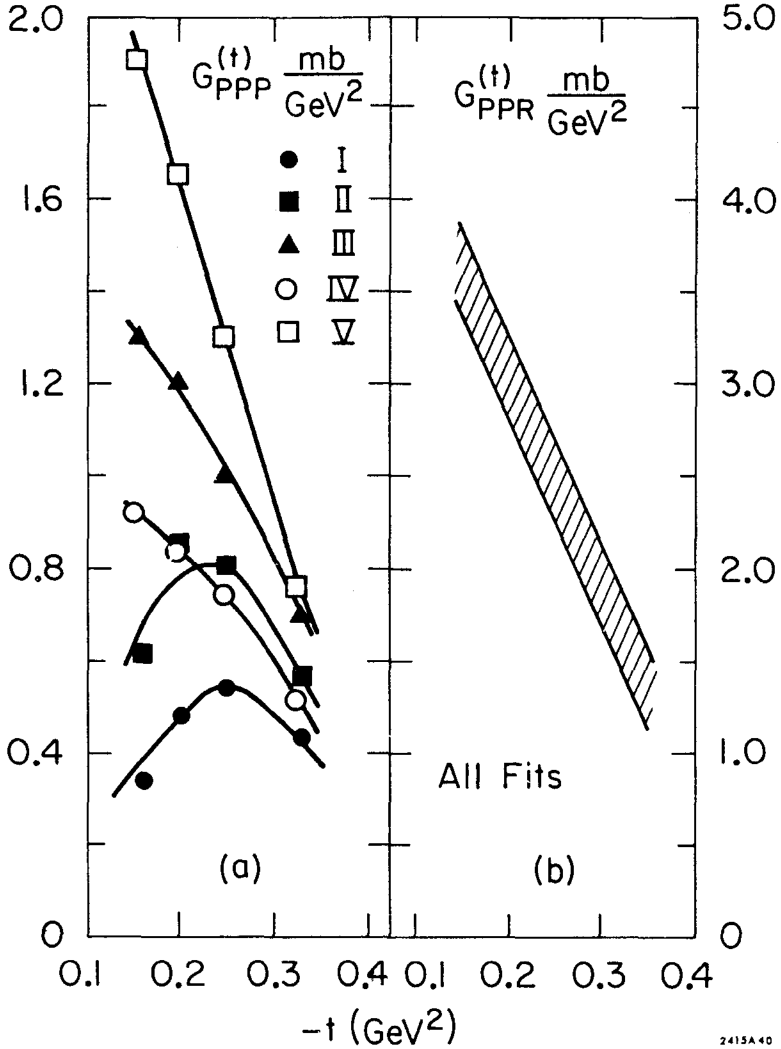

Figure 181

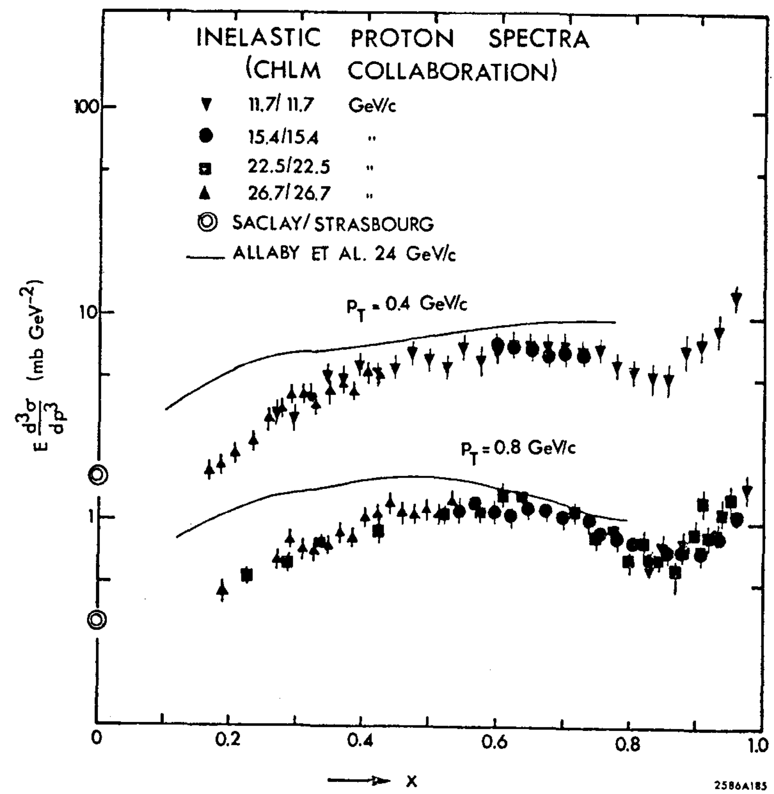

Figure 182

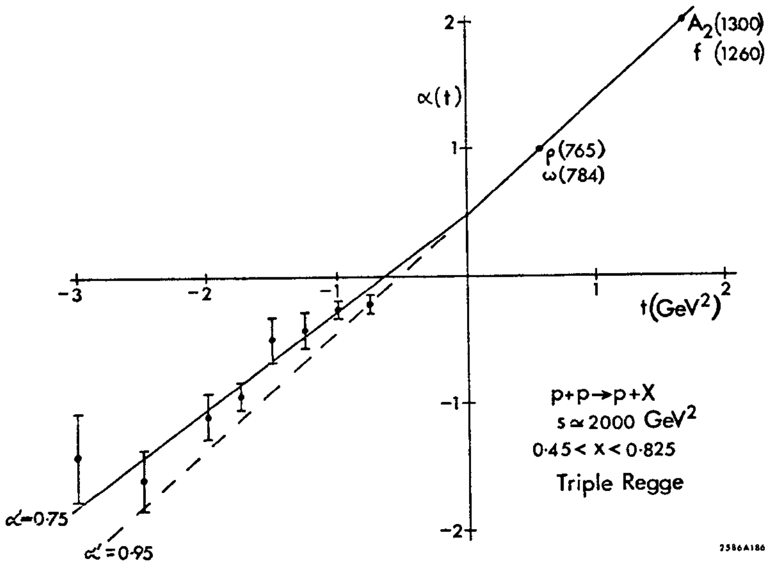

Figure 183

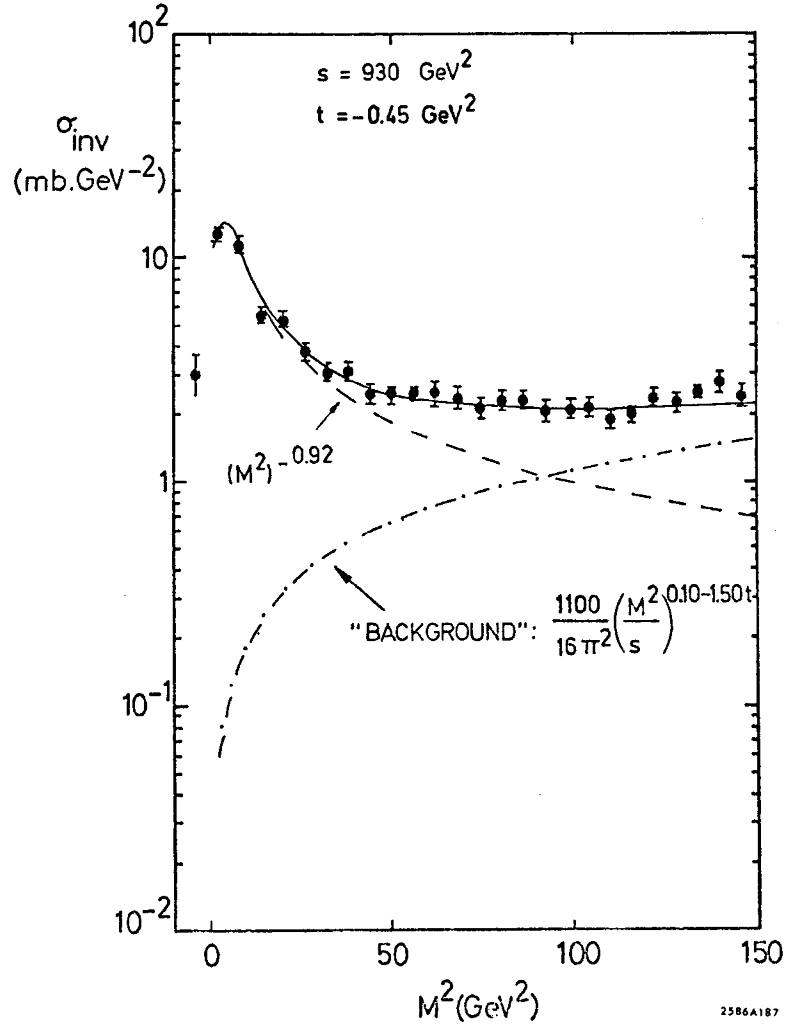

Figure 184

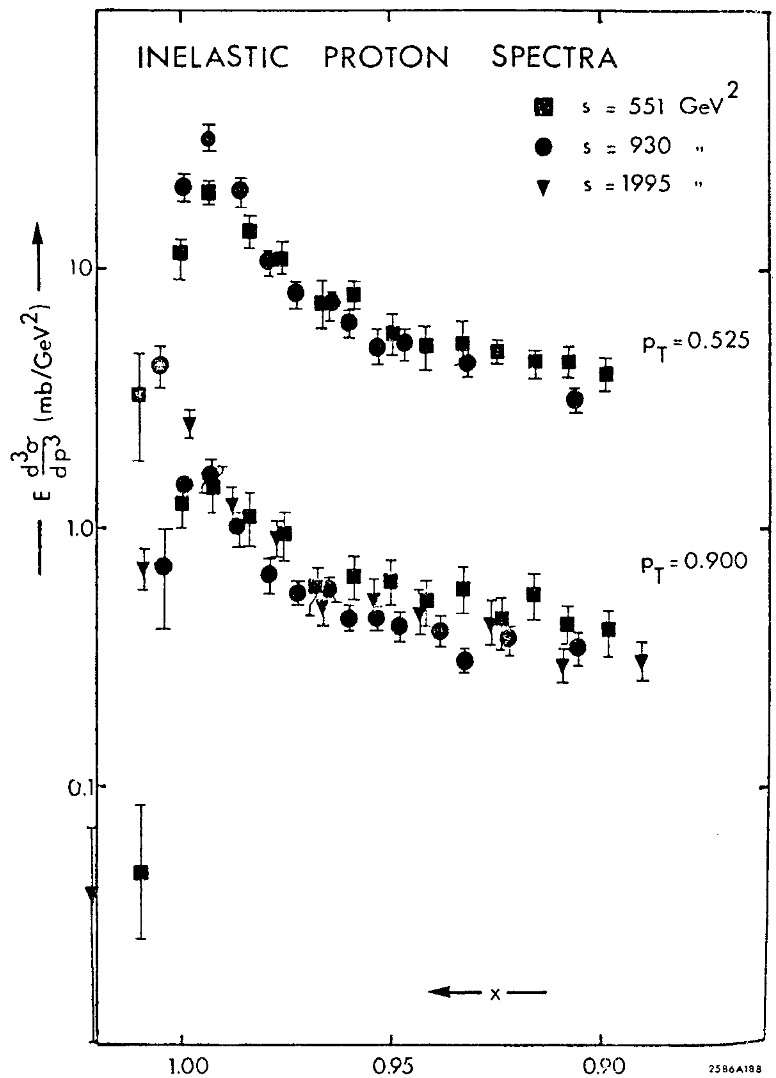

Figure 185

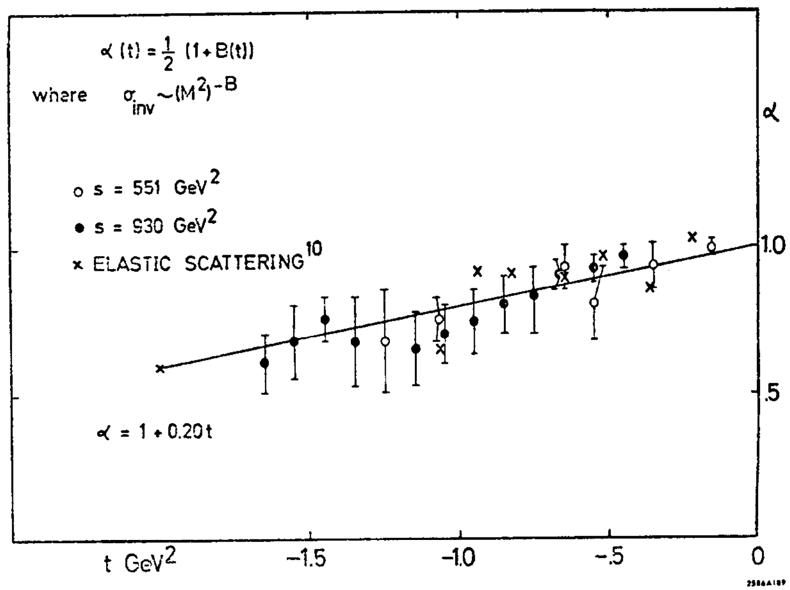

Figure 186

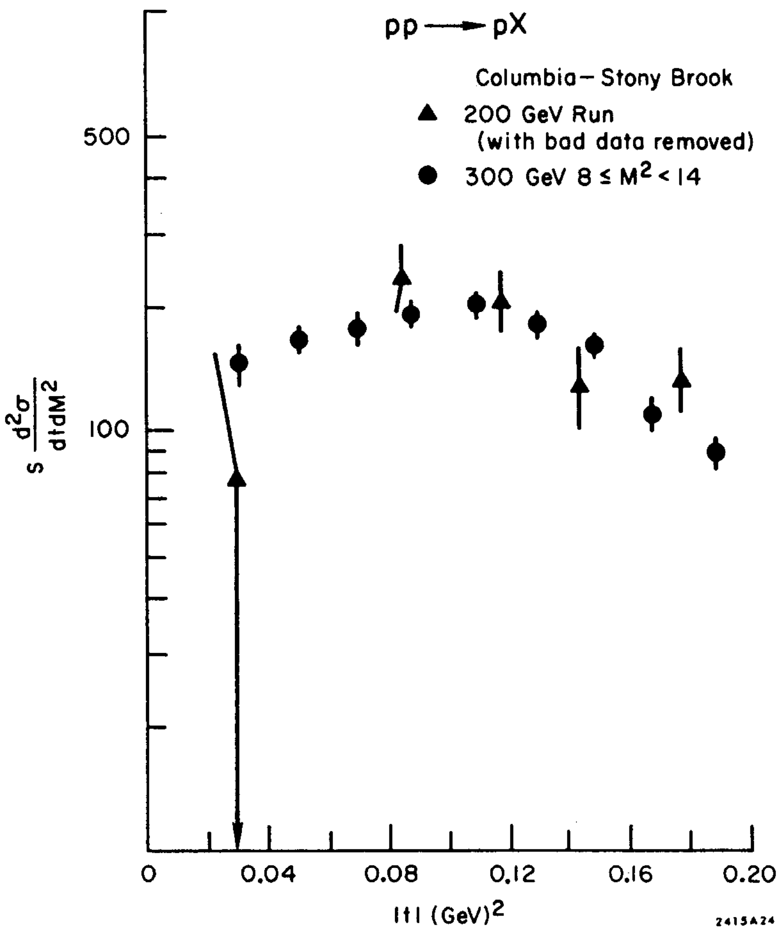

Figure 187

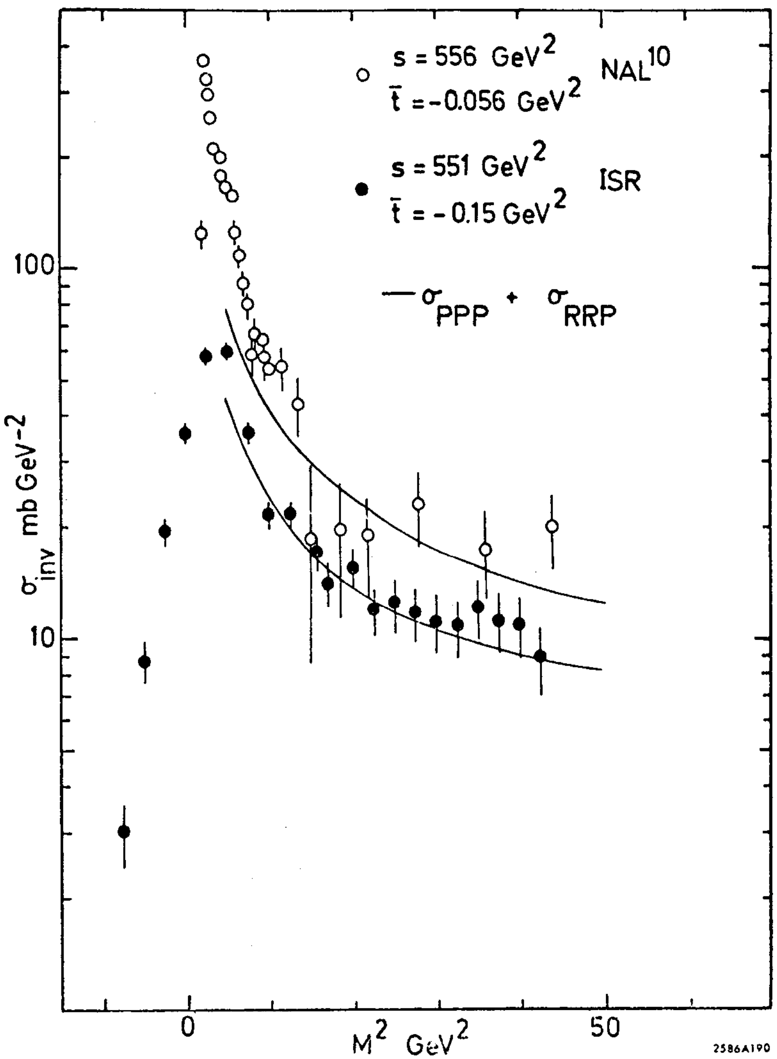

Figure 188

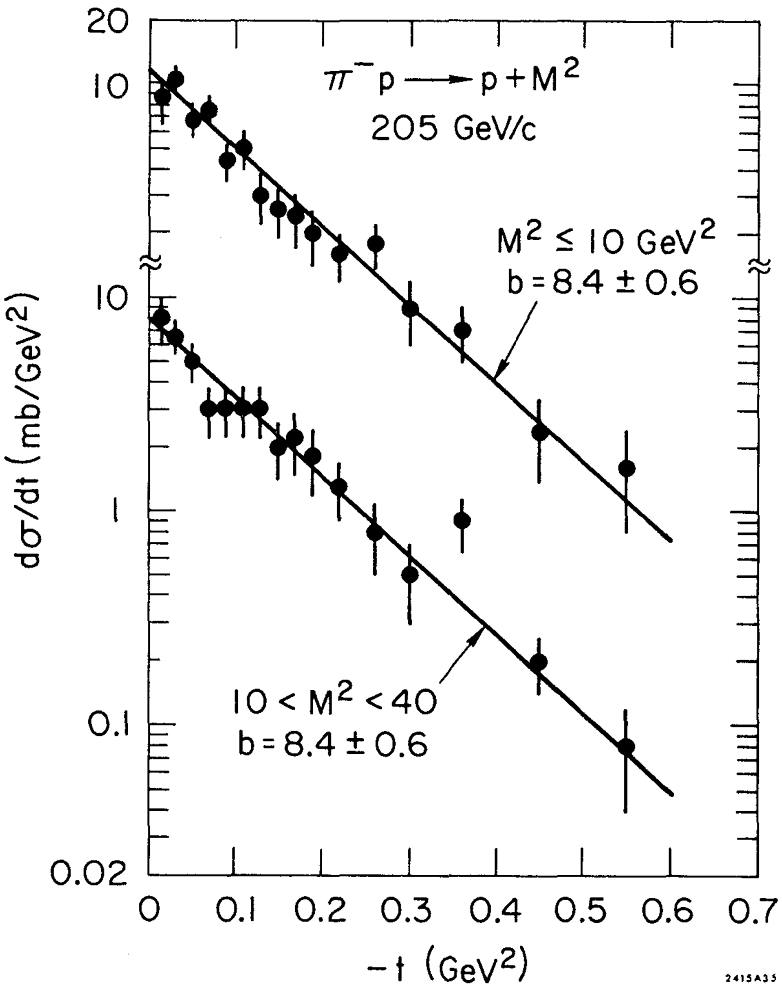

Figure 189

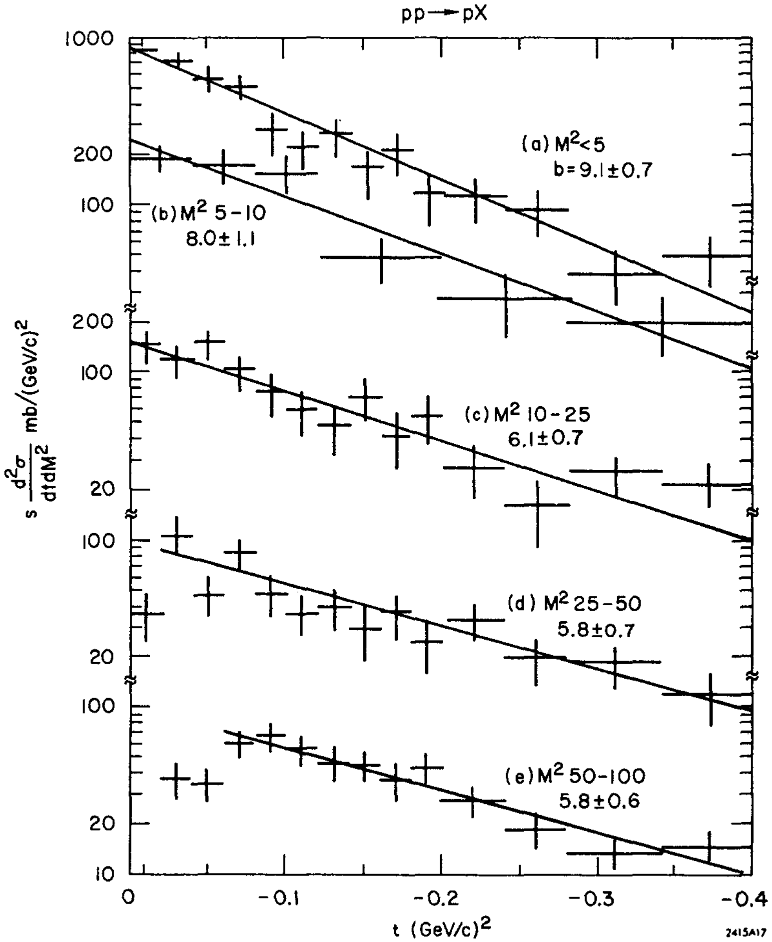

Figure 190

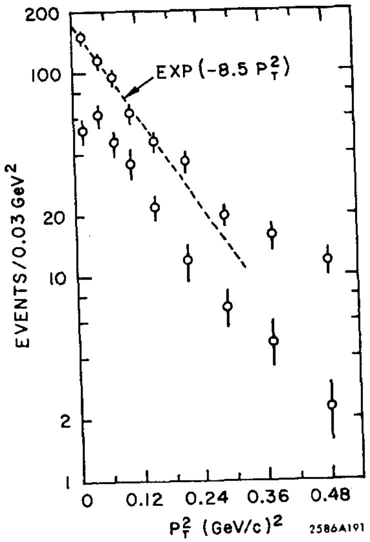

Figure 191

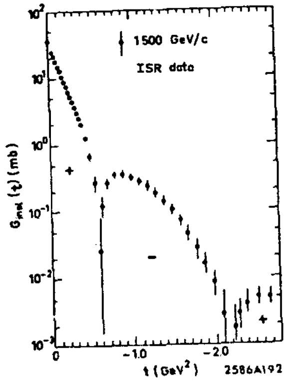

Figure 192

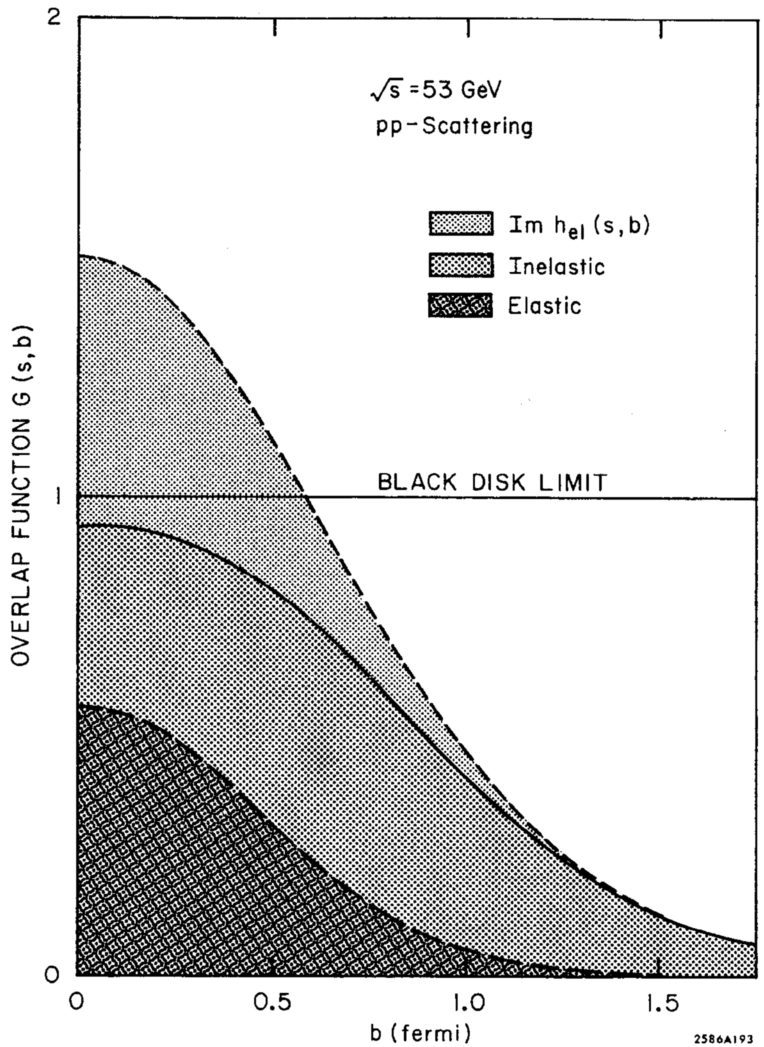

Figure 193

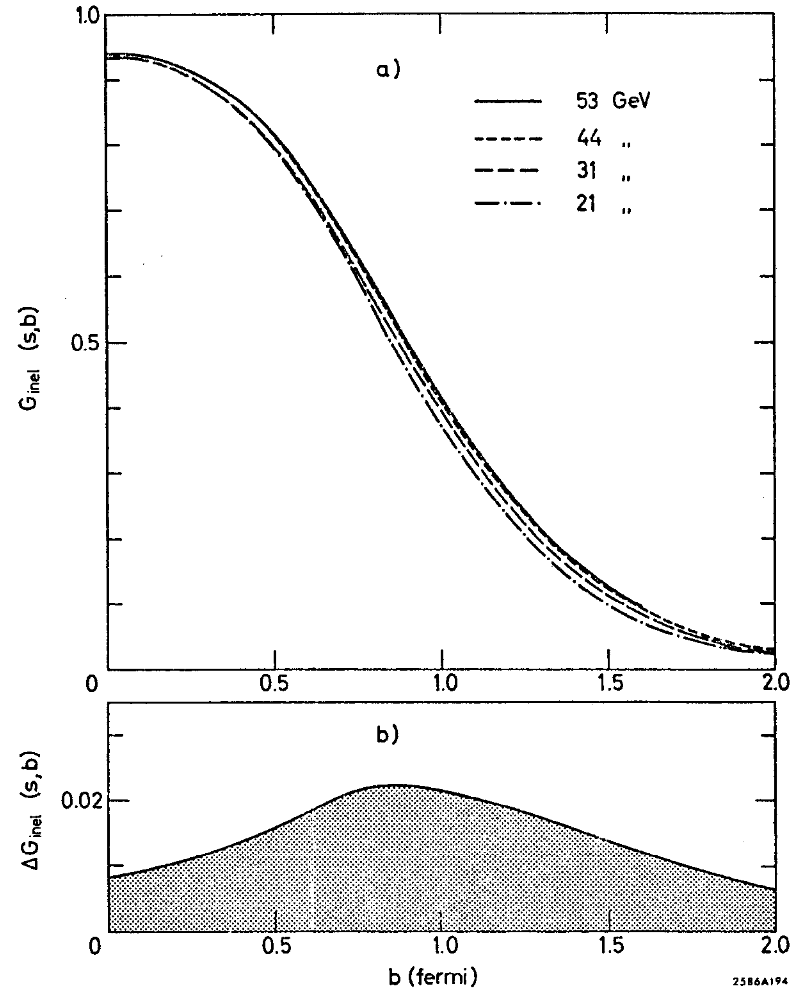

Figure 194

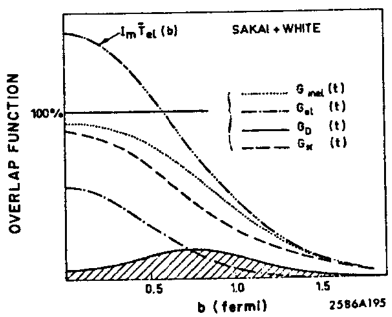

Figure 195

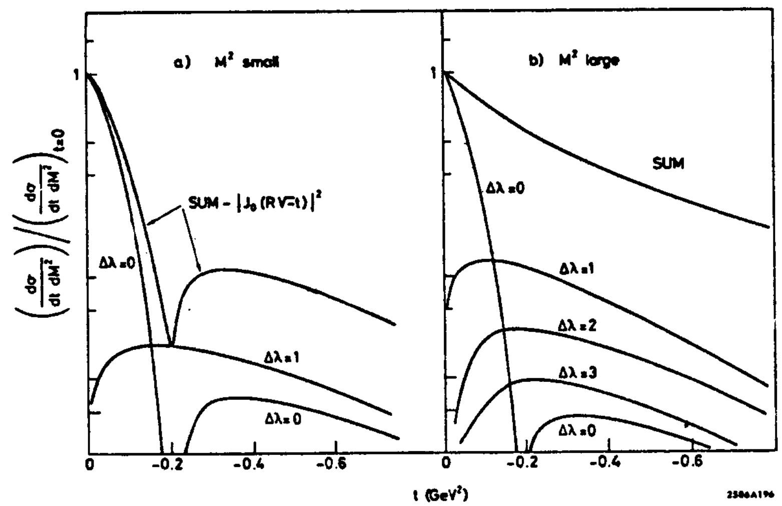

Figure 196

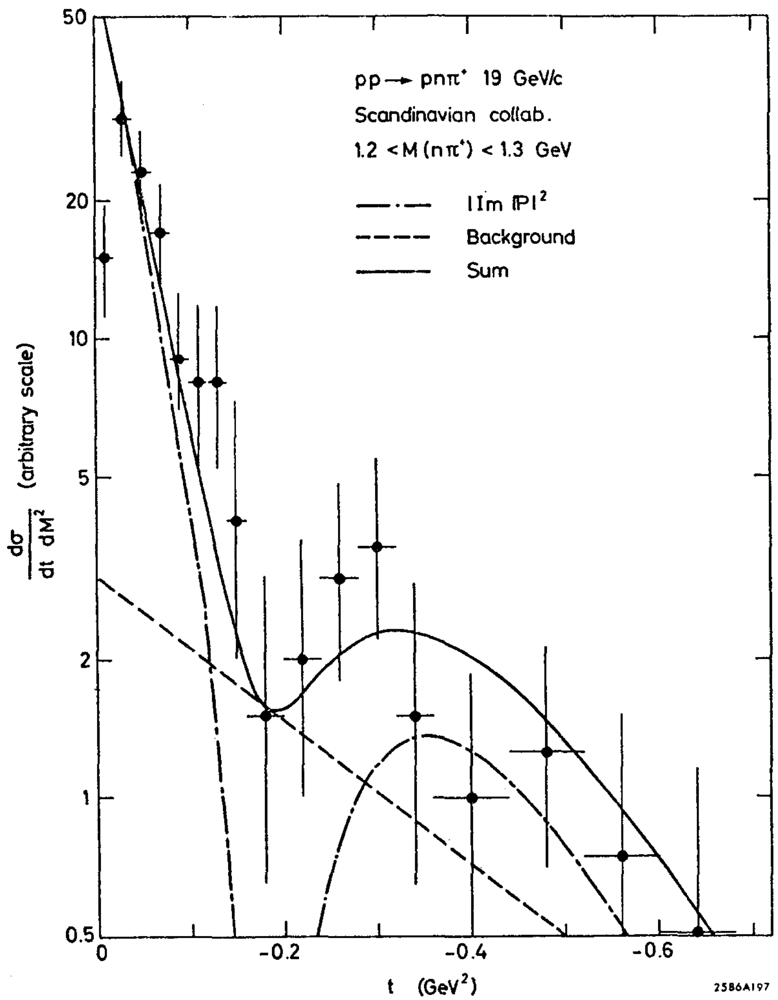

Figure 197

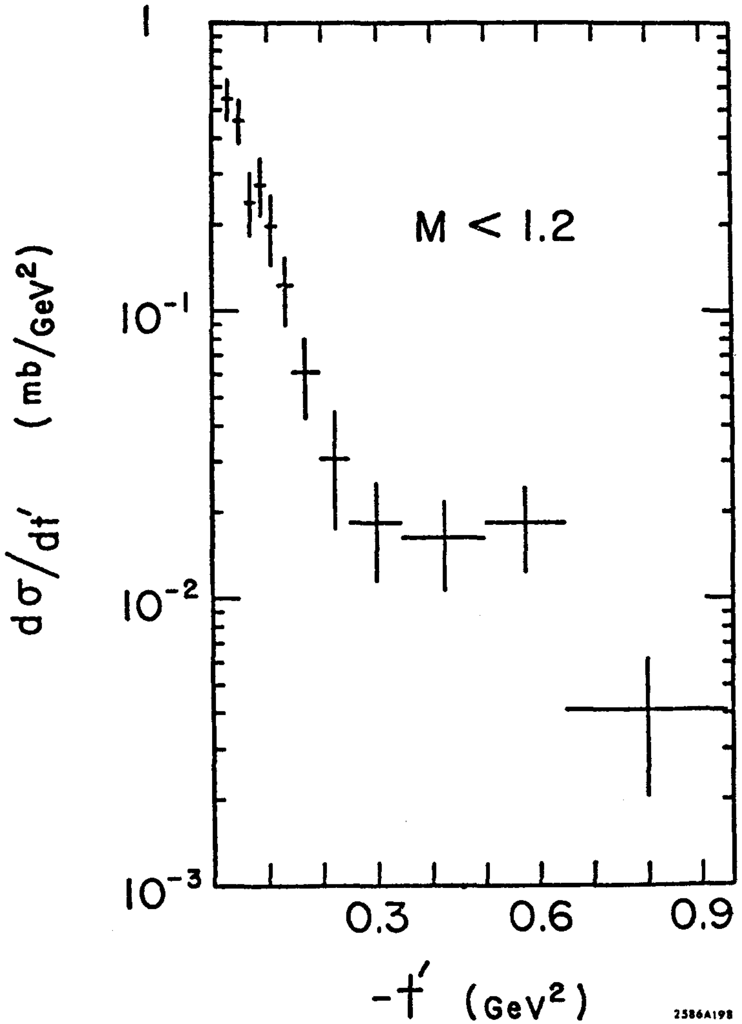

Figure 198a

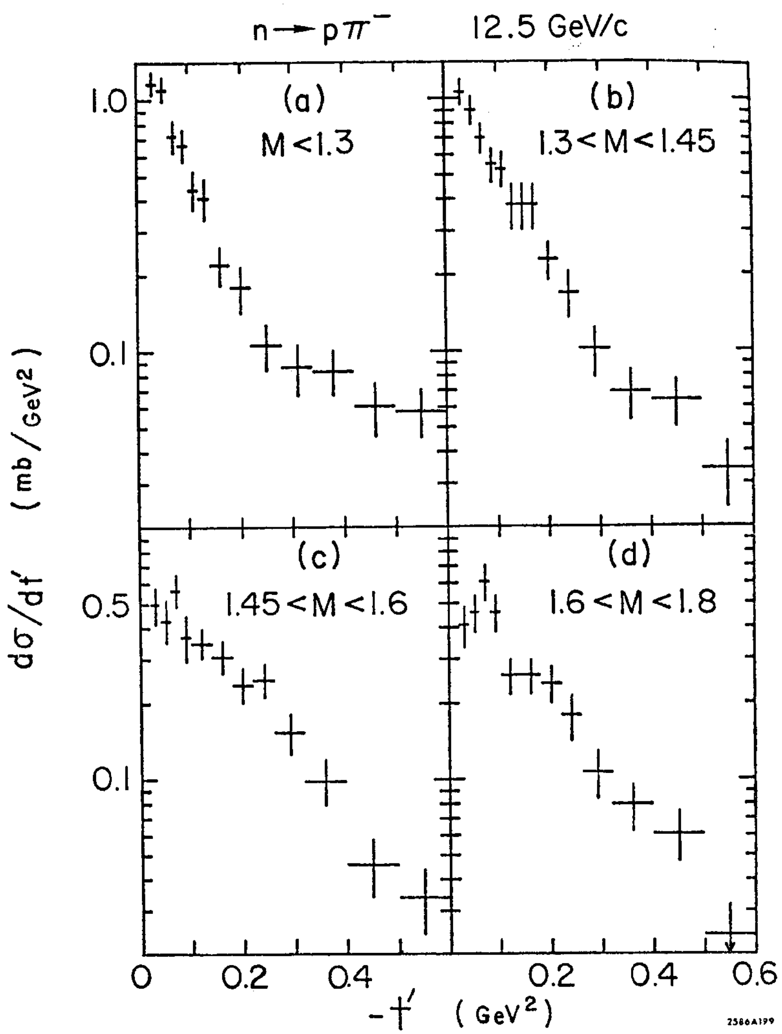

Figure 198b

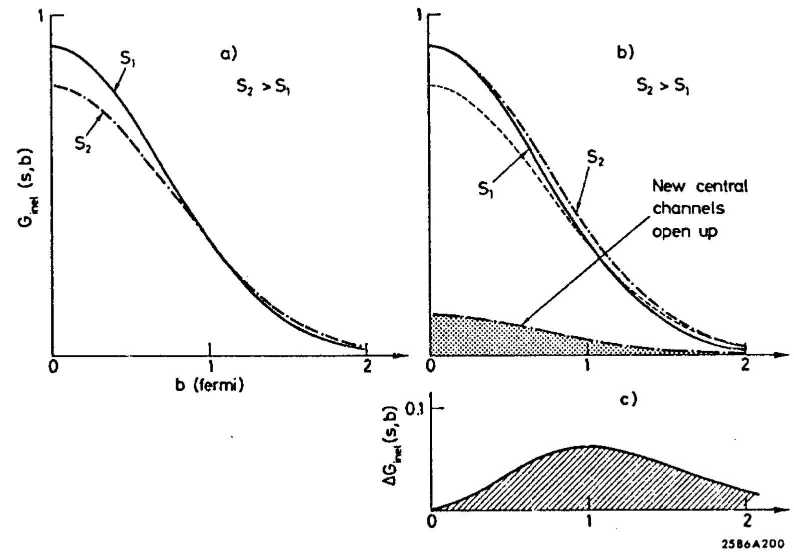

Figure 199

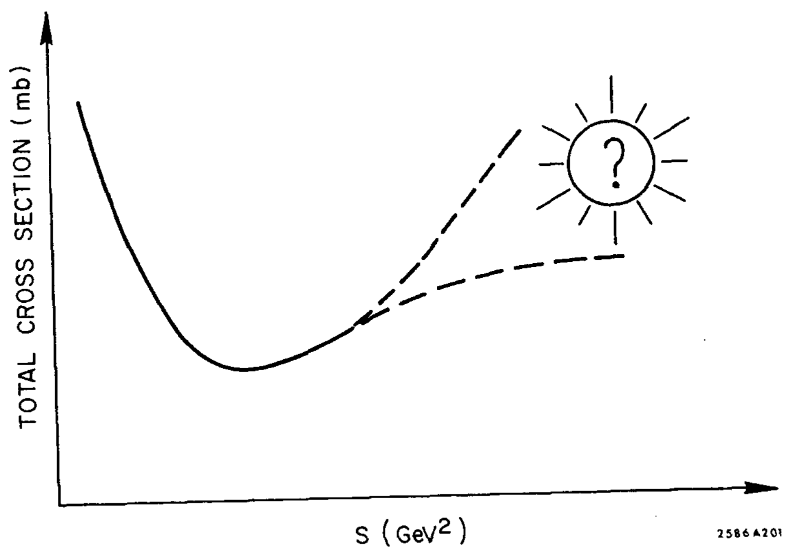

Figure 200

THE PHENOMENOLOGY OF DIFFRACTIVE PRODUCTION OF THREE-PION SYSTEMS

Lorella Jones

University of Illinois
Urbana, Illinois 61801

INTRODUCTION

The reaction $\pi^- p \to \pi^- \pi^- \pi^+ p$ has diffractive energy dependence when the mass of the three-pion system is above 1 GeV. Descriptions of the dynamics of this diffraction depend strongly, however, on whether or not the three pions originated from a resonance. Hence it is important to be able to separate the resonant and non-resonant production in the data.

As emphasized by Roger Cashmore, a resonance tends to produce both a bump in the mass spectrum and rapid phase variation in one partial wave as the mass moves through the region of the bump. Hence resonance separation requires a proper partial wave analysis of the produced 3-pion system. This was first carried out in an isobar model (FIT) by Ascoli and coworkers[1] who use as basis states $\epsilon^0\pi^-$, $\rho^0\pi^-$ and $f^0\pi^-$ in various orbital angular momenta. (Their ϵ^0 is a very broad $\pi^+\pi^-$ s-wave located somewhere near the ρ^0.) Their analysis program has also been applied by other groups; it is the program used to obtain the intensities and phases of three-pion partial waves shown by certain of the lecturers in this summer school.

Some of their many results may be summarized as follows:

i) The A_2 is a $\rho\pi$ D-wave with resonant phase variation
ii) The A_1 is a $\rho\pi$ S-wave without resonant phase variation
iii) The A_3 is an $f\pi$ S-wave without resonant phase variation
iv) There are some sizable $\epsilon\pi$ waves, also without resonant phases
v) Relative phases between all the large partial waves are determined as a function of $M_{3\pi}$
vi) The A_1 is predominantly t channel helicity zero.

These detailed results must now be confronted by phenomenologists.

In today's seminar I will neglect the resonant A_2, and focus on the various important non-resonant waves in the system. My message will be that a Reggeized Deck[1] model of relatively naive form works well for these non-resonant waves, and helps one to understand both their magnitudes and their phases. In the following section I outline the model, and point out certain features which bear directly on the partial waves obtained from it.

Deck Model

The basic idea in the Deck model is that pion exchange is important, and we think we can calculate it quantitatively. Deck[1] pointed out that the process depicted in Fig. 1 (where the hatched blob represents elastic $\pi^- p$ scattering) will produce a $\rho^0\pi^-$ state with diffractive energy dependence, with rather a lot of events in the A_1 region just above the $\rho\pi$ threshold.

Since his article, a number of improvements have been made which increase agreement with the data and allow comparison with final states other than $\rho^0\pi^-$. These are:

i) Reggeization of the pion exchange (Berger[1])
ii) Inclusion of all $\pi^+\pi^-$ partial waves from $\pi\pi$ phase shift analysis, instead of having just a ρ^0 resonance
iii) Inclusion of $\pi^-\pi^-$ scattering
iv) Symmetrization in the identical π^- particles, once improvement ii) has escalated the situation from a 3 body final state to a 4 body final state.

The diagrams to be calculated in this improved model are shown in Fig. 2. Here the hatched blobs represent $\pi\pi$ and πp elastic scattering, and the row of xxxxx represents exchange of a Reggeized pion.

At this stage, the actual calculation proceeds by Monte Carlo methods. However, certain of the important properties of the model can be understood with much less labor. In particular, one can show fairly simply that S waves and $M = 0$ (t-channel helicity zero) will predominate in the 3π final state.

Let θ_1 and φ_1 be the angles of the outgoing bachelor π^-, in the 3π rest frame, using the incident beam as the z axis. (The bachelor π^- is the one which is not in a $\pi^+\pi^-$ resonance.) Then the partial wave amplitudes may be computed as

$$F^{JM}_{IS,\rho\sigma}$$

$$= \begin{pmatrix}\text{Various}\\ \text{factors}\end{pmatrix} \sum_{\mu} \langle JM|IS,M-\mu,\mu\rangle \int_{-1}^{1} d(\cos\theta_1)$$

$$\times \int_0^{2\pi} d\phi_1\, e^{-iM\phi_1} d^L_{M-\mu,0}(\theta_1) d^S_{0\mu}(\delta) \begin{pmatrix}\text{scattering}\\ \text{amplitude}\end{pmatrix}_{\rho\sigma}$$

Here ρ and σ are nuclear spin indices, J is the total spin of the 3π system, S is the spin of the $\pi^+\pi^-$ system, and L is the orbital angular momentum between this dipion and the bachelor π^-. M is the z projection of the total spin J. Using the arguments of Gottfried and Jackson,[1] M is also the t channel helicity of the 3π system.

To begin with, disregard the factor $d^S_{0\mu}(\delta)$. It is then clear that if the amplitude has little θ_1 or ϕ_1 dependence, $L = 0$ and $M = 0$ will dominate. The rotation by δ is from the $\pi^+\pi^-$ rest frame into the 3π rest frame. It depends on θ_1, but not on φ_1. However, near the $\epsilon\pi$, $\rho\pi$, or $f\pi$ thresholds this dependence on θ_1 is not very strong, and our conclusion that $L = 0$, $M = 0$ should dominate is unaffected. Thus, in order that the model have some hope of describing the A_1 and A_3 regions, which data analysis shows are predominantly S-waves with t channel helicity zero, it must have little θ and φ dependence. More realistically, the amplitude should have little dependence on these angles in those regions of phase space where it is large.

A very clever argument invented by Stodolsky[1] can be used to show that the original Deck model amplitude has little dependence on these angles. Consider the process illustrated in Fig. 1. For high incident energy, when the $\rho^0\pi^-$ mass is held at a low value (1 or 2 GeV), the energy in the π^-p system can get quite large. In most of the phase space available, therefore, the π^-p scattering can be replaced by Pomeron exchange without serious loss. Furthermore, the amplitude for Pomeron exchange is peaked sharply forward; a large part of the overall process will thus occur near $t = 0$ (see Fig. 3). At $t = 0$, the amplitude for Pomeron exchange is up to numerical factors) $S_{\pi_0 p_0}$. Hence we see that

$$\text{Figure 3} \approx \frac{S_{\pi_0 p_0}}{t_x - \mu^2} \tag{2}$$

Now one must write out $S_{\pi_0 p_0}$ and t_x in terms of θ_1 and φ_1 (for $S_{\pi_0 p_0}$ and S large), to see how Eq. 2 behaves. In general this is laborious, and here is where Stodolsky's trick comes in. First calculate the kinematic boundary in t at the $\bar{p}p$ vertex, using an approximate formula good for large s

$$t_{min} \approx -\frac{(m^2_{3\pi} - m^2_{\pi})^2 M^2}{S^2} \tag{3}$$

The same formula can be used for the two body subreaction with π_0 and p_0 in the final state, if we treat t_x as the mass^2 of an incoming particle (and assume $S_{\pi_0 p_0}$ large).

$$t_{min} \approx \frac{-(m^2_{\pi} - t_x)^2 M^2}{S^2_{\pi_0 p_0}} \tag{4}$$

Equating these expressions, we find

$$\frac{S_{\pi_0 P_0}}{\mu^2 - t_x} \approx \frac{s}{m_{3\pi}^2 - \mu^2} \qquad (5)$$

One can see from the right hand side that there is no dependence on θ_1 and φ_1, so $L = 0$ and $M = 0$ ought to dominate in the partial wave analysis of the model (at least near $\epsilon^0\pi^-$, $\rho^0\pi^-$ and $f^0\pi^-$ threshold). These general conclusions are still true for the Reggeized and "improved" version, even though the arguments above are more approximate for this case.

Another important feature of the model is that the Reggeization provides a signature factor $(\exp[-i\pi\alpha_\pi(t_x)] + 1)$. Because t_x has angular dependence $(t_x = m_\pi^2 + S_{23} - 2E_A(M_{3\pi} - E_1) + 2p_1p_A \cos\theta_1$ in the 3π rest frame, where 2 and 3 are outgoing π's in the dipion, 1 is the outgoing bachelor π, and A is the incident π), different partial waves will automatically have different phases. These phases, first discussed by Froggatt and Ranft,[1] will vary from calculation to calculation depending on the overall θ_1 dependence of the amplitudes inserted. They can be compared with the detailed phases extracted from the data; this puts the model to a much more sensitive test than simply examining mass distributions.

A group at Illinois (Ascoli, Cutler, Jones, Kruse, Roberts, Weinstein and Wyld) have recently done a detailed comparison of the updated Deck model with the data. We used all the contributions shown in Fig. 2, and inserted the best available $\pi\pi$ and πN scattering amplitudes for the blobs. The agreement of both magnitudes and phases for most non-resonant partial waves is quite good, and hence the distributions in most mass variables are well reproduced. In particular the A_1 effect seems to be adequately described. I will restrain myself from showing slides of all possible distributions, and just refer you to our papers (Phys. Rev. D8, p. 3894; Phys. Rev. D9, p. 1963) for details. Instead of dwelling overlong on this one calculation, let me devote the rest of this seminar to some more general (and doubtless more important) questions in 3π phenomenology.

Recent Studies of the Partial Wave Analysis

The 3π partial wave analysis program has been subjected to a good deal of close scrutiny lately, and rightfully so. All our conclusions about the dynamics of the system hinge on the validity of the partial wave analysis; the question of A_1 phase variation in particular is of great interest. One can scrutinize the particular details of the Ascoli fitting routine; or, on a more general level, one can argue that the early implementations of isobar model analysis are hopelessly crude in that they neglect 3 body unitarity. Let us look at each of these in turn.

The isobar analysis is really written with the production and decay of resonances in mind. A state with spin J and projection M is produced, and it then decays into a dipion of spin S and a bachelor π in relative orbital angular momentum L. The two contributions shown in Fig. 4 are added for Bose symmetrization in the identical π^- particles. In order to have a finite number of parameters in FIT, various approximations are made, some of which are motivated by resonance considerations. One might wonder whether the program can adequately handle the sort of manifestly non-resonant situation given by the Deck model.

The Deck model can be used to test FIT, because it can be explicitly partial wave analyzed according to Eq. 1. The procedure is as follows:

i) Calculate the partial waves explicitly from the formula above

ii) Generate Monte Carlo data from the model, and run this data through FIT.

We find from the explicit partial waves that not all the approximations made in FIT are valid in the Deck model, although they are valid for the larger partial waves over much of the region. However despite the complications introduced by many small waves, the results of FIT agree well with the explicit partial wave analysis for the big waves. We conclude that FIT handles Deck-like situations well, even though it was written with resonances in mind. Hence there seems to be little point in worrying about changing details of the Ascoli fitting program; if some feature of the analysis is wrong it is probably in the original concept of the simple isobar model.

All of the information on relative phases of the partial waves depends, in the isobar method, on the assumption that the dipion mass dependence of the overall amplitude is properly approximated by Breit-Wigners. However, we know that this parametrization does not account for all $\pi^+\pi^-$ interactions; and hence it cannot provide a completely accurate description of the $\pi^+\pi^-$ cuts in the 3π amplitude. The reason is that rescattering, of the sort shown in Fig. 5, should be included. One might therefore desire to have a fitting function which automatically has unitarity, in the sense that it has the correct dipion cuts. Fits using such a function might possibly be better in the same way that the $(\eta_\ell\, e^{2i\delta_\ell} - 1)/2i$ parametrization is good for partial waves of two-body processes.

Two groups have been working on the implementation of these ideas:

L.B.L.: Goradia, Lasinski, Tabak, and Smadja

Illinois: Ascoli and Wyld

Although the two groups use rather different language in discussing their methods, both end up with the same equation and both have essentially the same results.[2)] Basically, they formulate an integral equation which the amplitude must satisfy if it has the correct discontinuity across the dipion cuts. They then solve this equation with isobar model input to find new states. These new states then include the rescattering, and fitting with these states essentially strips away the rescattering to get at the original production process.

Let R_1, R_2 be the old fitting functions, and S_1, S_2 the new fitting functions, where the index i indicates that the last scattering occurred between π_i^- and π^+. Then the integral equations to be solved may be written schematically as

$$S_1 = R_1 + it_1\rho\, A_{12}S_2$$

$$S_2 = R_2 + it_2\rho\, A_{21}S_1 \qquad (6)$$

Here t_i is the $\pi^+\pi_i^-$ scattering amplitude, ρ is a phase space, and A_{ij} is a recoupling coefficient in momentum and isospin space. The rescattering tends to "mix" states of a given J and parity, so that a state produced as a $1^+\rho\pi$ S-wave may emergy as a $1^+\epsilon\pi$ P-wave.

Fits with these new functions yield the following results:[2)]

i) The A_2 does exhibit a resonant phase

ii) The A_1 bump is still in the $1^+\rho\pi$ S-wave

iii) The A_1 does not exhibit a resonant phase.

Essentially, therefore, the qualitative conclusions are unchanged from those obtained with the original isobar model. Of course, numerous details of the results are different.

The fitters are somewhat unhappy with the new functions because the χ^2 is not as good as with the old isobar model, and not all the distributions are reproduced as well by the fit. Interpretation of these facts is still up in the air. A complete understanding of these "unitary" fits has not yet been reached, but it is unlikely that any further major improvement of the analysis can be achieved in the near future.

Where do we go from here?

Work is in progress by the fitters to understand the role of their various approximations, both using the isobar states and the new "unitarized" states. This will inevitably lead to refinements in the results; at present no one seems to believe that it will lead to a qualitative change in the results.

Theories like the Deck model, which have no rescattering, should really be compared with the results of the new analysis rather than the old. A cursory look at this indicates that agreement will improve in some regards and decrease in others, but that the overall impression of agreement will remain.

Similar experimental and theoretical remarks apply to the Q region.

References

1. All work mentioned in this seminar, except that discussed in Reference 2, is properly referenced in two papers by Ascoli *et al.*: Phys. Rev. D8, p. 3894; and Phys. Rev. D9, p. 1963. Needless to say, these papers also contain references to other important work which failed to find its way into the talk. The interested reader is thus urged to peruse the reference lists in the above papers (whether he reads the texts or not!).
2. Phase shifters are notoriously cautious and it is difficult to obtain written copies of their work until they have checked everything many times. This reference, therefore, of necessity refers to extant but unpublished work.

   Both Ascoli and Lasinski gave talks at the Meson Resonance Conference, Boston, 1974. Hence some of their work should appear in the proceedings of this conference.

   Both groups are also preparing a longer version for publication. As further fitting of data will probably be done before these papers reach the physical sheet, the time of publication is uncertain.

Figure Captions

Fig. 1. Original Deck Model.

Fig. 2. Glorified Deck Model.

Fig. 3. Labelling of Variables for Eq. 2.

Fig. 4. Basic Isobar Model

Fig. 5. A Possible Rescattering.

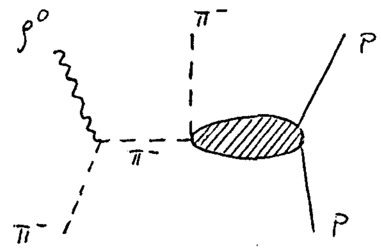

Figure 1

Original Deck Model

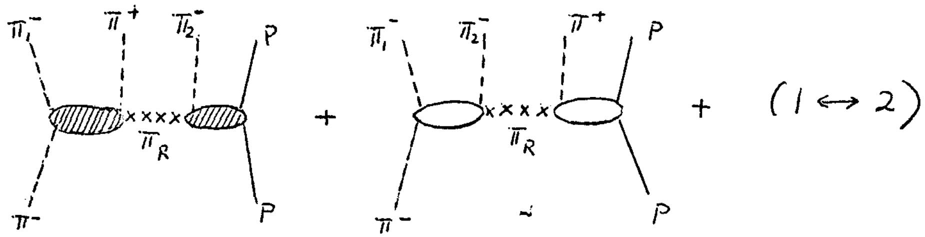

Figure 2

Glorified Deck Model

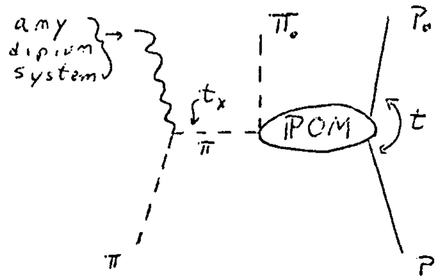

Figure 3

Labelling of variables for Eq.2

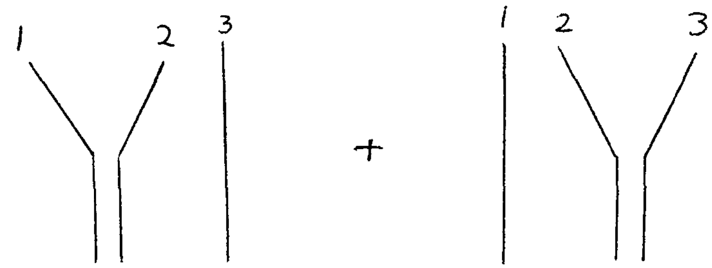

Figure 4

Basic Isobar Model

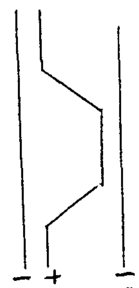

Figure 5

A Possible Rescattering

AMPLITUDE STRUCTURE IN TWO- AND QUASI-TWO-BODY PROCESSES

Michel Davier

Stanford Linear Accelerator Center
Stanford University, Stanford, California 94305

OUTLINE

II. GENERAL FEATURES OF EXCHANGE PROCESSES

1. Kinematic Dependence

(a) s dependence

(b) t dependence and helicity structure

2. Quantum Numbers Exchanged

(a) allowed exchange

(b) exotic exchanges

(c) SU(3) symmetry

3. Phases

(a) $t = 0$

(b) $t \neq 0$

III. EXTRACTING AMPLITUDES FROM INCOMPLETE DATA

1. Projection of one amplitude: exchanges in elastic scattering

(a) cross-over effect

(b) polarizations

2. Making Use of Analyticity Properties of Amplitudes

(a) application of dispersion relations to πN amplitude analyses

(b) derivative analyticity relations

(c) application of derivative analyticity relations to amplitude analyses

IV. DUALITY AND ABSORPTION

1. Duality

(a) two descriptions of 2-body scattering

(b) relating low and high energy descriptions: FESR

(c) two-component duality

(d) application of duality: exchange degeneracy

(e) duality and quarks

(f) semi-local duality ?

2. Absorption

(a) classical absorption

(b) absorption zeroes vs signature zeroes

(c) dual absorption

V. MODELS AND SPECULATIONS

1. Models for Two-Body Scattering

(a) dual absorptive model

(b) strong absorption models

2. Speculations on the Pomeron

(a) Pomeron from high energy pp data

(b) Can we extract $\mathrm{Im}\, P(s,0)$ at lower s?

(c) application to $\gamma p \to \phi p$

(d) implications for exchange degeneracy

OUTLOOK

INTRODUCTION

In this series of lectures we are concerned with the experimental determination of two-body amplitudes and their phenomenology. Even though two-body and quasi-two-body processes represent only a small fraction of the total interaction, their study is very important in several respects:

(1) They provide the simplest laboratory for studying the exchange forces between hadrons in a rather controllable way: energies, spins, particle identities and quantum numbers can be varied separately.

(2) Two-body processes constitute a testing ground for--as well as inducing--theoretical ideas in hadron dynamics. Concepts like Regge poles, duality, absorption have been brought forward in trying to understand exchange processes. In turn these new ideas have been applied to more complex situations involving multiparticle final states.

(3) Even at super-high energies where the cross sections for known identifiable two-body processes will become very small--except for elastic scattering--we still hope two-body scattering ideas will be relevant. Indeed in a multiparticle event subenergies will still be rather small and two-body exchanges will probably still happen.

In these lectures we would like to focus our interest on the structure of the amplitudes. Rather than discussing two-body scattering data in a general way, we are going to translate and summarize our knowledge in terms of amplitudes. In the first chapters, we shall try to make as little reference as possible to our sometimes preconceived theoretical ideas, but instead try to extract the maximum unbiased information from the data.

I - GENERALITIES AND COMPLETE EXTRACTION OF AMPLITUDES FROM DATA

1. Generalities on Amplitudes (Spinology)

(a) Helicity formalism.[1,2]

Consider the scattering process

$$1 + 2 \rightarrow 3 + 4$$

where each particle is labelled by a set of quantum numbers: λ_i (helicity), J_i (spin), η_i (parity), m_i (mass) and $\vec{p}_i$ (momentum). The naturality ξ is defined by:

$$\xi = (-1)^J \eta = \tau\eta$$

where τ is the signature. The process can be described in either the s or the t channel with helicity amplitudes:

s-channel

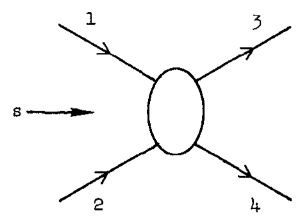

$$F^s_{\lambda_3\lambda_4\lambda_1\lambda_2}(s,t)$$

t-channel

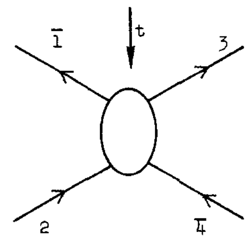

$$F^t_{\lambda_3\lambda_{\bar{1}}\lambda_{\bar{4}}\lambda_2}(s,t)$$

The amplitudes can be decomposed into amplitudes with well-defined total angular momentum J using the Jacob-Wick expansion:

$$F^s_{\lambda_3\lambda_4\lambda_1\lambda_2}(\theta,\phi) = \sum_J (2J+1)\, F^{s(J)}_{\lambda_3\lambda_4\lambda_1\lambda_2}\, e^{-(\lambda-\mu)\phi}\, d^J_{\lambda\mu}(\theta)$$

with $\lambda = \lambda_1 - \lambda_2$ and $\mu = \lambda_3 - \lambda_4$

At high energy amplitudes are built up by exchanges in the $t(u)$ channel. Usually a given exchange is characterized by a set of quantum numbers: η, τ, SU(3) quantum numbers, etc. ... . Although t-channel helicity amplitudes show simple relations for a well-defined t-channel exchange, s-channel amplitudes are more widely used now: kinematic constraints are easier to take into account in pole models and more importantly they probably have a more physical interpretation.

-exchange of well-defined naturality in the t-channel[3]

Consider an exchange with quantum numbers J, η in the t-channel.

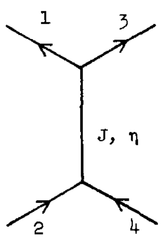

Parity conservation at vertex $2\bar{4}J$ reads:

$$F^{t(J)}_{\lambda_3\lambda_{\bar 1}\lambda_{\bar 4}\lambda_2} = \eta_2\eta_{\bar 4}\eta(-1)^{J+J_4-J_2}\, F^{t(J)}_{\lambda_3\lambda_{\bar 1}-\lambda_{\bar 4}-\lambda_2}$$

$$F^t_{\lambda_3\lambda_{\bar 1}\lambda_{\bar 4}\lambda_2} = (2J+1)\, d^J_{\lambda\mu}(\theta_t)\, F^{t(J)}_{\lambda_3\lambda_{\bar 1}\lambda_{\bar 4}\lambda_2}$$

$$\lambda = \lambda_{\bar 1} - \lambda_3, \qquad \mu = \lambda_2 - \lambda_{\bar 4}$$

At high energy (to leading order in s) we have

$$d^J_{-\lambda\mu}(\theta_t) = (-1)^\lambda\, d^J_{\lambda\mu}(\theta_t) + O(\tfrac{1}{s})$$

$$(\cos\theta_t \to 1)$$

leading to:

$$F^t_{\lambda_3\lambda_{\bar 1}\lambda_{\bar 4}\lambda_2} = \eta(-1)^J\,\eta_{\bar 4}\eta_2\,(-1)^{\lambda_{\bar 4}-\lambda_2}\,(-1)^{J_4-J_2}\, F^t_{\lambda_3\lambda_{\bar 1}-\lambda_{\bar 4}-\lambda_2} + O(\tfrac{1}{s})$$

where $\xi = \eta(-1)^J$ is the exchanged naturality. A similar relation holds for the $\bar{1}3J$ vertex. An important consequence of these formulae is that amplitudes with opposite naturality do not interfere in the unpolarized differential cross section.

To see the effect on the (J,η) exchange on s-channel amplitudes, one must make use of the s-t crossing matrix. After some more non-leading terms in s are dropped, the following relations hold:

$$F^s_{\lambda_3\lambda_4\lambda_1\lambda_2} = \xi\,\eta_2\eta_4(-1)^{J_4-J_2}(-1)^{\lambda_4-\lambda_2}\, F^s_{\lambda_3-\lambda_4-\lambda_1-\lambda_2} + O(\tfrac{1}{s})$$

$$= \xi\,\eta_1\eta_3(-1)^{J_3-J_1}(-1)^{\lambda_3-\lambda_1}\, F^s_{-\lambda_3\lambda_4-\lambda_1\lambda_2} + O(\tfrac{1}{s})$$

As an example, let us consider the processes $\pi N \to \rho N$ or ρN^*. At the $\pi\rho$ vertex, for high energies, one has the relation

$$F^s_{\lambda_\rho\lambda_4\lambda_2} = -\xi\,(-1)^{\lambda_\rho}\, F^s_{-\lambda_\rho\lambda_4\lambda_2}$$

so that $\xi = +1$ exchanges contribute only to helicities $\lambda_\rho = \pm 1$, while $\xi = -1$ exchanges populate all helicities $\lambda_\rho = 0, \pm 1$.

-number of independent helicity amplitudes

Restrictions on helicity amplitudes are imposed by invariance under discrete symmetries: parity, time-reversal, charge conjugation.

parity

$$F_{\lambda_3\lambda_4\lambda_1\lambda_2} = \eta_1\eta_2\eta_3\eta_4(-1)^{J_1+J_2+J_3+J_4}\,(-1)^{\lambda_1+\lambda_2+\lambda_3+\lambda_4}\,F_{-\lambda_3-\lambda_4-\lambda_1-\lambda_2}$$

time reversal (restricts the number of amplitudes only for elastic scattering

$$F_{\lambda_3\lambda_4\lambda_1\lambda_2} = F_{\lambda_1\lambda_2\lambda_3\lambda_4}$$

charge conjugation (for charge-conjugate reactions like $\bar{p}p \to \bar{\Lambda}\Lambda$)

$$F_{\lambda_3\lambda_4\lambda_1\lambda_2} = \epsilon_1\epsilon_2\epsilon_3\epsilon_4\,F_{\lambda_4\lambda_3\lambda_2\lambda_1}$$

Using these rules enables one to determine the number of independent amplitudes required to describe a given process: a few simple examples are shown in Table 1. A general remark is that except for reactions of the type $0\,\frac{1}{2} \to 0\,\frac{1}{2}$ with only 2 amplitudes, the number of amplitudes for processes of interest is large (≥ 4) and consequently the separation of individual amplitudes is a somewhat tedious experimental task.

(b) Invariant amplitudes

Helicity amplitudes refer explicitly to the centre-of-mass frame. When calculating scattering amplitudes from field theory, or when studying analytic properties, it is useful to write down explicitly invariant amplitudes.

If no spins are involved, the only Lorentz scalars are s and t (u) and the scattering amplitude is a scalar

$$T = f(s,t)$$

When some of the particles have spin, Lorentz invariants I_n can be constructed from 4-vectors and spin tensors:

$$T = \sum_n f_n(s,t)\,I_n$$

where the f_n are invariant amplitudes. Invariant amplitudes are related linearly to helicity amplitudes:

$$f_n(s,t) = \sum_{(\lambda)} A_{(\lambda)}(s,t)\,F_{(\lambda)}(s,t)$$

where (λ) represents a set of helicities and the $A_{(\lambda)}$ are known kinematic functions.

-example: $0^-\,\frac{1}{2}^+ \to 0^-\,\frac{1}{2}^+$ elastic scattering.

Using the 2 Dirac spinors, it is possible to form 2 invariants and the general form of the amplitudes in terms of the 2 invariant amplitudes A and B is:

$$T = \bar{u}_4\left[A(s,t) + \tfrac{1}{2}B(s,t)\,[\not{q}_2 + \not{q}_4]\right]u_2$$

Assuming $m_1 = m_3 \ll m_2 = m_4 = M$, one can express the s-channel helicity amplitudes in terms of the invariant amplitudes A and B:

$$\begin{cases} F_{++} = \dfrac{M}{4\pi\sqrt{s}}\cos\dfrac{\theta}{2}\left[A + \left(\nu - \dfrac{t}{4M}\right)B\right] \\[2ex] F_{+-} = \dfrac{M}{4\pi\sqrt{s}}\sin\dfrac{\theta}{2}\,\dfrac{M}{2\sqrt{s}}\left[\dfrac{4M\nu - t + 4M^2}{2M^2}A + \dfrac{4M\nu - t}{2M}B\right] \end{cases}$$

where $\nu = (s-u)/4M$ and the following notation has been used:

$$F_{++} \equiv F_{0\frac{1}{2}0\frac{1}{2}} \qquad\qquad F_{+-} \equiv F_{0-\frac{1}{2}0\frac{1}{2}}$$

$$\frac{d\sigma}{dt} = \frac{4\pi}{s}\left[|F_{++}|^2 + |F_{+-}|^2\right]$$

At high s and for t not too large, we have the simpler expressions:

$$\begin{cases} F_{++} \simeq \dfrac{M}{4\pi\sqrt{s}} (A + \nu B) = \dfrac{M}{4\pi\sqrt{s}} A' \\ F_{+-} \simeq \dfrac{M}{4\pi\sqrt{s}} \dfrac{\sqrt{-t}}{s} [(\nu + M)A + M\nu B] \xrightarrow[s\to\infty]{} \dfrac{\sqrt{-t}}{8\pi\sqrt{s}} A \end{cases}$$

so that

$$\left(\frac{d\sigma}{dt}\right)_{s\to\infty} = \frac{M^2}{4\pi s^2} \left[|A'^2| - \frac{t}{4M^2} |A|^2 \right]$$

$$= \frac{1}{s^2} \; [|M_{++}|^2 + |M_{+-}|^2]$$

The amplitudes A and B are free of kinematic singularities and possess simple properties under s-u crossing. Defining the amplitudes $A^{(\pm)}$ and $B^{(\pm)}$ for πN scattering:

$$A^{(+)} = \frac{1}{3} [A(I_s = \tfrac{1}{2}) + 2A(I_s = \tfrac{3}{2})] = \frac{1}{\sqrt{6}} A(I_t = 0)$$

$$A^{(-)} = \frac{1}{2} [A(I_s = \tfrac{1}{2}) - A(I_s = \tfrac{3}{2})] = \frac{1}{2} A(I_t = 1)$$

(and similar relations for $B^{(\pm)}$), s-u crossing means:

$$A^{(\pm)}(s,t,u) = \pm A^{(\pm)}(u,t,s)$$

$$B^{(\pm)}(s,t,u) = \mp B^{(\pm)}(u,t,s)$$

(c) Density matrices and polarizations

The initial state is described by a density matrix ρ^i with $\mathrm{Tr}\,\rho^i = 1$. If no polarization is observed in the final state, the differential cross section is expressed by

$$\frac{d\sigma}{dt} = \frac{1}{s^2} \mathrm{Tr}(M\rho^i M^\dagger) = \frac{1}{s^2} \sum_{\substack{\lambda_3\lambda_4 \\ \lambda_1\lambda_2\lambda_1'\lambda_2'}} M_{\lambda_3\lambda_4\lambda_1\lambda_2} \rho^i_{\lambda_1\lambda_2\lambda_1'\lambda_2'} M^\dagger_{\lambda_3\lambda_4\lambda_1'\lambda_2'}$$

For unpolarized initial state ρ^i is a diagonal unit matrix multiplied by a normalization constant:

$$\rho^i = \frac{I}{(2J_1 + 1)(2J_2 + 1)}$$

The polarization information on the final state is described by a density matrix ρ^f:

$$\left(\frac{d\sigma}{dt}\right) \rho^f = \frac{1}{s^2} M\rho^i M^\dagger$$

$$\rho^f = \frac{M\rho^i M^\dagger}{\mathrm{Tr}(M\rho^i M^\dagger)}$$

The expectation value of an observable A referring to the spins of the final state particles is given by:

$$\langle A \rangle = \frac{\mathrm{Tr}(\rho^f A)}{\mathrm{Tr}\,\rho^f}$$

For the construction of density matrices describing polarization states for arbitrary spins, see Ref. 4.

-examples.

$0\,\frac{1}{2} \to 0\,\frac{1}{2}$: the density matrix describing the nucleon polarization has the general form $\rho = \frac{1}{2} [I + \vec{P}\cdot\vec{\sigma}\,]$ corresponding to a polarization P_i of the nucleon along the axis i

$$P_i = \frac{1}{2} \; \frac{\mathrm{Tr}(\rho\sigma_i)}{\mathrm{Tr}\,\rho}$$

$\frac{1}{2}\frac{1}{2} \to \frac{1}{2}\frac{1}{2}$: the most general density matrix with correlations will involve the tensor products between I, $\vec{\sigma}_1$ and $\vec{\sigma}_2$:

$$\rho = \frac{1}{4}\left[I + \vec{P}_1\cdot\vec{\sigma} \otimes I + \vec{P}_2\cdot\vec{\sigma} \otimes I + \sum_{i,j=x,y,z} c_{ij}\sigma_i \otimes \sigma_j\right]$$

(d) <u>observables in</u> $0^- \frac{1}{2}^+ \to 0^- \frac{1}{2}^+$ <u>scattering</u> (such as $\pi N \to \pi N$, $\pi N \to K\Sigma$, $\bar{K}N \to K\Lambda$, etc.)

The amplitude is a 2×2 matrix in helicity space and parity conservation gives the form:

$$\begin{array}{cc} M = \begin{bmatrix} M_{++}e^{i(\phi/2)} & -M_{+-}e^{-i(\phi/2)} \\ M_{+-}e^{i(\phi/2)} & M_{++}e^{-i(\phi/2)} \end{bmatrix} & \longleftarrow \lambda_2 \\ \uparrow & \\ \lambda_4 & \end{array}$$

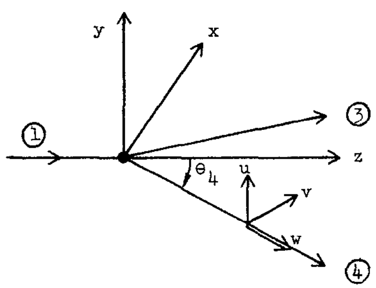

(axes convention; $\phi = 0$)

$\cos\phi = \hat{y}\cdot\hat{n}$

$$\rho^i = \frac{1}{2}\begin{bmatrix} 1+P_z^i & P_x^i - iP_y^i \\ P_x^i + iP_y^i & 1-P_z^i \end{bmatrix}$$

where $\vec{P}^i$ is the initial polarization vector of the nucleon. It is straightforward, although tedious, to compute the 3 components of polarization of the final baryon. Defining:

$$\frac{d\sigma}{dt} = \frac{1}{s^2}\left[|M_{++}|^2 + |M_{+-}|^2\right]$$

$$P = -\frac{2\,\mathrm{Im}\,M_{++}M_{+-}^*}{|M_{++}|^2 + |M_{+-}|^2}$$

$$A' = \frac{|M_{++}|^2 - |M_{+-}|^2}{|M_{++}|^2 + |M_{+-}|^2}$$

$$R' = -\frac{2\mathrm{Re}\,M_{++}M_{+-}^*}{|M_{++}|^2 + |M_{+-}|^2}$$

one finds the final polarization components:

$$P_z^f\,\mathrm{Tr}\,\rho^f = A'P_z^i + P_x^i[R'\cos\phi - P\sin\phi] + P_y^i\,[R'\sin\phi + P\cos\phi]$$

$$P_x^f\,\mathrm{Tr}\,\rho^f = -R'P_z^i + A'P_x^i + A'P_y^i$$

$$P_y^f\,\mathrm{Tr}\,\rho^f = P_y^i + P - P_x^i\sin\phi$$

with $\mathrm{Tr}\,\rho^f = 1 - PP_x^i\sin\phi + PP_y^i\cos\phi$.

For a stable baryon, polarization can be experimentally analyzed in a rescattering experiment: in this case only the transverse component of the polarization is measured and one must consider different orientations of the target polarization in order to separate A' and R'. Usually the rotated A and R parameters (corresponding to the transverse polarization) are measured:

$$A = A'\sin\theta_4^L + R'\cos\theta_4^L$$

$$R = -A'\cos\theta_4^L + R'\sin\theta_4^L \qquad \text{(lab angle)}$$

For small t, $\theta_4^L \to \pi/2$ and $A \to A'$, $R \to R'$. P, A and R are not 3 independent observables since $P^2 + R^2 + A^2 = 1$ and in general P and R measurements will suffice, except for the sign of A. Figure 1 shows schematically the experimental configurations in the scattering plane to measure A and R when only transverse polarization is measured for the outgoing baryon.

2. πN Amplitudes at 6 GeV/c

This represents the only case where all observables have been measured, therefore permitting the separation of all helicity amplitudes. It is worth looking with some detail since it represents, in principle, the only unbiased source of information on individual amplitudes.

(a) Data and observables

In addition to helicity subscripts, we will use the isospin exchange in the t-channel I_t to label amplitudes. We have:

$$F(\pi^\pm p \to \pi^\pm p) = F^0 \mp F^1$$

$$F(\pi^- p \to \pi^0 n) = \sqrt{2}\, F^1$$

In terms of "particle" exchange F^0 corresponds to (Pomeron + f) exchange while F^1 corresponds to ρ exchange. To describe the 3 reactions, one needs 4 independent amplitudes, therefore 8 real numbers for each t value. The observables for each reaction are:

$$\frac{d\sigma}{dt} = |F_{++}|^2 + |F_{+-}|^2$$

$$-P\,\frac{d\sigma}{dt} = 2\,\mathrm{Im}(F_{++}F^*_{+-})$$

$$-R\,\frac{d\sigma}{dt} = [|F_{++}|^2 - |F_{+-}|^2]\cos\theta_L + 2\,\mathrm{Re}(F_{++}F^*_{+-})\sin\theta_L$$

$$A\,\frac{d\sigma}{dt} = [|F_{++}|^2 - |F_{+-}|^2]\cos\theta_L - 2\,\mathrm{Re}(F_{++}F^*_{+-})\cos\theta_L$$

The measured observables around $P_L = 6$ GeV are:[5-12]

$$\begin{array}{ccc} \frac{d\sigma^+}{dt}, & \frac{d\sigma^-}{dt}, & \frac{d\sigma^0}{dt} \\ P^+, & P^-, & P^0 \\ R^+, & R^- & \\ & (A^-) & \end{array}$$

(b) Amplitude extraction

For $t \neq 0$ amplitudes can be determined up to an overall phase. Since F^0_{++} is the dominant diffractive amplitude, thus mostly imaginary, all other amplitudes are projected on F^0_{++}. Therefore at each t value there are 7 unknown real numbers to be determined: F^0_{++}, $(F^0_{+-})_\parallel$, $(F^0_{+-})_\perp$, $(F^1_{++})_\parallel$, $(F^1_{++})_\perp$, $(F^1_{+-})_\parallel$ and $(F^1_{+-})_\perp$ (where $\perp$, $\parallel$ denotes component orthogonal, collinear to F^0_{++}). It follows that:

F^0_{++} is mostly determined from $\frac{d\sigma^+}{dt} + \frac{d\sigma^-}{dt}$

$(F^0_{+-})_\parallel$ is mostly determined from R^-

$(F^0_{+-})_\perp$ is mostly determined from $P^+\frac{d\sigma^+}{dt} + P^-\frac{d\sigma^-}{dt}$

$(F^1_{++})_\parallel$ is mostly determined from $\frac{d\sigma^-}{dt} - \frac{d\sigma^+}{dt}$

and $(F^1_{+-})_\perp$ is mostly determined from $P^+\frac{d\sigma^+}{dt} - P^-\frac{d\sigma^-}{dt}$

$(F^1_{+-})_\parallel$ could be determined from $R^-(d\sigma^-/dt) - R^+(d\sigma^+/dt)$, but data on $R^\pm$ is not good enough to proceed in this way: so that, in practice, the remaining two amplitudes $(F^1_{+-})_\parallel$ and $(F^1_{+-})_\perp$ are determined by two quadratic equations involving $d\sigma^0/dt$ and P^0.

In general two solutions for the F^0 amplitudes are found, whereas 4 solutions emerge for $(F^1_{++})_\perp$ and $(F^1_{+-})_\parallel$. Continuity from $t = 0$ together with the sign of $R^-(d\sigma^-/dt) - R^+(d\sigma^+/dt)$ seem sufficient to remove the ambiguities. At larger t values ($-t > 0.5$ GeV^2) ambiguities appear again because of insufficient information on R.

(c) Experimental problems

Besides the difficult experiments to measure $R^\pm$ (it is significant that only one experimental group has performed that experiment so far), the determination of the πN amplitudes suffer from uncertainties of experimental origin.

--it is hard to measure $\frac{d\sigma^-}{dt} - \frac{d\sigma^+}{dt}$ and hence $F(^1_{++})_\parallel$.

At 6 GeV, $d\sigma^-/dt \sim 40\, e^{7.7t}$ and $d\sigma^+/dt \sim 37\, e^{7.1t}$ (in mb/GeV^2), giving a cross-over zero around $t_c = -\,0.15$ GeV^2 (approximately the zero of $(F^1_{++})_\parallel$). If normalization uncertainties are 5%, then the error in location of t_c is $\Delta t_c = 0.1$ GeV^2, namely, its accurate position is not known. This situation has been improved by the experiment of Ambats et al. who claimed a normalization uncertainty of $\pm$ 1.5% between π^+p and π^-p, giving a Δt_c error of $\pm$ .025 GeV^2.

--measured values of P^0 are spread over a wide range outside quoted errors. Argonne points[11] are typically lower (~ 0.2) than CERN points[10] (~ 0.4). This particularly affects the determination of $(F^1_{++})_\perp$ as its zero can be moved from $t = -0.25$ to -0.5 GeV^2 according to what P^0 measurements are used.

(d) Results

There have been several analyses,[13-16] all using essentially the same sets of data. We are going to discuss the latest analysis[5] by the Argonne group since it uses their new data on $d\sigma^\pm/dt$.

--$I_t = 0$ exchange $(P + f)$ (Fig. 2).

F^0_{++} is large and is the dominant amplitude; it is roughly exponential in t. F^0_{+-} is small, but predominantly imaginary so that s-channel helicity is approximately conserved. To express the deviation in a quantitative way, it is useful to consider the invariant amplitudes A and A':

$$\left|\frac{A_0}{A'_0}\right| = \frac{2M\,|F^0_{+-}|}{\sqrt{-t}\,|F^0_{++}|} = 0.32 \pm 0.04, \qquad 0.10 < -t < 0.5 \text{ GeV}^2$$

The same ratio computed from t-channel helicity amplitudes yields a value of 1.5.

It is important to note that P and f exchanges cannot be separated since they have the same quantum numbers and consequently they always appear together in the observables. It is only through the energy dependence of the F^0 amplitudes over a large s range that P and f could be disentangled; unfortunately we only have 6 GeV so far.

--$I_t = 1$ exchange (ρ), (Fig. 3).

$(F^1_{++})_\parallel$ has a zero at $-t \sim 0.15$ GeV^2 and is strongly peripheral. A Bessel-Fourier transformation into impact parameter space shows a broad peak centered at about 1 f. $(F^1_{++})_\perp$ also goes through zero in the same t range, although at a larger value than $(F^1_{++})_\parallel$: it occurs at $-t \sim 0.25$ GeV^2 with the Argonne polarization data[11] while it moves out to $-t \sim 0.4$ GeV^2 with the CERN data.[10] The modulus of F^1_{+-} vanishes around $-t \sim 0.6$ GeV^2. Ambiguities preclude from making a precise conclusion above 0.6: in particular (although there is a hint in the data) it is not possible to see if there is a single zero in $(F^1_{+-})_\parallel$ and a double zero in $(F_{+-})_\perp$ as would be expected from a ρ Regge pole amplitude. The behaviour of the phase difference between F^0_{++} and F^1_{+-} is interesting since it is essentially independent of t for $-t < 0.4$ GeV^2: if ρ exchange is Regge-behaved in the helicity-flip amplitude, it therefore means that the phase of F^0_{++} is changing significantly with t. This is important to keep in mind since F^0_{++} is the reference amplitude and consequently the correspondence between $\perp$ and $\parallel$ components and real and imaginary parts is unfortunately not straightforward.

(e) Future of complete amplitude analyses

In πN scattering, R^- measurements already exist at 16 and 40 GeV,[17] but P_0 measurements do not extend beyond 11 GeV. At 16 GeV some information can be obtained on F^0 amplitudes:

$$\frac{2M\,|F^0_{+-}|}{\sqrt{-t}\,|F^0_{++}|} = 0.26 \pm 0.06$$

i.e. not very much smaller than the value at 6 GeV.

In KN and $\overline{K}N$ scattering there are 8 independent amplitudes and therefore 15 unknown quantities (+ overall phase). Eight independent observables have so far been measured around 8 GeV:

$$\frac{d\sigma}{dt}(K^{\pm}p) \qquad \frac{d\sigma}{dt}(K^0_L p \to K^0_S p)$$

$$\frac{d\sigma}{dt}(K^- p \to \overline{K}^0 n) \qquad \frac{d\sigma}{dt}(K^+ n \to K^0 p)$$

$$P(K^{\pm}p) \qquad P(K^- p \to \overline{K}^0 n)$$

while a measurement of $P(K^+ n \to K^0 p)$ is underway at CERN. So at least 6 other experiments are needed to measure:

$$\frac{d\sigma}{dt}(K^{\pm}n) \qquad P(K^{\pm}n)$$

$$P(K^0_L p \to K^0_S p) \qquad R(K^+ p)$$

The complete extraction of KN and $\overline{K}N$ amplitudes at high energy will remain a dream still for some time.

3. Hypercharge Exchange Reactions

In hypercharge exchange processes the final baryon is a Λ^0, Σ^+ or a Y^* decaying into Λ or Σ. It is therefore possible to measure all the components of its polarization vector with the observation of the angular distribution of the weak decay (we exclude final states with Σ^0 which decays electromagnetically). Examples of such processes are:

$$\pi^+ p \to K^+\Sigma^+$$
$$K^- p \to \pi^0\Lambda^0$$
$$\pi^+ p \to K^+ Y_1^{*+}$$
$$\hookrightarrow \Sigma^+\pi^0,\ \Lambda^0\pi^+$$

(a) Decay angular distribution of an unstable baryon

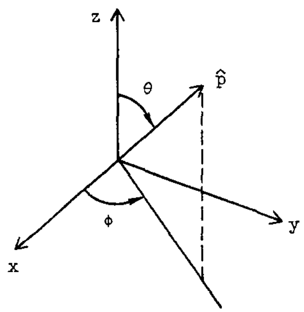

Generally the decay angular distribution is given by:

$$W(\hat{p}) = \sum_{\substack{\lambda\lambda' \\ (\mu)}} \rho^{(\mu\mu)}_{\lambda\lambda'}\ B^{\lambda\lambda'}(\hat{p})$$

where $\rho^{(\mu\mu')}_{\lambda\lambda'}$ is the density matrix for the final state plarization in the reaction (μ refers to the helicity state of the particles accompanying the hyperon in the final state).

For a weak two-body decay ($\Lambda^0 \to p\pi^-$, $\Sigma^+ \to p\pi^0$) where $\hat{p}$ can be taken along the final proton, the elements $B^{\lambda\lambda'}$ take the following form:

$$B^{\frac{1}{2}\,\frac{1}{2}} = \frac{1}{4\pi}(1 + \alpha\cos\theta)$$
$$B^{-\frac{1}{2}\,-\frac{1}{2}} = \frac{1}{4\pi}(1 - \alpha\cos\theta)$$
$$B^{\frac{1}{2}\,-\frac{1}{2}} = \frac{\alpha}{4\pi}e^{i\phi}\sin\theta$$
$$B^{-\frac{1}{2}\,\frac{1}{2}} = \frac{\alpha}{4\pi}e^{-i\phi}\sin\theta$$

where α is the decay parameter in the parity-violating weak decay, measuring the interference between S and P waves:

$$\alpha = \frac{2\,\mathrm{Re}\,S^*P}{|S|^2 + |P|^2}$$

Using the expression used previously for the density matrix elements of a spin 1/2 particle expressed in terms of the polarization vector, we get

$$W(\hat{p}) = \frac{1}{4\pi}\,(1 + \alpha\,\vec{P}_Y \cdot \hat{p})$$

where P_Y is the hyperon polarization vector. Experimentally the situation is hopeful:

$$\left.\begin{aligned} &\alpha(\Lambda^0 \to p\pi^-) = 0.65 \\ &\alpha(\Sigma^+ \to p\pi^0) = -0.98 \end{aligned}\right\} \quad \text{(very good analyzers)}$$

$$\alpha(\Xi^- \to \Lambda\pi^-) = -0.39$$

$$\alpha(\Xi^0 \to \Lambda\pi^0) = -0.44$$

$$\alpha(\Sigma^+ \to n\pi^+) = 0.07 \qquad \text{(useless)}$$

(b) Application to amplitude analysis

For an unpolarized target experiment, the observation of the hyperon decay measures the P parameter as defined in Section 1:

$$W(\theta,\phi) = \frac{1}{4\pi}\,(1 + \alpha\,P \sin\phi \sin\theta)$$

If the target is polarized along the direction $\vec{P}^i$ with components $P^i_x = P^i_\perp \cos\psi$, $P^i_y = P^i_\perp \sin\psi$, P^i_z with respect to the reaction plane (ψ azimuthal angle), then the complete observation of the angular distribution of the decay measures all three polarization parameters P, R', A':

$$\begin{aligned} W(\theta,\phi) &= \frac{1}{4\pi}\,[1 + \alpha P^i_y \sin\phi \sin\theta + P(\alpha \sin\phi \sin\theta + \alpha P^i_y) \\ &\quad + R'(\alpha P^i_y \cos\theta - \alpha P^i_z \cos\phi \sin\theta) + A'(\alpha P^i_x \cos\phi \sin\theta + \alpha P^i_z \cos\theta)] \end{aligned}$$

We note that P can be measured in two ways: observation of the hyperon decay with an unpolarized target[18] or left-right asymmetry with a polarized target.[19] It is comforting that the two experiments agree well.

An experiment designed to measure R' in the process $\pi^- p \to K^0\Lambda^0$ is planned at CERN.[20] Contrary to $R^\pm$ in elastic scattering, it is expected that R can be large in non-diffractive exchange reactions and therefore will be very useful to sort out the underlying amplitudes.

4. Generalization to Several Spins; Resonance Production and Joint-Decay Distributions

When higher-spin particles are produced, or when several particles in the final state have spin, the number of observables increases sharply and can exceed the number of independent real amplitudes. For example, in the process $\pi^- p \to$ (spin J meson)^0 + Λ^0 where the Λ^0 and meson decays are observed the number of observables with unpolarized target is $2(J+1)(2J+1)$ while there are only $4(2J+1)-1$ independent real amplitudes. There is therefore some degree of redundancy in the measurements and it becomes extremely important to understand the relations between all the observables and to define a set of independent observables to be measured with a minimum use of polarized targets.

Our purpose in this section is not to derive results in detail but rather to present a formalism to describe any two-body process with any spins in order to reconstruct amplitudes from experimental data in the most efficient way.

(a) Transversity amplitudes[21-23]

When several particles with spin are involved it becomes more interesting to use the transversity--rather than helicity--quantization axes.

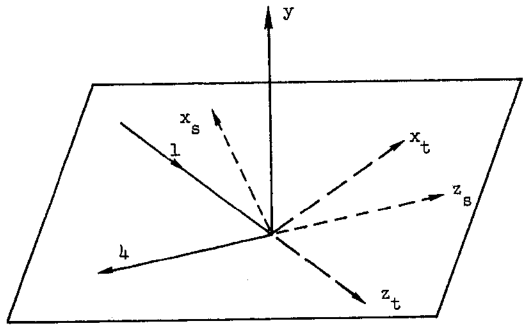

reaction plane and center-of-mass of particle 3

The following reference frames are defined:

$$\left.\begin{array}{lll} (x_s \quad y \quad z_s) & \text{s-channel} \\ (x_t \quad y \quad z_t) & \text{t-channel} \end{array}\right\} \text{helicity axes}$$

$$\left.\begin{array}{lll} (z_s \quad x_s \quad y\ ) & \text{s-channel} \\ (z_t \quad x_t \quad y\ ) & \text{t-channel} \end{array}\right\} \text{transversity axes}$$

In the s-channel helicity frame the third axis is collinear to the momentum $(\hat{z} \parallel \vec{p}_3)$, while they are orthogonal $(\hat{z} \perp \vec{p}_3)$ in the transversity frame. Going from helicity to transversity frames only involves a rotation with Euler angles $\pi/2$, $\pi/2$ and $-\pi/2$.

As we shall see, transversity amplitudes are very useful because they are much more closely related to the measured observables than helicity amplitudes: in particular the redundancy between several measurements is easier to see and it is simple to define a set of independent measurements, both problems not being very transparent in the helicity quantization.

-parity conservation: $H_{\lambda\ldots}$ helicity amplitudes

$T_{\tau\ldots}$ transversity amplitudes

$$H_{\lambda_3\lambda_4\lambda_1\lambda_2} = \eta(-1)^{\Sigma J - \Sigma\lambda}\, H_{-\lambda_3-\lambda_4-\lambda_1-\lambda_2}$$

for unpolarized initial state $\rho^{\lambda_3\lambda_3'}_{\lambda_4\lambda_4'} = (-1)^{\lambda_3-\lambda_3'+\lambda_4-\lambda_4'}\,\rho^{-\lambda_3-\lambda_3'}_{-\lambda_4-\lambda_4'}$

$$T_{\tau_3\tau_4\tau_1\tau_2} = 0 \quad \text{if} \quad \eta(-1)^{\tau_1+\tau_2-\tau_3-\tau_4} = -1$$

for unpolarized initial state $\rho^{\tau_3\tau_3'}_{\tau_4\tau_4'} = 0$ for $\tau_3-\tau_3'+\tau_4-\tau_4'$ odd

-naturality conserving amplitudes

With linear combination of helicity amplitudes, one can define naturality amplitudes to leading order in s as in Section 1 of this chapter.

$$N^{\pm}_{\lambda_3\lambda_4\lambda_1\lambda_2} = \frac{1}{\sqrt{2}}\left[H_{\lambda_3\lambda_4\lambda_1\lambda_2} \pm \epsilon(\lambda_3\lambda_1)\, H_{-\lambda_3\lambda_4-\lambda_1\lambda_2}\right]$$

$$\text{with} \quad \epsilon(\lambda_3\lambda_1) = \eta_1\eta_3 \exp[i\pi(v + J_3 - \lambda_3 + J_1 - \lambda_1)]$$

and $v = 0$ for boson exchange, $v = 1/2$ for baryon exchange.

Let us write down the transformation from helicity to transversity amplitudes:

$$T_{\tau_3\tau_4\tau_1\tau_2} = \sum_{\lambda_1\lambda_2\lambda_3\lambda_4} D^{J_1}_{\lambda_1\tau_1}(R)\, D^{J_2}_{\lambda_2\tau_2}(R)\, D^{J_3}_{\lambda_3\tau_3}(R^*)\, D^{J_4}_{\lambda_4\tau_4}(R^*)\, H_{\lambda_3\lambda_4\lambda_1\lambda_2}$$

where R is the rotation $R(\frac{\pi}{2}, \frac{\pi}{2}, -\frac{\pi}{2})$

$$= \frac{1}{2}\sum_{\lambda_1\lambda_2\lambda_3\lambda_4} D^{J_1} D^{J_2} D^{J_3}_{*} D^{J_4}_{*}\Big[H_{\lambda_3\lambda_4\lambda_1\lambda_2} + \xi\eta_1\eta_3 \exp[i\pi(v + J_1-\lambda_1+J_3-\lambda_3)] \times H_{-\lambda_3\lambda_4-\lambda_1\lambda_2}\Big]$$

We therefore have the important result that T amplitudes are naturality-conserving amplitudes with

$$\xi = \eta_1 \eta_3 \exp[i\pi(v + \tau_3 - \tau_1)]$$

In conclusion, transversity amplitudes are simpler to work with because of the parity relations (some amplitudes are plainly zero) and they correspond to well-defined naturality in the t channel. These properties make them closer to experimental data. However, helicity amplitudes have a more physical interpretation and one needs to know <u>all</u> of the transversity amplitudes to reconstruct any <u>one</u> of the helicity amplitudes.

(b) <u>Naturality of exchange</u>[23]

Since transversity amplitudes correspond to pure naturality exchange, they constitute the simplest description of a two-body process in terms of t or u channel exchanges. More practically, they tell us what measurements are needed to extract the different naturalities and their interference.

The transversity density matrix elements for particle 3 when the initial state is unpolarized, are:

$$\rho_{\tau_3\tau_3'} = \frac{1}{N} \sum_{\tau_1\tau_2\tau_4} T_{\tau_3\tau_4\tau_1\tau_2} T^*_{\tau_3'\tau_4\tau_1\tau_2}$$

and the only non-zero elements have $\tau_3 - \tau_3'$ even.

-With unpolarized initial state and measurement of one final polarization, all observables can be expressed by (superscript = naturality)

$$\sum [T^+_\lambda T^{+*}_\mu + T^-_\lambda T^{-*}_\mu]$$

and are therefore insensitive to the relative phase between opposite naturalities.

-When particle 1 has spin 0, $\rho_{\tau_3\tau_3'}$ is the form

$$\sum T^+_\lambda T^{+*}_\mu \qquad \text{or} \qquad \sum T^-_\lambda T^{-*}_\mu$$

and isolates the exchanged naturality. In the helicity description, one has to combine $\rho_{\lambda_3\lambda_3'}$ elements to project out a given exchanged naturality.

-If both particles 1 and 3 have spins, the naturality separation requires polarization of 1 and analysis of polarization of 3 through its decay or in a rescattering experiment. When particle 3 decays strongly some polarization information is obtained and allows the naturality separation when a meson is produced (1 = meson, 3 = meson) but not when a baryon is produced (1 = meson, 3 = baryon decaying strongly).

-To measure the interference between opposite naturality exchanges requires polarization measurements at opposite vertices; for example, measurement of the double density matrix elements $\rho^{\tau_4\tau_4'}_{\tau_3\tau_3'}$ with $\tau_3 - \tau_3'$ and $\tau_4 - \tau_4'$ both even.

These results are summarized below in a pictorial way[23] with diagrams representing incoming and outgoing particles; lines can be reversed at the same vertex. All particles have spin (otherwise indicated) and a vertical arrow has the meaning of a polarization measurement (either incoming polarized particle, or measurement of an outgoing particle polarization)

<u>measurements</u>	<u>amplitudes measured</u>
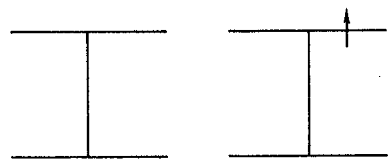	incoherent sum of naturalities $\lvert T^+_\lambda\rvert^2 + \lvert T^-_\lambda\rvert^2$
spin 0 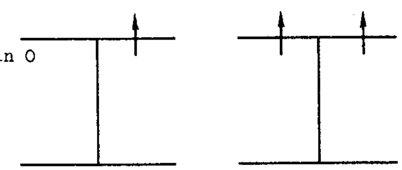	opposite naturalities separation $\lvert T^\pm_\lambda\rvert^2$

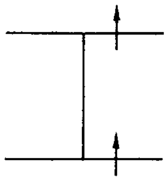

interference between opposite naturalities

$T^{+}_{\lambda} T^{-*}_{\mu}$

(c) Applications

(1)

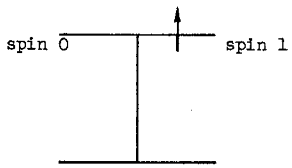

Exchanged naturality	Transversity density matrix elements	Helicity density matrix elements
$\xi = \eta_1\eta_3$	ρ^{T}_{00}	$\rho^{H}_{11} + \rho^{H}_{1-1}$
$\xi = -\eta_1\eta_3$	$\rho^{T}_{11} + \rho^{T}_{1-1}$	ρ^{H}_{00}
	$\mathrm{Re}\ \rho^{T}_{1-1}$	$\rho^{H}_{11} - \rho^{H}_{1-1}$
	$\mathrm{Im}\ \rho^{T}_{1-1}$	$\mathrm{Re}\ \rho^{H}_{10}$

$\pi N \rightarrow \rho N$

$\xi = +1$	$(\rho^{H}_{11} + \rho^{H}_{1-1}) \frac{d\sigma}{dt}$	"ω, A_2" exchange (helicity 1)
$\xi = -1$	$\rho^{H}_{00} \frac{d\sigma}{dt}$	"π" exchange (helicity 0)
	$(\rho^{H}_{11} - \rho^{H}_{1-1}) \frac{d\sigma}{dt}$	"π" exchange (helicity 1)

A complication which should be accounted for is due to the presence of an S-wave $\pi\pi$ which interferes with the ρ amplitudes. An example of the 3-amplitude separation is shown in Fig. 4.

$\gamma N \rightarrow \pi N$

The naturality separation is particularly clear in this reaction where it is achieved by using linearly polarized photons.

$$\left(\frac{d\sigma}{dt}\right)_{\xi=+1} = \frac{d\sigma_{\perp}}{dt} \qquad (P_{\gamma} \text{ perpendicular to the scattering plane})$$

$$\left(\frac{d\sigma}{dt}\right)_{\xi=-1} = \frac{d\sigma_{\parallel}}{dt}$$

The separation is shown in Fig. 5 for $\gamma p \rightarrow \pi^0 p$ at 6 GeV. Extensive measurements of that type have been carried out for $\pi^{\pm}$ photoproduction ($\gamma N \rightarrow \pi N$ and $\gamma N \rightarrow \pi\Delta$).[24]

(2)

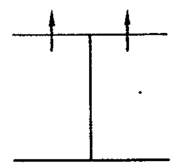

A well-known example is vector meson photoproduction with linearly polarized photons where the meson decay measures the amount of natural and unnatural parity exchange.[25] This is particularly striking in the case of ω production where around 5 GeV both π exchange and diffraction occur in similar magnitude and can be fully separated by this technique.

(3)

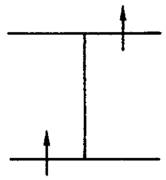

An experiment of this type is in progress at CERN[26] with $\pi^- p\uparrow \to \rho^0 n$. The upper vertex determines the exchanged naturality while correlations between proton polarization and ρ^0 decay distributions relate to the interference between opposite naturalities. Even ignoring the S-wave problem this experiment still does not measure all the helicity amplitudes in this process (see next section) since the ρ decay is parity-conserving.

(d) Joint-decay distributions; statistical tensors

If both particles 3 and 4 decay, the joint-decay distribution takes a simple form when expressed in terms of statistical tensors $t^{LL'}_{MM'}$:

$$W(\theta_3\phi_3\theta_4\phi_4) = \sum_{\substack{L_3L_4\\M_3M_4}} F_3(L_3)\, F_4(L_4)\, t^{L_3L_4}_{M_3M_4}\, Y^{L_3 *}_{M_3}(\theta_3\phi_3)\, Y^{L_4 *}_{M_4}(\theta_4\phi_4)$$

where $F(L)$ are known coefficients depending of the spin on the decaying particle and its decay mode. If parity is conserved in the decay, then $F(L) = 0$ for L odd: an important consequence is that strong decays only measure even polarization tensors (even L_3 and even L_4). Experimentally the elements $t^{L_3L_4}_{M_3M_4}$ are measured by evaluating moments:

$$F_3(L_3)\, F_4(L_4)\, t^{L_3L_4}_{M_3M_4} = \left\langle Y^{L_3}_{M_3}(\theta_3\phi_3)\;\; Y^{L_4}_{M_4}(\theta_4\phi_4) \right\rangle$$

The statistical tensors are related to the double density matrix elements:

$$\rho^{\lambda_3\lambda_3'}_{\lambda_4\lambda_4'} = \sum_{\substack{L_3L_4\\M_4M_4}} (-1)^{J_3+\lambda_3-L_3+J_4+\lambda_4-L_4} \langle J_3 - \lambda_3;\ J_3\lambda_3'|L_3M_3\rangle\langle J_4-\lambda_4; J_4\lambda_4'\ L_4M_4\rangle t^{L_3L_4}_{M_3M_4}$$

and have the following properties

normalization $\qquad t^{00}_{00} = \dfrac{1}{\sqrt{(2J_3+1)(2J_4+1)}}$

hermicity $\qquad \left(t^{L_3L_4}_{M_3M_4}\right)^* = (-1)^{M_3+M_4}\, t^{L_3L_4}_{-M_3-M_4}$

parity $\begin{cases} \text{helicity frame} & t^{L_3L_4}_{M_3M_4} = (-1)^{L_3+L_4-M_3-M_4}\, t^{L_3L_4}_{-M_3-M_4} \\ \text{transversity frame} & t^{L_3L_4}_{M_3M_4} = 0 \quad M_3 + M_4 \ \text{odd.} \end{cases}$

Let us see in one example how to use statistical tensors in the transversity frame.

$$\pi^+ p \to K^+ Y^*(1385)$$

$\frac{3}{2}^+$

$\quad \hookrightarrow \Lambda^0 \pi^+$

$\qquad \hookrightarrow p\pi^-$

Four amplitudes are necessary to describe this reaction and therefore we have seven unknown quantities to solve for at each t value. Here, since Λ decays weakly, both L odd and even components of t^L_M are non-zero; however due to parity conservation in the production all $M = 1$ components vanish in the transversity frame. So there are 6 non-vanishing tensor elements:

$$t_0^0 \quad t_0^1 \quad t_0^2 \quad t_0^3 \qquad \text{(real)}$$

$$t_2^2 \quad t_2^3 \qquad \text{(complex)}$$

To relate the amplitudes let us come back to the density matrix elements in the transversity frame. The following elements

$$\rho_{\frac{3}{2}\frac{3}{2}} = \left|T_{\frac{3}{2}-\frac{1}{2}}\right|^2$$

$$\rho_{\frac{1}{2}\frac{1}{2}} = \left|T_{\frac{1}{2}\frac{1}{2}}\right|^2$$

$$\rho_{-\frac{1}{2}-\frac{1}{2}} = \left|T_{-\frac{1}{2}-\frac{1}{2}}\right|^2$$

$$\rho_{-\frac{3}{2}-\frac{3}{2}} = \left|T_{-\frac{3}{2}\frac{1}{2}}\right|^2$$

are linear combinations of the t_0^L components and yields the magnitude of the 4 amplitudes while the elements

$$\rho_{\frac{3}{2}-\frac{1}{2}} = \rho^*_{-\frac{1}{2}\frac{3}{2}} = T_{\frac{3}{2}-\frac{1}{2}} T^*_{-\frac{1}{2}-\frac{1}{2}}$$

$$\rho_{\frac{1}{2}-\frac{3}{2}} = \rho^*_{-\frac{3}{2}\frac{1}{2}} = T_{\frac{1}{2}\frac{1}{2}} T^*_{-\frac{3}{2}\frac{1}{2}}$$

are linear combinations of the complex t_2^L components and measure two of the three relative phases. Without a polarized target it is thus possible to separate amplitudes up to an overall phase and to the phase between amplitudes with opposite target transversities.

The previous conclusion is quite general: with an unpolarized target one can at best (when all components of polarizations are measured, in a weak decay) measure $N-1$ real amplitudes with an arbitrary overall phase convention when N numbers are needed to extract all the amplitudes: this last unmeasured phase necessitates the use of a polarized target. When a polarized target is used, many more observables can be measured, providing constraints for the amplitude determination. The situation is summarized in Table 2 for typical reactions.[27] Reactions like $\pi N \to K^*\Lambda$ and $\pi N \to KY^*$ should be very helpful in our understanding of strong amplitudes: analyses of the type described previously will involve high-statistics experiments with large solid-angle systems to observe the decay correlations.

(e) polarized proton beams

Experiments are being done at ANL with a polarized proton beam; in particular elastic scattering in pure spin states has been measured.[28] To understand the meaning of the data in terms of the more familiar helicity amplitudes[29-30] it is necessary to transform spin states $|s_y = \pm\frac{1}{2}\rangle$ into helicity states $|s_z = \pm\frac{1}{2}\rangle$:

$$|{}^{\uparrow}_{\downarrow}\rangle = |s_y = \pm\tfrac{1}{2}\rangle = \frac{1}{\sqrt{2}}\left[|s_z = +\tfrac{1}{2}\rangle \pm i|s_z = -\tfrac{1}{2}\rangle\right]$$

Proton-proton elastic scattering is described by 5 helicity amplitudes:

$$\left.\begin{aligned} H_1 &= \langle ++|M|++\rangle \\ H_2 &= \langle ++|M|--\rangle \\ H_3 &= \langle +-|M|+-\rangle \end{aligned}\right\} \quad \text{overall no helicity flip}$$

$$H_4 = \langle +-|M|-+\rangle \qquad \text{double helicity flip}$$

$$H_5 = \langle ++|M|+-\rangle \qquad \text{single helicity flip}$$

One can then express the pure spin states cross-sections shown in Fig. 6 in terms of the amplitudes H_i or even better in terms of linear combinations of H_i isolating pure naturality exchange. It is then easy to show that $\frac{d\sigma}{dt}(\uparrow\uparrow \to \uparrow\uparrow)$, $\frac{d\sigma}{dt}(\downarrow\downarrow \to \downarrow\downarrow)$ and $\frac{d\sigma}{dt}(\uparrow\downarrow \to \uparrow\downarrow)$ only involve natural parity exchange, while $\frac{d\sigma}{dt}(\uparrow\uparrow \to \downarrow\downarrow)$ and $\frac{d\sigma}{dt}(\uparrow\downarrow \to \downarrow\uparrow)$ correspond to pure unnatural parity exchange.

The data at 6 GeV and $t = 0.5\ GeV^2$ shows that these unnatural parity cross sections are small, typically 10% or less of the dominant natural parity cross sections.

TABLE 1

Reaction type	Number of helicity amplitudes				
	no discrete symmetry	using P	using T	using C	using PTC
$\pi N \to \pi N$	4	2	2	-	2
$\pi N \to \pi \Delta$	8	4	-	-	4
$\gamma N \to \gamma N$	16	8	10	-	6
$\pi N \to \rho N$	12	6	-	-	6
$NN \to NN$	16	8	10	-	5
$\bar{N}N \to \bar{Y}Y$	16	8	-	12	6

TABLE 2

Reaction type	Number of amplitudes	Number of real independent observables	measured observables (+ constraints)		
			unpolarized target	polarized target: transverse	polarized target: longitudinal
$\pi N \to \pi N$	2	3	1	2	(+0)
$K\Lambda$	2	3	2	3(+3)	(+2)
ρN	6	11	4	10	(+2)
$K^*\Lambda$	6	11	10(+2)	11(+25)	(+12)
$\pi\Delta$	4	7	4	7(+3)	(+2)
KY^*	4	7	6(+2)	7(+17)	(+8)
$\rho\Delta$	12	23	20	23(+33)	(+16)
K^*Y^*	12	23	22(+26)	23(+121)	(+48)

II - GENERAL FEATURES OF EXCHANGE PROCESSES

We shall discuss almost exclusively non-diffractive two-body processes, although in some cases the diffractive part cannot be easily separated out, such as in elastic scattering for $I_t = 0$ exchange. We are going to summarize properties of data on two-body scattering in order to gather information on the behaviour of the underlying amplitudes. We have seen that our knowledge of single amplitudes is rather limited; on the other hand there is a wealth of data on cross sections and polarizations which can cast some light on our problem.

1. Kinematic Dependence

(a) s dependence

--t = 0

Very useful information on the behaviour at $t = 0$ of the imaginary parts of the amplitudes can be extracted from total cross section measurements. These measurements are rather complete--$\pi^\pm$, $K^\pm$ and $p^\pm$ on protons and neutrons--and cover a wide range of s values from threshold to $\sim 400\ GeV^2$. It is useful to project each forward amplitude onto t-channel quantum numbers, conveniently labelled by particles' names:

$$\sigma_T(\pi^\pm p) = P_\pi + f_\pi \mp \rho_\pi$$

$$\sigma_T(K^\pm p) = P_K + f_K \mp \omega_K \mp \rho_K + A_K$$

$$\sigma_T(K^\pm n) = P_K + f_K \mp \omega_K \pm \rho_K - A_K$$

$$\sigma_T(p^\pm p) = P_p + f_p \mp \omega_p \mp \rho_p + A_p$$

$$\sigma_T(p^\pm n) = P_p + f_p \mp \omega_p \pm \rho_p - A_p$$

Defining sums and differences

$$\Delta(Ap) = \sigma_T(A^-p) - \sigma_T(A^+p)$$

$$\Sigma(Ap) = \sigma_T(A^-p) + \sigma_T(A^+p)$$

we can express the pure t-channel exchanges in terms of the measured cross sections:

$$2\rho_\pi = \Delta(\pi p)$$

$$\left.\begin{aligned} 4\rho_K &= \Delta(KP) - \Delta(Kn) \\ 4\omega_K &= \Delta(Kp) + \Delta(Kn) \\ 4A_K &= \Sigma(Kp) - \Sigma(Kn) \end{aligned}\right\} \text{ and similar relations for } \bar{p}^{\pm}N$$

Experimental problems are obvious in these extractions: systematic differences between experiments show up, particularly in different energy regions; also neutron data comes from deuterium experiments where a Glauber correction has to be applied. In regard to the last remark it is interesting that a better determination of the s dependence of ω_K and ω_p comes from $\Delta(Kd)$ and $\Delta(pd)$ directly. We are not going to discuss here f and P exchanges since they cannot be separated simply; we shall come back to this problem in the last chapter.

The s-dependence of the imaginary part of exchange amplitudes at $t = 0$ has some remarkable properties:

(i) from well measured differences, amplitudes are seen to be power-behaved in s (or p_L) after a few oscillations at low energies. Energies around 3-4 GeV are typical lower limits for the simple power behaviour. We parameterize the s dependence in the form

for example $$\rho_\pi = \beta_\pi\, s^{\alpha_\rho^\pi - 1}$$

(ii) all the exponents α_i that can be isolated cluster around 0.5 ($\pm$ 0.1). Accurate values depend sensitively on low s cut-offs, uncertainties in neutron data and resolution of discrepancies between experiments. Values found using the data of Ref. 31-35 are shown in Table 3. A typical example of the power behaviour is displayed in Fig. 7 with $\Delta(Kd)$ and $\Delta(pd)$.

(iii) Same exchanges in different processes show a close similarity in their energy dependence. In particular α_ρ^π is equal to α_ρ^K within errors and is also consistent with the badly determined α_ρ^P. Also the very accurately determined α_ω^K and α_ω^p are the same, as can be seen directly in Fig. 7. One therefore concludes that, within the limited range of processes and exchanges afforded by elastic scattering, the power behaviour of a given t-channel exchange is not affected in a strong way by s-channel effects (like absorption) at $t = 0$.

The s dependence of amplitudes at $t = 0$ can also be obtained from measurements on differential cross sections, $(d\sigma/dt)_{t=0}$. Experimentally this is not always easy: if a recoil particle has to be observed, data will only exist up to some minimum $|t|$ value and extrapolation at $t = 0$ will be necessary with the corresponding uncertainties; if, on the other hand, no recoil is observed $t = 0$ can be easily reached, if not smeared by resolution effects or not affected by Coulomb effects, such as in elastic scattering where Coulomb scattering (γ exchange) has to be subtracted out. When well-defined t-channel quantum numbers can be isolated, information is thus obtained on the s dependence of the modulus of the corresponding amplitude and is therefore complementary to the information contained in total cross-sections.

Experimental determinations of the s dependence of some $(d\sigma/dt)_{t=0} \sim s^{2\alpha-2}$ are shown in Table 4. An immediate conclusion when results in Tables 3 and 4 are compared is that α values obtained from $(d\sigma/dt)_{t=0}$ and σ_T are consistent with one another when the same exchange is involved: this is very important because it means that the phase of the amplitude at $t = 0$ is essentially energy-independent. This, as we shall see in Chapter 3, is a consequence of analyticity in energy and power behaviour.

--$t \neq 0$

Data on differential cross sections have traditionally been parametrized using:

"slope" $\quad \frac{d\sigma}{dt} = A(s)\, e^{B(s)t}$

"α_{eff}" $\quad \frac{d\sigma}{dt} = As^{2\alpha_{eff}(t)-2}$

The experience has been that s dependence of slopes is not particularly illuminating for exchange reactions and the α_{eff} approach has been in general more fruitful. However we would like to warn against an abusive use of α_{eff}: if, in non-diffractive reactions, it seems that cross sections are reasonably well power-behaved (see $\pi^- p \to \pi^0 n$ in Fig. 8), it is not the case in elastic scattering and α_{eff} determinations depend on the energy range considered and can be very misleading.

The most reliable α_{eff} determination comes from $\pi^- p \to \pi^0 n$ over a very wide s range (with the new NAL data[39]) and shows a simple linear function $\alpha_{eff}(t)$[36]

$$\alpha_\rho(t) = (.56 \pm .02) + (.97 \pm .04)t$$

out to t values around $-1.5\ GeV^2$ (Fig. 9).

The situation is not so pretty for the case of A_2 exchange where a crude linear behaviour seems to exist for $0 > t \gtrsim -0.5\ GeV^2$ but larger $|t|$ data is too imprecise to pin down unambiguously the s dependence. Information on the ω α_{eff} is still very primitive.

(b) t dependence and helicity structure

Exchange amplitudes generally exhibit an exponential fall-off in t, but even some of the crudest characteristics of the t dependence are determined by the relative amount of the different helicity amplitudes present in a given process.

In the forward t region the presence of a peak or a turn-over immediately informs us of the relative importance of overall helicity non-flip amplitudes and flip amplitudes at small t, since flip amplitudes have to vanish kinematically at $t = 0$. We observe:

$\pi^- p \to \pi^0 n$: ρ exchange mostly helicity flip (confirmed by complete amplitude analysis)

$K^- p \to \bar{K}^0 n$: ρ, A_2 mostly helicity flip

$K^+ n \to K^0 p$: (Im ρ_{++} and Im A_{++} given by σ_T data and are small at $t = 0$)

$K_L^0 p \to K_S^P p$: from the peak at $t = 0$, ω mostly helicity no-flip.

Dips for $t \neq 0$ (or absence of dip) provide direct information on helicity amplitudes, although it is hard to translate the facts into statements on real or imaginary parts of the amplitudes:

-from πN amplitudes at 6 GeV, both Re ρ_{+-} and Im ρ_{+-} vanish for $-t \sim 0.6\ GeV^2$ producing a dip in $d\sigma/dt\ (\pi^- p \to \pi^0 n)$.

- $d\sigma/dt(\pi^- p \to \eta n)$ is dominated by A_{+-} but no dip is seen at 0.6, so that we do not know simply the behaviour of Re A_{+-} and Im A_{+-} there.

-$I_t = 0$ exchange can be isolated in $\pi N \to \rho N$:

$$\left(\frac{d\sigma}{dt}\right)_{I_t=0} = \frac{1}{2}\left[\frac{d\sigma}{dt}(\pi^- p \to \rho^- p) + \frac{d\sigma}{dt}(\pi^+ p \to \rho^+ p) - \frac{d\sigma}{dt}(\pi^- p \to \rho^0 n)\right]$$

and it is seen to be almost completely natural parity exchange as given by $(\rho^H_{11} + \rho^H_{1-1})(d\sigma/dt)_{I_t=0}$. It strongly resembles $|\rho_{+-}|^2$ (Fig. 10) with a forward turnover and a dip at $0.6\ GeV^2$. It therefore tells us that, because of the helicity flip at the upper vertex, ω exchange is predominantly non-flip at $N\bar{N}$ vertex--a fact we already knew from $K_L^0 p \to K_S^0 p$ forward peak.

A summary of our qualitative knowledge on dominant helicity couplings to baryon-antibaryon is indicated in Table 5.

One interesting phenomenological exercise is to follow the position of these dips as a function of s. It is remarkable that over a very large s range above a few GeV^2 their position is essentially at fixed t (or u) although the accuracy to detect a change is somewhat limited: for example the dip at 0.6 GeV^2 in $\pi^- p \to \pi^0 n$ is rather well measured but it is difficult to assign a precise value to its location at high energies because of the steep fall-off of $d\sigma/dt$. There are a few cases where a systematic dip displacement has been observed, all of them in the low energy region. One remarkable example is given by the dip at $u \sim -0.2$ GeV^2 in $\pi^+ p$ backward scattering[40] (see Fig. 11) which shows, not a fixed u position, but a fixed $u' = u - u_{min}$. More interestingly, the same phenomenon is seen in the crossed channel process $\bar{p}p \to \pi^- \pi^+$ where the dip appears at larger $|u|$ but is well accounted for by a constant u' position. Such an observation is consistent with a geometrical origin of this dip since u' is directly related to the scattering angle, $|u'| \sim p^2\theta^2$.

Measurements of polarization are very useful tools to study the helicity structure of amplitudes. However, besides elastic scattering, data are rather poor and most of the time not very informative regarding t dependence. On the other hand the s dependence has a characteristic feature:

(i) for elastic processes, fixed-t polarization is generally power-behaved in s corresponding to the interference between a dominant $(P + f)_{++}$ amplitude slowly varying in s with a flip amplitude (ρ_{+-}, A_{+-}) falling like a power.

(ii) for inelastic processes, P is rather independent of energy, as expected from the interference between helicity amplitudes falling with s at similar rates.

2. Quantum Numbers Exchanged

It is an experimental fact that exchange amplitudes are connected with the existence of particles with the same quantum numbers; in particular when t or u-channel quantum numbers do not correspond to any known particle the corresponding amplitudes are always small.

(a) Allowed exchange

We have so far mainly talked about $(P + f)$, ρ, ω and A_2 exchanges. Let us complete here a rapid survey of meson exchange.

K^* exchange

A large amount of data exist on hypercharge exchange cross sections and polarizations. Of particular importance, line-reversed reactions such as

$$\pi N \to K\binom{\Sigma}{\Lambda} \qquad\qquad \bar{K}N \to \pi\binom{\Sigma}{\Lambda}$$

have been measured over a wide range of energies. Unfortunately the measurements are not complete yet for an amplitude analysis and only model-dependent studies have been made. An interesting fact is the absence of a forward turn-over, such as in $\pi^- p \to \pi^0 n$ and $\pi^- p \to \eta n$ indicating that these reactions will be in principle very powerful tools to study non-flip amplitude with K^*_V and K^*_T exchange, and compare them with their non-strange SU(3) partners.

π exchange:

Good spectrometer data exist at 6 GeV[41] and 17 GeV.[26] Unnatural parity exchange as given by

$$\sigma_0 = \rho^H_{00} \frac{d\sigma}{dt} \qquad\qquad (\lambda_p = 0)$$

$$\sigma_- = (\rho^H_{11} - \rho^H_{1-1}) \frac{d\sigma}{dt} \qquad\qquad (\lambda_p = \pm 1)$$

is thought to be dominated by π exchange. As seen in Fig. 12, σ_0 shows no shrinkage between 6 and 17 GeV for $0 < -t < 0.5$ GeV^2 corresponding to a constant $\alpha_{eff} \simeq 0$.

Natural parity exchange

$$\sigma_+ = (\rho^H_{11} + \rho^H_{1-1}) \frac{d\sigma}{dt} \qquad (\lambda_\rho = \pm 1)$$

also has $\alpha_{eff} \simeq 0$ for $-t < 0.15$ GeV^2 but seems to behave more like expected A_2 exchange at larger $|t|$ although α_{eff} is a bit too large there.

Good data relevant to π exchange exist on $KN \to K^*N$ at 6[41] and 13 GeV,[42] π photoproduction[24] $\gamma\uparrow N \to \pi^\pm N$, and $\pi^\pm\Delta$ (mostly natural parity exchange) and $np \to pn$, $\bar{p}p \to \bar{n}n$.

Reactions with π exchange are rather complex in the fact they generally involve many exchanges,and it is clear that the underlying amplitudes can only be uncovered by complete measurements. There is however good evidence here that the identification of t-channel quantum numbers with "pure" exchanges fails, presumably because of large absorption correction to π exchange, spilling over to $\xi = +1$ amplitudes. Of course the proximity of the π pole from $t = 0$ makes π exchange something unique where some of the Regge character shown by other exchanges may be washed out. For practical purposes it is very important to understand π exchange since it is one of the most productive areas of meson spectroscopy through $\pi\pi$ and $K\pi$ scattering, and improved knowledge of the π exchange amplitudes will consolidate the process of extrapolating to the pion pole.

Baryon exchange

The experimental situation is rather poor since cross sections in the backward direction are small at high energy. For allowed baryon exchange, s dependence vary between $\alpha(0) = 0$ and $\alpha(0) = -0.7$. Looking at the s dependence of the backward peak over a large energy range (for example in Fig. 13), we notice that s channel effects are still present at energies ~ 5 GeV: a consequence of this fact is that data at higher energies are needed in order to see the distinct properties of "smooth" u-channel exchange. It is interesting that before the s dependence of baryon exchange sets in, the fall-off in s is fairly steep, s^{-7} to s^{-11}, averaging over resonances.

The closest we come to u-channel amplitudes is in πN scattering around 6 GeV where $\pi^\pm p \to p\pi^\pm$, $\pi^- p \to n\pi^0$ differential cross sections and $\pi^\pm p \to p\pi^\pm$ polarizations have been measured. In terms of $I_u = \frac{1}{2}$ (N) and $I_u = \frac{3}{2}$ (Δ) quantum numbers we have (summing over nucleon helicities)

$$\frac{d\sigma^+}{du} = \frac{d\sigma}{du}(\pi^+ p \to p\pi^-) = \frac{1}{9}|2N + \Delta|^2$$

$$\frac{d\sigma^0}{du} = \frac{d\sigma}{du}(\pi^- p \to n\pi^0) = \frac{2}{9}|N - \Delta|^2$$

$$\frac{d\sigma^-}{du} = \frac{d\sigma}{du}(\pi^- p \to p\pi^-) = |\Delta|^2$$

and therefore

$$|N|^2 = \frac{1}{2}\left[3\left(\frac{d\sigma^+}{du} + \frac{d\sigma^0}{du}\right) - \frac{d\sigma^-}{du}\right]$$

$$|\Delta|^2 = \frac{d\sigma^-}{du}$$

$$\mathrm{Re}(N^*\Delta) = \frac{3}{4}\left[\frac{d\sigma^+}{du} - 2\frac{d\sigma^0}{du} + \frac{1}{3}\frac{d\sigma^-}{du}\right]$$

From the data (Fig. 14) we see that $|N|^2$ possesses a dip at $u \sim 0.2$ GeV^2 while $|\Delta|^2$ is structureless. However accurate analyses of the data are not easy since they rely critically on the relative normalizations of the different sets of data.

Important information could be gathered from the line-reversed reactions observed in $\bar{p}p$ two-body annihilations, i.e., $\bar{p}p \to \pi^\pm\pi^\mp$, allowing one to separate the different signatures. Data exist at 4-5 GeV[43] but relative normalization with πN data is difficult and the energy probably not high enough. In any case s dependence of annihilation data is generally compatible with the corresponding backward data.

(b) Exotic exchanges

Two definitions of an exotic exchange can be adopted:

1st kind: when quantum numbers are different from those of the $\underline{1}$ and $\underline{8}$ SU(3) representations for mesons or $\underline{8}$ and $\underline{10}$ for baryons.

2nd kind: where quantum numbers cannot be generated by a simple quark model with $q\bar{q}$ for mesons and qqq for baryons (more restrictive definition)

-experimental evidence

I = 2, I = 3/2 meson exchange

Cross sections for forbidden centre-of-mass hemisphere for the processes:

$\pi^- p \to K^+\Sigma^-$ $\qquad$ $\pi^- p \to K^+ Y^{*-}$

$K^- p \to \pi^+\Sigma^-$ $\qquad$ $K^- p \to \pi^+ Y^{*-}$

$\bar{p}p \to \bar{\Sigma}^+\Sigma^-$

$\pi^- p \to \pi^+\Delta^-$

$K^- p \to K^0 \Xi^{*0}$

$K^- p \to K^+ \Xi^{*-}$

all show fast fall-off in s ($\sim s^{-6}$) and are typically of the same order of magnitude (~ 1 μb at 5 GeV), with the notable exception of $pn \to \Delta^-\Delta^{++}$ (~ 100 μb at 5 GeV). Almost all of these reactions do not show a peak at small momentum transfer, thus failing to show the usual distinctive appearance of crossed-channel exchange: an exception is $\bar{p}p \to \bar{\Sigma}^+\Sigma^-$ at 5.7 GeV/c although the slope is somewhat small (~ 1 GeV^2).

The s dependence of $(d\sigma/dt)_{t\simeq 0}$ shows a more interesting behaviour (Fig. 15), particularly for $\pi^- p \to K^+\Sigma^-$,[44] although only meagre information on t dependence is provided. A significant change in s dependence seems to occur near 4 GeV/c however from looking at the t dependence it is still possible that the flattening could come from fluctuations in the angular distributions (as caused by s channel resonances, for instance). Higher s data are needed before a clear-cut conclusion can be drawn. Concerning the order of magnitude, let us note that at 5 GeV

$$\left[\frac{\frac{d\sigma}{dt}(\pi^- p \to K^+\Sigma^-)}{\frac{d\sigma}{dt}(\pi^+ p \to K^+\Sigma^+)}\right]_{t\simeq 0} \sim 2\ 10^{-4}$$

In view of the smallness of exotic amplitudes, it seems more fruitful to look for them through their interference with allowed amplitudes. For example,

$$A(\pi^- p \to K^0\Sigma^0) = \frac{\sqrt{2}}{3} A_{1/2} + \frac{\sqrt{2}}{3} A_{3/2} \qquad (A_{I_t})$$

$$A(\pi^+ p \to K^+\Sigma^+) = -\frac{2}{3} A_{1/2} + \frac{1}{3} A_{3/2}$$

where $A_{3/2}$ is the exotic amplitude. It follows that:

$$\frac{\mathrm{Re}\, A_{1/2} A^*_{3/2}}{|A_{1/2}|^2} = -\frac{1}{2}\,\frac{\frac{d\sigma}{dt}(\pi^+ p \to K^+\Sigma^+) - 2\frac{d\sigma}{dt}(\pi^- p \to K^0\Sigma^0)}{\frac{d\sigma}{dt}(\pi^+ p \to K^+\Sigma^+) + \frac{d\sigma}{dt}(\pi^- p \to K^0\Sigma^0)}$$

At 3.6 GeV, this ratio is $.025 \pm .045$ with a systematic error of $\pm .017$ and therefore no evidence for $I_t = 3/2$ exchange is found at the 5% level if the two amplitudes are in phase; the limit could obviously be much worse if some large phase difference existed between $A_{1/2}$ and $A_{3/2}$.

Evidence for $I_t = 2$ and $I_t = 3/2$ exchanges comes from photoproduction[45] comparing the reactions:

$$\left.\begin{array}{l} \gamma p \to \pi^- \Delta^{++} \\ \gamma n \to \pi^- \Delta^{+} \\ \gamma p \to \pi^+ \Delta^{0} \\ \gamma n \to \pi^+ \Delta^{-} \end{array}\right\} \qquad \frac{\mathrm{Re}\, A_1 A_2^*}{|A_1|^2} = .10 \pm .015$$

$$\left.\begin{array}{l} \gamma p \to K^+ \Sigma^0 \\ \gamma n \to K^+ \Sigma^- \end{array}\right\} \qquad \frac{\mathrm{Re}\, A_{1/2} A_{3/2}^*}{|A_{1/2}|^2} = .05 \pm .01$$

Exotic baryon exchange

Fast s dependence ($\sim s^{-10}$) is seen for exotic baryon exchange (see Fig. 16 for $\bar{p}p \to K^+K^-$ and Fig. 17 for $K^-p \to pK^-$) compared with dependence like $s^{-3} - s^{-4}$ for allowed exchange. It is interesting that exotic channels continue the trend observed in the high-mass resonance region with no evidence of a change in trend observed so far. Nevertheless a backward peak has been observed at 5 GeV[43] in both $K^-p \to pK^-$ and $\bar{p}p \to p\bar{p}$ (Figs. 18 and 19) which is at least a good hint of some kind of exchange. It is unfortunate however that these healthy peaks have almost disappeared in the preliminary data of Ref. 46 at 6.2 GeV/c. So there again it seems that fluctuations (s-channel effects?) are occurring over and above a steeply falling s dependence which still prevail at 6 GeV. The ratio:

$$\left[\frac{\frac{d\sigma}{du}(K^-p \to pK^-)}{\frac{d\sigma}{du}(K^+p \to pK^+)}\right]_{u \simeq 0}$$

is $\sim 10^{-2}$ at 5 GeV/c, but has already fallen to $\sim 2 10^{-3}$ at 6.2 GeV/c.

-experimental difficulties

Some difficulties in interpreting an exotic peak have been pointed out when a resonance is produced.[47] As an example let us consider $\pi^-p \to \pi^+\Delta^-$.

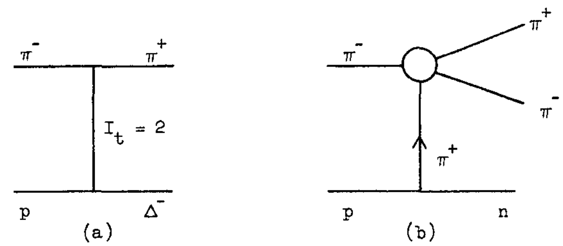

One would like to describe phenomena with diagram (a); however processes (b) can also contribute and reflect into the $(n\pi^+)$ mass spectrum at low mass simulating a false Δ peak. It is amusing that to achieve this effect $\pi^+\pi^- \to \pi^-\pi^+$ scattering has to occur--also an exotic backward process--but it will do so at a much lower s value and hence the process will still be dominated by $\pi\pi$ resonances. Since these reflections are still badly understood, we think it is safe to use data involving only stable particles, i.e., $\bar{p}p \to \bar{\Sigma}^+\Sigma^-$, $K^-p \to pK^-$ and $\bar{p}p \to p\bar{p}$.

-interpretations.

Real exotic particle exchange is not likely in view of the absence of a persistent peak at small t (u) although the s dependence of $K^-p \to pK^-$ $\alpha_{eff} \simeq -4$ does not rule out a 2^* of mass 2-2.5 GeV for a canonical $\alpha' = 1$ Regge trajectory and a spin of $1/2$ or $3/2$.

Direct channel effects could be responsible for fluctuations in the angular distribution around a collective steep s dependence. It is then expected that at some energy some exchange will take place in the crossed channel where the most likely candidate is double particle exchange which certainly is the cheapest way to generate exotic quantum numbers. However they have not been seen yet.

-violation of quark selection rules

In the simple quark model the ϕ meson is a $\lambda\bar{\lambda}$ system and therefore couples very weakly to non-strange particles. This is observed for example in backward scattering around 5 GeV where processes like $K^-p \to \Lambda\rho$ and $K^-p \to \Lambda\omega$ occur, but $K^-p \to \Lambda\phi$ has not been detected yet.

Recent results on ϕ forward production in $\pi^-p \to \phi n$ have been obtained recently[48] showing a very fast decrease of the cross section like s^{-8} (Fig. 20) where a corresponding allowed process $\pi^-p \to \omega n$ behaves as $s^{-2.4}$. The differential cross section is flatter for ϕ (slope 1.4 GeV^2 at 5 GeV) than ω (slope $\simeq$ 3 GeV^{-2}) production. This reaction is rather interesting because all channels are suppressed by the quark model: s-channel non-strange resonances will not couple to ϕn, u channel exchanges are prohibited by the same properties and t-channel exchanges are suppressed because they cannot couple to both upper and lower vertices. The only reasonable candidate to generate some amplitude seems to be two-particle exchange such as K-K^* which is not prohibited by the quark model. Although such an explanation would not be inconsistent with the ratio $\frac{\sigma(\pi^-p \to \phi n)}{\sigma(\pi^-p \to \omega n)} \sim 3.5\ 10^{-3}$ at 5 GeV, and the shape of $d\sigma/dt$, the steep s dependence is somewhat surprising.

(c) SU(3) symmetry.

We know that SU(3) can only be an approximate symmetry of the strong interactions but it is important to see how useful a tool it can be in understanding two body reactions. Even though it is not exact, it can still be helpful in organizing our systematic understanding of exchanges.

$t = 0$

The difference between $\alpha_\rho(0) = .57 \pm .01$ and $\alpha_\omega(0) = .40 \pm .03$ is not accounted for by the ρ-ω mass difference and linear trajectories of same slope since it yields $\alpha'_\rho = .97 \pm .04$ and $\alpha'_\omega = 1.2 \pm .1$. It therefore seems that ρ and ω exchanges break SU(3) symmetry, while ρ exchange with different external particles is consistent with symmetry $(\alpha_\rho^\pi(0) \simeq \alpha_\rho^K(0))$. On the other hand the residues show a 20% breaking

$$\frac{\rho_\pi}{\rho_K} = 1.6 \pm .1$$

instead of 2 for exact SU(3).

The relationship between the residues of ρ_π and ω_K cannot be tested well because, since $\alpha_\rho^\pi \neq \alpha_\omega^K$ the comparison depends on any scale factor s_0 in $(s/s_0)^\alpha$.

$t \neq 0$

SU(3) can be applied to two-body reactions and yields relations independent of any dynamics producing the reactions. For example, the following equalities between amplitudes are predicted:

$$A(K^-p \to K^0\Xi^0) = A(K^-p \to \pi^+\Sigma^-)$$
$$A(K^-p \to K^-p) = A(\pi^-p \to \pi^-p) + A(K^-p \to \pi^-\Sigma^+)$$
$$A(K^+p \to K^{*+}p) = A(\pi^+p \to \rho^+p) + A(\pi^+p \to K^{*+}\Sigma^+)$$
$$\sqrt{2}\ A(\gamma p \to \pi^+ n) = \sqrt{3}\ A(\gamma p \to K^+\Lambda^0) - A(\gamma p \to K^+\Sigma^0)$$

These relations are in general badly violated but they do not teach us a lot about the structure of the breaking. It is more useful to isolate t-channel exchanges in different reactions and relate them using SU(3). Such an exercise awaits some complete amplitude analysis such as in hypercharge reactions to compare K^* exchange to ρ and ω exchanges. Before this is done we can go a few steps in this direction in writing down SU(3) relations when some restrictions are imposed on the t-channel exchanges. In particular, if we assume exotic amplitudes identically vanish, then some new SU(3) relations can be found: for example, take the general SU(3) relation

$$A(K^+p \to K^0\Delta^{++}) + \sqrt{3}\,A(K^-p \to \pi^-\Sigma^+) = \sqrt{3}\,A(K^-n \to K^+\Xi^-) - A(K^-n \to K^0\Xi^-)$$

where the amplitudes on the right-hand side are exotic in the t-channel and can be set to zero; we obtain the simple relation:

$$\frac{d\sigma}{dt}(K^+p \to K^0\Delta^{++}) = 3\,\frac{d\sigma}{dt}(K^-p \to \pi^-\Sigma^+)$$

expressing SU(3) symmetry between (ρ, K_V^*) and (A_2, K_T^*) exchanges. However this kind of relation is expected to be more reliable when there is a dominant helicity amplitude such as for ρ and A_2 exchange:

$$\frac{d\sigma}{dt}(K^-p \to \bar{K}^0n) + \frac{d\sigma}{dt}(K^+n \to K^0p) = \frac{d\sigma}{dt}(\pi^-p \to \pi^0n) + 3\,\frac{d\sigma}{dt}(\pi^-p \to \eta n)$$

Such a prediction is successfully compared to experiment[49] in Fig. 21.

SU(3) symmetry applied to vertices can help us understand the empirical helicity couplings which we have derived from experiment. The coupling of vector and tensor mesons to $B\bar{B}$ is expressed in terms of a symmetric octet coupling (d), an antisymmetric octet coupling (f) and a singlet coupling. Expressing the fact that ϕ and f' completely decouple from $N\bar{N}$ leads to SU(3) couplings depending only on f and d for each helicity amplitude. Table 6 shows the couplings for vector mesons and their numerical values, as compared to $\rho\bar{p}p$ helicity non-flip, obtained with $(f/d)_{++} = -3$ (in order to reproduce $(\rho\bar{p}p/\omega\bar{p}p)_{++}$), $(f/d)_{+-} = 1/3$ (so that $(\omega\bar{p}p)_{+-} = 0$) and $(\rho\bar{p}p)_{+-}/(\rho\bar{p}p)_{++} = 3$ from πN amplitude analysis at 6 GeV. We see that, as is experimentally observed, the K_V^* couplings--also the K_T^* couplings--do not show a dominant helicity transfer.

3. Phases

The phase of an amplitude is in general hard to measure experimentally. At $t = 0$, the optical theorem give one method while, at $t \neq 0$, one need some interference with a known amplitude.

(a) t = 0

Coulomb interference

Existing measurements are still very fragmentary. $\pi^\pm p$ is the only systematic study from 8 to 20 GeV[50] and the data can be used to measure the phase of $(P + f)$ and ρ exchange at $t = 0$. It shows that the phase is given correctly by dispersion relations, hence checking the analyticity properties of the forward amplitude. The phase of the even-crossing part $(P + f)$ is $\sim 100°$, while for the odd-crossing part no more than the sign is really measured $(\mathrm{Re}\,\rho/\mathrm{Im}\,\rho > 0)$.

At 2 GeV/c in the $\pi^\pm p$ system, a new piece of data[51] yields:

$$\begin{cases} \mathrm{Re}(P + f) = -(6.2 \pm .45)\ \mathrm{mb} \\ \mathrm{Im}(P + f) = 32.45\ \mathrm{mb} \end{cases}$$

$$\left\{\begin{matrix} \mathrm{Re}\,\rho = (2.25 \pm .45)\ \mathrm{mb} \\ \mathrm{Im}\,\rho = 3.35\ \mathrm{mb} \end{matrix}\right\} \qquad \phi = (34 \pm 6)°$$

where the ρ Regge phase is 39°.

The situation in $K^\pm p$ is still worse, since we have only a few good low energy points[52] and very questionable high energy determinations. Below 3 GeV, $\mathrm{Re}(K^+p)$ is large and negative ($\alpha = \mathrm{Re}/\mathrm{Im} = -0.44$ at 2.6 GeV) while $\mathrm{Re}(K^-p)$ oscillates in the resonance region and then seems to settle to very small values. The corresponding phases are found to be:

$P_{L(\mathrm{GeV/c})}$	$\phi^{(+)}(P + f + A_2)$	$\phi^{(-)}(\rho + \omega)$
1.2	97°	(22 ± 5)°
1.8	98°	(35 ± 2)°
2.6	100°	(38 ± 3)°

where the ω Regge phase (ω dominates over ρ at $t = 0$) is 53° for $\alpha_\omega(0) = 0.41$. Reliable high energy determinations of the forward phases in $K^\pm p$ are particularly wanting.

Special Case of $K_L^0 p \to K_S^0 p$

One can use the CP violating decay $K_L^0 \to \pi^+\pi^-$ to interfer with K_S^0 regenerated from a hydrogen target. Knowing the decay phase ϕ_{+-}, both the regeneration amplitude and its phase are measured at $t = 0$ by observing the interference pattern as a function of the K^0 decay time. The probability distribution of events is:

$$\frac{dN}{d\tau} = |R|^2 \exp(-\Gamma_S\tau) + |\eta_{+-}|^2 \exp(-\Gamma_L\tau) + 2|R\eta_{+-}| \exp[-(\Gamma_S+\Gamma_L)\tfrac{\tau}{2}] \cos(\delta\tau + \phi - \phi_{+-})$$

where $[A(K_L^0 p \to K_S^0 p)]_{t=0} = Re^{i\phi}$, $\eta_{+-}e^{i\phi_{+-}}$ is the CP violating amplitude, δ the $K_L^0 K_S^0$ mass difference and Γ_S and Γ_L the K_L^0 and K_S^0 inverse lifetimes.

The results show[53] that between 10 and 50 GeV:

-ϕ is roughly independent of s

$$\phi = (-131 \pm 8)° = \pi + (49 \pm 8)°$$

-$\alpha_{eff}(0) = .47 \pm .13$ in agreement with the s dependence of $\sigma_T(K^-n) - \sigma_T(K^+n)$ related by SU(2) invariance to $\sigma_T(\bar{K}^0 p) - \sigma_T(K^0 p)$, the imaginary part of $K_L^0 p \to K_S^0 p$ at $t = 0$.

Using the optical theorem

Measurements at $t = 0$ of $d\sigma/dt$ yields $(\mathrm{Re}\,A)^2 + (\mathrm{Im}\,A)^2$ and using the optical theorem ($\mathrm{Im}\,A \sim \sigma_T$) on can deduce the absolute value of Re A. This approach has not been very successful in elastic scattering because of the smallness of the real parts and problems connected with relative normalization and possible curvature of $d\sigma/dt$ at small t. However the approach has been most fruitful for odd-crossing amplitudes.

$$\mathrm{Im}\,A(\pi^-p \to \pi^0 n) = -\frac{k}{4\sqrt{2}\,\pi}[\sigma_T(\pi^-p) - \sigma_T(\pi^+p)]$$

$$\mathrm{Im}\,A(K_L^0 p \to K_S^0 p) = -\frac{k}{8\pi}[\sigma_T(K^-n) - \sigma_T(K^+n)]$$

Figure 22 shows the ratio $\alpha = \mathrm{Re}\,A/\mathrm{Im}\,A$ for $\pi^-p \to \pi^0 n$, yielding a phase $\phi = \pi + (43.5 \pm 2.5)°$ corresponding to a Regge $\alpha_\rho(0) = .52 \pm .04$ in good agreement with the s dependence of the imaginary part. In $K_L^0 p \to K_S^0 p$ the phase is $\phi + (40 \pm 10)°$ giving $\alpha_\omega(0) = .55 \pm .11$ in accord with direct phase measurements and the s dependence of the corresponding total cross sections.

A more interesting exercise can be carried through for the KN and $\bar{K}N$ change exchange reactions:

$$[\mathrm{Im}(K^-p \to \bar{K}^0 n)]^2 = \frac{1}{16\pi}[\sigma_T(K^-n) - \sigma_T(K^-p)]^2$$

$$[\mathrm{Im}(K^+n \to K^0 p)]^2 = \frac{1}{16\pi}[\sigma_T(K^+p) - \sigma_T(K^+n)]^2$$

In Fig. 23 we compare the values of $[\mathrm{Im}\,A]^2$ to the differential cross sections at $t = 0$: it strikingly shows that the process $K^-p \to \bar{K}^0 n$ is purely imaginary at $t = 0$, while its counterpart $K^+n \to K^0 p$ is purely real. This result confirms some of the duality ideas that we are going to discuss in Chapter IV.

(b) $t \neq 0$

A very attractive method which can be used in ρ and ω production is provided by $\rho - \omega$ electromagnetic mixing as observed in the $\pi^+\pi^-$ decay channel, leading to the exciting possibility of measuring the production phase difference between ρ and ω.

Corresponding to the production amplitudes:

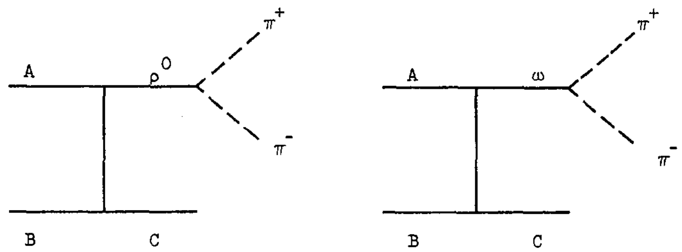

one can observe interferences of the form:

$$\sum_\lambda M_\lambda(\rho)\, M_\lambda^*(\omega) = \xi \sqrt{\left(\sum_\lambda M_\lambda(\rho)^2\right)\left(\sum_\lambda M_\lambda(\omega)^2\right)}\; e^{i\phi}$$

where ξ is a coherence factor and ϕ is the phase difference including the phase of $\omega \to \pi^+\pi^-$ (known and checked in e^+e^- production or ρ and ω photoproduction where the hadronic phase difference is small). Ideally if all the amplitudes were sorted out one could measure the phase difference for each helicity state; however experiments have not reached that point yet and several helicity states are still summed over so that a coherence factor has still to be used.

This method has been used recently by an Argonne group in a rather elegant way.[54] They measured the charge-symmetric processes

$$\pi^- p \to \pi^+\pi^- \, n$$
$$\pi^+ n \to \pi^-\pi^+ \, p$$

which should have equal cross sections except for SU(2) electromagnetic breaking. The interference pattern is striking in the mass spectrum of Fig. 24, showing a constructive interference for $\pi^- p \to \pi^+\pi^- n$ and a destructive one for $\pi^+ n \to \pi^-\pi^+ p$. The interference term can be projected out:

$$\Delta = \sigma(\pi^- p \to \pi^-\pi^+ n) - \sigma(\pi^+ n \to \pi^+\pi^- p) = 4\,\mathrm{Re}(\rho^*\omega)$$

for different $\lambda_{\pi\pi}$ and naturalities ξ.

Figure 25 shows the t-dependence of the phases and some idea of the s dependence. The phase of the unnatural parity exchange Δ^0 is $(122 \pm 6)°$ where one would expect 90° for π - B exchange degeneracy (π in ρ production and B in ω production). The phase Δ^+, the amplitude with natural parity exchange, is changing with t going from 90° at $t = 0$ to about 0° at $t = -0.3$, there, ρ - A_2 exchange degeneracy would predict - 90° and so, again, we see a strong departure at small t from the expected exchanges, a discrepancy already noticed with the behaviour of $\alpha_{eff}(t)$.

A ρ - ω interference analysis has been carried out by the CERN-Munich group[55] observing only $\pi^- p \to \pi^+\pi^- n$ at 17 GeV/c. Their results for the phase of the natural parity exchange is in agreement with the previous analysis, but they disagree on the phase of the unnatural parity exchange with $\lambda_{\pi\pi} = 0$: with the phase convention of the Argonne group, they find phases below 90°, showing either an unsuspected s dependence or some experimental disagreement.

Similar measurements could be extended to other reactions such as

$$K^- p \to (\rho, \omega)\Lambda$$

where the interference effects could be even more visible due to about equal cross sections for ρ and ω production; in constrast ρ production in πN is larger than ω production and the smallness of the decay rate $\omega \to \pi^+\pi^-$ renders the observations rather difficult.

TABLE 3

Amplitude	P_L range (GeV/c)	β (mb)	α
ρ_π	4-200	3.43 ± 0.07	.57 ± .01
ρ_K	3-200	2.16 ± 0.12	.57 ± .03
ω_K	3-200	13.0 ± 2.6	.39 ± .01
A_K	3-200	1.8 ± 0.2	.48 ± .05
$\Delta(Kd) \sim \omega_K$	6-200		.41
$\Delta(pd) \sim \omega_p$	6-200		.41

TABLE 4

Reaction	exchanges	α (t = 0)	Ref.
$\pi^- p \to \pi^0 n$	ρ	.58 ± .03	36
$\pi^- p \to \eta n$	A_2	.47 ± .07	37
$K^- p \to \bar{K}^0 n$	$\rho + A_2$		
$K^+ n \to K^0 p$	$\rho - A_2$		
$K_L^0 p \to K_S^0 p$	$\rho + \omega$		
$K_L^0 d \to K_S^0 d$	ω	.43	38

TABLE 5

Exchange	Dominant helicity coupling to $B\bar{B}$
P + f	++
ω	++
ρ	+-
A_2	+-
π	+-
$K_V^* K_T^*$	? (++ important)

TABLE 6

$VB\bar{B}$ vertex	SU(3) coupling	helicity non-flip coupling	helicity flip coupling
$\rho p\bar{p}$	$\frac{1}{\sqrt{2}}(f + d)$	1.	3.
$p\bar{p}$	$\frac{1}{\sqrt{2}}(-3f + d)$	-5.	0.
$K^*\Lambda\bar{p}$	$\frac{1}{\sqrt{6}}(3f + d)$	2.3	2.6
$K^*\Sigma^+\bar{p}$	- f + d	-2.8	2.1

III - EXTRACTING AMPLITUDES FROM INCOMPLETE DATA

There is so much data in incomplete form and so little information on amplitudes, that it seems worthwhile to try methods where a few amplitudes can be extracted out in an approximate way. On the other hand we have treated real parts and imaginary parts as two independent sets of observables where we know that analyticity relates them: so it seems that analyticity can be used in amplitude analyses in order to reduce the number of measurements to be carried out.

1. Projection of One Amplitude: Exchanges in Elastic Scattering

Amplitude analyses at 6 GeV tell us that the $I_t = 0$, πN amplitude is, to a good approximation, helicity non-flip. This point is also established in ρ^0 photoproduction, a process with very similar amplitudes $(P + f)$. Furthermore, from the energy dependence of elastic scattering we know that the dominant part of this amplitude is contributed for by the Pomeron at energies above a few GeV. We also know that the phase at $t = 0$ is very close to $\pi/2$ and we do not suspect that it will change drastically away from $t = 0$, as long as we stay in the very forward region. (We shall come back later on to this assumption.) With these experimental facts (and one assumption) in mind, it is easy to see that elastic processes will provide very direct and interesting information on exchange amplitudes from their interference with the dominant (imaginary, helicity non-flip, $I_t = 0$) diffractive amplitude.

(a) Cross-over effect

Consider the elastic scattering of particle A and antiparticle $\bar{A}$ on protons, expressed in terms of even and odd-crossing amplitudes $F^{\pm}$:

$$\frac{d\sigma}{dt}(\bar{A}p) = \sum_{\lambda} |F_\lambda^+ + F_\lambda^-|^2$$

$$\frac{d\sigma}{dt}(Ap) = \sum_{\lambda} |F_\lambda^+ - F_\lambda^-|^2$$

$$\frac{d\sigma}{dt}(\bar{A}p) - \frac{d\sigma}{dt}(Ap) = \sum_{\lambda} 4\,\mathrm{Re}(F_\lambda^+ F_\lambda^{-*})$$

$$\frac{d\sigma}{dt}(\bar{A}p) + \frac{d\sigma}{dt}(Ap) = \sum_{\lambda} 2[|F_\lambda^+|^2 + |F_\lambda^-|^2]$$

At high energy F_{++}^+ becomes the dominant amplitude and we are going to project all amplitudes onto it. We shall further neglect $|F^-|^2$ in front of $|F^+|^2$ and F_{+-}^+ in front of F_{++}^+. We have therefore

$$\frac{d\sigma}{dt}(\bar{A}p) - \frac{d\sigma}{dt}(Ap) = 4\,F_{++}^+(F_{++}^-)_{\parallel} + 4(F_{+-}^+)_{\parallel}\,(F_{+-}^-)_{\parallel} + 4(F_{+-}^+)_{\perp}\,(F_{+-}^-)_{\perp}$$
$$\simeq 4F_{++}^+(F_{++}^-)_{\parallel}$$

$$\frac{d\sigma}{dt}(\bar{A}p) + \frac{d\sigma}{dt}(Ap) = 2(F_{++}^+)^2 + 2|F_{+-}^+|^2 + 2|F_{++}^-|^2 + 2|F_{+-}^-|^2$$
$$\simeq 2(F_{++}^+)^2$$

leading to

$$(F_{++}^-)_{\parallel} = \frac{\frac{d\sigma}{dt}(\bar{A}p) - \frac{d\sigma}{dt}(Ap)}{\sqrt{8[\frac{d\sigma}{dt}(\bar{A}p) + \frac{d\sigma}{dt}(Ap)]}} = \Delta_A$$

Δ_A can be measured in 3 processes isolating the following amplitudes:

$\pi^{\pm} p$	$\mathrm{Im}\,\rho^{\pi}_{++}$
$K^{\pm} p$	$\mathrm{Im}(\rho + \omega)^{K}_{++} \simeq \mathrm{Im}\,\omega^{K}_{++}$
$p^{\pm} p$	$\mathrm{Im}(\rho + \omega)^{p}_{++} \simeq \mathrm{Im}\,\omega^{p}_{++}$

This method was applied first to $K^{\pm}p$ scattering at 5 GeV/c[56] and clearly showed that $\mathrm{Im}\,\omega^{K}_{++}$ had zeroes at $t = -0.2$ and $\sim -1.3\ \mathrm{GeV}^2$ (Fig. 26) and could be fitted rather well to an expression

$$\mathrm{Im}\,\omega^{K}_{++} = F(t) = Ae^{Bt}\, J_0(R\sqrt{-t})$$

with $R \simeq 1f$. It is rather illuminating to transform the amplitude into impact parameter space using a Fourier-Bessel transformation:

$$\tilde{F}(b) = \int_0^{\infty} dt\, F(t)\, J_0(b\sqrt{-t})$$

With the parametrization for $\mathrm{Im}\,\omega^{K}_{++}$, we find

$$\widetilde{\mathrm{Im}\,\omega^{K}_{++}} = \frac{A}{B}\exp\left(-\frac{R^2 + b^2}{4B}\right) I_0\left(\frac{Rb}{2B}\right)$$

where $I_0(x)$ is a Bessel function of an imaginary argument. $\widetilde{\mathrm{Im}\,\omega^{K}_{++}}$ has a strong peak around $b \sim R$ and most of its strength is given by the impact parameters around this value. Alternatively, it is probably better to use the exact Legendre expansion at lower energies:

$$\mathrm{Im}\,\omega^{K}_{++} = \frac{\sqrt{\pi}}{k^2}\sum_J \left(J + \frac{1}{2}\right) d^J_{\frac{1}{2}\frac{1}{2}}(\theta)\, a_J$$

The partial wave amplitude a_J is then given by

$$a_J = \frac{1}{\sqrt{\pi}\,(2J+1)} \int dt\ \mathrm{Im}\,\omega^{K}_{++} \cos\frac{\theta}{2}\left(P'_{J+\frac{1}{2}} - P'_{J-\frac{1}{2}}\right)$$

Figure 27 shows the a_J amplitudes from the data of Ref. 43: the peripheral nature of $\mathrm{Im}\,\omega^{K}_{++}$ is very dramatic. This is to be contrasted with the impact parameter structure of the Pomeron amplitude which is best approximated by the K^+p amplitude itself.[56] Figure 28 shows that the Pomeron amplitude receives contributions from all partial waves up to the most peripheral waves, consistent with an optical picture of diffraction. Notice that $\widetilde{\mathrm{Im}\,\omega^{K}_{++}}$ in Fig. 28 appears as a relatively minor correction to the dominant diffractive term.

More information can be gathered from the systematic data between 3 and 6 GeV obtained by the Argonne group,[5] an example of which can be seen in Fig. 29. All the measured "amplitudes" $\Delta_{\pi,K,p}$ are fitted well with the form $Ae^{Bt}\, J_0(R\sqrt{-t})$ for $0 < -t < 0.8\ \mathrm{GeV}^2$ (Fig. 30). Of course, Δ_π is small and and its t dependence is not well measured and suffers most of all from systematic uncertainties between π^+ and π^- data. Beyond $-t > 0.8\ \mathrm{GeV}^2$ the data deviate considerably from the low t fit especially at lower energies: we ascribe these failures to helicity-flip amplitudes and real parts and expect the effect to decrease with energy. Already at 6 GeV, the fitted form for Δ works well up to $-t \sim 1.2\ \mathrm{GeV}^2$, namely, the second cross-over zero. It is hard at these rather low energies to make a quantitative study of the s dependence of $\mathrm{Im}\,\omega^{K}_{++}$ and $\mathrm{Im}\,\omega^{p}_{++}$ since s-dependent effects affect the extraction of the amplitude. Qualitatively we have the following behaviour:

-R is approximately constant at about 1f and does not change too much between the three processes.

-The shrinkage question is not settled (s dependence of B).

$-\text{Im}\ \omega^K_{++}$ and $\text{Im}\ \omega^p_{++}$ are becoming more and more similar in shape as the energy increases, up to a constant factor of 3 predicted by the quark model.

It is interesting that the peripherality of the ω exchange amplitude has the consequence that total elastic cross sections for K^+p and K^-p on one hand, and pp and $\bar{p}p$ on the other hand, are nearly equal, although the differential cross sections are very different. Indeed we have:

$$\int dt\ [\frac{d\sigma}{dt}(\bar{A}p) - \frac{d\sigma}{dt}(Ap)] = 4AA'\int dt\ e^{(B+B')t}\ J_0(R\sqrt{t})$$

where

$$\frac{1}{2}[\frac{d\sigma}{dt}(\bar{A}p) + \frac{d\sigma}{dt}(Ap)] \simeq A'\ e^{B't}$$

giving

$$\sigma_{el}(\bar{A}p) - \sigma_{el}(Ap) = \frac{4AA'}{B+B'}\exp\left(-\frac{R^2}{4(B+B')}\right)$$

Numerically at 5 GeV the difference amounts to .3 mb for $K^{\pm}p$ (8%) while it is 3.3 mb for $p^{\pm}p$ (23%).

This method of extracting the imaginary part of the odd-crossing amplitude through elastic scattering has limitations of both theoretical and experimental origins.

-on the theoretical side, limitations occur from 2 opposite directions. On one hand, if $\text{Im}\ F^{(-)}_{++}$ is small (as in $\pi^{\pm}p$), then its extraction becomes sensitive to neglected amplitudes (flip); on the other hand, if $\text{Im}\ F^{(-)}_{++}$ becomes too large, one can no longer safely neglect $|F^{(-)}|^2$ involving the knowledge of $\text{Re}\ F^{(-)}_{++}$ in particular. Therefore we can say that qualitatively the method will work best for $K^{\pm}p$, will improve with energy for $p^{\pm}p$ and could be questionable for $\pi^{\pm}p$. It is fortunate that the worst case of $\pi^{\pm}p$ can be tested against the results of the complete amplitude analysis at 6 GeV: in Fig. 31 we see that Δ_π agrees very well with the "exact" amplitude $(F^1_{++})_{\parallel}$ giving us some confidence in the method. For πN however, one does not need even to neglect $|F^{(-)}|^2$ in the sum since it is measured by $d\sigma/dt\ (\pi^-p \to \pi^0 n)$ and can be subtracted out:

$$\frac{d\sigma}{dt}(\pi^-p \to \pi^-p) + \frac{d\sigma}{dt}(\pi^+p \to \pi^+p) - \frac{d\sigma}{dt}(\pi^-p \to \pi^0 n) = 2|F^{(+)}|^2$$

-on the experimental side, relative normalization between Ap and $\bar{A}p$ measurements is of crucial importance for measuring the shape of $\Delta(t)$ and in locating the position of the zeroes. The uncertainty in the cross over position t_c is

$$\Delta t_c = \frac{\Delta N/N}{b_{\bar{A}} - b_A}$$

where $\Delta N/N$ is the relative normalization uncertainty and $b_{\bar{A}}$, b_A are the elastic slopes. For example, $\pi^{\pm}p$ at 6 GeV have the following slopes:

$$b_+ = 7.1\ , \qquad b_- = 7.7 \qquad (\text{in GeV}^{-2})$$

yielding an uncertainty $\Delta t_c = .04\ \text{GeV}^2$ for a 2% relative normalization uncertainty.

Detailed studies of elastic scattering will teach us several important features of the peripherality picture we have of $\text{Im}\ F^{(-)}_{++}$. To see that, let us consider the successful parametrization $\text{Im}\ F^{(-)}_{++} = Ae^{Bt}\ J_0(R\sqrt{t})$: the peak position in b space is determined by R and the width of the distribution is controlled by B. Then for a given amplitude, say $\text{Im}\ F^{(-)}_{++}(Kp)$, one would like to know the s dependence of R and B: for example, if B increases with s (shrinkage), does R also increase, thus preserving the peripherality picture? Also the comparison of $\pi^{\pm}$, $K^{\pm}$ and $p^{\pm}$ at an energy higher than 6 GeV would be very interesting since these processes have different interaction volumes, as indicated by the wide range in the total cross section values. The indications, at 6 GeV, are that there does not seem to be any simple relationship between the absorption radius R and the interaction radius as measured by the total elastic slope. New experiments are in progress at SLAC and NAL and it is interesting that, from the preliminary measurements, the method of extracting $\mathrm{Im}\, F_{++}^{(-)}$ will probably work in $K^{\pm}p$ and $p^{\pm}p$ up to rather large energies (~ 100 GeV) since the difference in slopes does not decrease too fast with s (Fig. 32).

(b) Polarizations in elastic scattering

Let us consider polarizations for elastic scattering of particle A and antiparticle $\bar{A}$ on protons and isolate leading terms in the sums and the differences.

$$P\frac{d\sigma}{dt}(\bar{A}p) = -2\,\mathrm{Im}[(F_{++}^{+} + F_{++}^{-})(F_{+-}^{+} + F_{+-}^{-})^{*}]$$

$$P\frac{d\sigma}{dt}(Ap) = -2\,\mathrm{Im}[(F_{++}^{+} - F_{++}^{-})(F_{+-}^{+} - F_{+-}^{-})^{*}]$$

$$\begin{aligned}\Delta P &= P\frac{d\sigma}{dt}(\bar{A}p) - P\frac{d\sigma}{dt}(Ap)\\ &= -4\,\mathrm{Im}[F_{++}^{+}F_{+-}^{-*} + F_{++}^{-}F_{+-}^{+*}]\\ &= -4[F_{++}^{+}(F_{+-}^{-})_{\perp} + (F_{++}^{-})_{\parallel}(F_{+-}^{+})_{\perp} - (F_{++}^{-})_{\perp}(F_{+-}^{+})_{\parallel}]\\ &\simeq -4\,F_{++}^{+}(F_{+-}^{-})_{\perp}\end{aligned}$$

$$\begin{aligned}\Sigma P &= P\frac{d\sigma}{dt}(\bar{A}p) + P\frac{d\sigma}{dt}(Ap)\\ &= -4\,\mathrm{Im}[F_{++}^{+}F_{+-}^{+*} + F_{++}^{-}F_{+-}^{-*}]\\ &= -4[F_{++}^{+}(F_{+-}^{+})_{\perp} + (F_{++}^{-})_{\parallel}(F_{+-}^{-})_{\perp} - (F_{++}^{-})_{\perp}(F_{+-}^{-})_{\parallel}]\\ &\simeq -4F_{++}^{+}(F_{+-}^{+})_{\perp}\end{aligned}$$

In the case of $\pi^{\pm}p$ scattering, one gets the exact relation:

$$P\frac{d\sigma}{dt}(\pi^{-}p) + P\frac{d\sigma}{dt}(\pi^{+}p) - P\frac{d\sigma}{dt}(\pi^{-}p \to \pi^{0}n) = -4F_{++}^{+}(F_{+-}^{+})_{\perp}$$

These relations can be applied to $\pi^{\pm}p$ and $K^{\pm}p$ data and teach us the following properties:

-πN scattering

$(F_{+-}^{-})_{\perp}$ is approximately equal to $\mathrm{Re}\,\rho_{+-}$, in excellent agreement with the complete amplitude analysis, as seen in Figs. 33 and 34. It has a double zero at $-t \sim 0.6\ \mathrm{GeV}^2$, like a pure Regge pole amplitude

$$\mathrm{Re}\,\rho_{+-} = \tan\frac{\pi\alpha}{2}\,\mathrm{Im}\,\rho_{+-}$$

where both $\mathrm{Im}\,\rho_{+-}$ and $\tan(\pi\alpha/2)$ vanish at $-t = 0.6\ \mathrm{GeV}^2$. The energy dependence of $(F_{+-}^{-})_{\perp}$ between 3 and 14 GeV shows a slightly faster fall-off than given by the ρ trajectory as measured in charge-exchange scattering. However $(F_{+-}^{-})_{\perp}$ is not quite $\mathrm{Re}\,F_{+-}^{-}$ since the phase of F_{++}^{0} can be changing with t, hence inducing a false t dependence in $(F_{+-}^{-})_{\perp}$.

$(F_{+-}^{+})_{\perp}$ is obtained from the exact relation between polarizations and shows no clear structure (Fig. 35); an f Regge pole would not have structure either since

$$\mathrm{Re}\,f_{+-} = -\cot\frac{\pi\alpha}{2}\,\mathrm{Im}\,f_{+-}$$

Accurate polarization data at 10 and 14 GeV seem to indicate a single zero around $-t = 0.8\ \mathrm{GeV}^2$. It is not clear whether this is due to the Pomeron, f exchange, or both.

-KN scattering

$(F_{+-}^{-})_{\perp}$ is dominated by ρ exchange since ω is mainly helicity non-flip; it is rather poorly determined from the data, but it is consistent with $\mathrm{Re}\,\rho_{+-}^{\pi}$ data scaled using SU(3) symmetry (Figs. 36 and 37).

Contrary to πN, the amplitude $(F_{+-}^{+})_{\perp}$ is large indicating a large coupling of A_2 exchange to helicity-flip (as we already knew). The data clearly show that $\mathrm{Re}\,A_{+-}$ does not vanish for $0 < -t < 1.2\ \mathrm{GeV}^2$ unlike $\mathrm{Re}\,\rho_{+-}$ (this is consistent with the Regge phase even if $\mathrm{Im}\,A_{+-} = 0$ at $-0.6\ \mathrm{GeV}^2$).

2. Making Use of the Analyticity Properties of Amplitudes

Fixed -t analyticity provides in principle a very powerful constraint on amplitude analyses. This constraint is generally expressed as a dispersion relation satisfied by the invariant amplitudes where the real part at $s = s_0$ is related to an integral over the imaginary part as a function of s. Thus knowing $\mathrm{Im}\, F(s,t)$ over a large range of s values from threshold to s_{max} determines $\mathrm{Re}\, F(s,t)$ for $s \ll s_{max}$, therefore halving the number of independent real amplitudes in that interval.

Dispersion relations have been experimentally tested at $t = 0$ only and in a few cases: $\pi^{\pm}p$ between 8-20 GeV and pp over a larger energy range. We will assume the validity of the analyticity properties of the amplitudes at all t values.

(a) Application of dispersion relations to πN amplitude analyses[57-59]

The main idea is to develop an iterative procedure using the data on $d\sigma/dt$ and the dispersion relations. Starting from the fact that $d\sigma/dt$ is predominantly $(\mathrm{Im}\, A_+')^2$, one can use $\sqrt{d\sigma/dt}$ as a zeroth order input to the dispersion integral, which result is used to correct $d\sigma/dt$ and so on. Schematically,

$$\frac{d\sigma}{dt} \simeq (\mathrm{Im}\, A_+'^{(0)})^2$$

$$\Downarrow$$

$$\mathrm{Im}\, A_+'^{(0)} \xrightarrow{\text{Dispersion relation}} \mathrm{Re}\, A_+'^{(0)}$$

$$\Downarrow$$

$$\cdots \Longleftarrow \mathrm{Im}\, A_+'^{(1)} = \sqrt{\frac{d\sigma}{dt} - \mathrm{Re}[A_+'^{(0)}]^2}$$

For the A_+' even amplitude, the dispersion relation reads:

$$\mathrm{Re}\, A_+'(\nu,t) = \frac{\nu F_B^+(\nu,t)}{1 - \frac{t}{4M^2}} + C_+(t) + \frac{2\nu^2}{\pi} P \int_{\nu_0}^{\infty} \frac{d\nu'}{\nu} \frac{\mathrm{Im}\, A_+'(\nu',t)}{\nu'^2 - \nu^2}$$

with
$$\nu_0 = m_\pi + \frac{t}{4M}$$

$$\nu = \frac{s - u}{4M} = E_L + \frac{t}{4M}$$

$$F_B^+(s,t) = \frac{g^2}{M} \frac{\nu}{\nu^2 - \nu^2} \qquad \text{(Born term)}$$

$$\nu_B = -\frac{m_\pi^2}{2M} + \frac{t}{4M}$$

and where g is the πNN coupling constant $(g^2/4\pi \sim 14.6)$ and $C_+(t)$ is a subtraction function.

These analyses make use only of $d\sigma/dt\ (\pi^+p)$, $d\sigma/dt\ (\pi^-p)$, $d\sigma/dt\ (\pi^-p \to \pi^0 n)$, $P(\pi^+p)$ and $P(\pi^-p)$. They do not use any data on $P(\pi^-p \to \pi^0 n)$, nor do they rely on A and R measurements. The main conclusions reached by these studies are:

-the t dependence of $\mathrm{Re}\, A_+'$ shows a slow variation with t of the phase: ϕ_{++} increases from 101° to 117° when $-t$ increases from 0 to 0.4 GeV^2 (Fig. 39) corresponding to a flatter t dependence for $\mathrm{Re}\, A_+'$ as compared to $\mathrm{Im}\, A_+'$ (Fig. 38). Uncertainties in $\mathrm{Re}\, A_+'$ arise mainly from the low-energy part of the dispersion integrals.

-the determination of $\mathrm{Re}\, B_+(s,t)$ is not so reliable and does involve some assumptions. However good agreement is found with $R^{\pm}$ data at 6 GeV. It is interesting to note that, in general, only using P and $d\sigma/dt$ data leaves an ambiguity between flip and nonflip amplitudes; this problem is solved here since in the phase shift region the full amplitudes can be reconstructed and propagated to high energy.

-Re A'_- shows a zero much closer to the cross over zero of the imaginary part than indicated by amplitude analysis; this effect could come from the t dependence of ϕ_{++} since conventional analyses assume $\phi_{++} = \pi/2$ independent of t. This shows a much closer similarity between the t dependences of Re F^1_{++} and Im F^1_{++}, with <u>both</u> zeroes around $-t = 0.15$ GeV^2. Also, since the behaviour of Re F^1_{++} was mostly derived, in the 6 GeV amplitude analyses, from the charge exchange polarization--a weak measurement--we suspect this new result to be more reliable. Actually this analysis can be used to <u>predict</u> P_0 and it is seen in Fig. 40 that it prefers the Argonne results to the CERN results (in agreement with our discussion of amplitudes at 6 GeV).

-Re B_- shows a remarkable Regge phase (Fig. 38) as we already knew from just looking at ΔP.

This method using analyticity appears most interesting in that it provides solid constraints for amplitude analyses and does not use the weaker and most controversial sets of data. However the use of dispersion relations is cumbersome, really dependent on low energy data, suffering from inconsistencies between different sets of data over these large energy ranges and finally not very transparent.

(b) <u>Derivative analyticity relations</u>

We will show that at high energy the nonlocal connection between real and imaginary parts can be replaced by a quasilocal relation between the real part and the derivatives of the imaginary part at the same energy.

<u>-derivation</u>[60]

Consider an even-crossing amplitude $F_+(s,t)$ normalized to

$$\text{Im}\, F_+(s,0) = s\sigma_T^+$$

It satisfies a subtracted dispersion relation where the subtraction constant $C_+(t)$ and Born terms have been omitted for simplicity:

$$\text{Re}\, F_+(s,t) = \frac{2s^2}{\pi} P \int_{s_0}^{\infty} \frac{ds'}{s'} \frac{\text{Im}\, F_+(s',t)}{s'^2 - s^2}$$

$$= \frac{2s^2}{\pi} \lim_{\substack{\epsilon \to 0 \\ (\epsilon > 0)}} \left[\int_{s_0}^{s-\epsilon} \frac{ds'}{s'} \frac{\text{Im}\, F_+(s',t)}{s'^2 - s^2} + \int_{s+\epsilon}^{\infty} \frac{ds'}{s'} \frac{\text{Im}\, F_+(s',t)}{s'^2 - s^2} \right]$$

Integrating by parts, we get

$$\int_{s_0}^{s-\epsilon} \frac{ds'}{s'} \frac{\text{Im}\, F_+(s',t)}{s'^2 - s^2}$$

$$= -\frac{1}{2s} \left[\ln\left(\frac{s+s'}{|s-s'|}\right) \frac{\text{Im}\, F_+(s',t)}{s'} \right]_{s_0}^{s-\epsilon}$$

$$+ \frac{1}{2s} \int_{s_0}^{s-\epsilon} \frac{ds'}{s'} \ln\left(\frac{s+s'}{|s-s'|}\right) \left[-\frac{1}{s'} + \frac{d}{ds'} \right] \text{Im}\, F_+(s',t)$$

where the first term disappears when taking the principal value except for a term

$$\frac{1}{2s} \ln\left(\frac{s+s_0}{s-s_0}\right) \frac{\text{Im}\, F(s_0)}{s_0}$$

which is negligible for $s \gg s_0$. The dispersion integral then reads:

$$\text{Re}\, F_+(s,t) = \frac{s}{\pi} P \int_{s_0}^{\infty} \frac{ds'}{s'} \ln\left(\frac{s+s'}{|s+s'|}\right) \left[\frac{d}{ds'} - \frac{1}{s'} \right] \text{Im}\, F_+(s',t)$$

Introduce the rapidity variable $e^y = s$

$$\text{Re}\, F_+(y,t) = \frac{e^y}{\pi} P \int_{y_0}^{\infty} dy'\, e^{-y'} \ln\left(\coth \frac{|y-y'|}{2}\right) \left[\frac{d}{dy'} - 1 \right] \text{Im}\, F_+(y',t)$$

More generally we can rewrite this last equation as:

$$\text{Re}\, F_+(y,t) = \frac{e^y}{\pi} P \int_{y_0}^{\infty} dy'\, e^{(\alpha-1)y'} \ln\left(\coth \frac{|y-y'|}{2}\right) \left[\alpha - 1 + \frac{d}{dy'} \right] (\text{Im}\, F_+(y',t) e^{-\alpha y'})$$

which is very useful since it allows us to use $\operatorname{Im} F(s,t)\, s^{-\alpha}$ as our working function and we can choose α in order to minimize its s dependence

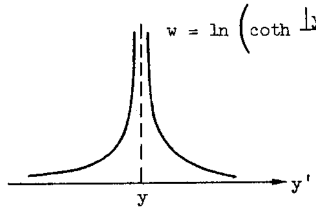

$$w = \ln\left(\coth \frac{|y-y'|}{2}\right)$$

$$y' \to \infty, \qquad w \sim 2e^{-|y-y'|}$$

The rest of the derivation is tedious, but straightforward. We expand $\operatorname{Im} F_+(y',t)$ in power series of $(y'-y)$ and we extend the lower limit of the integral to $-\infty$ (for y large enough). We finally get

$$\operatorname{Re} F_+(y,t) = e^{\alpha y} \tan\left[\frac{\pi}{2}\left(\alpha - 1 + \frac{d}{dy}\right)\right] \left(e^{-\alpha y} \operatorname{Im} F_+(y,t)\right)$$

$$= \tan\left[\frac{\pi}{2}(\alpha-1)\right] \operatorname{Im} F_+(y,t) + \frac{\pi}{2} \frac{e^{\alpha y}}{\cos^2\left[\frac{\pi}{2}(\alpha-1)\right]} \frac{d}{dy}\left(\operatorname{Im} F_+(y,t) e^{-\alpha y}\right) + \cdots$$

For an odd-crossing amplitude we would have instead:

$$\operatorname{Re} F_-(y,t) = e^{\alpha y} \tan\left[\frac{\pi}{2}\left(\alpha + \frac{d}{dy}\right)\right] \left(e^{-\alpha y} \operatorname{Im} F_-(y,t)\right)$$

$$= \tan\left(\frac{\pi\alpha}{2}\right) \operatorname{Im} F_-(y,t) + \frac{\pi}{2} \frac{e^{\alpha y}}{\cos^2(\pi\alpha/2)} \frac{d}{dy}\left(\operatorname{Im} F_-(y,t)\, e^{-\alpha y}\right) + \cdots$$

These relations should not apply at too low an energy since the lower limit of integration y_0 was moved to $-\infty$ and threshold terms have been dropped. On the other hand, pole terms can be added to the final answer. We can choose the parameter α to minimize the s dependence of the function to be differentiated. Conveniently we take

$$\text{even amplitude} \qquad \alpha = 1 \qquad \operatorname{Re} F_+ = s \tan\left(\frac{\pi}{2}\frac{d}{dy}\right) \frac{\operatorname{Im} F_+}{s}$$

$$\text{odd amplitude} \qquad \alpha = 0 \qquad \operatorname{Re} F_- = \tan\left(\frac{\pi}{2}\frac{d}{dy}\right) \operatorname{Im} F_-$$

Whereas an integral dispersion relation is a sum over the imaginary part involving a large range of energies, these new relations necessitate the knowledge of the derivatives of the imaginary part taken locally. In practice, however, one will need some range of energies to measure the derivatives. It is obvious that this approach will only be fruitful if only a small number of terms can approximate the true answer--a result to be investigated on the data.

Before going further, let us present a more intuitive way of deriving these derivative relations. Analyticity in energy allows one to write the amplitude in terms of a Mellin transform in the complex J plane (t-channel analyticity)[61]:

$$M^{\pm}(s,t) = \int dJ [s^J \pm (-s)^J]\, T(J,t)$$

with $\operatorname{Im} M = s\sigma_T$

$$s^J \pm (-s)^J = s^J \pm (se^{-i\pi})^J = 2e^{-i(\pi/2)J} s^J \begin{Bmatrix} \cos\frac{\pi}{2}J \\ i \sin\frac{\pi}{2}J \end{Bmatrix}$$

Any real constant can be incorporated into the real function $T(J,t)$:

$$M^{\pm}(s,t) = \begin{Bmatrix} 1 \\ i \end{Bmatrix} \int dJ\, s^J e^{-i(\pi/2)J}\, T^{\pm}(J,t)$$

<u>For an even amplitude</u>:

$$\frac{M^+(s,t)}{s} = \int dJ\, s^{J-1} e^{-i(\pi/2)J}\, T^+(J,t)$$

$$= -i \int dJ\, e^{(J-1)y}\, T'^{+}(J,t) \left[1 - i \tan\left[\frac{\pi}{2}(J-1)\right]\right]$$

$$\frac{\text{Re } M^+(s,t)}{s} = -\int dJ\, e^{(J-1)y}\, T'^+(J,t) \tan[\tfrac{\pi}{2}(J-1)]$$

$$= -\tan(\tfrac{\pi}{2}\tfrac{d}{dy})\int dJ\, e^{(J-1)y}\, T'^+(J,t)$$

leading to

$$\frac{\text{Re } M^+}{s} = \tan(\tfrac{\pi}{2}\tfrac{d}{dy})\,(\frac{\text{Im } M^+}{2})$$

For an odd amplitude:

$$M^-(s,t) = i\int dJ\, s^J\, T^-(J,t)\,[1 - i\tan(\tfrac{\pi}{2}J)]$$

$$\text{Re } M^-(s,t) = \int dJ\, s^J\, T^-(J,t)\tan(\tfrac{\pi}{2}J)$$

$$= \tan(\tfrac{\pi}{2}\tfrac{d}{dy})\int dJ\, s^J\, T^-(J,t)$$

giving

$$\text{Re } M^- = \tan(\tfrac{\pi}{2}\tfrac{d}{dy})\,\text{Im } M^-$$

-application to total cross sections.[60]

Separating into symmetric and antisymmetric parts we have:

$$\text{Re } F^+ = s\tan(\frac{\pi}{2}\frac{d}{d\ln s})\,\sigma_T^+(s)$$

$$\text{Re } F^- = \tan(\frac{\pi}{2}\frac{d}{d\ln s})\,s\sigma_T^-(s)$$

Above the resonance region $\sigma_T^+(s)$ is a smooth function and retaining only the first derivative is a good approximation (Fig. 41). Good agreement is found with calculations using dispersion relations.

We have seen in Chapter II that in general $\sigma_T^-(s)$ was power-behaved, $\sigma_T^-(s) \sim s^{\alpha-1}$ and consequently:

$$\frac{\text{Re } F^-}{\text{Im } F^-} = \tan(\frac{\pi\alpha}{2})$$

a result generally labelled "Regge" but in fact following directly from power behaviour and analyticity.

If asymptotically $\sigma_T^+ \sim (\ln s)^\beta$ $(\beta \leq 2)$ it follows that:

$$\frac{\text{Re } F^+}{\text{Im } F^+} \sim \frac{\pi\beta}{2\ln s}$$

showing that (i) if σ_T rises asymptotically, then the real part becomes positive (as observed in pp scattering above 300 GeV) and (ii) the real part increases with $\ln s$ one power down compared to the total cross section.

(c) Applications of derivative analyticity relations to amplitude analysis[62]

With quasi-local analyticity relations, we are now in a position to incorporate the analyticity constraints in a convenient form, most suited to amplitude analyses.

-formalism

Let us consider for simplicity a process with one even amplitude:

$$s^2\frac{d\sigma}{dt} = (\text{Re } F_+)^2 + (\text{Im } F_+)^2$$

$$\frac{\text{Re } F_+}{s} = \tan(\frac{\pi}{2}\frac{d}{d\ln s})\,\frac{\text{Im } F_+}{s}$$

The iterative method outlined in paragraph (a) on dispersion relations can be implemented now in its most convenient form. For our purposes it is somewhat more practical to use a phase-magnitude relation. Writing the amplitude explicitly with modulus and phase:

$$F_+(s,t) = R_+(s,t)\, e^{i\phi_+(s,t)}$$

the relation between R and ϕ reads:

$$\phi_+(s,t) = -\frac{\pi}{2}\frac{d}{d\ln s}(\ln R_+)$$

or

$$\phi_+ = -\frac{\pi\alpha}{2} - \frac{\pi}{2}\frac{d}{dy}[\ln(R_+ s^{-\alpha})]$$

similarly for an odd amplitude:

$$\phi_-(s,t) = \frac{\pi}{2} - \frac{\pi}{2}\frac{d}{d\ln s}(\ln R_-)$$

or

$$\phi_- = \frac{\pi}{2}(1+\alpha) - \frac{\pi}{2}\frac{d}{dy}[\ln(R_- s^{-\alpha})]$$

For amplitudes with pure power-behaviour we find the "Regge" phases:

$$R \sim s^{\alpha} \Longrightarrow \phi_+ = -\frac{\pi}{2}\alpha$$

$$\phi_- = \frac{\pi}{2}(1-\alpha)$$

corresponding to Regge amplitudes $(e^{-i\pi\alpha} \pm 1)$.

In the single amplitude case we have, for positive signature:

$$s\sqrt{\frac{d\sigma}{dt}} = R_+(s,t)$$

$$\phi_+(s,t) = -\frac{\pi}{2} - \frac{\pi}{2}\frac{d}{dy}(\ln\frac{R_+}{s})$$

These simple equations have the following important physical consequence for elastic scattering at sufficiently high energy where Pomeron exchange (even amplitude) dominates. One expects the differential cross sections to increase in the forward direction and the t-slope to increase also. This means that there is a finite value of t at which the function (R_+/s) is essentially constant. This "cross over" in the same amplitude at different energies tells us that the real part has a zero at this t value (see Chapter V).

Let us now turn to a case with two helicity amplitudes, where both the differential cross section and polarization are measured. It is always possible to combine the different measured quantities in order to project out amplitudes with well-defined signature. Therefore consider two even-signatured amplitudes F_{++} and F_{+-} with modulii R_{++}, R_{+-} and phases ϕ_{++}, ϕ_{+-}. We have the two equations:

$$A^2 = R_{++}^2 + R_{+-}^2 = s^2\frac{d\sigma}{dt}$$

$$A^2P = 2R_{++}R_{+-}\sin(\phi_{++} - \phi_{+-})$$

Using the derivative relations, R_{+-} can be eliminated and a differential equation is obtained for R_{++}:

$$\frac{d}{dy}\left(\ln\frac{R_{++}}{A}\right) = -\frac{2}{\pi}\frac{(A^2 - R_{++}^2)}{A^2}\sin^{-1}\left(\frac{A^2P}{2R_{++}\sqrt{A^2 - R_{++}^2}}\right)$$

Given data as a function of s, $A(s)$ and $P(s)$, this equation can be solved numerically at each t value and F_{++} and F_{+-} can be reconstructed. There is an arbitrary integration constant which depends only on t and must be determined at one energy value from A and R measurements. An even more attractive approach is to extend the analysis down to energies where complete phase-shift solutions exist and amplitudes can be fully reconstructed.

It is well known that the arbitrary constant is related to an arbitrary rotation in the flip no-flip plane which arises as a consequence of using only $d\sigma/dt$ and P as input. To see that explicitly, let us define

$$R_{++} = A\cos\theta \qquad (\theta = \text{flip no-flip rotation angle})$$
$$R_{+-} = A\cos\theta$$

and solve for θ

$$\pi\frac{d\theta}{dy} = -\sin 2\theta\,\sin^{-1}\left(\frac{P}{\sin 2\theta}\right)$$

If the polarization is small (one amplitude is small or they both have the same s dependence) then one has the approximate solution

$$\theta(y,t) = \theta_0(t) - \frac{1}{\pi}\int_{y_0}^{y} dy'\ P(y')$$

where $\theta_0(t)$ is the s-independent integration constant which corresponds physically to a rotation in the helicity plane and must be determined at $y = y_0$.

-mathematical examples

Before using this method on real data, it is very instructive to test it on a few examples in order to learn about possible pitfalls.

(i) difference of two Regge poles

$$M_+ = \beta_1 s^{\alpha_1} e^{-i(\pi/2)\alpha_1} - \beta_2 s^{\alpha_2} e^{-i(\pi/2)\alpha_2}$$

A numerical comparison of the exact phase with the approximate one is shown in Fig. 42 for the values $\beta_1 = 1$, $\beta_2 = 0.5$, $\alpha_1 = 0.9 + t$ and $\alpha_2 = 0.5 + 0.6t$. The zeroes of the amplitude are at

$$\ln s = \frac{\ln(\beta_2/\beta_1)}{\alpha_1 - \alpha_2} + i\,\frac{\pi}{2}$$

One sees that the approximately reconstructed amplitudes follow quite well the input functions except when the latter have dips which have been completely smeared out. Away from the zeroes, the procedure is quite accurate.

(ii) absorbed Regge pole (Pomeron)

$$M_+ = s e^{-i(\pi/2)} \left[e^{Bt} - \frac{A}{A+B}\ e^{(ABt/A+B)}\right]$$

with $B = 0.5(\ln s - i\,\frac{\pi}{2})$ and $A = 4$. This amplitude is predominantly imaginary and the differential cross section resulting from it somewhat realistic.

The simple phase method gives good results except where M_+ has zeroes (Fig. 43). Since $\mathrm{Re}\, M_+$ is quite small, it is sensitive to details of the procedure and is reconstructed quite well except for the point where $\mathrm{Im}\, M_+$ and the differential cross section have a dip and vary rapidly.

The above two examples are of value to show that the method is workable and particularly to help develop an intuition about how to proceed with real data.

-applications to data

(i) $K_L^0 p \to K_S^0 p$.

The amplitude for this process has odd signature only and therefore it is straightforward to use our method. In general the amplitude will have helicity flip and non-flip parts, respectively dominated by ρ and ω exchange and, since no polarization data are available one cannot perform a general amplitude analysis. However the helicity-flip contribution vanishes at $t = 0$ and presumably $t \simeq -0.5\ \mathrm{GeV}^2$ and therefore we can hope to measure the phase of the helicity non-flip amplitude at these t values.

At $t = 0$ there are actually two independent ways of measuring the phase: (1) from the s dependence of $(d\sigma/dt)_{t=0}$

$$\phi_{++}^{(-)} = -\frac{\pi}{4}\frac{d}{dy}\left[\ln\left(\frac{d\sigma}{dt}\right)_{t=0}\right]$$

or (2) from the s dependence of the imaginary part of the amplitude as given by the optical theorem

$$\frac{8\pi}{k}\,\mathrm{Im}\, F_{++}^{(-)} = \sigma_T(K^+n) - \sigma_T(K^-n) < 0$$

It is remarkable that experimentally both $(d\sigma/dt)_{t=0}$ and $\mathrm{Im}\, F_{++}^{(-)}$ are power-behaved from a few GeV/c to 60 GeV/c (see Chapter II) and therefore the phase can be obtained most easily. The results for methods (1) and (2) are shown in Fig. 44 and are in good agreement with independent measurements using $K_L^0 - K_S^0$ interference or optical point extrapolations.

At $t = -0.5\ \mathrm{GeV}^2$ we have[63]

$$\phi_{++}^{(-)} = -\frac{\pi}{4}\frac{d}{dy}\left(\ln\frac{d\sigma}{dt}\right) = \frac{\pi}{2}\,(1.02 \pm .22)$$

indicating a very small real part in qualitative agreement with $\mathrm{Re}\ \rho_{+-}$ in πN scattering.

(ii) $\gamma p \to \gamma p$.

Compton scattering is a nice example with an even-signatured amplitude. The helicity non-flip amplitude is large and dominated by P and f exchange, while the flip amplitude is much smaller. In the forward direction, $I_t = 1$ exchange (mostly A_2, flip) has been measured to be small by comparing γp and γd Compton scattering. There is no direct experimental information on the helicity structure of $I_t = 0$ exchange, however, we know from πN scattering and $\gamma p \to \rho^0 p$ that it is helicity non-flip to a good approximation and we expect γp to exhibit the same character. We therefore neglect helicity-flip contributions and assume the phase we obtain from $d\sigma/dt$ is that of the dominant helicity non-flip amplitude. Using the data of Ref. 64-66, the real part is obtained at mean momenta of 4 and 10 GeV (Fig. 45). The comparison between the two momenta shows a marked energy dependence, indicating that probably f exchange dominates the real part at these energies, as one would expect a priori. Comparing $\mathrm{Im}\ F_{++}$ and $\mathrm{Re}\ F_{++}$ at 10 GeV (Fig. 46) reminds us very strongly of the πN, $I_t = 0$ amplitudes at the same energy (Fig. 38). Between $t = 0$ and $-t = 0.8\ \mathrm{GeV}^2$ the phase ϕ_{++} changes from 102° to 110°, in good agreement with πN scattering.

(iii) further applications in progress

The πN system is currently being investigated using only $(d\sigma/dt)\,(\pi^{\pm}p)$, $(d\sigma/dt)\,(\pi^- p \to \pi^0 n)$ and $P(\pi^{\pm}p)$. The flip no-flip ambiguity $(\theta_0(t))$ can be fixed at 6 GeV using the known amplitudes or at lower energies using phase shifts.

Hypercharge exchange reactions constitute an interesting area for applications since signature can be dealt with using the appropriate line-reversed pairs of reactions. Denoting even-signatured amplitudes by T_λ (mostly K_T^* exchange) and odd-signatured amplitudes by V_λ (mostly K_V^* exchange) we have

$$\frac{d\sigma}{dt}(\pi N \to KY) = \sum_\lambda |T_\lambda + V_\lambda|^2$$

$$\frac{d\sigma}{dt}(\bar{K}N \to \pi Y) = \sum_\lambda |T_\lambda - V_\lambda|^2$$

leading to the four equations:

$$\frac{1}{2}\Sigma = |T_{++}|^2 + |T_{+-}|^2 + |V_{++}|^2 + |V_{+-}|^2$$

$$\frac{1}{2}\Delta = \mathrm{Re}(T_{++}V_{++}^* + T_{+-}V_{+-}^*)$$

$$\frac{1}{4}(\Sigma P) = \mathrm{Im}(T_{++}T_{+-}^* + V_{++}V_{+-}^*)$$

$$\frac{1}{4}(\Delta P) = \mathrm{Im}(T_{++}V_{+-}^* + V_{++}T_{+-}^*)$$

When the phase-magnitude relations are taken into account, one obtains a system of 4 differential equations which can be solved numerically at each t value, giving back the amplitudes with some ambiguities.

We have tried to show how analyticity can, in a powerful and very practical way, improve our tools to extract amplitudes from incomplete data.

IV - DUALITY AND ABSORPTION

In this chapter we are going to briefly review some of the most important ideas and concepts in the phenomenology of two-body scattering, as they relate in a relevant way to the experimental facts we have gathered through the course of the preceding sections.

1. Duality

(a) Two descriptions of two-body scattering

At low energy ($\sqrt{s} \lesssim 2$ GeV), our knowledge of two-body scattering is embodied in s-channel phase-shifts describing the data with resonant and non-resonant (background) waves. As s increases this description ceases to be practical because of too many waves.

At high energy we have seen that amplitudes are clearly related to t-channel exchanges and that, in general, only a few exchanges are required to describe the experimental situation.

If at low energy there is little uncertainty in the analytical description of s-channel resonances, the situation is less clear at high energy: we know most amplitudes manifest some kind of Regge behaviour, with the phase-energy relation and trajectories approximately related to the particle spectrum. Hence, as a starting point, it is not too unreasonable to assume that t-channel exchanges are mediated by Regge poles. Later, considering some of the difficulties encountered, we shall come back on this assumption.

(b) Relating low and high energy descriptions: FESR[67]

There must be some relation between low s and high s regions since the scattering amplitude is analytic in energy. Using analyticity and Regge behaviour for high energy one can derive a finite energy sum rule (FESR).

Consider a scattering amplitude $F(\nu)$ which is supposed to be a real analytic function of the variable ν every where in the ν plane except for inelastic cuts from $-\infty$ to $-\nu_0$ and from ν_0 to ∞ and some isolated poles on the real axis. We assume a Regge behaviour at high energy:

$$F(\nu) = \sum_k \beta_k \frac{1 + \tau_k e^{-i\pi\alpha_k}}{\sin \pi\alpha_k} \nu^{\alpha_k}$$

$$|\nu| > N, \ \beta_k, \ \alpha_k \ \text{functions of } t.$$

Now if we apply Cauchy's theorem to the closed contour Γ:

$$\int_\Gamma F(\nu) \nu^n d\nu = 0$$

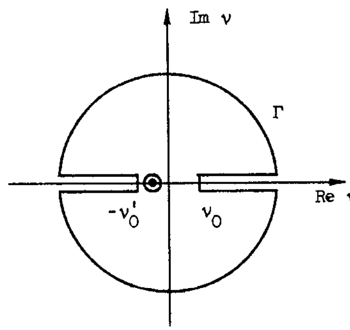

$$\int_{-N}^{-\nu_0'} \mathrm{Im}\, F(\nu) \nu^n d\nu + \int_{\nu_0}^{N} \mathrm{Im}\, F(\nu) \nu^n d\nu + \sum_k \beta_k \frac{N^{\alpha_k+n+1}}{\alpha_k+n+1} [\tau_k - (-1)^n] = 0$$

where pole terms are formally included in the dispersion integrals. The expression becomes simpler if $F(\nu)$ has a well-defined signature; if $F(\nu)$ is odd

$$F(\nu) = -F(-\nu) \qquad \text{and} \qquad \tau_k = -1$$

then the FESR reads

$$\int_{\nu_0}^{N} \mathrm{Im}\, F(\nu) \nu^n d\nu = \sum_k \beta_k \frac{N^{\alpha_k+n+1}}{\alpha_k+n+1} \qquad (n \ \text{even})$$

Thus if we know (from phase-shifts) the behaviour of $\text{Im } F(\nu)$ below $\nu = N$, we have a way to use analyticity in order to get some information on high energy parameters, provided (i) the asymptotic form chosen was correct and (ii) the cut-off N is taken high enough for this asymptotic form to be valid. This procedure has indeed been applied with some success.

The limitation that phase-shifts data exist only for low s, well below the "asymptotic" Regge region has been actually a rather favourable situation since it led to the concept of duality. Dolen, Horn and Schmid[68] investigated the πN charge exchange amplitudes taking $N = 1.1$ GeV as their cut-off: they were able to reproduce the main features of t-channel ρ exchange (dominance of B, ρ trajectory, zeroes) even though N was low and resonance behaviour was still seen at higher energies at $t = 0$ (Fig. 47): the high energy amplitude is behaving like the average of the s-channel resonances. An important aspect of the result is that s-channel resonances actually dominate the left-hand side of the FESR with no noticeable background, leading to the powerful idea that, s-channel resonances or t-channel poles are alternate descriptions of the same process with the smooth high s, t-channel pole amplitudes averaging out the s-channel resonant structures.

A powerful use of FESR is realized when both s and t channel descriptions make use of the same singularities; in this case it provides a way of bootstrapping these singularities. Consider, for example, the process $\pi^+\pi^0 \to \pi^0\pi^+$ where ρ exchange occurs in both s and t channel: requiring the first zero of both amplitudes to coincide leads to $1/\alpha' \simeq \frac{3}{2} m_\rho^2$ or $\alpha' \simeq 1.1 \text{ GeV}^2$, a value rather close to the experimental number.

Many applications of FESR have followed for πN, KN, photoproduction etc. .... It would be very interesting to have reliable FESR analyses to learn about those amplitudes not easily accessible at high energy in the t channel. For example we know very little about even crossing amplitudes (in particular, f exchange in πN elastic scattering, f and A_2 exchanges in KN, $\bar{K}N$ elastic scattering). In principle we can learn about A_2 exchange using FESR and low energy KN and $\bar{K}N$ data: however, in practice, this is somewhat unreliable since $K^{\pm}n$ low energy data are not yet very complete, nor very accurate and consequently the phase shifts with proper quantum numbers cannot be completely trusted.

For example a recent FESR analysis[69] of KN and $\bar{K}N$ scattering with a cutoff $p_L = 1.5$ GeV/c shows the expected features for the dominant amplitudes like $\text{Im } \omega_{++}$ and $\text{Im } \rho_{+-}$ while $\text{Im } A_{++}$ and $\text{Im } A_{+-}$ seem to behave differently from $\text{Im } \omega_{++}$ and $\text{Im } \rho_{+-}$ respectively. One must keep in mind however that the cutoff is rather low, the phase shifts solutions not always reliable and some of the amplitudes are quite small in magnitude and subject to uncertainties. Such methods will be nevertheless very useful, as the quality of the KN phase shifts improves, to study specific exchanges in the intermediate energy region.

Let us emphasize at this point the dominance of the FESR integral by resonances is expected to make sense only for the imaginary part of the amplitude, while real parts of resonances can contribute to very distant energies, even outside the physical domain.

(c) Two-component duality

The generalization of the duality concept to elastic scattering has been made.[70-71] While s-channel resonances are dual to t-channel exchanges, the background under the resonances builds up the diffractive amplitude--the exchange of the Pomeron.

s-channel resonances <===> t-channel exchanges

s-channel background <===> Pomeron exchange

The consequences of this principle are well known:

--if the s-channel has exotic quantum numbers, no resonances will contribute and high energy exchanges will only involve Pomeron exchange, at least in the imaginary part

$$\text{Im } F_{s \text{ large}} \simeq \text{Im } P$$

In order to achieve that, allowed t-channel exchanges have to cancel each other (exchange degeneracy). For example K^+p scattering is exotic in the s-channel and we expect that, at high energy,

$$\text{Im } f^K = \text{Im } \omega^K$$
$$\text{Im } \rho^K = \text{Im } A^K$$

so that

$$\text{Im } A(K^+p) \simeq P$$

$$\text{Im } A(K^-p) \simeq P + 2 \text{ Im } \omega^K + 2 \text{ Im } \rho^K$$

This result is only expected to hold for the imaginary part since the real part of K^+p scattering can receive contribution from the distant Y^* resonances of the s-u crossed channel and is seen experimentally to be large. It is amusing to see that for Regge exchanges with some $\alpha(t)$ we have

$$\text{Re } A_R(K^+p) = 2(\beta^K_\omega + \beta^K_\rho)\, s^\alpha$$

$$\text{Im } A_R(K^+p) = 0$$

$$\text{Re } A_R(K^-p) = 2(\beta^K_\omega + \beta^K_\rho) \cos \pi\alpha\, s^\alpha \qquad (\simeq 0 \text{ at } t = 0)$$

$$\text{Im } A_R(K^-p) = -2(\beta^K_\omega + \beta^K_\rho) \sin \pi\alpha\, s^\alpha$$

In Fig. 48 it is shown that indeed the low energy part of $\text{Im}(\rho + A)^K$ is large and dominated by resonances while $\text{Im}(\rho - A)^K$ is much smaller and structureless.

--if the s-channel is exotic and no Pomeron exchange is allowed, we expect the scattering amplitude to be essentially real. This is the case in K^+N charge exchange scattering: we have seen in Chapter II that the phase of the forward amplitude for $K^+n \to K^0p$ was very close to zero. We expect similar results for $K^+p \to K^0\Delta^{++}$, $pn \to np$ and $pp \to n\Delta^{++}$. At the same time the corresponding non-exotic channels are expected to be mostly imaginary, as observed in $K^-p \to \bar{K}^0n$.

--imaginary parts of amplitudes for non-diffractive scattering should be dominated by resonances. This is observed in πN scattering[72] where clean Argand loops show up in $I_t = 1$ amplitudes (no Pomeron) (Fig. 49); the aspect of $I_t = 0$ diagrams is different with a large imaginary background (Pomeron) superimposed to resonance patterns.

(d) application of duality: exchange degeneracy (EXD)

The following set of assumptions (duality) leads to very strong consequences for t-channel exchanges:

$$\left.\begin{array}{l}\text{(1) analyticity}\\ \text{(2) asymptotic Regge behaviour}\end{array}\right\} \quad \text{FESR}$$

(3) absence of exotic amplitudes (for imaginary parts only in non-diffractive channels)

--trajectories

Consider exotic $\pi^+\pi^+$, K^+K^+, K^+K^0 scattering. Exchange degeneracy tells us that the ρ and f trajectories should be the same and the same result should hold for (f,ω) and (ρ,A_2) leading to a unique trajectory for ρ, ω, f and A_2 exchange. A look at the Chew-Frautschi plot shows that it is rather well satisfied by the particle spectrum (Fig. 50). From the mass spectrum alone we would deduce a linear trajectory:

$$\alpha(t) = 0.46 + 0.9t$$

when compared to experimental trajectories $\alpha(t) = \alpha(0) + \alpha' t$ measured in the space-like region

	$\alpha(0)$	α'	
ρ	.56	.97	$-t < 1.5\ \mathrm{GeV}^2$
A_2	.48	.9	$-t < 0.4\ \mathrm{GeV}^2$
ω	.40	?	
f	?	?	

we see that the agreement is not overwhelming. In Fig. 51 we directly compare $\alpha_\rho(t)$ and $\alpha_A(t)$ from $\pi^- p \to \pi^0 n$ and $\pi^- p \to \eta n$.

--residues

Duality imposes equality between residues in exotic channels.

--line-reversed reactions

Consider the pair of s-u crossed reactions:

$$a + b \to c + d \qquad (1)$$

$$\bar{c} + b \to \bar{a} + d \qquad (2)$$

asymptotically the two amplitudes have to be equal, but EXD makes some very strong requirements at any s (sufficiently large). Let us separate out odd and even amplitudes:

$$A_+ = \beta_+(1 + e^{-i\pi\alpha})s^\alpha = 2\beta_+ e^{-i\pi(\alpha/2)} \cos\frac{\pi\alpha}{2} s^\alpha$$

$$A_- = \beta_-(1 - e^{-i\pi\alpha})s^\alpha = 2i\beta_- e^{-i\pi(\alpha/2)} \sin\frac{\pi\alpha}{2} s^\alpha$$

A_+ and A_- are $\pi/2$ out of phase and consequently

$$\left(\frac{d\sigma}{dt}\right)_1 = \left(\frac{d\sigma}{dt}\right)_2$$

with

$$\left(\frac{d\sigma}{dt}\right)_{1,2} = \frac{1}{s^2}|A_+ \pm A_-|^2 = 4s^{2\alpha-2}(\beta_+^2 + \beta_-^2)$$

This result follows uniquely from the identity between the two trajectories α_+ and α_-.

Let us now explicitly show helicity amplitudes:

$$A_{+}^{\substack{++\\+-}} = 2e^{-i\pi(\alpha/2)} s^\alpha \left[\beta_{+}^{\substack{++\\+-}} \cos\frac{\pi\alpha}{2} + i\beta_{-}^{\substack{++\\+-}} \sin\frac{\pi\alpha}{2}\right]$$

leading to a polarization:

$$P\frac{d\sigma}{dt} = 4s^{2\alpha-2} \sin\pi\alpha[\beta_+^{+-}\beta_-^{++} - \beta_-^{+-}\beta_+^{++}]$$

The equality of residues, $\beta_{+}^{\substack{++\\+-}} = \beta_{-}^{\substack{++\\+-}}$, imposed by duality, leads to no polarization in both processes.

It is interesting to compare processes involving the same EXD exchanges and one expects:

$$\frac{\frac{d\sigma}{dt}(ab \to cd)}{\frac{d\sigma}{dt}(\bar{c}b \to \bar{a}d)} = \frac{\frac{d\sigma}{dt}(a'b' \to c'd')}{\frac{d\sigma}{dt}(\bar{c}'b' \to \bar{a}'d')}$$

--experimental tests of line-reversal

We have experimental information on:

$$\frac{d\sigma}{dt}(K^- p \to \bar{K}^0 n,\ K^+ n \to K^0 p) \qquad \text{(Fig. 52)}$$

$$\frac{d\sigma}{dt}(\pi N \to KY,\ \bar{K}N \to \pi Y)$$

$$P(K^- p \to \bar{K}^0 n)$$

$P(\pi N \to KY, \bar{K}N \to \pi Y)$

$$\frac{\frac{d\sigma}{dt}(K^- p \to \bar{K}^0 n,\ K^- n \to K^0 \Delta^-)}{\frac{d\sigma}{dt}(K^+ n \to K^0 p,\ K^+ p \to K^0 \Delta^{++})} \qquad \text{(Fig. 53)}$$

Agreement with EXD is not good in general. However one does not have to blame duality as a whole since some other assumptions were used in particular the assumed Regge pole behaviour with its factorization properties. Since we have numerous examples where the simple Regge-pole description breaks down, mostly through factorization, one may still hope to retain basic dual properties once the structure of the singularities is better understood. Along this direction it is instructive to compare the non-zero polarizations in $K^- p \to \bar{K}^0 n$ (duality + Regge pole behaviour predicts zero polarization) and in $\pi^- p \to \pi^0 n$ (Regge pole assumption leads to zero polarization).

--dip mechanisms

In a Regge amplitude

$$A_+ = \beta_+ \frac{1 + e^{-i\pi\alpha}}{\sin \pi\alpha} s^\alpha$$

the residue function $\beta_+(t)$ must have zeroes to cancel the possible poles of $\sin \pi\alpha$.

$$\alpha = 0 \qquad \sin \pi\alpha = 0 \qquad \Longrightarrow \beta_+(\alpha = 0) = 0$$

Then exchange degeneracy forces the same zero on the corresponding exchange

$$\beta_-(\alpha = 0) = 0$$

where the pole is already cancelled and therefore the amplitude has a zero.

For example, at $\alpha_\rho = \alpha_{A_2} = 0$ we have

$$\mathrm{Im}\ \rho_{+-} = 0$$

$$\mathrm{Re}\ \rho_{+-} = 0$$

but $\mathrm{Re}\ A_{+-} \neq 0$.

These results are in good agreement with experiment for the flip amplitudes. The following processes are dominantly helicity-flip and should be related by EXD and SU(3):

$$\frac{d\sigma}{dt}(\pi^- p \to \pi^0 n) \sim \beta_\pi^2 \sin^2 \frac{\pi\alpha}{2} \sim 2 \sin^2 \frac{\pi\alpha}{2}$$

$$\frac{d\sigma}{dt}(\pi^- p \to \eta n) \sim \beta_\eta^2 \cos^2 \frac{\pi\alpha}{2} \sim \frac{2}{3} \cos^2 \frac{\pi\alpha}{2}$$

$$\frac{d\sigma}{dt}(K^- p \to \bar{K}^0 n) \sim 2\beta_K^2 \qquad \sim 1$$

In Fig. 54 these relations are compared to experimental data: we see that there is good agreement between the shapes (a statement about duality and Regge behaviour for flip amplitudes) and even in magnitude (SU(3) symmetry). The same qualitative agreement is found in vector meson production[73]

$$KN \to K^* N, \quad \bar{K}N \to \bar{K}^* N, \quad \pi N \to \rho N$$

where $I_t = 0$ exchange (f,ω) can be isolated.

This nice systematics obviously will not work for helicity non-flip amplitudes with their zeroes completely uncorrelated with wrong-signature points.

(e) duality and quarks

Duality and the absence of exotic states leads to properties usually attributed to the quark model:

--in meson-meson scattering with SU(3) symmetry, duality leads to nonet structure for t-channel exchanges.

--considering K^+K^+ and K^+K^0 scattering, we find the canonical quark-model mixing angle between $\omega - \phi$ and $f - f'$

$$\cos^2\lambda = \frac{1}{3}$$

This intriguing correction has been exploited in the duality diagrams,[74-75] but will not be developed here.

(f) semi-local duality?

It is interesting to see how resonances can average and build up the smooth Regge behaviour: in particular let us find experimentally what is a typical momentum range for cancellations to occur. For example, consider backward $K^- p \to \bar{K}^0 n$ scattering[76] which has exotic quantum numbers: Fig. 55 shows the energy dependence of the imaginary part of the amplitudes showing resonance-produced oscillations around the zero value predicted by duality. A typical range $\Delta P_L \sim 1$ GeV/c corresponds to the short-range cancellation between resonances.

This semi-local duality can be exploited as a method to learn about t-channel amplitudes. Having a complete description in terms of phase-shifts over some (low) energy domain, we can reconstruct s-channel helicity amplitudes with well-defined t-channel quantum numbers in a local sense. Then, by observing the s-dependence of these amplitudes over some range of momenta (~ 1 GeV/c) we can hope to learn about them.

--example: $\bar{K}N$ scattering[77]

This type of study is particularly interesting and important for $\bar{K}N$ scattering where phase-shifts exist and are usually parametrized in terms of resonances superimposed to a background: each partial wave is taken as the sum of background and resonant parts

$$f_{\ell\pm} = f^R_{\ell\pm} + f^B_{\ell\pm}$$

The amplitudes reconstructed from the background shows dominance of the helicity non-flip, $I_t = 0$, imaginary part in accordance with Pomeron exchange properties (Fig. 56). It is remarkable that the background only contributes a negligible amplitude to $I_t = 1$ exchange in strong support of the Harari-Freund proposal.

Helicity amplitudes reconstructed from the resonant parts of the $\bar{K}N$ partial wave amplitudes are shown in Fig. 57. Even at momenta 1-1.3 GeV/c the features of high energy t channel exchange are well established with a zero at $t \sim -0.2$ GeV^2 for Im F_{++} (both $I_t = 0$ and $I_t = 1$) and a zero at $t \sim -0.5$ for Im F_{+-} ($I_t = 0, 1$).

As a final remark, let us note that a linear separation between background and resonances

$$\text{Im } F = \text{Im } P + \text{Im } R$$

does not obey unitarity. Indeed for a given partial wave P, we have the S-matrix:

$$S^\ell = \underset{\text{background}}{S^\ell_B}\ \underset{\text{resonance}}{S^\ell_R}$$

and consequently

$$T^\ell = T^\ell_B + T^\ell_R(1 + 2iT^\ell_B)$$

$$\text{Im } T^\ell = \text{Im } T^\ell_B + \text{Im } T^\ell_R + 2\ \text{Re}(T^\ell_R T^\ell_B)$$

The last term is generally ignored in most analyses.

2. Absorption

(a) classical absorption

In a scattering process, both the incident and outgoing waves can be absorbed out and it is convenient to describe the overall scattering amplitude in the impact parameter space:

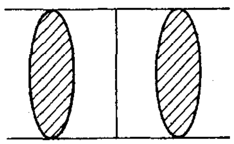

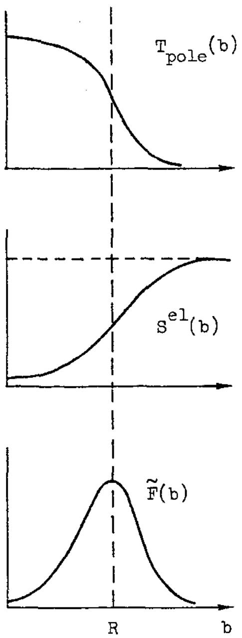

$F_{\Delta\lambda}(s,t)$

$$= \int b\, db\, T^{\Delta\lambda}_{pole}(b,s)\, S^{el}(b,s)\, J_{\Delta\lambda}(b\sqrt{-t})$$

where $S^{el}(b,s)$ is the transmission at the impact parameter b, and $\Delta\lambda$ the overall helicity change.

$$S^{el}(b,s) = 1 + iT^{el}(b,s)$$
$$\simeq 1 - |T^{el}(b,s)|$$

Therefore the dominant effect of absorption is the removal of low partial waves leading to peripherality of the absorbed amplitude in b space.

For a purely imaginary elastic amplitude with $\Delta\lambda = 0$

$$F_{el} = \frac{i\sigma_T}{4\sqrt{\pi}}\, e^{(B/2)t}$$

we have

$T_{el}(b)$

$$= \frac{1}{\sqrt{\pi}} \int_0^\infty \sqrt{-t}\; d\sqrt{-t}\; F_{el}(t)\; J_0(b\sqrt{-t})$$

$$= \frac{i\sigma_T}{4\pi B}\, e^{-b^2/2B}$$

and therefore total absorption of low partial waves if

$$\frac{\sigma_T}{4\pi B} = 1$$

Typically $\sigma_T = 25$ mb, $B = 7\ \text{GeV}^{-1}$ leading to $\sigma_T/4\pi B \sim 0.7$; so that in order to absorb completely the central waves one needs some additional absorption. For example it has been suggested[78] that all the inelastic diffractive states should be included as intermediate states leading to an increase in absorption.

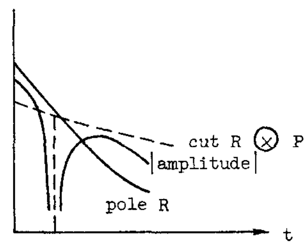

For strong enough an absorption the t-distribution can present dips due to the interference between the bare pole amplitude and the cut resulting from the convolution integral. The cut is destructive at $t = 0$ since T_{el} is imaginary.

Absorption has a qualitatively different effect on different helicity amplitudes due to the kinematic zero at $t = 0$ for flip amplitudes. Schematically we have:

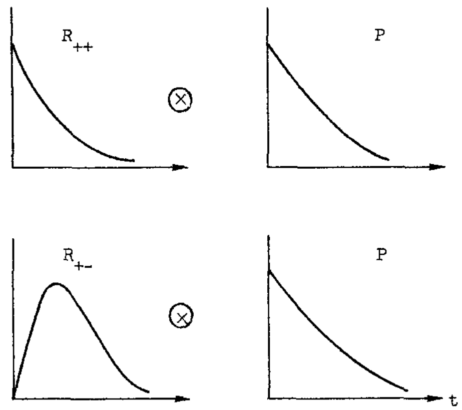

cut large

cut less
(less overlap)

This can also be seen by transforming the pole input into impact parameter space: one then finds that helicity flip amplitudes are in general already peripheral and therefore absorption of low waves is of little effect.

--general form for an absorbed amplitude

$$F_{\Delta\lambda}(t) = \int b\, db\, T(b)\, J_{\Delta\lambda}(b\sqrt{-t})$$

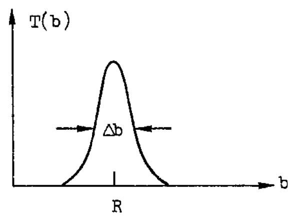

if $T(b) = \delta(b-R)$

$$F_{\Delta\lambda}(t) \sim J_{\Delta\lambda}(R\sqrt{-t})$$

if $T(b)$ peaks at $b \sim R$ with some width Δb, then $F_{\Delta\lambda}(t)$ retains the zeroes of $J_{\Delta\lambda}(R\sqrt{-t})$ for Δb not too large

$$\sqrt{-t} \ll \frac{\pi}{\Delta b}$$

A realistic form is $F_{\Delta\lambda}(t) = Ae^{Bt} J_{\Delta\lambda}(R\sqrt{-t})$ where R is the peak value and B is related to Δb.

$$\Delta b \sim 2\sqrt{B}$$

(b) absorption zeroes versus signature zeroes

Wrong signature occur typically for $t \sim -0.6\ GeV^2$ where $\alpha(t)$ passes through zero. Experimentally helcity-flip amplitudes have zeroes around $0.6\ GeV^2$; however absorption can also produce similar effects: $J_1(R\sqrt{-t})$ vanishes at the same place for $R = 1f$, a very realistic value. Therefore we have the following dilemma in trying to explain these dips:

$$\Delta\lambda = 1 \begin{cases} \text{Regge pole amplitude with signature zeroes} \\ \text{structureless pole} \otimes \text{absorption} \sim J_1(R\sqrt{-t}) \end{cases}$$

For $\Delta\lambda = 0$, there is no question: we have to invoke strong absorption to obtain a zero at $-0.2\ GeV^2$ and there is no trace of Regge zeroes.

A possible way to distinguish between absorption and wrong-signature zeroes arises if R shows some variation with s: in that case the J_1 zero will move with energy while the Regge zero, being a t-channel effect, should stay fixed.

(c) "dual" absorption

We know that s-channel resonances will produce dips in angular distributions due to their well-defined angular momentum. Since duality relates these resonances to the t-channel exchanges, we are interested in the relationship between these dips and the high energy t-channel dips (with or without absorption).

First of all let us see how resonances can produce dips at fixed t values. This will occur if there is a definite relationship between the mass and the spin of the dominant resonances. As an example, consider $\pi\pi$ scattering with no Pomeron ($\pi^+\pi^- \to \pi^0\pi^0$):

$$R(s,t) = \sum_J A_J P_J(\cos\theta)$$

For $J \gg 1$ and $\epsilon < \theta < \pi-\epsilon$

$$P_J(\cos\theta) \sim 2(2\pi J \sin\theta)^{-1/2} \cos\left[(J+\tfrac{1}{2})\theta - \tfrac{\pi}{4}\right]$$

and the first zero of the angular distribution is at:

$$(J+\tfrac{1}{2})\theta = \frac{3\pi}{4}$$

$$\theta \simeq \frac{3\pi}{4J}$$

Since $t = 2q^2(1-\cos\theta)$, a fixed t dip will occur if

$$s \sim \frac{1}{1-\cos\theta} \sim \frac{1}{\theta^2} \sim J^2$$

Thus the looked-for relationship is:

$$J \sim \sqrt{s}$$

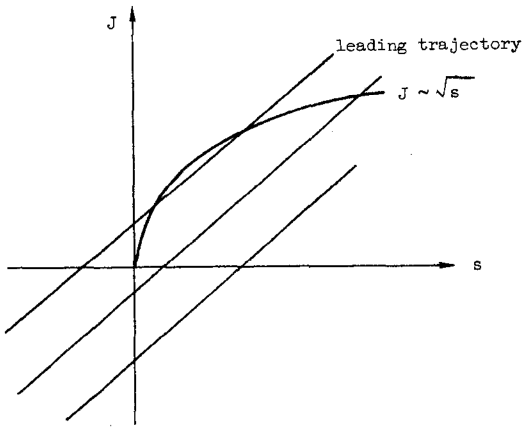

Above the curve $J \sim \sqrt{s}$ we expect angular momentum barrier effects, while below the amplitude is suppressed by absorption of low partial waves leading to the overall peripheral picture.

This behaviour can be checked against the observed N^* and Y^* baryon spectrum in Figs. 58 and 59. It seems satisfied although the deviation from the leading trajectory is still not clearly perceived. There is nevertheless a noticeable lack of low spin resonances at large mass: it seems that one should look experimentally a little harder into this question of low-lying "daughter" resonances, in order to pin down the idea of peripherality. In Fig. 60 we plot the location of the first zero of the $\Delta\lambda = 0$ and $\Delta\lambda = 1$ helicity amplitude from the prominent Y^* resonances: fixed t structures occur already in the lower mass states.

We have seen therefore that the dominance of "peripheral" resonances leads to a peripheral Im R while no insight is gained on the real part. On the other hand, classical absorption has for consequence that <u>both</u> real and imaginary parts are peripheral.

--<u>discussion</u>

It is an experimental fact that known resonances (log J) contribute a zero at 0.2 GeV^2 in Im R_{++} and that Im R_{++} at high energy also possesses such a zero (at least for the observed vector exchanges) as a result of absorption. The most logical connection between these two facts is to assume that <u>resonances are dual to Regge poles + absorption cuts</u>.[79]

Alternatively one could still have resonances dual to poles alone. If central resonances continue to be excited, dips can occur at larger t (~ 0.6 GeV^2) corresponding to the signature zeroes of Regge poles. Also at high energy absorption moves zero down to 0.2 GeV^2 thereby breaking duality. This alternative seems much less natural, but cannot be completely excluded at the present time.

This situation has an immediate consequence for exchange degeneracy: in the first case EXD will be satisfied at the same level than duality itself while in the second case there will be strong violations of duality due to absorption corrections.

Even though we are not yet seeing overwhelming evidence for peripheral high-mass resonances (in the $J \sim \sqrt{s}$ sense), the low mass resonances do exhibit striking peripheral properties in b space:[80] see, for example Fig. 61 where the $\bar{K}N$ resonant partial wave amplitudes are used to reconstruct Im R_{++}. The peripheral resonance contributions peak around 1f in a clear way almost outside the diffractive impact parameter distribution (Fig. 62). This feature is not unique to $\bar{K}N$ scattering and is also observed in πN phase shifts: Fig. 63 shows the full amplitude Im R_{++} + Im P where the resonance contribution is clearly visible on the edge of the diffractive background distribution of central character. From the same $\bar{K}N$ analysis it is interesting to follow the zero positions at 0.2 and 0.5 GeV^2 of the resonant amplitudes Im $R_{++}^{(I_t=0)}$ and Im $R_{+-}^{(I_t=1)}$ which are essentially constant within the accuracy of the different phase-shift analyses (Fig. 64).

V - MODELS AND SPECULATIONS

1. Models for Two-Body Scattering

From what we have seen in the preceding chapters it is clear that any model for high energy scattering should incorporate or possess the following properties:

- some Regge features, in particular in $\Delta\lambda = 1$ amplitudes
- strong absorption of the bare exchanges by Pomeron cuts
- duality for the imaginary parts
- approximate SU(3) symmetry for residues

Different models will have their emphasis on a few properties and will generally try to "explain" the remaining properties. Pure pole models are not reliable, except for flip amplitudes, and cannot yield a complete description of two-body processes. Strong absorption appears to be an important ingredient which has to be included in any realistic model.

We are not going to review all potentially successful models but rather select two of them in order to illustrate different assumptions and problems: on one hand, the dual absorptive model where duality and absorption are strongly linked together; on the other hand the strong absorption model where the accent is put on calculating strong-absorption cuts with no relationship to duality.

(a) Dual absorptive model (Harari[81])

--rules

The imaginary part of a non-diffractive t-channel exchange is built up by peripheral resonances. The $J \sim \sqrt{s}$ peripheral resonances are dual to the sum of poles and their absorption cuts:

$$\text{Resonances} \Longleftrightarrow R + R \otimes P$$

For a change $\Delta\lambda$ of helicity the imaginary part of an amplitude has a zero structure approximately given by $J_{\Delta\lambda}(R\sqrt{-t})$ where R is around 1 f

$$\mathrm{Im}\, F_{\Delta\lambda} \sim J_{\Delta\lambda}(R\sqrt{-t})$$

For $\Delta\lambda = 0$ the cut correction is large while it is much smaller for $\Delta\lambda = 1$.

The structure of the real parts is not given by duality requirements, but one can invoke analyticity: if $\mathrm{Im}\, F \sim s^{\alpha}$ then

$$\frac{\mathrm{Re}\, F}{\mathrm{Im}\, F} \sim \begin{cases} -\cot\frac{\pi\alpha}{2} & \text{(even exchange)} \\ \tan\frac{\pi\alpha}{2} & \text{(odd exchange)} \end{cases}$$

These crossing relations are claimed to work only for $\Delta\lambda = 1$ amplitudes where the s^{α} dependence is not perturbed too much by cuts; in $\Delta\lambda = 0$ amplitudes strong cuts can introduce log factors in the amplitude and the crossing relation could fail.

The Pomeron amplitude is assumed to be structureless in t, central in impact parameter space, mostly imaginary and helicity no-flip.

--comparison with experiment

(i) dips in inelastic processes ($\Delta\lambda = 1$ amplitudes)

Imaginary parts behave like $J_1(R\sqrt{-t})$ while real parts are

$$\tan\left(\frac{\pi\alpha}{2}\right) J_1(R\sqrt{-t}) \qquad \text{or} \qquad -\cot\left(\frac{\pi\alpha}{2}\right) J_1(R\sqrt{-t})$$

according to the signature:

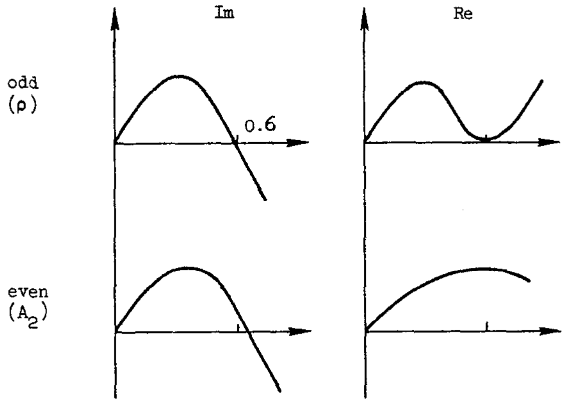

$$\frac{d\sigma}{dt} \sim \frac{J_1^2}{\cos^2 \frac{\pi\alpha}{2}}$$

$$\frac{d\sigma}{dt} \sim \frac{J_1^2}{\sin^2 \frac{\pi\alpha}{2}}$$

The most simple way to produce dips at $-t \sim 0.6$ GeV^2 in differential cross sections is when $\Delta\lambda = 1$ amplitudes with zero dominate. If other helicity amplitudes are important they are likely to wash out any indication of a dip: for example $[J_0(R\sqrt{-t})]^2$ has a bump in this t region. In order to see if a given process will have a dip or not, it is sufficient to apply the helicity coupling rules derived empirically in Chapter II and find out if $\Delta\lambda = 1$ dominates. If this latter condition is true, a dip will be observed if the exchange is odd under crossing since $d\sigma/dt$ has the zero of $[J_1(R\sqrt{-t})]^2$.

The dip is predicted and observed for the processes:

$$\pi^- p \to \pi^0 n, \quad \pi N \to \pi\Delta, \quad \gamma p \to \pi^0 p, \quad (\pi N \to \rho N)_{I_t=0} \;.$$

For reaction dominated by $\Delta\lambda = 1$ even exchanges, no such dip is observed: $\pi^- p \to \eta n$, $\pi N \to \eta\Delta$. This is also true when both even and odd exchanges occur such as in $K^- p \to \bar{K}^0 n$, $K^+ n \to K^0 p$, $KN \to K\Delta$ and $\bar{K}N \to \bar{K}\Delta$.

When $\Delta\lambda = 1$ does not dominate, no dip is expected as in $\gamma p \to \eta p$, $\pi N \to \omega N$, despite a strong ρ exchange.

The behaviour of elastic polarizations is also in good agreement with the dual absorptive model, as a test of Re $R_{\Delta\lambda=1}$.

(ii) elastic scattering ($\Delta\lambda = 0$ amplitudes)

The (dominant) imagainary part of an elastic scattering amplitude receives contributions from resonances (or t channel poles) and the Pomeron. For exotic channels, only the Pomeron term survives, as in K^+N and NN scattering:

$$F \sim P \sim \mathrm{Im}\, P$$

while for non-exotic processes, such as K^-N and $\bar{N}N$ scattering, we have the complete form

$$\mathrm{Im}\, F = \mathrm{Im}\, P + \mathrm{Im}\, R$$

For s high enough, the $\Delta\lambda = 0$, imaginary Pomeron amplitude dominates so that the leading terms in the differential cross section are:

$$\frac{d\sigma}{dt}\,(\text{exotic}) \simeq P^2$$

$$\frac{d\sigma}{dt}\,(\text{nonexotic}) \simeq P^2 + 2P\,\mathrm{Im}\, R_{\Delta\lambda=0}$$

where Im $R_{\Delta\lambda=0}$ behaves like a $J_0(R\sqrt{-t})$ function. We therefore expect the following pattern:

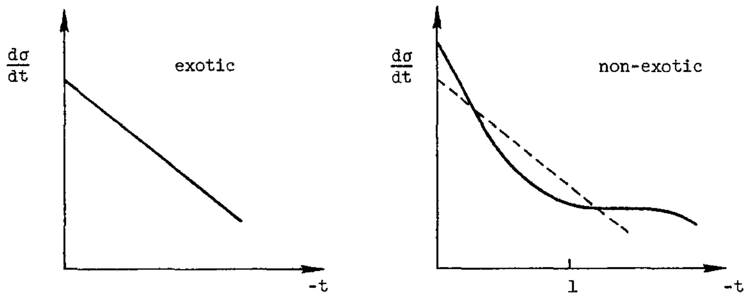

This behaviour is clearly seen in the data in the intermediate energy region for $\pi^{\pm}p$ (both non-exotic), $K^{\pm}p$ and up to ~ 10 GeV for $p^{\pm}p$ where the resonance contribution is larger. Obviously as the contribution from the resonances slowly decreases as the energy goes up, we expect the two patterns to become more and more similar and the "dip" in the non-exotic channel to fade away. We can translate this effect in terms of the exponential slope of the forward differential cross section which energy dependence comes from the proper s dependence of the Pomeron slope (which shrinks according to K^+p and pp data) and the disappearance of the Regge term (producing an apparent anti-shrinkage). The following trends are therefore expected in the dual absorptive model:

$$\frac{d\sigma}{dt} \sim e^{Bt}$$

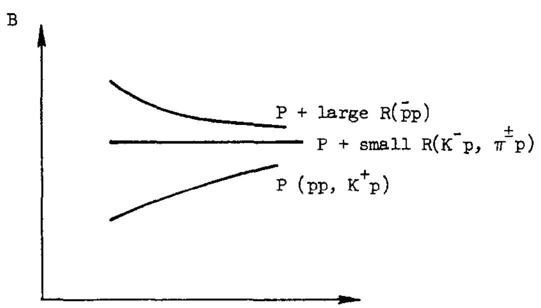

and are in good agreement with experimental data.

--questions and problems

Dips at $t \sim -0.6\ \mathrm{GeV}^2$ in $\Delta\lambda = 1$ amplitudes are explained by zeroes of $J_1(R\sqrt{-t})$; at the same time the complete systematics of the dips requires some connection with wrong signature zeroes ($\alpha = 0$): in particular for even exchanges there is a delicate cancellation between J_1 and $\sin(\pi\alpha/2)$ where the J_1 zero is completely determined by the absorption radius R. In order for this effect to happen at every energy, α and R should have the same s dependence. Now experimentally α is pretty independent of s at least for ρ exchange for $-t < 1\ \mathrm{GeV}^2$ and other exchanges at $t = 0$. It then follows that R should be more or less constant with s and it is hard to correlate this fact with the expanding radius of the shrinking Pomeron.

The peripherality picture receives also a warning from the new NAL data[39] on $\pi^-p \to \pi^0 n$, still showing a dip at approximately the same value $-t \sim 0.6\ \mathrm{GeV}^2$. A flip amplitude

$$\mathrm{Im}\, F_1(t) = Ae^{Bt}\, J_1(R\sqrt{-t})$$

corresponds in b space to:

$$\mathrm{Im}\, \tilde{F}_1(b) = \frac{A}{2B} \exp\left(-\frac{(R^2+b^2)}{4B}\right) I_1\left(\frac{Rb}{2B}\right)$$

$$\simeq \frac{A}{2B}\sqrt{\frac{B}{\pi R b}} \quad \exp\left(-\frac{(b-R)^2}{4B}\right)$$

for $b \gg 2B/R$.

If B shows shrinkage as in the $\pi^-p \to \pi^0 n$ data, the impact parameter distribution becomes wider and the peripheral character slowly disappears. In Fig. 65(a), $\mathrm{Im}\,\tilde{\rho}_{+-}(b)$ is plotted from the exact formula and

$$B(s) = B_0 + \alpha' \ln s \qquad\qquad \alpha' \simeq 1\ \mathrm{GeV}^{-2}$$

Since for a flip amplitude $\mathrm{Im}\,\tilde{F}_1(0)$ vanishes kinematically at $b = 0$, peripherality is maintained in an artificial way. If the same shrinkage occurs for a $\Delta\lambda = 0$ amplitude where no kinematic suppression operates at small b, peripherality is lost rather quickly (see Fig. 65(b)). It will be of crucial interest to check whether $\Delta\lambda = 0$ amplitudes show shrinkage properties.

Another possible problem is connected with even exchanges (f, A_2, K_T^*) which are predicted to be peripheral. There is no model-independent analyses of these amplitudes for $\Delta\lambda = 0$ and therefore it is very difficult to make any sensible statement; however there exist now some evidence from FESR analyses in KN and hypercharge exchange reactions indicating that tensor exchanges may be less peripheral than vector exchanges. It would be very important to confirm this experimentally by a direct test: this could be done for A_2 exchange by studying the differences

$$\Delta_A^K = \frac{d\sigma}{dt}(K^+p) + \frac{d\sigma}{dt}(K^-p) - \frac{d\sigma}{dt}(K^+n) - \frac{d\sigma}{dt}(K^-n)$$

$$\Delta_A^\gamma = \frac{d\sigma}{dt}(\gamma p \to \omega p) - \frac{d\sigma}{dt}(\gamma n \to \omega n)$$

It is remarkable that $I_t = 0$ exchange in πN scattering can be explained[82] by a peripheral f

$$\mathrm{Im}\, f_{++} = A_f\, e^{B_f t}\, J_0(R\sqrt{-t})$$

if the Pomeron amplitude shrinks. There is then a nice consistency between $\pi^\pm p$ and $K^\pm p$ elastic scattering, all being described with peripheral exchanges and a shrinking Pomeron at energies 3-20 GeV (Fig. 66). This harmonious situation is unfortunately shaken by data[83,84] on ϕ photoproduction where Pomeron exchange is expected to dominate in the t channel since non-strange exchanges do not couple strongly to ϕ: the data shows essentially no s dependence for $d\sigma/dt\ (\gamma p \to \phi p)$ at $-t = 0.6\ \mathrm{GeV}^2$. Even including some s dependence for $(d\sigma/dt)_{t=0}$ leaves little shrinkage

$$\alpha_P' \simeq 0.1 - 0.2\ \mathrm{GeV}^{-2}$$

in the range 2 to 19 GeV. This is to be contrasted with Fig. 66 where in the same energy range $\alpha_p' \simeq 0.6\ \mathrm{GeV}^{-2}$. Regardless of the ϕ data, it is also possible that a slope $\alpha_p' \simeq 0.6\ \mathrm{GeV}^{-2}$ leads to some inconsistencies in the dual absorptive model analyses since it corresponds to a sizeable real part of the Pomeron amplitude at larger t values-- ~ 50% of the imaginary part at $-t \sim 0.5\ \mathrm{GeV}^2$.

(b) Strong absorption models (Kane et al.[84])
--calculating $R \otimes P$ cuts

In these models the cut is calculated explicitly as a convolution integral over the pole amplitude and the Pomeron amplitude:

$$R_{abs}(s,t) = R_{pole}(s,t) + i\int dt'\, dt''\, K(t,t',t'')\, R_{pole}(s,t')\, P(s,t'')$$

where $R_{pole}(s,t)$ is a structureless amplitude, having no relationship to exchange degeneracy or duality and $K(t,t',t'')$ is a real positive function. All dips seen in differential cross sections are explained as absorption zeroes coming from the destructive interference between pole and cut.

In its early forms the model suffered from not representing correctly real parts. If P is an imaginary amplitude, both the real and imaginary parts of the pole term are equally strongly absorbed giving a $\sim J_1(R\sqrt{-t})$ behavior for both:

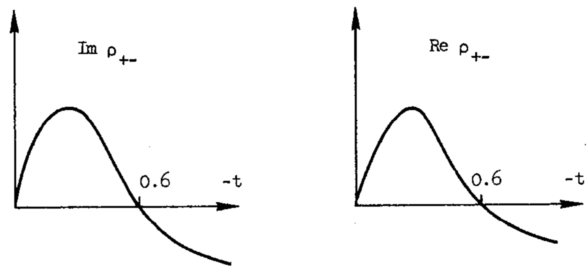

Such a form for Re ρ_{+-} is ruled out by polarization data on $\pi^{\pm}p$ so that a new version of the model was developed.

--<u>a new model</u>

Since the trouble seemed to come from the assumption of a purely imaginary Pomeron (believing the procedure to compute cuts) an easy cure is to allow for a Pomeron real part. This was originally motivated by the steepening forward differential cross section observed in pp scattering at the ISR: parametrizing the imaginary Pomeron amplitude with a dominant central part and a peripheral part with expanding radius

$$\text{Im } P = Ae^{Bt} + Ce^{Dt} J_0(R\sqrt{-t})$$

$$R \sim R_0 \sqrt{\ln s} = R_0 \sqrt{y}$$

one obtains via analyticity a real part proportional to the derivative of J_0

$$\text{Re } P \sim \frac{d}{dy} J_0(R\sqrt{-t}) \sim J_1(R\sqrt{-t})$$

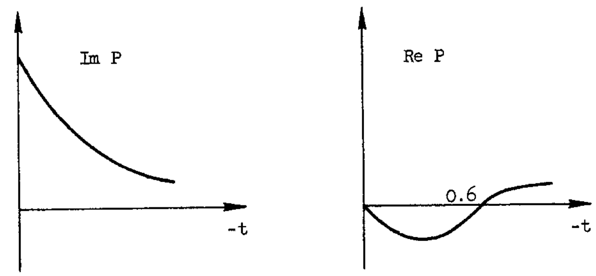

It is easy to understand how the real part of P changes the conclusions about real and imaginary absorbed amplitudes:

$$\text{Re } R_{abs} = \text{Re } P_{pole} - \text{Re } P_{pole} \otimes |\text{Im } P| + \text{Im } R_{pole} \otimes |\text{Re } P|$$

$$\text{Im } R_{abs} = \text{Im } R_{pole} - \text{Re } P_{pole} \otimes |\text{Re } P| - \text{Im } R_{pole} \otimes |\text{Im } P|$$

The result of absorption will now depend on the relative sign of Re P_{pole} and Im P_{pole}, leading to a qualitatively different conclusion for odd and even exchanges:

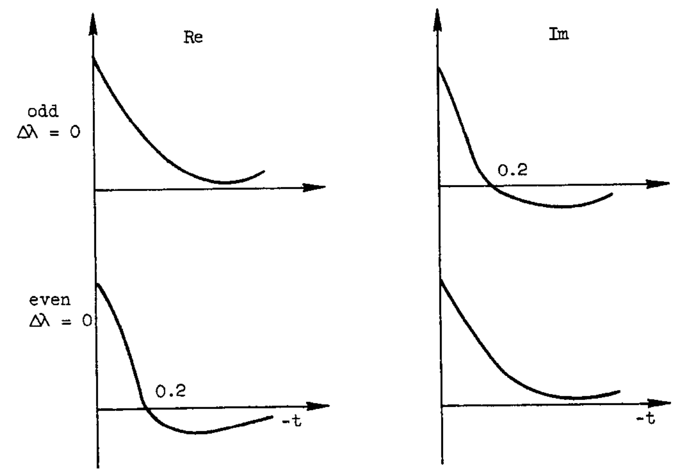

Therefore real parts of even exchanges and imaginary parts of odd exchanges are peripheral (first zero around 0.2 GeV^2) while imaginary parts of even exchanges and real parts of odd exchanges are rather central (with a broad minimum around 0.4 GeV^2).

Using these prescriptions, a zeroth order fit to the available data can be obtained with a few parameters, SU(3) symmetry and some assumptions of simplicity.

--problems

First of all duality is never satisfied at any level and would sadly appear as a mere accident. At the end the absorbed amplitudes have some kind of resemblance to exchange-degenerate amplitudes, but it is only approximate, at any rate worse than the data actually shows: for example $d\sigma/dt$ for $K^{\pm}p$ are not too different with K^+p showing a sizeable curvature which is not supported by the data.

The rise in K^+p total cross section (also pp) is explained by different energy dependences of f and ω amplitudes. Since Im ω is more peripheral than Im f, the model predicts that

$$\alpha^{\omega}_{eff}(0) > \alpha^{f}_{eff}(0)$$

The data from NAL and ISR indicate that P is a rising term as well and there seems to be little evidence for a large effect from f-ω energy dependence.

Since absorption has a larger effect in non-flip amplitudes, one expects in this model

$$\alpha^{eff}_{\Delta\lambda=0} > \alpha^{eff}_{\Delta\lambda=1}$$

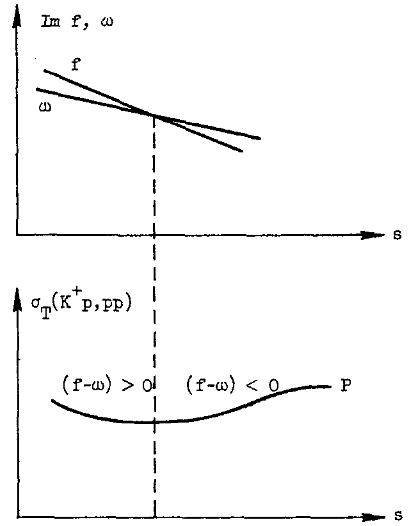

since

$$R_{abs} \sim R_{pole} - R_{cut}$$

$$\sim s^{\alpha}\left[1 - \frac{\lambda}{\ln s}\right]$$

$$\sim s^{\alpha+\epsilon}$$

$$(\epsilon > 0)$$

for a limited s range

where data on $\pi^- p \to \pi^0 n$ and $\Delta(\pi^{\pm}p)$ do not seem to indicate a significant effect. It is interesting to see that the cut term has a strong effect on the phase of the amplitude at $t = 0$: if

$$\text{Im } R^- = As^{\alpha}\left[1 - \frac{\lambda}{\ln s}\right] = Ae^{\alpha y}\left[1 - \frac{\lambda}{y}\right]$$

$$\Longrightarrow \text{Re } R^- \simeq Ae^{\alpha y}\tan\left(\frac{\pi\alpha}{2}\right)\left[1 - \frac{\lambda}{y} + \frac{\lambda}{\alpha y^2}\right]$$

$$\frac{\text{Re } R^-}{\text{Im } R^-} \simeq \tan\left(\frac{\pi\alpha}{2}\right)\left[1 + \frac{\lambda}{y(y-\lambda)\alpha}\right]$$

So that one expects a larger real part at low s from the pole term alone: while the data show a small effect in this direction (see Fig. 22) it seems too small considering the large size of the absorptive cut. It is instructive to notice that the phase of an amplitude, being related to derivatives of the modulus with respect to s, is a rather sensitive indicator of any change in the s dependence.

At a more fundamental level, the magnitude of Re P required to fit the data may be too large. In Chapter III we have seen that the real parts of $I_{t=0}$ $\pi^{\pm}p$ and γp elastic scattering were strongly s-dependent and probably related more to f exchange rather than Pomeron exchange. It does mean of course that f exchange should be not ignored in calculating cut diagrams but the whole problem has to be investigated separately--whether and how to compute $R \otimes R'$ cuts. We have seen that for exotic quantum numbers these amplitudes are rather small and this should be understood before engaging in a systematic program to include pole-pole cuts in two-body processes. The half-success of the strong absorption models seems to indicate the need for real part effects in rescattering and $R \otimes R'$ cuts are likely to play a role in them.

2. Speculations on the Pomeron

We have seen in many occasions that it is crucial to learn more about the Pomeron amplitudes at lower energies since it relates to the problems of understanding of elastic amplitudes, separation of f exchange, exchange degeneracy and absorption. Since experimentally the Pomeron is most accesible at very high energies, we shall try to start there and gather the relevant properties of Pomeron exchange.

(a) Pomeron from high-energy pp data (ISR)

We take the following points as clear experimental facts:[85]

- Im $P(s, t = 0)$ is rising with s
- Re $P(s, t = 0)$ is small, crossing zero and becoming positive
- Im $P(s,t)$ is dominantly central, but has a distinct peripheral piece (~ J_0 may be a good parameterization)
- Im $P_{\text{central}}(s,t)$ changes very slowly with s (α' small)
- Im $P_{\text{peripheral}}(s,t)$ is growing

The stronger shrinkage seen at small t can be induced by any of 3 effects or a mixture of them:

- the growth at $t = 0$
- the shrinkage of the peripheral part
- an expanding radius R in $J_0(R\sqrt{-t})$

Since the first effect we mention is already clearly observed in the data, it is interesting to see if, by itself, one can achieve a good description of pp elastic scattering with other parameters only slowly varying. In this simple model we write

$$\text{Im } P(s,t) = Ae^{Bt} + C(s)\, e^{Dt}\, J_0(R\sqrt{-t})$$

with A, B, D and R are slowly changing with s and the main s dependence comes from $C(s)$, growing with s.

Analyticity requires that

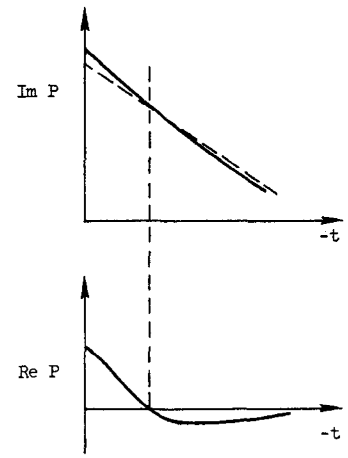

$$\text{Re } P = \tan\left(\frac{\pi}{2}\frac{d}{dy}\right) \text{Im } P$$

$$\simeq \frac{dC}{dy}\, e^{Dt}\, J_0(R\sqrt{-t})$$

with $dC/dy > 0$.

If $C = C_0 y$, then Re P is essentially s-independent while Im P grows like ln s.

An excellent fit to the available ISR data yields

$$B = 4.4 \text{ GeV}^{-2}$$
$$D = 4.7 \text{ GeV}^{-2}$$
$$R = 4.7 \text{ GeV}^{-2} \sim 1 \text{ f}$$

showing a rather broad peripheral distribution in b space. Let us note at this point that our picture is quite orthogonal to Kane's[84] where the main s dependence comes from the s dependence of R in the J_0 argument.

At lower energies we expect real parts from Regge exchange to contribute since, although $\text{Im } R$ is not very large, $\text{Re } P$ can be quite substantial--as seen in Chapter IV.

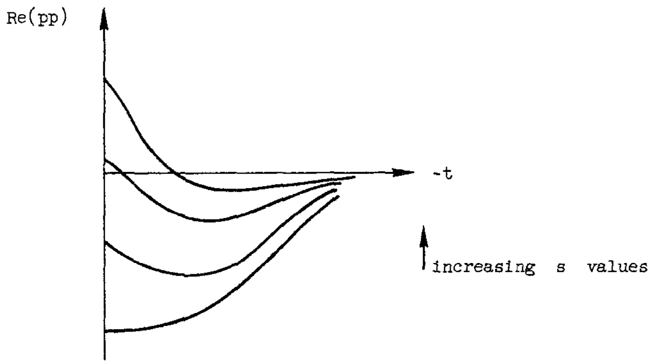

We expect the same qualitative behaviour for meson scattering with R scaled geometrically with $\sim\sqrt{\sigma_T}$ and the peripheral piece will lead to some curvature in $d\sigma/dt$ at high energy.

(b) Can we extract $\text{Im } P(s,0)$ at lower s?

We can isolate the combination $(P + f)$ in πN, KN and NN elastic scattering. How to eliminate f exchange? Let us recall the following properties of exchange amplitudes:

-ρ, ω and A_2 exchange is power-behaved at $t = 0$ and probably the same will hold for f exchange.

-within the experimental uncertainty it appears that $\alpha(0)$ for a given exchange is independent of the process; for example, $\alpha_\rho^\pi(0) \sim \alpha_\rho^K(0) \sim \alpha_\rho^p(0)$.

-SU(3) symmetry is approximately true for residues at the 20% level (ρ_π/ρ_K for example).

Guided by these facts we shall assume that the f amplitude has similar properties at $t = 0$:

- $\text{Im } f = fs^{\alpha_f - 1}$
- $\alpha_\pi^f = \alpha_f^K \; (= \alpha_f^N)$
- $2f_K = f_\pi$ as given by SU(3).

It is then possible to use cross sections data on $\pi^\pm p$, $K^\pm p$ and $K^\pm n$ to eliminate the f amplitude and obtain a "Pomeron" amplitude. The relation is

$$\frac{1}{2}\left[\Sigma(Kp) + \Sigma(Kn) - \Sigma(\pi p)\right] = 2P_K - P_\pi$$

and is evaluated using total cross section data in Fig. 67. Since we do not a priori expect a marked difference between the s dependence of P_K and P_π, it is fair to assume that we are seeing in Fig. 67 the s dependence of either P_K or P_π: data shows a rising Pomeron contribution from a momentum of 3 GeV up. Thus the asymptotic behaviour seen at the ISR for pp scattering and also for $K^\pm p$ scattering at lower energies ($\gtrsim$ 20 GeV) seems to persist to quite low energies, once Regge terms have been removed.

Before going further we must check the stability of our result against the most crucial assumption of an SU(3)-symmetric f coupling to pseudoscalar mesons. From the branching ratio

$$\frac{\Gamma(f \to K\bar{K})}{\Gamma(f \to \pi\pi)} = .025 \pm .01$$

obtained from an analysis[86] including a proper treatment of f-A_2 interference in the $K\bar{K}$ channel, we obtain

$$\frac{2f_K}{f_\pi} = .94 \pm .2$$

in good agreement with SU(3). Since this last result is only accurate to $\pm$ 20%, it is important to see the effect of such variations on the s dependence of the Pomeron amplitude. This is studied in Fig. 68 where the quantity

$$\frac{1}{2}\left[\Sigma(Kp) + \Sigma(Kn) - \left(\frac{2f_K}{f_\pi}\right)\Sigma(\pi p)\right]$$

is evaluated for different values of $2f_K/f_\pi = 1 \pm .2$. Within this range of values, our result stands that the Pomeron amplitude is rising with s, the rise being more linear in $\ln s$ for the values of the ratio closest to symmetry.

More quantitatively there is internal consistency between a linear $\ln s$ growth of the Pomeron term and the ratio f_K/f_π given by SU(3). Parametrizing cross sections as

$$\frac{1}{2}\Sigma(\pi p) = P_\pi^0 + P_\pi' y + f_\pi e^{(\alpha_f - 1)y}$$

$$\frac{1}{2}\Sigma(KN) = P_K^0 + P_K' y + f_K e^{(\alpha_f - 1)y}$$

yields reasonable values for the parameters:

$$P_\pi = (14.2 \pm 2.5) + (1.4 \pm .3)y$$

$$P_K = (11.3 \pm 1.4) + (1.34 \pm .2)y$$

$$\left.\begin{aligned} f_\pi &= 39.4 \pm 1.1 \\ f_K &= 21.6 \pm 7 \end{aligned}\right\} \frac{2f_K}{f_\pi} = 1.10 \pm .05$$

$$\alpha_f = .44 \pm .07$$

to be compared to

$$\alpha_K = 13.0 \pm 2.6$$

$$\alpha_\omega \sim 0.41$$

The fact that $P_\pi \neq P_K$ indicate that Pomeron exchange is not a pure SU(3) singlet[87] in agreement with vector meson photoproduction:

$$\left[\frac{\frac{d\sigma}{dt}(\gamma p \to \phi p)}{\frac{d\sigma}{dt}(\gamma p \to \rho^0 p)}\right]_{t=0} \sim \frac{f_{\gamma\phi}^2}{f_{\gamma\rho}^2}\left(\frac{\sigma_T(\phi p)}{\sigma_T(\rho p)}\right)^2 - \frac{1}{60}$$

leading to $\sigma_T(\phi p) \sim 10$ mb around 10 GeV. Experimentally $\sigma_T(\phi N)$ has been directly measured by nuclear absorption to be 12 mb at 6 GeV[88] showing a large reduction compared to $\sigma_T(\rho N) \simeq \sigma_T(\pi N)$. Assuming the SU(3) breaking occurs through octet exchange

$$P = P_1 \cos\alpha + P_8 \sin\alpha$$

measured by a mixing angle α, we can evaluate the Pomeron contribution to forward elastic amplitudes:

$$\left.\begin{aligned} P_\pi &= \left(\cos\alpha + \frac{1}{\sqrt{2}}\sin\alpha\right)P_0 \\ P_K &= \left(\cos\alpha - \frac{1}{2\sqrt{2}}\sin\alpha\right)P_0 \end{aligned}\right\} \text{pseudoscalar nonet}$$

$$\left.\begin{aligned} P_\rho = P_\omega &= \left(\cos\alpha + \frac{1}{\sqrt{2}}\sin\alpha\right)P_1 \\ P_\phi &= (\cos\alpha - \sqrt{2}\sin\alpha)P_1 \end{aligned}\right\} \text{vector nonet}$$

where we have used the canonical ω-ϕ mixing angle. Since $\sigma_T(\rho N) \sim \sigma_T(\pi N)$ we know that $P_0 \sim P_1$ and consequently

$$\sigma_T(\phi N) \sim \frac{1}{2}\,[\Sigma(Kp) + \Sigma(Kn) - \Sigma(\pi p)]$$
$$\sim 2P_K - P_\pi$$

This serves as an independent check of the f_K/f_π ratio since values for $\sigma_T(\phi N)$ in agreement with data occur for the SU(3) ratio (Fig. 68). We therefore expect $\sigma_T(\phi N)$ to show a linear rise with $\ln s$ from as low a momentum as 3 GeV and up: this can be experimentally checked by studying the s dependence of $(d\sigma/dt)_{t=0}$ $(\gamma p \to \phi p)$ and would be clear-cut confirmation of the Pomeron behaviour at low energies.

(c) Application to $\gamma p \to \phi p$

ϕ photoproduction is dominated by Pomeron exchange and the study of the t distribution of this process should have some similarities with pp elastic scattering as seen at the ISR. Let us parametrize the ϕ photoproduction amplitude in the same way

$$F \sim \text{Im } P = Ae^{Bt} + C(s)\, e^{Dt}\, J_0(R\sqrt{-t})$$

where

-- B, R and D are scaled geometrically from pp scattering leading to $R \sim 3.5\ \text{GeV}^{-1}$ (less peripheral than pp)

-- C(s) is given by $2\sigma_T(KN) - \sigma_T(\pi p)$

In Fig. 69, the above parameter-free description (except for overall s independent scale approximately given by vector dominance and $f^2_{\gamma\phi}$ from e^+e^- colliding beam data) is compared favorably with the data on $\gamma p \to \phi p$ from 2 to 12 GeV. There is shrinkage at small $-t \lesssim 0.3\ \text{GeV}^{-2}$ while the large t cross section is dominated by the central part and is quite independent of s (Fig. 70) in agreement with experiment. In Fig. 71 we show the different amplitudes making up the full Pomeron contribution at 12 GeV.

It is clear that the effects are not very large and that we need new accurate experiments measuring forward ϕ photoproduction down to $t = 0$ and concentrating on the careful study of s dependence. At an easier level it should be verified that the integrated cross section is a growing function of s.

(d) Implications for exchange degeneracy

--$t = 0$

A Pomeron s dependence of the form $A + B \ln s$ implies a breaking of exchange degeneracy since $\sigma_T(K^+p)$ and $\sigma_T(pp)$ show some extra contributions at lower energies. At $s \sim 10\ \text{GeV}^2$ we have approximately

$$\text{Im } R(K^-p) \simeq \text{Im}(f + \omega) \sim 10 \text{ mb}$$

$$\text{Im } R(K^+p) \simeq \text{Im}(f - \omega) - 1 - 2 \text{ mb}$$

indicating a small violation $\lesssim 20\%$ of exchange degeneracy. If the breaking comes from absorption effects, then the f cut is weaker than the ω cut, as expected from the new strong absorption model (see Section 1(b) of this chapter); but breaking could also come from the pole terms, since the respective values for $\alpha(0)$ are not too different where a strong absorption difference would have an important effect.

--$t \neq 0$

If exchange degeneracy is broken in K^+p and pp elastic scattering, $\text{Im}(f - \omega)$ is going to contribute to the shape of $d\sigma/dt$ since it interferes with the dominant Pomeron amplitude:

-if $\text{Im } f_{++}$ and $\text{Im } \omega_{++}$ have zeroes at the same t value ($\sim -0.2\ \text{GeV}^2$), then $d\sigma/dt\ (K^+p)$ will be of the form $P^2 + 2P.\text{"}J_0\text{"}$ with a "J_0" term about 5 times smaller than in K^-p. Since the P term is essentially non-shrinking for $-t > 0.2$-$0.3\ \text{GeV}^2$ the effect of the "J_0"

produces a slight anti-shrinking, at variance with the trend of experimental data showing a pronounced shrinkage.

-if $\mathrm{Im}\, f_{++}$ and $\mathrm{Im}\, \omega_{++}$ have different zeroes the shape of $\mathrm{Im}(f-\omega)_{++}$ will depend on the separation between their zeroes.

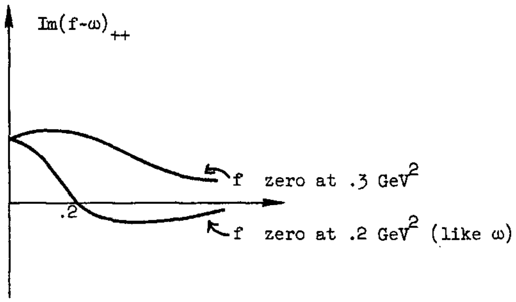

Even for slightly displaced zeroes (0.2 and 0.3 GeV^2), $\mathrm{Im}(f - \omega)_{++}$ can be very different from a J_0 shape, leading to a much flatter amplitude. This results in an apparent shrinking of the K^+p differential cross section since this rather flat amplitude is decreasing with energy:

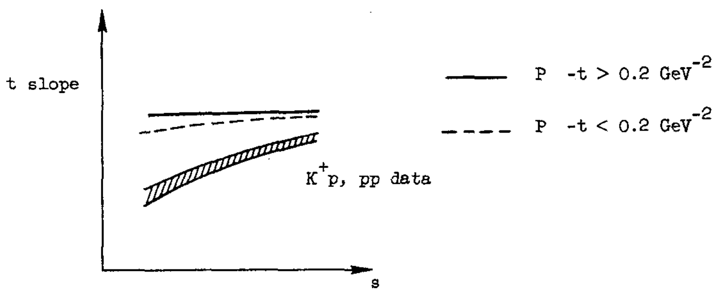

It is interesting to notice that such a small change in the first zero has important consequences for the peripherality of the amplitude: if $\mathrm{Im}\, f_{++} = 0$ at $-t \sim 0.3\ \mathrm{GeV}^2$ it means that $\langle R \rangle \sim 0.5$ f rather than $\langle R \rangle \sim 1$ f for $\mathrm{Im}\, \omega_{++}$ and that $\mathrm{Im}\, f_{++}$ is qualitatively central in agreement with strong absorption with important real parts, a convincing mechanism for which being still lacking.

It thus seems that our picture of a mostly central Pomeron with very slow energy dependence with a growing peripheral (but wide) part leads to a consistent description of elastic processes and vector meson photoproduction. Small breaking of exchange degeneracy follows and has significant effects on the slopes of the differential cross sections; the breaking of exchange degeneracy is strong enough to allow the imaginary part f exchange to become significantly central. To verify these conclusions it is important to carry out accurate measurements of $\gamma p \to \phi p$, and also have some model-independent look at the even exchanges such as in hypercharge exchange reactions and may be $\gamma p \to \omega p$ and $\gamma n \to \omega n$.

OUTLOOK

There has been a qualitative change in understanding two-body reactions when experiments have been geared to extract individual amplitudes instead of just bi-linear products such as cross sections. Information gathered so far is very limited and new experiments should expand our knowledge considerably. Major areas are:

1) energy dependence of πN amplitudes
2) getting closer to KN, $\bar{K}N$ complete amplitude separation
3) measuring even-crossing amplitudes through $K^{\pm}d$, $\gamma N \rightarrow \omega N$ and hypercharge exchange reactions
4) production of resonances observing their correlated decays; mostly for lower spins
5) accurate elastic scattering and polarization measurements at high energy (up to ~ 100 GeV) to determine the energy dependence of a few important amplitudes
6) improving experimental knowledge of the Pomeron amplitude at lower energies, mostly through detailed measurements of $\gamma p \rightarrow \phi p$
7) determine the importance of non-exotic Regge $\otimes$ Regge cuts through accurate comparison of processes sensitive to interferences.

We also need to develop methods to incorporate the constraints of analyticity into amplitude analyses: while the derivative analyticity relations look promising, one has to understand their limitations more fully. It is possible that a clever use of analyticity will relieve some of the burden of carrying out complete experiments--a task out of sight in most cases.

When unambiguous experimental measurements of even amplitudes are done it will become essential to understand absorption effects, the structure of Pomeron amplitudes and the importance of Regge cuts.

The present picture of a high energy amplitude is aesthetically not particularly pleasing; for example SU(3) symmetry and concepts like exchange degeneracy are only appproximately verified by experiment to about 20%. However we feel that much will be learnt when the breaking mechanisms are understood and then, may be, a simpler picture will emerge.

Bibliography

1. M. Jacob and G. Wick, Annals of Phys. 7, 404 (1959).
2. G. Cohen-Tannoudji et al., Nuovo Cimento 48A, 1077 (1967).
3. G. Cohen-Tannoudji et al., Nuovo Cimento 55A, 412 (1968).
4. J. Werle, Relativistic Theory of Reactions, North Holland (1966), p. 264.
5. I. Ambats et al., ANL/HEP 7329 (1973).
6. A. Stirling et al., Phys. Rev. Lett. 14, 763 (1965).
7. P. Sonderegger et al., Phys. Lett. 20, 75 (1966).
8. M. Whalig and I. Mannelli, Phys. Rev. 168, 1515 (1968).
9. M. Borghini et al., Phys. Lett. 31B, 405 (1970).
10. P. Bonamy et al., Nucl. Phys. B52, 392 (1973).
11. D. Hill et al., Phys. Rev. Lett. 30, 239 (1973).
12. A. DeLesquen et al., Phys. Lett. 40B, 277 (1972).
13. F. Halzen and C. Michael, Phys. Lett. 36B, 367 (1971).
14. R. Kelly, Phys. Lett. 39B, 635 (1972).
15. G. Cozzika et al., Phys. Lett. 40B, 281 (1972).
16. P. Johnson et al., Phys. Rev. Lett. 30, 242 (1973).
17. L. Van Rossum, Proceedings of the 1973 KEK Summer School, KEK 73-10.
18. D. Yovanovitch et al., contribution to the XVI International Conference on High Energy Physics, Chicago (1972).
19. W. Beusch et al., CERN preprint (1974).
20. CERN-ETH-Helsinki-London collaboration (5 GeV/c).
21. A. Kotanski, Proceedings of the 1970 Herceg-Novi School.
22. A.D. Martin, Proceedings of the 1972 Rencontre de Moriond.
23. J.P. Ader et al., CERN preprint TH 1768 (1973).
24. See for example, D.J. Sherden et al., Phys. Rev. Lett. 30, 1230 (1973).
25. J. Ballam et al., Phys. Rev. Lett. 24, 960 (1970).
26. CERN-Munich group; R. Cashmore, private communication.
27. M.G. Doncel et al., CERN/D.Ph.II/Phys 74-7 (1974).
28. R.C. Fernow et al., University of Michigan preprint UMHE 74-21 (1974).
29. F. Halzen and G.H. Thomas, ANL/HEP 7402 (1974).
30. G.L. Kane and U.P. Sukhatme, UMHE 73-30 (1974).
31. W. Galbraith et al., Phys. Rev. 138B, 913 (1965).
32. K. Foley et al., Phys. Rev. Lett. 19, 330 (1967).
33. S. Denisov et al., Phys. Lett. 36B, 415 and 528 (1971).
34. S. Denisov et al., Nucl. Phys. B65, 1 (1973).
35. A.S. Carroll et al., Phys. Rev. Lett. 33, 932 (1974).
36. V.N. Bolotov et al., IHEP 73-52 (1973).
37. V.N. Bolotov et al., IHEP 73-57 (1973).
38. U. Amaldi, Rapporteur's talk, Proceedings of the International Conference on Elementary Particles, Aix-en-Provence (1973).
39. R. Walker, these proceedings.
40. V. Barger et al., preprint (1973).
41. R. Diebold, Proceedings of the International Conference on Elementary Particles, Aix-en-Provence (1973).
42. R.C. Carnegie, these proceedings.
43. A. Eide et al., Nucl. Phys. B60, 173 (1973).
44. C. Akerlof et al., Phys. Rev. Lett. 33, 119 (1974).
45. A. Boyarski et al., Phys. Rev. Lett. 25, 695 (1970).
46. C. Baglin et al., to be published; F. Richard, private communication.
47. C. Berger, Phys. Rev. Lett. 23, 1139 (1969).
48. D. Ayres et al., Phys. Rev. Lett. 32, 1463 (1974).
49. I. Ambats et al., ANL/HEP 7367 (1973).
50. K. Foley et al., Phys. Rev. Lett. 19, 193 and 622 (1967).
51. P. Baillon et al., Phys. Lett. 50B, 387 (1974).
52. P. Baillon et al., Phys. Lett. 50B, 377 (1974).
53. V.K. Birulev et al., Phys. Lett. 38B, 452 (1972).
54. S. Kramer et al., Phys. Rev. Lett. 33, 505 (1974).

55. P. Estabrooks et al., CERN preprint (June 1974).
56. M. Davier and H. Harari, Phys. Lett. 35B, 239 (1971).
57. E. Pietarinen, Nucl. Phys., B49, 315 (1972).
58. H. Hecht et al., CERN preprint TH-1722 (1973).
59. G. Höhler and H. Jakob, Karlsruhe preprint TKP 13/73 (1973).
60. J. Bronzan et al., Phys. Lett. 49B, 272 (1974).
61. F. Zachariasen, Physics Reports, 1 (1971).
62. U. Sukhatme et al., to be published.
63. A.D. Brody et al., Phys. Rev. Lett. 26, 1050 (1971).
64. G. Buschorn, et al., Phys. Lett. 37B, 207 (1971).
65. R.L. Anderson et al., Phys. Rev. Lett. 25, 1218 (1970).
66. A. Boyarski et al., Phys. Rev. Lett. 26, 1600 (1971).
67. K. Igi and S. Matsuda, Phys. Rev. Lett. 18, 625 (1967).
A. Logunov et al., Phys. Lett. 24, 181 (1967).
68. R. Dolen et al., Phys. Rev. 166, 1768 (1968).
69. F. Elvekjaer and B. Martin, CERN preprint TH 1806 (1974).
70. H. Harari, Phys. Rev. Lett. 20, 1395 (1968).
71. P. Freund, Phys. Rev. Lett. 20, 235 (1968).
72. H. Harari and Y. Zarmi, Phys. Rev. 187, 2230 (1969).
73. C. Michael, CERN preprint TH-1627 (1973).
74. H. Harari, Phys. Rev. Lett. 22, 562 (1969).
75. J. Rosner, Phys. Rev. Lett. 22, 689 (1969).
76. C. Bricman et al., CERN preprint (1970).
77. M. Fukugita and T. Inami, Nucl. Phys. B44, 490 (1972).
78. M. Ross et al., Nucl. Phys. B23, 269 (1970).
79. M. Harari, Annals of Physics 63, 432 (1971).
80. M. Fukugita et al., Rutherford preprint RPP/T/32 (1972).
81. H. Harari, Phys. Rev. Lett. 26, 1400 (1971) and Ref. 79.
82. M. Davier, Phys. Lett. 40B, 369 (1972).
83. R.L. Anderson et al., Phys. Rev. Lett. 30, 149 (1973).
84. G. Kane, Phys. Lett. 40B, 363 (1972).
85. D. Leith, these proceedings.
86. A. Irving and C. Michael, CERN preprint TH-1825 (1974).
87. M. Davier, Phys. Rev. Lett. 20, 952 (1968).
88. H. Alvensleben et al., Phys. Rev. Lett. 27, 444 (1971) and references therein.
89. G. Grayer et al., Proceedings of the 3rd International Conference on Experimental Meson Spectroscopy, Philadelphia (1972) and CERN preprint (1973).
90. R.L. Anderson et al., SLAC-Pub 925 (1971).
91. Abrams et al., BNL 14046 preprint (1969).
92. W. Michael and G. Gidal, LBL-744 preprint (1972).
93. B. Haber et al., Contribution to the 1973 APS Meeting, Berkeley
94. D. Crennel et al., Phys. Rev. Lett. 27, 1674 (1971).
95. W.T. Kaune et al., SLAC-Pub 1079 (1972).
96. R. Carnegie, et al., to be published.
97. Y. Antipov et al., IFVE 74-99 (1974).
98. C. Akerlof et al., UMHE 74-20 (1974).
99. W.T. Meyer et al., Contribution to the 1973 APS Meeting, Berkeley.
100. R. Diebold et al., Phys. Rev. Lett. 32, 904 (1974).
101. G. Ferro Fontan, CERN preprint TH 1490 (1972).

Table Captions

Table 1. Number of independent helicity amplitudes for typical processes.

Table 2. Observables and measured quantities for reaction types with and without a polarized target.

Table 3. Energy dependence of forward t-channel amplitudes from total cross section data with a parametrization $\beta s^{1-\alpha}$.

Table 4. Energy dependence of forward differential cross sections parametrized with $s^{2\alpha-2}$.

Table 5. Dominant helicity couplings of mesons to baryon-antibaryon as deduced from experimental data.

Table 6. SU(3) symmetry for $VB\bar{B}$ vertices and helicity couplings.

Figure Captions

Figure 1. Recoil baryon polarization in $0^- \frac{1}{2}^+ \to 0^- \frac{1}{2}^+$ scattering with a polarized target.

Figure 2. $I_t = 0$ πN amplitudes at 6 GeV/c from Ref. 5.

Figure 3. $I_t = 0$ πN amplitudes at 6 GeV/c from Ref. 5.

Figure 4. Naturality amplitudes in $\pi N \to \rho N$ at 17.2 GeV/c from Ref. 86, using data from Ref. 89.

Figure 5. Separation of naturality in $\gamma p \to \pi^0 p$ using linearly polarized photons (Ref. 90).

Figure 6. pp elastic scattering at 6 GeV with measurements of 2 or 3 spins (Ref. 28).

Figure 7. Differences of total cross sections between $K^\pm d$ and $p^\pm d$ using data from Refs. 31, 33, 34, 35 and 91.

Figure 8. s dependence of $\frac{d\sigma}{dt}(\pi^- p \to \pi^0 n)$ at fixed t values (Ref. 36).

Figure 9. ρ Regge trajectory from data on $\frac{d\sigma}{dt}(\pi^- p \to \pi^0 n)$ (Ref. 36).

Figure 10. Separation of $I_t = 0$ exchange in $\pi N \to \rho N$; data from Refs. 92, 93, 94 and 94.

Figure 11. Location of dip for nucleon exchange in $\pi^+ p \to p\pi^+$ and $\bar{p}p \to \pi^- \pi$ from Ref. 40.

Figure 12. Differential cross sections for $\pi^- p \to \rho^0 n$ with well-defined naturality in the t channel at 6 and 17.2 GeV/c (Ref. 41).

Figure 13. s dependence of the differential cross-sections for $\bar{p}p \to \pi\pi$ at fixed t (u); data from Ref. 43.

Figure 14. Differential cross sections for backward πN scattering around 6 GeV/c (from Ref. 101).

Figure 15. Cross sections for exotic quantum number exchange in $\pi^- p \to K^+\Sigma^-$ and $K^- p \to \pi^+\Sigma^-$ (Ref. 44).

Figure 16. s dependence of the differential cross section for $\bar{p}p \to K^- K^+$ at fixed t (u); data from Ref. 43.

Figure 17. s dependence of backward $K^\pm p$ differential cross sections ($u = 0$) from Ref. 43.

Figure 18. Complete angular distribution for $K^\pm p$ elastic scattering at 5 GeV (Ref. 43) and "exotic" $K^- p$ backward peak.

Figure 19. Complete angular distribution for $\bar{p}p$ elastic scattering at 5 GeV (Ref. 43) and "exotic" backward peak.

Figure 20. Energy dependence of the cross section for $\pi^- p \to \phi n$ (Ref. 48).

Figure 21. Test of SU(3) symmetry for amplitudes dominantly helicity flip (from Ref. 49).

Figure 22. Ratio of real to imaginary parts in $\pi^- p \to \pi^0 n$ at $t = 0$ as a function of beam momentum (Ref. 36).

Figure 23. Differential cross sections at $t = 0$ for $K^+ p \to K^0 n$ and $K^- p \to \bar{K}^0 n$ and contributions of the imaginary parts obtained from total cross section data.

Figure 24. $\rho - \omega$ interference in the $\pi^+\pi^-$ mass spectrum for $\pi^- p \to \pi^+\pi^- n$ (σ^-) and $\pi^+ n \to \pi^-\pi^+ p$ (σ^+); data from Ref. 54.

Figure 25. Phase differences between ρ and ω production amplitudes in $\pi N \to (\rho,\omega)N$, for different t-channel exchanges (Ref. 54).

Figure 26. Odd-crossing helicity non-flip amplitude parallel to Pomeron exchange ($\sim \mathrm{Im}\, \omega^K_{++}$) in $K^\pm p$ elastic scattering at 5 GeV (Ref. 56).

Figure 27. Impact parameter distribution of amplitude shown in Fig. 26.

Figure 28. Impact parameter profiles in $K^\pm p$ elastic scattering at 5 GeV (Ref. 56).

Figure 29. Differential cross-sections for particle and antiparticle elastic scattering at 5 GeV/c from Ref. 5.

Figure 30. Difference $\Delta(s,t)$ as defined in the text for $\pi^\pm p$, $K^\pm p$ and $p^\pm p$ elastic scattering at 3, 3.65, 5 and 6 GeV/c (Ref. 5).

Figure 31. $(F^1_{++})_\parallel$ amplitude obtained from cross-over data only and compared to result of complete amplitude analysis; data from $\pi^\pm p$ at 6 GeV (Ref. 5).

Figure 32. Difference between exponential slopes in $K^\pm p$ elastic scattering as a function of beam momentum; data from Refs. 5, 96, 97 and 98.

Figure 33. Difference of $\pi^\pm p$ polarizations at 10 GeV as a function of t (Ref. 9).

Figure 34. $(F^1_{+-})_\perp$ and $(F^0_{+-})_\perp$ obtained from polarization and cross section data only and comparison to results of full amplitude analysis.

Figure 35. Sum of $\pi^\pm p$ polarizations at 10 GeV (Ref. 9).

Figure 36. Sum and difference of $K^\pm p$ polarizations at 10 GeV (Ref. 9).

Figure 37. Sum and difference of $K^\pm p$ polarizations at 14 GeV (Ref. 9).

Figure 38. Even-crossing non-flip amplitudes in πN elastic scattering at 10 GeV; real and imaginary parts are separated using analyticity through dispersion relations (from Ref. 58).

Figure 39. Phases of F^0_{++} and F^1_{+-} in πN elastic scattering at 6 GeV (from Ref. 58).

Figure 40. Predicted πN charge-exchange polarization from Ref. 58.

Figure 41. Real and imaginary parts of elastic processes at $t = 0$ using derivative analyticity relations (Ref. 60).

Figure 42. Derivative analyticity relations: difference of 2 Regge poles reconstructed with first derivative only. The solid curve is the input amplitude while the dashed curve represents the reconstructed amplitude. (a) real part (b) imaginary part as a function of s (Ref. 62).

Figure 43. Same as Figure 42 for an absorbed amplitude, as a function of t.

Figure 44. Phase of $K^0_L p \to K^0_s p$ at $t = 0$. Hatched area is the result of derivative relations; data from Refs. 63 and 53.

Figure 45. Real parts of helicity non-flip amplitude in $\gamma p \to \gamma p$ scattering at 4 and 10 GeV using derivative analyticity relations and data from Refs. 64 and 65.

Figure 46. Real and imaginary parts of helcity in non-flip amplitude in $\gamma p \to \gamma p$ at 10 GeV.

Figure 47. Im A' for πN charge exchange at $t = 0$ from Ref. 68.

Figure 48. $\mathrm{Im}(\rho \pm A_2)_{++}$ from $\sigma_T(K^{\pm}N)$ data (Ref. 91).

Figure 49. πN phase shifts projected on t-channel $I_t = 0, 1$ exchanges (Ref. 72).

Figure 50. Meson spectrum and exchange degeneracy of Regge trajectories.

Figure 51. ρ and A_2 trajectories in the scattering region (Refs. 36 and 37).

Figure 52. Test of exchange degeneracy in $K^- p \to \bar{K}^0 n$ and $K^+ n \to K^0 p$ (Ref. 100).

Figure 53. Test of exchange degeneracy in $K^+ p \to K^0 \Delta^{++}$ and $K^- n \to \bar{K}^0 \Delta^-$ (Ref. 99).

Figure 54. Test of exchange degeneracy (dips) and SU(3) for processes dominated by helicity flip amplitudes.

Figure 55. Test of local duality in backward $K^- p \to \bar{K}^0 n$ scattering (Ref. 76).

Figure 56. Helicity amplitudes reconstructed from the background in $\bar{K}N$ phase shifts (Ref. 77).

Figure 57. Helicity amplitudes reconstructed from resonances in $\bar{K}N$ low energy scattering (Ref. 77).

Figure 58. Chew-Frautschi plot for N^* resonances; the number inside the circles is equal to 10 times the elasticity of each resonance.

Figure 59. Chew-Frautschi plot for Y^* resonances and peripheral curve (Ref. 80).

Figure 60. First zeroes in the decay angular distribution of Y^* resonances as contributed to helicity flip and non-flip amplitudes.

Figure 61. Impact parameter profile for the imaginary part of the helicity non-flip amplitude reconstructed from the background in $\bar{K}N$ low energy phase-shifts; the 3 plots correspond to analyses in different energy regions (Ref. 80).

Figure 62. Same as Fig. 61 for the resonant part of $\bar{K}N$ scattering.

Figure 63. Same as Fig. 61 for the sum of background and resonances in πN scattering at low energy.

Figure 64. Zeroes of helicity amplitudes in $\bar{K}N$ low energy scattering (Ref. 77).

Figure 65. (a) Impact parameter profile of $\mathrm{Im}\, F_{+-}$ from $\pi^- p \to \pi^0 n$ using experimental shrinkage; (b) same distribution for $\mathrm{Im}\, F_{++}$ assuming similar shrinkage and constant zero location.

Figure 66. Slope of Pomeron amplitude from a dual absorptive model analysis of πN elastic scattering (Ref. 82); the hatched region corresponds to the slope of K^+p elastic scattering.

Figure 67. Total cross sections and s dependence of Pomeron amplitude.

Figure 68. Dependence of Pomeron amplitude on the ratio $2f_K/f_\pi$.

Figure 69. Differential cross section for $\gamma p \to \phi p$ between 2 and 12 GeV.

Figure 70. s dependence of $\frac{d\sigma}{dt}(\gamma p \to \phi p)$ at fixed t.

Figure 71. Central and peripheral Pomeron amplitudes in $\gamma p \to \phi p$ at 12 GeV.

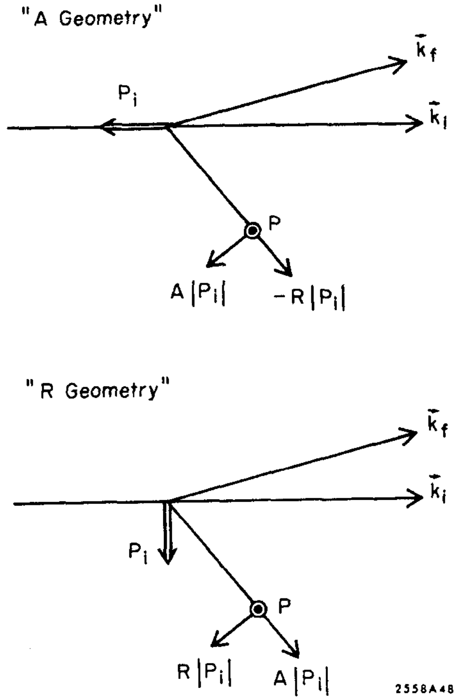

Figure 1

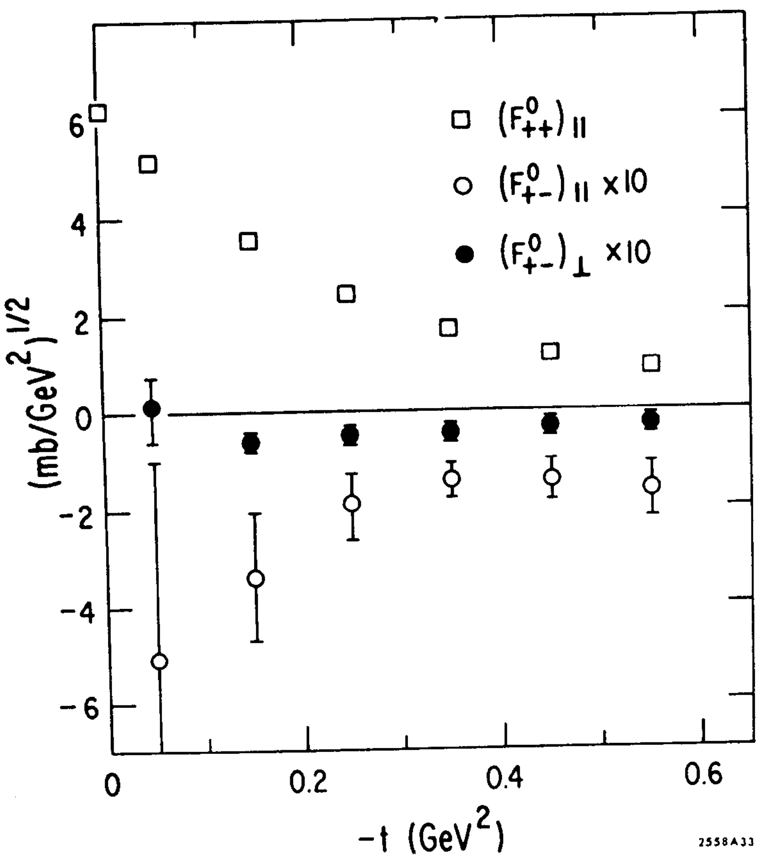

Figure 2

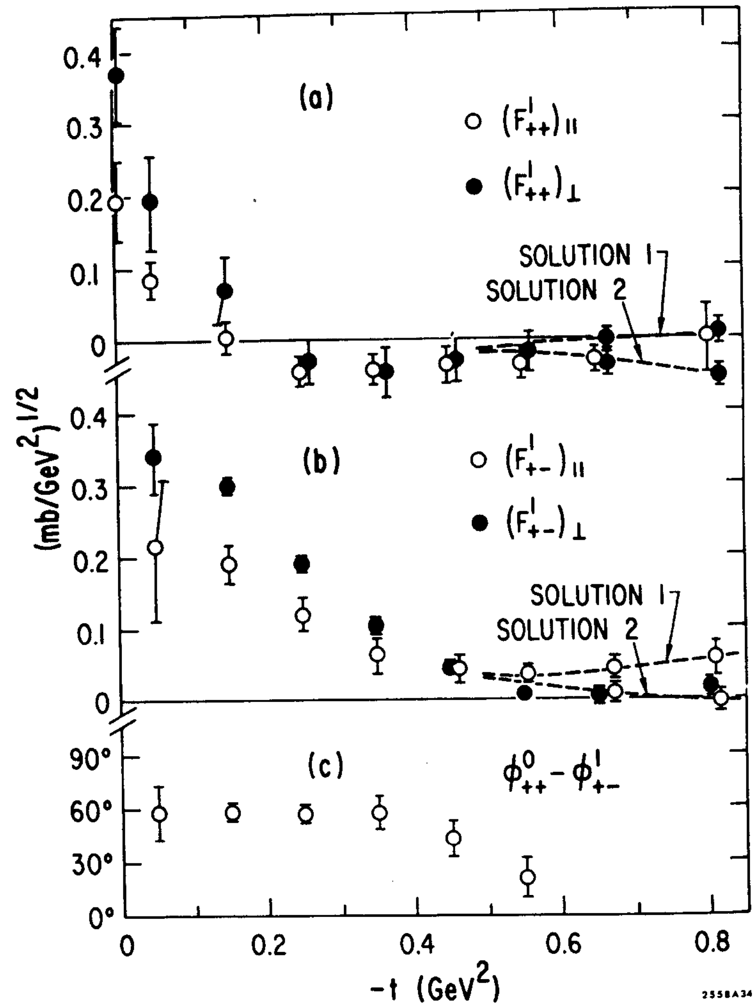

Figure 3

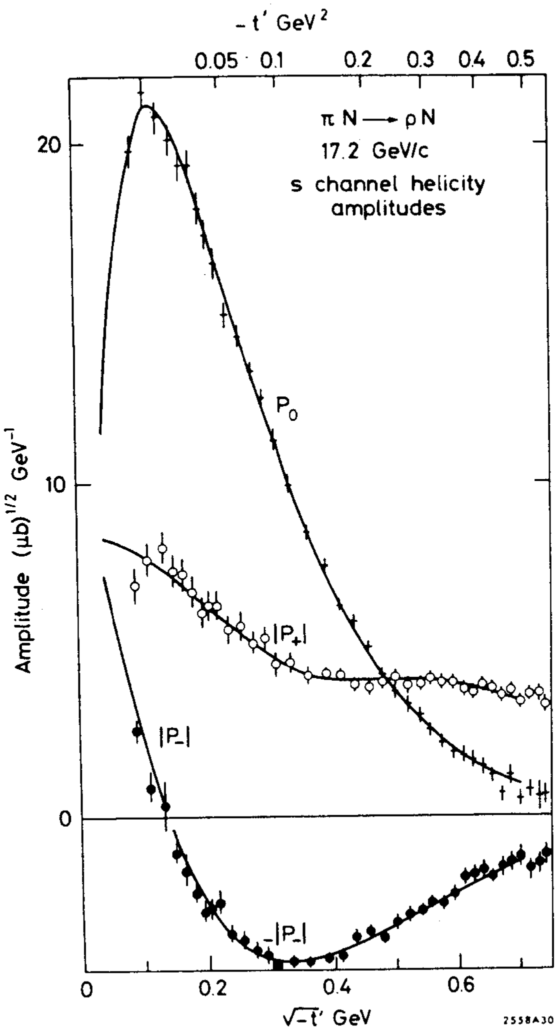

Figure 4

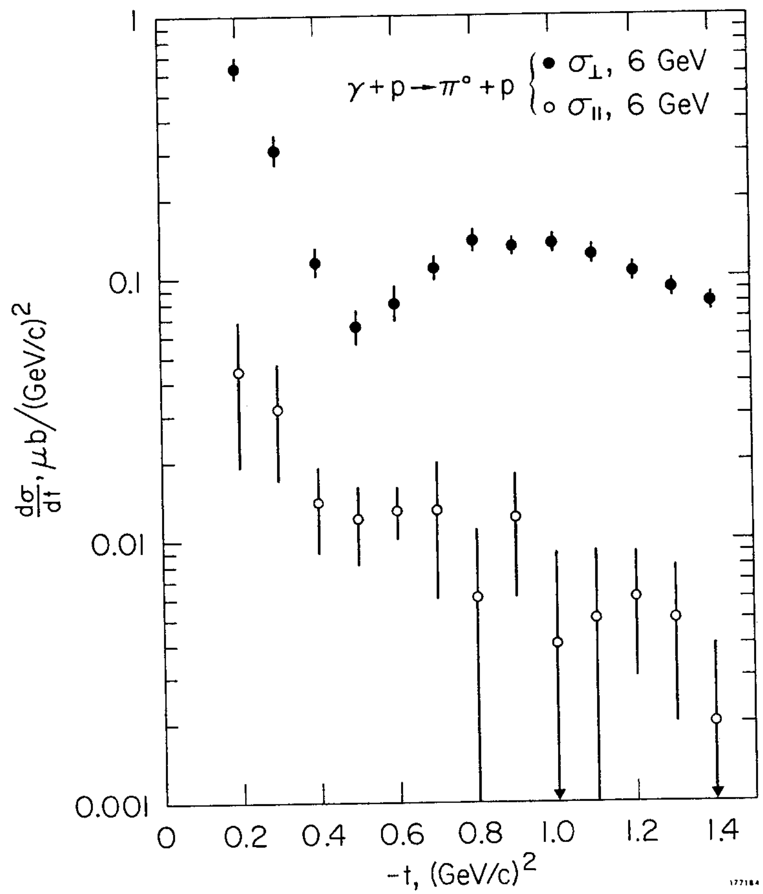

Figure 5

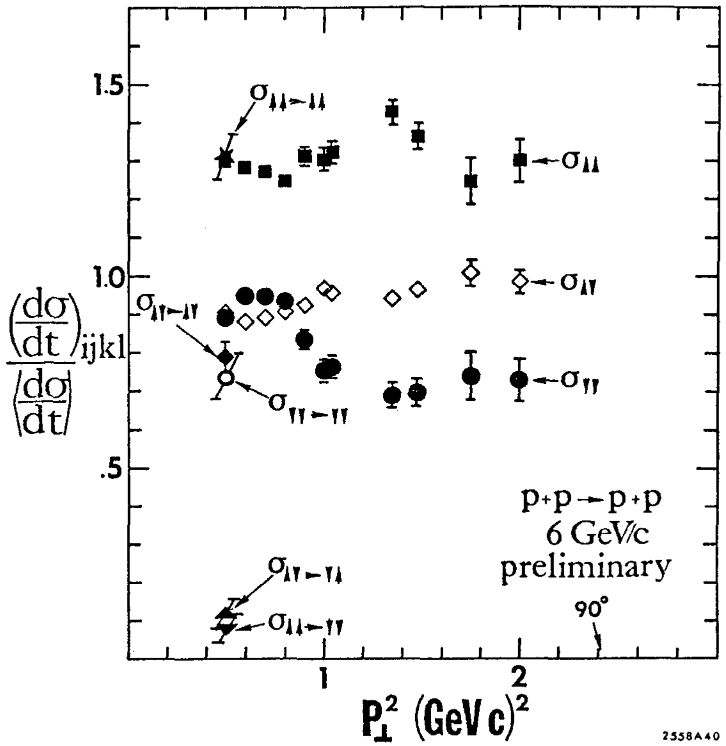

Figure 6

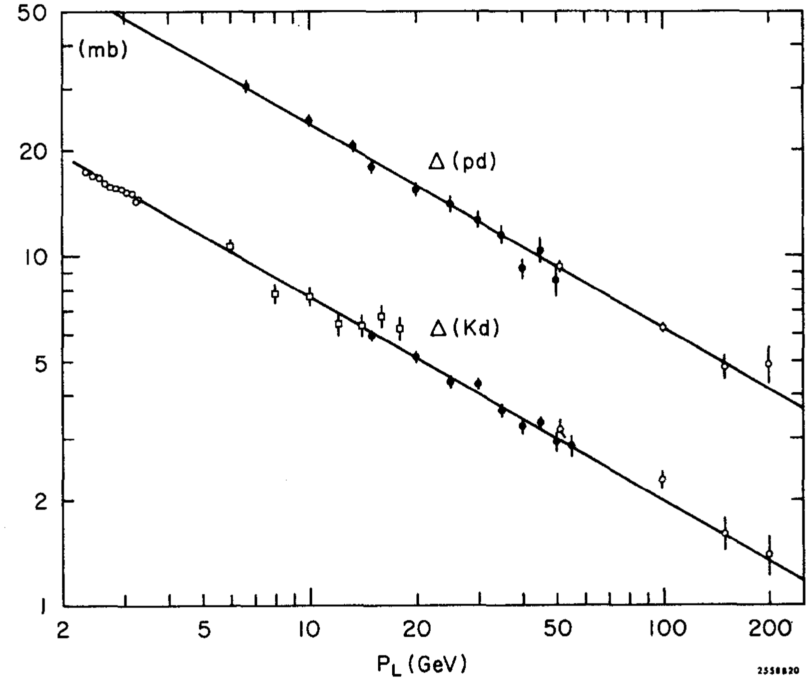

Figure 7

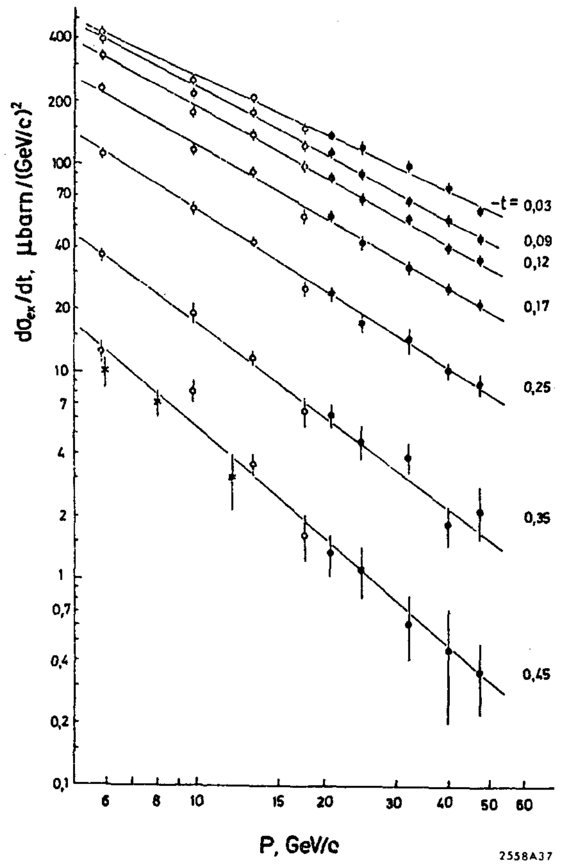

Figure 8

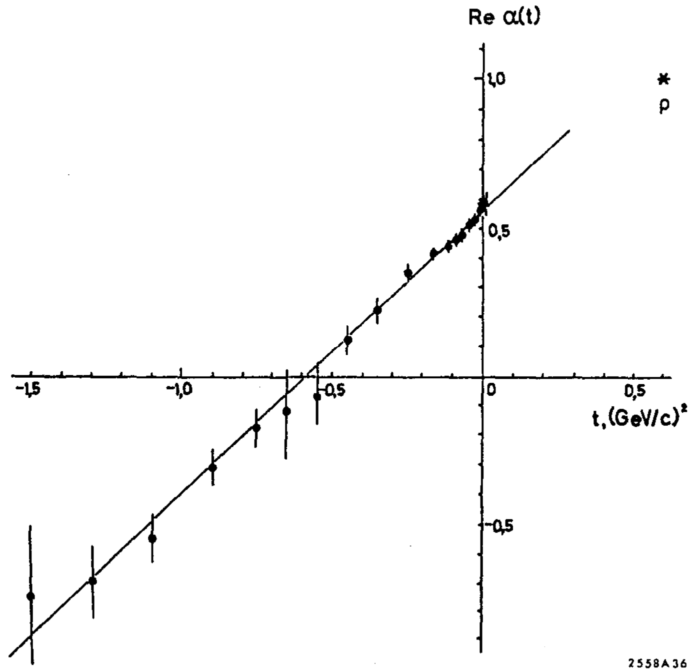

Figure 9

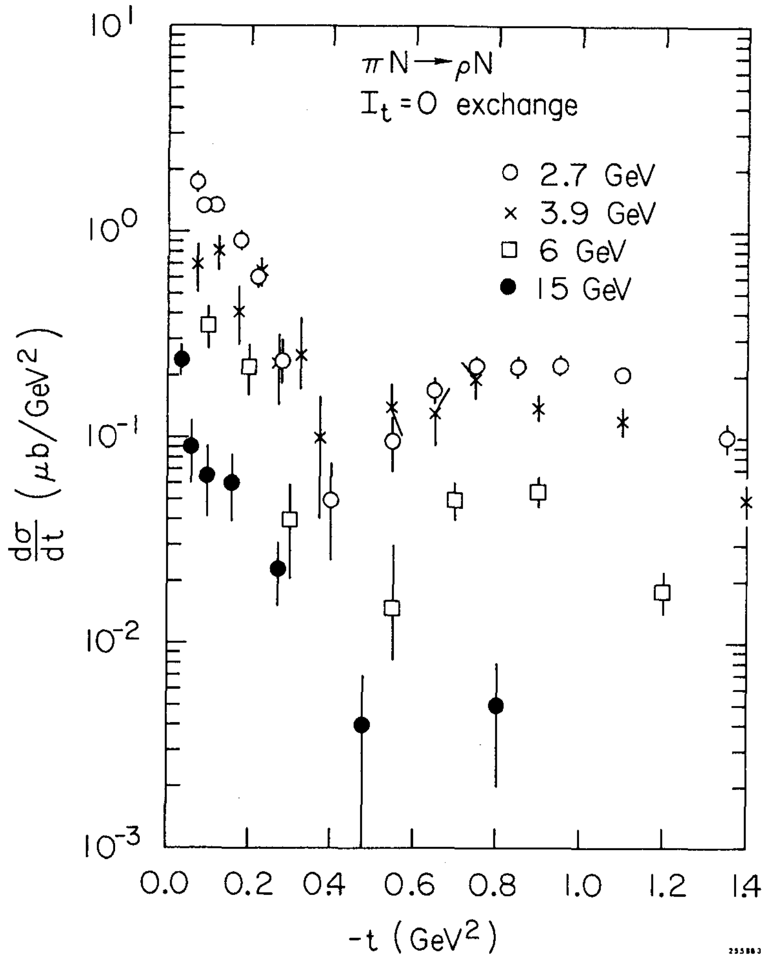

Figure 10

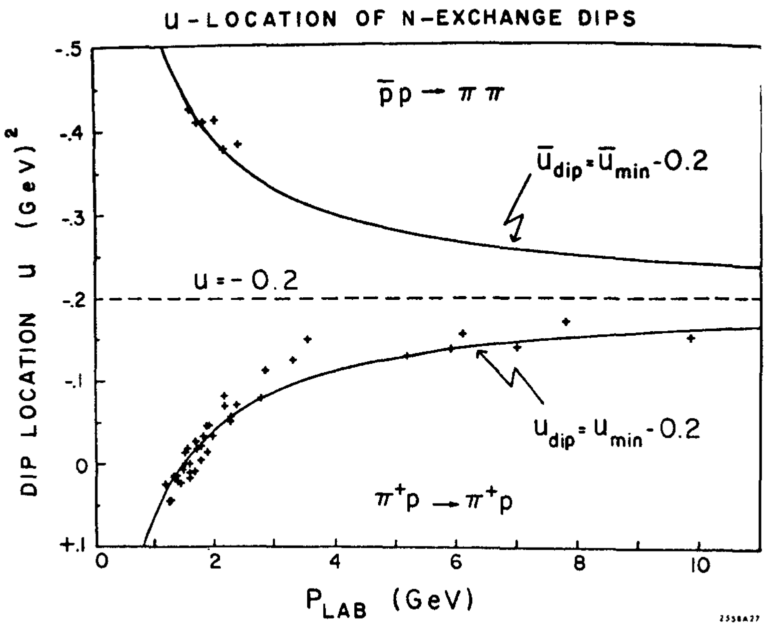

Figure 11

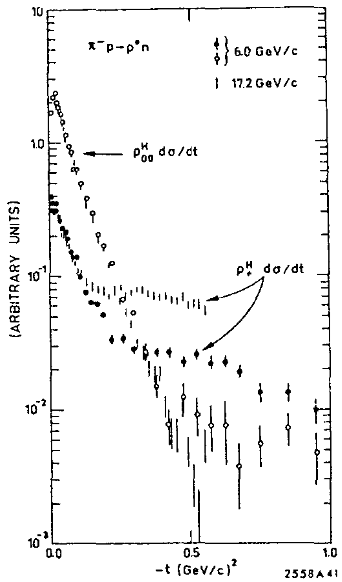

Figure 12

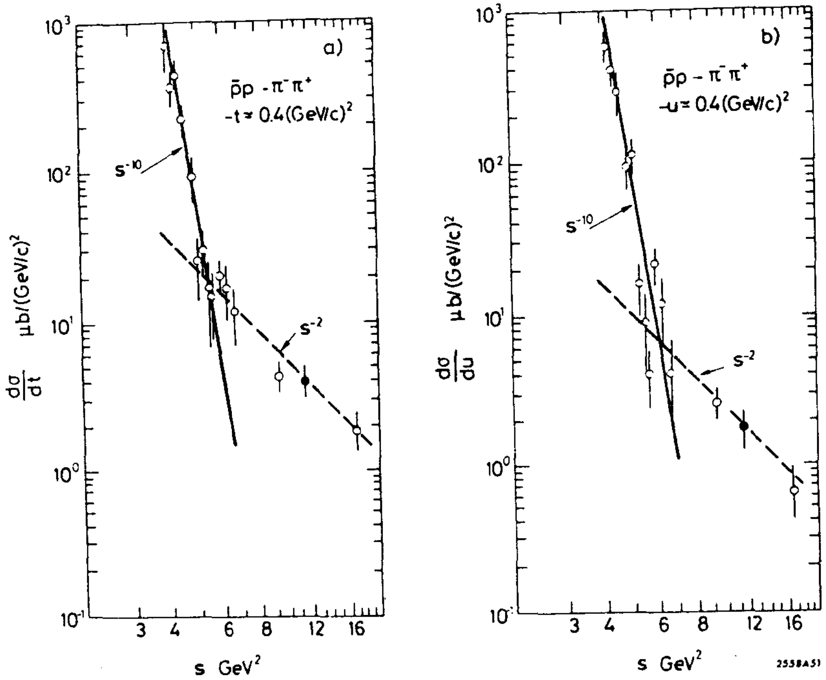

Figure 13

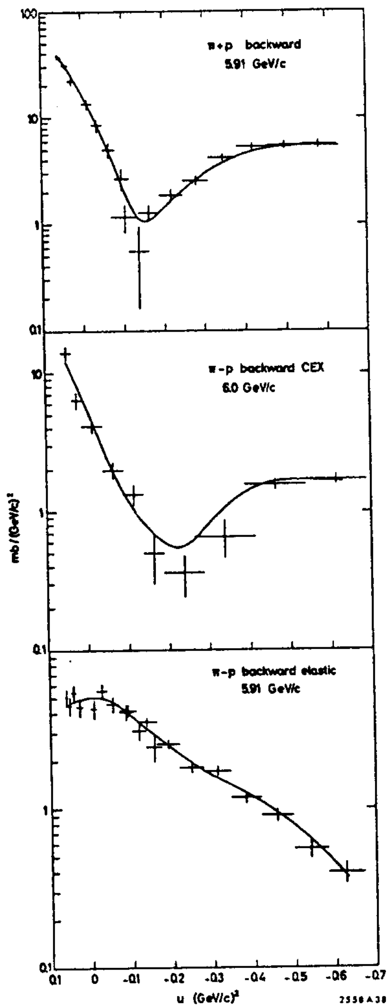

Figure 14

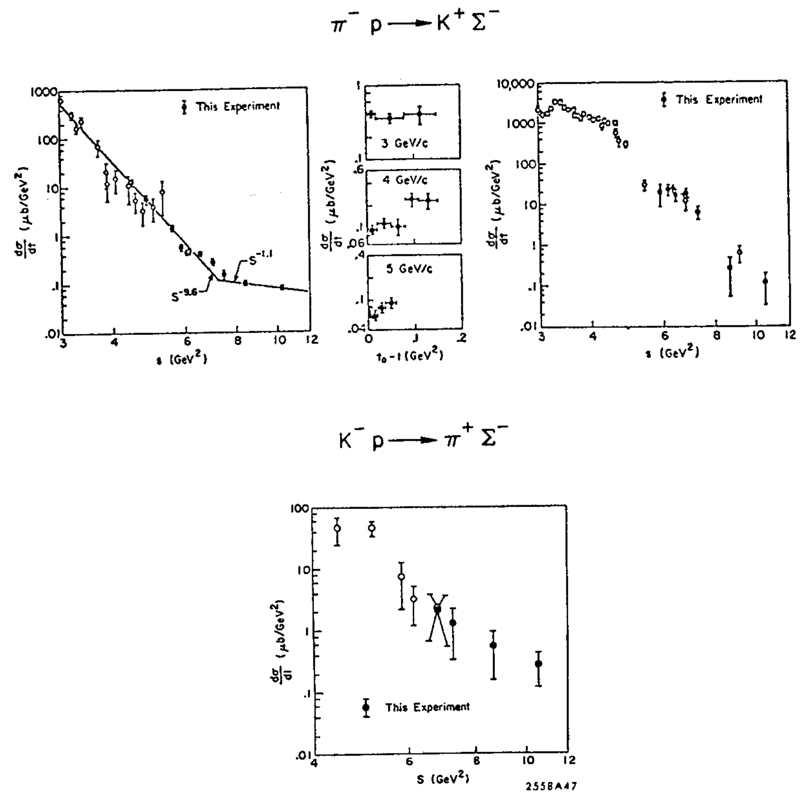

Figure 15

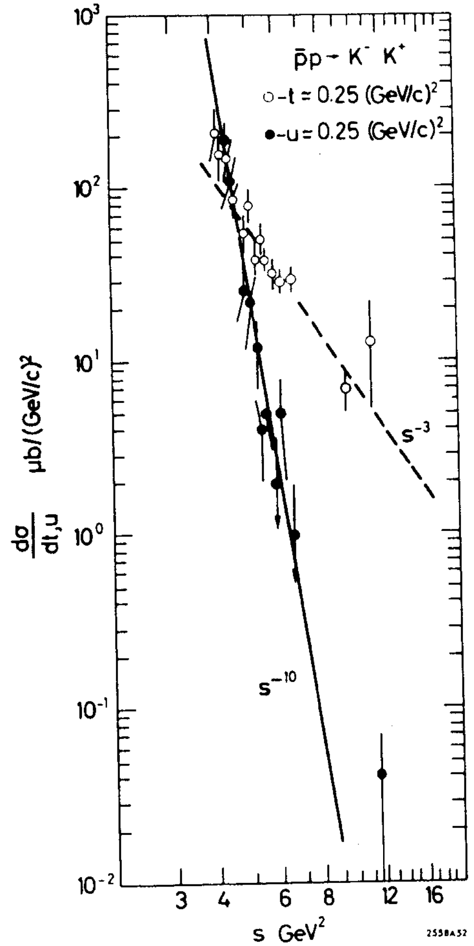

Figure 16

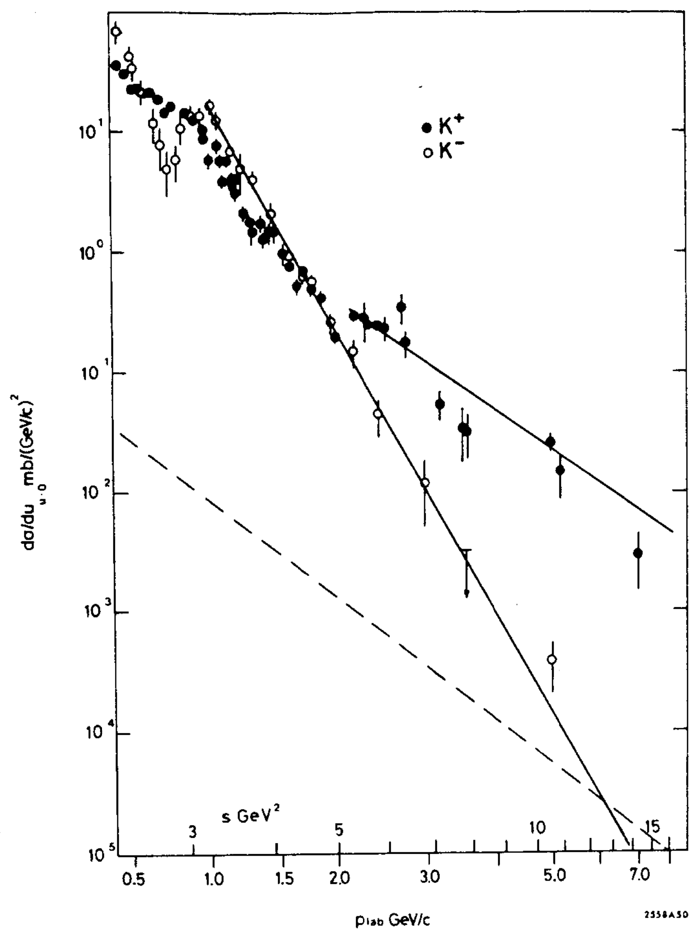

Figure 17

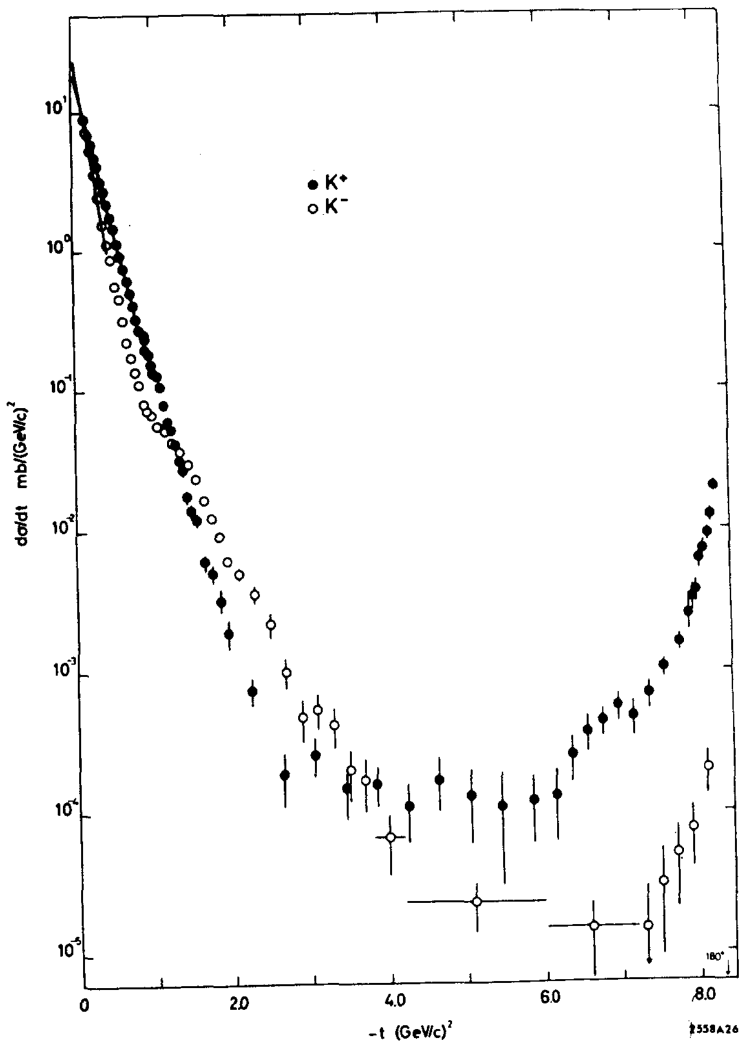

Figure 18

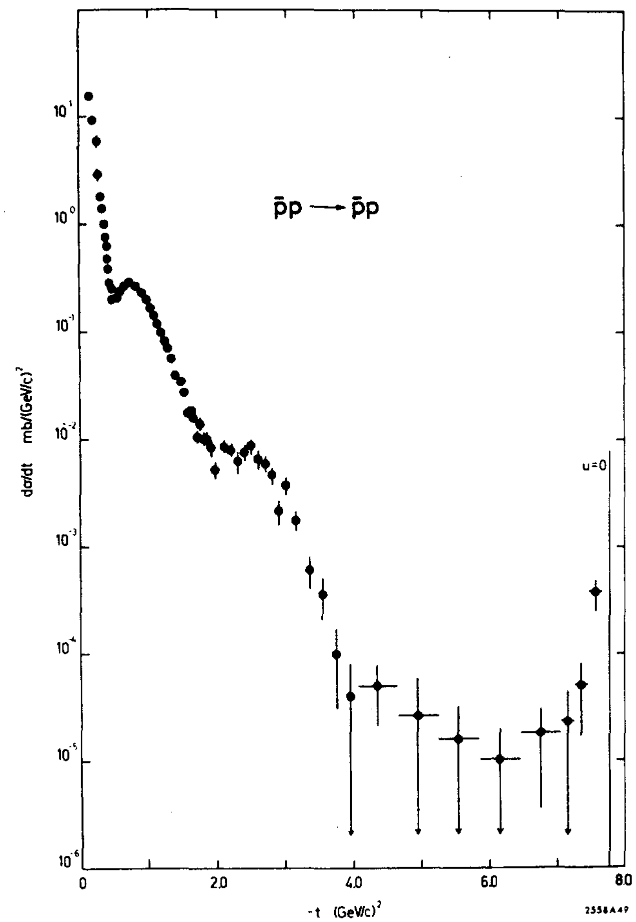

Figure 19

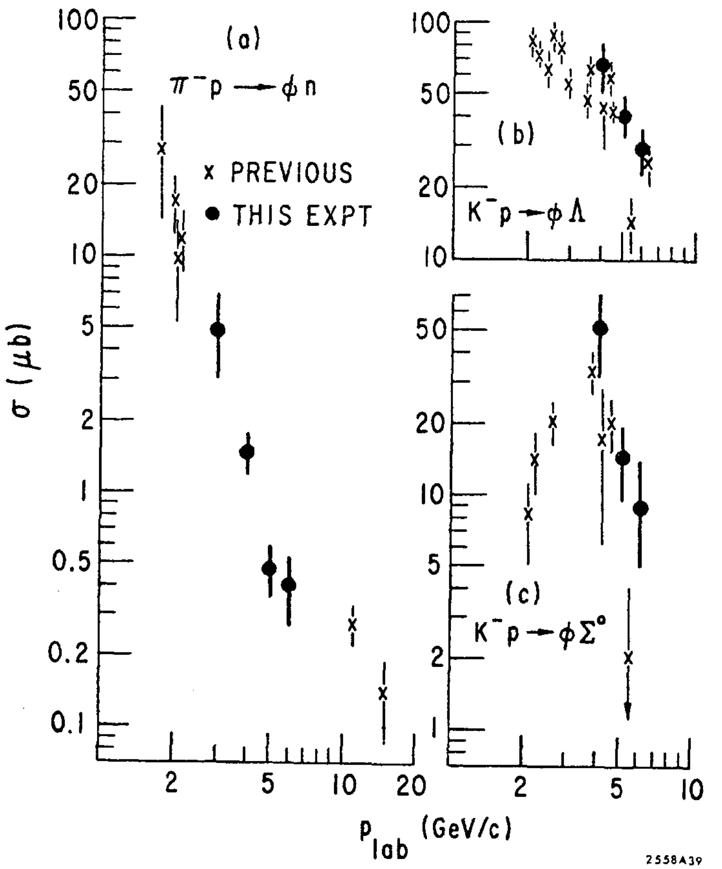

Figure 20

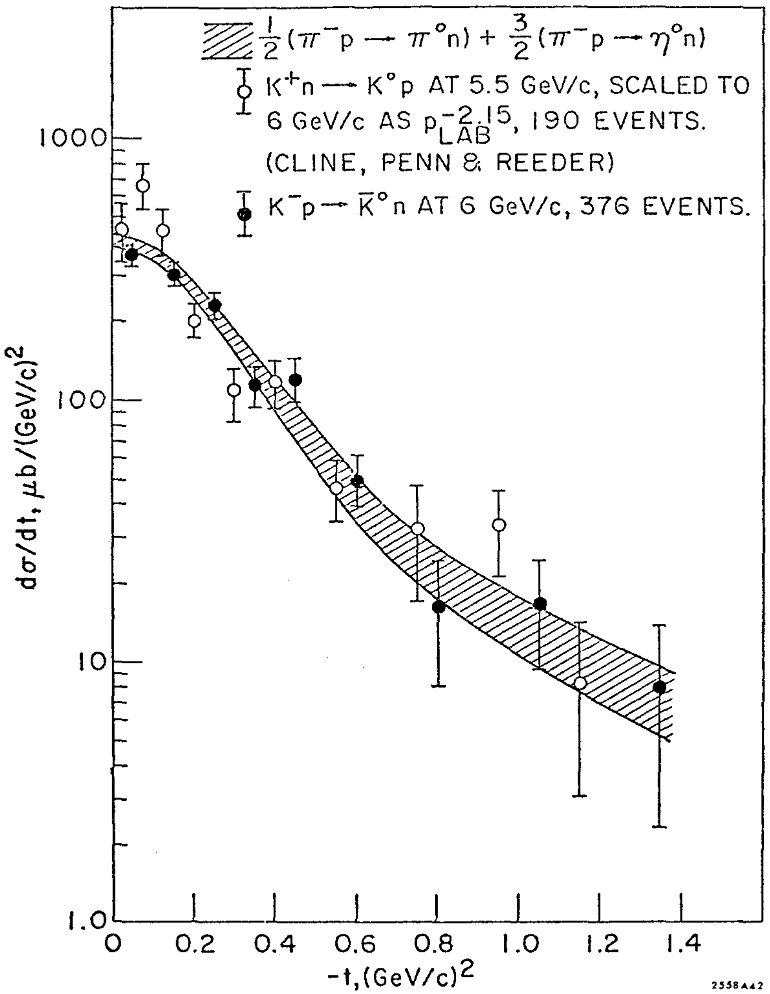

Figure 21

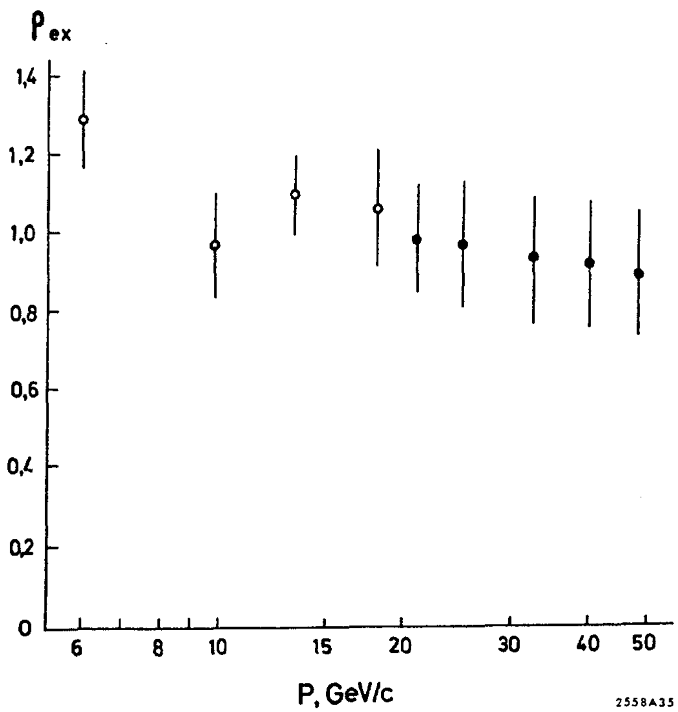

Figure 22

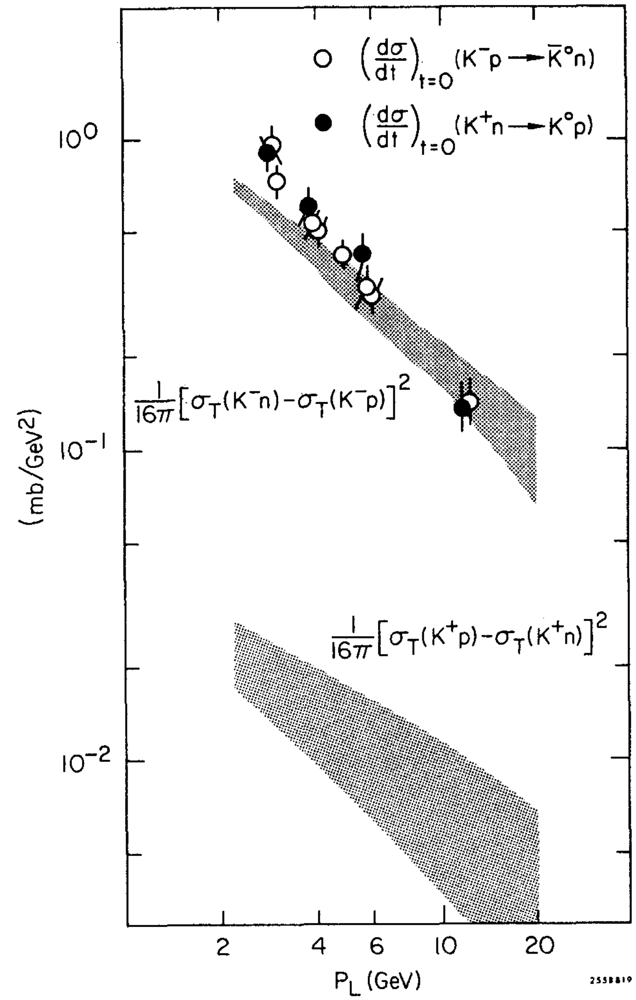

Figure 23

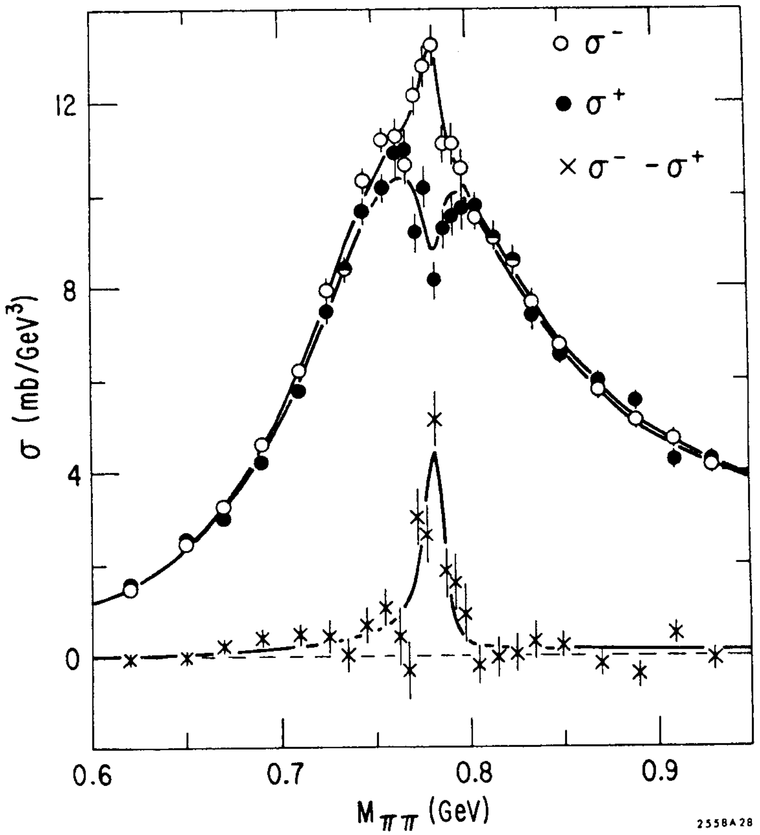

Figure 24

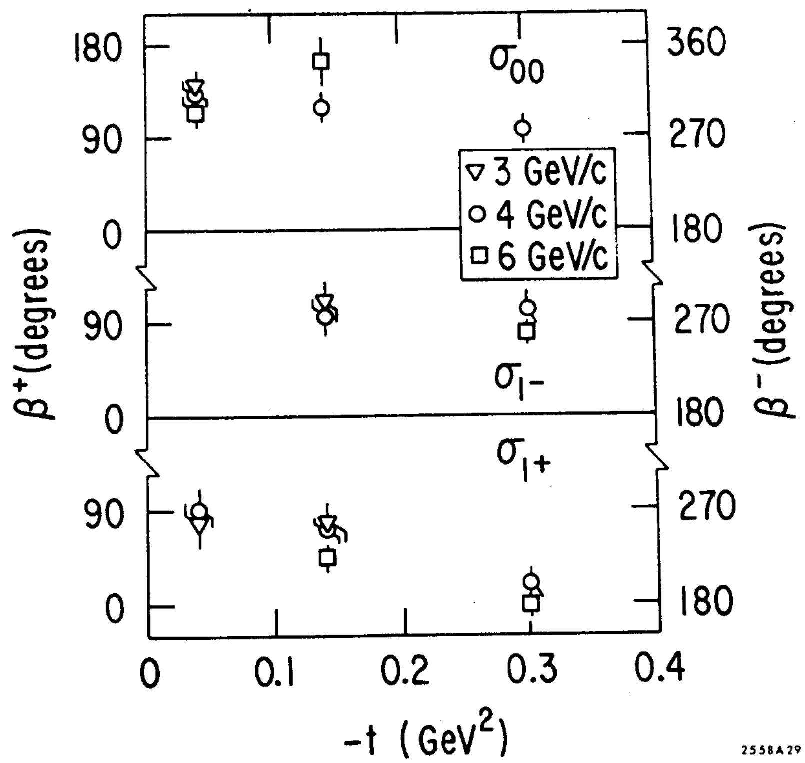

Figure 25

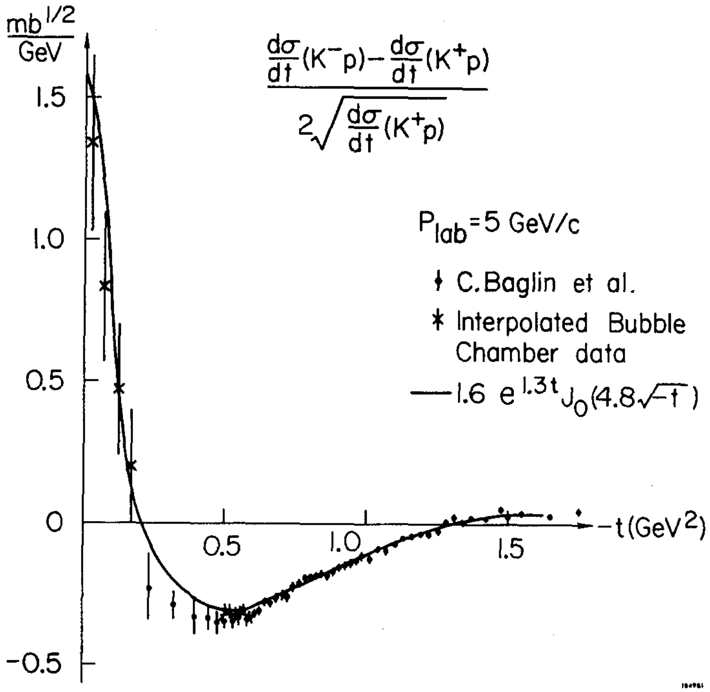

Figure 26

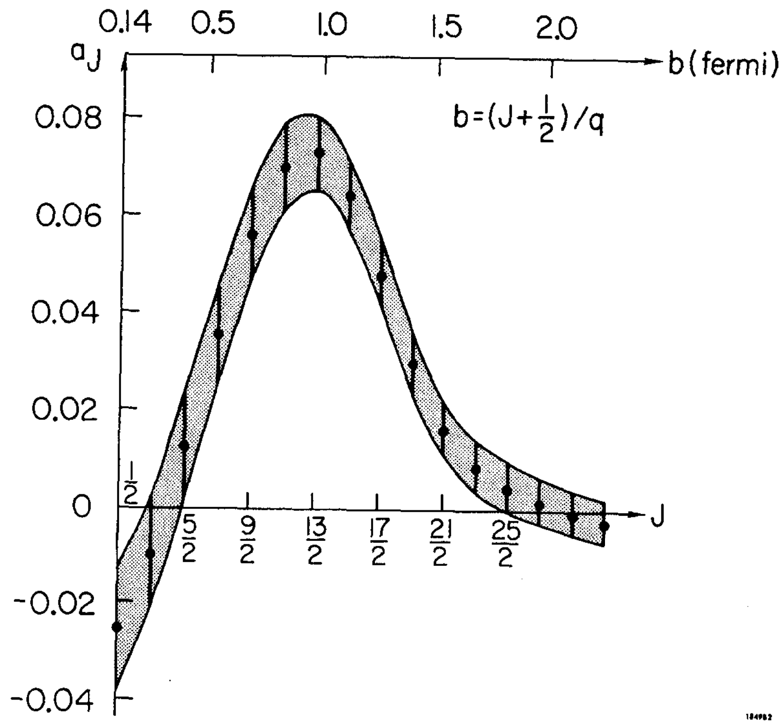

Figure 27

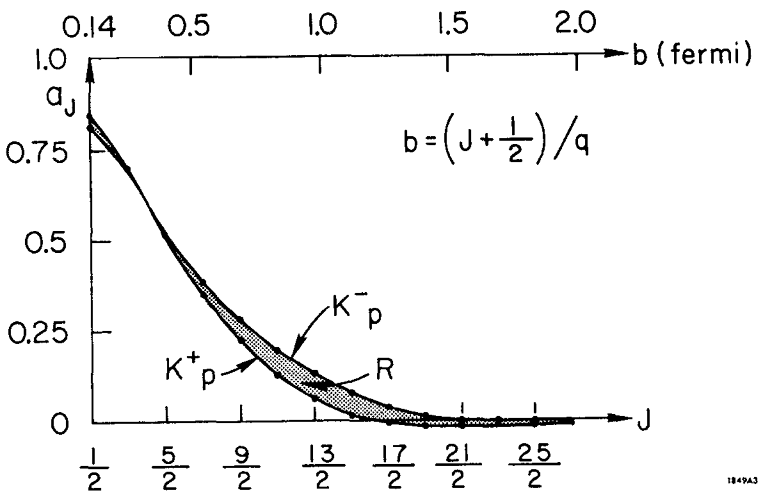

Figure 28

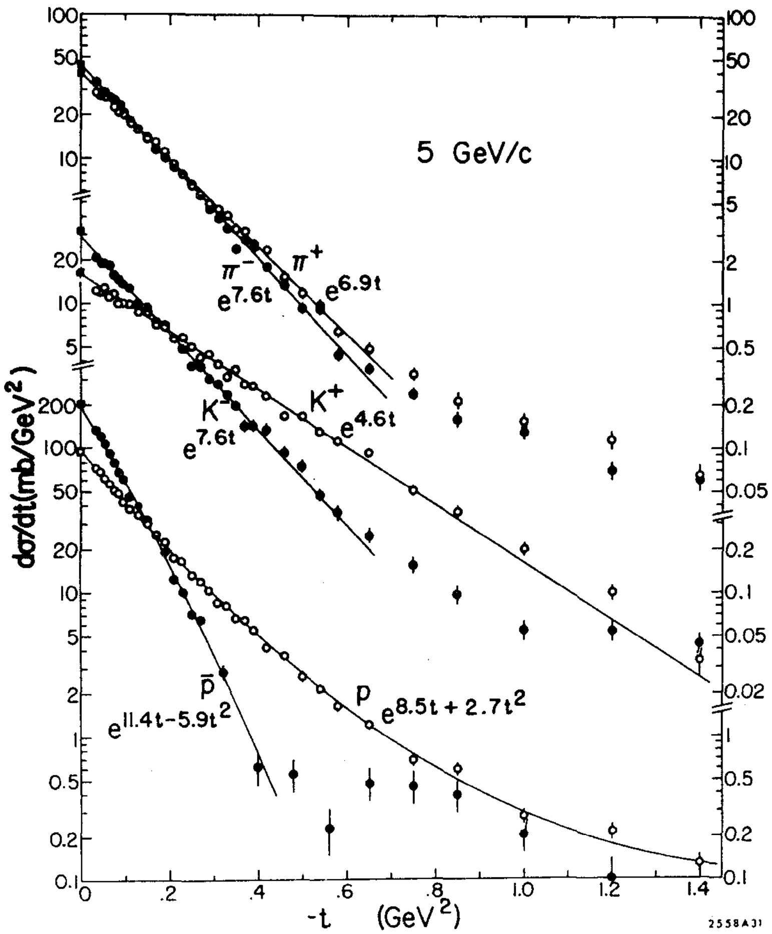

Figure 29

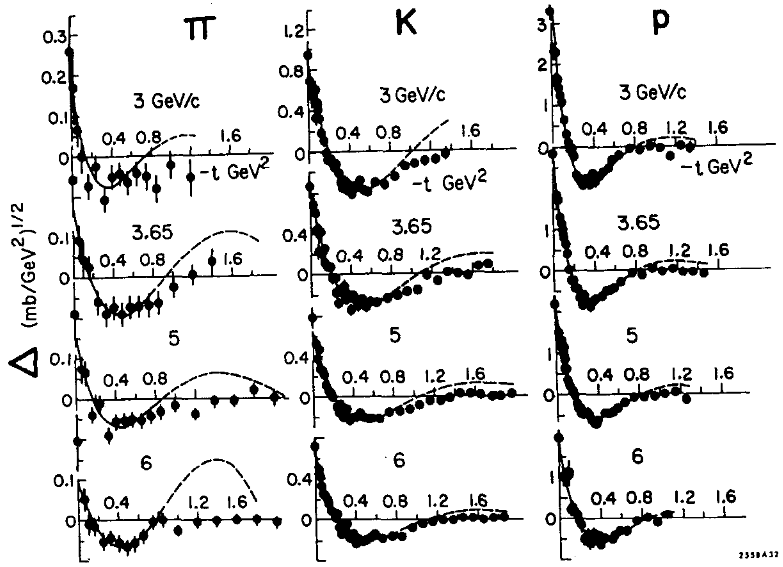

Figure 30

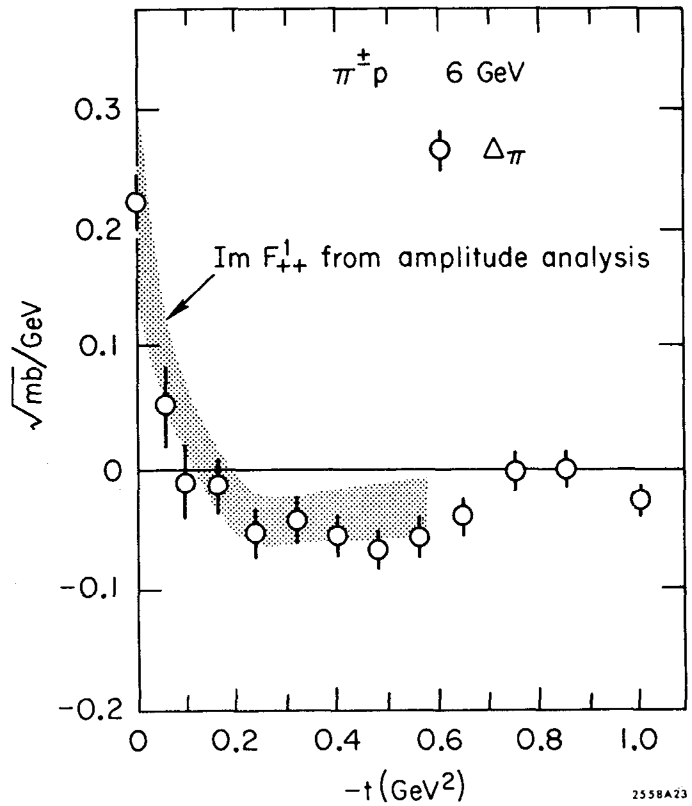

Figure 31

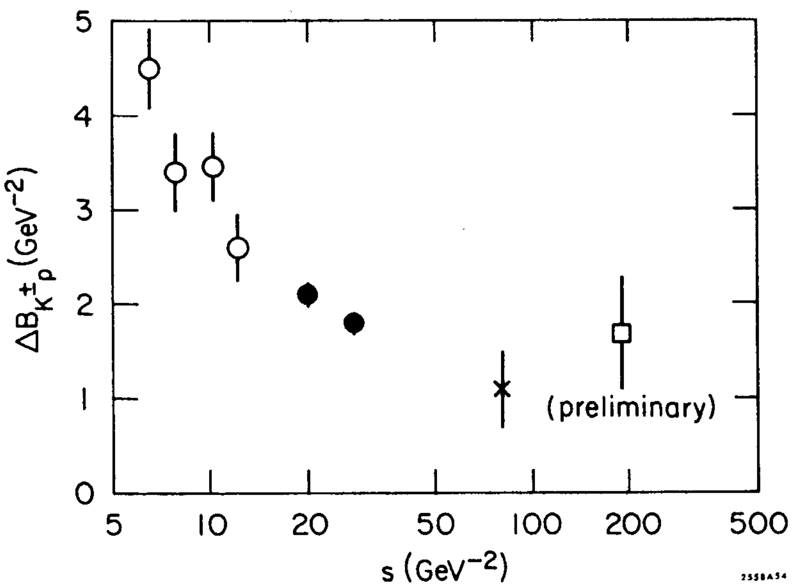

Figure 32

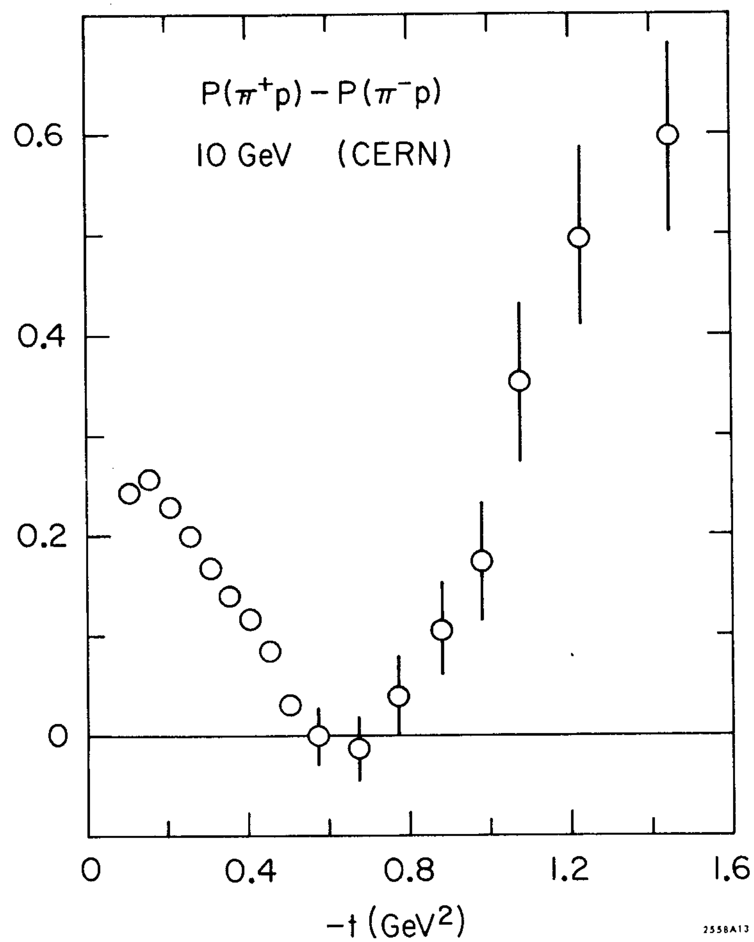

Figure 33

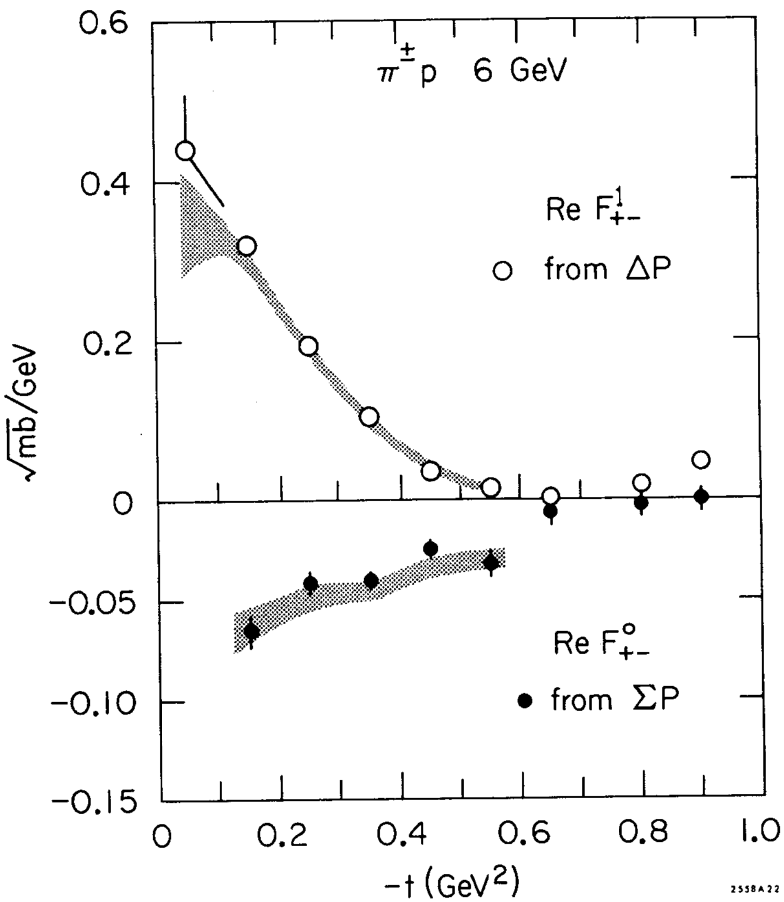

Figure 34

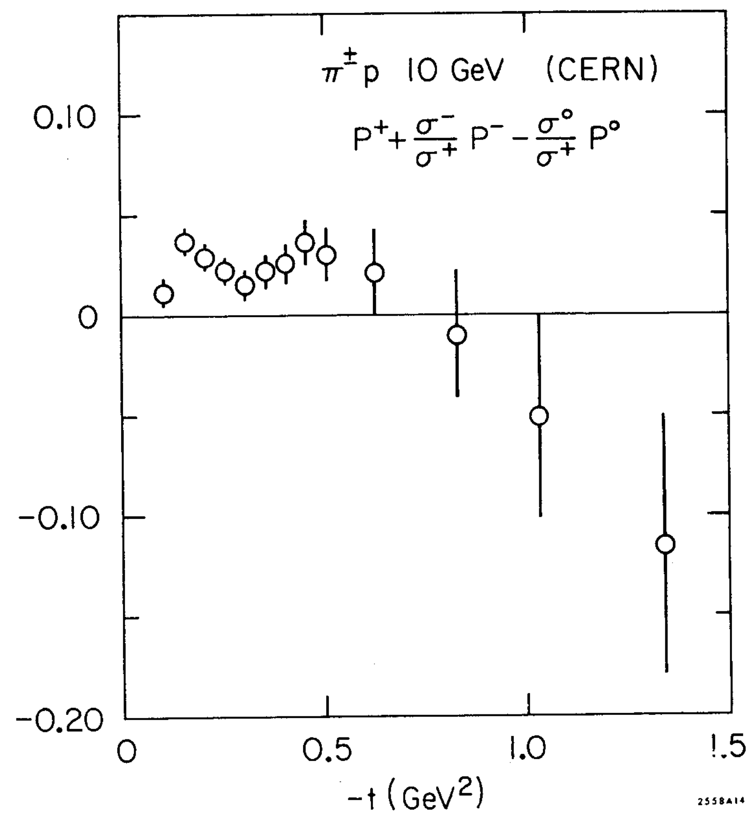

Figure 35

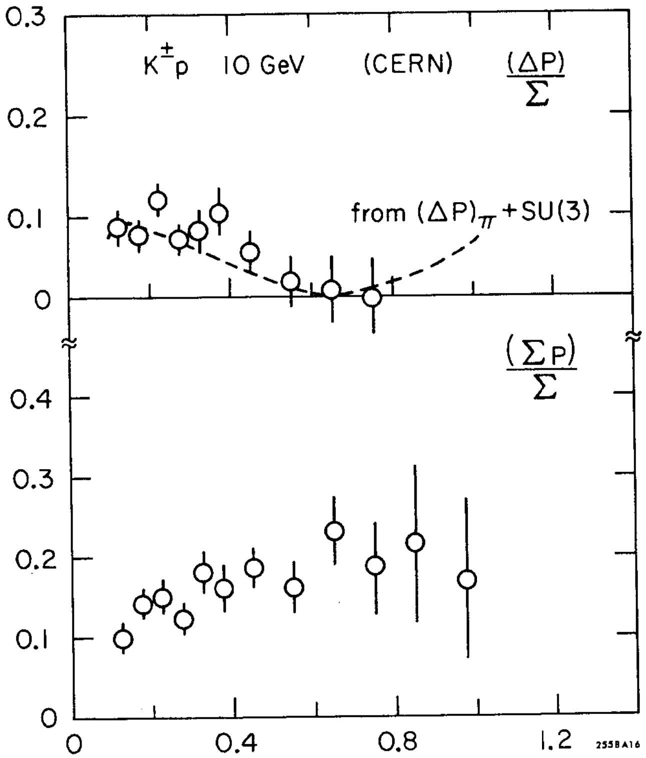

Figure 36

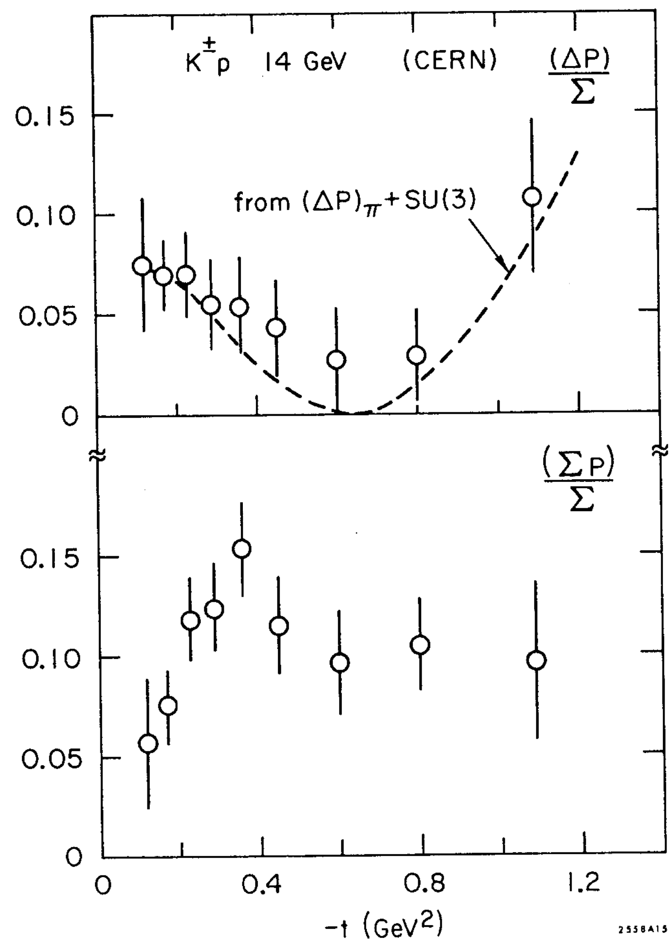

Figure 37

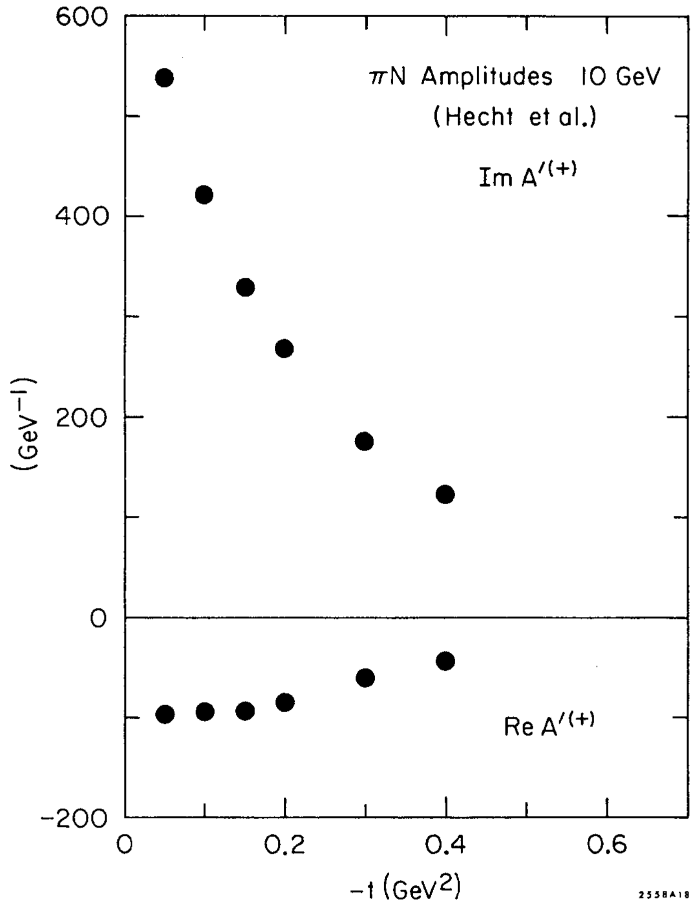

Figure 38

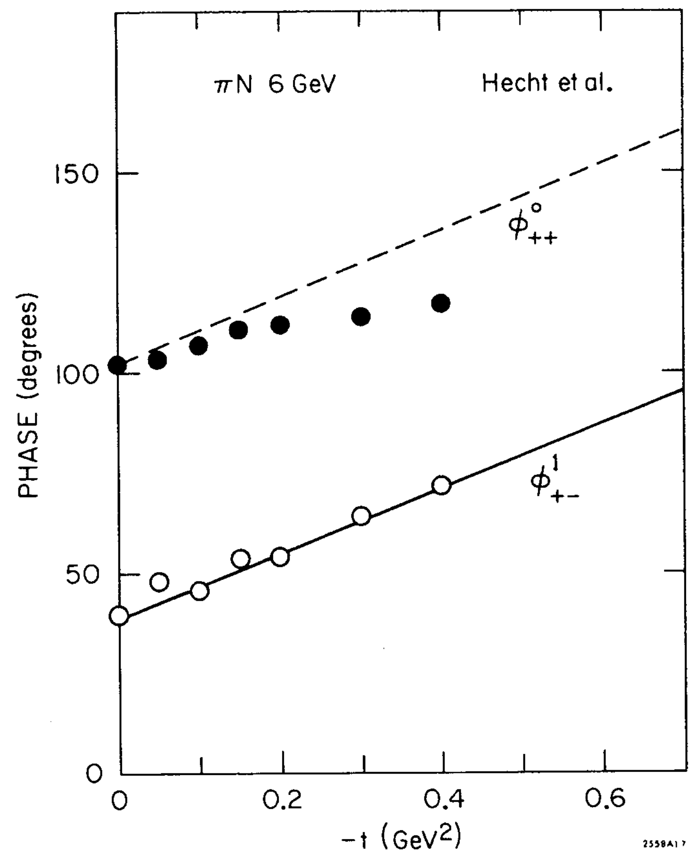

Figure 39

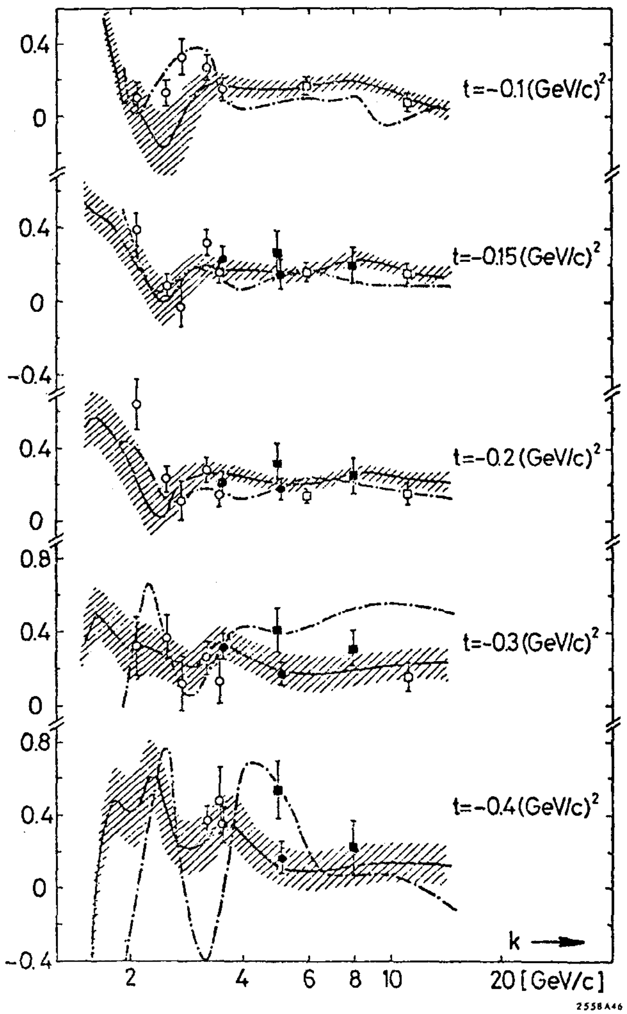

Figure 40

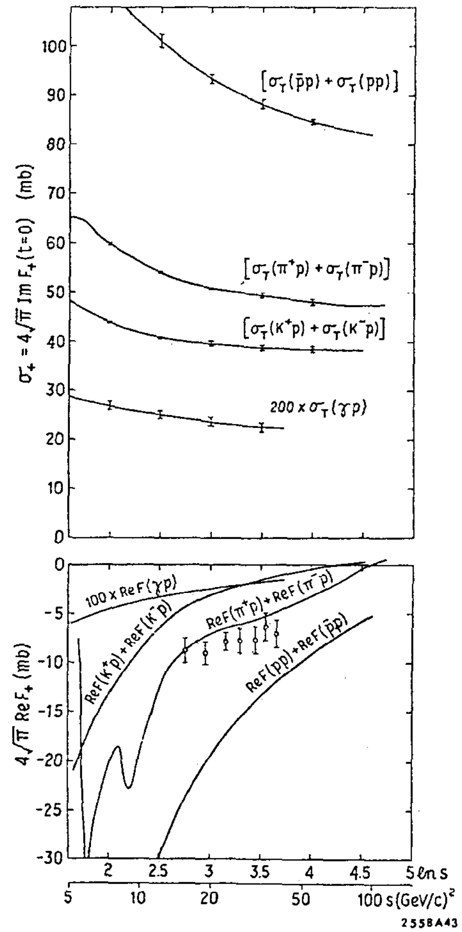

Figure 41

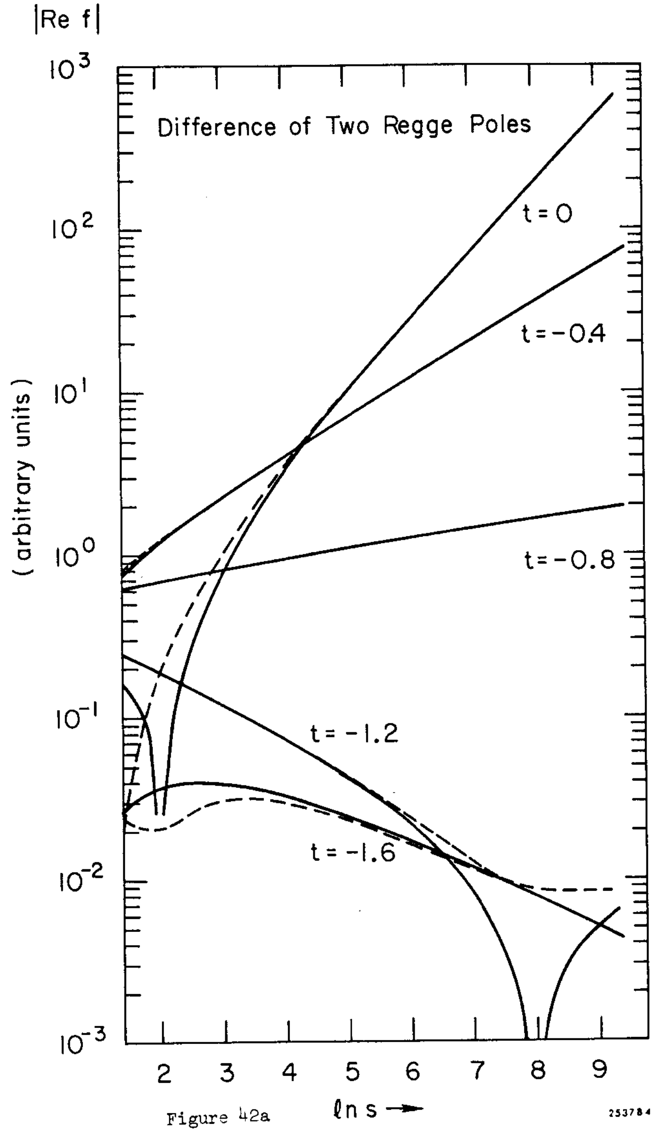

Figure 42a

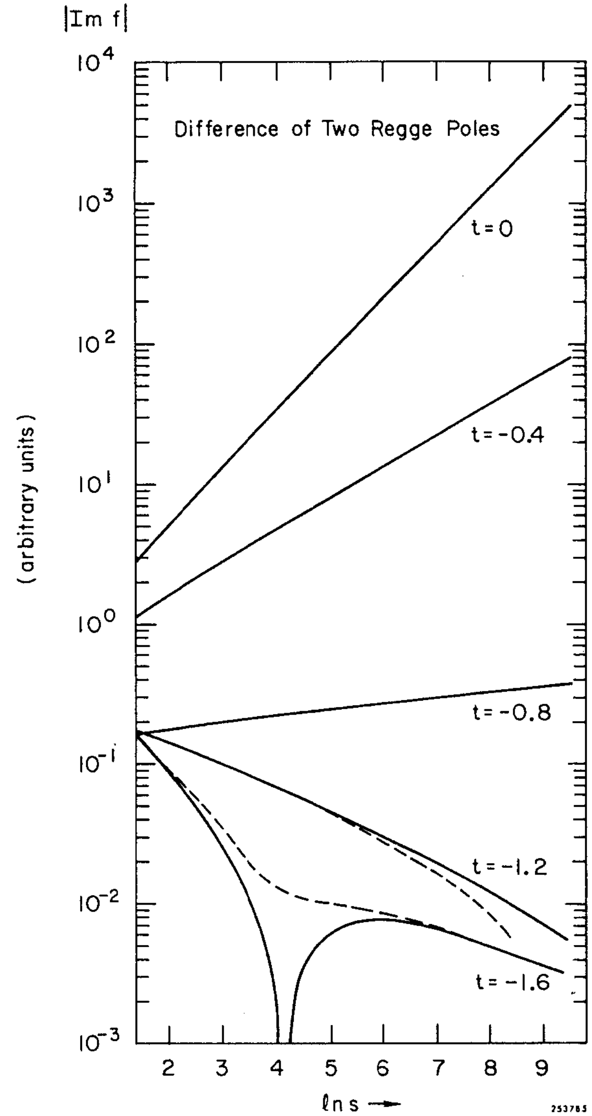

Figure 42b

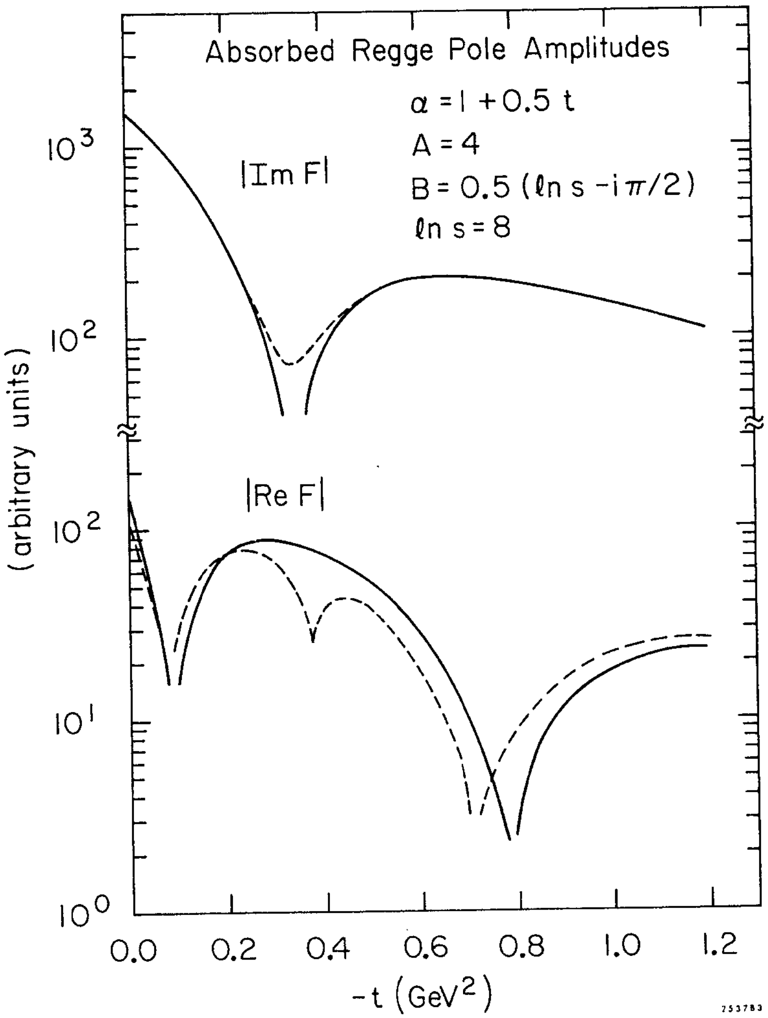

Figure 43

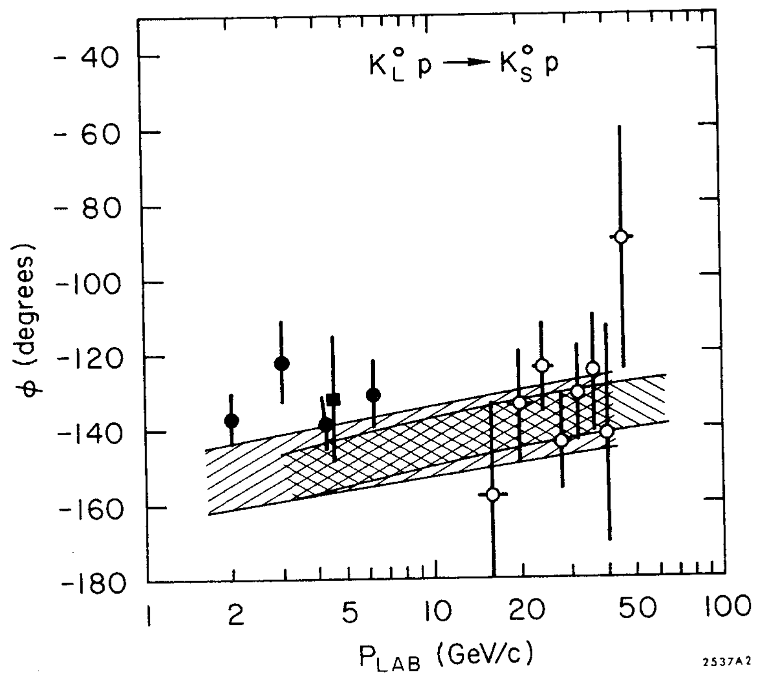

Figure 44

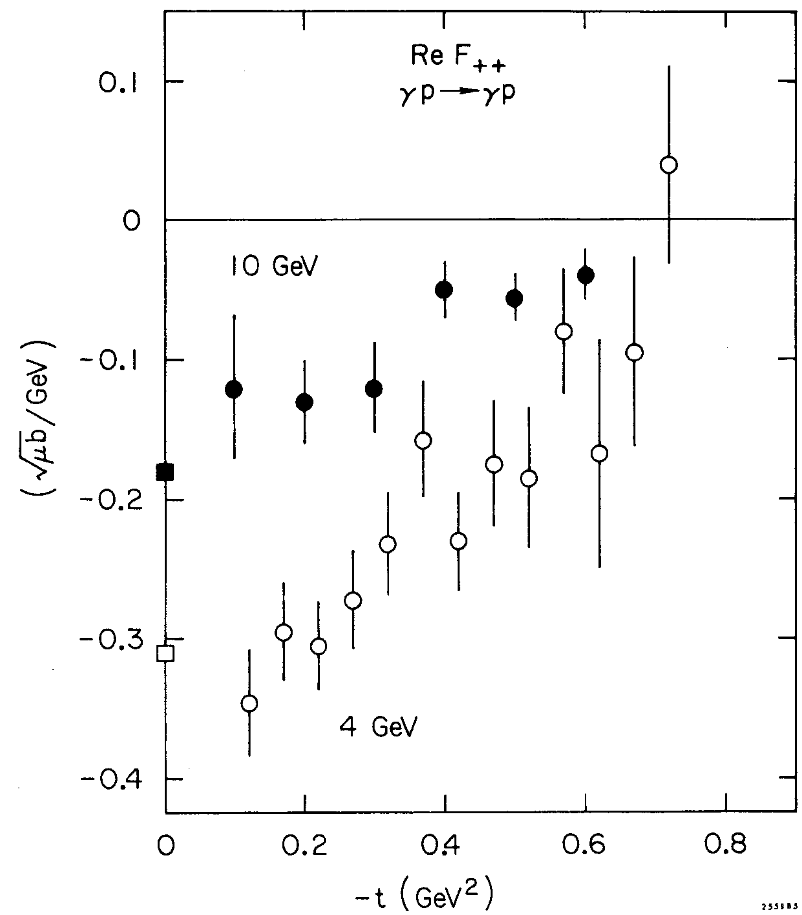

Figure 45

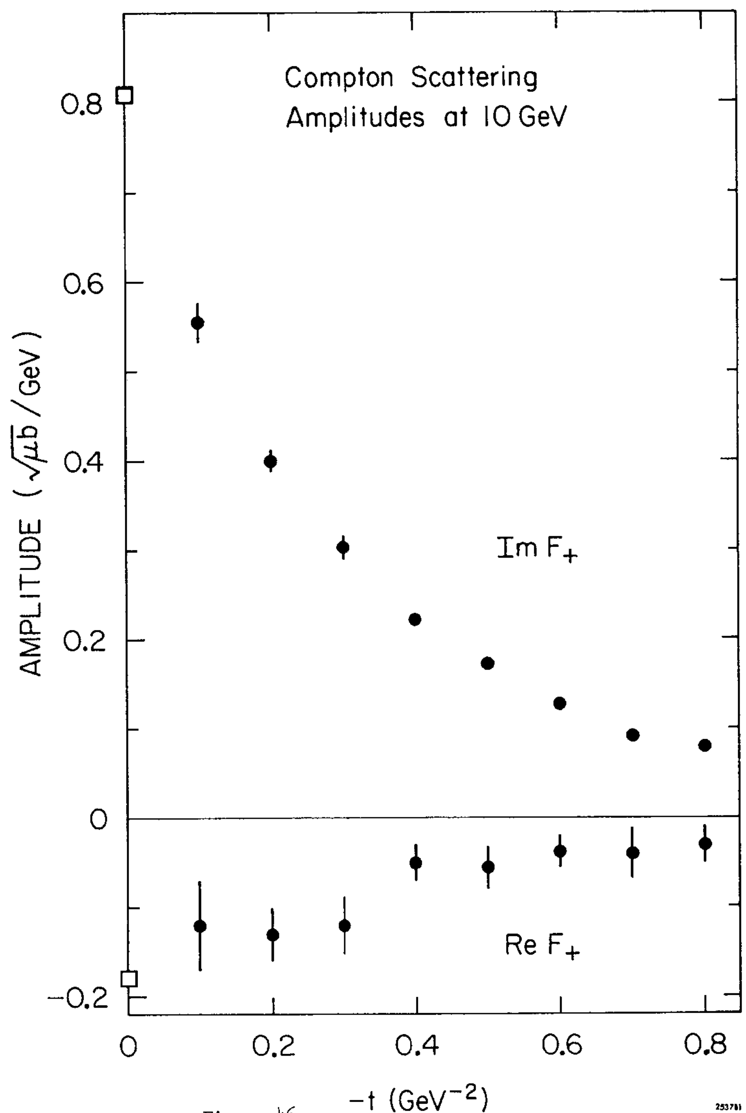

Figure 46

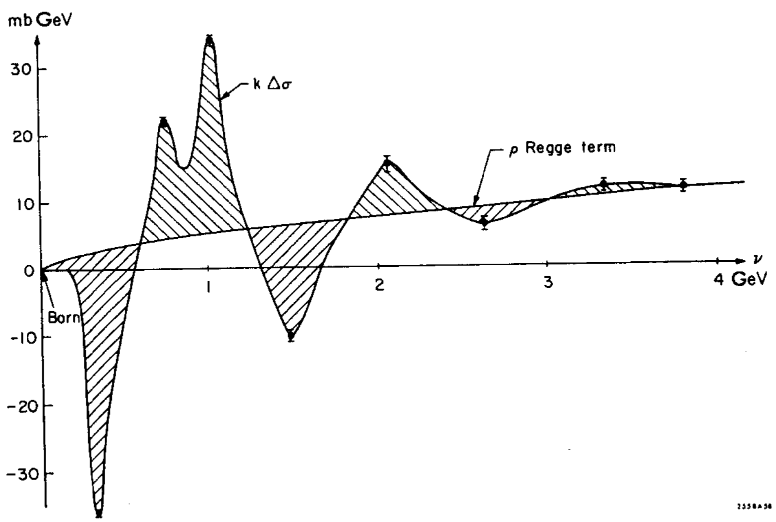

Figure 47

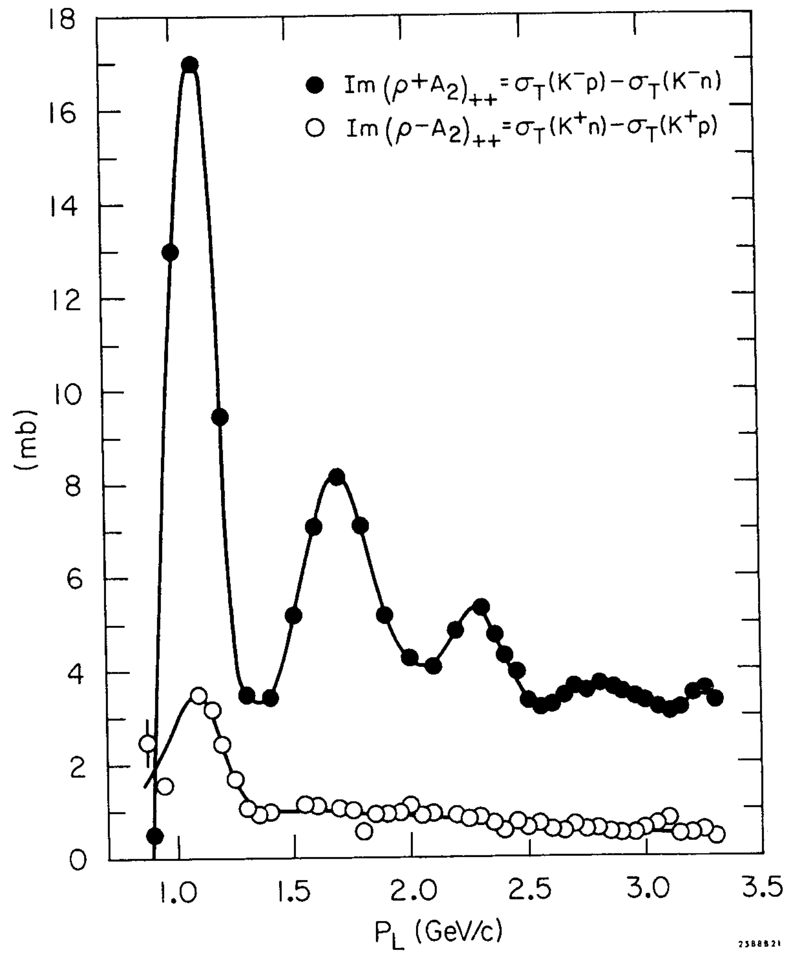

Figure 48

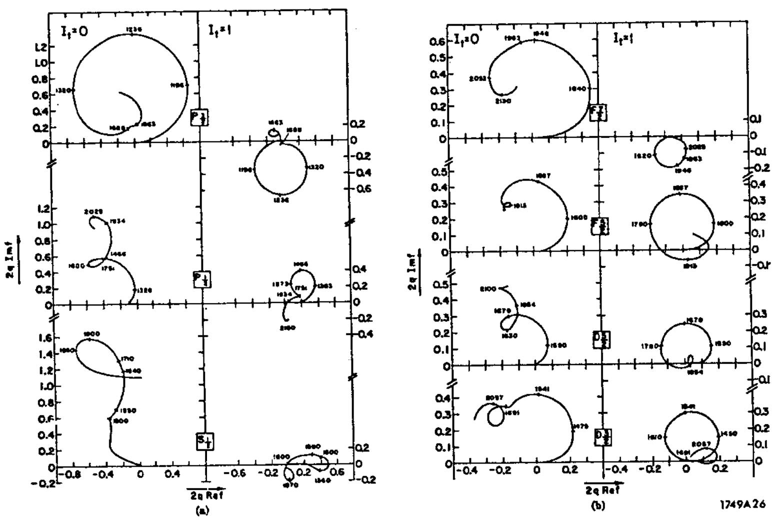

Figure 49

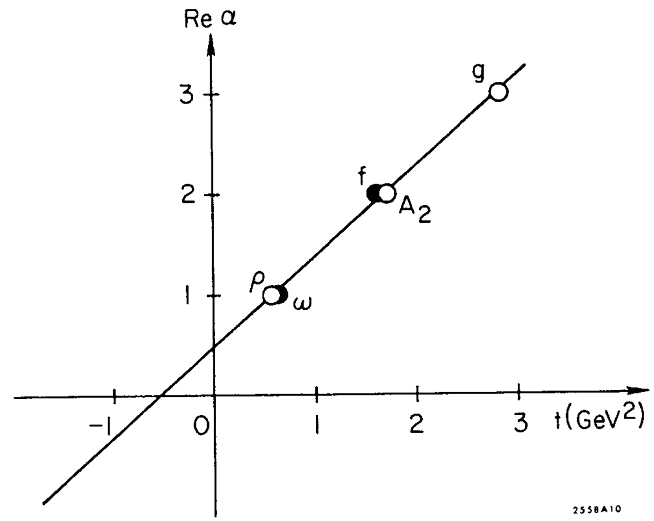

Figure 50

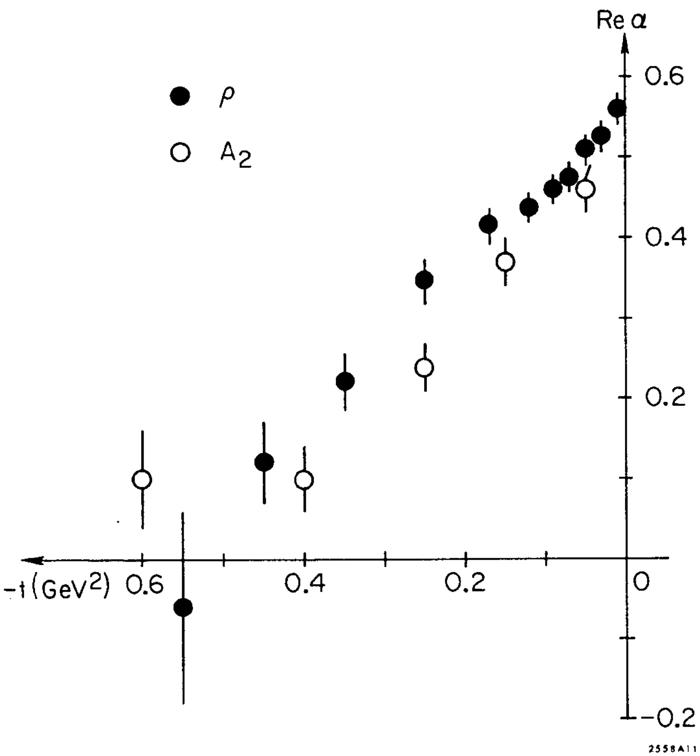

Figure 51

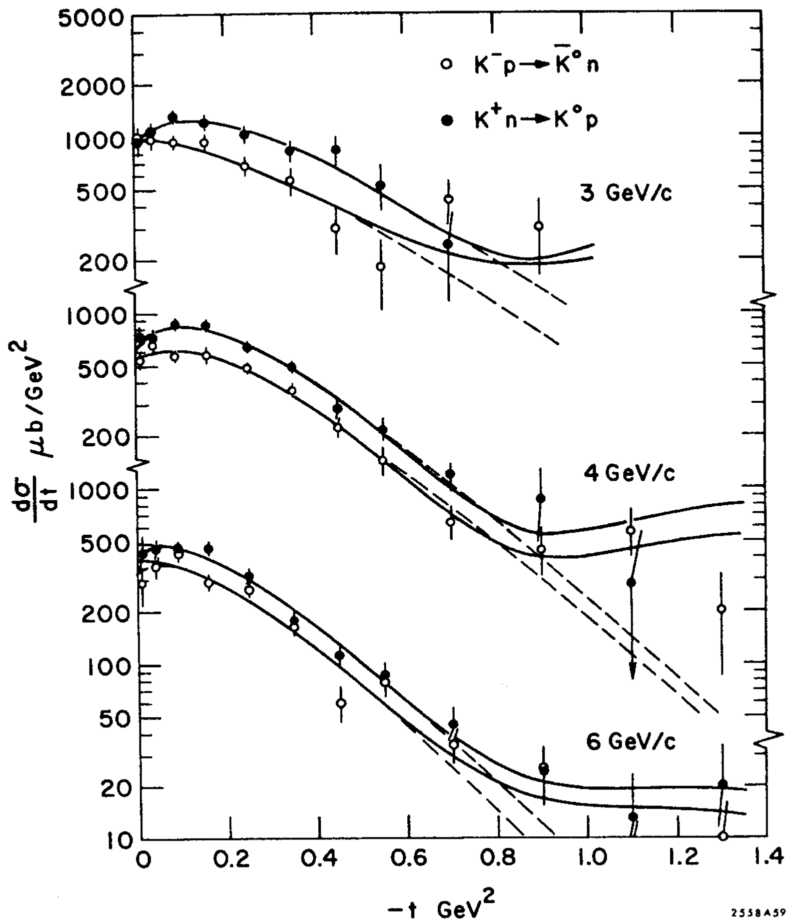

Figure 52

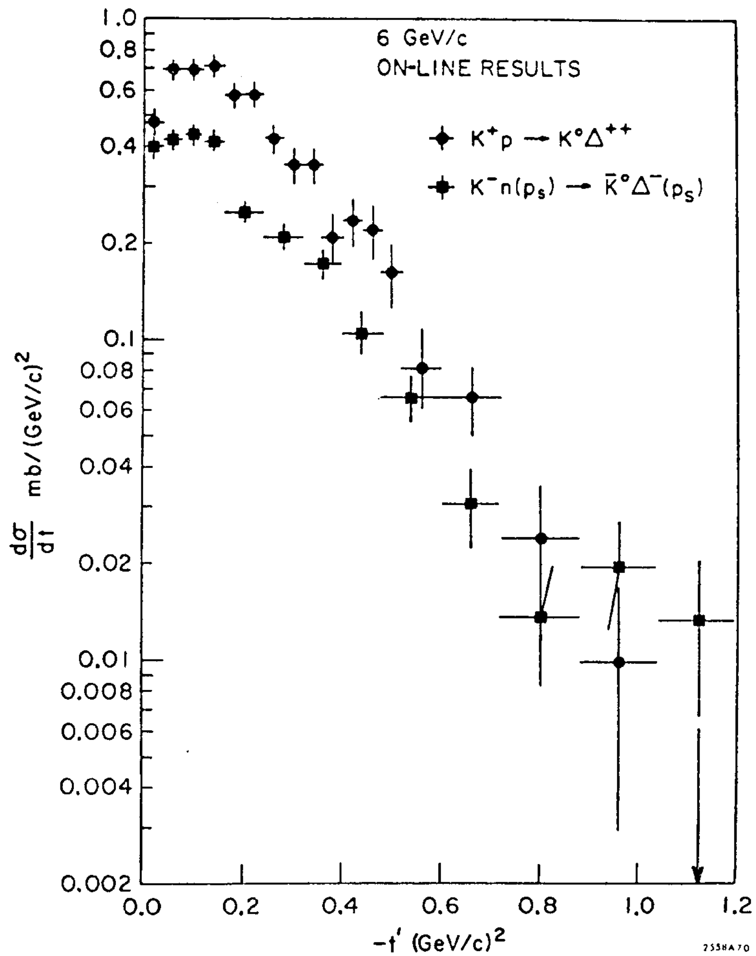

Figure 53

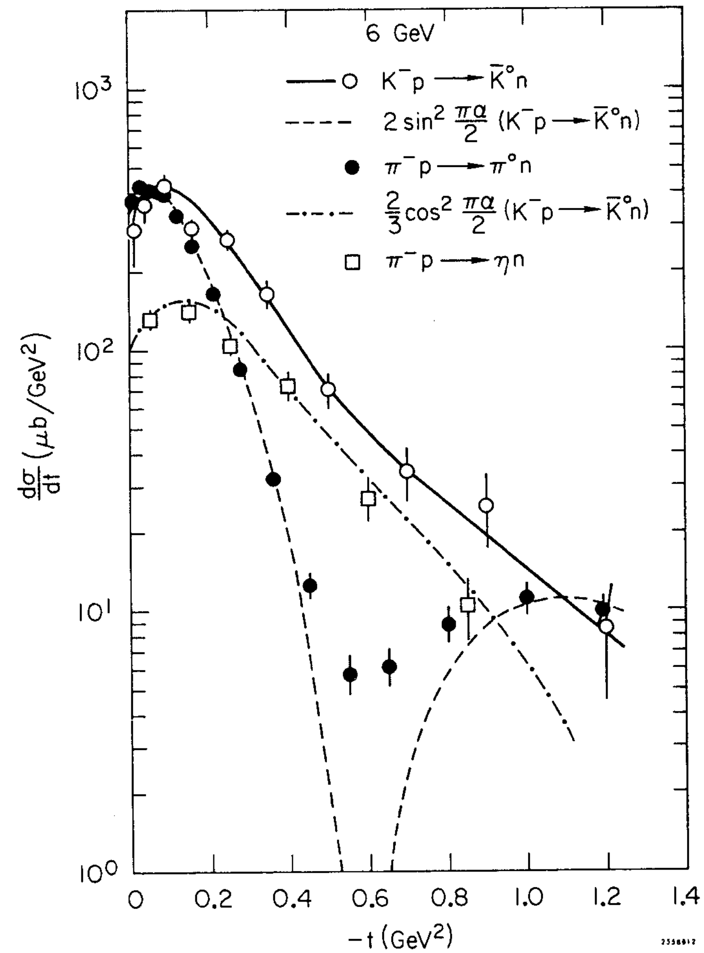

Figure 54

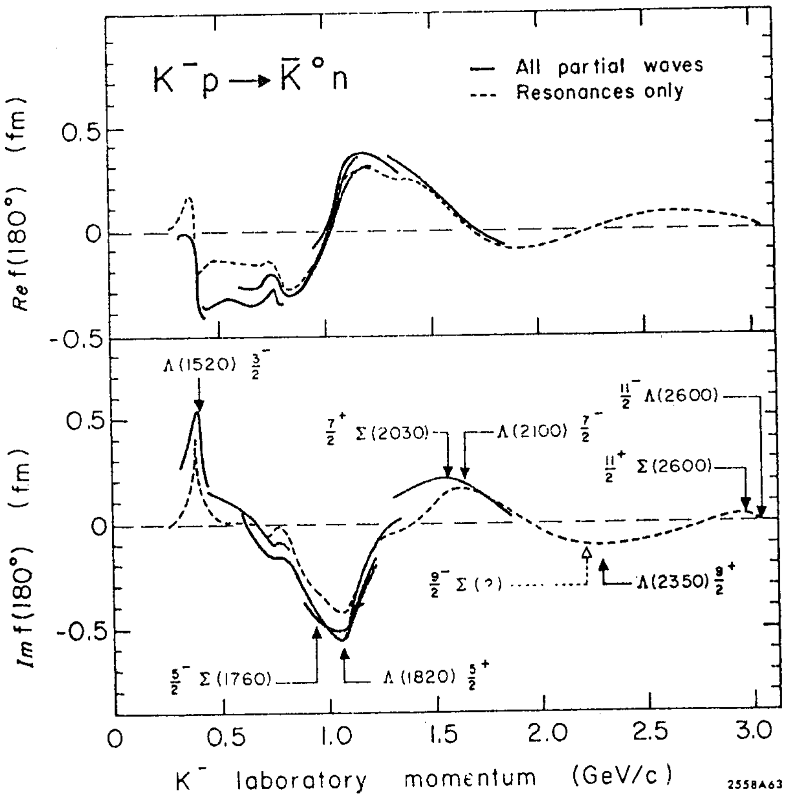

Figure 55

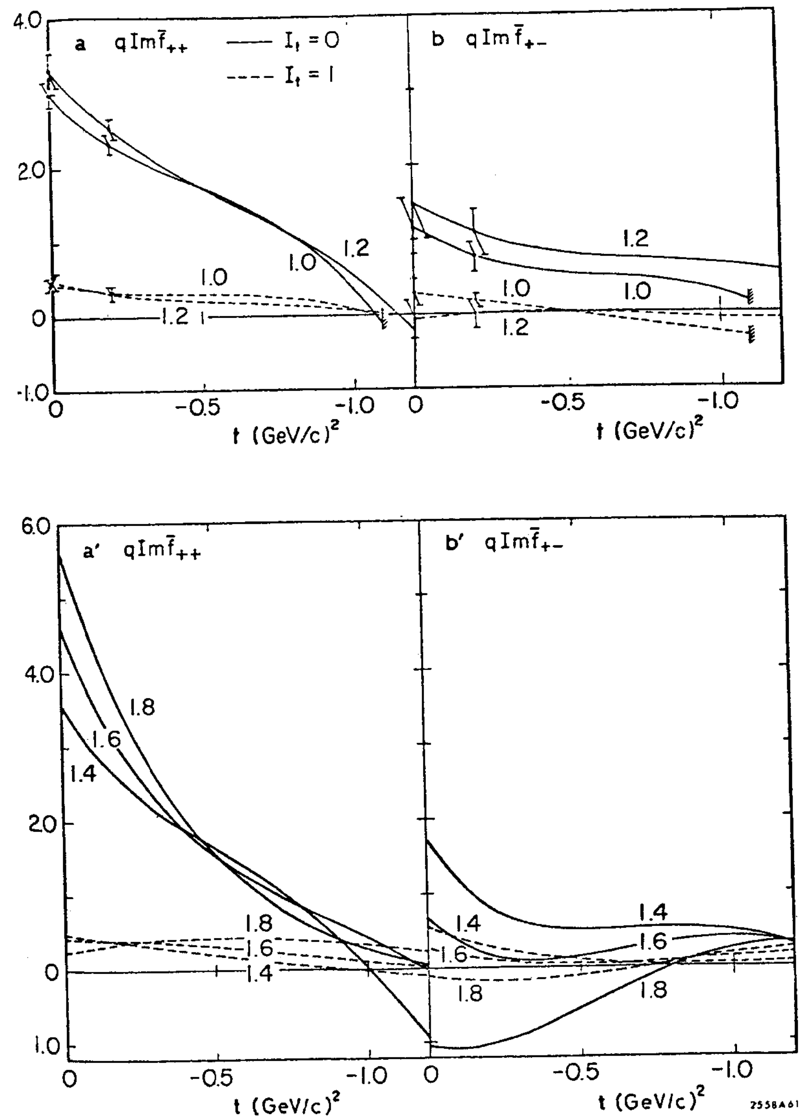

Figure 56

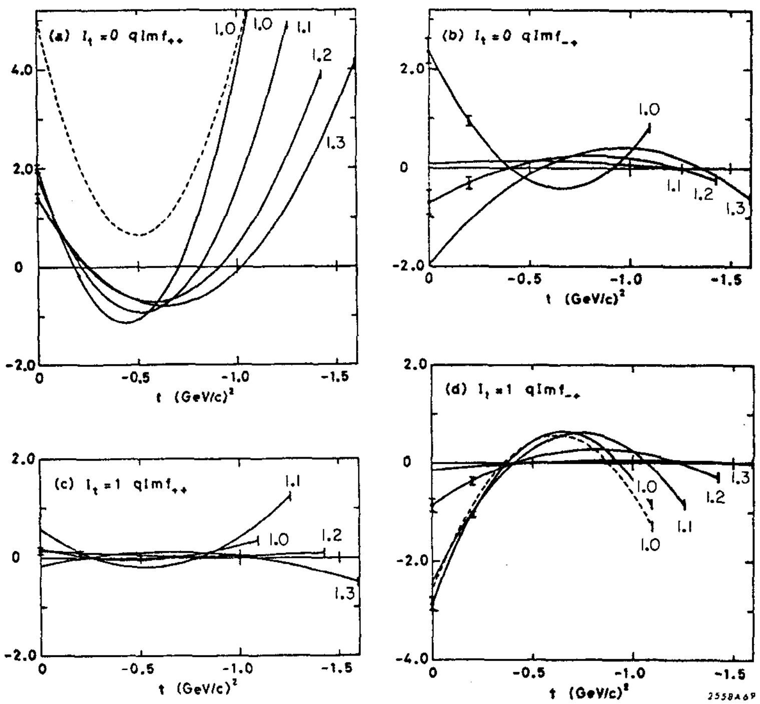

Figure 57

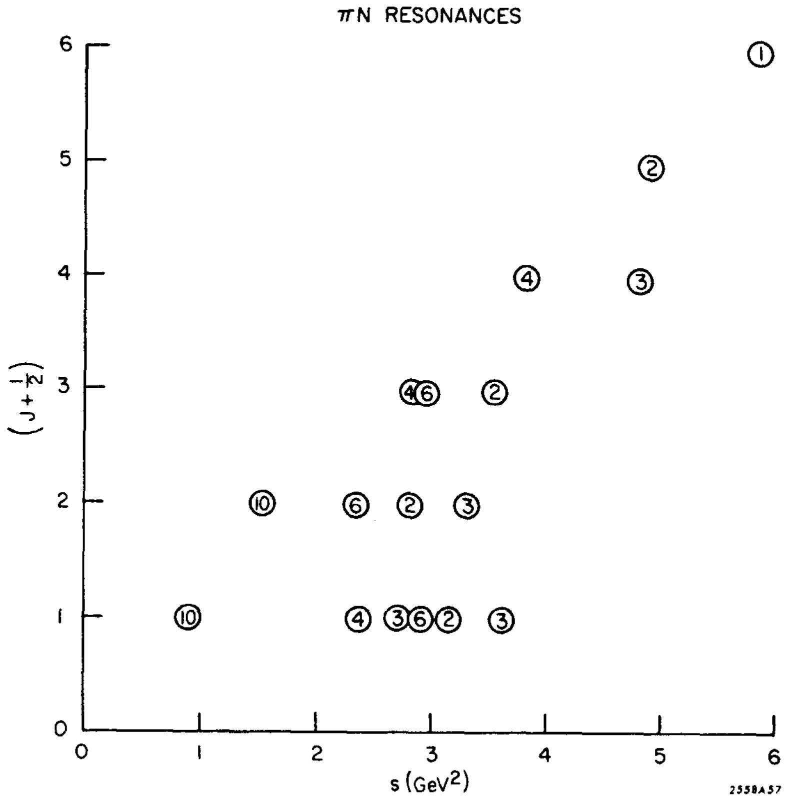

Figure 58

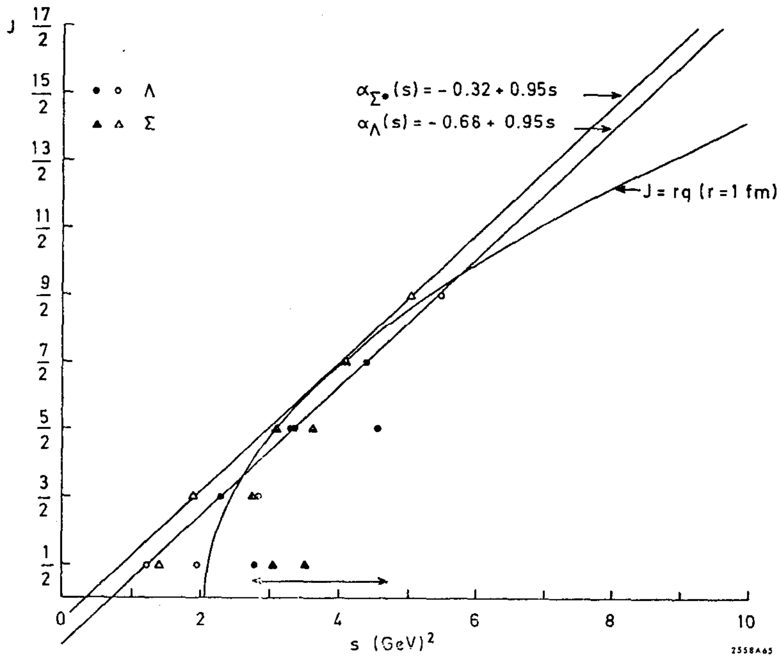

Figure 59

PROMINENT Y* RESONANCES

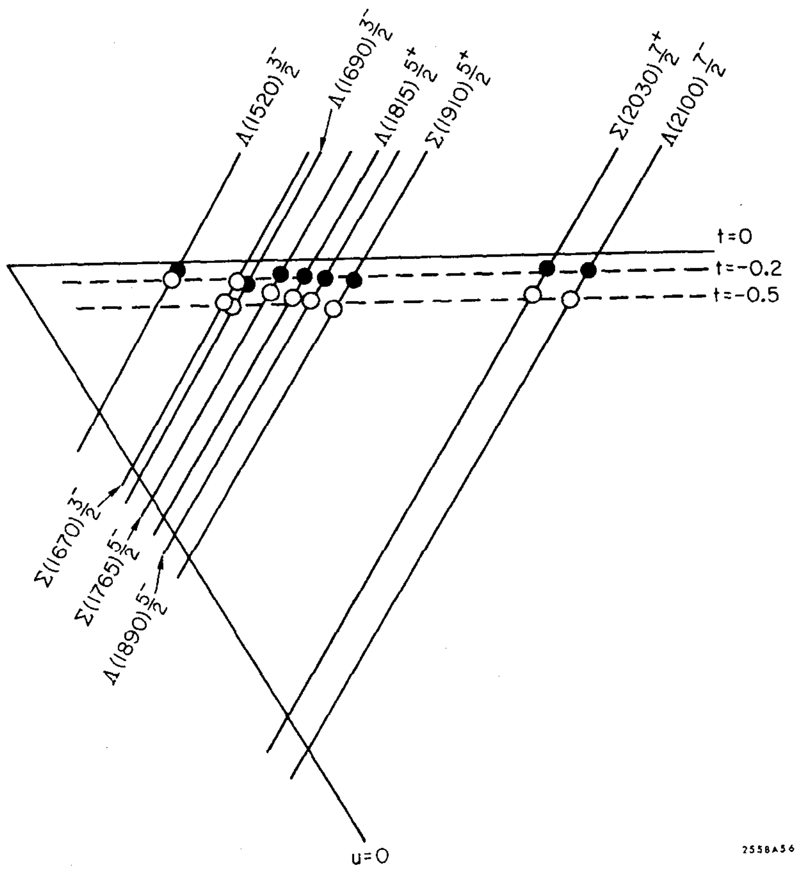

Figure 60

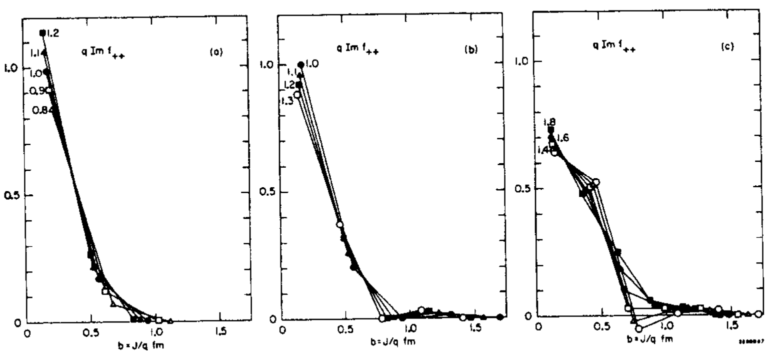

Figure 61

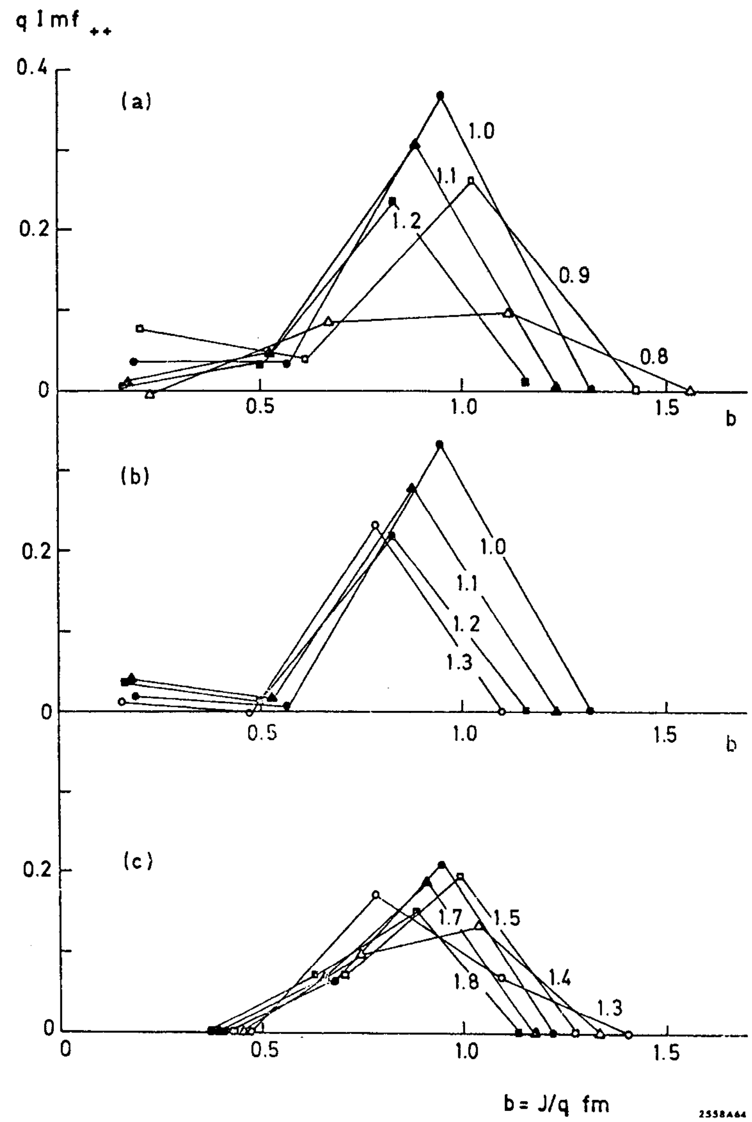

Figure 62

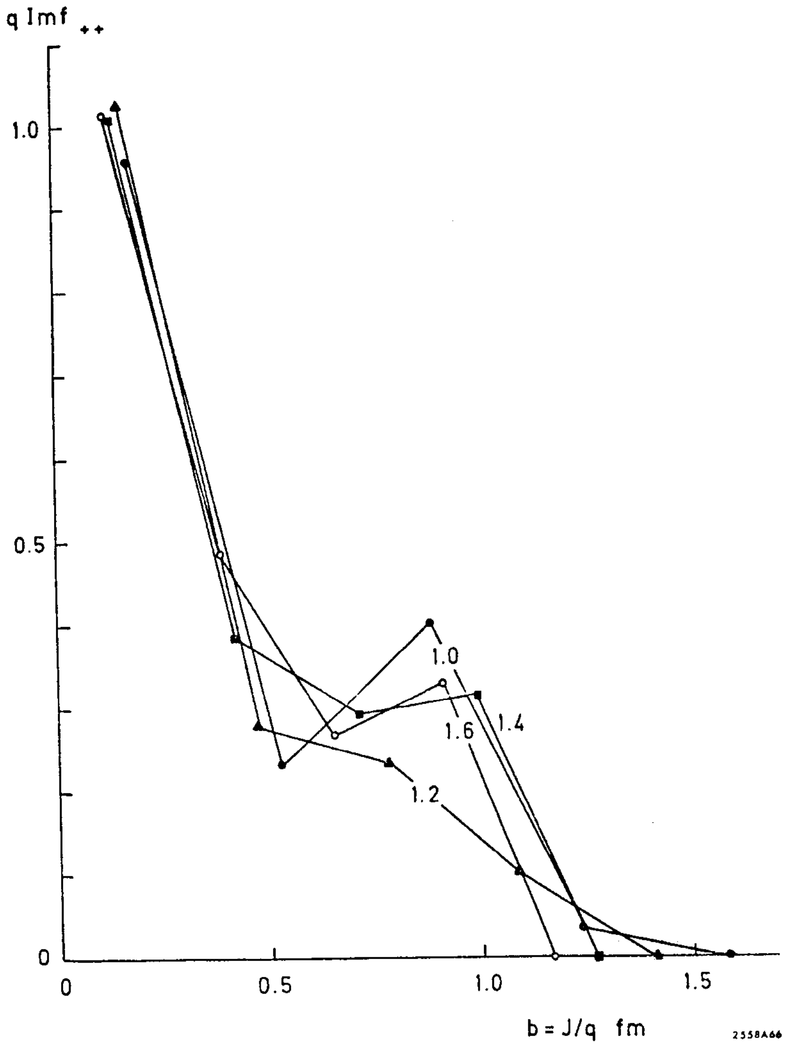

Figure 63

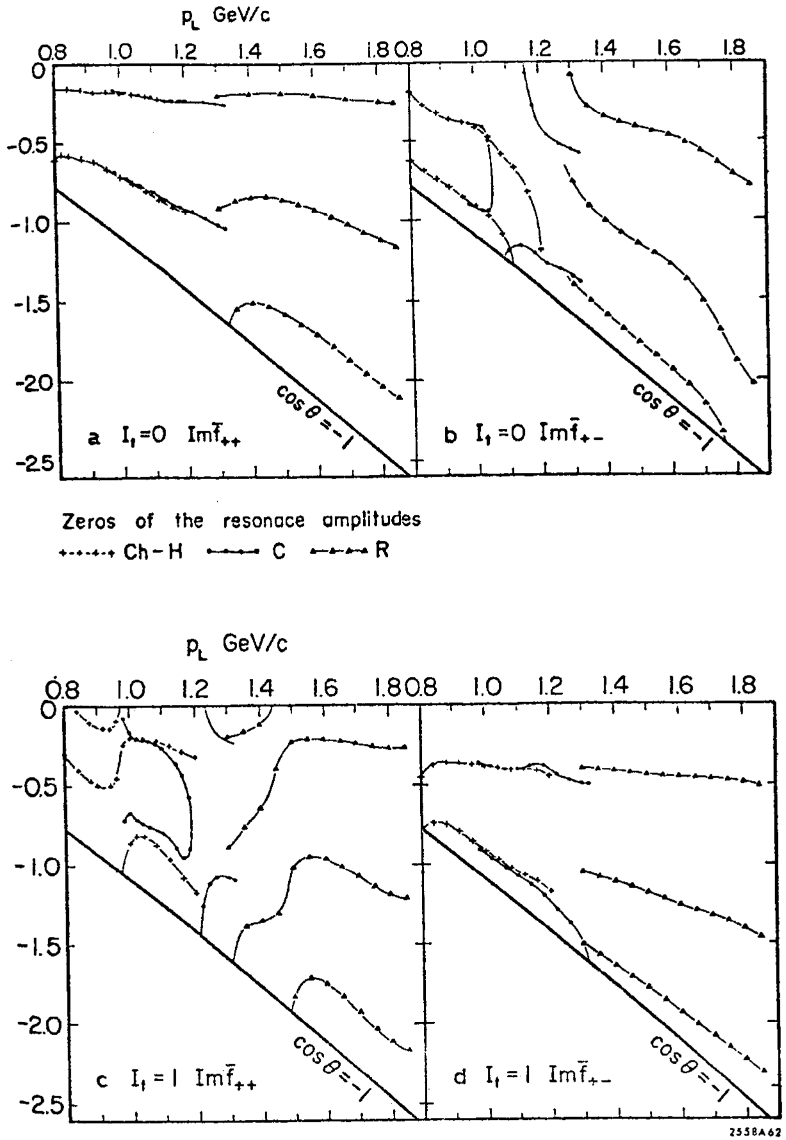

Figure 64

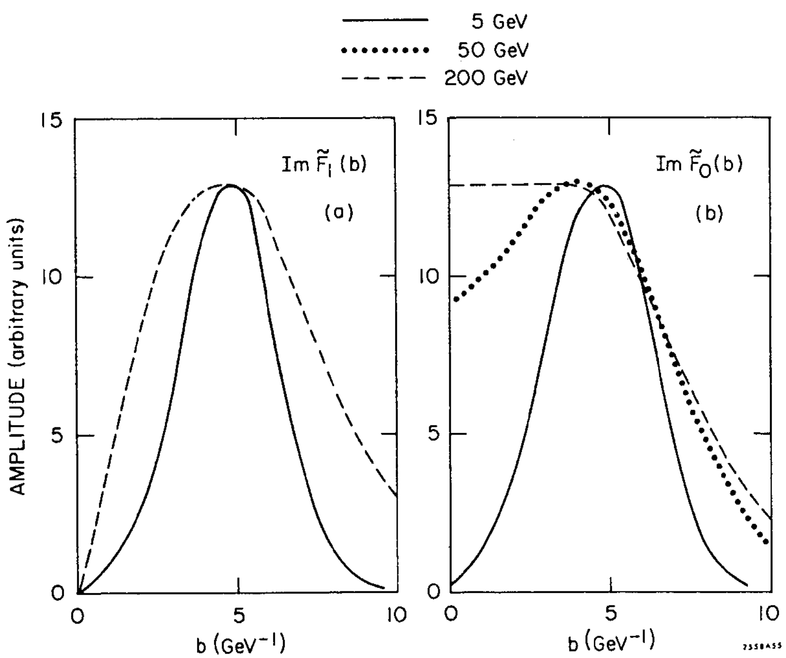

Figure 65

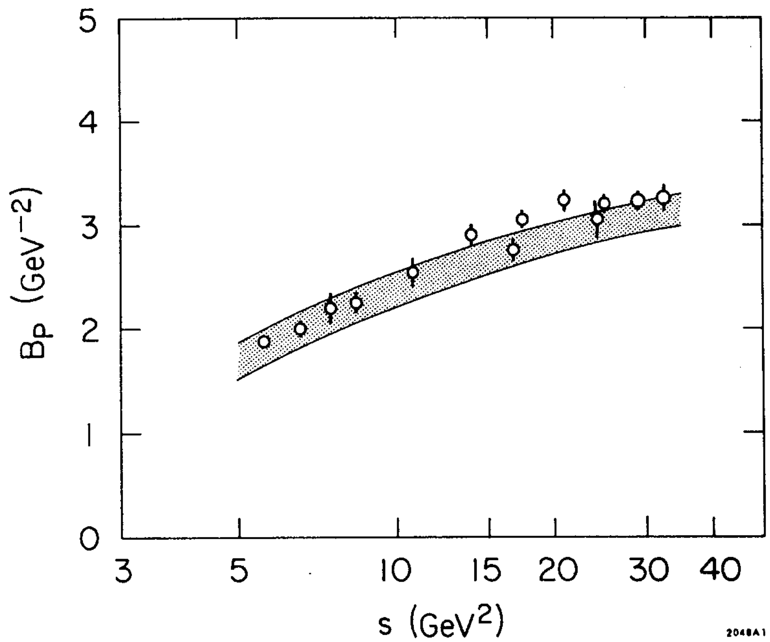

Figure 66

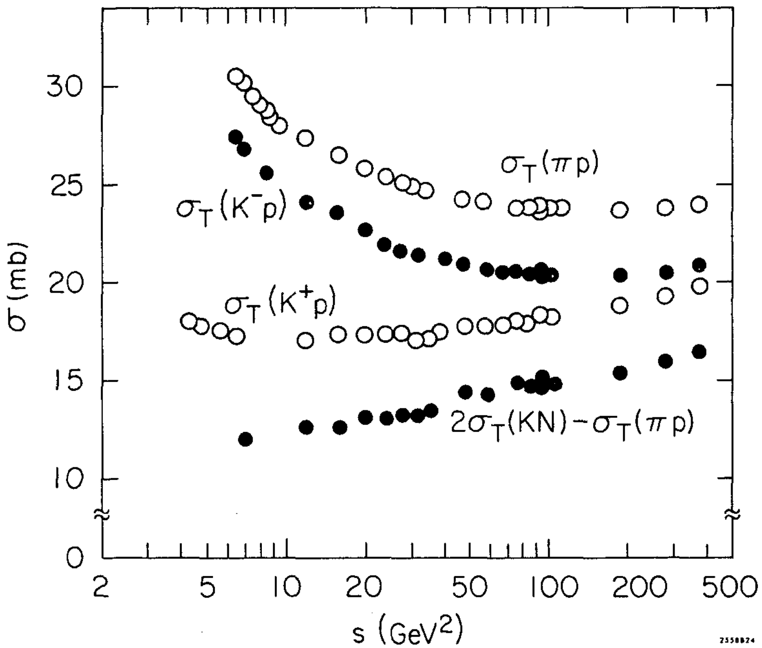

Figure 67

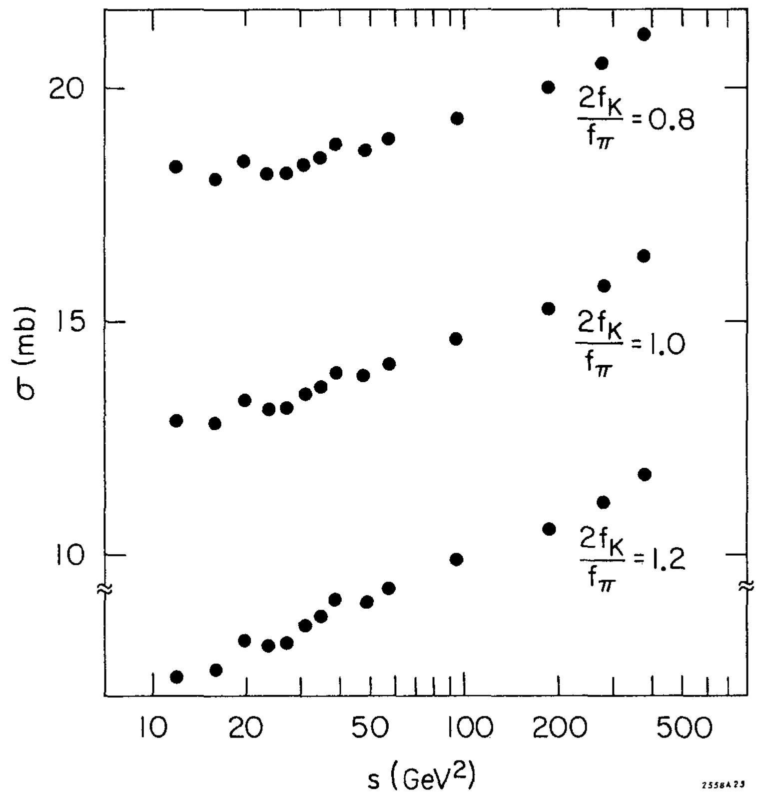

Figure 68

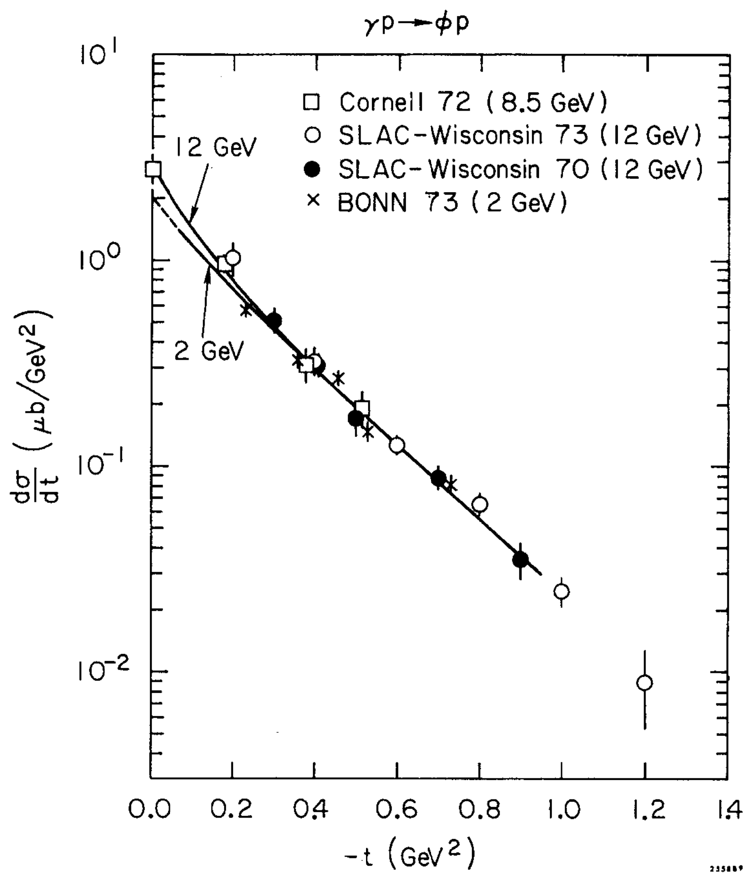

Figure 69

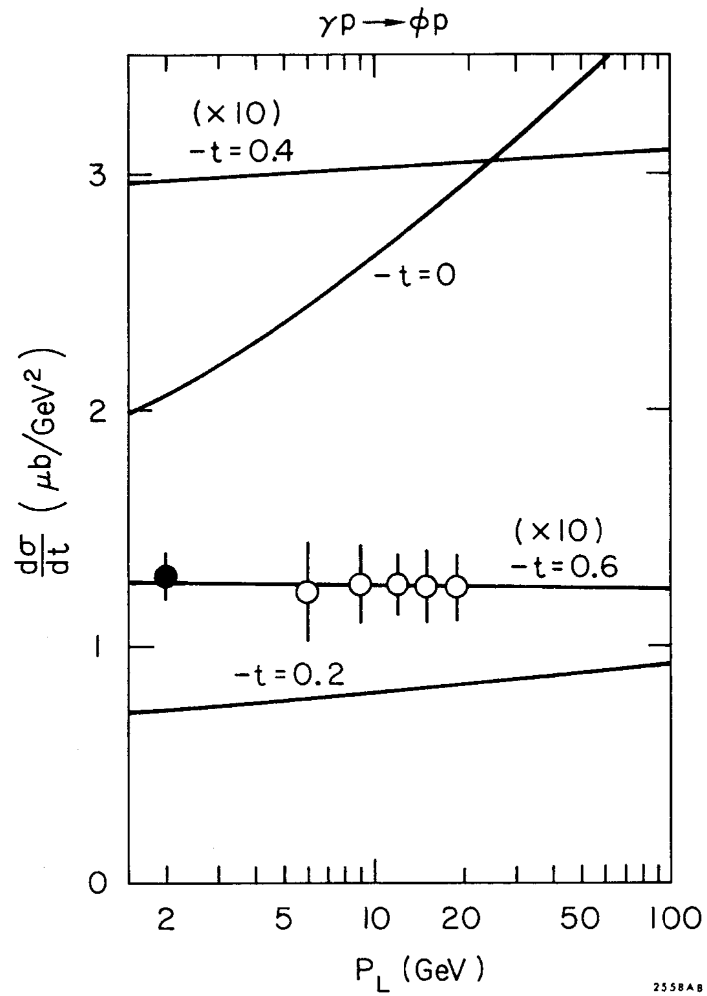

Figure 70

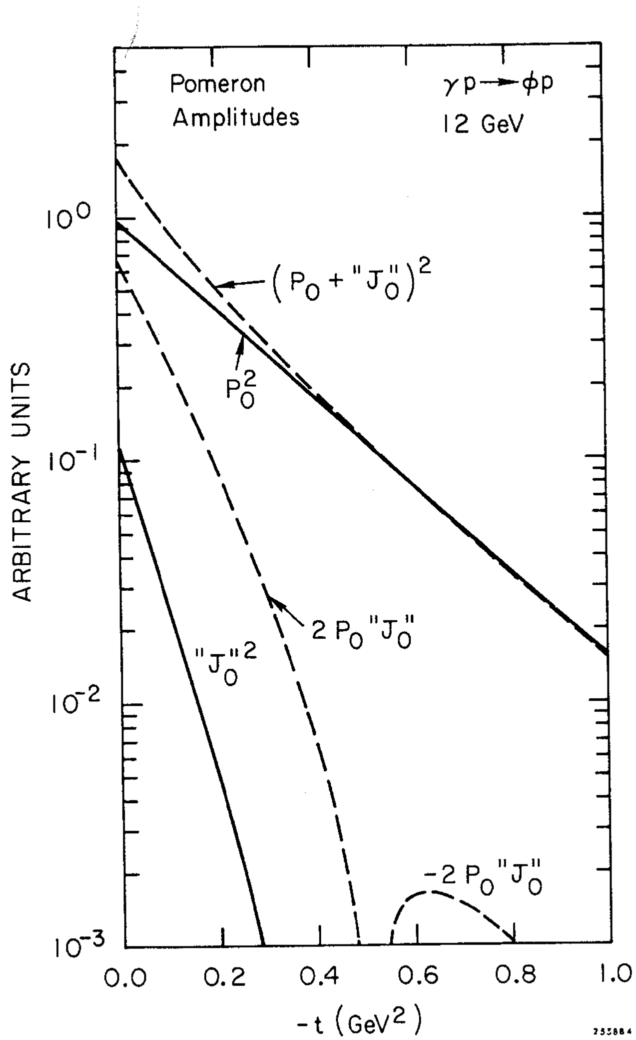
Pomeron
Amplitudes
γp → φp
12 GeV
ARBITRARY UNITS
10^0
10^{-1}
10^{-2}
10^{-3}
$(P_0 + "J_0")^2$
P_0^2
$2 P_0 "J_0"$
$"J_0"^2$
$-2 P_0 "J_0"$
0.0
0.2
0.4
0.6
0.8
1.0
$-t$ (GeV^2)

Figure 71

RESONANCES: EXPERIMENTAL REVIEW

Roger J. Cashmore

Oxford University
Oxford, England

INTRODUCTION

The object of these first two lectures is to describe the experimental measurements and methods used to identify resonances and give their parameters. The following lectures (by F. Gilman) will give some idea of the order in these resonances and our present understanding of their properties (mass, widths, couplings, etc.). However before beginning such a discussion I want to emphasize the motivations behind studying resonances, the properties we actually wish to determine and then give a rough outline of the plan I want to follow. Finally a little background is necessary in order to bring some sense into the bevy of states that exist.

(a) Motivations

The observation of resonances and their decays give us an insight into the underlying symmetries of the strong interaction. Indeed they have already lead to many of the conerstones in our present understanding of the strong interaction--SU(3), quarks, Regge trajectories, FESRs, etc. Even within the last year or so the first tests of Melosh transformation were made with resonance measurements, and that has once again helped us to see a little more clearly the symmetry structure of the strong interaction. As these resonances and their parameters become better and better known we can expect similar improvements in our understanding. Thus the pursuit of resonances continues to be a worthwhile task.

(b) Properties

Besides the sheer existence of a resonant state the other properties we would like to know are its spin, parity, isospin, mass, widths, decay channels and decay couplings. The first three properties are important for any schemes which attempt to classify states while the latter are necessary for any dynamical models of these decays.

(c) Plan

I intend to describe just how these results are obtained and the reliability to be associated with the measurements. Due to the limited sorts of beams and targets which are available for experiment we are immediately forced into a discussion of two different types of experiments:

(i) formation experiments: these are basically concerned with baryon states

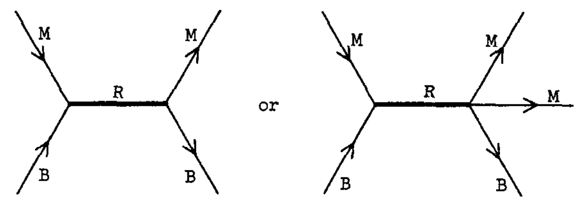

M-meson, B-baryon, R-resonance.

(ii) production experiments: basically meson systems but also Ξ's.

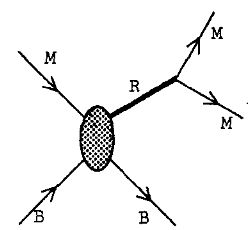

The data from (i) are far more extensive and complete than from (ii) and this has resulted in the healthier state of baryon spectroscopy, compared with meson spectroscopy.

(d) Some Background

We have to introduce some framework in order to be able to keep some sense in the large number of states we observe and direct us to what are significant measurements that have to be made.

(i) SU(3)--all hadronic states so far observed lie in irreducible representations of SU(3). In particular the baryons always appear in $\underline{1}$, $\underline{8}$, $\underline{10}$, while the mesons lie in $\underline{1}$ and $\underline{8}$ representations. Thus if one of the states in such a representation is observed then we must necessarily see the other members. If we do not then we either have to invoke some specific mechanism for its absence or question the validity of SU(3) (heresy!).

(ii) Quarks and SU(6)--Baryons lying in $\underline{1}$, $\underline{8}$, $\underline{10}$s and mesons in $\underline{1}$, $\underline{8}$s, suggested the quark model for hadrons. Baryons are qqq states and in group theory language we have

$$\underline{3} \times \underline{3} \times \underline{3} = \underline{1} + \underline{8} + \underline{8} + \underline{10}$$

while mesons are $q\bar{q}$ states

$$3 \times \bar{3} = \underline{1} + \underline{8}$$

If we now assume the quarks have spin 1/2 we have for baryons in SU(6) (SU(3) $\times$ SU(2))--

$$6 \times 6 \times 6 = \underline{20} + \underline{70} + \underline{70} + \underline{56}$$

The 20 is purely antisymmetric in quark labels, the $\underline{70}$'s have mixed symmetry and the $\underline{56}$ is purely symmetric. An example of a $\underline{20}$ state has never been observed, while we have prolific examples of $\underline{70}$'s and $\underline{56}$'s. This is due to the fact that selection rules prevent the decay of a $\underline{20}$ into any of the easily observed particles (and hence their production also). Thus we do not give up the idea of SU(6) because of the nonobservation of a $\underline{20}$ but rather give a plausible argument for the apparent absence. It is interesting to note the SU(3) $\times$ SU(2) breakdown of these larger representations

$$56 \text{ -- } {}^{2}8,\ {}^{4}10$$

$$70 \text{ -- } {}^{2}1,\ {}^{2}8,\ {}^{4}8,\ {}^{2}10$$

(notation ${}^{2s+1}$SU(3) where s is the spin of the system). For the mesons we have

$$6 \times \bar{6} = \underline{1} + \underline{35}$$

and here the SU(3) $\times$ SU(2) composition is

$$\underline{1} \text{ -- } {}^{1}1$$

$$\underline{35} \text{ -- } {}^{1}8,\ {}^{3}1,\ {}^{3}8$$

Finally in order to obtain the J^{PC} quantum numbers of the quark system we add internal orbital angular momentum to the system and use the quantum mechanical rules of angular momentum addition to give the total spin.

Thus we expect baryons to be in 56's and 70's with varying amounts of internal angular momentum while the mesons should lie in $\underline{1}$'s and $\underline{35}$'s.

FORMATION EXPERIMENTS AND $s = 0, -1$ BARYON STATES

In this section we discuss the information which exists on $s = 0$ and $s = -1$ baryon states from the reactions

$$s = 0: \quad \pi N \longrightarrow N^*_{1/2} \text{ or } N^*_{3/2} \longrightarrow \pi N,\ \eta N,\ \Lambda K,\ \Sigma K,\ \pi\pi N \ldots$$

$$\gamma N \longrightarrow N^*_{1/2} \text{ or } N^*_{3/2} \longrightarrow \pi N,\ \eta N,\ \ldots$$

$$s + -1: \quad \bar{K}N \longrightarrow Y^*_0 \quad \text{or} \quad Y^*_1 \longrightarrow \bar{K}N,\ \Lambda\pi,\ \Sigma\pi,\ \Lambda\eta,\ \Sigma\pi\pi,\ \Lambda\pi\pi \ldots ,$$

and deal with the different types of measurement, analysis and interpretation.

(1) Crudest measurements which can be made are the total, elastic and inelastic cross sections. These usually have shapes as in the figure and are given by

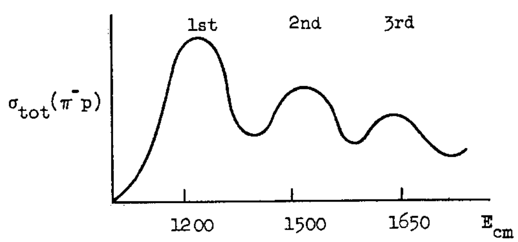

$$\sigma = 4\pi\lambda\!\!\!^{-2}\left(\frac{j+1}{2}\right)\frac{1}{4}\,\frac{\Gamma_i\,\Gamma_{tot}}{(m-m_0)^2 + \frac{\Gamma^2_{tot}}{4}}$$

when

$$m = m_0, \quad \sigma = 4\pi\lambda\!\!\!^{-2}\left(j + \tfrac{1}{2}\right)x_{el}$$

so that we measure m_0, Γ_{tot}, $(j+1/2)x_{el}$, I. This can be a dangerous activity. We now know that the 2nd bump contains two resonances while the 3rd contains ≥ 7 resonances!!

(2) Differential cross sections, polarizations, in two body reactions-- $0^- + 1/2^+ \longrightarrow 0^- + 1/2^+$.

These represent the greatest source, of information to date on baryon resonances. They are conventionally analyzed using partial wave expansions.

(a) The differential cross section is given by

$$\frac{d\sigma}{d\Omega} = |f(\theta)|^2 + |g(\theta)|^2, \quad F(\theta,\varphi) = f(\theta) + i\ \underline{\sigma}\cdot\underline{n}\ g(\theta)$$

where $f(\theta)$ and $g(\theta)$ have the partial wave expansions

$$f(\theta) = \frac{1}{q}\sum_L \{(L+1)a_{L+} + La_{L-}\}\ P_L(\cos\theta) \qquad \text{spin non flip}$$

$$g(\theta) = \frac{1}{q}\sum_L \{a_{L+} - a_{L-}\}\ \sin\theta\ P'_L(\cos\theta) \qquad \text{spin flip}$$

and

$$a_{L+}: j = L + 1/2; \quad a_{L-}: j = L - 1/2 .$$

(b) The polarization is given by $P(d\sigma/d\Omega) = 2\ \mathrm{Im}(fg^*)$

The object is to determine the a_L's--these give us information on what is happening on each J^P state at the c.m. energies at which we have data. There are two distinct methods of doing this

(a) The analysis is done separately at each energy and then one spots continuous solutions from energy to energy--energy independent.

(b) To make a model for a_L's and then fit a large number of energies at once--energy dependent (continuity is assured in this case of course), e.g.

$$a_L(E) = a^0_L(E - E_0) + \cdots \quad \text{or} \quad a_L(E) = \frac{1}{2}\,\frac{\sqrt{\Gamma_i\Gamma_0}}{m_0 - m - i\,\frac{\Gamma_t}{2}}$$

if a resonance is believed to be present.

(3) Two $\rightarrow$ 3 body reactions

These represent the latest addition in information. Reactions which have been analyzed are

$$\pi N \longrightarrow \pi\pi N$$

$$K^- p \longrightarrow \Lambda\pi\pi \ .$$

Here the method of analysis $(\pi\pi N)$ is to write the reaction amplitude as

$$\text{Amp} = \sum \text{quasi-two body amp.}$$

$$= \underbrace{\pi\Delta + N\rho + N\epsilon}_{\text{used to date}} \quad + \cdots$$

and then

(i) to make a partial wave expansion of each quasi two body amplitude.

(ii) to describe the $M(\pi n)$ variation by Δ Breit-Wigner or δ^3_3. (through the Watson final state interaction theorem $-e^{i\delta}(\sin\delta)/q^{L+1}$).

(iii) to make a maximum likelihood fit to all the data to determine

$$a_L^{\pi\Delta},\ a_L^{N\rho},\ \ldots \ \text{etc.}$$

in an energy independent manner.

This method of analysis is not as sound as the 2 body analysis but describes the data well. It is a model and the problems associated with double counting and the exact form of the final state interaction are worrisome points.

(4) Properties of partial wave amplitudes.

The a_L's are related to the T-matrix. From unitarity we have that

$$S = 1 + 2iT \qquad \text{with} \quad S^+S = 1$$

For the cases of

(i) pure elastic scattering we have

$$T = \frac{e^{2i\delta} - 1}{2i}$$

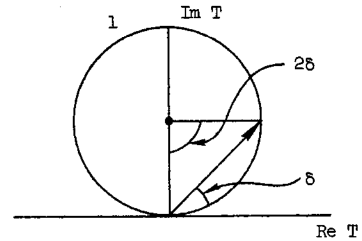

δ is the phase shift

with the simple description in the Argand diagram. δ is the phase shift. T is constrained to lie inside the unitary circle.

(ii) elastic scattering when an inelastic channel has opened up (e.g. $K^-p \to K^-p$ when $K^-p \to \Lambda\pi$ exists)

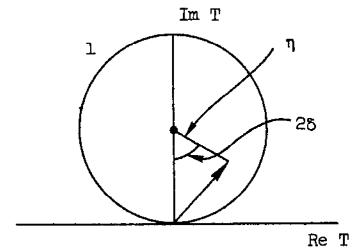

$$T = \frac{\eta\, e^{2i\delta} - 1}{2i}$$

and η is the inelasticity. T is always constrained to be within the circle shown. Furthermore

$$\sigma_{el} \propto \frac{1}{4}\,[1 + \eta^2 - 2\eta\cos 2\delta]$$

$$\sigma_{tot} \propto \frac{1}{2}\,[1 - \eta\cos 2\delta]$$

(from the optical theorem)

which implies

$$\sigma_{inel} \propto \frac{1}{4}\,[1 - \eta^2]$$

(iii) the presence of a resonance

$$a = \frac{1}{2}\frac{\sqrt{\Gamma_i\Gamma_0}}{m_0 - m - i\frac{\Gamma_{tot}}{2}}$$

Γ_i -- partial width to incoming channel

Γ_0 -- partial width to outgoing channel

If the resonance is purely elastic we have

$$\Gamma_i = \Gamma_0 = \Gamma_{el} = \Gamma_{tot}$$

and

$$a_L = \frac{1}{2}\frac{\Gamma_{tot}}{m_0 - m - i\frac{\Gamma_{tot}}{2}}$$

This means that $\text{Im } T > 0$.

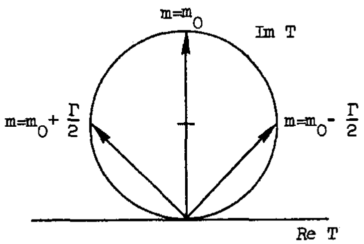

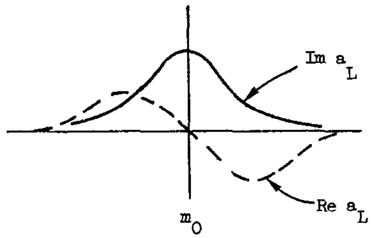

However if the resonance is inelastic we can have the following result for an inelastic channel

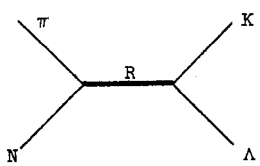

$$T \propto \frac{g_{\pi N}\, g_{\Lambda K}}{m_0 - m - i\frac{\Gamma_{tot}}{2}}$$

Whereas in $\pi N \to \pi N$, $\text{Im } T > 0$ $(g^2_{\pi N})$ we can now have either positive or negative sign for $\text{Im } T$ depending on the sign of the product $g_{\pi N} g_{\Lambda K}$ (in general $g_{in}\, g_{out}$). In this case the partial wave amplitude must lie in the region indicated and a resonance would behave as shown, i.e. the resonance circle can be above or below the real axis. In general we have that

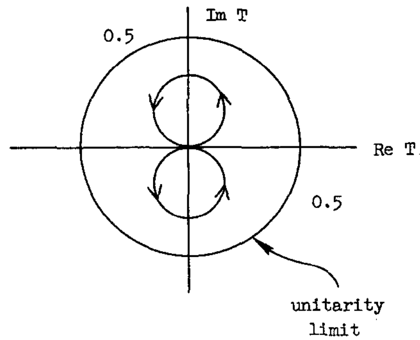

$$a = \frac{1}{2}\frac{\gamma}{m_0 - m - i\frac{\Gamma_t}{2}}$$

where $\gamma = \sqrt{\Gamma_i\Gamma_0} = g_i g_0 \sqrt{(PS)_i\ (PS)_0}$ and PS is the phase space in the decay. This formula has the following properties:

(a) It describes a circle with centre $(0,\ \gamma/2\Gamma_t)$ and radius $\gamma/2\Gamma_t$.

(b) The amplitude moves most rapidly in the vicinity of $m = m_0$.

(c) $\gamma/\Gamma_t = \pm\sqrt{x_i x_0}$ where x_i, x_0 are the branching fractions and the $\pm$ (couping sign) is determined by where the resonance loop lies in the Argand diagram.

(d) The resonance amplitude moves in a counterclockwise direction (this corresponds to having the time development corresponding to a decaying state).

Three examples are given of $T(\pi N \to \pi N)$ which demonstrate the different loops associated with resonances of different elasticities. Many more examples of such resonance loops can be found in Figs. 1, 2, 3 and 4.

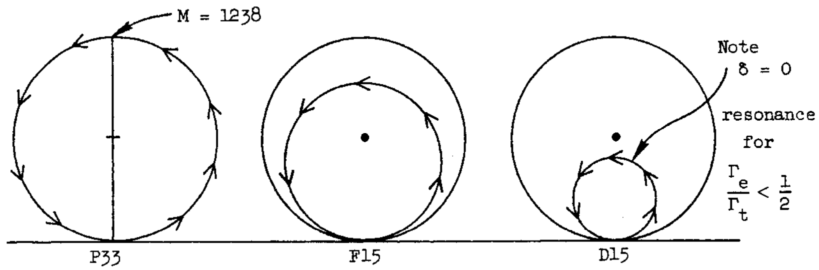

[The notation used is in general, L, 2I, 2J where L is the incident orbital angular momentum, I the isospin and J the total angular momentum.]

(iv) a resonance and a background: we find that

$$T = T_B + e^{2i\delta_B} T_R \qquad (\text{from } s = s_B s_R)$$

The rotation induced by $e^{2i\delta_B}$ is just enough always to keep a resonance loop (in T_R) within the unitary limit. An excellent example of this is found in the S31 wave of πN scattering (see Fig. 1).

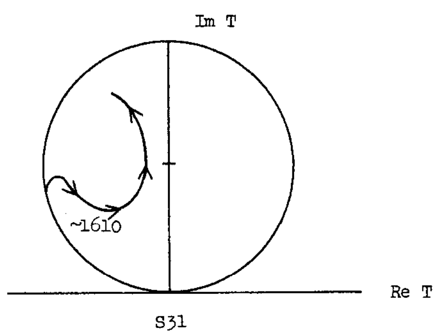

(v) Backward moving amplitudes: there is a maximum backward speed set by causality (Wigner Condition)

$$\frac{d\delta}{dk} > -\frac{1}{a}$$

where a is the diameter of the region of interaction.

(5) How to identify a resonance and its properties

We now list the points used in this process

(a) Identification --loop structure in the Argand diagram

(b) J^P,I --relevant partial wave amplitude

(c) Mass --δ = 0, $\pi/2$, maximum 'speed' of amplitude

(d) Width --shape of amplitude as function of centre of mass energy

(e) Partial Widths --γ/Γ_t from diameter of resonance circle. This gives $|\sqrt{x_i x_0}|$

(f) Coupling Sign --position of resonance loop in Argand diagram.

(6) Results and Practical Estimation

πN system

(a) πN final state--Here many resoances are observed as can be seen in Figs. 1 and 2.

(b) $\pi\pi N$ final state--Here the same resonances are observed as in (a) (see Fig. 3) together with some other states, e.g. a D13(1700), P13(~ 1700)

Here we see the value of studying inelastic channels. If a resonance has a small coupling (branching fraction) to the elastic channel then its strength in $\pi N \to \pi N$ is proportional to g_i^2 whereas its strength in an inelastic channel is $g_i g_0$, i.e. if g_0 is large we have a much better chance of observing it. This is particularly the case with $D_{13}(1700)$.

$K^- N$ system

(a) 2 body final states--Again many resonances are observed but due to the greater complexity expected and the harder experiments the state of Y_0^*'s and Y_1^*'s (s = -1 baryons) is not as well defined.

(b) 3 body final states--These have not as yet yielded any new resonances.

As can be seen from Table 1 we now have all the N^*, Δ states falling in the $[56,0^+]_{n=0}$, $[70,1^-]_{n=2}$, $[56,0^+]_{n=2}$ and all but one in the $[56,2^+]$. To compliment this we have observed all the Y_0^*, Y_1^* states necessary to fill the

$\underline{1}$, $\frac{1}{2}^-, \frac{3}{2}^-$

$\underline{8}$, $\frac{1}{2}^+, \frac{1}{2}^-, \frac{3}{2}^-, \frac{5}{2}^-, \frac{5}{2}^+$

$\underline{10}$, $\frac{3}{2}^+, \frac{7}{2}^+$

If we look at less well identified states (usually high mass states) together with those of Table 1 we have the impression that the following rule may be appearing

Positive parity states lie in [56]'s

Negative parity states lie in [70]'s.

Only the observation of further states will or will not verify this conjecture.

So far I have only summarized the identification and IJ^P for each state. These are important for classifications but the couplings are essentia for dynamical schemes. Unfortunately these are hard to measure although in general it is fairly simple to give the coupling sign. This only relies on observing whether the resonance loop is up or down rather than on a detailed understanding of the variation of the amplitude with mass.

(7) How difficult is it to measure masses and widths?

In general it is very difficult and even the PDG now quote a range. These problems are well demonstrated by the results below for two well known resonances, the D15 and F35 in πN scattering.

D15 M	D15 Γ	F35 M	F35 Γ	
1670	141	1890	260	estimate
1666	159	1824	282	T-matrix pole
1692	176	1907	324	unitarity (BW background)
fairly clean elastic resonance		high inelastic resonance		

i.e., differences ~ 10 - 100 MeV.

Thus a warning is in order: Always be wary of any quoted masses and widths or any fits to them.

Poles in the T-matrix

(a) An argument existed for a long while over the parameters of the P33(1238) resonance. Values for the mass and width varied by 10-20 MeV. This was all resolved when searches were made for the position of the pole in the T-matrix in the complex energy plane. All analyses gave the same pole to within 1 MeV. Thus we see that the results were parametrization dependent but the pole was common to every analysis.

(b) This result is also true for other resonances, e.g., $P_{11}(1470)$... Thus we appear to have a better way of describing resonances but there is an open question as to whether they are physically more sensible than Breit-Wigner type parameters. This will only be resolved by further quantitative investigation.

Finally I would like to repeat my statement that these problems do not apply to the coupling signs and this is why they have played such a significant role in discussing baryon decay mechanisms.

(8) Summary

In summary we have a good understanding (although by no means complete) of the resonances observed in the reactions

$$\pi N \longrightarrow \pi N,\ \eta N,\ \Lambda K,\ \Sigma K,\ \pi\pi N$$
$$\gamma N \longrightarrow \pi N,\ \eta N$$
$$\bar{K}N \longrightarrow \bar{K}N,\ \Lambda\pi,\ \Sigma\pi,\ \Lambda\pi\pi$$

i.e., S = 0, S = -1 baryons and their couplings.

PRODUCTION EXPERIMENTS: s = -2 BARYONS, MESONS

In general the analysis of these reactions is complicated by the presence of other particles. Unfortunately it is in many cases the only way we can observe certain states.

(1) s = -2, -3 Baryons, e.g. Ξ^*, Ω's

Ξ^*'s and Ω^*'s have to be observed in reactions of the type

$$K^-p \to K^+ \Xi^{*-},\quad \Xi^{*-} \to \Xi\pi,\ \Lambda\bar{K} \quad\longrightarrow\quad \left\{\begin{array}{l} K^+\Xi\pi \\ K^+\Lambda K^- \end{array}\right.$$

$$K^-p \to K^+K^0\Omega^{*-},\quad \Omega^{*-} \to \Xi\bar{K},\ \Omega\pi \quad\longrightarrow\quad \left\{\begin{array}{l} K^+K^0\,\Xi\bar{K} \\ K^+K^0\Omega\pi \end{array}\right.$$

Clearly these data are very difficult to obtain and this accounts for the paucity of information on these states. Indeed only the $\Xi^*(1530)$ is reasonably well measured. Thus all we can hope for is the identification of possible Ξ^* states (e.g. from bumps in mass spectra) and in general the J^P assignment will be unknown, i.e. the Ξ's are in bad shape and always will be. Of course similar comments apply to Ω^*'s!!

(2) Meson resonances and formation reactions

Before proceeding directly to production experiments I do want to point out that it is possible to observe meson states in formation experiments. However the drawbacks are large.

(a) e^+e^- annihilation:

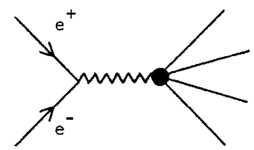

In this case we are limited to mesons in the sequence $J^{PC} = 1^{--}$, i.e., the vector mesons

(ρ, ω, φ, ρ'? ...)

(b) $\bar{p}p$ reactions

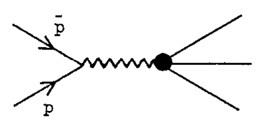

Here the limitations are of mass, i.e. $M_R \geq 2M_p$.

Thus we see that the limitations are large and production reactions are of vital importance in the observation of meson resonances.

(3) $\pi\pi$ and $K\pi$ resonances or 'nearly formation reactions'

Pion exchange is well known to be an important factor in many hadronic reactions and to dominate often in the forward direction (the pole is then near the physical region) e.g.,

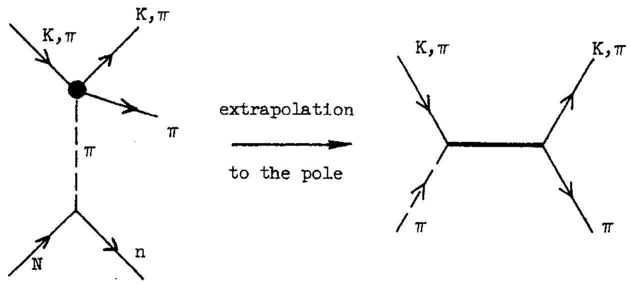

(or $\pi\pi \to K\bar{K}$)

Thus by extrapolation to the pole we can effectively obtain information on

$$\pi\pi \to \pi\pi\ ,\ K\bar{K}$$
$$K\pi \to K\pi$$

and then apply all the techniques we have developed for dealing with formation experiments, i.e., partial wave analyses.

The quality of the data on this type of reaction is demonstrated in Fig. 4. The presence of the ρ, f, g mesons is clearly indicated in the Y_2^0, Y_4^0 and Y_6^0 moments and detailed partial wave analyses of Fig. 5 confirm these besides producing evidence for new states (ρ'?). In the future we can expect similar results on $K\pi$ scattering (see Carnegie Topical Conference).

There are however limitations even to these reactions. One can only observe mesons in the natural spin parity series $J^P = 0^+, 1^-, 2^+, \ldots$. Furthermore if we consider pions, Bose symmetry imposes the further restrictions that $G = +1$ and $(I = 0, C = +)$ or $(I = 1, C = -)$ states only are possible. To identify such states we have to turn to other reactions.

Even so many of the best identified states (see Table 2) in the meson system, the 1^-, 2^+, 3^- states, are found in these reactions. This accounts for the firmer standing of these meson resonance SU(3) multiplets. The 0^+ octet of Table 2 is not yet satisfactorily identified. This suffers from one of the common problems of spectroscopy, i.e., identifying low spin states $(J = 0)$ in the presence of high spin states $(J \geq 1)$ which produce the major angular structure.

(4) Meson resonances in 3 particle final states

The observation of 3π or $K\pi\pi$ final states allows study of resonance in the unnatural spin parity series 0^-, 1^+, 2^- although again for 3π one is restricted to $G = -1$ states.

The importance of the 1^+ states can be seen from inspection of Table 2, two such states being required. Unfortunately such unnatural spin-parity states can be produced by diffractive excitation and thus any analysis will have a confused interpretation--is it resonance or is it a dynamical effect that produces the large 1^+ cross section?

The analysis technique is essentially that described earlier for the similar formation experiments, i.e., the reaction is analyzed as

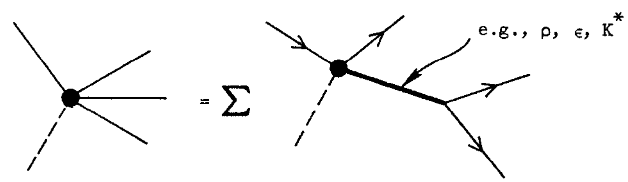

Let me immediately turn to the results.

(i) In Fig. 6 the A_2 resonance is clearly observed in the variation of both modulus and phase of the 2^+ $\pi\rho D$ wave.

(ii) In Fig. 7 we see results for the 1^+ $\pi\rho s$ wave which should contain the A1 resonance. Even though the cross section is large the phase shows no similar variation to that exhibited by the A2. This has been an outstanding problem of meson spectroscopy for 10 years--no clear observation of an A1 resonance. Indeed the cross section is almost accounted for by a dynamical mechanism (the Deck mechanism) although it fails in specific details. Recently models have been made in which three terms are considered (a) the Deck diagram (b) rescattering in the Deck diagram (c) direct resonance production.

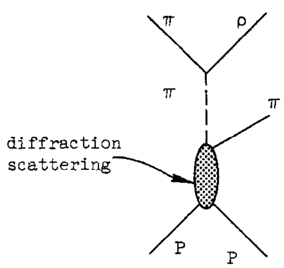

(a) Deck Diagram

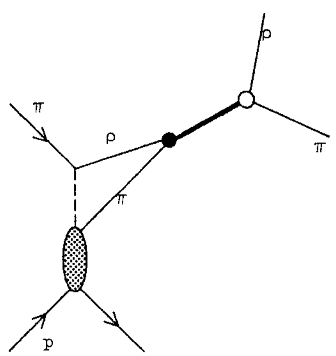

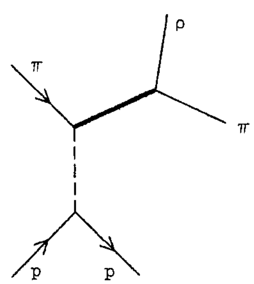

(b) Rescattering in Deck Diagram

(c) Direct resonance production

The total amplitude can then be written

$$\text{Amp} = D + D\, i \sin\delta\, e^{i\delta} + R \sin\delta\, e^{i\delta}$$

$$= D \cos\delta\, e^{i\delta} + R \sin\delta\, e^{i\delta}$$

Now if $R \sim -iD$ we see that

$$\text{Amp} \sim De^{i\delta}(\cos\delta - i \sin\delta) \sim D\ ,$$

i.e. all phase variation has been suppressed. Thus even though the usual signature of a resonance (its phase/amplitude variation) is not observed it may still be there. The parameters required are however rather unusual $M \sim 1300$ MeV, $\Gamma \sim 200$ MeV. Such a state should be observed in other reactions, e.g. $\pi^+ p \to \pi^+\pi^-\pi^0\Delta^{++}$ but unfortunately the indications are that it is absent. Thus we are once again faced with the problem of the A1. Its failure to appear would be interesting on quark model grounds since the D meson is present. However SU(3) does not require the A1 since the D could be classified as a singlet.

(iii) A similar discussion occurs for the 2^- state the A3. Once again it can be produced by a Deck type of mechanism.

(iv) The situation in $K\pi\pi$ states is even more confusing at this time. Both Q mesons (1^+, s = +1 states) should appear here as there is no G-parity selection rule. However no definite observation of resonance behavior has been made. In this case failure to observe at least one Q would be bad since such a state is demanded by the existence of the B meson. A recent high statistics spectrometer experiment here at SLAC should resolve this situation (if at all possible).

Once again it might be hoped that study of charge exchange or hypercharge exchange reactions would bring some insight since then we remove diffraction dissociation as a possible strong mechanism.

(5) Mesons in 4π final states

Here we can obtain $G = +1$ states of all spin parities (except 0^-). Indeed studies of the $\pi\omega$ system ($\omega \to 3\pi$) indicate the presence of the 1^+ meson, the B. This is the best identified 1^+ state. The g meson (see Fig. 4) is also observed to decay to 4 pions. At this time little other information is available.

(6) Summary of status of meson states

At present only the leading trajectory meson states are really well known. In general one has measurements of IJ^{PC} and estimates of the mass and total width from mass spectra and partial wave analyses. Some partial widths are known but there are no measurements of relative coupling signs. More sophisticated experiments and analyses will be required for this.

In Table 2 we see the present reliable states. The difference between that and Table 1 demonstrates the much poorer level of knowledge of mesons compared with baryons. When one realizes that the couplings are even more poorly known it is clear that baryons will be the major spectroscopy laboratory for a substantial time. We can only hope that mesons will soon be brought to the same status.

CONCLUSIONS

The information on baryon states is abundant whereas the mesons need substantial improvement. With the continued increase of our knowledge we should be better placed to understand the systematics of the strong interaction.

In the following lectures F. Gilman will demonstrate the present state of the art.

References

Many further sources can be found within the following references.

Review of Resonances

J. Rosner, SLAC-PUB-1931 (submitted to Physics Reports).

Systematics and Decays

F.J. Gilman, This Summer Institute.

Properties of Partial Wave Amplitudes

R. H. Dalitz, Ann. Rev. Nucl. Sci. 13 (1963), 339.

Problems of Measurement of Resonance Parameters

R. J. Cashmore, Purdue Conference on Baryon Spectroscopy, p. 53 (Purdue University, Lafayette, Indiana, 1973).

Experimental Analyses

R. Ayed and P. Bareyve, P.L. 31B, 598, 1970: Aix en Provence Conference, 1973.

R.J. Cashmore et al., LBL-2634, SLAC-PUB-1387.

P. Estabrooks, A.D. Martin, CERN/MUNICH, 1973 Tallhasse Conference, p. 37.

Yu. M. Antipov et al., N.P. B63, 141 (1973), N.P. B63, 153 (1973).

TABLE 1

Baryon States Observed

States of the $[56,0^+]_{n=0}$

$^4 10$	$\frac{3}{2}^+$	$\Delta(1236)$,	$\Sigma(1385)$,	$\Xi(1530)$	
$^2 8$	$\frac{1}{2}^+$	$N(940)$,	$\Lambda(1120)$,	$\Sigma(1180)$,	$\Xi(1310)$

States of the $[70,1^-]$

$^2 10$	$\frac{3}{2}^-$	$\Delta(1700)$,	$\Sigma(1580)$	
$^2 10$	$\frac{1}{2}^-$	$\Delta(1610)$,	$\Sigma(1740)$	
$^4 8$	$\frac{5}{2}^-$	$N^*(1670)$,	$\Sigma(1765)$	$\Lambda(1830)$
$^4 8$	$\frac{3}{2}^-$	$N^*(1710)$,	$\Sigma(1940)$,	$\Lambda(\quad)$
$^4 8$	$\frac{1}{2}^-$	$N^*(1660)$,	$\Sigma(\quad)$,	$\Lambda(1670)$
$^2 8$	$\frac{3}{2}^-$	$N^*(1520)$,	$\Sigma(1660)$,	$\Lambda(1690)$
$^2 8$	$\frac{1}{2}^-$	$N^*(1510)$,	$\Sigma(\quad)$,	$\Lambda(\quad)$
$^2 1$	$\frac{3}{2}^-$			$\Lambda(1520)$
$^2 1$	$\frac{1}{2}^-$			$\Lambda(1405)$

TABLE 1 cont.

States of the $[56,2^+]$

$^4 10$	$\frac{7}{2}^+$	$\Delta(1925)$,	$\Sigma(2030)$	
$^4 10$	$\frac{5}{2}^+$	$\Delta(1860)$,	Σ	
$^4 10$	$\frac{3}{2}^+$	$\Delta(1900)$?,	Σ	
$^4 10$	$\frac{1}{2}^+$	$\Delta(1850)$,	Σ	
$^2 8$	$\frac{5}{2}^+$	$N^*(1680)$,	$\Sigma(1905)$,	$\Lambda(1820)$
$^2 8$	$\frac{3}{2}^+$	$N^*(1730)$,	Σ ,	$\Lambda(1890)$

Other States

$[56,0^+]$ radial excitation

$\frac{1}{2}^+$	$N^*(1470)$	$\Sigma(\quad)$,	$\Lambda(\quad)$
$\frac{3}{2}^+$	$\Delta^*(\sim 1600)$,	$\Sigma(\quad)$	

$[56,2^+]$ radial excitation

$\frac{5}{2}^+$	F_{15} (~ 2000),	$\Sigma(\quad)$	$\Lambda(\quad)$
$\frac{3}{2}^+$	?		

TABLE 2

MESON STATES

L = 0 1, 35	
0^-	π, K, η, X
1^-	ρ, K^*, ω, φ
L = 1 1, 35	
0^+	π_N, $K\pi(\sim 1200)$, ϵ?, S^*
1^+	B, ... ,
1^+	A1?, ... , D, E(?)
2^+	A_2, $K^*(1400)$, f, f'
L = 2 1, 35	
1^-	p'? , ...
2^-	A3?, ...
2^-	
3^-	g, $K^*(\sim 1800)$, $\omega(1670)$?

RADIAL EXCITATIONS? ρ'?

Figure Captions

Fig. 1. I = 3/2 πN partial wave amplitudes.

Fig. 2. I = 1/2 πN partial wave amplitudes.

Fig. 3. Argand plots for $\pi\pi N$ Partial wave amplitudes.

Fig. 4. Unnormalized moments for $\pi^+\pi^- \to \pi^+\pi^-$ from the reaction $\pi^- p \to \pi^+\pi^- n$ at 17.2 GeV/c.

Fig. 5. $\pi\pi$ Partial Waves.

Fig. 6. The variation of the amplitude and phase of the $2^+ \pi\rho D$ wave.

Fig. 7. The variation of the amplitude and phase of the 1^+ $\pi\rho$ s-wave.

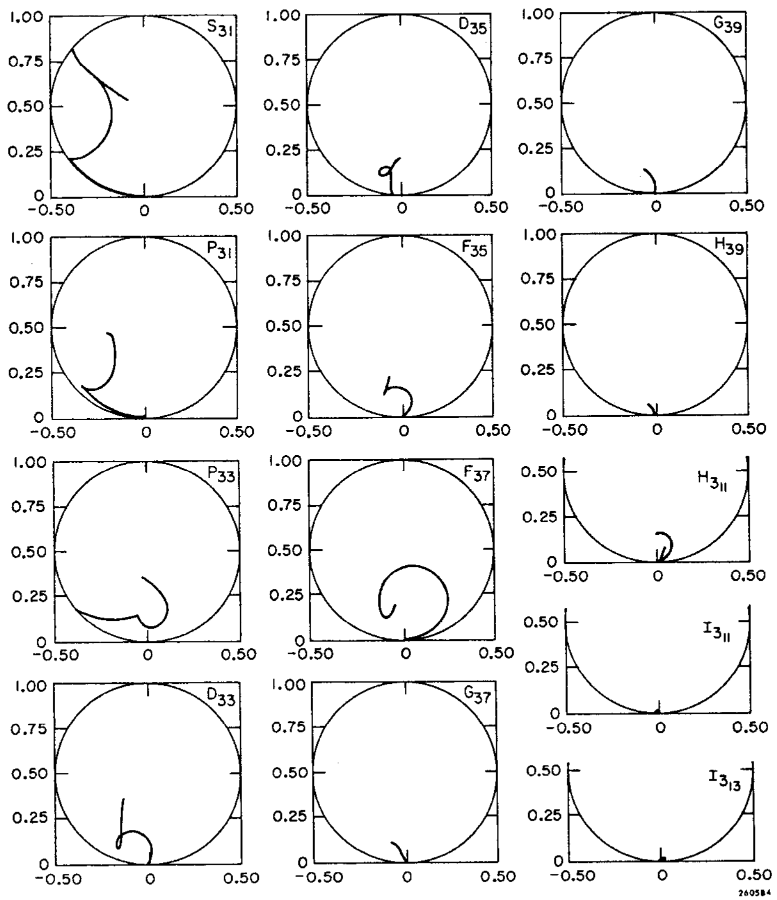

Figure 1

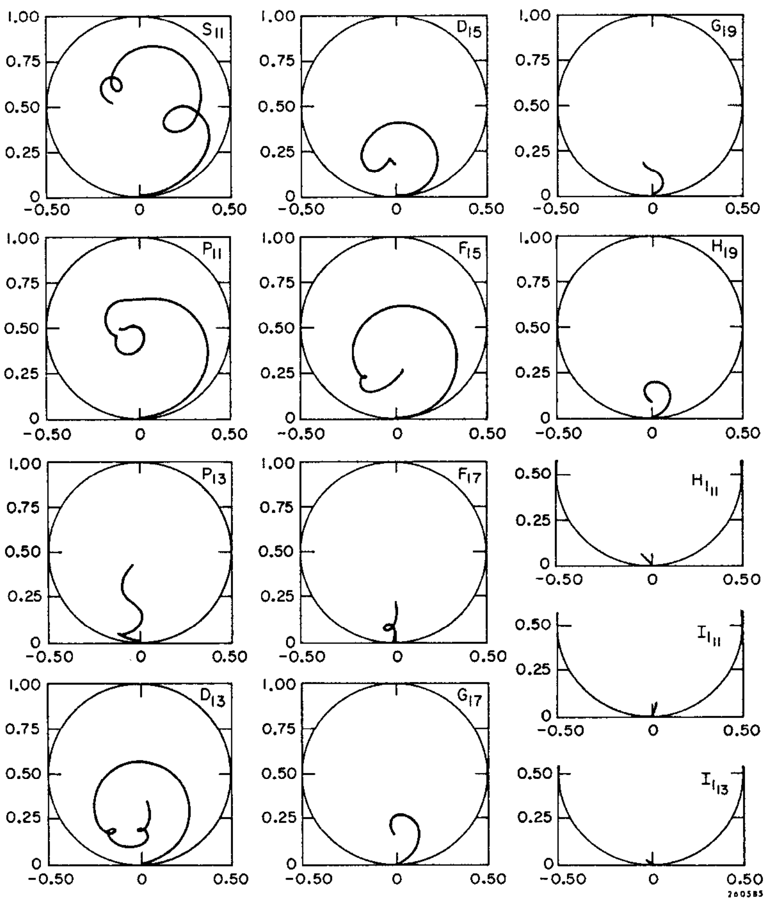

Figure 2

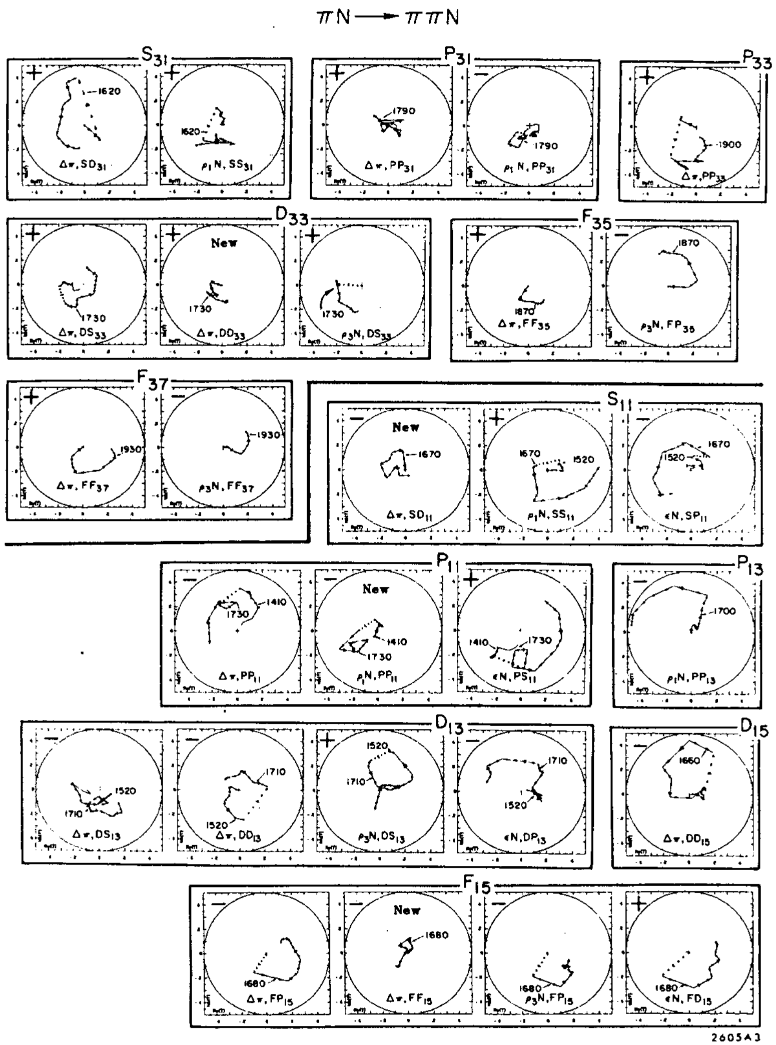

Figure 3

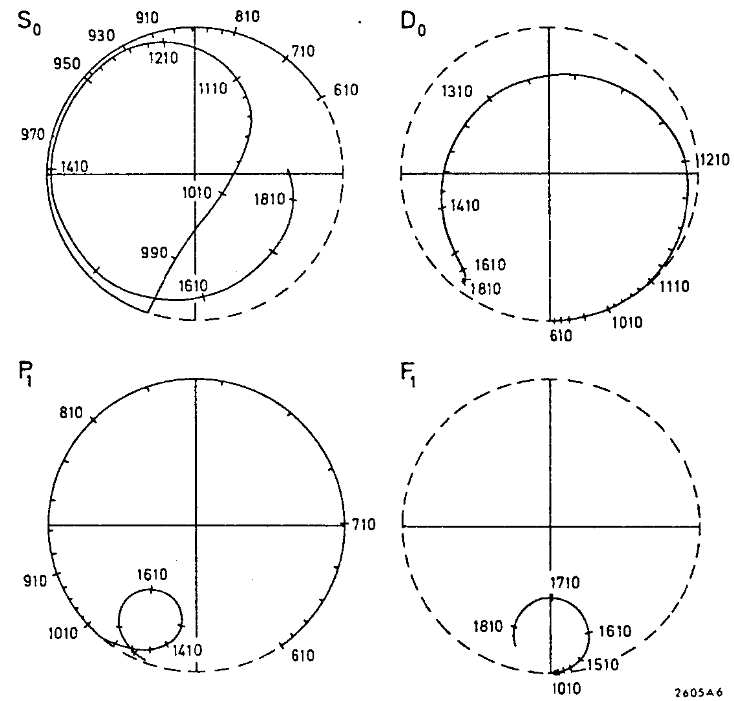

Figure 4

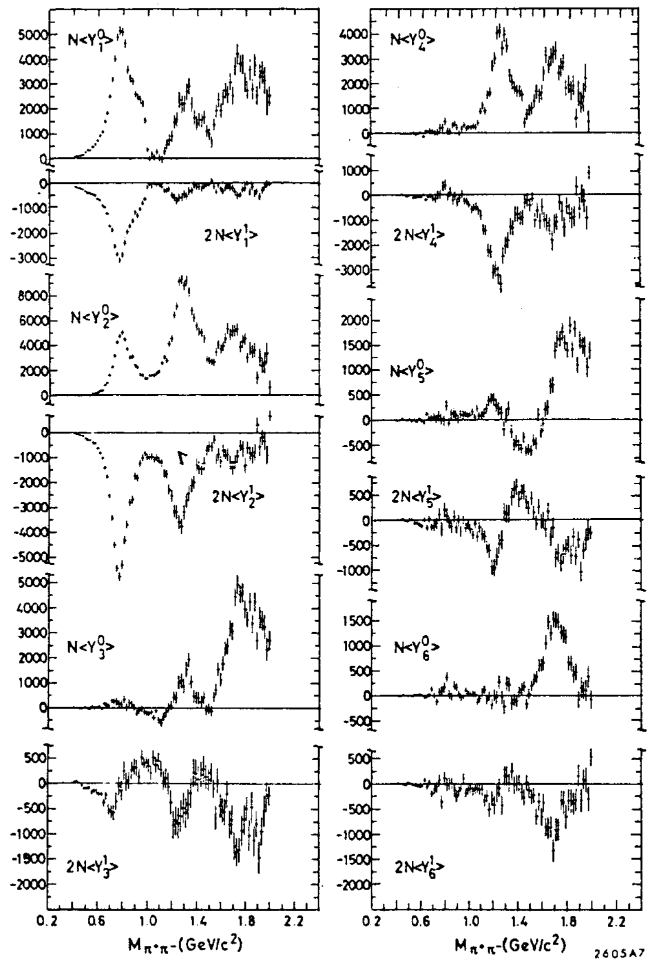

Figure 5

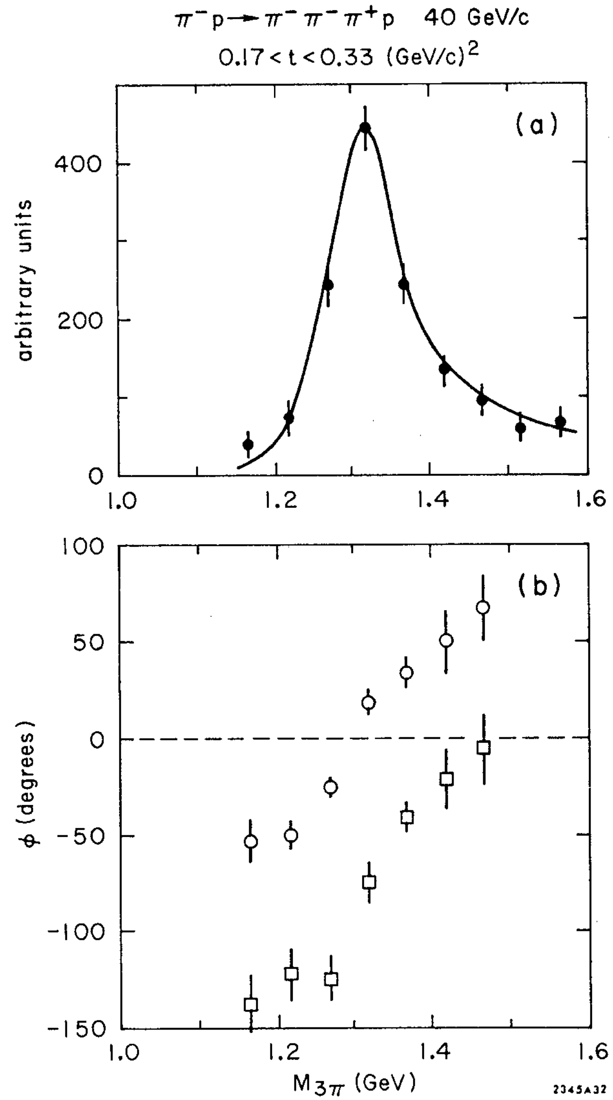

Figure 6

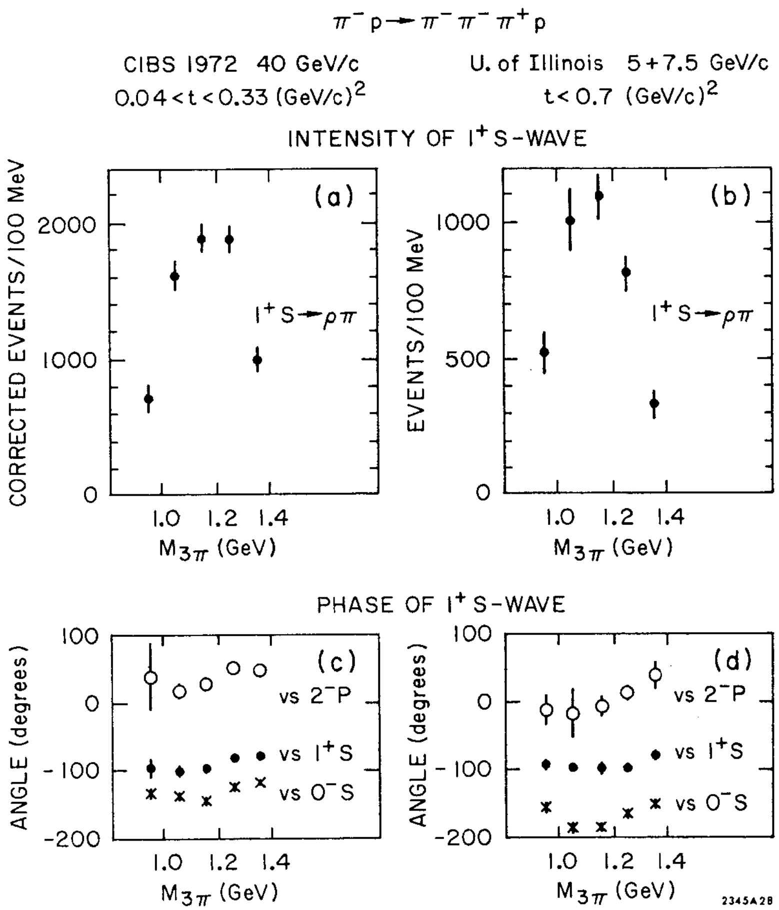

$\pi^- p \rightarrow \pi^- \pi^- \pi^+ p$
CIBS 1972 40 GeV/c
$0.04 < t < 0.33$ (GeV/c)^2
U. of Illinois 5+7.5 GeV/c
$t < 0.7$ (GeV/c)^2
INTENSITY OF 1^+ S-WAVE
CORRECTED EVENTS/100 MeV
EVENTS/100 MeV
(a)
(b)
$1^+ S \rightarrow \rho\pi$
$M_{3\pi}$ (GeV)
PHASE OF 1^+ S-WAVE
ANGLE (degrees)
(c)
(d)
vs 2^-P
vs 1^+S
vs 0^-S
2345A28

Figure 7

RESONANCES: A QUARK VIEW OF HADRON SPECTROSCOPY AND TRANSITIONS

Frederick J. Gilman

Stanford Linear Accelerator Center
Stanford University, Stanford, California 94305

I. INTRODUCTION

At this time, when so much of our concern is already focused on what is happening in the TeV energy region for strong interactions, why be interested in resonances? Of course, one might answer that the enumeration of what hadronic states exist and their quantum numbers is one of many subject areas within particle physics, and an incomplete one at that, which should be studied like any other as part of our understanding of physical phenomena. But this increasingly neglected area is still of great interest and importance for reasons other than that of completing a catalogue of states and their properties.

First, the arrangement of states tells us about the symmetries of strong interactions. As we all know, internal symmetry groups like isospin and SU(3), when realized in the normal manner, imply that single particle states fall into multiplets which correspond to irreducible representations of the appropriate group. Further, the existence of such a symmetry group implies relations among amplitudes, e.g., among three point functions appropriate to resonance decays.

Second, if hadrons are "made" of still simpler constituents like quarks,[1,2] this structure may be reflected in a recognizable way in the spectrum of states. In fact, on the basis of a non-relativistic picture of building hadrons out of quarks, an $SU(6) \times O(3)$ description of the hadronic spectrum has arisen. Furthermore, one may employ this to calculate relations among transition amplitudes, although to do so it is necessary to understand both the structure of the states involved and the nature of the operators that induce the appropriate transitions. In such a picture the existence of additional "charmed" quarks should result in "charmed" hadronic states, which remain to be found.[3]

Third, resonances and their properties can tell one about the dynamics of strong interactions at many levels. At a fundamental level, those aspects of the spectrum and amplitudes which point toward an underlying quark basis for strong interactions require one to consider the question of quark confinement. Some very interesting recent approaches to this problem involve either the use of "infrared slavery" arising in asymptotically free gauge theories[4] or the "bag" model.[5] Particularly in the latter case, a number of properties of the low-lying hadron states come simply from the confinement of the quarks.

At a less fundamental level, the multiplet structure, the ordering of states, and the mass splittings between multiplets give us information on the "forces" involved between constituents. A popular model for many years has been that of quarks in a harmonic oscillator potential.[6,7]

Given a hadronic spectrum and two body decay amplitudes, then one may proceed to the next level of dynamics by building up the (non-diffractive) four-point function. According to duality one may obtain the imaginary part of such a non-diffractive amplitude either in terms of a complete sum of resonant states in the direct or crossed channel. In fact, many of the major successes of the duality approach arise from considering cases where one channel is exotic, i.e., where there are no resonances possible according to the quark model. Thus, results of imposing duality such as exchange degeneracy follow from the resonance spectrum, and more particularly, from the absence of exotic states. Finally, the hadron states may be used as "Born terms" in the t-channel to calculate elastic and inelastic two-body and multiparticle scattering amplitudes. As such, what happens at very low energies and how the hadronic resonance spectrum and couplings are organized has a very direct effect on what happens even in the TeV region.

II. SYMMETRIES AND NON-SYMMETRIES

Throughout the following we shall assume that the SU(2) group of isotopic spin transformations is an exact symmetry of strong interactions. Evidence for this comes both from the observation of nearly degenerate isospin multiplets and from amplitude relations. Whatever breaking of the mass or amplitude relations occurs is of order α and therefore seemingly attributable to electromagnetic effects, although these have not actually been calculated since their magnitude depends on the details of strong interactions themselves.

The larger symmetry group[8] of SU(3) is clearly broken at the 10 to 20% level in masses, but it still gives rise to many clearly identifiable SU(3) multiplets among mesons and baryons. With more than a dozen identified baryonic multiplets being slowly filled with states, no one seriously doubts the applicability and usefulness of SU(3) as a strong interaction symmetry.

SU(3) has also had some success when applied to amplitudes. In particular, application to matrix elements of currents, yielding relations among baryon magnetic moments and among the vector and axial-vector couplings in weak decays,[9] are in striking agreement with experiment. Results for decay amplitudes,[10] say for baryon$'$ $\rightarrow$ meson + baryon, are in fair agreement with experiment, although there is often some leeway in the choice of barrier factors and mixing parameters when comparison is made with experiment. More striking are the relative signs of amplitudes in reactions like $\bar{K}N \rightarrow \pi\Lambda$ and $\bar{K}N \rightarrow \pi\Sigma$ which agree very well with SU(3). For four point functions there are major discrepancies when a naive comparison is made with SU(3), but this is well understood in terms of kinematic effects induced by SU(3) breaking on the masses of exchanged particles or on thresholds and barrier factors.[11]

Combining the SU(2) of quark spin with SU(3) gives one an SU(6)--usually called $SU(6)_S$ where S stands for spin. In a non-relativistic picture of quarks bound in a spin and SU(3) independent potential, with total orbital angular momentum L, one could classify the bound states in terms of $SU(6) \times O(3)$. Much investigation a decade ago showed that SU(6) <u>cannot</u> be a true symmetry in a relativistic theory.[12] Nevertheless, it has increasingly proven to be a very useful algebra with which to classify the hadron states we observe. Although other theoretical approaches (e.g. the bootstrap) presumably have some applicability to hadron spectroscopy, and may well be complementary, it is the quark model which up to now has shown the most promise of a general and basic understanding of the subject. In the following, we shall examine in some detail the consequences of such a quark viewpoint as a basis of both hadron spectroscopy and transitions.

The quark model rules for constructing states go as follows. Mesons are constructed out of a $q\bar{q}$ pair. Adding internal orbital angular momentum, $\vec{L}$, to the quark spin, $\vec{S}$, gives the total $\vec{J}$ of the state. As quarks have spin 1/2, S can only take the values 0 and 1. Given that quarks are in the basic 6 representation of SU(6), and antiquarks in a $\bar{6}$, all meson states are then in the representations contained in $6 \times \bar{6} = 35 + 1$. These have the SU(3) and quark spin content:

$$\begin{array}{rl} 35: & 8 \text{ of } SU(3) \text{ with } S = 1 \\ & 8 \text{ of } SU(3) \text{ with } S = 0 \\ & 1 \text{ of } SU(3) \text{ with } S = 1 \\ 1: & 1 \text{ of } SU(3) \text{ with } S = 0\ . \end{array} \qquad (1)$$

Since fermion and antifermion have opposite intrinsic parity, one has $P = (-1)^{L+1}$ for the $q\bar{q}$ state. For neutral, non-strange mesons, $C = (-1)^{L+S}$ and $G = (-1)^{L+S+I}$.

With these rules there are two kinds of meson states which cannot be formed, i.e., exotic meson states:

1. SU(3) exotics--only 1 and 8 representations of SU(3) are allowed. The 10, $\overline{10}$ and 27 representations, for example, are exotic.
2. CP exotics--only CP = +1 natural spin parity ($J^P = 0^+, 1^-, 2^+, \ldots$) states are allowed. There is no state with $J^{PC} = 0^{--}$.

Up to this point, neither type of exotic meson has been found.[13]

For baryons one constructs states from three quarks with a wave function which has overall symmetry in SU(3), L, and S. The antisymmetry expected for fermions may be avoided by postulating quarks to be parafermions[6] (of rank 3), or more simply, by introducing the new quantum number of color.[14] Insisting that all hadrons are singlets under the SU(3)' of color forces the three fermion quarks in a baryon into an antisymmetric 1 representation of color, leaving the remaining part of the wave function to be symmetric.

From the standpoint of SU(6) one would then expect baryons to fall in the representations spanned by $6 \times 6 \times 6 = 56 + 70 + 70 + 20$, whose SU(3) and total quark spin S content are given by:

56: (symmetric)	: 8 of SU(3) with $S = 1/2$	
	10 of SU(3) with $S = 3/2$	
70: (mixed symmetry)	: 1 of SU(3) with $S = 1/2$	
	8 of SU(3) with $S = 1/2$	
	10 of SU(3) with $S = 1/2$	(2)
	8 of SU(3) with $S = 3/2$	
20: (antisymmetric)	8 of SU(3) with $S = 1/2$	
	1 of SU(3) with $S = 3/2$	

The parity will be simply given by $P = (-1)^L$. Since only the 1, 8, and 10 representations of SU(3) are contained above, any other representation (e.g. $\overline{10}$, 27) is exotic for baryons. Evidence for exotic baryons is not conclusive.[15]

III. MESON STATES

Let us then proceed to see how the known meson states compare with the SU(6) × O(3) picture outlined above. We do so with the vague idea that any reasonable "potential" will have states with small values of L lying lowest.

For $L = 0$ we expect $35 + 1$ states, all with parity $P = -1$, including $8 + 1$ vector and $8 + 1$ pseudoscalar mesons. The observed lowest mass mesons exactly fill this multiplet structure as shown[16] in Table I. As is well known, the physical ω and φ are mixtures of the octet and singlet states with a "magic" mixing angle $\theta = \cos^{-1}(2/3)$. The η may also be slightly mixed with the η' or higher mass states. Another candidate for the slot occupied by the η' (or mixed with it) is the E (1422). Although it is usually forgotten, it is entirely non-trivial that the lowest mass mesons have negative parity and that exactly those states required by the quark model are found, and no more!

TABLE I

Meson States with $L = 0$

SU(6)	SU(3)	S	J^{PC}	States[17]
35	8	0	0^{--}	π (140) K (495) η (550)
35	8 + 1	1	1^{--}	ρ (770) K^* (890) ω (784) φ (1020)
1	1	0	0^{--}	probably mainly η' (958)

The next principal set of states we expect are those with $L = 1$, all of which have positive parity. We first examine those with quark spin $S = 1$, shown in Table II. The B is now well established[18] from massive π^+p bubble chamber experiments and has $\pi\omega$ as a main decay mode. None of the other states is established, with the K^* state being lost in the non-resonant

"Q-bump" in $K^{\pm}N$ reactions. However, SU(3) tells us that the rest of the octet had better be there. Nondiffractive processes are the obvious place to look. The H and/or H' may be very broad (decaying into $\pi\rho$), and correspondingly difficult to find.[19]

TABLE II

Meson States[17] with L = 1 and S = 0

SU(6)	SU(3)	S	J^{PC}	States
35	8	0	1^{+-}	B (1235) K^* (1320?)
1	1	0	1^{+-}	H ? } may be mixed H' ?

The S = 1 states with L = 1 are even more problematic, as shown in Table III.

TABLE III

Meson States[17] with L = 1 and S = 1

SU(6)	SU(3)	S	J^{PC}	States
35	8 + 1	1	2^{++}	A_2 (1310) K^* (1420) f (1270) f' (1514)
35	8 + 1	1	1^{++}	A_1 (1100?) K^* (1240?) D (1285) D' ?
35	8 + 1	1	0^{++}	δ (970) K^* (1300?) ϵ (700) ? S^* (997) ϵ' (1300) ?

Here the $J^{PC} = 2^{++}$ states are all found, with the f and f' again being mixed octet and singlet states like the ω and φ. The 1^{++} states are an embarassment with only the D now well established. The famous A_1 and its K^* SU(3) partner are not found as resonances in the dominantly diffractive reactions $\pi p \to (3\pi)p$ or $Kp \to (K\pi\pi)p$. While there are hints of a $K\pi\pi$ state at ~ 1240 MeV in $\bar{p}p$ annihilations and in $\pi^- p \to (K\pi\pi)\Lambda$, these results are not conclusive by any means. A much more intensive look at nondiffractive channels is needed to search for these states, and in the process we should not be prejudiced by the "masses" for the corresponding diffractively produced non-resonant bumps.

The scalar mesons[18] are in fair shape now that the δ (970) is established, with $\pi\eta$ as principle decay mode. With the s-wave $K\pi$ phase shift rising through 90° at ~ 1300 MeV, it seems likely there is an appropriate K^* near that mass. At present there are too many I = 0 candidates, although both the ϵ and ϵ' may not survive as resonant states. One possibility, explored by Morgan,[20] is to form the scalar octet plus singlet out of δ, K^*, S^* and ϵ', with the S^* and ϵ' mixed.

Candidates to fill out the L = 2 multiplets are lacking in most cases. As seen in Table IV, only the 3^{--} states have been mostly established. The K^* (1800) has only recently been established by a SLAC group investigating $K\pi$ scattering.[21] The assignment, and even existence, of the F_1, ρ', and A_3 is somewhat speculative.

There are hints of a few other multiplets for mesons.[22] One possibility is a radial excitation of the ground state 35 + 1 with L = 0. Candidates for this include the E (1420) and a proposed ρ' (1250) or the ρ' (1600). Note that given the quark model, not only does the proposal of a new state require in general the remainder of its SU(3) multiplet be found, but all of its SU(6) partners. Here one needs to see a π', an ω', a φ', etc.--a nontrivial requirement which should make one somewhat skeptical on the existence of all these unseen states.

TABLE IV

Meson States[17] with L = 2

SU(6)	SU(3)	S	J^{PC}	States
35	8 + 1	1	3^{--}	g (1680) K^* (~ 1800) ω_3 (1675) φ_3 (?)
35	8 + 1	1	2^{--}	F_1 (1540)? ?
35	8 + 1	1	1^{--}	ρ' (1680) ? ?
35	8	0	2^{-+}	A_3 (1640) ? ?
1	1	0	2^{-+}	?

At still higher mass there is now evidence[18] from $\pi\pi \to K\bar{K}$ for the first of the 4^{++} states expected for L = 3. And then there are indications from $\bar{p}p$ reactions for bumps in the T (2190) and U (2360) regions. The particularly interesting possibility of towers of states has been raised from a recent analysis[23] of $\bar{p}p \leftrightarrow \pi\pi$, although evidence could already be deduced[24] for this from the spectrum of states at lower mass. How and if the quark model states coexist with a pattern of towers or of Regge daughter states is one of many unsettled questions concerning the spectrum of hadron states.

IV. BARYON STATES

Because of extensive phase shift analyses, baryon spectroscopy is a much richer experimental area with which to compare our theoretical expectations. Even so, only the nucleon resonances below about 2 GeV in mass can be said to have been investigated with any claim of completeness. As such, we shall only list N^* candidates for each SU(3) multiplet, with the exception of the ground state. The Y^*'s are still only in fair shape, while the status of Ξ^*'s can only be described as poor.

The full set of states in the ground state 56 with L = 0 was completed ten years ago with the discovery of the Ω^-. They appear[16] in Table V.

TABLE V

Baryons in the 56 L = 0 Ground State

SU(6)	SU(3)	S	J^P	States[17]
56	8	1/2	$1/2^+$	N (940) Λ (1115) Σ (1193) Ξ (1317)
56	10	3/2	$3/2^+$	Δ (1232) Σ^* (1385) Ξ^* (1530) Ω^- (1672)

The next highest mass states observed all have negative parity, as befits L = 1, and they fit nicely into a 70 of SU(6). As Table VI shows, the established negative parity N^*'s below 2 GeV provide all the candidates for the SU(3) and J^P multiplets in a 70 L = 1 with no omissions or additions. Mixing of the two $J^P = 1/2^-$ N^*'s, $3/2^-$ N^*'s, and three $1/2^-$ Λ^*'s, $3/2^-$ Σ^*'s, etc., can, and presumably does, take place. A recent discussion of candidates for the Y^* states (most of which are now known) and the possible mixings can be found in Cashmore et al.[25]

Also essentially complete in having candidates for all the nonstrange states is a 56 with L = 2 and P = +1, as shown in Table VII.

TABLE VI

Non-Strange Baryons in the 70 L = 1

SU(6)	SU(3)	S	J^P	States
70	1	1/2	$1/2^-$	[Λ^* (1405)]
			$3/2^-$	[Λ^* (1520)]
	8	1/2	$1/2^-$	S_{11} (1535)...
			$3/2^-$	D_{13} (1520)...
	10	1/2	$1/2^-$	S_{13} (1650)...
			$3/2^-$	D_{33} (1670)...
	8	3/2	$1/2^-$	S_{11} (1700)
			$3/2^-$	D_{13} (1700)...
			$5/2^-$	D_{15} (1670)...

TABLE VII

Baryons in the 56 with L = 2

SU(6)	SU(3)	S	J^P	States[17]
56	8	1/2	$5/2^+$	F_{15} (1688)...
			$3/2^+$	P_{13} (1810)...
	10	3/2	$7/2^+$	F_{37} (1950)...
			$5/2^+$	F_{35} (1890)...
			$3/2^+$	P_{33} (~1900 ?)...
			$1/2^+$	P_{31} (1910)...

The remaining P_{33} state below 2 GeV we classify with the Roper resonance as forming a radially excited 56 with L = 0 (Table VIII).

TABLE VIII

Baryons in a radially excited 56 with L = 0

SU(6)	SU(3)	S	J^P	States[17]
56	8	1/2	$1/2^+$	P_{11} (1470)...
	10	3/2	$3/2^+$	P_{33} (1690)...

We do this both for reasons of mass and because of inelastic amplitude signs, to be discussed later.

Some other possible multiplets can be proposed on the basis of picking through the relatively few nonstrange baryon states remaining in the tables.[17] First, the P_{11}(1780) probably belongs in a second radially excited 56 L = 0. This requires finding yet another P_{33} state, presumably around 2100 MeV, to be its non-strange companion in a 56.

There are several negative parity states in the 2000-2200 MeV range which are good candidates for members of a 70 L = 3 multiplet. In particular the G_{17} (2190) and D_{15} (2100) states fit the S = 1/2 octet slots in such a multiplet, while the D_{35} (1960) and an undiscovered G_{37} state could be the decuplet S = 1/2 members. That leaves D_{13}, D_{15}, G_{17}, and G_{19} states to be found, presumably several hundred MeV higher in mass, to fit into the required S = 3/2 octets.

There are also several candidates for a radially excited 70 L = 1 multiplet in the same region. The D_{13} (2040) and S_{11} (2100) fit in as the octet S = 1/2 states. The S_{31} (1900) and a D_{33} would be in the S = 1/2 decuplet, leaving S_{11}, D_{13}, and D_{15} states to be found at ~ 2200 MeV to fill the octets with S = 3/2.

As for higher mass positive parity states, there is the beginning of a 56 L = 4 multiplet containing the H_{19}(2200) and F_{17}(1990) as octet S = 1/2 members, and the $H_{3,11}$(2420) as the highest spin Δ^*, with H_{39}, F_{37}, and F_{35} states yet to be found for the remaining $S = 3/2$ slots. Finally another F_{15} state at ~ 2000 MeV would be the beginning of a radially excited 56 $L = 2$ multiplet.

On looking back over the above classification of baryons into multiplets there is an obvious pattern:[15,22] 56 representations have even L, 70 representations odd L. While one could classify the observed states in a way which breaks this "rule," they fit it well and there is no compelling reason to do so. Note that this "rule" and the baryon spectrum are then not consistent with the states expected from a three dimensional harmonic oscillator potential where, for example, one expects[6] a 70 $L = 2$, 70 $L = 0$, 56 $L = 0$, and 20 $L = 1$ in the same mass region as the 56 $L = 2$. If the spectrum of baryons is as simple as it now seems to be, one hopes there would be a deeper reason for that simplicity. Another interesting way of looking at the $I = 1/2$ N^* states we have been discussing is shown in Fig. 1. Is it possible we have a tower structure developing? And if so, as for mesons, what is its relation to the quark model picture we have been discussing?

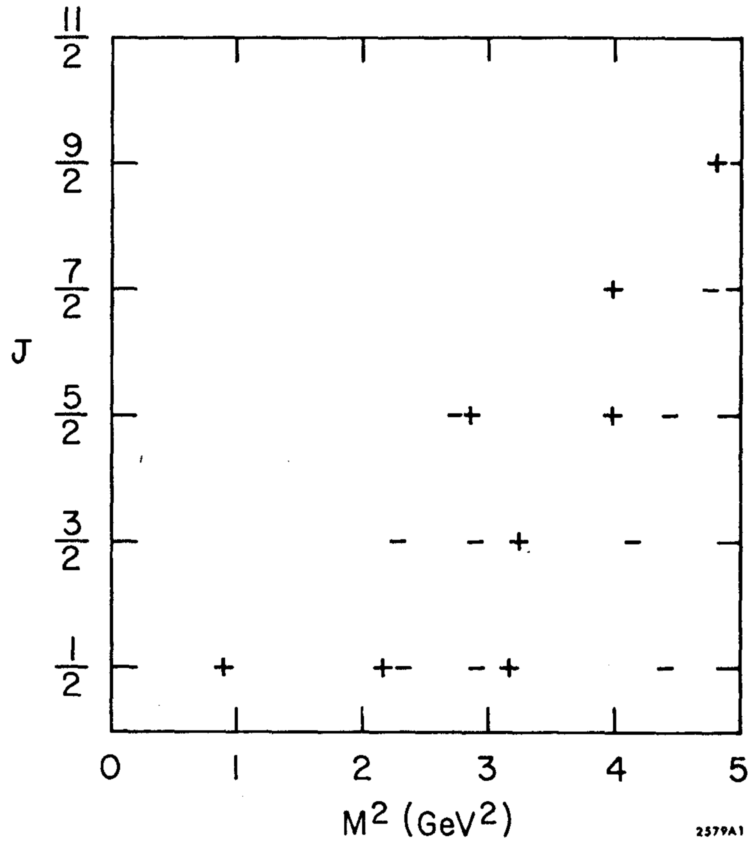

Figure 1

Spins vs. mass squared for the known $I = 1/2$ N^* resonances. Positive (negative) parity states are denoted by + (-).

V. TRANSITIONS AMONG HADRONS

Given the spectroscopy of hadrons in terms of quark constituents which we have built up in the preceeding sections, we now turn to transitions between these states. We restrict ourselves to matrix elements of currents at $q^2 = 0$. For the vector current, such matrix elements are directly related to the amplitudes for one photon decay or excitation. The axial-vector current presents more of a problem in that few weak axial-vector transitions are measured. But via the PCAC hypothesis,[26] one may relate such matrix elements to pion amplitudes, which are the mainstay of strong interaction decays.

However, to be able to carry out a calculation of such matrix elements we must actually solve two problems at once. First, we must understand the currents, their symmetry properties, and commutation relations. Second, we must understand hadron spectroscopy, how different hadron states are related, and how these currents "flow" inside them. These two problems in fact have been partially solved in recent times by relating them, i.e. by finding a *transformation* between the quarks *seen* by currents and those which we used earlier as the building blocks of hadrons.

The result is an approximate theory of photon and pion transition matrix elements within the context of the quark model. The theory yields many relations among decay widths and predicts with great success the relative amplitude signs in inelastic processes like $\pi N \to N^* \to \pi\Delta$ and $\gamma N \to N^* \to \pi N$. The agreement with experiment that is found leads one to have further confidence in the quark model for spectroscopy, particularly if the assignment of observed resonances to the states in the model, and lends support as well to the theory of current-induced transitions.

VI. CURRENTS AND QUARKS

In order to formulate a theory of current-induced-transitions among hadrons composed of quarks we need a group theoretic frame work for labeling the states and operators involved. For this purpose it is natural to turn to an algebra of charges formed by integrating weak and electromagentic current densities over all space.

To start with, consider vector and axial-vector charges:

$$Q^{\alpha}(t) = \int d^3x \, V_0^{\alpha}(\vec{x},t) \tag{3a}$$

$$Q_5^{\alpha}(t) = \int d^3x \, A_0^{\alpha}(\vec{x},t) \tag{3b}$$

where α is an SU(3) index which runs from 1 to 8 and $V_\mu^{\alpha}(\vec{x},t)$ and $A_\mu^{\alpha}(\vec{x},t)$ are the local vector and axial-vector current densities with measurable matrix elements. The vector charges are just the generators of SU(3). These integrals over the time components of the current densities are assumed to satisfy the equal-time commutation relations proposed by Gell-Mann[8]

$$\begin{aligned}
[Q^{\alpha}(t), Q^{\beta}(t)] &= if^{\alpha\beta\gamma} Q^{\gamma}(t) \\
[Q^{\alpha}(t), Q_5^{\beta}(t)] &= if^{\alpha\beta\gamma} Q_5^{\gamma}(t) \\
[Q_5^{\alpha}(t), Q_5^{\beta}(t)] &= if^{\alpha\beta\gamma} Q^{\gamma}(t) \, ,
\end{aligned} \tag{4}$$

where $f^{\alpha\beta\gamma}$ are the structure constants of SU(3). Sandwiched between nucleon states at infinite momentum, the last of Eqs. (4) gives rise to the Adler-Weisberger sum rule.[27] From this point on, we shall always be considering matrix elements to be taken between hadron states[28] with $p_z \to \infty$.

For the purposes at hand we need a somewhat larger algebraic system then that provided by the measurable vector and axial-vector charges in Eqs. (3), which form the algebra of SU(3) × SU(3) according to Eqs. (4). To obtain the larger algebra we adjoin to the integrals over all space of[29] $V_0^\alpha(\vec{x},t)$ and $A_z^\alpha(\vec{x},t)$, those of the tensor current densities $T_{yz}^\alpha(\vec{x},t)$ and $T_{zx}^\alpha(\vec{x},t)$. In the free quark model these charges have the form:

$$\begin{aligned}
\int d^3x\, V_0^\alpha(\vec{x},t) &\sim \int d^3x\, \psi^+(x)\, (\tfrac{\lambda^\alpha}{2})\, \mathbb{1}\, \psi(x) \\
\int d^3x\, A_z^\alpha(\vec{x},t) &\sim \int d^3x\, \psi^+(x)\, (\tfrac{\lambda^\alpha}{2})\, \sigma_z\, \psi(x) \qquad (5) \\
\int d^3x\, T_{yz}^\alpha(\vec{x},t) &\sim \int d^3x\, \psi^+(x)\, (\tfrac{\lambda^\alpha}{2})\, \beta\sigma_x\, \psi(x) \\
\int d^3x\, T_{zx}^\alpha(\vec{x},t) &\sim \int d^3x\, \psi^+(x)\, (\tfrac{\lambda^\alpha}{2})\, \beta\sigma_y\, \psi(x)
\end{aligned}$$

where $\psi(x)$ is the Dirac (and SU(3)) spinor representing the quark field. When commuted using the free quark field commutation relations, these charges act algebraically like the product of SU(3) and Dirac matrices $(\lambda^\alpha/2)\mathbb{1}$ $(\lambda^\alpha/2)\sigma_z$, $(\lambda^\alpha/2)\beta\sigma_x$, and $(\lambda^\alpha/2)\beta\sigma_y$ respectively.[30] The Dirac matrices $\beta\sigma_x$, $\beta\sigma_y$, and σ_z form the so-called W-spin.[31] They are invariant under boosts in the z-direction and the corresponding charges are "good," in the sense that they have finite (generally non-vanishing) matrix elements between states as $p_z \to \infty$. This makes them the correct set of charges to use to label states in terms of their internal quark spin components. If we let $\alpha = 0$ correspond to the SU(3) singlet representation (and λ^0 be a multiple of the unit matrix), then Eqs. (5) consists of 36 charges which close under commutation. They act like an identity operator plus 35 other generators of an SU(6) algebra. We call this algebra the $SU(6)_W$ of currents[30] because of its origin. Q^α and Q_5^α then essentially[29] form a chiral SU(3) × SU(3) subalgebra of this larger algebra.

Given such an algebra, we define the smallest representations of it (other than the singlet), the 6 and $\bar{6}$ representations, as the current quark (q) and current antiquark $(\bar{q})$ respectively. We may build up all the larger representations of $SU(6)_W$ out of these basic ones.

Can then real baryons be written as three current quarks, qqq, and real mesons as current quark and antiquark, $q\bar{q}$, with internal angular momentum L, as in the constituent quark model used for hadron spectroscopy? While possible in principle, it is a disaster when compared with experiment. For it leads to $g_A = 5/3$, zero anomalous magnetic moment of the nucleon, no electromagnetic transition from the nucleon to the 3-3 resonance (Δ), no decay of ω to $\gamma\pi$, etc. It would also yield results for masses like $M_N = M_\Delta$, $M_\pi = M_\rho$, etc. The hadron states we see cannot be simple in terms of current quarks. They must lie in mixed representations of the $SU(6)_W$ of currents. Work in past years has shown directly that hadron states are quite complicated when viewed in terms of current algebra.[32]

We may restate this complication in terms of the definition of an operator V for any hadron:

$$\begin{aligned}
|\text{Hadron}\rangle &\equiv V|\text{simple } qqq \text{ or } q\bar{q} \text{ state of current quarks}\rangle \\
&= |\text{simple } qqq \text{ or } q\bar{q} \text{ state of constituent quarks}\rangle \qquad (6)
\end{aligned}$$

All the complication of real hadrons under the $SU(6)_W$ of currents (i.e., in terms of current quarks) has been swept into the operator V. On the other hand, real hadrons are supposed to be simple in terms of the "constituent quarks" used for spectroscopy purposes, as indicated by the second equality in Eq. (6). In other words, the transformation V connects the two simple descriptions in terms of current quarks and constituent quarks.[33] It is for this reason that it is sometimes called the "transformation from current to constituent quarks."[34,35]

Up to this point we have only managed to restate the problem via Eq. (6). But as often happens, phrasing the problem right is a major way toward the solution. For what we are after in the end are matrix elements of various current operators, $\mathcal{O}$. Using Eq. (6) and assuming V is unitary we may write

$$\langle \text{Hadron}' | \mathcal{O} | \text{Hadron} \rangle$$

$$= \langle (\text{simple current quark state})' | V^{-1} \mathcal{O} V \, | (\text{simple current quark state}) \rangle \tag{7}$$

This has two important advantages. First, we may study the properties of $V^{-1}\mathcal{O}V$ in isolation, and then apply what we learn to the matrix elements of $\mathcal{O}$ between any two hadron states. Second, even though V itself is very complicated and contains (by definition) all information on the current quark composition of each hadron, it is possible that the object $V^{-1}\mathcal{O}V$ for some operators $\mathcal{O}$ may be relatively simple in its algebraic transformation properties.

This last possibility is of course exactly what we shall assume on the basis of calculations done in the free quark model. In that model, Melosh[36] and others[37,38,39] have been able to formulate and explicitly calculate the transformation V. While one would not take the details of the transformation found there as correctly reflecting the real world, one might try to abstract the algebraic properties of some transformed operators $V^{-1}\mathcal{O}V$, from such a calculation. In cases of interest, this turns out to be equivalent to assuming that the transformed operators $V^{-1}\mathcal{O}V$ have the algebraic properties of the most general combination of single quark operators consistent with SU(3) and Lorentz invariance.

Thus, while Eq. (5) shows that Q_5^α itself behaves under the $SU(6)_W$ of currents as simply

$$\int d^3x \, \psi^+(x) \left(\frac{\lambda^\alpha}{2}\right) \sigma_z \, \psi(x) \, ,$$

a direct calculation in the free quark model shows that algebraically $V^{-1}Q_5^\alpha V$ behaves as a sum of two terms.[40]

$$V^{-1} \, Q_5^\alpha \, V$$

$$\sim \left(\frac{\lambda^\alpha}{2}\right) \sigma_z + \left(\frac{\lambda^\alpha}{2}\right) \left[(\beta\sigma_x + i\beta\sigma_y)(v_x - iv_y) - (\beta\sigma_x - i\beta_y)(v_x + iv_y)\right] \, , \tag{8}$$

where the products of Dirac and SU(3) matrices are understood to be taken between quark spinors (and integrated over all space). Here v_μ is a vector in configuration space, so that $v_x \pm iv_y$ raises (lowers) the z component of angular momentum (L_z) by one unit. The particular combination of Dirac matrices and vector indices in the two terms in Eq. (8) is dictated by the demands that the total $J_z = 0$ and the parity be odd for the axial-vector charge, Q_5^α, and for $V^{-1} \, Q_5^\alpha V$.

For the vector charge, Q^α, we must have

$$V^{-1}Q^\alpha V = Q^\alpha \, , \tag{9}$$

since we want these charges to be the generators of SU(3), both before and after the transformation. However, the first moment of the charge density,[41]

$$D_+^\alpha = i \int d^3x \left(\frac{-x-iy}{\sqrt{2}} \right) V_0^\alpha(\vec{x},t) \, , \tag{10}$$

is not a generator and is transformed non-trivially by V. One finds in the free quark model that in algebraic properties $V^{-1} \, D_+^\alpha V$ behaves as a sum of four terms under the $SU(6)_W$ of currents:[42]

$$V^{-1}D_+^\alpha V$$

$$\sim (\frac{\lambda^\alpha}{2})\, \mathbb{I}(v_x + iv_y) + (\frac{\lambda^\alpha}{2})\,(\beta\sigma_x + i\beta\sigma_y) + (\frac{\lambda^\alpha}{2})\,\sigma_z(v_x + iv_y)$$

$$+ (\frac{\lambda^\alpha}{2})\,(\beta\sigma_x - i\beta\sigma_y)(v_x + iv_y)(v_x + iv_y)\ , \tag{11}$$

where again the Dirac and SU(3) matrices are understood to be taken between quark spinors.

We abstract the algebraic properties of $V^{-1}Q_5^\alpha V$ and $V^{-1}D_+^\alpha V$ given in Eqs. (8) and (11) from the free quark model and assume them to hold in the real world. We are then able to treat matrix elements of Q_5^α and D_+^α between hadron states as follows:

(1) We identify the hadrons with qqq or $q\bar{q}$ states of the constituent quark model where the total quark spin S is coupled to the internal angular momentum L to form the total J of the hadron. The states so constructed fall into $SU(6)_W \times O(3)$ multiplets.

(2) Since very few weak axial-vector transitions are measured, given a matrix element of Q_5^α, we use PCAC to relate it to a measured pion transition amplitude. Application of the golden rule then yields:

$$\Gamma(H' \to \pi^- H) = \frac{1}{4\pi f_\pi^2}\,\frac{p_\pi}{2J'+1}\,\frac{(M'^2 - M^2)^2}{M'^2}\,\sum_\lambda |\langle H',\lambda|\ (1/\sqrt{2})\ (Q_5^1 - iQ_5^2)|\ H,\lambda\rangle|^2\ , \tag{12}$$

where $f_\pi \simeq 135$ MeV. The factors in Eq. (12) are forced on us by PCAC and kinematics--there are no arbitrary phase space factors.

For real photon transitions, matrix elements of $D_+^3 + (1/\sqrt{3})D_+^8$ are directly proportional to the corresponding Feynman amplitudes. The width for $H' \to \gamma H$ is given by[41]

$$\Gamma(H' \to \gamma H) = \frac{e^2}{\pi}\,\frac{p_\gamma^3}{2J'+1}\sum_\lambda |\langle H',\ \lambda|\ D_+^3 + (1/\sqrt{3})\ D_+^8|H,\ \lambda-1\rangle|^2\ . \tag{13}$$

(3) Given a matrix element of Q_5^α or D_+^α between hadron states which is related to measurements by either Eq. (12) or (13), we transform using V from simple constituent to simple current quark states. The particular matrix element is thus rewritten in terms of $V^{-1}Q_5V$ or $V^{-1}D_+V$, and simple current quark states. We know the algebraic properties of all these quantities under the $SU(6)_W$ of currents via abstraction of Eqs. (8) and (11) from the free quark model and our identification of hadrons with quark model states. We may then apply the Wigner-Eckart theorem to each term to express it as a Clebsch-Gordan coefficient[43] (of $SU(6)_W$) times a reduced matrix element. Since the same reduced-matrix element occurs in many different transitions, relations among the corresponding transition amplitudes follow.

VII. CONSEQUENCES FOR TRANSITION AMPLITUDES

The experimental consequences of the theory outlined in the last section have been considered by a number of authors.[36,44-53] These consequences fall into the following three categories:

(1) Selection Rules. For transitions by pion or photon emission from states (either mesons or baryons) with internal angular momentum L' to those with L, one finds[46,47]

$$\big||L' - L| - 1\big| \le \ell_\pi \le L + L' + 1 \tag{14a}$$

$$\big||L' - L| - 1\big| \le j_\gamma \le L + L' + 1\ , \tag{14b}$$

where ℓ_π and j_γ are the total angular momentum carried off by the pion and photon in the overall transition.

For example, ℓ_π can be 0 or 2 ($\ell_\pi = 1$ is forbidden by parity), but not 4 for a pion decay from $L' = 1$ to $L = 0$. Thus the decay of the $D_{15}(1670)$, the $J^P = 5/2^- N^*$ resonance with $L' = 1$, into $\pi\Delta$ is forbidden in g-wave ($\ell_\pi = 4$), although otherwise allowed by kinematical considerations. Similarly, only $j_\gamma = 1$ is allowed for $L' = 0$ to $L = 0$ photon transitions, although

$j_\gamma = 2$ (and even $j_\gamma = 3$ for $\Delta' \to \gamma\Delta$) is generally permitted by kinematics. This particular rule is well-known for $\Delta \to \gamma N$, where it is just the successful quark model result[54] that the transition is purely magnetic dipole in character, i.e. the possible electric quadrupole amplitude is forbidden. The inequalities in Eqs. (14) might be regarded as the generalization of these particular results to all L and L' in the present theoretical context.

Note that for $|L - L'| \geq 3$ the lower limit of the inequalities becomes operative in a non-trivial way, forbidding low values of ℓ_π or j_γ which would otherwise have been favored kinematically. Unfortunately, the relevant hadron states which would provide an interesting test of this have not yet been found.

Selection rules of a different sort govern the number of independent reduced matrix elements. For pion transitions from a hadron multiplet with internal angular momentum L' down to the ground state hadrons with $L = 0$, there are at most two independent reduced matrix elements, corresponding to the two terms in Eq. (8). For real photon transitions between the same two multiplets there are at most four independent reduced matrix elements, corresponding to Eq. (11).

In general structure, the theory described above includes various concrete quark model calculations, both non-relativistic[55] and relativistic.[56] In fact, a one-to-one correspondence exists between the quantities calculated in such models and the reduced matrix elements in the present theory. However, such models are usually much more specific, with parameters like the strength of the "potential," quark masses, etc. fixed. Since the quantities corresponding to reduced matrix elements are expressed explicitly in terms of such parameters, they are computable numerically and the scale of the reduced matrix elements is determined.

Also included in the general structure of the theory are the results following from assuming strong interaction $SU(6)_W$ conservation.[31] For pion transitions, this corresponds in the present theory to retaining only the first term in $V^{-1}Q_5^\alpha V$. Since this hypothesis fails experimentally, various ad hoc schemes for breaking $SU(6)_W$ have been proposed.[57] Such schemes still fall within the general structure of amplitudes presented above,[58] and they are similar in giving relations between amplitudes while not setting their absolute scale.[59] However, as we shall see below, they are generally more restrictive in that they tie together pion and rho decay amplitudes.

(2) Decay Widths. The simplest such set of relations are those for pion transitions from $L' = 0$ to $L = 0$ mesons. Here there is only one reduced matrix element (the second term in Eq. (6) has $\Delta L_z = \pm 1$ and so cannot contribute when $L' = L = 0$), so that the amplitudes for $\rho \to \pi\pi$, $K^*(890) \to \pi K$, and $\omega \to \pi\rho$ are all proportional. The ratio of the amplitudes for the first two processes may be obtained from $\Gamma(\rho \to \pi\pi)/(K^* \to \pi K)$, while the amplitude for the latter is obtainable from $\omega \to 3\pi$ and rho dominance. Within errors, the ratio of the three amplitudes is that predicted by the theory.[60]

For pion transitions from mesons with internal angular momentum $L' = 1$ to those with $L = 0$, both terms in Eq. (8) are possible and there are consequently two independent reduced matrix elements which describe all such decays. Rather than performing a fit to all the data, we choose two measured widths as input and thereby determine all the other decay rates. For this purpose we take $\Gamma(A_2 \to \pi\rho) = 71.5$ MeV, from the latest particle data tables,[17] and $\Gamma_{\lambda=0}(B \to \pi\omega) = 0$. This latter condition, the vanishing of the helicity zero (longitudinal) decay of $B \to \pi\omega$, is suggested by high statistics experiments[61] which find the transverse decay to be strongly dominant. While probably not exactly zero, we take this as a very reasonable first approximation to the data. Exact vanishing of $\Gamma_{\lambda=0}(B \to \pi\omega)$ corresponds to only the second term in $V^{-1}Q_5^\alpha V$, with the algebraic properties of $(\lambda^\alpha/2)[(\beta\sigma_x+i\beta\sigma_y)(v_x-iv_y) - (\beta\sigma_x-i\beta\sigma_y)(v_x + iv_y)]$, having a non-zero reduced matrix element. This well illustrates the experimental necessity of a non-trivial transformation V; for if $V = \mathbb{1}$, only the term behaving as $(\lambda^\alpha/2)\sigma_z$ would be present and the predicted helicity structure for $B \to \pi\omega$ would be completely opposite that observed.

The results[62] can be seen in Table IX. The correct values for $\Gamma(A_2 \to \pi\rho)/\Gamma(K^*(1420) \to \pi K^*)$ and $\Gamma(f \to \pi\pi)/\Gamma(K^*(1420) \to \pi K)$ may be regarded as testing the SU(3) component of the theory, while, for example, the value of $\Gamma(A_2 \to \pi\rho)$ or $\Gamma(K^*(1420) \to \pi K^*)$ relative to $\Gamma(f \to \pi\pi)$, $\Gamma(K^*(1420) \to \pi K)$ or $\Gamma(A_2 \to \pi\eta)$ tests the full theory, including the phase space factors in Eq. (12), since one is relating d-wave pion decays into pseudoscalar vs. vector mesons. As for the other decays in the table, we note that: (a) other strong interaction decay modes of the B meson very likely exist, although $\pi\omega$ is certainly dominant; (b) the "real" A_1 resonance still remains to be found for comparison with the theory; (c) the now established $I = 1$ scalar meson, δ, only has $\pi\eta$ as a possible strong decay channel, so the total width should almost coincide with that into $\pi\eta$; (d) we have chosen 1300 MeV, the mass where the s-wave πK phase shift goes through 90°, as the mass of the strange, $J^P = 0^+$ meson.[63] The overall agreement found in Table IX between theory and experiment is quite good, with the exception of $\Gamma(A_2 \to \pi\eta')$. While mixing of the pseudoscalar mesons is such as to alleviate this discrepancy, reasonable mixing angles do not change the width appreciably from the value in Table IX. A more likely source of trouble lies in the theoretical assignment of the η' to be dominantly that SU(3) singlet pseudoscalar meson associated with the octet containing the pion and eta. In any case, an actual measurement of the $A_2 \to \pi\eta'$ decay width, rather than an upper limit, would be an interesting quantity to determine experimentally.

For $L' = 2$ mesons decaying by pion emission to the $L = 0$ states, there are again two independent reduced matrix elements. About the only decay width determined with any certainty is $g \to \pi\pi$. The meagre information available on other decays is consistent with the theory within the large experimental errors.[47]

For photon decays of mesons the data are even more sparse, although there are plenty of theoretical predictions.[52] In fact, only a few decays among $L' = 0$ mesons are actually measured, where there is just one possible reduced matrix element. Fixing this from $\Gamma(\omega \to \gamma\pi)$, the predictions[64] are collected in Table X. What widths have been measured are consistent with the predictions of the theory, although at the limits of the error bars in several cases.

TABLE IX

Decays of $L' = 1$ Mesons to $L = 0$ Mesons by Pion Emission.[62]

Decay	Γ(predicted) (MeV)	Γ(experimental)[17] (MeV)
$A_2(1310) \to \pi\rho$	71.5 (input)	71.5 ± 8
$K^*(1420) \to \pi K^*$	27	29.5 ± 4
$f\ (1270) \to \pi\pi$	112	141 ± 26
$K^*(1420) \to \pi K$	55	55 ± 6
$A_2(1310) \to \pi\eta$	16	15 ± 2
$A_2(1310) \to \pi\eta'$	5	< 1
$B\ (1235) \to \pi\omega$, $\lambda = 0$	0 (input)	$\Gamma_{total} = 120 \pm 20$
$\lambda = 1$	75	$\pi\omega$, with $\lambda = 1$ strongly dominant, only mode seen
$A_1(1100) \to \pi\rho$, $\lambda = 0$	63	??
$\lambda = 1$	31	
$\delta\ (970) \to \pi\eta$	41	50 ± 20
$\kappa(1300) \to \pi K$	380	?, broad

TABLE X

Decays of $L' = 0$ Mesons to Other $L = 0$ Mesons by Photon Emission

	Γ(predicted) no mixing (KeV)	Γ(predicted) $\theta_p = -10.5°$ (KeV)	Γ(experimental)[17] (KeV)
$\omega \to \gamma\pi$	870 (input)	870 (input)	870 ± 60
$\rho \to \gamma\pi$	92	92	$30 \pm 10 \leq \Gamma \leq 80 \pm 10$ (Ref. 65)
$\varphi \to \gamma\pi$	0	0	< 14
$\rho \to \gamma\eta$	36	56	< 160
$\omega \to \gamma\eta$	5	7	< 50
$\varphi \to \gamma\eta$	220	170	126 ± 46
$\eta' \to \gamma\rho$	160	120	$0.27\Gamma(\eta' \to \text{all})$
$\eta' \to \gamma\omega$	15	11	
$\varphi \to \gamma\eta'$	0.5	0.6	

There are a large number of pion and photon transitions among baryons which are predicted by the theory. They are compared with experiment elsewhere.[46,47,52,25] Overall there is fair agreement between theory and experiment, with a number of predicted pion widths "right on the nose," but others off by factors of 2 to 3. In many of these cases there are large experimental uncertainties, as well as the theoretical uncertainty inherent in using the narrow resonance approximation to compute decays of one broad resonance into another.

(3) Relative Signs. In the process $\pi N \to N^* \to \pi\Delta$, the couplings to both πN and $\pi\Delta$ of all the N^*'s with a given value of L are related by $(SU(6))_W$ Clebsch-Gordan coefficients to the same reduced matrix element(s). The signs of the amplitudes for passing through the various N^*'s in $\pi N \to \pi\Delta$ are then computable group theoretically. The correctness of these sign predictions is crucial, for while, for example, one may be willing to envisage a small amount of mixing of the constituent quark states, and corresponding corrections of say, 20%, to amplitudes (and 40% to widths), this will not change their signs. A wrong sign prediction could well spell the end of the theory!

This in fact seemed to be the case last year[66] when a comparison of the theoretical predictions[46,67] was made with the amplitude signs observed in an earlier phase shift solution of $\pi N \to \pi\Delta$ by the LBL-SLAC collaboration.[68] Since then a newer solution[69,70] with much better χ^2 has been found--in fact, the new solution is the only one left once additional data in the previous energy "gap" between 1540 and 1650 MeV is used as a constraint.[71]

The present situation with regard to amplitude signs for intermediate N^*'s with $L = 1$ in $\pi N \to N^* \to \pi\Delta$ is shown[72] in Table X. Aside from an overall phase (chosen so as to give agreement with the sign of the $DD_{15}(1670)$ amplitude), there is one other free quantity. This is the relative size of the reduced matrix elements of the two terms in $V^{-1}Q_5^\alpha V$ or, what turns out to be equivalent, the sign of an s-wave relative to a d-wave transition amplitude. In Table XI we have fixed this by using the sign of the $SD_{31}(1640)$ amplitude. All other signs for N^*'s in the 70 L = 1 multiplet are then predicted theoretically. The seven other signs determined experimentally agree with these predictions. The sign of the s-wave relative to d-wave amplitude is such as to show that the reduced matrix element of the second term in $V^{-1}Q_5^\alpha V$ with the algebraic properties of $(\lambda^\alpha/2)\ [(\beta\sigma_x + i\beta\sigma_y)(v_x - iv_y) - (\beta\sigma_x - i\beta\sigma_y)(v_x + iv_y)]$, is dominant for $L' = 1$ to $L = 0$ pion transitions of baryons, just as it is for $L' = 1$ to $L = 0$ pion transitions of mesons.

TABLE XI

Signs of Resonant Amplitudes[72] in $\pi N \to N^* \to \pi\Delta$ for N^*'s in the 70 L = 1 multiplet of $SU(6)_W \times O(3)$. Amplitudes are labeled by $(\ell_{\pi N}\ell_{\pi\Delta})_{2I,2J}$ and the resonance mass in MeV.

Resonant Amplitude	Theoretical Sign	Experimental Sign[70]
$DS_{13}(1520)$	-	-
$DD_{13}(1520)$	-	-
$SD_{11}(1550)$	+	?
$SD_{31}(1640)$	+ (input)	+
$DS_{33}(1690)$	-	-
$DD_{33}(1690)$	-	-
$DD_{15}(1670)$	+ (input)	+
$DS_{13}(1700)$	-	-
$DD_{13}(1700)$	+	+
$SD_{11}(1715)$	+	+

For N^*'s with $L = 2$, many of the amplitudes have not been seen experimentally. As the overall phase is already fixed, there is just one parameter free. Again this is the relative size of the two possible reduced matrix elements, only now it corresponds to the sign of a p-wave relative to an f-wave pion decay amplitude. We use the FP_{15} (1688) amplitude in Table XII to fix this sign[72] it corresponds to the reduced matrix element of the first term in $V^{-1}Q_5^{\alpha} V$ behaving algebraically as $(\lambda^{\alpha}/2)\sigma_z$, being dominant. All other signs (3) which are measured in Table XII agree with the theory.

TABLE XII

Signs of Resonant Amplitudes[72] in $\pi N \to N^* \to \pi\Delta$ for N^*'s in the 56 L = 2 Multiplet of $SU(6)_W \times O(3)$. Amplitudes are labeled as in Table XI.

Resonant Amplitude	Theoretical Sign	Experimental Sign[70]
$FP_{15}(1688)$	- (input)	-
$FF_{15}(1688)$	+	+
$PP_{13}(1860)$	-	?
$PF_{13}(1860)$	+	?
$FF_{37}(1950)$	-	-
$FP_{35}(1880)$	-	?
$FF_{35}(1880)$	-	-
$PP_{33}(\quad)$	+	?
$PF_{33}(\quad)$	+	?
$PP_{31}(1960)$	+	?

The signs of amplitudes for resonances in the radially excited 56 L = are given in Table XIII. The sign of the $PP_{33}(1690)$ amplitude is in fact the principal reason for its previous assignment as the partner of the Roper resonance, since the alternative assignment to a 56 L = 2 leads to an opposite sign prediction.

TABLE XIII

Signs of Resonant Amplitudes[72] in $\pi N \to N^* \to \pi\Delta$ for N^*'s in a Radially Excited 56 L = 0 Multiplet of $SU(6)_W \times O(3)$. Amplitudes are Labeled as in Table XI.

Resonant Amplitude	Theoretical Sign	Experimental Sign[70]
$P_{11}(1470)$	+	+
$P_{33}(1690)$	-	-

Another reaction where relative signs are predicted is $\gamma N \to N^* \to \pi N$. This involves the theory at both the $\gamma N N^*$ and $\pi N N^*$ vertices. Although the situation is more complicated, there are also more amplitudes determined experimentally. An analysis[50,52] of the situation shows that not only are there 15 or so signs correctly predicted, but the information on the $\pi N N^*$ vertex so obtained agrees with that from $\pi N \to N^* \to \pi\Delta$ as to which term in $V^{-1}Q_5^\alpha V$ has the dominant reduced matrix element.

What emerges from all this is another possible systematics: for pion amplitudes, both meson and baryon show that the term transforming as $(\lambda^\alpha/2)\sigma_z$ is dominant in known L' even $\to L = 0$ transitions, while $(\lambda^\alpha/2)[\beta\sigma_+ v_- - \beta\sigma_- v_+]$ is dominant for $L' = 1 \to L = 0$ transitions. This might generalize to all L' even and L' odd decays. If it does, we will have yet another simple regularity to explain.

VIII. CONCLUSION

The theory of pion and photon transitions which we have outlined has had great success in predicting the signs of amplitudes--more than 25 relative signs are correctly predicted in the reactions $\pi N \to N^* \to \pi\Delta$ and $\gamma N \to N^* \to \pi N$. There is also at least fair success in predicting the relative magnitude of decay amplitudes, particularly for mesons.

This success lends support both to the theory of current-induced-transitions we have presented and to the assignment of hadron states to constituent quark model multiplets. In particular, the amplitude signs found to be in agreement with experiment mean that, at least in a rough sense, the relationship between the wave functions of different hadrons is that of the quark model. At $q^2 = 0$ one sees evidence for a quark picture of hadrons which is just as compelling as that obtained in a very different way as $q^2 \to \infty$ in deep inelastic scattering.

Aside from pushing further on questions like masses, the extension[53] to $q^2 \neq 0$ current induced transitions, the relationship[73] of V and PCAC, etc., what is most needed is a deeper understanding of why we can get away with such simple assumptions--why can we abstract anything relevant about transformed current operators from the free quark model? Even given that, why can we recognize so clearly the hadrons corresponding to the constituent quark model states? Why aren't the multiplets more badly split in mass and mixed? Most of all, to answer these and other questions we need at least part of the dynamics at which point we might be able to calculate magnitudes of the matrix elements as well. Then we truly will have a quark picture of hadron structure, spectroscopy, and amplitudes.

References

1. M. Gell-Mann, Phys. Letters 8, 214 (1964).
2. G. Zweig, CERN preprints TH. 401 and TH. 412, 1964 (unpublished).
3. See S. Glashow, invited talk presented at the IV International Conference on Experimental Meson Spectroscopy, Northeastern University, Boston, 1974 (unpublished).
4. See, for example, the discussion at last year's Summer Institute by D. Gross, Proceedings of the Summer Institute on Particle Physics, SLAC Report No. 167, Vol. II, p. 251 (1973).
5. MIT bag: A. Chodos et al., Phys. Rev. D9, 3471 (1974) and A. Chodos et al., MIT preprint MIT-CTP-417, 1974 (unpublished).
   SLAC bag: W. Bardeen et al., to be published.
6. O.W. Greenberg, Phys. Rev. Letters 13, 598 (1964). See also D. Faiman and A.W. Hendry, Ref. 55.
7. See the recent review by R.H. Dalitz in Baryon Resonances-73, E.C. Fowler, editor (Purdue University, West Lafayette, 1973), p. 393.
8. M. Gell-Mann, Phys. Rev. 125, 1067 (1962).
9. See the review of weak leptonic decays of K. Kleinknecht, invited talk at the XVII International Conference on High Energy Physics, London, July, 1974 (unpublished).
10. See, for example, N.P. Samios et al., Rev. Mod. Phys. 46, 49 (1974).
11. For a discussion of SU(3) as applied to scattering amplitudes see A.H. Rosenfeld in Particle Physics (Irvine Conference-1971), M. Bander, G.L. Shaw, and D.Y. Wong, editors (American Institute of Physics, New York, 1972), AIP Conference Proceedings No. 6, Particles and Fields Subseries, No. 2, pg. 1.
12. This work is reviewed in A. Pais, Rev. Mod. Phys. 38, 215 (1966).
13. See D. Cohen, invited talk at the IV International Conference on Experimental Meson Spectroscopy, Northeastern University, Boston, 1974 (unpublished).
14. W. A. Bardeen, H. Fritzsch, and M. Gell-Mann in Proceedings of the Topical Meeting on Conformal Invariances in Hadron Physics, Frascati, 1972, p. 139.
15. See P.J. Litchfield, invited talk at the XVII International Conference on High Energy Physics, London, 1974 (unpublished).
16. We indicate the mass of a state in MeV/c^2 in parentheses, e.g. $\pi(140)$ as in Ref. 17. For baryons the subscripts are 2I, 2J, e.g. P_{11} (940) is the nucelon.
17. N. Barash-Schmidt et al., "Review of Particle Properties," Phys. Letters 50B, No. 1 (1974).
18. Meson spectroscopy is reviewed by F. Wagner, invited talk at the XVII International Conference on High Energy Physics, London, 1974 (unpublished).
19. See F.J. Gilman, invited talk at the IV International Conference on Experimental Meson Spectroscopy, Northeastern University, Boston, 1974 and SLAC-PUB-1436 (unpublished).
20. D. Morgan, Rutherford preprint RL-7-063, 1974 (unpublished).
21. See R. Carnegie, these Proceedings.
22. See also J. Rosner, invited talk at the XVII International Conference on High Energy Physics, London, 1974 (unpublished).
23. B.D. Hyams et al., CERN preprint, 1973 (unpublished).
24. See D. Leith, invited talk at the IV International Conference on Experimental Meson Spectroscopy, Northeastern University, Boston, 1974 and SLAC-PUB-1440 (unpublished).
25. R.J. Cashmore, A.J.G. Hey, and P.J. Litchfield, CERN preprint CERN/D.Ph.II/PHYS 74-19, 1974 (unpublished).
26. M. Gell-Mann and M. Levy, Nuovo Cimento 16, 705 (1960).
27. S.L. Adler, Phys. Rev. Letters 14, 1051 (1965); W.I. Weisberger, Phys. Rev. Letters 14, 1047 (1965).

28. The theory may alternately be formulated in terms of light-like charges and hadron states at rest. This more modern language makes clearer some of the theoretical questions which arise, but for the charges and operators we consider here the two formulations give equivalent results.

29. Between states with $p_z \to \infty$, the z and t components of the vector and axial-vector currents have equal matrix elements. Therefore, the integral over all space $A_z^\alpha(\vec{x},t)$ has the same matrix elements as $Q_5^\alpha(t)$.

30. R. Dashen and M. Gell-Mann, Phys. Letters 17, 142 (1965).

31. H.J. Lipkin and S. Meshkov, Phys. Rev. Letters 14, 670 (1965), and Phys. Rev. 143, 1269 (1966); K.J. Barnes, P. Carruthers, and F. von Hippel, Phys. Rev. Letters 14, 82 (1965).

32. Older work on current algebra representation mixing is reviewed by H. Harari in Spectroscopic and Group Theoretical Methods in Physics (North Holland, Amsterdam, 1968), p. 363, particularly for baryons, and in F.J. Gilman and H. Harari, Phys. Rev. 165, 1803 (1968) for mesons. For some recent results see A. Casher and L. Susskind, Phys. Rev. D9, 436 (1974); M. Ida, Kyoto preprint RIFP-182, 1973 (unpublished); and T. Kuroiwa, K. Yamawaki, and T. Kugo, Kyoto preprint KUNS-277, 1974 (unpublished).

33. M. Gell-Mann, in Elementary Particle Physics, P. Urban, ed. (Springer-Verlag, New York, 1972), p. 733.

34. Such a transformation was suggested by R.F. Dashen and M. Gell-Mann, Phys. Rev. Letters 17, 340 (1966) in connection with saturating local current algebra. The free quark model transformation given there is just that finally settled on by Melosh, Ref. 36.

35. A phenomenological scheme for transforming charges is discussed by F. Buccella et al., Nuovo Cimento 69A, 133 (1970) and 9A, 120 (1972).

36. H.J. Melosh, IV, Caltech thesis (1973) (unpublished); and Phys. Rev. D9, 1095 (1974). See also Ref. 34.

37. S.P. de Alwis, Nucl. Phys. B55, 427 (1973); S.P. de Alwis and J. Stern, CERN preprint TH. 1679, 1973 (unpublished); E. Eichten, J. Willemsen and F. Feinberg, Phys. Rev. D8, 1204 (1973).

38. W.F. Palmer and V. Rabl, Ohio State University preprint, 1974 (unpublished). See also E. Celeghini and E. Sorace, Firenze preprint, 1974 (unpublished); and T. Kobayashi, Tokyo preprint TUETP-73-29, 1973 (unpublished).

39. H. Osborn, Caltech preprint CALT-68-435, 1974 (unpublished).

40. Under the chiral SU(3) × SU(3) subalgebra of the $SU(6)_W$ of currents, the two terms in Eq. (8) transform as $(8,1)$-$(1,8)$ and $(3,\bar{3})$-$(\bar{3},3)$, respectively.

41. The operators D_+^α have $J_z = +1$. The corresponding operators D_-^α with $J_z = -1$, and all their matrix elements, are related (up to a sign) by a parity transformation. Hence we need only consider the properties of D_+^α.

42. Under the chiral SU(3) × SU(3) subalgebra of the $SU(6)_W$ of currents the four terms in Eq. (11) transform as $(8,1) + (1,8)$, $(3,\bar{3})$, $(8,1) - (1,8)$, and $(\bar{3},3)$ repsectively.

43. J.C. Carter, J.J. Coyne, and S. Meshkov, Phys. Rev. Letters 14, 523 (1965) and S. Meshkov, private communication; C.L. Cook and G. Murtaza, Nuovo Cimento 39, 531 (1965). W-spin Clebsch-Gordan coefficients are just those of SU(2).

44. F.J. Gilman and M. Kugler, Phys. Rev. Letters 30, 518 (1973).

45. A.J.G. Hey and J. Weyers, Phys. Letters 48B, 263 (1973).

46. F.J. Gilman, M. Kugler and S. Meshkov, Phys. Letters 45B, 481 (1973).

47. F.J. Gilman, M. Kugler and S. Meshkov, Phys. Rev. D9, 715 (1974).

48. A.J.G. Hey, J.L. Rosner, and J. Weyers, Nucl. Phys. B61, 205 (1973).

49. A. Love and D.V. Nanopoulos, Phys. Letters 45B, 507 (1973).

50. F.J. Gilman and I. Karliner, Phys. Letters 46B, 426 (1973).

51. A.J.G. Hey and J. Weyers, Phys. Letters 48B, 69 (1974).

52. F.J. Gilman and I. Karliner, Stanford Linear Accelerator Center Report No. SLAC-PUB-1382, 1974 (unpublished).

53. F.E. Close, H. Osborn, and A.M. Thomson, CERN preprint TH. 1818, 1974 (unpublished).

54. C. Becchi and G. Morpurgo, Phys. Letters 17, 352 (1965).

55. D. Faiman and A.W. Hendry, Phys. Rev. 173, 1720 (1968); ibid 180, 1572 (1969); L.A. Copley, G. Karl, and E. Obryk, Phys. Letters 29B, 117 (1969) and Nucl. Phys. B13, 303 (1969).

56. See, for example, R.P. Feynman, M. Kislinger and F. Ravndal, Phys. Rev. D3, 2706 (1971).

57. Such schemes center around adding an L = 1 "spurion" in a 35: see J.C. Carter and M.E.M. Head, Phys. Rev. 176, 1808 (1968); D. Horn and Y. Ne'eman, Phys. Rev. D1, 2710 (1970); R. Carlitz and M. Kislinger, Phys. Rev. D2, 336 (1970). Specific broken $SU(6)_W$ calculational schemes with the same general algebraic structure as the theory considered here have been developed by L. Micu, Nucl. Phys. B10, 521 (1969); E.W. Colglazier and J.L. Rosner, Nucl. Phys. B27, 349 (1971); W.P. Petersen and J.L. Rosner, Phys. Rev. D6, 820 (1972); W.P. Petersen and J.L. Rosner, Phys. Rev. D7, 747 (1963). See also D. Faiman and D. Plane, Nucl. Phys. B50, 379 (1972).

58. The algebraic structure of broken $SU(6)_W$ schemes and their relation to the present theory are discussed in Ref. 48.

59. The relation between various quark model, $SU(6)_W$, broken $SU(6)_W$, and constituent to current quark transformation calculations of pion decay amplitudes is discussed by H.J. Lipkin, NAL preprint NAL-PUB-73/62-THY, 1973 (unpublished).

60. See the discussion in Ref. 44, particularly footnote 13.

61. S.U. Chung et al., Brookhaven preprint BNL 18340, 1973 (unpublished); V. Chaloupka et al., CERN preprint, 1974 (unpublished); U. Karshon et al., Weizmann Institute preprint WIS-73/44-Ph, 1973 (unpublished) and references to previous work therein.

62. This is essentially an updated version of results found in F.J. Gilman, M. Kugler, and S. Meshkov, Refs. 46 and 47, and also in J.L. Rosner, Phys. Reports (to be published) and Stanford Linear Accelerator Center Report No. SLAC-PUB-1391, 1974 (unpublished). The decay widths are calculated from the expressions in Table I of ref. 47, with quark model assignments as described there.

63. We have not treated the decay of the $I = 0$ scalar mesons into $\pi\pi$ in Table III because of the unclear situation in assigning the observed states to the quark model multiplet. For recent assessments see J.L. Rosner, Ref. 62 and D. Morgan, Ref. 20.

64. This is an updated version of Table II of F.J. Gilman and I. Karliner, Ref. 52. The decay widths can be calculated from Table I of Ref. 52, with the quark model assignments as described there.

65. See J. Rosen, invited talk at the IV International Conference on Experimental Meson Spectroscopy, Northeastern University, Boston, 1974 (unpublished).

66. F.J. Gilman, in Baryon Resonances-73, E.C. Fowler, Ed. (Purdue University, West Lafayette, 1973), p. 441.

67. The relative signs of these resonant amplitudes in theories with the same general algebraic structure have been considered by R.G. Moorhouse and N.H. Parsons, Nucl. Phys. B62, 109 (1973) in the context of the quark model and by D. Faiman and J.L. Rosner, Phys. Letters 45B, 357 (1973) in the context of broken $SU(6)_W$.

68. D. Herndon et al., LBL Report No. LBL-1065, 1972 (unpublished); see also U. Mehtani et al., Phys. Rev. Letters 29, 1634 (1973).

69. R.J. Cashmore, lectures presented at the Scottish Universities Summer School in Physics, Stanford Linear Accelerator Center Report No. SLAC-PUB-1316, 1973 (unpublished).

70. A.H. Rosenfeld et al., Stanford Linear Accelerator Center/LBL preprint SLAC-PUB-1386/LBL 2633, 1974 (unpublished); R.S. Longacre et al., Stanford Linear Accelerator Center/LBL preprint SLAC-PUB-1390/LBL 2637, 1974 (unpublished).

71. R.J. Cashmore et al., Stanford Linear Accelerator Center/LBL preprint SLAC-PUB-1387/LBL 2634, 1974 (unpublished).

72. Tables XI and XII update the comparison of theory and experiment contained in Table VIII of Ref. 47 (see also Ref. 67). The ordering in angular momentum and isospin Clebsch-Gordan coefficients is the same as in Ref. 47 (see particularly footnote 59) even though there is a changed isospin convention in the new experimental papers, Ref. 70.

73. The connection of chiral representation mixing and the Nambu-Goldstone mechanism of chiral symmetry realization is explored by R. Carlitz and W.K. Tung, University of Chicago preprint EFI 73/19, 1974 (unpublished).

LECTURES ON INCLUSIVE HADRONIC PROCESSES

Dennis Sivers

Stanford Linear Accelerator Center
Stanford University, Stanford, California 94305

These are "low profile" lectures intended to present some ideas on inclusive processes with a minimum of extraneous formalism. We discuss how many features of the data are empirically described by simple rules common to many models. Important questions in Mueller-Regge phenomenology are presented and some aspects of cluster models are introduced.

I. INTRODUCTION

For a spell, the study of hadronic interactions was restricted largely to the properties of $2 \to 2$ collisions even though, at high energies, such collisions constitute only a small fraction of events. (For example, the ratio $\sigma_{pp}^{el}/\sigma_{pp}^{tot} \cong .18$ at the CERN ISR so that there is particle production more than 80% of the time.) For various reasons, people realized the importance of confronting the problem of particle production even before there were effective methods of dealing with many-body final states. Some rationales for paying particular attention to production processes can be noted:

1. Hadrons have structure resembling that of a simple quark model. However, when they are struck we do not see the quarks, just more hadrons. This intriguing fact makes hadronic collisions something intrinsically different than a high-energy rerun of atomic or nuclear collisions. The many-hadron final states confront the physicist with a unique new type of phenomenon.

2. The unitarity equation makes important connections between processes with different numbers of final-state particles. Experience suggests that it is doubtful we can anticipate an approximate understanding of a process if we try to deal with it in isolation. Unitarity forces us to worry about everything.

3. Hadron resonances with much in common with the stable particles have alternate decay schemes with different numbers of particles.

Now, through the efforts of many people, we have developed what seems to be a powerful set of tools for the systematic exploitation of data on particle production. We have the concept of an inclusive measurement, the probability of detecting a particle emerging from a collison with a specified momentum without regard to other collision products, and a theoretical framework to deal with this concept. In the meantime we are steadily improving our understanding of exclusive processes where each particle emerging from the collision is analyzed. In addition, we are beginning to understand ways to deal with <u>mixed</u> or <u>semi-inclusive</u> measurements where something, but not all (no strange particles, $n_{ch} \gtrsim 8$, etc.), is known about the other particles in the final state.

Many of the early questions about production processes, such as whether short-range-order or diffractive-dominated mechanisms explain the bulk of the data, have been answered empirically by experiment. (See the reviews of Berger and Jackson for some historical perspective.) In other instances, experimental "surprises" such as the results on inelastic diffraction or the production of particles with large transverse momentum, have generated enough interest to spin-off into separate realms of specialization. I will not deal here with well known facts or with the new fads but will concentrate on some topics in "garden variety" inclusives which have been, by comparison, neglected. I have chosen to further restrict attention to topics which can be approached with a minimum of formalism. I ask the experts to bear with me because I think the topics demonstrate to what extent some very fundamental questions remain unanswered. Impatient theorists who have assumed one answer and gone on to calculate more complex problems are subject to embarrassment by vindictive experimentalists.

II. A PRELIMINARY SURVEY OF THE DATA

There are several features of the data on high energy production processes which can be approached with a minimum of theoretical preparation. Not everyone agrees what this minimum theoretical input is, but let me list some empirical features of the data which are obviously important:

1. Quantum number conservation. The final states are constrained by energy momentum conservation and by the conservation of additive quantities such as charge, baryon number, etc.

2. Transverse momentum cutoff. The spectra of all particles is rapidly damped in transverse momentum.

3. The leading particle effect. A large fraction of the energy in a typical collison is not "available" for particle production. For example, in pp collisions the leading protons carry off, on the average something near half the c.m. energy even at the ISR. It is important to note that this feature should be largely absent from the quasi-inclusive processes $\bar{p}p|_{annih} \to \pi + X$.

4. Clustering. Most observed particles are π's, but these π's are not produced individually but are often found in resonances or clusters.

The fact that these empirical facts already put strong constraints on inclusive spectra has long been known (Kryzwicki [1964]). They are present in all the available models for inclusive processes. See, for example, the discussion in the review of Morrison. It is an interesting exercise to see to what extent the features (1)-(4) constitute input of the models and to what extent they may follow from more fundamental theoretical ideas but we will not delve into that question here. Our interest in 1)-4) can be attributed to the fact that they explain quite directly several common features of hadronic production processes.

The first such feature is the fact that hadronic prong cross sections show striking regularities. Figs. II.1 and II.2 show the topological cross sections for pp and π-p plotted against lab momentum. The energy dependence of a typical production cross section does not seem to be too sensitive to the quantum number of the beam. Figure II.3 shows the associated multiplicity distribution for the process $pp \to p + (N \text{ charged})$ plotted against the missing mass associated with the charged particles. Except for the fact that we have an odd number of charged particles the behavior is quite similar to the direct pp prong cross sections.

The gross features of the energy dependence of the prong cross sections can be understood from simple multiperipheral models or from one-dimensional phase space (DeTar, 1971).

An important question which is still not entirely resolved involves the asymptotic behavior of the various prong cross sections. Experiments suggest that all total and elastic cross sections rise slowly through the NAL-ISR energy regime. The question whether exclusive production cross sections exhibit a similar rise is quite important for our conception of "diffraction." So far there is no evidence for an increase, or even a flattening, of any of the prong cross sections. This corresponds to a certain lack of experimental support for the result

$$\sigma_n(S) \to \text{const.}(\text{mod logs}) \qquad \text{(II.1)}$$

which is an important aspect of the so-called two-component models. We won't discuss two-component models here because we don't have time to go too deeply into diffractive dissociation and the topic of Professor Leith's lectures. An excellent treatment of the topic can be found in the review of Harari.

Because the moments of the multiplicity distribution are given by integrals of the corresponding inclusive cross sections, e.g.,

$$\langle n_{ch} \rangle = \sigma_{inel}^{-1} \int \left(\frac{d^3p}{E}\right) \frac{d\sigma(ab \to cX)}{d^3p/E} \qquad (II.2)$$

$$\langle n_{ch}(n_{ch} - 1) \rangle = \sigma_{inel}^{-1} \int \left(\frac{d^3p_2}{E_1}\right) \left(\frac{d^3p_2}{E_2}\right) \frac{d\sigma(ab \to c_1c_2X)}{(d^3p_1/E_1)(d^3p_2/E_2)}$$

etc.

the measurement of the multiplicity distribution at a given incident energy constitutes a crude set of distributions (with one momentum bin). The multiplicity distribution therefore provides an important first hurdle for theoretical model-making types since it doesn't pay to spend too much time on the fine grained structure of a model which can't get the coarse structure correct.

One possibility which emerges from comparing the multiplicity distributions of $\bar{p}p$ annihilation and pp collisions is that part of the broad dispersion in the latter may be due to the spread in inelasticities of the leading protons observable in the flat x distribution for $pp \to p$ anything. If we assume that the dominant process is $pp \to pp + (n\pi)$ and denote by Q^2 the (invariant mass)^2 associated with pion system, we can write

$$D^2(S) = \int F(Q^2,S)\, D^2(Q^2)\, dQ^2 + \int F(Q^2,S)\, [\bar{n}(Q^2) - \bar{n}(S)]^2\, dQ^2 \qquad (II.3)$$

where $F(Q^2,S)$ is the normalized inclusive distribution for $pp \to pp + (Q^2)$. If we let $\epsilon = Q^2/S$ and assume $F(Q^2,S) \simeq \frac{1}{S}\hat{F}(\epsilon)$ we can write the second term

$$\langle n(S) \rangle^2 \int \hat{F}(\epsilon)\, d\epsilon \left(1 - \frac{\bar{n}(\epsilon S)}{\bar{n}(S)}\right)^2 \qquad (II.4)$$

and we may get a large positive contribution to the dispersion in (II.3) even if the $D^2(Q^2)$ is small. It would be very instructive to compare the multiplicity distribution for the process $pp \to pp + n(Q^2)$ with that of $\bar{p}p_{annih} \to n(Q^2)$ in order to discern whether the annihilation process contains the same kind of clustering effects as other production mechanisms. This question is important for the bootstrap theories of inclusive spectra (Krzywicki and Peterson, 1972; Finkelstein and Peccei 1972).

Note that, in (II.4) above, if the average multiplicity is strictly logarithmic we do not get a growth of $D^2(S)$ proportional to $\langle n(S) \rangle^2$ since

$$\left(1 - \frac{\bar{n}(\epsilon S)}{\bar{n}(S)}\right)^2 = \left(1 - \frac{a\,\ell n(\epsilon S) + b'}{a\,\ell n(S) + b}\right)^2 = O\left(\frac{1}{\langle n(S) \rangle^2}\right) \qquad (II.5)$$

If there are regions with substantial corrections to logarithmic multiplicities we may have $D \propto \langle n \rangle$.

One approach to the multiplicity distribution which has generated a great deal of theoretical speculation is the hypothesis of Koba-Nielsen-Olesen (1972) (KNO) scaling. Simply stated (see, for example, Van der Velde, 1974), the assumption of KNO scaling is that the probability for producing n particles, $P_n = \sigma_n/\sigma_{inel}$, depends on the average separation of the particles in one-dimensional phase space. If we denote $Y = \ell n(S/m^2)$ then the statement is that P_n depends on n through the ratio n/Y. Putting in normalization we get

$$P_n = Y^{-1} f\left(\frac{n}{Y}\right) \qquad (II.6)$$

or as it is sometimes written

$$P_n = \frac{1}{\langle n \rangle} \tilde{f}\left(\frac{n}{\langle n \rangle}\right) \qquad (II.6')$$

There is good solid evidence for the approximate validity of (II.6). See Fig. II.4 or for a more complete discussion the reviews of Boggild and Ferbel and of Wrobleski. This provides a good example of how an empirical result can have a profound effect on the way we think about collision processes. The prediction (II.6) can be contrasted to the Poisson distribution expected in the simplest multiperipheral schemes,

$$P_n = e^{-gY} \frac{g^n Y^n}{n!} . \qquad (II.7)$$

with KNO scaling we necessarily have strong long range correlations since the multiplicity moments $f^{(n)}$ which measure the integrals of correlation functions

$$f^{(n)}(Y) = \int C^{(n)}(y_1 \cdots y_n)\, dy_1 \cdots dy_n \propto Y^n \qquad (II.8)$$

The difference between SRO models and KNO scaling doesn't begin to show up until, at very high energies, the $f^{(n)}$ of the former begin to be proportional to Y. For example, in a SRO model

$$f^{(3)} \cong CY \int \exp[-\lambda|y_1 - y_2|]\, d(y_1 - y_2) \exp[-\lambda|y_2 - y_3|]\, d(y_2 - y_3)$$
$$\cong CY \frac{1}{\lambda^2}(1 - e^{-\lambda\Delta Y})^2 \cong \frac{CY}{\lambda^2}\left(\lambda\Delta Y - \frac{\lambda^2\Delta Y^2}{2!} + \cdots\right)^2 \qquad (II.9)$$

where ΔY is the maximum spacing between particles allowed kinematically. For moderate energies (II.9) looks more like Y^3 than Y so all SRO models exhibit a kind of low energy KNO scaling. Thomas (1973) has discussed in more detail how a SRO may mock up an apparent KNO scaling result. There is a great deal of controversy, then, over whether the multiplicity scaling (II.6) will continue to find experimental support at higher energies.

If we want to follow up on the KNO hypothesis, one promising approach might be the geometrical models which provide a relatively natural accommodation with (II.6). Geometrical models rely on the fact that the impact parameter is a hidden variable in production processes. Our intuition suggests that since hadrons are fragile objects central collisions might produce different final states than glancing or peripheral collisions. Let's write the n-particle cross section as a superposition of the n-particle cross section at fixed impact parameter

$$\sigma_n = \int d^2b\, \sigma_n(b)$$
$$\sigma(b) = \sum_n \sigma_n(b) \qquad (II.10)$$

where $\sigma(b)$ is the impact parameter representation of the overlap function (van Hove, 1964) which can be determined from unitarity and elastic scattering data. However, the $\sigma_n(b)$ cannot be determined since they are sensitive to phases in the n-particles production amplitude. (See, for example, Henyey, 1974.) We can make the assumption that

$$\langle n(b,S)\rangle = \langle n(S)\rangle\, w(b) \qquad (II.11)$$

and that we have a narrow distribution of multiplicities at a given impact parameter

$$\sigma_n(b) \cong \sigma(b)\, \delta(n - \langle(b,S)\rangle) \qquad (II.12)$$

so that

$$\sigma_n(S) \cong \int d^2b\, \sigma(b)\, \delta(n - \langle n(b,S)\rangle)$$
$$\cong \frac{2\pi b_0\, \sigma(b_0)}{\left|\frac{d\langle n(b)\rangle}{db}\right|} \qquad (II.13)$$

where b_0 is determined by $n = \langle n(b_0,S)\rangle$. This can be rewritten

$$\frac{\sigma_n}{\sigma_{inel}} = \frac{1}{\langle n(S)\rangle} \frac{2\pi b_0\, \sigma(b_0)}{\sigma_{inel}} \frac{1}{\left|\frac{dw(b)}{db}\right|}\Bigg|_{b=b_0} \qquad (II.14)$$

which, given (II.11), is equivalent to KNO scaling (II.6). Simple intuitive arguments suggest that $w(b)$ should be determined from the amount of matter overlap between the two hadrons (Barshay, 1973; Buras and Koba, 1973) and thus be a decreasing function of b. However, the interpretation of the multiperipheral model as a random walk in rapidity space can lead to an increasing $\langle n(b) \rangle$ (Moreno, 1973). Using (II.14) we can actually solve for $w(b)$ using the experimental $\sigma(b)$ and the KNO scaling function. Because of the absolute value of dw/db is all that is determined we are unable to determine from (II.14) whether $w(b)$ should increase or decrease with increasing impact parameter. Solutions for $w(b)$ taken from Bialas and Bialas (1974) are shown in Fig. II.5.

One thing which this simple geometrical exercise tells us is that to achieve KNO scaling we need a narrow multiplicity distribution at a given impact parameter, (II.12). There is no room for a coherent contribution, such as diffraction, which contributes to a given n-particle final state from all impact parameters. This provides one way of seeing the basic incompatibility between KNO scaling and two-component models, which have (II.1). Before serious theoretical models based on KNO scaling can emerge, they must be prepared to deal with the existence of inelastic diffraction. Strong evidence for the importance of the diffractive component in the multiplicity distribution can be seen in the dip in $\sigma(n_L, \text{tot})$ shown in Fig. II.6.

The experimentally observed cutoff in the transverse momentum of the hadrons produced in strong interaction processes provides an important dynamical constraint. Dick Blankenbecler will discuss in considerable detail the few tenths of a millibarn of cross section associated with the creation of large transverse momentum secondaries. Whatever hard mechanism turns out to be the explanation for these large-p_T collisions it's important to keep in mind the fact that it usually doesn't happen. It may be important for the development of certain models but it's rare. Experimentally, the average transverse momentum of a produced pion either becomes constant asymptotically

$$\langle p_T \rangle_\pi \sim 0.35(1 + O(1/\ell n\, S))\ \text{GeV/c} \qquad \text{(II.15)}$$

or grows very slowly. The energy dependence of $\langle p_T \rangle_\pi$ can be found in Fig. II.7. If we try to deal carefully with transverse momentum spectra we have to admit that the prediction of the Hagedorn thermodynamic model [Hagedorn (1950); Ranft (1970)] usually quoted as

$$\left.\frac{E\, d^3\sigma}{d^3p}\right|_{\text{therm}} \propto e^{-6p_T} \qquad \text{(II.16)}$$

can work only in a very small range of p_T, $0.15 \lesssim p_T \lesssim 1.0$ GeV/c. The actual shape of the spectrum depends in a nontrivial way on x. Some NAL data are shown in Fig. II.8. It may turn out that ability to get the details of the p_T structure correct will prove a decision test of models for the production processes. As far as I am aware, there are no good candidates and I regret my inability to deal in more detail with this problem.

Figure Captions, Section II

Fig. II.1 Topological cross sections for pp scattering. Compilation of data from the review of Whitmore.

Fig. II.2 Topological cross sections for $\pi^- p$ scattering notable for their similarity to those of pp. Figure from the review of Whitmore.

Fig. II.3 (a) Comparison of $\langle n_c \rangle$ in pp collisions with $\langle n_c - 1 \rangle$ in $pp \to p + M^2$.

(b) Comparison of $\langle n_c \rangle$ in $\pi^- p$ collisions with $\langle n_c - 1 \rangle$ for $\pi^- p \to p + M^2$.

(c) Prong cross sections for pp collisions (dashed lines) compared to Prong cross sections for $pp \to pM^2$.

Fig. II.4 Experimental evidence for KNO scaling.

Fig. II.5 Behavior of $\bar{n}(b)/\bar{n}$ inferred from geometrical model assuming KNO scaling and using data on $\sigma(b)$. Figure is from Bialas and Bialas (1974).

Fig. II.6 Cross sections for pp collisions at 205 GeV/c as a function of the number of particles going in C.M. hemisphere along beam direction. Dip structure can be attributed to diffractive dissociation as discussed by Sivers and Thomas (1974).

Fig. II.7 Average transverse momentum as a function of incident energy (Whitmore).

Fig. II.8 Compilation of data on the p_T distribution of $pp \to \pi^-$ (Whitmore

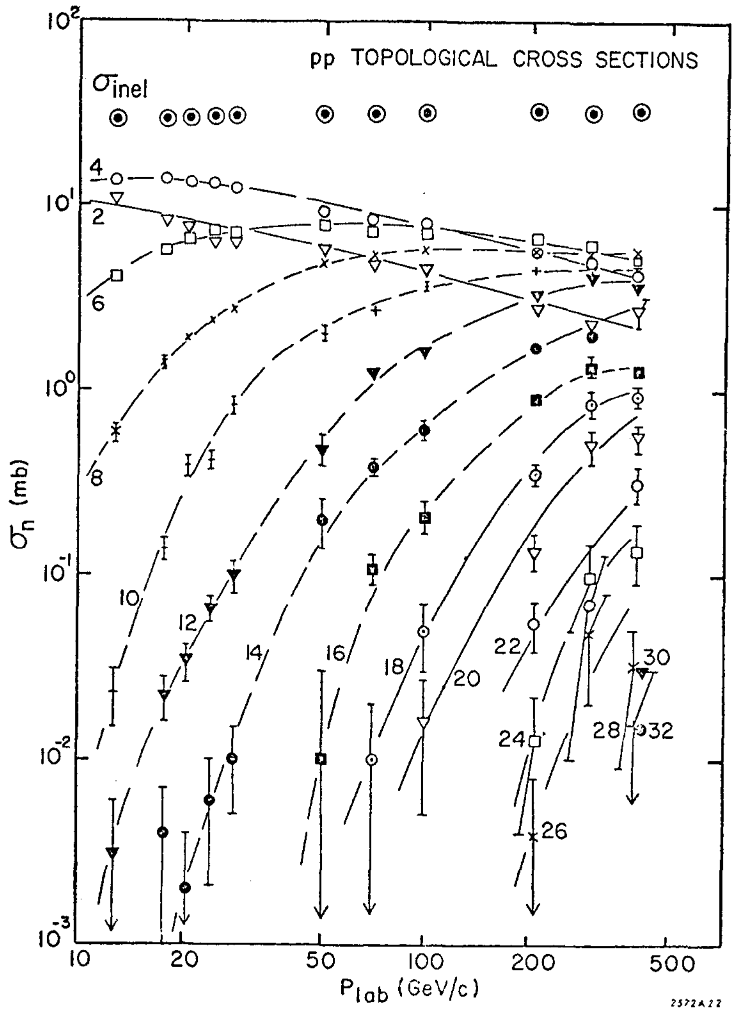

Fig. II.1

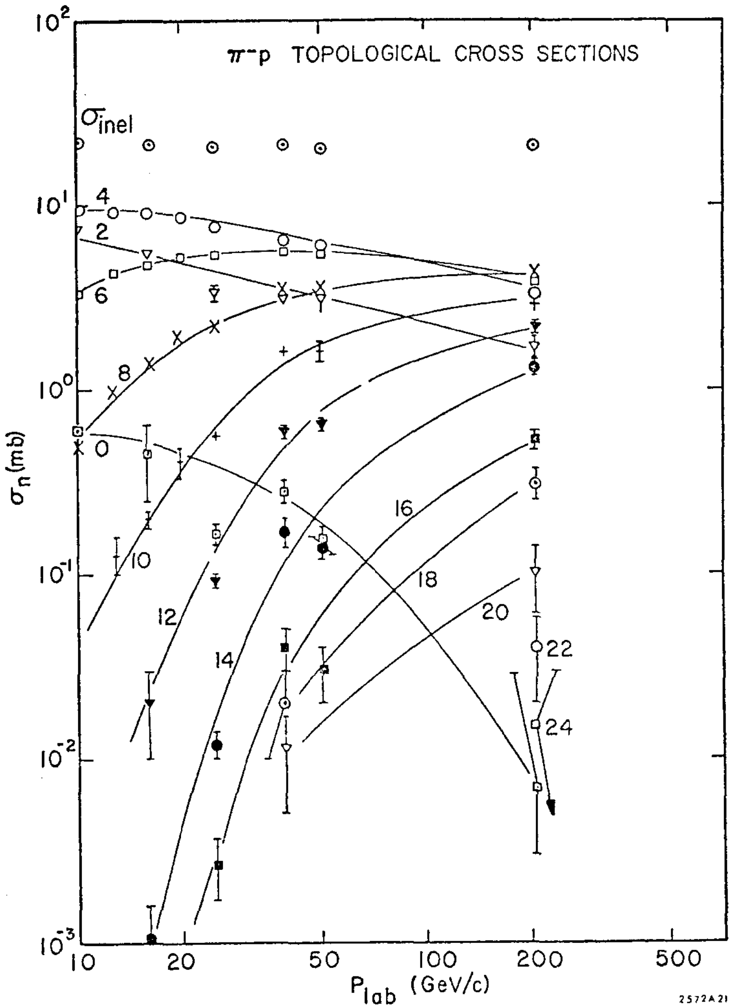

Fig. II.2

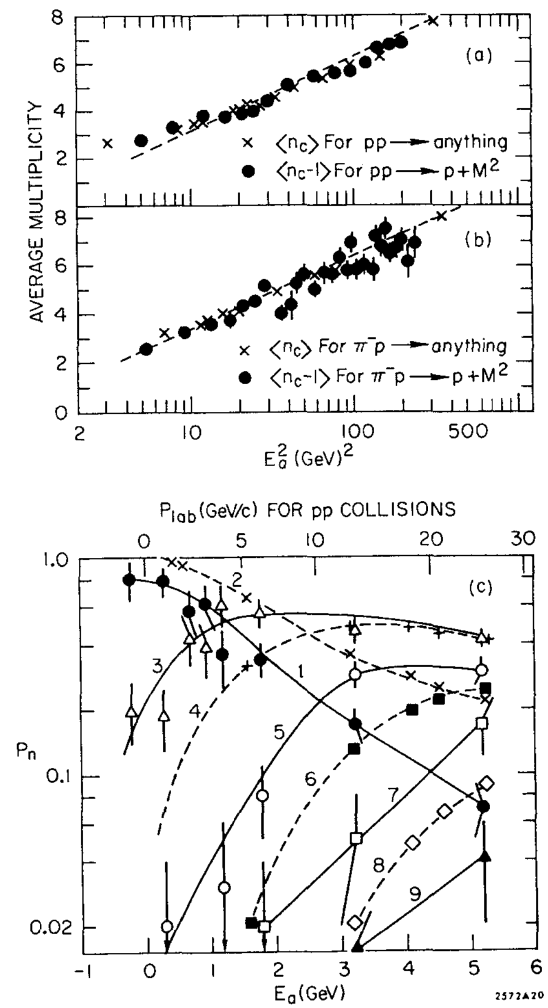

Fig. II.3

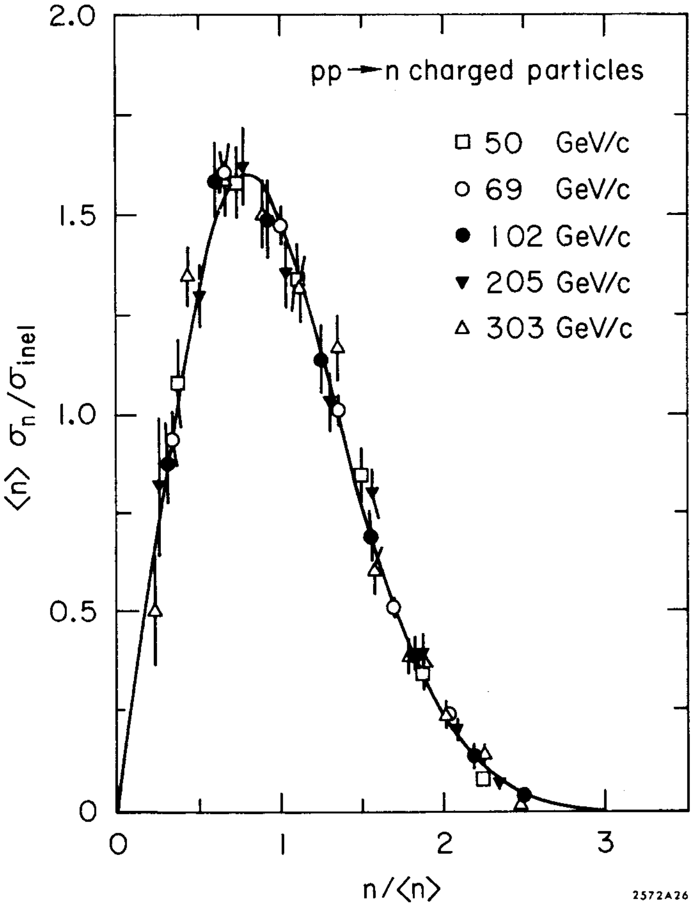

Fig. II.4

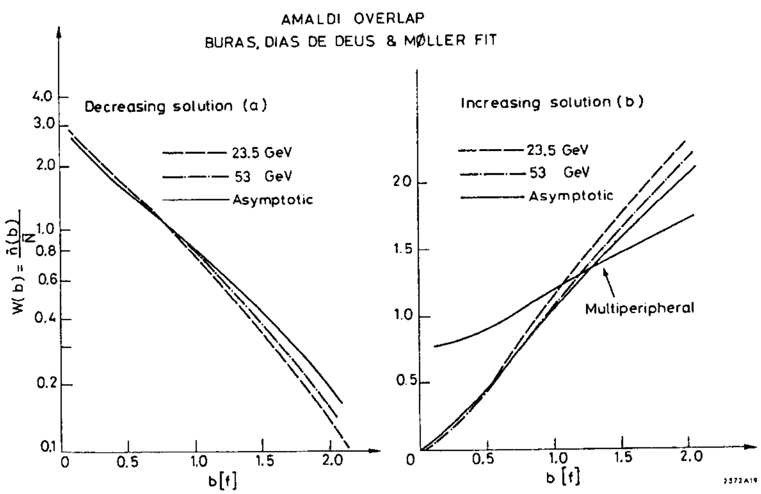

Fig. II.5

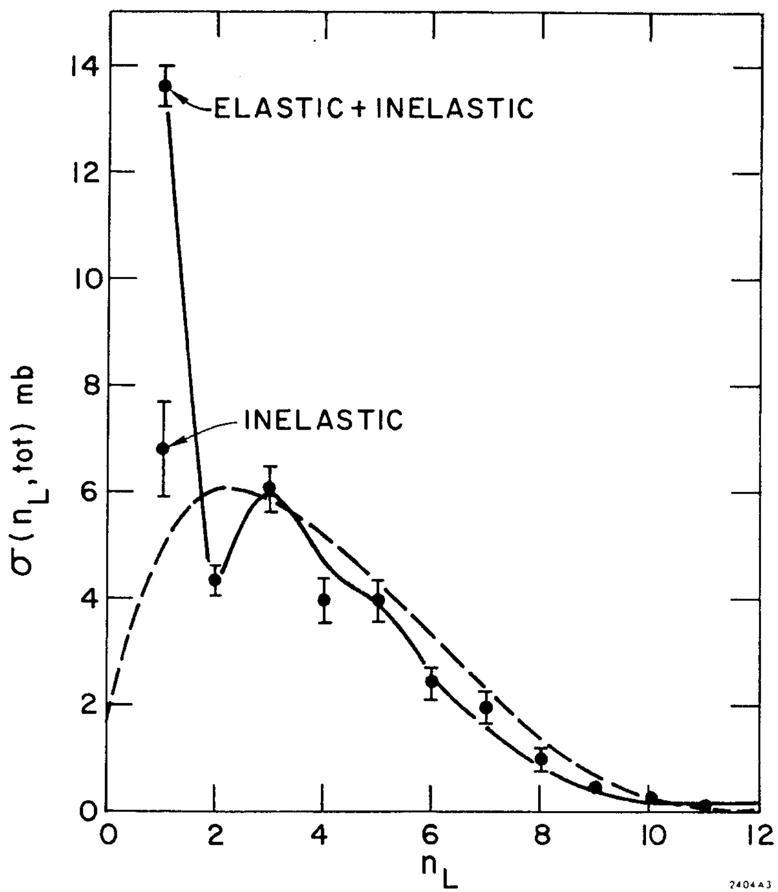

Fig. II.6

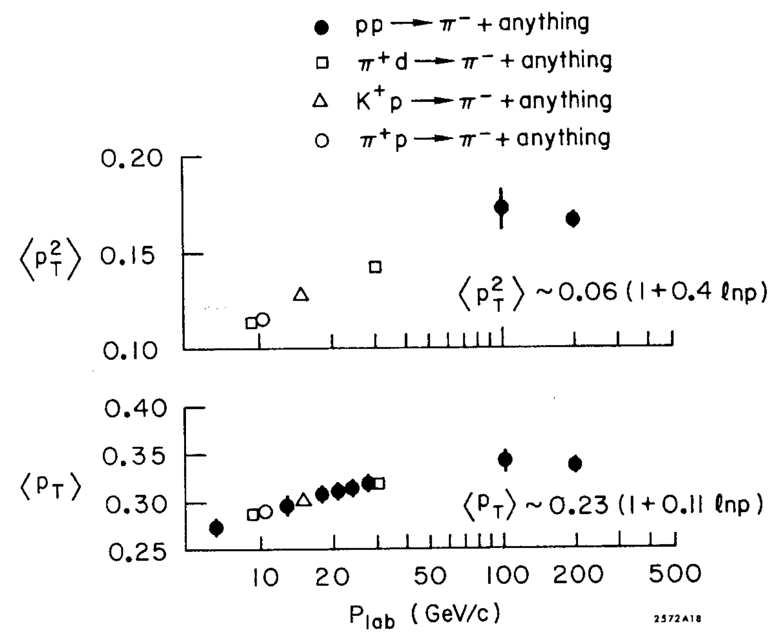

Fig. II.7

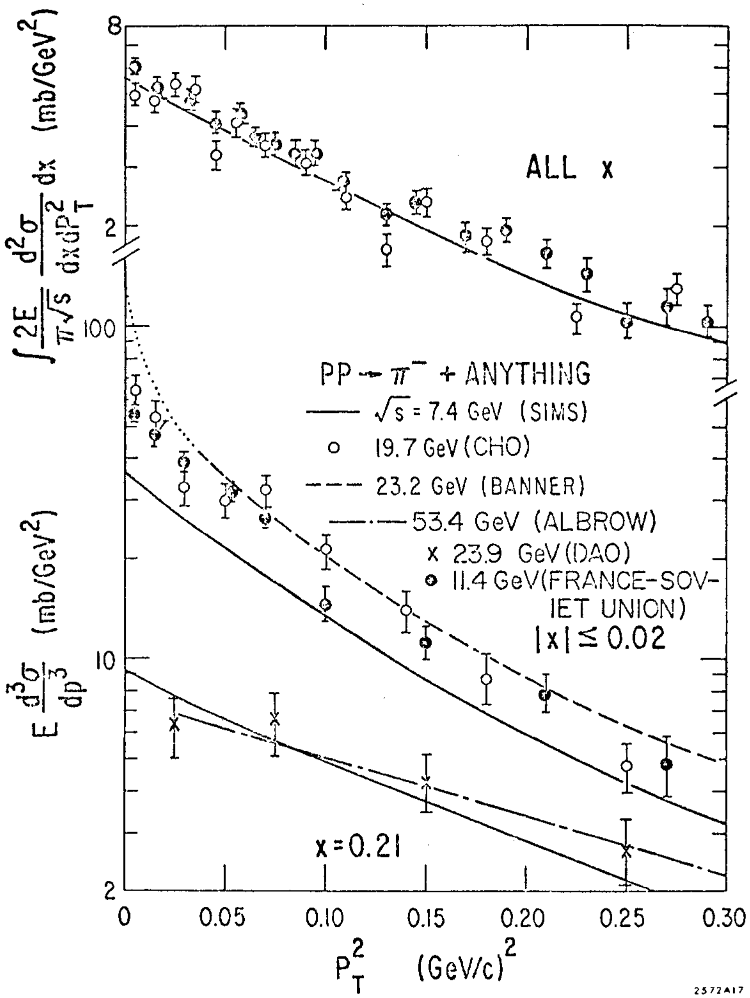

Fig. II.8

III. DIRECT MODELS FOR INCLUSIVE PROCESSES

Much in the same manner we connect, through unitarity, the total cross section with the discontinuity of the forward elastic amplitude,

$$\sigma_{tot}^{ab}(S) = \frac{1}{\lambda^{1/2}}\ \frac{1}{2i}\ \mathrm{disc}_S\ A^{ab\rightarrow ab}(S,0) \qquad \text{(III.1)}$$

where $\lambda = \lambda(S,\ m_a^2,\ m_b^2) \sim S^2$, the single-particle inclusive cross section is related to a discontinuity of an (unphysical) forward 3-3 amplitude. The relation, indicated schematically by the sketch below

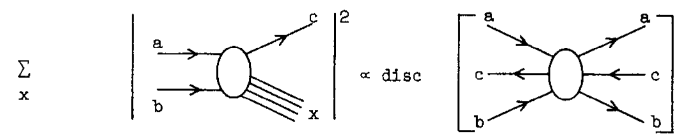

can be written

$$E_c\ \frac{d^3\sigma^{ab\rightarrow c}}{d^3p_c}(S,\vec{p}_c) = \frac{1}{\lambda^{1/2}}\ \frac{1}{2i}\ \mathrm{disc}_{m^2}\ A_{ab\bar{c}\rightarrow ab\bar{c}}(S,\ \vec{p}_c;\ \text{all}\ \ \Delta^2 = 0) \qquad \text{(III.2a)}$$

This generalization of the optical theorem was first hypothesized by Mueller (1970). Strictly speaking, it remains a hypothesis and has not been rigorously been proved. There are some subtleties in the definition of the discontinuity. The variables related to the various subenergies have to be specified carefully and there are problems related to the presence of anomolous thresholds in M^2. These points will not conern us much here but are discussed in detail by several authors (Stapp, 1971; Polkinghorne, 1972; Tan, 1971; Cahill and Stapp, 1972).

The practical use of (III.2) is that it enables us to model directly the functional dependence of the inclusive cross section by making a Regge expansion for the 3-3 amplitude. This means we can forget about the complicated behavior of the various exclusive components of the single-particle inclusive cross section. Check back and see how the dependence with energy of the individual prong cross sections in Figs. II.1 and II.2 disappears when they are summed to form a total cross section which can be fit by a simple Regge expansion. A similar cancellation can occur in the inclusive single particle distribution although we have no guarantee that it will. By making the appropriate Regge expansion of the 6-pt-function it may be possible to achieve a simple expression for the behavior of the invariant cross section. Notice that we can shortcircuit some of the problems with Regge expansions of multiparticle amplitudes by making asymptotic expansions directly for the discontinuity in (III.2) and neglecting phase problems.

For reference, the appropriate generalization of the optical theorem for the two-particle inclusive cross section is

$$\frac{E_c E_d d^6\sigma^{ab\to cd}}{d^3p_c\, d^3p_d}(S, \vec{p}_c, \vec{p}_d)$$

$$= \frac{1}{\lambda^{1/2}} \frac{1}{2i} \operatorname{disc}_{m^2} A_{ab\bar{c}\bar{d}\to ab\bar{c}\bar{d}}(S, \vec{p}_c, \vec{p}_d;\ \text{all } \Delta^2 = 0) \qquad \text{(III.2b)}$$

By extension, we can play all the games with Regge expansions of the 8-pt function that we can with the 6-point function. An important new feature in (III.2b) involves possible dependence on the azimuthal angle, $\cos\phi = \hat{p}_{Tc}\cdot\hat{p}_{Td}$ of the two-particle distribution. We will return to this point later.

Approach to Asymptotic Behavior

The most direct use of Mueller-Regge ideas lies in the study of the *energy dependence of inclusive spectra using a Regge expansion for the* 3-3 amplitude based on singularities known from 2-2 phenomenology. We have to be careful we don't let conventional wisdom concerning things we don't really understand in 2-2 reactions mislead us but this approach can obviously simplify things.

I will not discuss in detail the central region indicated by the diagram

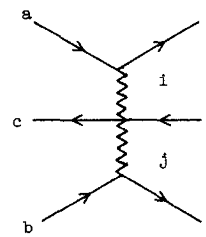

where the expansion

$$E\frac{d^2\sigma}{d^3p} \approx \sum_{i,j} \beta_{ij}\, u^{\alpha_i(0)-1}\, t^{\alpha_j(0)-1} \qquad \text{(III.3a)}$$

is valid with

$$t = (p_a - p_c)^2 \qquad \text{(III.3b)}$$

$$u = (p_b - p_c)^2 \qquad \text{(III.3c)}$$

$$\frac{tu}{S} = K^2 = (m_c^2 + p_T^2) \qquad \text{(III.3d)}$$

since, if we require $t \gtrsim 10\ \text{GeV}^2$, $u \gtrsim 10\ \text{GeV}^2$ and take into consideration that the bulk of the data occurs for $K^2 \lesssim 0.1\ \text{GeV}^2$ we see that we need $S \gtrsim 10^3\ \text{GeV}^2$ for the expansion to be useful. We just don't have the lever arm in energy to say much of interest about the central region.

Let's instead examine the simplest aspects of the Mueller-Regge hypothesis. In the limit

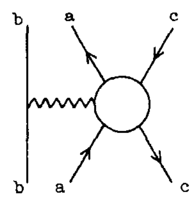

$y_a - y_c$ fixed $\quad \bar{p}_T$ fixed

$y_a - y_b = Y \to \infty$

$y_c - y_b \to \infty$

$$E\frac{d^3\sigma}{d^3p} \sim \frac{1}{S}\sum_k \beta_k^{b\bar{b}}(0)\left(\frac{S}{S_0}\right)^{\alpha_k(0)} F_k^{a\to c}(\vec{p}_T;\ y_a - y_c) \qquad \text{(III.4a)}$$

or in terms of Feynman's variable

$$E\frac{d^3\sigma}{d^3p} \sim \frac{1}{S}\sum_k \beta_k^{b\bar{b}}(0)\left(\frac{S}{S_0}\right)^{\alpha_k(0)} \hat{F}_k^{a\to c}(\vec{p}_T;x) \qquad \text{(III.4b)}$$

Some important points have to be made concerning the application of (III.4a) or (III.4b):

1. All singularities which have the quantum numbers appropriate for coupling to the $b\bar{b}$ channel have to be included. This, of course, includes the vacuum, Pomeranchuk, singularity. In the usual case the Pomeron leads to Feynman scaling, or something like it.
2. As written, (II.4) contains only pole contributions. The contribution of Regge cuts is more complicated, containing logarithmic factors and a possible continuum of powers. It is naive to believe that the Regge cut contributions to this 6-point function need have very much to do with the Regge cuts in 2-2 amplitudes. Of course, it often doesn't hurtto be naive when you can't think of any improvements to the simple form.
3. The usual trick is to keep only two terms in (III.4), a Pomeron pole and a term associated with the leading meson poles with intercept,

$$E\frac{d^3\sigma}{d^3p} \sim \beta_{\mathbb{P}}^{b\bar{b}}(0)\, F_{\mathbb{P}}^{a\to c}(p_T;\ y_c - y_a) + \beta_M^{b\bar{b}}(0)\, F_M^{a\to c}(\vec{p}_T;\ y_c - y_a)\left(\frac{S}{S_0}\right)^{-1/2}$$

(III.4c)

This represents an "approximate" asymptotic expansion with <u>unknown</u> corrections. There are possible correction terms to (III.4c) associated with the Pomeron which are depressed by a single power of S. These are sometimes referred to as attributable to the <u>kinematic daughters</u> of the Pomeron. These corrections cannot be disentangled in general from true, low-lying J-plane singularities, and are not necessarily the most important but they seem crucial in comparing $pp \to \bar{p}$ with with $pp \to \pi$ (Sivers, 1973).

It is important to remember that these corrections should be larger for a given reaction as we go to larger p_T since they are responsible for most of the energy dependence of the large-p_T cross sections. (See Cronin's presentation at the Topical Conference.)

4. After all these warnings the most important thing about (III.4c) is that it can be tested quite easily. Because few experiments have been done the evidence for its validity is neither very strong nor very poor.

Schindler, et al. (1974), have looked at the processes $pp \to \pi^\pm$ in the target fragmentation region, $y_{lab} \leq 0$. Their plots are shown in Figs. III.1 and III.2. It is not too hard to fit a portion of these graphs with a straight line but there is some suggestion we might need corrections. It seems important to try to do better--to decide whether we should include kinematic corrections, more terms, or try logarithmic factors. It is important for several theories concerning the relevant patterns of exchange degeneracy that the data are approaching the asymptotic limit from above. For a thorough discussion of these theories I suggest the review of Roberts (1973).

One reason for doing fits of the form (III.4c) for a large number of different reactions and different ranges of the kinematic variables is that it would be useful for a systematic study of Pomeron factorization. If we can isolate the Pomeron term in many different reactions we can test

$$\frac{\beta_{\mathbb{P}}^{b\bar{b}}(0)\, F_{\mathbb{P}}^{a\to c}(\vec{p}_T,x_c)}{\beta_{\mathbb{P}}^{b\bar{b}}(0)\, \beta_{\mathbb{P}}^{a\bar{a}}(0)} = \frac{\beta_{\mathbb{P}}^{b'\bar{b}'}(0)\, F_{\mathbb{P}}^{a\to c}(\vec{p}_T,x_c)}{\beta_{\mathbb{P}}^{b'\bar{b}'}(0)\, \beta_{\mathbb{P}}^{a\bar{a}}(0)}. \qquad \text{(III.5)}$$

with

$$b,\ b' \in (\pi^+,\ \pi^-,\ K^+,\ K^-,\ p,\ \bar{p},\ \gamma,\ \ldots)$$
$$c \in (\pi^+,\ \pi^-,\ K^+,\ K^-,\ p,\ \Lambda,\ \Sigma,\ n,\ \ldots)\ .$$

The fact that there are many different tests at different values of X and $\vec{p}_T$ is important since we now have strong evidence from the rising cross sections and long range azimuthal correlations that the Pomeron is not even approximately a simple pole. Violation of factorization must show up at some level and it is interesting to know whether they can be small in single particle inclusives as they evidently are in total cross sections. Preliminary studies of factorization have been done by M.S. Chen et al. (1971), Miettenen (1971) as well as by Ellis, Finkelstein and Peccei (1972).

Energy Fractions

Using energy conservation, we have the sum rule

$$\sqrt{s} = \sum_c \int \frac{d^3p_c}{E_c}\,(E_c)\ f^c_{ab}(S,\ \vec{p}_c) \qquad \text{(III.6a)}$$

where $f_{ab} = \sigma^{-1}_{ab}\, E_c\, d^3\sigma/d^3p_c$. The individual terms in (3.6) are recognized as giving the average amount of c.m. energy per collision carried off by the constituents of type c. We therefore define the average fraction of c.m. energy per event as

$$\eta_c = \int \frac{d^3p_c}{E_c} \left(\frac{E_c}{\sqrt{s}}\right) f^c_{ab}(S,\vec{p}_c) \qquad \text{(III.6)}$$

or using Feynman's scaling parameter

$$\eta_c(S) = \frac{1}{2} \int_{-1}^{+1} dx\ d^2p_T\ f^c_{ab}(X,\vec{p}_T;S) \qquad \text{(III.7)}$$

These energy fractions seem to me to be terribly important numbers. They can be interpreted as giving the particle content of hadronic energy. When we take into account the fact that the distributions in transverse momentum are sharply peaked so that the integration over d^2p_T in (III.7) although nominally dependent on S, become independent of energy, we see that the behavior of the energy fractions is important for the approach to asymptotic behavior.

Now that the evidence has come into indicate that total cross sections rise so that it is not so convenient to think of the Pomeron as a simple pole, the question arises how this might affect the Feynman-Yang scaling hypothesis. If the normalized distributions, f_{ab}, become independent of energy for all stable particles then the energy fractions all go to constants. This is a natural way that scaling could occur but--surprise--it doesn't have to be so simple.

Putting complicated Pomeron singularities into Mueller-Regge diagrams indicates the strong possibility that the normalized distributions should change slowly with energy. One thing that can happen is that the diffractive processes, such as $pp \to p$, have a singularity at $x = 1$ near the kinematic limit

$$|x|_{max} = 1 - \frac{(m_N + m_\pi)^2 + M_N^2 + 2p_T^2}{S} \qquad \text{(III.8)}$$

of the integral in (III.7). The energy fraction associated with the protons then rises slowly to one as the fraction of energy associated with "produced" particles slowly falls to zero. This occurs as the normalized distributions for nonleading particles is a nonzero constant only in a vanishing small neighborhood of $x = 0$,

$$f^c_{ab}(S,X) = O(1/\ln S)\ , \qquad x \neq 0,\ c \neq a,\ b \qquad \text{(III.9)}$$

There is some indirect evidence for this exciting possibility from triple-regge phenomenology but the experimental energy fractions, Fig. (III.3), are consistent with approaching asymptotic constants. For comparison, particle multiplicities are shown in Fig. III.4.

Triple-Regge Region

There's been a great deal of study of the "diffractive" triple-regge region as several papers have gotten involved in extracting a triple-Pomeron coupling. Let's back off and look at the case where a and c have different quantum numbers

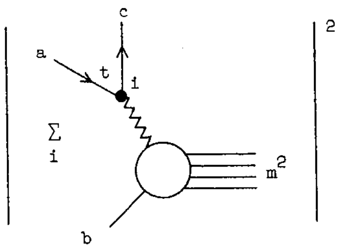

Recall the standard "derivation" of the triple-regge formula in terms of the diagram above. We first presume we can isolate the Regge poles, $\alpha_i(t)$ in the $a\bar{c}$ channel

$$E\frac{d^3\sigma}{d^3p} \sim \frac{1}{S}\sum_{\ell} \beta^i_{a\bar{c}}(t)\left(\frac{S}{m^2}\right)^{2\alpha_i(t)+1} g^i_b(m^2) \qquad \text{(III.10)}$$

The next order of business is based on the assumption that the bottom part of the diagram represents something like the Reggeon-α_i-particle-b cross section

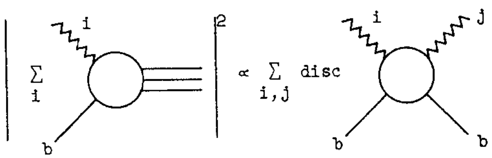

which, in the limit of large M^2 is presumed to Reggize

$$E\frac{d^3\sigma}{d^3p} \sim \frac{1}{S}\sum_{i,j,k} \gamma_{ijk}(t,t,0)\left(\frac{S}{m^2}\right)^{\alpha_i(t)+\alpha_j(t)} (m^2)^{\alpha_k(0)} \qquad \text{(III.11)}$$

Let's go back and look at a simple case where we have π-exchange--say $\gamma\to\pi^+$. Here, from analogy to exclusive photoproduction $\gamma p\to\pi^+ n$, we guess that it may not be trivial to isolate the π Regge pole from the absorptive cut corrections. Fables say the absorptive cuts are as big as the pole itself. Just for the fun of playing with the diagram let's try to represent the absorptive cut as something like a two-body state in the $a\bar{c}$ channel

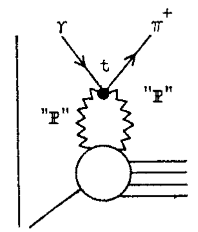

Thus we no longer have Reggeon + particle $\to M^2$ but "π"+Pomeron + particle $\to M^2$ which doesn't even have to be connected. There's a piece which looks like

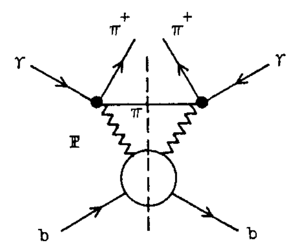

We now have no reason to "reggeize" the bottom vertex when M^2 large since the effective energy of the process $Pp\to Pp$ is not necessarily related to M^2. Everyone has probably already noticed that what's going on in the last diagram is something like inclusive ρ production where the ρ gives a in the triple regge region. This can produce a problem for experimenters. Should they try to remove ρ events from the data before looking at (III.11)? The simple things we've done here suggest that such "containimation" is only one piece of the absorptive corrections to π exchange in the $\gamma\pi$ channel.

Similar arguments can help us understand baryon exchange in $p \to \pi^{\pm}$, $\pi^{\pm} \to p$ and $K^{-} \to \Lambda$. Consistently, analyses of (heavy $\to$ light) processes (Fig. III.5) find trajectories with intercepts lower than the same trajectory in (light $\to$ heavy) processes. Because of the different kinematics we are not always as close to t_{min} when heavy $\to$ light and we can get contributions to the triple-regge region from multiperipheral graphs like

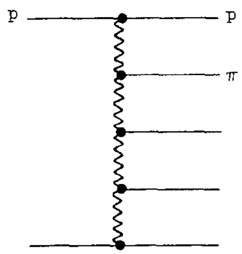

Azimuthal Correlations

Freedman, Jones, Low and Young (1971) have discussed two particle azimuthal correlations in terms of the diagram

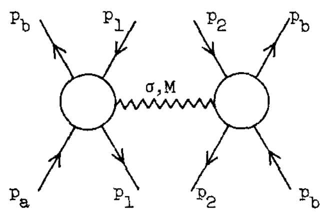

$$t_1 = (p_a - q_1)^2 \qquad \cos\phi = \hat{p}_1 \cdot \hat{p}_2$$

$$t_2 = (p_0 - q_2)^2$$

$$\frac{s_2}{m^2} = (1 - x_1)^{-1}$$

$$\frac{s_2}{m^2} = (1 + x_2)^{-1}$$

$$\frac{s}{m^2} = (1 - x_1)^{-1}(1 + x_2)^{-1}$$

Since there is zero four-momentum transfer between the two sides of the diagram, Lorentz invariance implies that the scattering amplitude, and presumably the M^2 discontinuity, has an $O(3,1)$ expansion analogous to that of an equal mass forward 2-2 amplitude

$$A_{ab\bar{c}_1\bar{c}_2 \to ab\bar{c}_1\bar{c}_2}$$

$$= \delta_{\lambda\lambda'} \sum_{M,r,r'} \int d\sigma(M^2 - \sigma^2)\, A_{ab\bar{c}_1\bar{c}_2}(M,\sigma,r,r')\, e^{i\lambda'\phi}\, d^{M\sigma}_{r\lambda' r'}(\eta) \tag{III.12}$$

where $d^{M\sigma}_{r\lambda r'}$ is an $SO(3,1)$ rotation matrix and $\cosh\eta = (m^2 - t_1 - t_2)/2(t_1 t_2)^{1/2}$. The leading contribution of the d function is to helicity flip

$$d^{M\sigma}_{r\lambda r'}(\eta) \sim (m^2)^{(\sigma - 1 - |M-\lambda|)} \tag{III.13}$$

The contribution of a Lorentz pole with σ, M to the 8-point amplitude at large M^2 is then

$$A_{ab\bar{c}_1\bar{c}_2 \to ab\bar{c}_1\bar{c}_2} \sim (M^2)^{\sigma-1} F_M(t_1,t_2,x_1,x_2)\cos(M\phi) \tag{III.14}$$

A Lorentz pole with $M \neq 0$ cannot correspond to a simple Regge pole since it contains a mixture of parities. A Regge pole with intercept $\alpha(0)$ leads to dependence suppressed by an extra power of M^2

$$A^{\text{Regge}} \sim (M^2)^{\alpha(0)} F_0(t_1,t_2,x_1,x_2)\left[1 + \frac{\cos\phi}{M^2} g_1 + \cdots\right] \tag{III.15}$$

Data on azimuthal correlations at high has recently become available. If we parametrize

$$\frac{E_1 E_2\, d^6\sigma}{d^3p_1\, d^3p_2} = a(y_1, y_2) + b(y_1, y_2)\cos\phi \tag{III.16}$$

and the value of b is shown as a function of the rapidity gap between particles 1 and 2 in Fig. III.   . The data indicate a long-range correlation which is important since it is among the best evidence for a Pomeranchuk singularity which is not a simple pole. The dependence of the correlation on the magnitude of the transverse momenta is in good agreement with the expectations of simple momentum conservation in the uncorrelated jet model (longitudinal phase space). We do not have the "local" conservation of transverse momentum expected from the multiperipheral model.

Figure Captions, Section III

Fig. III.1. Invariant cross sections for π^+ and π^- production, integrated overall transverse momenta, displayed as a function of $s^{-1/2}$: (a) The differential cross section at the value of laboratory rapidity equal to zero, (b) the integrated cross section for negative values of laboratory rapidity. Taken from Schindler et al. (1974).

Fig. III.2. Invariant cross sections for π^+ and π^- production, integrated overall transverse momenta, displayed as a function of $s^{-1/2}$: (a) The differential cross section at the value of laboratory rapidity equal to $-.5$, (b) the integrated cross section for values of laboratory rapidity less than $-.5$. Taken from Schindler et al. (1974).

Fig. III.3. Fraction of C.M. energy in pp collisions carried off by a given type of particle.

Fig. III.4. Particle multiplicities in pp collisions.

Fig. III.5. Effective N trajectory from $K^- \xrightarrow{p} \Lambda$ compared with trajectory from $p \xrightarrow{p} \pi^+$. Taken from Palev et al. (1973).

Fig. III.6. Fit of azimuthal correlations by Dibon et al. (1973) to a form $a + b \cos \phi$ showing long range correlations.

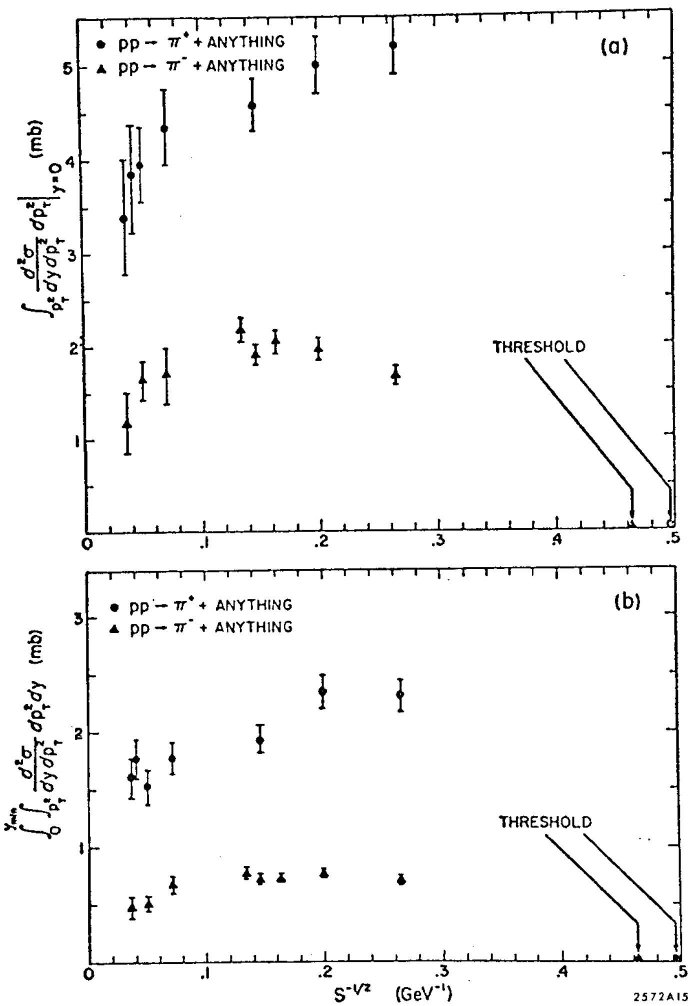

Fig. III.1

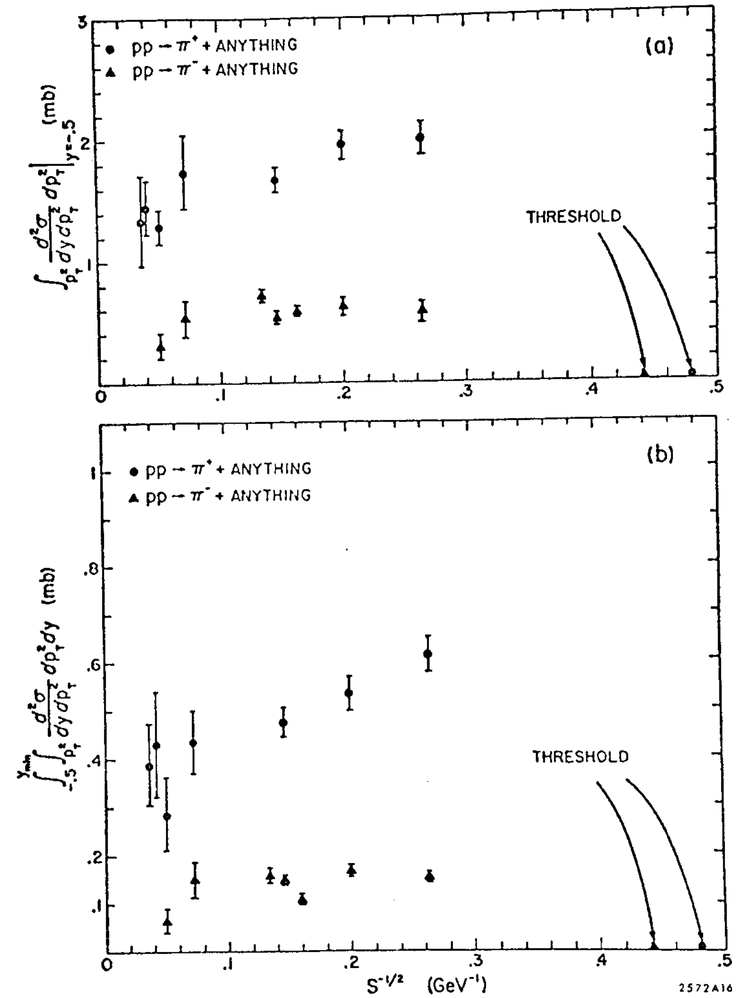

Fig. III.2

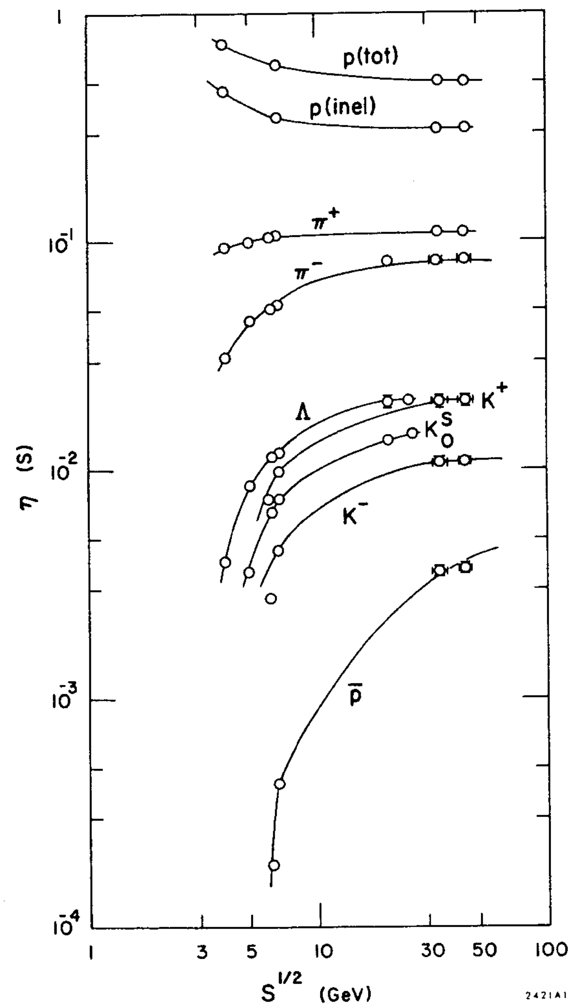

Fig. III.3

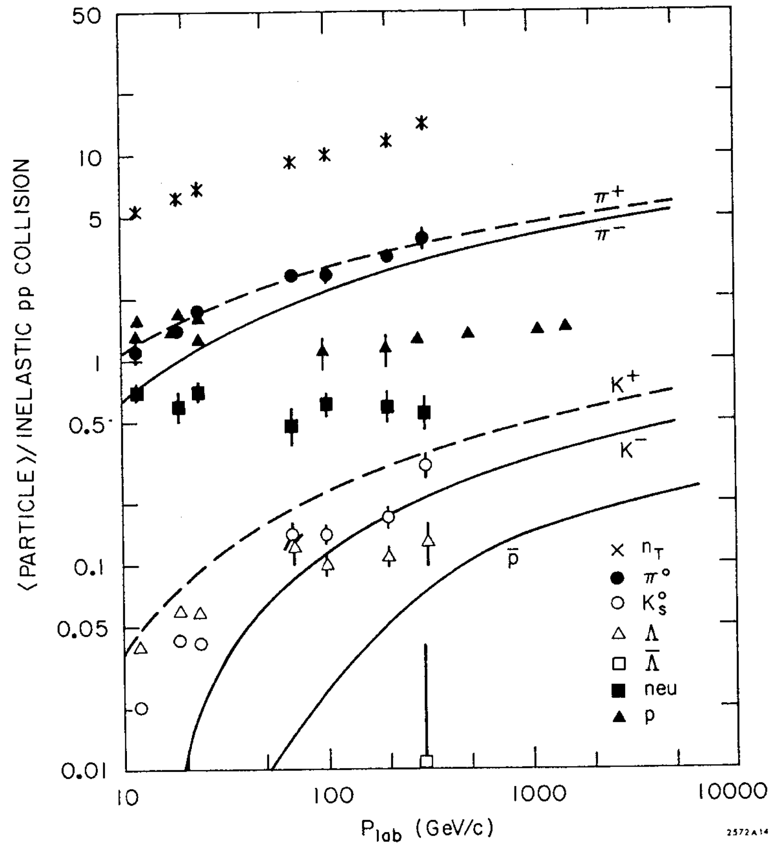

Fig. III.4

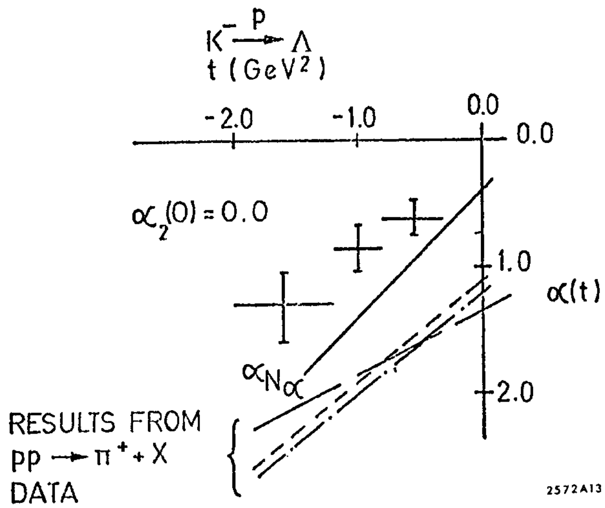

Fig. III.5

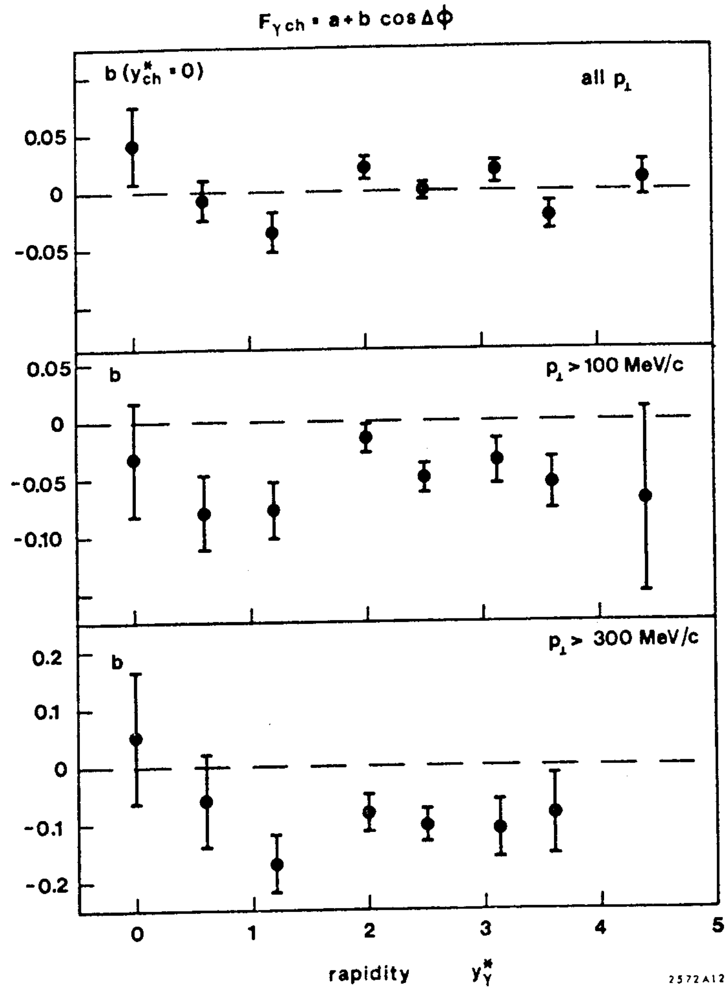

Fig. III.6

IV. MODELS FOR EXCLUSIVE PROCESSES

Instead of dealing directly with inclusive processes through the generalized optical theorem and Regge approximations for the appropriate 6-pt and 8-pt functions, we have the option of constructing models for the various exclusive reactions which contribute to an inclusive distribution. In order to be able to deal with multiparticle-phase-space integrals these models will be crude and will involve many simplifying assumptions. However, since the exclusive models can embody kinematic effects directly and can deal properly with conserved quantum numbers (e.g. implement the fact that antibaryons are produced in $B\bar{B}$ pairs instead of alone) they can provide a useful supplement to the Mueller-Regge approach. Basically, we hope that averaging over the unseen particles will enable the crude model to produce a reasonable inclusive cross section.

The simplest model for the exclusive production processes is probably also the most familiar, the Chew-Pignotti (1968) multiperipheral model. This model is usually dealt with in the strong-ordered approximation where the outside particles on the multiperipheral chain take essentially all the energy. This sort of drastic truncation of multiparticle kinematics removes much of the advantage of dealing with an exclusive model. One important feature of this model is the fact that the exclusive cross sections can be calculated exactly (DeTar, 1971) and we can see that there is a formal analogy between the Chew-Pignotti model and a classical one-dimensional non-interacting gas.

The gas analog has proved very useful as several people have explored the possibility that the techniques developed to deal with realistic gases and fluids can give some insight into hadron dynamics. This kind of approach allows us to combine two disparate phenomena under a single formalism and is very educational. An introduction to the ideas underlying the analogy can be found in the review lectures of Arnold, and further discussion can be found in Harari's review.

Let's reflect a bit on the properties we want to require of an exclusive model. It should certainly be required to be consistent with the properties (1)-(4) which were listed at the beginning of Section II. The best try so far to get all these things right while still retaining enough simplicity so that complicated Monte Carlo calculations are not needed for most results comes from work on a class of "cluster models." (See, for example Hamer and Peierls (1973), Bassetto et al. (1972),)Chiu and Wang (1973), Berger and Fox (1973), Bialas et al. (1973).) Current usage roughly equates the terms, "clusters," "fireballs" and "generalized resonances." Of these terms, the use of the word cluster probably carried the least extra connotation. Instead of trying to give a complete review of these cluster models here I will concentrate on those calculations which can be done with cluster models which supplement or improve our understanding of inclusive spectra based on Mueller-Regge analysis. A more complete discussion can be found in the review of Bialas.

Let's consider the independent emission of m neutral clusters in the central region with a matrix element squared

$$|T(p_a,p_b;\ p_1,p_2;q_1,\ldots,q_m)|^2 = g^m\ F(p_1)\ F(p_2)\ G(q_1,m_1)\cdots G(q_m,m_m) \qquad (IV.1)$$

where $F(p_i)$ represent "leading" clusters with the quantum numbers of the incident particles and $G(q_i,m_i)$ describes the production of a neutral cluster with sharply limited transverse momentum. This simple form allows us to calculate rather directly the average cluster multiplicity under the assumption that the leading particles take a large fraction of the energy (Sivers and Thomas, 1972).

If $\langle J\rangle$ denotes the average cluster multiplicity, we have approximately

$$\langle J\rangle \cong \pi g \int dm \int d(q_T^2)\ G(q_T,m)\ K_0(2\lambda s^{-1/2}m) \qquad (IV.2)$$

where $G(q_T,m)$ is the probability of producing a cluster of mass m and transverse momentum q_T and the K_0 is an associated Bessel function. If the probability for the decay of the cluster into different kinds of particles is not a function cluster mass we would have the average mass of the cluster determining the energy scale for the approach to asymptotic behavior of π's, K's, $\bar{p}$'s, etc.

One advantage of the cluster model over Mueller-Regge approaches can be found in two-particle correlations. Based on diagrams like

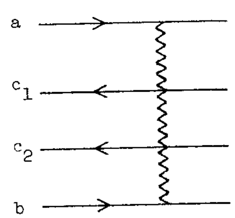

we can predict that two-particle correlation functions for y_1, y_2 in the central region should behave as

$$C(y_1, y_2) \propto \exp\{-|y_1-y_2|\cdot[\alpha_{\mathbb{P}}(0)-\alpha_M(0)]\} \tag{IV.3}$$

which is something like what is seen in the data where correlation length

$$\Lambda \cong (\alpha_{\mathbb{P}}(0) - \alpha_M(0))^{-1} \approx 2 \tag{IV.4}$$

is observed (see Fig. IV.1). The problem is, of course, that the requirement that both particles be in the central region is rather severe and we would prefer a calculation which dealt with all regions of phase space on a more equivalent footing. Cluster models fit this requirement.

The first order of business in discussing correlation functions is to get the multiplicity distribution correct. In a cluster model where the clusters themselves are independent, we have $f_2^- = \langle n_-(n_- - 1)\rangle - \langle n_-\rangle^2$ given by

$$f_2^- = \frac{\langle h_-(h_- - 1)\rangle}{\langle h_-\rangle} \langle n_-\rangle$$

where $\langle h_-\rangle$ is the average number of negative hadrons emerging from a single cluster and $\langle h_-(h_- - 1)\rangle$ is the average number of negative pairs from a cluster. Assuming a narrow probability distribution

$$P(h_i) \cong \delta(h_i - \langle h_i\rangle) \tag{IV.6}$$

and taking as a crude parametrization of the data

$$f_2^- \cong (0.7 \pm 0.1) \langle n_-\rangle \tag{IV.7}$$

we see that with hadronic clusters containing

$$\langle h_-\rangle \cong 1.7$$

negative particle we get the integral of the correlation function correct.

Once we get the multiplicity distribution right we are well on our way to getting the one and two particle distributions. Let's transform to the cluster rest frame and look at the rapidity distribution of particles <u>assuming</u> isotropic decay:

In this frame

$$\frac{dy}{\cosh^2 y} = \frac{p\ d\cos\theta}{E}$$

$$\frac{d^3p}{E} = \frac{dp^2\ d\Phi\ dy}{\cosh^2 y}$$

and we have

$$\frac{dh}{dy} \propto (\cosh y)^{-2} \langle q\rangle^2 \int_{[u \sinh y/\langle q\rangle]}^{\infty} dx\, n(x) \qquad (IV.8)$$

If we neglect the dependence of the integral on the lower limit we have the normalized single cluster decay distribution

$$g(y) \cong 0.5(\cosh y)^{-2} \qquad (IV.9a)$$

which can be approximated in turn by

$$g(y) \cong \frac{1}{\delta(2\pi)^{1/2}} \exp(-y^2/2\delta^2) \qquad (IV.9b)$$

with $\delta \cong 0.8$-0.9.

The inclusive angle particle distribution is given by

$$\frac{1}{\sigma_{tot}} \frac{d\sigma_h}{dy} = \int dy'\, \rho(y')\, \langle h\rangle\, g(y - y') \qquad (IV.10)$$

where $\langle h\rangle$ is the average number of hadrons of type h in the cluster and $\rho(y)$ is the density of clusters. The correlation function is given by two hadrons from the same cluster

$$C(y_1, y_2) = \int dy'\, \rho(y')\langle h(h-1)\rangle\, g(y' - y_1)\, g(y' - y_2) \qquad (IV.11)$$

of if $\rho(y')$ is slowly varying

$$C(y_1, y_2) \cong \frac{\langle h(h-1)\rangle}{2\delta\pi^{1/2}} \left(\frac{1}{\sigma} \frac{d\sigma}{dy}\bigg|_{y=0} \frac{1}{\langle h\rangle}\right) \exp\left(\frac{-(y_1 - y_2)^2}{4\delta^2}\right) \qquad (IV.12)$$

The effective "correlation length" is very similar to that in Mueller-Regge analysis, $\lambda^R = 2$,

$$\lambda = 2\delta \cong 1.6 - 1.8 \qquad (IV.13)$$

Notice that if we form an N-particle correlation function we get a factor

$$C(y_1, \ldots, y_n) \propto \exp\left[- \sum_{i > j} \frac{(y_i - y_j)^2}{2n\delta^2}\right] \qquad (IV.14)$$

so that the correlation length increases with the number of particles to be correlated. Equation (IV.14) offers an opportunity to distinguish between cluster models and a more realistic Mueller-Regge approach than (IV.3) since in the latter the correlation length should not depend on the number of particles. Until 3 and 4 particle correlations become available the two approaches can be considered complementary. A Gaussian may hold for small Δy while (IV.3) is more relevant at large Δy. The advantage of cluster models in the fragmentation region is obvious in the work of Ranft and Ranft (1973).

Contour plots of two particle correlation functions from the NAL bubble chamber case show in Figs. IV.1 and IV.2.

The cluster model can deal with diffractive dissociation, and, in essence, become a 2-component model by careful treatment of the clusters containing the leading particles. We usually have to give up the assumption of isotropic decay for this cluster. This is discussed by Pokorski and van Hove (1970).

By fitting the average multiplicity we can calcúlate the density of clusters and we find, on the average, that our assumptions predict an average spacing of something more than one unit of rapidity between clusters. This is uncomfortably small since the clusters each spread particles over two units of rapidity and we must therefore have considerable overlap. This overlap makes it difficult to decide whether it makes sense experimentally to determine the average quantum numbers of clusters and this is unfortunate. If clusters had turned out to be easily observable with well-defined quantum numbers they would be perfect candidates for the long-spurred role of fundamental hadrons.

One of the simplest-things to calculate in a cluster model is mean square charge transfer. If a neutral cluster is produced at y_0 and decays into N_+ positive and $N_- = N_+$ negative particles then assuming a binomial distribution of particles going left and right the mean square charge in the right hemisphere of the cluster is

$$\langle U^2 \rangle_{\text{cluster}} = \frac{1}{2} N_+ = \frac{1}{4} N_{ch} \qquad (IV.15)$$

This result can be used in the framework of neutral cluster models (Quigg and Thomas, 1973) to predict

$$\langle U^2(y) \rangle = \frac{2}{3} \delta \frac{d\sigma_{ch}}{dy} \qquad (IV.16)$$

where δ is the dispersion parameter in (IV.9b). The prediction that $\langle U^2(y) \rangle$ is proportional to $d\sigma_{ch}/dy$ is in remarkable agreement with the data (Chao and Quigg, 1974) and the data indicate a universal constant of proportionality. Comparison with (IV.16) is indicated in Fig. IV.3. The observed size of $\langle U^2(y) \rangle$, however, predicts a value of $\delta \cong 1.2$ which is too large to explain rapidity correlations. Better agreement can be obtained using charged clusters but the approach then loses a great deal of the predictive power. It would be interesting to compare (IV.16) with data from $\bar{p}p$ annihilations, $e^+e^- \to$ hadrons and deep inelastic electroproduction (Newmeyer and Sivers, 1974) to investigate to what extent clustering properties of hadrons are independent of the production mechanism.

Rapidity correlations at fixed charge multiplicity have been proposed as a severe test of the assumptions of cluster models (Berger, 1974). As emphasized by Berger, if we restrict attention to $n \gtrsim \langle n \rangle/2$ the semi-inclusive distributions are comparatively free of diffractive events and we can obtain cleaner insight into the properties of the nondiffractive production mechanism. By studying the n-dependence of the semi-inclusive correlations we can obtain a new type of information (Arnold and Thomas, 1974). The correlation function at fixed charged multiplicity can be written

$$C_n(y_1, y_2)$$
$$= A_0 \left(\frac{1}{\sigma_n} \frac{d\sigma_n}{dy} (y_1 + y_2) \right) \frac{1}{2\delta\pi^{1/2}} \exp\left(- \frac{(y_1 - y_2)^2}{4\delta^2} \right)$$
$$- \frac{(A_0 + 1)}{n} \left(\frac{1}{\sigma_n} \frac{d\sigma_n}{dy} (y_1) \right) \left(\frac{1}{\sigma_n} \frac{d\sigma_n}{dy} (y_2) \right) \qquad (IV.17)$$

where A_0 is defined

$$A_0 = \left. \frac{\langle h(h - 1) \rangle}{\langle\langle h \rangle\rangle} \right|_n \qquad (IV.18)$$

in terms of the average number of hadrons per cluster at fixed multiplicity. If the multiplicity distribution from a cluster is narrow then (IV.18) should be approximately independent of n while for a broad distribution it should increase with n. Data from an NAL bubble chamber experiment (Singer et al. 1974). The implication of the data is that there is some variation of A_0 with n.

Although I mentioned the advantages of keeping exclusive models simple enough so that extensive Monte Carlo calculations are not required this was not intended to downplay the possible value of Monte Carlo techniques. One very important application of Monte Carlo calculations consists of making model-independent tests of the data. For example, Ludlam and Slansky (1973) have constructed a way to measure event by event fluctuations around the mean particle densities in various regions of phase space. They show how this measurement is sensitive to the existence of clustering in the production mechanism and demonstrate the existence of clusters in the data. A similar application of "nonparametric" methods has been demonstrated by Freedman (1974) who, among other things, tests the hypothesis that the matrix element for $pp \to pp + 4\pi$ is independent of azimuthal angles.

Figure Captions, Section IV

Fig. IV.1. Data on $R^{\pi^+\pi^-}(y_1, y_2)$ from pp collisions of 400 GeV/c. From Ferbel, topical conference.

Fig. IV.2. Data on $R^{cc}(y_1, y_2)$ from pp collisions at 400 GeV/c. From Ferbel, topical conference.

Fig. IV.3. Data on $\langle U^2(y)\rangle$ compared with $d\sigma_{ch}/dy$. From Chao and Quigg (1974).

Fig. IV.4. Data on $R_n(y_1, y_2)$ from Singer et al. (1974).

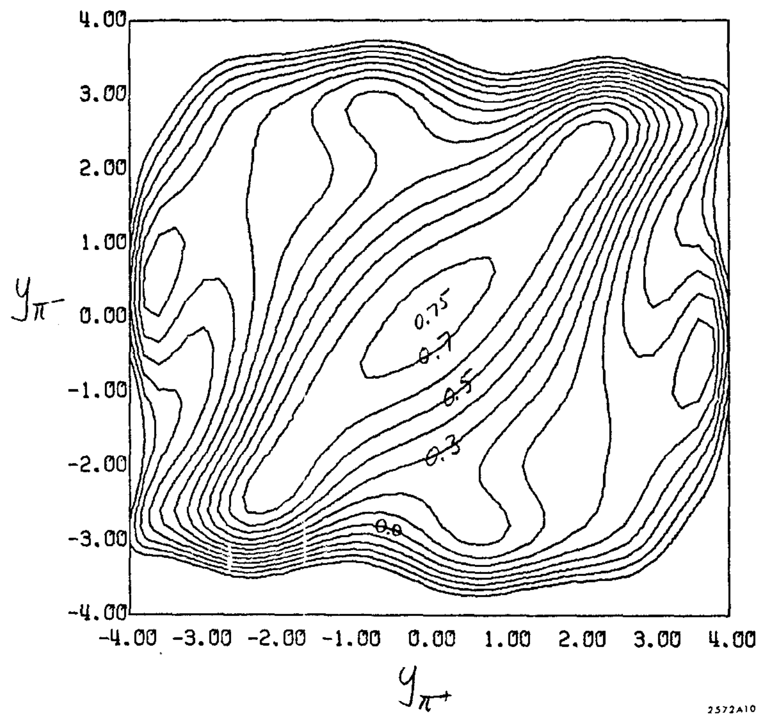

Fig. IV.1

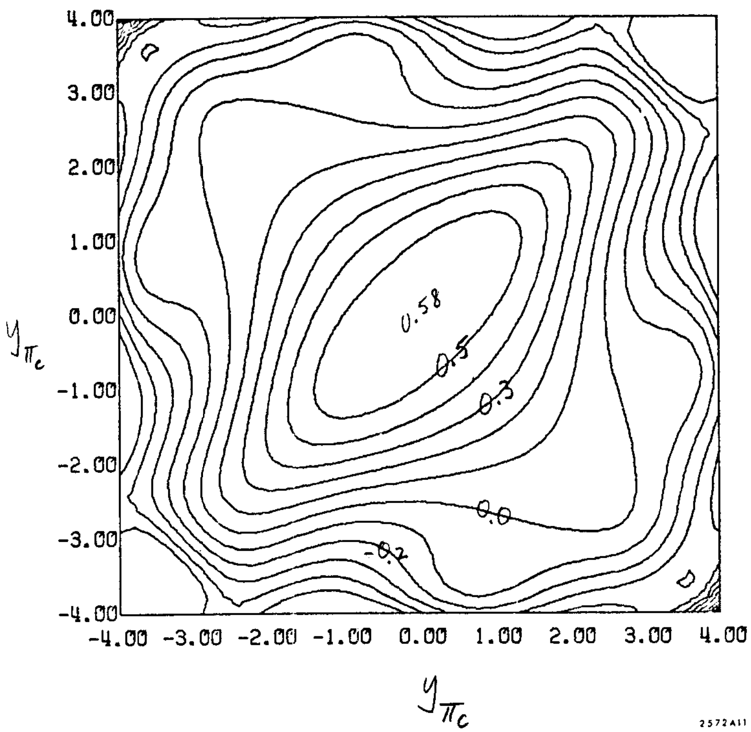

Fig. IV.2

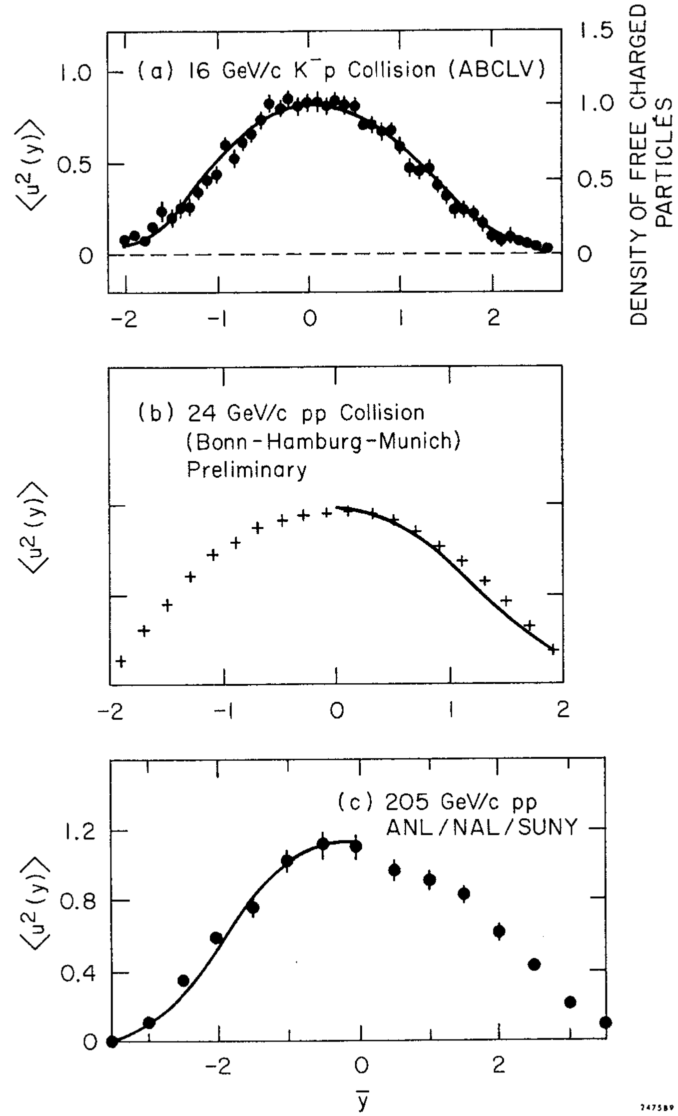

Fig. IV.3

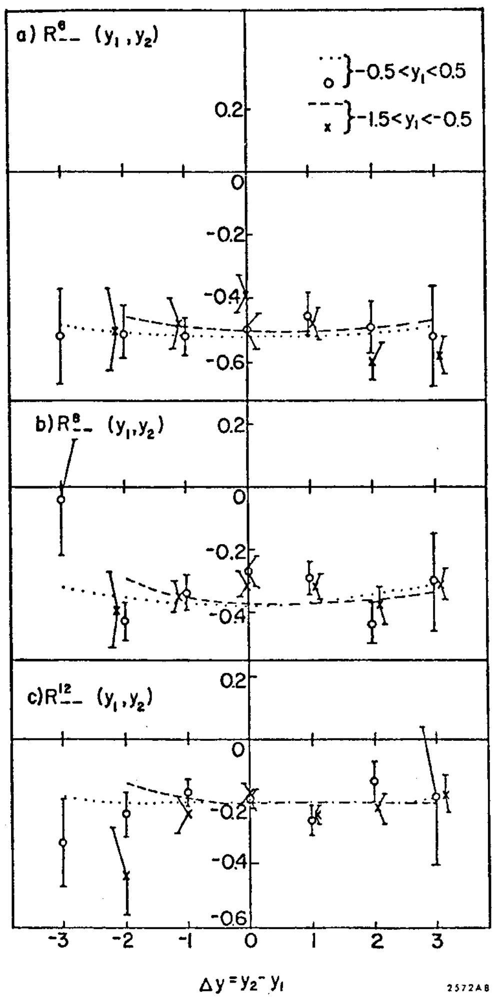

Fig. IV.4a

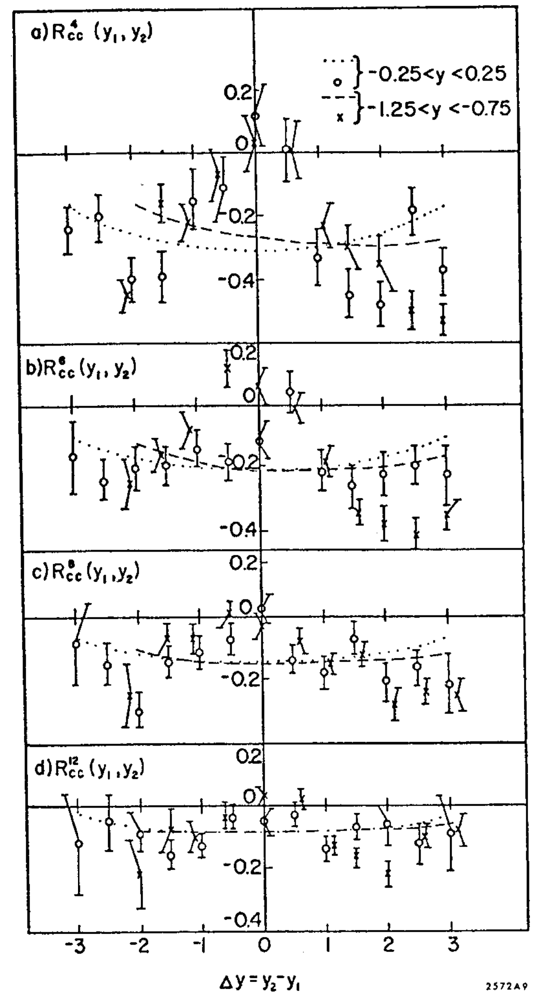

Fig. IV.4b

APPENDIX A

Variables in Single Particle Inclusives

The inclusive $ab \to cX$, indicated schematically as,

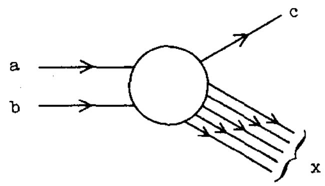

is commonly represented in the literature in terms of one of 3 sets of kinematic variables. The effective use of the literature requires a familiarity with all 3 sets and the relationships between them. The following brief summary of inclusive kinematics may prove convenient. For a more complete discussion of the relative advantage of plotting data in a particular way see, J.D. Jackson, "Scottish Universities Summer School Lectures."

1. The variables (s, t, u, M^2)

The use of any 3 of the variables

$$\begin{aligned} s &= (p_a + p_b)^2 \\ t &= (p_a - p_c)^2 \\ u &= (p_b - p_c)^2 \\ M^2 &= (p_a + p_b - p_c)^2 \end{aligned} \tag{A.1}$$

subject to the constraint

$$s + t + u = M^2 + m_a^2 + m_b^2 + m_c^2 \tag{A.2}$$

is a direct extension of familiar two-body kinematics. These variables are naturally most convenient when it makes sense to treat the particles carrying away the unseen momentum as something like a normal single hadron state. For example, they appear naturally in the formulation of the triple-Regge expansion. Figure (A.1) shows some data on $pp \to p$ plotted as M^2 and t.

2. The variables (s, p_t, x)

In the c.m. frame, let's denote the components of the momentum of particle c longitudinal or transverse to the beam direction as p_L and p_t respectively. For unpolarized beams and targets the azimuthal direction of p_t is not important. The Feynman scaling parameter will be defined as

$$x' = p_L/s^{1/2} \tag{A.3}$$

Experimental results are often expressed in terms of

$$x' = p_L/p_L^{max}\,(p_t, s^{1/2}) \tag{A.4}$$

at low incident energies there can be substantial differences between x and x'. The variable x' has the property that its range of values is always (-1,+1). Some inclusive cross sections appear to scale more rapidly in terms of x' than in x but this doesn't mean x' is "better" than x. It is accepted that the Feynman scaling conjecture

$$\sigma_{ab}^{-1}\, E_c \frac{d^3\sigma}{d^3p_c}\,(x, p_T; s^{1/2}) \sim f_{ab}^c(x, p_T) \tag{A.5}$$

is intended to be an asymptotic expression. The finite energy corrections to (A.5) have to be studied and for the purpose of this study the variable x will usually be just as convenient or more convenient than x'. Keep on your toes, always pays to be aware of whether x or x' is being used in a given plot. Figure A.2a shows inclusive $pp \to \pi^-$ plotted against x' and Fig. A. 2b some data plotted against x.

3. The variables (s, κ, y)

The rapidity variable

$$y = \frac{1}{2} \ell n \frac{E + p_L}{E - p_L} \tag{A.6}$$

where the energy and the momentum are measured, for example, in the c.m. frame is useful for many types of analysis of high energy production processes. It defines the boost from the c.m. frame to the frame in which the momentum of particle c has only a transverse component. If two particles came from a cluster or resonance with longitudinal velocity β they will each have rapidity near

$$y \text{ cluster} = \tanh^{-1} \beta \tag{A.7}$$

This is true irrespective of the masses of the particles. For this reason the rapidity variable is useful in defining the concept of short range order. For the present short range order simply implies that particles with quite different rapidities are, in some sense, produced independently. It is convenient to define an effective transverse mass

$$\kappa = (m^2 + p_T^2)^{1/2} \tag{A.8}$$

which can be used to relate the energy and momentum separately to the rapidity,

$$\begin{aligned} p_L &= \kappa \sinh y \\ E &= \kappa \cosh y \end{aligned} \tag{A.9}$$

For two particles c_1 and c_2 the invariant $s_{12} = (p_1 + p_2)^2$ is given by

$$s_{12} = m_1^2 + m_2^2 + 2\kappa_1\kappa_2 \cosh(y_1 - y_2) - 2\vec{p}_{T1} \cdot \vec{p}_{T2} \tag{A.10}$$

Another convenience of the rapidity variable is that invariant phase space can be written

$$\frac{d^3p}{E} = d^2p_T \, dy \tag{A.11}$$

Various single particle inclusive distributions from pp collisions at the ISR as a function of Y_{lab} are shown in Fig. A.3. The connection between the lab rapidity and the c.m. rapidity is a simple translation

$$\begin{aligned} y_{lab} &= y_{cm} + \cosh^{-1}\left(\frac{s - m_a^2 + m_b^2}{2m_b s^{1/2}}\right) \\ &\cong y_{cm} + \log \frac{s^{1/2}}{m_b} \end{aligned} \tag{A.12}$$

4. Connections between the variables

The reader is invited to try his hand at the following simple exercises in order to convince himself of his dexterity with manipulations of the kinematic variables.

(a) Show that for positive x, and large s, the momentum transfer t in (A.1) can be written

$$t \cong m_a^2(1 - x) + m_c^2(1 - \frac{1}{x}) - \frac{p_T^2}{x} \tag{A.13}$$

What is the connection for $x < 0$?

(b) Verify that for $x < 0$ the missing mass can be written

$$M^2 = s(1 - x) + m_c^2(1 - \frac{2}{x}) - \frac{2p_T^2}{x} \tag{A.14}$$

when $P_L \neq 0$. What is the appropriate expression for $p_L = 0$?

(c) If $M_a^2 \neq M_c^2$ verify that for $x \neq 1$

$$t_{min} \cong \frac{(m_a^2 - m_c^2)m^2}{s} \tag{A.15}$$

(d) Verify the approximate relations between M^2 and c.m. rapidities.

$$M^2 \cong \begin{cases} s\left[1 - \frac{\kappa}{m_a}\exp(|y_c - y_a|)\right] & y_c > 0 \\ s\left[1 - \frac{\kappa}{m_b}\exp(|y_c - y_b|)\right] & y_c < 0 \end{cases}$$

(e) In Figs. A.4 and A.5, single particle distributions for $pp \to cX$ are shown for various particle at the ISR. Assuming approximate scaling, sketch these distributions as x and as y at $s^{1/2} = 10^4$. ($Y = \ln s = 2 \ln s^{1/2} = 13.82$.)

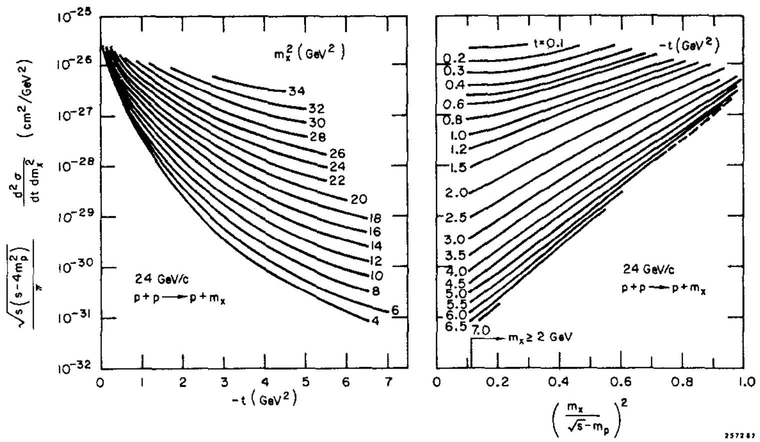

Fig. A.1

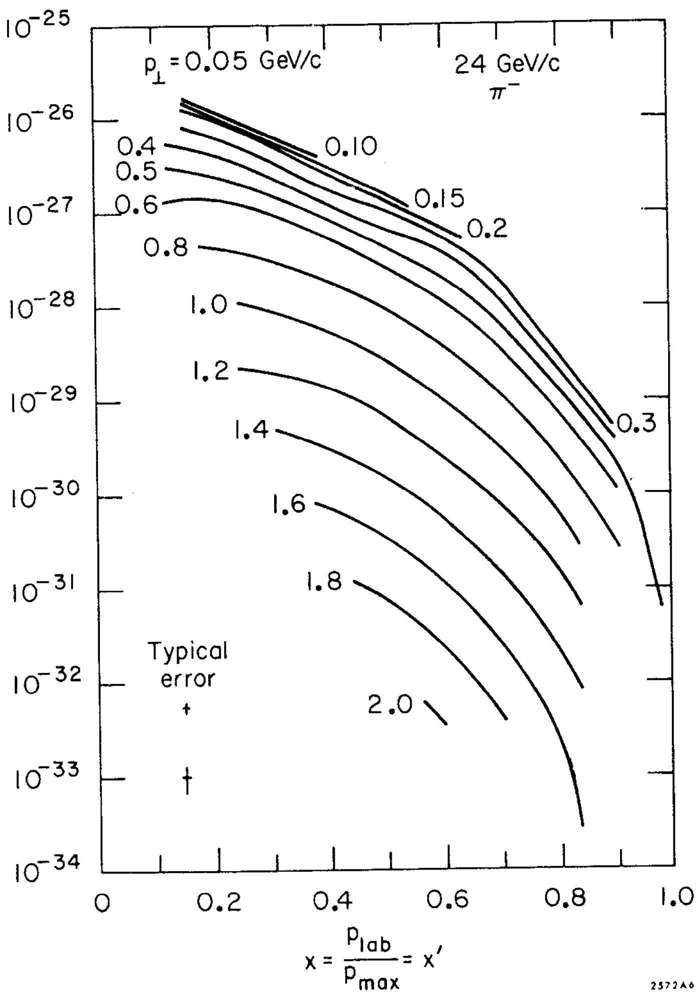

$p_\perp = 0.05$ GeV/c
24 GeV/c
π^-
0.10
0.15
0.2
0.3
0.4
0.5
0.6
0.8
1.0
1.2
1.4
1.6
1.8
2.0
Typical error
$x = \frac{p_{lab}}{p_{max}} = x'$

Fig. A.2

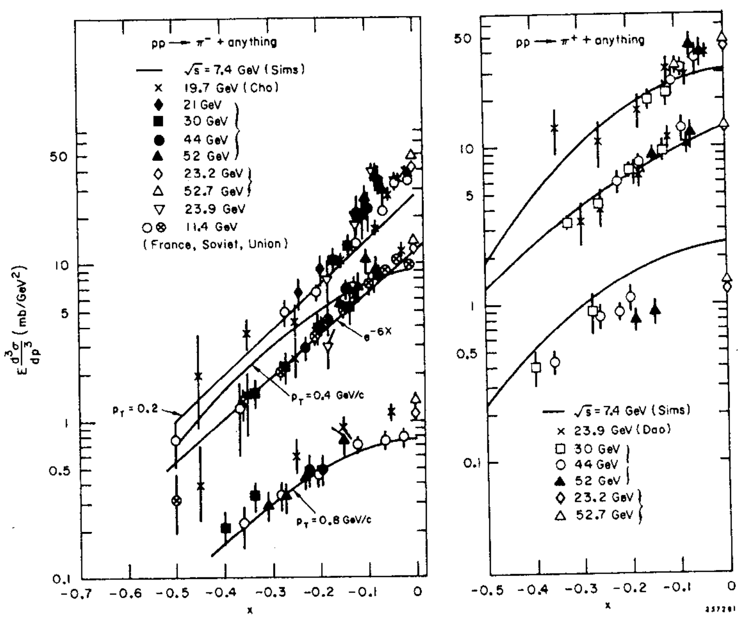

pp → π^- + anything
$\sqrt{s}$ = 7.4 GeV (Sims)
19.7 GeV (Cho)
21 GeV
30 GeV
44 GeV
52 GeV
23.2 GeV
52.7 GeV
23.9 GeV
11.4 GeV
(France, Soviet, Union)
$p_T = 0.2$
$p_T = 0.4$ GeV/c
$p_T = 0.8$ GeV/c
e^{-6X}
$E\frac{d^3\sigma}{dp^3}$ (mb/GeV^2)
x
pp → π^+ + anything
$\sqrt{s}$ = 7.4 GeV (Sims)
23.9 GeV (Dao)
30 GeV
44 GeV
52 GeV
23.2 GeV
52.7 GeV

Fig. A.3

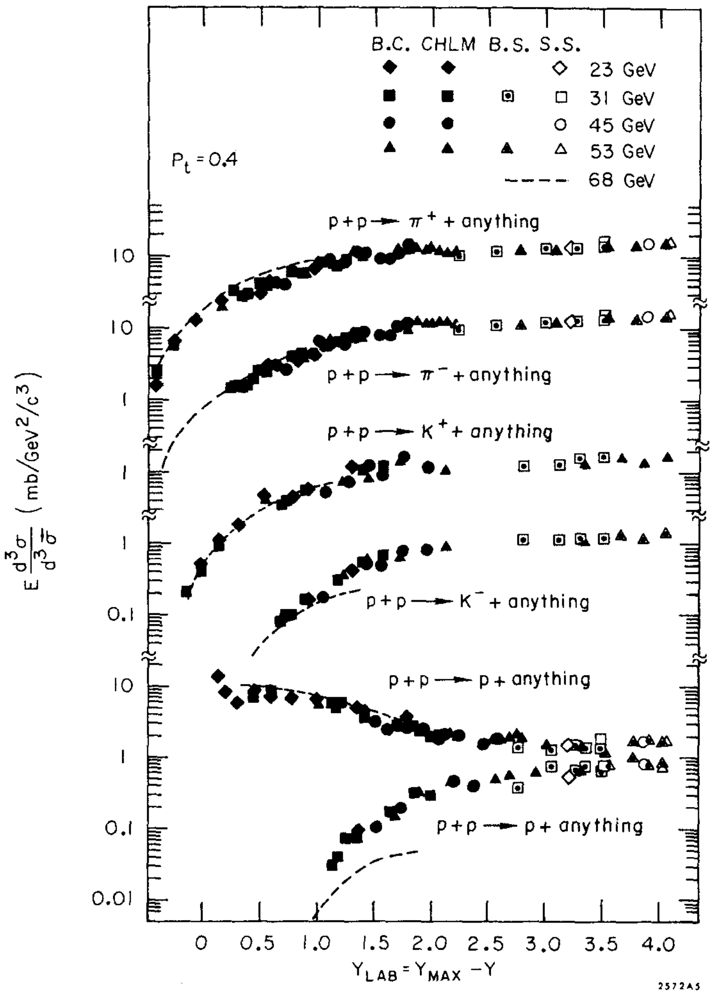

B.C. CHLM B.S. S.S.
23 GeV
31 GeV
45 GeV
53 GeV
68 GeV
$P_t = 0.4$
p+p → π⁺ + anything
p+p → π⁻ + anything
p+p → K⁺ + anything
p+p → K⁻ + anything
p+p → p + anything
p+p → p̄ + anything
$E\frac{d^3\sigma}{d^3\bar{\sigma}}$ (mb/GeV²/c³)
$Y_{LAB} = Y_{MAX} - Y$
2572A5

Fig. A.4

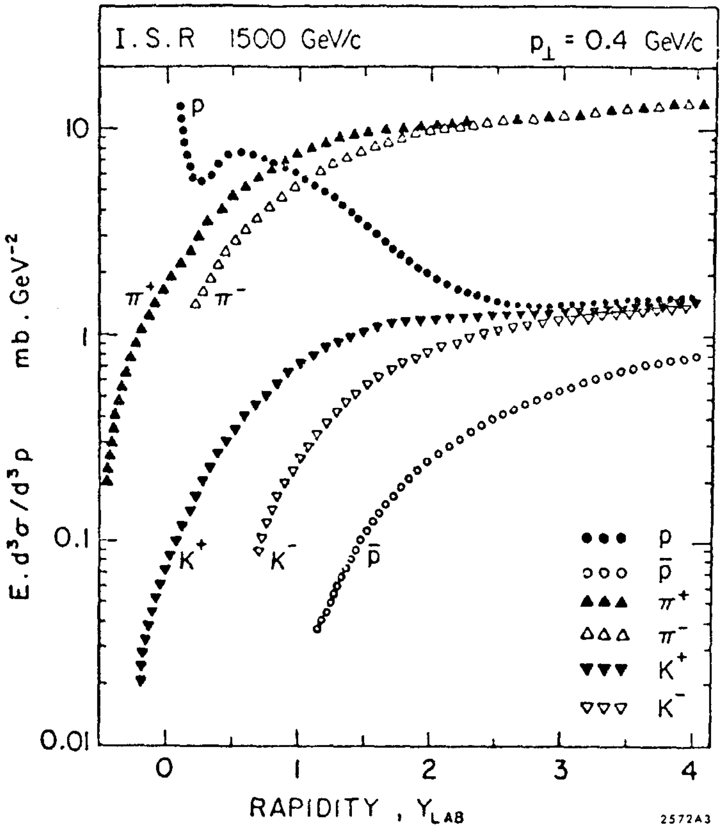

I.S.R 1500 GeV/c
$p_\perp$ = 0.4 GeV/c
$E . d^3\sigma / d^3p$ mb . GeV⁻²
RAPIDITY , Y_{LAB}
2572A3

Fig. A.5

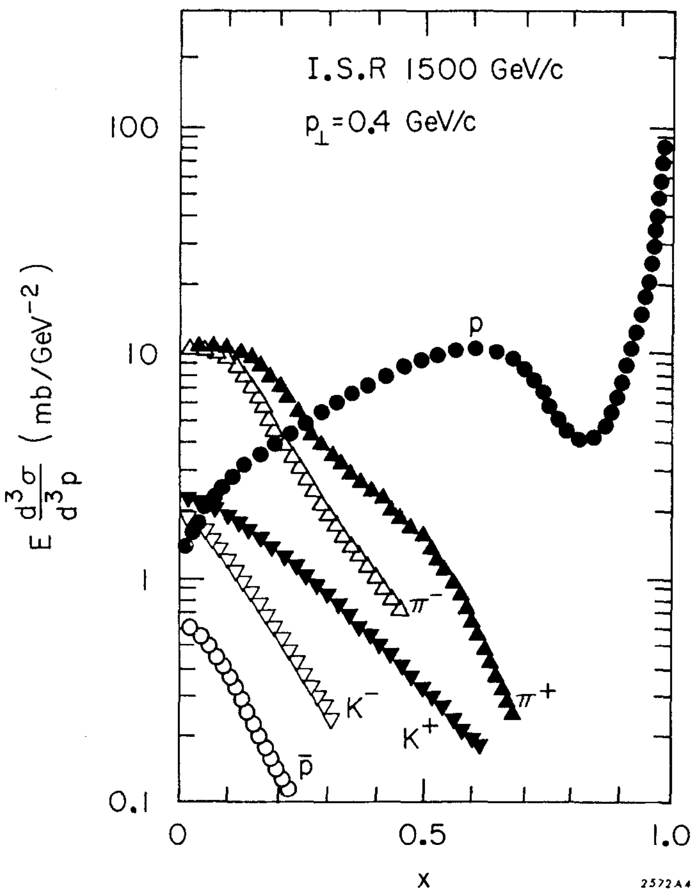

Fig. A.6

Bibliography

Experimental Summaries

H. Boggild and T. Ferbel, "Inclusive Reactions" to appear in Ann. Reviews of Nuclear Science.

A.N. Diddens, "Very High Energy Experiments" Lectures given at Barcelona.

M.E. Law, J. Kasman, R.S. Panvini, W.H. Seims and T. Ludlam (LBL-80, 1972) "A Compilation of Data on Inclusive Reactions."

D.R.O. Morrison, "Experimental Review of Strong Interactions at High Energy." (From 1973 Hawaii Topical Conference.)

J.C. Sens, "Review of Recent Results from the European Centre for Nuclear Research ISR."

J. Whitmore, "Experimental Results on Strong Interactions in the NAL Hydrogen Bubble Chamber." (Submitted to Physics Reports.)

Phenomenological

R. Arnold, "Lectures on the Feynman Wilson Fluid Analogy," ANL/HEP 7317.

E.L. Berger, "Multiparticle Production Processes at High Energy", Ref. TH. 1734-CERN.

A. Bialas, "Correlations in Particle Production at High Energies." Ref. TH.1745-CERN.

Chan Hong-Mo, "Duality and the Regge Approach to Inclusive Reactions." RL-73-062, Lectures given at Barcelona, 1973.

H. Harari, "Multi Hadron Production at High Energies∑ Phenomenology and Theory." (Scottish Universities Summer School.)

J.D. Jackson, "Introduction to Hadronic Interactions at High Energies," LBL-2079 (Scottish Universities Summer School, 1973).

R.G. Roberts, "Phenomenology in Inclusive Reactions," (Scottish Universities Summer School).

Strictly Formal

R.C. Brower, C.E. DeTar, and J.H. Weis, "Regge Theory for Multiparticle Amplitudes." MIT-CTP-395 (to be published in Physics Reports).

References

R. Arnold and G. Thomas (1974), Argonne Preprint.

A. Basseto, et al. (1972), Nuovo Cim. Letters 5, 655.

J. Benecke, T.T. Chou, C.N. Yang, and E. Yen (1969), Phys. Rev. 188, 2129.

E.L. Berger (1974), CERN/D.Ph.II/Phys 74-17.

E.L. Berger and G.C. Fox (1973), CERN-TH-1700.

A. Białas and E. Białas (1974), Ref. TH-1788-CERN, submitted to Acta Physica Polonica B.

A. Białas et al. (1973), Phys. Letters 45B, 337.

Buras (1973), A.J. Buras and Z. Koba, Nuovo Cim. Letters 6, 629.

K. Cahill and H. Stapp (1972), Phys. Rev. D6, 1007.

A.W. Chao and C. Quigg (1974)

M.S. Chen et al. (1971), Phys. Rev. Letters 26, 1585.

G.F. Chew and A. Pignotti (1968), Phys. Rev. 176, 2112.

C.B. Chiu and K. Wang (1973), Phys. Rev. D8, 2929.

C. DeTar (1971), Phys. Rev. D3, 128.

H. Dibon et al. (1973), Phys. Letters 44b.

J. Ellis, J. Finkelstein and R.D. Peccei (1972), Nuovo Cim. 12A, 763.

R.P. Feynman (1969), Phys. Rev. Letters 23, 1415.

J. Finkelstein and R. Peccei (1972), Phys. Rev. D6, 2606.

D.Z. Freedman, C.E. Jones, F.E. Low and J.E. Young (1971), Phys. Rev. Letters 26, 1197.

J.H. Freidman (1974), Phys. Rev. D9, 3053.

R. Hagedorn (1970), Nucl. Phys. B24, 93.

C.J. Hamer and R.F. Peierls (1973), Phys. Rev. D8, 1358.

Z. Koba, H.B. Nielson and P. Olesen (1972), Nucl. Phys. B40, 317.

A. Krzywicki (1964), Nuovo Cim. 32, 1067.

A. Krzywicki and B. Peterson (1972), Phys. Rev. D6, 924.

T. Ludlam and R. Slansky (1973), Yale preprint.

H.I. Miettenen (1971), Phys. Letters 38B, 431.

H. Moreno (1973), Phys. Rev. D8, 268.

A.H. Mueller (1970), Phys. Rev. D2, 2963.

J.L. Newmeyer and D. Sivers (1974), SLAC-PUB-1393.

K. Paler et al. (1973), Phys. Lett. 43B, 437 (1972).

S. Pokorski and L. van Hove (1974), CERN-TH-1772.

J. Polkinghorne (1972), Nuovo Cim. 7A, 555.

C. Quigg and G. Thomas (1973), Phys. Rev. D7, 2752.

G. Ranft and J. Ranft (1974), Phys. Letters 49B, 286.

J. Ranft (1970), Phys. Letters 31B, 529.

D. Schindler et al. (1974), Rochester preprint.

D. Sivers (1973), Phys. Rev. D8, 4004.

D. Sivers and G. Thomas (1972), Phys Rev. D6, 1961.

H. Stapp (1971), Phys. Rev. D3, 3177.

C.-I. Tan (1971), Phys. Rev. D4, 2412.

J. Van der Velde (1974), CERN preprint.

L. van Hove (1964), Rev. Mod. Phys. 36, 526.

LARGE MOMENTUM TRANSFER PROCESSES

R. BLANKENBECLER

Stanford Linear Accelerator Center
Stanford University, Stanford, California 94305

I. INTRODUCTION

In these lectures we shall attempt to present an overall and hopefully unified description of large momentum transfer processes and the way in which it joins smoothly onto the familiar descriptions of the Regge and resonance regions at small momentum transfer. I shall try to give physically motivated arguments rather than mathematical detail. The theoretical picture that I shall utilize is the constituent interchange model, or CIM, developed by J. Gunion, S. Brodsky and myself.[1,2] Since we shall be dealing with a model, we must enumerate its ad hoc calculational rules and give either a theoretical or experimental motivation for them. The ultimate test of all recipes is the final result, however. The reason for introducing such ad hoc rules at this stage is two fold; it should allow us to relate quite different experimental results, and it should give us clues as to the ultimate underlying theory. We shall discuss strong interaction processes at two levels: the first is at an internal or basic level, in which possible internal structure of hadrons, constituents, binding forces, etc., are considered, and the second is at an external or hadronic level in which the emission on bremsstrahlung (both real and virtual) of hadrons is taken into account. In other words, the first level is the short range behavior and the second is the long range behavior of hadronic matter.

The first level will be called hadron irreducible since there are no extra inessential hadrons involved, and will yield dimensional counting rules[3] that simply state that the more constituents there are, the more "fragile" is the particle. We shall need to develop rules for calculating the behavior of generalized structure (or probability) functions and the fixed angle behavior of irreducible, basic processes.[4] Using these two results, we can then operate at the hadronic level and join things together to make predictions about physical processes. If one is willing to assume arbitrarily the first two results, or to relate them in some way to form factor behavior, etc., then one need not ever work with constituents, and this is a very popular approach. The "soft gluon" model of Fried and Gaisser[5] is such an example, and while it is indeed different in detail from the CIM, these two pictures need not be fundamentally at odds with each other.

Let us consider, in transverse impact space, the collison of two composite hadrons. At large momentum transfer, the relevant impact parameters will be as small as possible and the finite sized hadrons will overlap in impact space. It is natural to expect then that an important force will be that between the constituents of one hadron and the containment field of the other hadron. This will naturally give rise to constituent interchange as a dominant force between hadrons in this large t region. Indeed, the CIM assumes that any other interaction can be neglected.

As the momentum transfer decreases, the collison will not necessarily be between the incident hadrons but can occur between secondaries emitted by them (which must then be reabsorbed on the way out after the collision in an exlcusive process). These secondaries will be predominantly hadrons since they are the lightest states and possess the longest compton wave lengths and have large coupling constants associated with their emission amplitude. Due to the finite size of the particles involved, these emissions and reabsorption processes occur at small average transverse momenta, and can become more and more important as the momentum transfer decreases. Furthermore, if the basic interchange process falls with increasing incident momenta, as most reasonable models suggest, then collisions between secondaries carrying only a small fraction of the incident momenta and hence small relative energy will dominate. This physical picture has therefore led us to a rather conventional explanation of the origin of Regge behavior in the subenergies--the interaction between "wee" components of the incident particles to use Feynman's term. Furthermore, note that if more than one pair of secondaries interact, it will give rise to multiple exchange contributions, absorption effects with all the requisite nonplanar graphs, etc.

The advantage of this picture of the interaction is that it forces us to recognize that the Regge behavior in the forward direction must join smoothly and continuously onto the fixed angle behavior.[6] Since the backward Regge behavior must also join onto this same fixed angle behavior, there must also exist continuity relations between the forward Regge parameters and the backward Regge parameters. In practice, this leads to relations between the leading forward Regge trajectories and the leading backward Regge residues, and vice versa.[7]

II. MOTIVATION

One important empirical motivation for the CIM is the fact, which at SLAC is called the "J. Matthews theorem," that all meson-baryon cross sections are equal (more or less) at 90°. In Figs. 1, 2, 3, we see[8] that at 90° and $s \sim 10\ (\text{GeV})^2$,

$$\frac{d\sigma}{dt}\,(M + B \to M' + B') \sim 0.1\mu b/(\text{GeV}/c)^2$$

and also, for the crossed process $\bar{p}p \to \pi\pi$, one sees that

$$\frac{d\sigma}{dt}\,(\bar{p}p \to \pi\pi) \sim 0.05\mu b/(\text{GeV}/c)^2 \ .$$

One simple way to interpret this remarkable fact is that if hadrons are composite objects, then once they are forced into a short enough range collision so that they overlap in impact space (by requiring a large angle scattering), then one simply has to rearrange the constituents and let the final particles emerge. If one rearranges the same number of constituents for all reactions, then the resultant cross sections should be roughly equal. Detailed calculations support this argument.

In addition, one should note that at 90°,

$$\frac{d\sigma}{dt}\,(pp \to pp)\Big/\frac{d\sigma}{dt}\,(\pi p \to \pi p) \sim 10^2$$

at 5 GeV/c. This means that nucleons must be coupled to the dominant short ranged force much more strongly than pions, because in this energy range, both theory and experiment suggest that pp scattering falls faster than πp scattering (s^{-10} vs. s^{-8}, respectively). This will be important to keep in mind when we try to pick out the most important graphs or subprocesses contributing to a particular reaction.

The CIM predicts that at fixed angle,

$$\frac{d\sigma}{dt} \sim \sum_i s^{-N_i}\, F_i(\theta) \ ,$$

where $N_0 < N_1 < N_2$, ... and hence as $s \to \infty$,

$$\frac{d\sigma(\theta)}{dt}\Big/\frac{d\sigma}{dt}\,(90°) \sim F_0(\theta)/F_0(90°) \ ,$$

and it is interesting to see if the data behaves this way. This ratio is shown for π^+p and K^+p elastic scattering[9] at 5 and 10 GeV/c in Fig. 4. The energy independence of $F_0(\theta)$ is consistent with this data. However, it would be nice to have such data on many more reactions and over a larger energy range. The interesting question is whether can we develop simple rules for computing the N_i and the $F_i(\theta)$. The neatest way to do this seems to be to assume a constituent model of the hadrons. This is the point where quarks enter our discussion, since to predict the angular distributions, quantum numbers must be assigned to the "point" constituents.

Our purpose here is to develop a description that works at large p_T but that also joins smoothly onto normal and familiar Regge behavior at small p_T. This is a non-trivial requirement for a theory, but it yields many unexpected relations between a priori independent Regge parameters, and thereby many experimental checks.

III. KINEMATICS

For the most part, we shall be interested in describing exclusive and single particle inclusive reactions of the type

$$A + B \to C + D$$

and

$$A + B \to C + X ,$$

although we shall also briefly discuss correlations in inclusive reactions. For later purposes, it is convenient to define the momenta as

$$\begin{aligned} p_A &= p + q + r \\ p_B &= p \\ p_C &= p + r \\ p_D &= p + q \end{aligned}$$

so that $s = (2p + q + r)^2$

$$t = q^2 \simeq -\frac{1}{2} s(1 - \cos\theta)$$

$$u = r^2 \simeq -\frac{1}{2} s(1 + \cos\theta)$$

and, of course, $s + t + u = M_A^2 + M_B^2 + M_C^2 + M_D^2$ for the exclusive case. However, for an inclusive reaction, one introduces the missing mass (squared) as

$$\mathcal{M}^2 = (p + q)^2$$

and the dimensionless ratio

$$\epsilon = \frac{\mathcal{M}^2}{s} \cong 1 - \frac{|\vec{P}_C|}{|\vec{P}_C|_{max}} ,$$

where $|\vec{P}_C|$ is the magnitude of particle C's spatial momentum in the center of mass and finite particle masses have been neglected compared to s, t, u $\mathcal{M}^2$. It will prove convenient to define the transverse and longitudinal momentum fraction variables of particle C as

$$x_T = \frac{P_T}{|\vec{P}|_{max}} \simeq \frac{2P_T}{\sqrt{s}}$$

$$x_L = \frac{P_L}{|\vec{P}_C|_{max}} \simeq \frac{(t-u)}{s}$$

and then

$$\epsilon = 1 - (x_T^2 + x_L^2)^{1/2} .$$

These are easily described and visualized in the Peyrou plot shown in Fig. 5, where the x_T and x_L are fractional distances, and ϵ is the (fractional) distance to the boundary which corresponds to $\epsilon \to 0$ or exclusive scattering.

The reason for choosing the particle momenta as we have done is because in a particular class of frames, they have a simple parametrization.[6] This way of writing four-vectors we will call the finite momentum frame:

$$k = \left(xP + \frac{k^2 + \vec{k}_T^2}{4xP} , \vec{k}_T, xP - \frac{k^2 + \vec{k}_T^2}{4xP} \right) .$$

The parameter P is arbitrary (its value determines the frame) and one easily finds

$$\int d^4k = \int dk^2\, d^2k_T \frac{dx}{2|x|} ,$$

to within delta functions arising from the Jacobian which usually don't contribute.

The usual infinite momentum frame variables are

$$k_+ = \frac{1}{2}(k_c + k_z) = xP$$

$$k_- = \frac{1}{2}(k_0 - k_z) = \frac{k^2 + k_T^2}{4xP} = \frac{M_r^2}{4k_+} ,$$

and the usual infinite momentum frame is the limit

$$k_3 = xP - \frac{k^2 + \vec{k}_T^2}{4xP} \longrightarrow \infty$$

$$k_0 = k_3 + \frac{k^2 + \vec{k}_T^2}{2xP} \longrightarrow k_3 + \frac{M_T^2}{2k_3} + \mathcal{O}(k_3^{-2})$$

In what we shall do here, this limit is not taken, and P is left arbitrary.

The four-momenta in the exclusive case can be shown to be (see all external masses equal for convenience)

$$p = \left(P + \frac{M^2}{4P} , \vec{0}_T, P - \frac{M^2}{4P} \right)$$

$$q = \left(\frac{q \cdot p}{2P} , \vec{q}_T, - \frac{q \cdot p}{2P} \right)$$

$$r = \left(\frac{r \cdot p}{2P}, \vec{r}_T , - \frac{r \cdot p}{2P} \right)$$

where $2q \cdot p = \vec{q}_T^{\,2}$, $2r \cdot p = \vec{r}_T^{\,2}$, and $\vec{q}_T \cdot \vec{r}_T = 0$. The same basic parametrization will be used in the inclusive case, but, of course, since $\mathcal{M}^2$ is arbitrary, the subsidiary conditions on the vectors q and r are modified.

IV. DIMENSIONAL COUNTING RULES

One of the more important recent developments in dyanmics has been the formulation of the dimensional counting rules by Brodsky and Farrar.[3] These rules allow one to quickly estimate the behavior of exclusive and inclusive reactions, form factors, structure functions, etc., at large momentum transfers. These rules have not been derived rigorously, indeed there are some exceptions to them in certain theories and certain reactions, but in the type of model of hadrons that we need to describe the present data, they seem to be consistent with both theory and experiment.

These rules will predict, in agreement with our intuition, that the more constituents that are involved in a coherent fashion, the faster the fall off of the matrix element at large values of all kinematic variables. This means that the simplest configuration in bound states with the minimum number of constituents will contribute the leading terms. Now the pion wave function, in the quark model for example, surely involves a sum over arbitrary numbers of quark paris, but at large angles, only the single $(\bar{q}q)$ configuration contributes to the leading behavior.

A. Form Factors

The two particle bound state wave function will be described by a covariant wave function with particle of momenta k and p-k as shown in Fig. 6a, with p and k written using the finite momentum variables x, $\vec{k}_T$, k^2, and P as described earlier. Consider first the matrix element of a single particle operator Q_q, such as the current operator, which brings a momentum transfer q into the system. We will ignore the algebraic complication due to spin and discuss only spin zero constituents. The quality of interest in the large q^2 behavior of the matrix element

$$M(q^2) = \langle p + q | Q_q | p \rangle$$

which is illustrated in Fig. 6b. The states are wave functions and the operator Q_q contains the requisite spectator particle propagators G_i, such as, for example, $Q_Q = j_1 G_2^{-1}$. Now the wave functions will satisfy a Bethe-Salpeter type of equation with an interaction kernel K, where

$$\langle p | = \langle p | \, KG_1G_2 .$$

Using this result into the matrix element M allows it to be written in terms of a "well-tempered" operator $\tilde{Q}_q$, where

$$\tilde{Q}_q = KG_1G_2Q_q = Q_qG_1G_2K \ .$$

$\tilde{Q}_q$ is a connected operator with the same matrix elements in the bound state as Q_q. It has the advantage that since it treats all the particles in the bound state on the same footing, it is straightforward to estimate its magnitude, especially for large q^2.

Choosing the interaction between the constituents to be <u>renormalizable</u>, such as $\lambda\varphi^4$, or a vector gluon theory, the lowest order term in K is a constant at large momentum transfer (fixed angle scattering). Using Fig. 7a, which illustrates the momentum flow in $\tilde{Q}_q$ and the two regions that contribute to the final result, the matrix element defining the form factor is

$$M = \iint \psi(y,k',p+q)\ \lambda\ \frac{\epsilon\cdot(2k+q)}{(M^2-(k+q)^2)}\ \psi(x,\ k,\ p+q)\ .$$

Using $(k+q)^2 = q^2(1-x) + O(k)$, and assuming that the wave functions fall sufficiently fast so that all components of k are finite, the form factor F and the matrix element become

$$M = \epsilon(2p+q)\ F_2(q^2)$$

where

$$F_2(q^2) \simeq \frac{\lambda}{q^2}\ \langle\frac{x}{1-x}\rangle\ [\ \int \psi\ d^4k]^2$$

and $\langle\rangle$ means average value in the bound state. This now leads us to the next fundamental assumption that the above averages and integers $\int \psi\ d^4k = \psi(x_\mu = 0)$ are finite, hence $F_2 \sim \lambda(\vec{q}_T^{\,2})^{-1}$. If there is a divergence, then one has to go back and carry out a more careful estimate of the q^2 behavior. Logarithmic modifications are probably to be expected and can arise from the $(1-x)$ factor.

The three particle bound state can be treated in the same fashion. Referring to Fig. 7b, we see immediately that the bound state equation must be iterated twice in order to spread the momentum transfer q among the final particles. The three particle form factor F_3 will then fall as

$$F_3(q^2) \sim \lambda^2(\vec{q}_T^{\,2})^{-2}\ .$$

The behavior of F_3 has been discussed carefully and in detail by C. Alabiso and G. Schierholtz who used a relativistic bound state equation and included the effects of spin. They discuss the general case and agree with the above in the limit of a renormalizable interaction.

In an N-particle bound state, an obvious extension of the previous discussion yields the result

$$F_N \sim \lambda^{N-1}(\vec{q}_T^{\,2})^{1-N}\ .$$

The above discussion assumed that the interaction between the constituents was of a renormalizable type. A super-renormalizable interaction yields a different result. For example, a $(\nu\varphi^2\chi)$ theory produces a kernel K that falls as ν^2/t, and the two particle form factor then behaves as $\nu^2(\vec{q}_T^{\,2})^{-2}$.

The present data is not very decisive, but $e^+e^- \to \pi^+\pi^-$ data suggests that the pion form factor behaves as a monopole and hence that the appropriate model of the pion is a $(\bar{q}q)$ bound state, with the q's interacting via a renormalizable interactions.

The present data for the nucleon form factor is consistent with a dipole falloff and hence there are <u>two</u> possible models for the baryons:

(1) $B = (3q)$, interacting via a renormalizable interaction.

(2) $B = (q + \text{"core"})$, interacting via a super-renormalizable interaction.

The first model obeys the simple dimensional counting rules and will be used throughout these lectures for simplicity. The second model is consistent with most of the data and has some virtues. However, one cannot choose between them at the moment on the basis of the large t data. The second model is the one used in our first papers on the CIM, and it will be referred to occasionally during our discussion. It has several interesting theoretical features and experimental advantages.

B. Scattering Amplitudes

The limiting behavior of scattering amplitudes at fixed angle can be handled by the same type of argument. The basic problem is to iterate the bound state equations so that the large momenta (q and r) are evenly distributed among the final particles so that they can bind. Consider a pion-pion scattering graph as depicted in Figs. 8a and 8b. If the vector k is parametrized in terms of x, k_r and k^2 as before, the invariant scattering amplitude can be easily estimated after iterating K three times as

$$M_a \sim \frac{\lambda^2}{q_T^2 r_T^2} \left\langle \frac{1}{x(1-x)} \right\rangle \psi_n^4(0)$$

$$M_a \sim s^{-2} f_2(\theta) \ .$$

The diagram in Fig. 8b is given directly in terms of the pion form factor as

$$M_b = \lambda F_n^2(t) \sim s^{-2} f_b(\theta)$$

It is seen that the exchange graphs of the form given by Fig. 8a, and the terms which can be obtained by permutation of p_A, p_B, p_C and p_D all fall with the same rate as the more familiar gluon exchange diagrams. While the contributions M_a and M_b both fall as s^{-2}, they have a quite different angular dependence. The resulting differential cross section a fixed angle falls as $d\sigma/dt \sim s^{-2}|M^2| \sim s^{-6}$.

The scattering of a two body (pion) state off of a three body (baryon) state can be handled in the same fashion. Using the momenta as shown in Fig. 8c, and describing k' in terms of x', k_T', and k'^2, this diagram behaves as

$$M_c \sim \frac{\lambda^4}{r_T^2 (q_T^2)^2} \left\langle \frac{1}{x(1-x)(1-x')} \right\rangle \left\langle \frac{1}{1-x} \right\rangle \psi_n^2(0)\, \psi_B^2(0,0)$$

$$\sim s^{-3} f_c(\theta)$$

and hence $d\sigma/dt \sim s^{-8}$. A similar treatment of a three body state off a three body state can be carried out in a similar fashion and one finds that $d\sigma/dt \sim s^{-10}$. In general, one can show by induction that

$$\frac{d\sigma}{dt} \sim s^{2-N_{tot}} f_{ABCD}(\theta) \ ,$$

where

$$N_{tot} = n_A + n_B + n_C + n_D \ .$$

This is a general result and will be useful in all our subsequent discussion.

It should be pointed out that if the nucleon is a $(q + \text{"core"})$, then the pion-proton cross section falls as s^{-8} which is the same as the $(3q)$ case. However, the proton-proton cross falls as s^{-12} rather than s^{-10} as in the $(3q)$ model.

In the following table, the predictions for some selected processes are given together with the experimental values of the s falloff where it is known with sufficient accuracy.

TABLE 1

Process	$d\sigma/dt$	exp. power
$\gamma p \to \gamma p$	s^{-6}	
$\gamma p \to \pi p$	s^{-7}	7.3 ± 0.4
$\to \pi\Delta$	s^{-7}	$\sim 7\text{-}8$
$\pi p \to \pi p$	s^{-8}	7.7 ± 0.6 ($\bar{\pi}p \to \bar{\pi}p$) 9.3 ± 0.5 (CEX)
$\to \pi\Delta^*$	s^{-8}	
$\to \rho p$	s^{-8}	
$\bar{p}p \to \pi\pi$	s^{-8}	
$pp \to pp$	s^{-10} or s^{-12}	10 ± 0.7
$\to pN^*$	s^{-10} or s^{-12}	$10 \sim 12$
$\bar{p}p \to \bar{p}p$	s^{-10} or s^{-12}	?

C. Limiting Regge Behavior

A full theory, or a complete model, should determine the angular behavior $f(\theta)$ as well as the power of s. It must be able to separate behaviors in s from t from u. It will be shown later that the graphs that involve interaction between constituents in different hadrons such as in Fig. 8b do not seem to contribute significantly to the experimental cross sections. If these graphs are discarded, then the variables can be separated by a more careful graphical analysis[4] and one finds that for fixed t, as $s \simeq -u$ gets large, scattering amplitudes approach the form (only dominant graphs are considered)

$$M \sim s^{\alpha_{AC}(-\infty)} \beta_{BD}(t) + \cdots$$

where

$$\alpha_{AC}(-\infty) = \frac{1}{2}(4 - n_A - n_B - n_I)$$

$$\beta_{BD}(t) \sim (-t)^b, \qquad b \equiv \frac{1}{2}(n_I - n_B - n_D)$$

and n_I is the number of constituents exchanged in the t channel. Examples of this predicted behavior are (all are evaluated at $t = -\infty$):

$\alpha_{nn} = -1$	I = 0 and 1
$\alpha_{pp} = -2$	I = 0 and 1
$\alpha_{\bar{p}p} = -4$	exotic
$\alpha_{\pi^+\pi^-} = -2$	double CEX
$\alpha_{\pi p} = -2$	baryon, Δ exchange
$\alpha_{\gamma\gamma} = 0$	J = 0 fixed pole
$\alpha_{\gamma\pi} = -1/2$	
$\alpha_{\gamma p} = -3/2$	

In the original CIM model of the baryon as a (q + "core"), the pp trajectory has the limiting value $\alpha_{pp}(-\infty) = -3$. The effective trajectory for pp scattering is shown in Fig. 9 and for $\pi^- p$ scattering in Fig. 10. Even though the errors are large, the trend is apparent.

An interesting application of the above formulae is to large angle and backward $\bar{p}p$ scattering. Backward scattering should be described by double baryon exchange which is predicted to behave as $\alpha_{\bar{p}p}(-\infty) = -4$, and $b = 0$. Since $\alpha_{\bar{p}p}$ is an exotic channel, it is natural to assume that it does not rise very far above its asymptotic value even at $t \cong 0$. If $\alpha_{\bar{p}p}(t) \simeq -4$ for all $t < 0$, then one predicts $d\sigma/dt \sim s^{-10}$ in the entire large angle and backward regions. This behavior is entirely consistent with the deuteron lying at $t \cong 4M^2$ on this trajectory.

D. Distribution Functions

The second fundamental result that we shall need, besides the fixed angle behavior, is the threshold behavior of the particle distribution functions which are simply related to what might be called generalized structure functions. We shall define $G_{H/A}(z)$ to be the probability of finding an (off-shell) particle H in the momenta (defined in the usual finite momentum frame). Now momentum conservation is expressible as

$$\sum_H \int dz\, z\, G_{H/A}(z) = 1$$

and the deep inelastic structure functions are expressible as

$$F_{2A}(x) = x \sum_q \lambda_q^2\, G_{q/A}(x)$$

where λ_q is the charge of the quark of type q.

A quark q can arise directly from the guts of particle A (which will be called hadron irreducible) or from a secondary hadron H which has been emitted by A (this will be called hadron reducible). Therefore, one clearly has the formula corresponding to these words

$$G_{q/A}(x) = \int_x^1 \frac{dz}{z} \sum_H G^I_{q/H}(x/z)\, G_{H/A}(z) ,$$

where the superscript I means hadron irreducible, and serves to avoid possible double counting. The full deep inelastic structure function can be written using this decomposition in the transparent form

$$F_{2A}(x) = \int_x^1 \sum_H F^I_{2H}(x/z)\, G_{H/A}(z) .$$

These formulae require that the probability function contain a delta function, i.e. $G_{A/A} \sim \delta(1-z)$.

Using an extension of the arguments used previously in our discussion of the dimensional counting rules, the threshold behavior $(x \sim 1)$ is found to be (see Refs. 4 and 10 for details)

$$G_{q/B}(x) \sim G^I_{q/B}(x) \sim (1-x)^{g(q/B)}$$

where

$$g(q/B) = 2n(\bar{q}B) - 1$$

and $n(\bar{q}B)$ is the minimum number of quarks in the state $(\bar{q}B)$, and, of course, $1 + n(\bar{q}B)$ is the minimum number of quarks in the state B. This is consistent with the Drell-Yan-West relation, since the form factor of B behaves as $F_B \sim (\sim q^2)^{-n(\bar{q}B)}$.

Using the above equations, the only consistent threshold behavior of the probability functions for finding hadron H in hadron B is

$$G_{H/B}(z) \sim (1-z)^{g(H/B)}$$

where

$$g(H/B) = 2n(\bar{H}A) - 1$$

and $n(\bar{H}B)$ is the minimum number of quarks in the hadronic state $(\bar{H}B)$. This remarkable result depends on the assumption of an underlying scale invariant theory at the constituent level and on the number of constituents.

Some typical values of $g(H/B)$ which will be useful later are the familiar results for quark $g(q/\pi) = g(\bar{q}/\pi) = 1$, $g(q/P) = 3$, $g(\bar{q}/P) = 7$, and the new results for hadrons, $g(B/B) = -1$ or 3, $g(\pi/p) = 5$, $g(K^+/p) = 5$, $g(K^-/p) = 9$, and $g(\bar{p}/p) = 11$. The value $g(B/B) = -1$, actually corresponds to the $\delta(1-z)$ term that is present in $G_{B/B}$. The physical interpretation of the systematics of these results is clear--the rate of vanishing of G depends on the number of degrees of freedom of the debris left behind (near the threshold) in producing the leading particle H. The number $n(\bar{H}B)$ is the number of constituents that must be stopped if H is to have x near 1.

The Regge behavior of the probability functions shows up in the power behavior for small z, i.e. $G \sim z^{-\alpha(0)}$. Throughout our discussion we shall therefore set

$$G_{H/A}(z) = z^{-\alpha_A(0)} (1-z)^{g(H/A)} ,$$

where $\alpha_A(0) = 1$ (Pomeron), but this could be multiplied by any smooth function of z (better data will certainly require this modification) without affecting our results on the general behavior of amplitudes.

E. Hadron Decays

The probability function $G_{H/A}(z)$ describes the fractional longitudinal momentum distribution which is perhaps most easily interpreted in the infinite momentum frame of A. It is possible, however, to determine some interesting properties of G by measurements in a general frame, including the rest frame of A. This may be very interesting in relating the decays of system with a large Q value, such as annihilation processes, and the decay of coherent states produced by diffractive excitation reactions.[4] Consider the decay $A \to a + X$ in the rest frame of A and the rate

$$\frac{d\Gamma}{d\omega} \equiv d_{a/A}(\omega), \qquad \omega = \frac{2E_a}{M_A} .$$

The decay can also be described in terms of the infinite momentum frame variable $x = (E_a + k_a^z)/M$, which leads to the spectrum

$$\frac{d\Gamma}{dx} \equiv D_{a/A}(x) = \int_0^1 d\omega \left[\omega^2 - \frac{4a^2}{M_A^2}\right]^{-1/2} d_{a/A}(\omega)\ \theta\ \omega\left[- x - \frac{a^2}{M_A^2 x}\right]$$

Now it has been shown in a quite general model (and it is what one would expect) that if $G_{a/A}(x) \sim (1-x)^g$, then $D_{a/A} \sim (1-x)^g$. Therefore as $\omega \sim 1$

$$d_{a/A}(\omega) \simeq (1-x)^{g(a/A)^{-1}}$$

The example of $(\bar{N}N)$ annihilation into a leading pion has been analyzed by Pelaquier[11] and the data seems to be consistent with the prediction $g(\pi/\bar{N}N) = 3$. Many other examples need to be analyzed and their threshold behavior extracted, especially excitation reactions. The familiar parton prediction

$$d_{\pi/(e^+e^-)} \sim (1-\omega)$$

follows after the photon spin is taken into account.

F. Angular Distribution

While the dimensional counting rule giving the energy falloff depends on the inter-constituent force and their number, the expected angular distributions depend on the quantum numbers of the constituents. For example, if the incident hadrons can exchange constituents and produce the final state, then this (ut) contribution illustrated in Fig. 11a will yield an amplitude of the general form $M_a \sim (-u)^{-A} (-t)^{-B}$, which produces an angular distribution characterized by a forward and backward peak.

If antiparticles are present, such as in pion-nucleon scattering, the (st) contribution of Fig. 11b will produce only a forward peak. The gluon exchange process of Fig. 11c will produce a forward peak only, and $M_c \sim (-t)^{-B}$ or $s(-t)^{-B}$ for a spin zero and spin one gluon respectively. In both cases, this term produces a high effective trajectory value and essential equality of particle-particle and particle-antiparticle scattering. Both of these behaviors are in disagreement with the present data and its trends. This is the reason why it was necessary to exclude these types of diagrams from the original CIM. As we shall see, this exclusion rule allowed a correct prediction of the large p_T behavior subsequently found in the ISR data.

Since there are no antiquarks present in the lowest configuration in the proton's wave function, only the (ut) term can contribute to pp scattering (also true for K^+p) and one expects that for finite t,

$$s^2 \frac{d\sigma}{dt}(pp) \sim (-u)^{2\alpha(t)} \beta^2(t) ,$$

where $\alpha(t)$ is an effective trajectory and $\alpha(-\infty) = -2$ (or -3 in (q + "core") model). From crossing, only the (st) term can contribute to $\bar{p}p$ scattering (and K^-p)

$$s^2 \frac{d\sigma}{dt}(\bar{p}p) \sim (s)^{2\alpha(t)} \beta^2(t)$$

and hence

$$R(\theta) = \frac{d\sigma(pp)}{d\sigma(\bar{p}p)} \sim \left(\frac{s}{-u}\right)^{-2\alpha(t)} \sim \left(\frac{2}{1 + \cos\theta}\right)^{-2\alpha(t)}$$

Thus a characteristic difference in angular distributions is expected in the model, and furthermore, $R(90°) \sim 2^4$ or 2^6, depending on the nucleon model assumed ($\alpha = -2$ or -3 respectively).

Predictions for the angular distribution of the processes $\pi^\pm p \to \pi^\pm p$, $K^\pm p \to K^\pm p$, $\pi^- p \to \pi^0 n$, and $K_L p \to K_S p$ are in reasonable agreement with the data.[12]

V. BASIC PROCESSES

The CIM model for inclusive and exclusive reactions begins with a basic irreducible process and then adds on the possibility of hadronic bremsstrahlung to "dress" and Reggeize the process. As the transverse momentum in the overall process of interest increases, the bremsstrahlung is suppressed and the basic process will dominate the reaction. Consider the irreducible contribution to elastic scattering illustrated in Fig. 12a, in which the projectile A scatters from a constituent q in the target particle B. The differential cross section can be written in the obvious form

$$\frac{d\sigma}{dt} \sim \sum_q \left(F^q_{BD}(t)\right)^2 \frac{d\sigma}{dt}(A + q \to C + q)\Bigg|_{\substack{s' = \langle x\rangle s \\ t'=t}}$$

where the cross section for $A + q \to C + q$ is evaluated at an averaged reduced energy because constituent q is carrying only a fraction x of the momenta of the state B. The function $F^q_{BD}(t)$ is a "form factor" whose asymptotic dependence can be computed using the dimensional counting rules.

Now consider the inclusive reaction $A + B \to C + X$ at a missing $(\text{mass})^2$ of $\mathcal{M}^2$. Again one of the basic scattering processes is $A + q \to C + q$ is shown in Fig. 12b, and the generalized structure functions of the target B obviously come in to the amplitude. One finds after an elementary calculation

$$E\frac{d\sigma}{d^3p} = \sum_q \frac{s}{\pi(s+u)}\, x\, G_{q/B}(x) \frac{d\sigma}{dt}(A + q \to C + q)\Bigg|_{\substack{s'=xs \\ u'=xu \\ t'=t}} ,$$

where $x \equiv -t/(s + u) = -t/(\mathcal{M}^2 - t)$, (x is the familiar Bjorken scaling variable). If particles A and C were electrons, this reduces to the usual scattering answer and since a factor of the $(\text{charge})^2$ of the constituent factors out of each of the basic cross sections, the sum over q then leads to the E and M structure function:

$$E\frac{d\sigma}{d^3p} = \frac{s}{\pi(s+u)} F_{2B}(x) \frac{d\sigma}{dt}(e + q \to e' + q')\Bigg|_{\substack{s'=xs \\ t'=t}} .$$

Since there is a relation between the probability functions G and the form factors F expressed by the Drell-Yan-West relation,[13] one might expect that there will be a relation connecting the inclusive and exclusive cross sections for small missing mass. In the resonance region for electroproduction, a relation has been found and is called Bloom-Gilman duality.[14] A similar sort of relation might be expected to hold in the hadronic case, and it does.[15]

For small missing mass, x approaches unity since $x = 1 - \mathcal{M}^2/(\mathcal{M}^2 - t)$. The probability functions G vanish as a calculable power given by dimensional counting. Using the relation

$$\frac{d^2\sigma}{dt\, d\mathcal{M}^2} = \frac{\pi}{s} E \frac{d\sigma}{d^3p} ,$$

the cross section into a differential mass bin at $\mathcal{M}^2$ is proportional to

$$\frac{d^2\sigma}{dt} \propto \frac{d\mathcal{M}^2}{\mathcal{M}^2}\left[\frac{\mathcal{M}^2}{\mathcal{M}^2-t}\right]^{g(q/B)+1} \frac{d\sigma}{dt}(A + q \to C + q)\Bigg|_{\substack{s'=s\\ u'=u\\ t'=t}} ,$$

and one recognizes that the large t dependence is the same as for elastic scattering since

$$\left[\frac{\mathcal{M}^2}{\mathcal{M}^2-t}\right]^{g(q/B)+1} \simeq (F^q_{BD}(t))^2 .$$

These two processes therefore have the same behavior on the kinematic variables in this limit but unfortunately a calculation of the relative normalization is difficult. One of the difficulties is the fact that at small missing mass, many of the final states in inclusive scattering become coherent so that one cannot just perform the incoherent sum over them as in the above formulas which hold at larger missing mass. In any case, we see that there is a smooth connection between inclusive and exclusive processes both at fixed $|t|$ and at fixed scattering angle.

VI. REGGE BEHAVIOR

We have seen that the typical basic scattering process between hadrons falls with energy at fixed angle rather rapidly in the CIM. This is true even at fixed momentum transfer unless there is a direct vector gluon force (which we have argued must be negligible). The basic scattering process can be considered as in Fig. 13a. If it falls as s increases at fixed t, then the system will prefer to scatter through diagrams of the form shown in Fig. 13b. In this virtual bremmstrahlung diagram, particle A converts to H with a fraction x of the incident momentum and other coherent "stuff" with momentum (1-x). The basic process is thereby converted to $H + B \to H' + D$ scattering at the reduced effective energy $s' \simeq xs$. If x can be small, then this process is not suppressed much if H' can pick up the momentum fraction (1-x) and convert to C. This latter process is suppressed as t increases, so that in the large t and eventual fixed angle limit, the irreducible process (Fig. 13a) will dominate. This is the physical origin of Regge behavior in this model at small t. It is dominated by the emission and absorption of the less massive hadronic states. They therefore control the long distance or small t behavior of the amplitudes.

The above discussion can be made more precise[6] and one finds that such graphs produce a Regge trajectory of the form

$$\alpha(t) = \alpha(-\infty) + A(t) ,$$

where A(t) vanishes in a calculable way as $|t|$ increases (the power can be calculated by dimensional counting). A similar result holds for the residue function. This behavior assures that the fixed angle behavior joins smoothly to the Regge behavior.

However, one should note that the earlier predictions were $\alpha_{\pi p}(-\infty) = -1$, and $\alpha_{pp}(-\infty) = -2$. Since factorization should hold, how can this behavior be tolerated? Fortunately, the equations are very clever and make these behaviors consistent in the simplest way possible. When one treats the coupled channel system (which must be done in order to check factorization) of $\pi\pi \leftrightarrow \bar{p}p$ in the t-channel, one finds that there must be at least 3 important trajectories which are related.

The matrix elements for $\pi\pi$, πp, and pp scattering must have the form (neglect signature here)

$$M = \beta_+(t)(-u)^{\alpha_+(t)} + \beta_-(t)(-u)^{\alpha_-(t)} + \beta_0(t)(-u)^{\alpha_0(t)} + \cdots$$

where $\alpha_+(-\infty) = \alpha_-(-\infty) = -1$, and $\alpha_0(-\infty) = -2$ (or -3). For $\pi\pi$ and πp scattering, there is no particular relation between the residues. However, in the pp case, one finds that at large t, $\beta_+(t) = -\beta_-(t)$ and the first two terms cancel, leaving a residue which is smaller than the third term which then produces the expected fixed angle behavior.

The theoretical calculation leads one to expect that $\alpha_+(t)$ rises at small t and should be identified with the familiar Regge trajectories there. However, α_- should deviate only slightly from its asymptotic value (probably below it). It was predicted in Ref. 6 that when $\alpha_+(t)$ drops to ~ -1, the first two terms should cancel and the fixed angle result should hold. Since $\alpha_+(t)$ should control πp scattering, the effective trajectory behavior shown in Fig. 11 leads us to expect that for $|t| > 2$ or 3, the fixed angle result should hold. For somewhat smaller $|t|$, one expects the power behavior to be more like that found in πp scattering. These predictions seem to be in rough agreement with the data but a more extensive analysis is clearly needed to see if this cancellation mechanism is occurring. If cuts become important, which may well be the case in pp scattering at ISR energies, the effective trajectory will drop even slower to its asymptotic value.

VII. TRIPLE REGGE REGION

Let us reexamine the inclusive formula given in Section V by including the Regge effects just discussed. The contribution from a single particle q is of the form

$$E\frac{d\sigma^q}{d^3p} = \frac{s}{\pi(s+u)}\, xG_{q/B}(x)\, \frac{d\sigma}{dt}(A + q + C + q)\Bigg|_{\substack{s'=xs\\ u'=xu\\ t'=t}}$$

where in light of our Regge analysis we now have

$$\frac{d\sigma}{dt}(A + q \to C + q) = \left|\gamma(t')(-u')^{\alpha_{AC}(t')} + \tilde{\gamma}(t')(-u)^{\alpha_{AC}(t')}\right|^2 / s'^2$$

and $\gamma(-\infty)$ = constant. Retaining only the γ-term for simplicity (one needs both terms to get the angular distribution correct), the inclusive cross section achieves the form $(\alpha_B(0) = 1)$.

$$E\frac{d\sigma^q}{d^3p} = \left(-\frac{u}{s}\right)^2 \frac{\gamma^2(t)}{(p_T^2 + M^2)}\, xG_{q/B}(x) \left[\frac{\mathcal{M}^2 - t}{s(p_T^2 + M^2)}\right]^{1-2\alpha_{AC}(t)}$$

where $x = -t/(s+u)$.

In the triple Regge limit defined by $s \approx |u| \gg \mathcal{M}^2 \gg |t|$, x goes to zero, $p_T^2 \sim -t$, and one finds the familiar Mueller-Regge form[16]

$$E\frac{d\sigma^q}{d^3p} = \beta_q(t)\, (xG_{q/B}(x))_{x=0} \left(\frac{\mathcal{M}^2 - t}{s}\right)^{1-2\alpha_{AC}(t)},$$

In this limit, the inclusive cross section is independent of the threshold $(x \sim 1)$ behavior of the probability functions. However, we have already seen that it is this threshold behavior which allows a smooth connection to the exclusive $(\mathcal{M}^2 \sim 0)$ limit for both fixed t and fixed angle. The triple Regge formula does not allow for this smooth connection. It is guaranteed by multiplying by the simple function $xG_{q/B}(x)$. We have therefore identified an important correction to the triple Regge formula for small missing mass (which has the virtue of being particularly simple).

VIII. BRIEF REVIEW AND ASIDE

It is important to keep in mind the division we have made between internal or short distance properties (which predicts the irreducible processes discussed before) and the long distance or hadronic sector of strong interactions. Any theory that gives results for the irreducible processes that can be written in the following forms

1. Exclusive $\frac{d\sigma}{dt} \propto (F^q_{BD}(t))^2 \frac{d\sigma}{dt}(A + q \to C + q)\Big|_{\substack{s'=\langle x\rangle s\\ u'=\langle x\rangle u\\ t'=t}}$

2. Inclusive $E\frac{d\sigma}{d^3p} \propto \frac{s}{s+u}\sum_q xG_{q/B}(x)\frac{d\sigma}{dt}(A + q \to C + q)\Big|_{\substack{s'=xs\\ u'=xa\\ t'=t}}$

3. Probability function $G_{H/A}(z) \propto z^{-\alpha(0)}(1-z)^{q(H/A)}$,

(where the quantity $d\sigma/dt\ (A + q \to C + q)$ is power behaved) will produce all the predictions for elastic single particle inclusive to be discussed shortly. If one is willing to assume the above forms, or to assume a model that relates them to simple quantities such as form factors, then the concept of constituent need never be used. However, the constituent interchange model has the virtue of predicting very simple relations between the limiting forms of all the functions involved which are quite specific since they depend only on the number of constituents involved.

One of the most puzzling aspects of the CIM (aside from the fact that no constituents have been seen) is the fact that even though there is strong binding involved, the constituents of one hadron do not seem to interact strongly with those in another hadron. This was first suggested in our original paper on the subject to explain the large ratio of pp to $\bar{p}p$ and K^+p to K^-p scattering at large angles, and then used to predict a leading p_T^{-8} behavior in $pp \to \pi X$ rather than the naturally expected scaling behavior of p_T^{-4}.[17] There is no fundamental understanding of how this happens. One possibility is that the basic theory has quarks and enjoys asymptotic freedom or is only asymptotically scale-free but it is not yet clear how this would work in detail. Another possibility is a class of quark containment theories (that might be termed container theories) in which the quarks interact strongly with the box that they are in but not with each other. Constituent interchange is then the natural force in such theories. There seems to be many analogies between such theories and independent particle models of the nucleus.

It is hoped that by examining models and their calculational rules, one can get clues as to the required behavior of a fundamental and complete theory of hadrons and their interactions. From this point of view, the "odder" the calculational rule, perhaps the better the clue.

IX. CENTRAL REGION

In order to get particles into the central region, it is advantageous to let both incident particles A and B bremsstrahlung, lose momentum and collide at a low relative effective energy. This type of inclusive process is conveniently decomposed into peripheral interactions, hadronic bremsstrahlung and the basic irreducible process as illustrated in Fig. 14. A very large class of theories can be decomposed in this fashion; for example, many of the statistical models can be so written. The resulting cross section is obviously of the form

$$E\frac{d\sigma}{d^3p}(A + B \to C + x)$$
$$= \sum_{a,b}\int dx\, dy\, G_{a/A}(x)\, G_{b/B}(y)\, E\frac{d\sigma^I}{d^3p}(a + b \to C + d^*)\Big|_{\substack{s'=xys\\ t'=xt\\ u'=yu}}$$

and

$$M_a^2 + M_b^2 + M_C^2 + M_{d^*}^2 = xys + xt + yu\ .$$

The irreducible process $a + b \to C + d^*$ (no extra hadrons are allowed to be emitted) can be conveniently separated into contributing graphs as depicted in Fig. 15. The first term on the right is the pure fixed power behaved amplitudes previously discussed while the second term gives rise to Regge behavior for the process $a + q \to C + q$. The third term corresponds to the production of a state c in the basic interaction that subsequently decays to the observed particle C.

Using the relation between the irreducible and total probability functions,

$$G_{q/B}(x) = \int_x^1 \frac{dz}{z} \sum_b G^I_{q/b}\left(\frac{x}{z}\right) G_{b/q}(z) ,$$

the inclusive cross section can be written in the convenient but unsymmetrical form

$$E\frac{d\sigma}{d^3p}(A + B \to C + x) = \int_{z_c}^1 dz \sum_a G_{a/A}(z)\, E\frac{d\sigma}{d^3p}(a + B \to C + x) ,$$

where $z_0 = -u/(s+t)$ and the inclusive cross section under the integral is evaluated at $s' = zs$, $u' = u$, and $t' = zt$. In this formula, small intermediate transverse momenta have been neglected, and the required symmetrization between the particles has not been explicitly denoted. This is easily handled in any specific reaction of interest.

The general behavior of the inclusive cross section can be understood from quite simple kinematic arguments that are of course implicitly contained in the above formula. The basic (internal) process is $a + q \to C + q$ and it has an $(\text{energy})^2$ of

$$s_{eff} = xys \sim \frac{x^2(-u)s}{xs + t} \geq 4p_T^2 ,$$

if the missing mass M_{d^*} is kept finite. Therefore this process is operating at a fixed angle and at an $s_{eff} \sim 4p_T^2$, and one expects

$$\frac{d\sigma}{dt}(a + q \to C + q) \sim (p_T^2)^{-N} f(\theta)$$

where N is related to the total number of constituents involved in this subreaction. Thus the p_T dependence of the inclusive cross section is related to and determined by the number of constituents involved in the basic process. Let us now discuss the behavior of the cross section given by the above integral more carefully in various kinematic regions.

Let us first examine the central region where $p_T^2 \sim tu/s \sim$ constant, and $\epsilon = \mathcal{M}^2/s \sim 1$. The integral over z is easily estimated in the above formula and one finds

$$E\frac{d\sigma}{d^3p} = \sum_a g_a(x_L, \epsilon)(p_T^2)^{-N_a}$$

where $N_a \equiv 2(1 - \alpha_{AC}(\langle z\rangle t))$, and $\langle z\rangle$ is the average value of z involved in the integral. For large $|t|$, $\alpha_{HC} \approx \alpha_{HC}(-\infty)$ which is a number determined by counting. For example, $\alpha_{AC} = -1$ yields p_T^{-8} terms, $\alpha_{AC} = -2$ yields p_T^{-12} terms, etc.

A second interesting region is the threshold region defined by $\epsilon \to 0$. This limit should suppress the bremsstrahlung contributions and one finds that this is indeed the case. Note that the suppression works from both ends of the integral since $z_0 = 1 - \epsilon/(1 + t/s) \to 1$, and also, the x variable in the inclusive process under the integral is

$$x' = -\frac{t'}{s' + u'} = \frac{(z - z_0)(s+t)}{(zs + u)} .$$

Thus in the integrand, $z \sim z_0$ is suppressed and of course $z \sim 1$ is suppressed by the explicit $G(z)$ probability function. One finds

$$E\frac{d\sigma}{d^3p} \simeq \sum_{a,b} \epsilon^{F(a,b)}\, \gamma_{ab}(p_T, u/s)$$

where

$$F(a,b) = g\left(\frac{a}{A}\right) + g\left(\frac{b}{B}\right) + 1 .$$

A more careful analysis of the integral yields the behavior for the a, b contribution

$$\sim \epsilon^{F(a,b)}(p_T^2 + M^2)^{-N_a} \left(\frac{1}{4} x_T^2 + \bar{y}\epsilon\right)^{1-g(b/B)-2\bar{\alpha}} f(p_T, \theta)$$

where $0 < \bar{y} < 1$ (using the mean value theorem)and $\bar{\alpha} \equiv \alpha(\langle z \rangle t)$. Note that if $x_T^2 \gg \epsilon$, which is true in the deep scattering regions, then the ϵ dependence is given by the first factor; however, if $x_T^2 \ll \epsilon$, which is true as one approaches the triple Regge region, then one finds a different power of ϵ. This can be interpreted as a triple Regge formula with an effective trajectory given by

$$\alpha_{eff}(t) = \alpha_{AC}(\langle z \rangle t) - \frac{1}{2}[1 + g(a/A)]$$

which can be described as a nonleading Regge (disconnected cut) contribution.

We have now identified a second important correction to the triple Regge formula which should become important at large missing mass and provides the correct extrapolation into the central region. An analysis of reactions of the form $pp \to CX$, where $C = p, \pi^{\pm}, K^{\pm}, \bar{p}$, has been carried out by Chen, Wang, and Wong.[19] As discussed in more detail in Ref. 4, their results for the effective trajectory provide evidence for the type of correction we are discussing and for the quantum number dependence predicted by the above formula for α_{eff}.

X. CHARACTERIZATION OF CROSS SECTIONS

It is convenient to have a simple way to characterize the possible behaviors of the inclusive cross section arising from different basic processes. If one includes the case in which the final particle C is a decay product of particle c, then one finds at large p_T that

$$E\frac{d\sigma}{d^3p} = \sum_{a,b,c} \frac{\epsilon^F}{(p_T^2 + M^2)^N} I_{a,b}\left(\epsilon, \frac{u}{s}\right)$$

where

$$F = 2(n(\bar{a}A) + n(\bar{b}B) + n(\bar{c}C)) - 1$$

$$N = n_a + n_b + n_c + n_{d^*} - 2$$

and $I_{a,b}$ is a slowly varying function. It will be set equal to a constant from now on in our discussion but is needed in any detailed numerical fit,[20] especially for values of x_L not near zero.

Some sample values of F and N are given in Tables I and II. The two numbers F and N have a simple physical interpretation. The power N measures the number of fundamental fields in the basic interaction that must act coherently in order to produce the observed large p_T. The power F measures the forbiddeness, or the number of fields that must be radiated by the incident systems A and B to arrive at the given subprocess plus the number that must be radiated in the final state produce the observed particle C.

In order to clarify these tables, consider some basic processes and the types of reactions that they can contribute to (M = any nonexotic meson state):

N = 4 (6 quarks involved):

$M + q \to \pi + q$

$\bar{q} + q \to \pi + M$

$q + q \to B + \bar{q}$

N = 6 (8 quarks involved):

$M + M \to \pi + M^*$

$q + (qq) \to \pi + B^*$

$B + q \to B + q$

N = 8 (10 quarks involved)

$B + M \to B + M^*$

$B + (qq) \to B + (qq)$.

TABLE I

Inclusive Process	Exclusive Limit Channel	Subprocesses	$\frac{d\sigma}{d^3p/E}$ $(\theta \sim 90°)$
$M + B \to M + X$	$M + B \to M + B^*$	$\underline{M + q \to M + q}$	$(p_\perp^2)^{-4}\ \epsilon^3$
	$(n = 10)$	$\bar{q} + B \to M + qq$	$(p_\perp^2)^{-6}\ \epsilon^1$
		$M + B \to M + B$	$(p_\perp^2)^{-8}\ \epsilon^{-1}$
$B + B \to B + X$	$B + B \to B + B^*$	$\underline{B + q \to B + q}$	$(p_\perp^2)^{-6}\ \epsilon^3$
	$(n = 12)$	$B + (qq) \to B + qq$	$(p_\perp^2)^{-8}\ \epsilon^1$
		$B + B \to B + B$	$(p_\perp^2)^{-10}\ \epsilon^{-1}$
	$B + B \to B + B^* + M^*$	$\underline{q + q \to B + \bar{q}}$	$(p_\perp^2)^{-4}\ \epsilon^7$
	$(n = 14)$	$q + (qq) \to B + M$	$(p_\perp^2)^{-6}\ \epsilon^5$
		$(qq) + B \to B + M + qq$	$(p_\perp^2)^{-10}\ \epsilon^1$
		$B + B \to B + B + M$	$(p_\perp^2)^{-12}\ \epsilon^{-1}$

The expected dominant subprocesses for selected hadronic inclusive reactions at large transverse momentum. The second column lists the important exclusive processes which contribute to each inclusive cross section at $\epsilon \sim 0$. The basis subprocesses expected in the CIM, and the resulting form of the inclusive cross section $Ed\sigma/d^3p \sim (p_\perp^2)^{-N}\ \epsilon^P$ for $p_\perp^2 \to \infty$, $\epsilon \to 0$, and fixed θ_{cm} are given in the last columns. The subprocesses that have the dominant $p_\perp$ dependence at fixed ϵ are underlined.

TABLE I Cont.

Inclusive Process	Exclusive Limit Channel	Subprocesses	$\frac{d\sigma}{d^3p/E}$ $(\theta \sim 90°)$
$B + B \to M + X$	$B + B \to M + B^* + B^*$	$\underline{q + (qq) \to M + B^*}$	$(p_\perp^2)^{-6}\ \epsilon^6$
	$(n = 14)$	$q + B \to q(\to M + q) + B^*$	$(p_\perp^2)^{-6}\ \epsilon^5$
		$q + B \to M + q + B^*$	$(p_\perp^2)^{-8}\ \epsilon^3$
		$(qq) + B \to M + B^* + qq$	$(p_\perp^2)^{-10}\ \epsilon^1$
		$B + B \to M + B^* + B^*$	$(p_\perp^2)^{-12}\ \epsilon^{-1}$
	$B + B \to M + M^* + B^* + B^*$	$\underline{M + q \to M + Q}$	$(p_\perp^2)^{-4}\ \epsilon^9$
	$(n = 16)$	$q + q \to \bar{q}(\to M + \bar{q}) + B^*$	$(p_\perp^2)^{-4}\ \epsilon^9$
		$q + q \to M + B^* + \bar{q}$	$(p_\perp^2)^{-6}\ \epsilon^7$
		$M + B \to M + B^*$	$(p_\perp^2)^{-8}\ \epsilon^5$
	$B + B \to M + M^* + M^* + B^* + M^*$	$\underline{q + \bar{q} \to M + M^*}$	$(p_\perp^2)^{-4}\ \epsilon^{11}$
	$(n = 18)$	$q + M \to q(\to M + q) + M^*$	$(p_\perp^2)^{-4}\ \epsilon^{11}$
$B + B \to \bar{B} + X$	$B + B \to \bar{B} + B^* + B^* + B^*$	$\underline{q + q \to B^* + \bar{q}(\to \bar{B} + qq)}$	$(p_\perp^2)^{-4}\ \epsilon^{11}$
	$(n = 18)$	$q + q \to B^* + \bar{B} + qq$	$(p_\perp^2)^{-8}\ \epsilon^7$
		$q + (qq) \to \bar{B} + B^* + B^*$	$(p^2)^{-10}\ \epsilon^5$

TABLE II

Inclusive Process	Exclusive Limit Channel	Subprocesses	$\frac{d\sigma}{d^3p/E}$ $(\theta \sim 90°)$
$\gamma + B \to \gamma + X$	$\gamma + B \to \gamma + B^*$	$\underline{\gamma + q \to \gamma + q}$	$(p_\perp^2)^{-2}\ \epsilon^3$
	$(n = 8)$	$\gamma + B \to \gamma + B^*$	$(p_\perp^2)^{-6}\ \epsilon^1$
		$\bar{q} + B \to \gamma + qq$	$(p_\perp^2)^{-5}\ \epsilon^0$
	$\gamma + B \to \gamma + B^* + M^*$	$q + (qq) \to B^* + \gamma$	$(p_\perp^2)^{-5}\ \epsilon^2$
	$(n = 10)$	$q + B \to B^* + \gamma + q$	$(p_\perp^2)^{-7}\ \epsilon^0$
		$\bar{q} + q \to M + \gamma$	$(p_\perp^2)^{-3}\ \epsilon^4$
		$\gamma + (qq) \to B^* + \gamma + \bar{q}$	$(p_\perp^2)^{-6}\ \epsilon^1$
$\gamma + B \to M + X$	$\gamma + B \to M + B^*$	$\underline{\gamma + q \to M + q}$	$(p_\perp^2)^{-3}\ \epsilon^3$
	$(n = 9)$	$\bar{q} + B \to M + qq$	$(p_\perp^2)^{-6}\ \epsilon^0$
		$\gamma + B \to M + B^*$	$(p_\perp^2)^{-7}\ \epsilon^{-1}$
	$\gamma + B \to M + M^* + B^*$	$\gamma + (qq) \to B^* + M + \bar{q}$	$(p_\perp^2)^{-7}\ \epsilon^1$
	$(n = 11)$	$\bar{q} + q \to M + \bar{M}^*$	$(p_\perp^2)^{-4}\ \epsilon^4$
		$q + (qq) \to M + B^*$	$(p_\perp^2)^{-6}\ \epsilon^2$

The expected dominant subprocesses for selected electromagnetically induced reactions at large transverse momentum. (See Table I.)

TABLE II Cont.

Inclusive Processes	Exclusive Limit Channel	Subprocesses	$\frac{d\sigma}{d^3p/E}$ $(\theta \sim 90°)$
$\gamma + B \to B + X$	$\gamma + B \to B + M^*$	$\underline{\gamma + (qq) \to B + \bar{q}}$	$(p_\perp^2)^{-5}\ \epsilon^1$
	$(n = 9)$	$q + B \to B + q$	$(p_\perp^2)^{-6}\ \epsilon^0$
		$\gamma + B \to B + M^*$	$(p_\perp^2)^{-7}\ \epsilon^1$
	$\gamma + B \to B + M^* + M^*$	$\underline{q + q \to B + \bar{q}}$	$(p_\perp^2)^{-4}\ \epsilon^4$
	$(n = 11)$	$\gamma + q \to B + \bar{q}\bar{q}$	$(p_\perp^2)^{-5}\ \epsilon^3$
		$q + (qq) \to B + M^*$	$(p_\perp^2)^{-6}\ \epsilon^2$
$e + B \to e + X$	$e + B \to e + B^*$	$e + q \to e + q$	$(p_\perp^2)^{-2}\ \epsilon^3$
	$(n = 8)$		
	$e + B \to e + B^* + M^* + M^*$	$e + \bar{q} \to e + \bar{q}$	$(p^2)^{-2}\ \epsilon^7$
	$(n = 12)$		

The dominant terms in the reactions of the type $pp \to CX$, where $C = \pi^{\pm,0}$, K^+, $\rho^{\pm,0}$, etc. are expected to be of the form shown in Fig. 16, with $N = 4$, 6, and 4 respectively. It is a simple matter to count the minimum possible bremsstrahlung states and one finds

$$E\frac{d\sigma}{d^3p} = (p_T^2 + M^2)^{-4}\,[h_1\epsilon^9 + h_2\epsilon^{11}] + (p_T^2 + M^2)^{-6}\,h_3\epsilon^5 + \cdots$$

The constants h_1, h_2, and h_3 vary from process to process. For the reaction $pp \to K^-X$ on the other hand, the initial state has no quarks in common with those in K^- and more bremsstrahlung is necessary, hence

$$E\frac{d\sigma}{d^3p}(K^-) = (p_T^2 + M^2)^{-4}\,[h_1\epsilon^{13} + h_2\epsilon^{11}] + (p_T^2 + M^2)^{-6}\,h_3\epsilon^9 .$$

Note that if the h_2 term dominated both the K^- and K^+ reactions, their ratio (K^-/K^+) would be independent of $x_\perp$. In general, however, one expects that this ratio will fall as $\epsilon \to 0$ (or increasing $x_\perp$) by a factor of ϵ^2 or ϵ^4 (if one had to guess). This latter behavior agrees with the qualitative behavior of the Chicago-Princeton data.[21]

This characterization of the data emphasizes that there are two distinct limits involved here. They are:

(1) p_T large (ϵ fixed), where the minimum value of N dominates

(2) $\epsilon \to 0$ (p_T fixed), where the minimum value of F dominates.

It is often stated that the parton model (whatever that is) predicts a factorization of the form ($x_L = 0$, p_T large and N = constant)

$$E\frac{d\sigma}{d^3p} \simeq (p_T^2 + M^2)^{-N} f(\epsilon) .$$

We see that this statement has a grain of truth but is not correct. It is oversimplified both physically and mathematically. However, a single term may happen to dominate in a certain regime. In any case, it is convenient to analyze data by assuming the above form and determining the effective value of N as a function of s, p_T, or ϵ. Defining N_{eff} by varying p_T^2 (or s) at fixed ϵ,

$$N_{eff} \equiv -\,p_T^2\frac{\partial}{\partial p_T^2}\ln\left(E\frac{d\sigma}{d^3\rho}\right) ,$$

one finds by using a single term form that

$$N_{eff} = N\left(1 + \frac{M^2}{p_T^2}\right)^{-1} .$$

This simple curve has the qualitative features of the N_{eff} extracted by the Chicago-Princeton group (see also the talk by Cronin in these proceedings) if M^2 is a few $(GeV)^2$. One also sees that more than one term is probably needed to accurately fit the data.

Let me now show you some rough fits to the data that I have carried out. These are not optimum fits in any sense, the parameters were simply varied until the theoretical curves looked something like the data for $pp \to \pi^-X$. The procedure used was as follows. I arbitrarily set $h_2 = 0$ even though by retaining it, a better fit could be achieved at intermediate values of p_T. The constants h_1 and h_3 were fit to the Chicago-Princeton-FNAL data[21] at large p_T (~ 5-6 GeV/c) and then the mass parameters associated with the p_T^2 denominators were chosen to agree with the data for $p_T \sim 1$ GeV/c. The resultant curves for the 200, 300, and 400 GeV/c data is shown in Fig. 17 along with the experimental points. Roughly speaking, the p_T^{-8} and the p_T^{-12} terms are comparable throughout this regime but the p_T^{12} term always wins at large p_T due to its slower falloff in ϵ. If one uses only the p_T^{-8} term, the fit is as shown in Fig. 18. One should take note of the fact that there are important nuclear effects in the data which effect the lower p_T range and primarily the magnitude of h_3. Take all details of these "fits" with a grain of salt.

In the upper ISR range of energies, the p_T^{-12} term is negligible ($\epsilon > 0.6$ for this data), and the agreement with the data[22] is excellent for $\sqrt{s} \gtrsim 30.6$ GeV as is shown in Fig. 19. An important question is whether low energy accelerator data is exploring the same physics as the ultra high energy data discussed above. The answer seems to be in the affirmative but low energy data does not exist for the most part, and much more is needed. In Figs. 20 and 21, the predictions of the theory using the same parameters as determined above are shown as dotted lines and compared with the data of Allaby, et al.[23] at 24 GeV/c. These curves check two aspects of the theory, the overall normalization (and its (scaling) energy dependence) and the behavior away from $x_L = 0$. The agreement is much better than could be expected. For increasing $x_L \gtrsim 0.5$, triple Regge and leading particle effects come in as expected and the agreement rapidly worsens. In fitting this data, the function $I(x,y)$ is quite important in determining the $x_L \neq 0$ behavior. Finally, the predictions at 69 GeV/c are in quite good agreement with the recent results of the Saclay-Serpuhkov collaboration[24] for $p_T < 1.25$ GeV/c and $x_L = 0$ as is shown in Fig. 22. When the effects of nuclear absorption on the Chicago-Princeton data are accurately understood, it will be necessary to go back and perform a careful fit of all of this data. It should be stressed that the low energy data is a powerful constraint on the theory and should not be ignored (as most theorists in this game seem to do).

B.

The reaction $pp \to pX$ is an interesting one because it involves a more coherent final state particle and has quite a few subprocesses that can contribute significantly to it (see Table I). The basic process $q + q \to B + \bar{q}$ will ultimately produce a p_T^{-8} behavior if it is present at all. However, since the original process may be in some sense close to its exclusive limit, one would expect that the diagrams that were shown to dominate the exclusive process should be important in the inclusive case, particularly for small ϵ. The dominant exclusive diagrams are shown in Fig. 23 and their immediate inclusive analogues in Fig. 23b. Notice that the two final states are different and incoherent for fixed ϵ since one involves a recoil q while the other involves a recoil "core." These will contribute terms of the order of p_T^{-12} and p_T^{-16} respectively. Retaining these three basic contributions only (which may be too drastic), the cross section in the central region should be characterized by the form

$$E \frac{d\sigma}{d^3p}(p)$$
$$= (p_T^2 + M^2)^{-4} h_1\epsilon^7 + (p_T^2 + M^2)^{-6} [h_2\epsilon^3 + h_4\epsilon^5] + (p_T^2 + M^2)^{-8}[h_3\epsilon^1 + h_6\epsilon^3] + \cdots ,$$

where h_4 and h_6 are additional (Feynman) scaling contributions arising from bremsstrahlung of the initial beam protons. The N_{eff} analysis of the data by Cronin at this conference indicates that the h_3, h_6 terms seems to dominate the amplitude for $\epsilon < 1/2$. This process has not been carefully analyzed, and one should be able to learn a lot from it. Perhaps large p_T data from the ISR will tell us whether the very interesting h_1 term is present, for example. Note also that in the exclusive limit, the h_2 and h_3 terms contribute to order s^{-10} while the h_1, h_4, and h_6 terms are nonleading at s^{-12}. A detailed discussion of the particle ratios will shortly be published.[25]

C.

One of the most interesting features of the CIM is the strong dependence of the predicted powers on the quantum numbers of the particles involved. In the previous sections, we have seen how the powers vary as a function of the detected particle. Similar effects should occur if various beam particles are utilized, and this should provide a severe test of the entire approach. For example, the reaction $\pi p \to \pi X$, the presence of antiparticles in the initial state means that less bremsstrahlung is required and the process is less forbidden than $pp \to \pi X$ but it involves the same basic processes. The cross section is expected to be of the form

$$E \frac{d\sigma}{d^3p} (\pi p \to \pi X)$$

$$= (p_T^2 + M^2)^{-4} [h_1\epsilon^7 + h_2\epsilon^5 + h_3\epsilon^3] + (p_T^2 + M^2)^{-6} [h_4\epsilon^3 + h_5\epsilon] + \cdots .$$

The h_3 and h_5 terms do not Feynman scale and contribute to the exclusive limit s^{-8} behavior. They involve the subprocesses $(\pi + q \to \pi + q)$ and $(\bar{q} + p \to \pi + \text{core})$ respectively, and an extra factor of $x_T^2 = (1-\epsilon)^2$ should be included for all such nonscaling terms but has been dropped for simplicity.

Another interesting case is the reaction $\bar{p}p \to \pi X$, which involves some new possibilities for the subprocesses. The cross section takes the form

$$E \frac{d\sigma}{d^3p} (\bar{p}p \to \pi X)$$

$$= (p_T^2 + M^2)^{-4} [h_1\epsilon^9 + h_2\epsilon^7] + (p_T^2 + M^2)^{-6} [h_3\epsilon^3 + h_4\epsilon^5 + h_5\epsilon^1] + \cdots .$$

The term h_3 arises from the interesting and unusual process $\text{core} + \overline{\text{core}} \to \pi + \pi$, and h_4 from $\bar{q} + \text{core} \to \pi + q$. The h_5 term (which does not Feynman scale) is the only one that contributes to an s^{-8} behavior in the exclusive limit and involves the processes $(\bar{p} + \text{core} \to \pi + \bar{q})$ and $(p + \overline{\text{core}} \to \pi + q)$.

D.

Processes involving photons are particularly important since they should most clearly probe the point-like nature of the constituents. The parton concept was invented in the first place to explain Bjorken scaling of the deep inelastic structure functions! A glance at Table II should convince you that there are a large number of experimental and theoretical possibilities here also. Let me confine my remarks to a brief discussion of two inclusive processes, photo-pion production and compton scattering although exclusive processes are extremely interesting. In Fig. 24 the conventional and expected contributions to these processes arising from (a) $\gamma + q \to \pi + q$ and (b) $\gamma + q \to \gamma + q$ are illustrated with the additional, nonleading terms arising from the subprocesses $\bar{q} + B \to \pi + \text{core}$ and $\bar{q} + B \to \gamma + \text{core}$. Just as in the hadronic case, these types of diagrams are expected to be important, especially at small ϵ. They are perhaps easiest thought of as arising from the baryon scattering off of the $(\bar{q}q)$ components of a target photon. Actually all of these contributions arise from the same basic type of diagrams, but evaluated in different regions of phase space with different particles being far off mass shell, etc.

The expected cross sections are

$$E \frac{d\sigma}{d^3p} (\gamma p \to \pi X) = (p_T^2 + M^2)^{-3} J_1\epsilon^3 + (p_T^2 + M^2)^{-6} J_2\epsilon^0 + \cdots$$

and

$$E \frac{d\sigma}{d^3p} (\gamma p \to \gamma X) = (p_T^2 + M^2)^{-2} J_1'\epsilon^3 + (p_T^2 + M^2)^{-5} J_2'\epsilon^0 + \cdots$$

The ϵ^0 terms would be ϵ^1 if the photon were pure vector meson dominated (so that it would act like a $\bar{q}q$ state rather than a fundamental field).

The photoproduction process has been analyzed by Eisner et al.[27] at 21 GeV/c for π^0 and they find $N_{eff} \sim 6$-7 and $F_{eff} \sim 0.5$ with $M^2 \sim 0.5$-1.2. Boyarski et al.[28] have analyzed $\pi^\pm$, $K^\pm$, and $p^\pm$ data at 18 GeV/c and for the charged pion case find a reasonable fit with $N_{eff} \sim 6$ and $F_{eff} \sim 1$. The best fit varies slightly with the particular process under consideration.

The compton process is very interesting and a basic one for any parton model. The J_1' term is the Bjorken-Paschos process[29] which they showed can be used to measure the ratio $\langle Q_i^4\rangle/\langle Q_i^2\rangle$ where $\langle Q_i\rangle$ is average quark charge in the proton. However, one expects that sizable and even dominant (at present energies) corrections will arise from terms of the form of the J_2' contribution. The J_1' term could still be extracted by a careful fitting of good data and this would be a very worthwhile project.

E.

In this section I would like to briefly review the general structure expected in inclusive final states that is expected on the basis of our previous discussion. A more extensive discussion will be given by Stan Brodsky in these proceedings and a numerical discussion will be published soon by J. Gunion. I will restrict myself to some qualitative remarks.[30] The general decomposition of the inclusive process is illustrated in Fig. 14 and Fig. 15. The basic interaction where the large p_T is generated involves the collision of two components of the incident hadrons. For example, the dominant term in the ISR range was shown to arise from the collision of a quark and a meson. In the overall center of mass, since the quark distribution function vanishes as $(1 - z)^3$ while the meson's vanishes as $(1-z)^5$, the quark will tend to have a higher average momentum than the meson. Therefore one does not expect back-to-back angular distributions in this frame--the quark will retain its excess longitudinal momentum if the pion is detected at 90°. The details of the distribution will depend on the angular behavior of the basic $q + \pi$ processes. When the recoiling quark connects to hadrons, they will smear out this already smeared out distribution. The events tend to be planer except that at each stage of extracting one particle from another (which must occur at least three times in a correlation experiment) there is a small transverse momentum introduced at each stage (this small transverse momentum was neglected in our discussion of the single particle inclusive case). We therefore see from the above arguments how particles correlated with a large p_T particle on the opposite side are expected to have a wide x_L (or rapidity) distribution and to be nonplaner. Only detailed fits to the data can find out if the physical picture works.

Notice that since one expects (Matthew's Theorem) that resonances (or perhaps even "clusters") are produced with roughly the same cross section as pions, there will be correlations on the same side with the large p_T particle as well. This is a very interesting point to check since it is a rather severe test of the theory. More detailed tests have been proposed by Sivers and Newmeyer for this region.[31]

We have found that the Chicago-Princeton data seems to be dominated by the subprocess with a meson-B^* final state. Therefore one expects to find large p_T pions correlated with baryons on the <u>opposite</u> and the <u>same</u> side (arising from the B^* decay).

XI. CONCLUSIONS

What has been achieved by the picture of strong interactions that we have been describing? Perhaps the most impressive point is a simple analytical description of inclusive and exclusive reactions valid at fixed angle and fixed momentum transfer. There are few parameters since dimensional counting (applied to one's favorite nucleon model) determines all limiting behaviors in a simple way. This, together with the fact that the CIM joins smoothly onto normal Regge theory at fixed t, puts many constraints on the forms the model can predict. The new dynamics has been isolated in the irreducible processes, and it was shown that if one gives the form of

(A) the exclusive basic process at fixed angle

(B) the probability functions $G_{H/A}(z)$,

the inclusive can be built up from the above and then the full amplitude constructed by using only the long range hadron states.

What are some of the important questions raised?

1. No fundamental deviation of the calculational rules, and reasons for:
   (a) weak q-q force, especially between hadrons,[32]
   (b) dimensional counting rules, especially in light of (a).

(c) What is the rule for "allowed" basic processes? For example, is $q + q \to B + \bar{q}$ and/or $q + (qq) \to q + (qq)$ allowed?

(d) How should hadron cores or the (qq) system be handled?

2. Can one calculate absolute normalizations of various subprocesses and then related different reactions absolutely? One needs to understand absorption processes and their effects for these calculations.

3. Who, what, where, and why are the constituents, if any?

References

1. J.F. Gunion, S.J. Brodsky, and R. Blankenbecler, Phys. Rev. D6, 2652 (1972); Phys. Letters 42B, 461 (1972); to help settle questions of co-variance in the approach used above, see M. Schmidt, Phys. Rev. D9, 40 (1974).

2. J.F. Gunion, S.J. Brodsky, and R. Blankenbecler, Phys. Letters 39B, 649 (1972); Phys. Rev. D8, 287 (1973).

3. S.J. Brodsky and G.R. Farrar, Phys. Rev. Letters 31, 1153 (1973); V. Matveev, R. Muradyan, and A. Tavkhelidze, Nuovo Cimento Lettere 7, 719 (1973). See also Z.F. Ezawa, DAMPT preprint 7415 (1974).

4. R. Blankenbecler and S.J. Brodsky, SLAC-PUB-1430, Phys. Rev. (to be published).

5. H.M. Fried and T.K. Gaisser, Phys. Rev. D7, 741 (1973); H.M. Fried, B. Kirby, and T.K. Gaisser, Phys. Rev. D8, 3210 (1973). A.P. Contogouris, J.P. Holden, and E.N. Argyres, Plattsburgh preprint, 1974.

6. R. Blankenbecler, S.J. Brodsky, J.F. Gunion, and R. Savit, SLAC-PUB-1294 and 1378, Phys. Rev. D 4117 (1973). For a phenomenological investigation of Regge behavior, see J. Tran Thanh Van, J.F. Gunion, D. Coon and R. Blankenbecler, SLAC-PUB-1483 (to be published).

7. R. Savit and R. Blankenbecler (in preparation).

8. The data are from C. Baglin et al., Phys. Letters 47b, 85 and 98 (1973). A. Eide, et al., Nucl. Phys. B60, 173 (1973).

9. A. Lundby, CERN preprint 73-3788, submitted to the Fifth International Conference on High Energy Collisons, Stony Brook, New York (1973).

10. J.F. Gunion, University of Pittsburgh preprint (to be published).

11. The idea that the decay of the $(N\bar{N})$ system should be related to the nucleon structure function was introduced and discussed by E. Pelaquier, contribution to IX Rencontre de Moriond (1974), and Montpellier preprint PM/74/7.

12. W.S. Brockett et al., Phys. Letters B51, 390 (1974). I wish to thank W.R. Frisken for discussions about this data and its analysis. G.W. Brandenburg et al., Phys. Letters 44B, 305 (1973).

13. S.D. Drell and T.M. Yan, Phys. Rev. Letters 24, 181 (1970); G.B. West, Phys. Rev. Letters 24, 1206 (1970).

14. E.D. Bloom and F.J. Gilman, Phys. Rev. Letters 25, 1140 (1970).

15. Slightly different versions of this connection are given in J.D. Bjorken and J. Kogut, Phys. Rev. D8, 1341 (1973); D.M. Scott, DAMTP Preprint 73/37. Our result for diffraction scattering is different from the above treatments at small t.

16. A. Mueller, Phys. Rev. D2, 2693 (1970).

17. S.M. Berman, J.D. Bjorken, and J.B. Kogut, Phys. Rev. D4, 3388 (1971). See also D. Horn and M. Moshe, Nucl. Phys. B48, 557 (1972); 139 (1973); J. Kogut, G. Frye, L. Susskind, Phys. Letters 49B, 469 (1972); R.M. Barnett and D. Silverman, UCI Preprint, December 1973. See also W.R. Theis, Phys. Letters 42B, 246 (1972).

18. I wish to thank D. Sivers for pointing this out.

19. Min-Shih Chen, Ling-Lie Wang and T.F. Wong, Phys. Rev. D5, 1667 (1972).

20. D.C. Carey et al., NAL-PUB-74/48 and 74/49--submitted to Phys. Rev. Letters. Their fit would not seem to work at larger transverse momenta.

21. J.W. Cronin et al., Phys. Rev. Letters 31, 1426 (1973).

22. F.W. Busser et al., Phys. Letters 46B, 471 (1973). M. Banner et al., Phys. Letters 44B, 537 (1973). B. Alper et al., Phys. Letters 44B, 521 (1973). See also the FNAL data of J.A. Appel et al., Phys. Rev. Letters 33, 719 (1974).

23. J.V. Allaby et al., CERN Report No. CERN-TH-70-11 (1970), unpublished. E.W. Anderson et al., Phys. Rev. Letters 19, 198 (1967).

24. Collaboration France-Soviet Union, Phys. Letters 50B, 283 (1973).

25. J.F. Gunion, S.J. Brodsky, and R. Blankenbecler (in preparation).

26. R. Anderson et al., Phys. Rev. Letters 30, 627 (1973).

27. A.M. Eisner et al., UCSR preprints, July 1974.

28. A. Boyarski et al., contribution to the Cornell conference, 1972, and D. Sherden (private communication). A SLAC-PUB is in preparation.

29. J.D. Bjorken and E. Paschos, Phys. Rev. 185, 1975 (1969).

30. See also the brief discussion by S. Ellis, contribution to the XVII International Conference on High Energy Physics (London), July 1974 and CERN preprint Th.1908.

31. J.L. Newmeyer and Dennis Sivers, SLAC-PUB-1425, May 1974, submitted to Phys. Rev.

32. Interesting speculations in this regard have been recently discussed by Z.F. Ezawa and J.C. Polkinghorne, Cambridge preprint DAMTP74/20 and A. Weldon (unpublished).

Figure Captions

Fig. 1. Elastic scattering cross section at 5 GeV/c. Note size of pp relative to meson-proton scattering and the qualitatively different angular distribution of $\bar{p}p$ and K^-p scattering.

Fig. 2. Inelastic scattering cross sections at 5 GeV/c. Note that they become roughly equal at large $|t|$ but differ by orders of magnitude in the forward direction.

Fig. 3. Annihilation process at 5 GeV/c. The cross section for $\bar{p}p \to K^-K^+$ is roughly equal to the above in the forward hemisphere but has a small backward peak as expected.

Fig. 4. Test of factorizability of s and angle dependence and of the predicted angular distribution in the CIM.

Fig. 5. The Peyrou plot illustrating the main kinematic regions of interest.

Fig. 6. Wave function and form factor diagrams.

Fig. 7. Even-tempered operator for the form factor for (a) a two-particle state and (b) a three-particle state.

Fig. 8. Typical scattering diagrams for the even tempered scattering operator. Meson-meson scattering is illustrated in (a) and (b), with the latter showing a direct quark-quark interaction. Meson-baryon is illustrated in (c).

Fig. 9. Effective trajectory for pp scattering for s between 20 and 40 $(\text{GeV})^2$ assuming $M \sim (-u)^{\alpha(t)}\ \beta(t)$.

Fig. 10. Effective trajectory for π^-p scattering for s between 10 and 20 $(\text{CeV})^2$ assuming a linear combination of $(-u)^\alpha$ and $(-s)^\alpha$ terms.

Fig. 11. Diagrams given rise to characteristic angular distributions. The (ut) terms arise as in (a), the (st) terms as in (b), and the (t) (or s(t)) terms as in (c).

Fig. 12. Illustrating the close relation between (a) exclusive and (b) inclusive scattering.

Fig. 13. The irreducible interaction (a) and its iteration in the t-channel (b) which gives rise to Regge behavior.

Fig. 14. The general separation of an inclusive process into beam fragmentation $X(A\bar{a})$, target fragmentation $X(B\bar{b})$ and the irreducible process.

Fig. 15. Simplest diagrams contributing to the irreducible process.

Fig. 16. Main diagrams expected to contribute to the reaction $pp \to \pi X$. Note the different final states arising from these contributions.

Fig. 17. Rough fit to the Chicago-Princeton-FNAL data using p_T^{-8} and p_T^{-12} terms.

Fig. 18. Same as Fig. 17 but using only a p_T^{-8} term.

Fig. 19. The fit used in Fig. 17 and compared with the ISR results of the CCR collaboration.

Fig. 20. Some parameters as in Fig. 17 compared with the data of Allaby, et al. The solid curves are data at constant p_T and the dashed lines are the theory for negative pions.

Fig. 21. Same as above but for the positive pion final states.

Fig. 22. Same parameters as in Fig. 17 compared with the negative pion data of the France-Soviet Union collaboration.

Fig. 23. Expected dominant diagram for (a) pp elastic scattering and (b) their corresponding form for inelastic scattering.

Fig. 24. Expected dominant diagrams for inclusive (a) photo-meson production and (b) compton scattering. The last diagram in each row is a type of important but nonleading process that seems to dominate the present data.

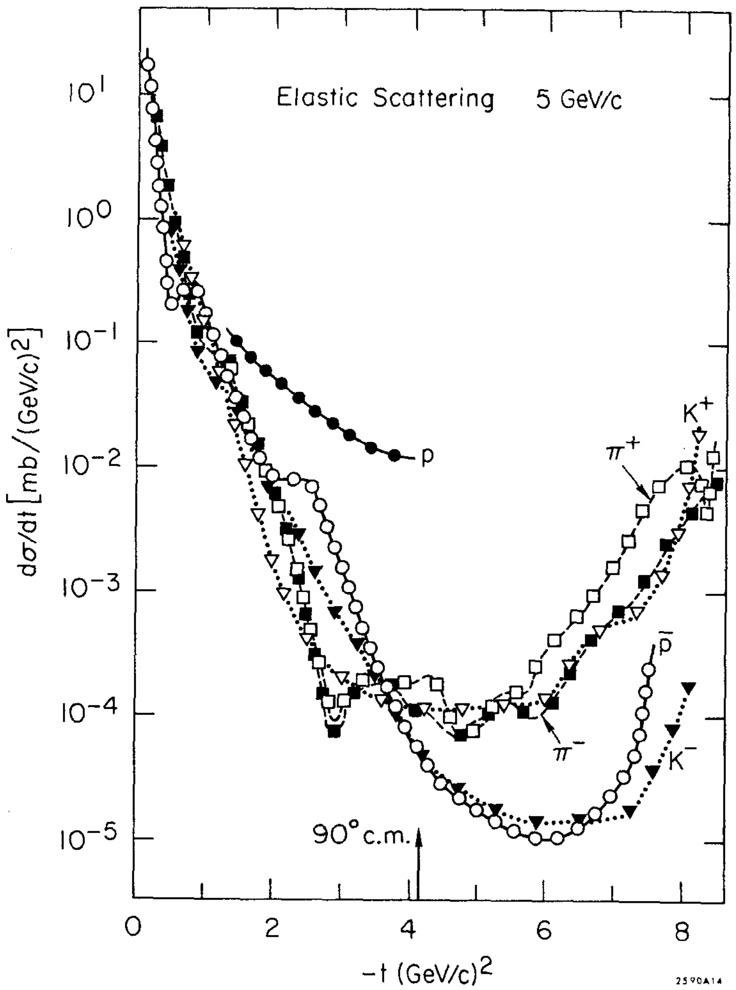

Figure 1

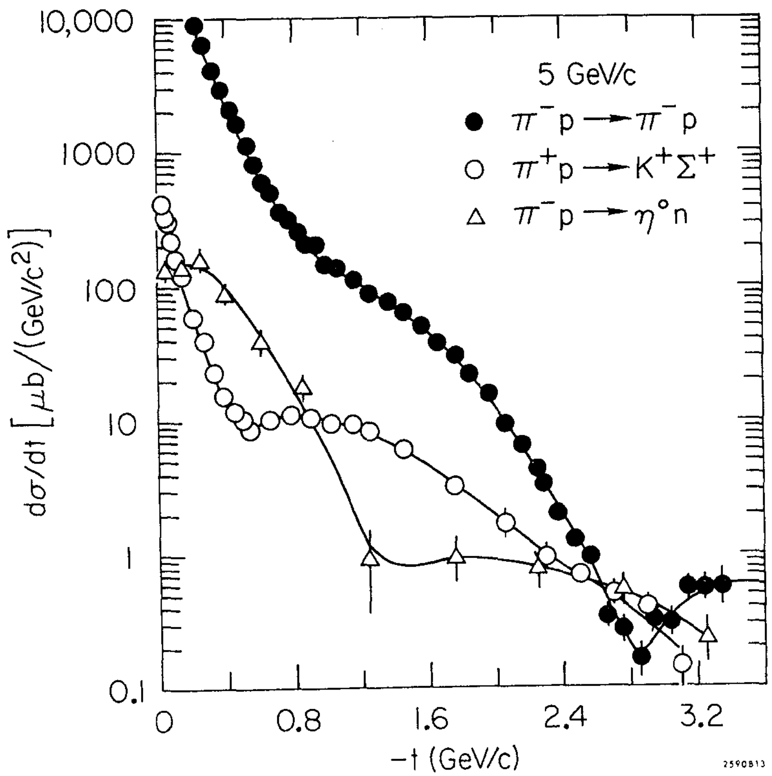

Figure 2

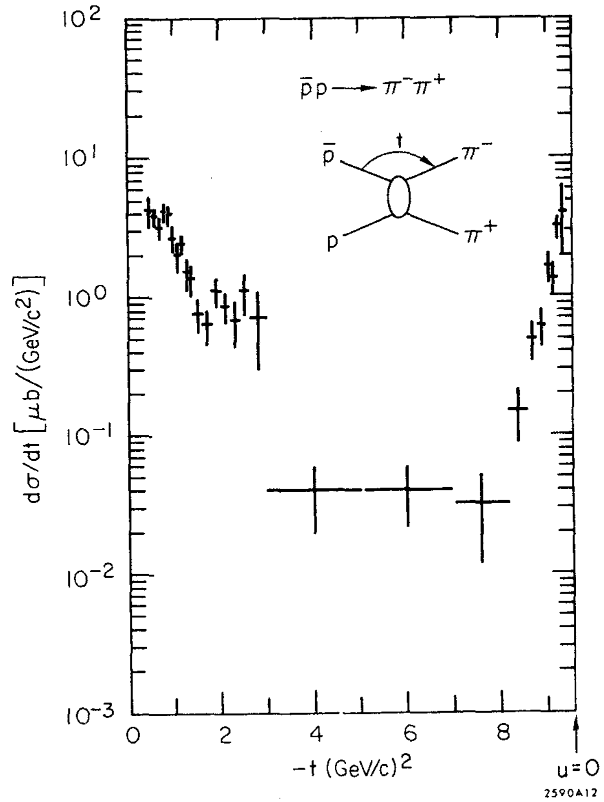

Figure 3

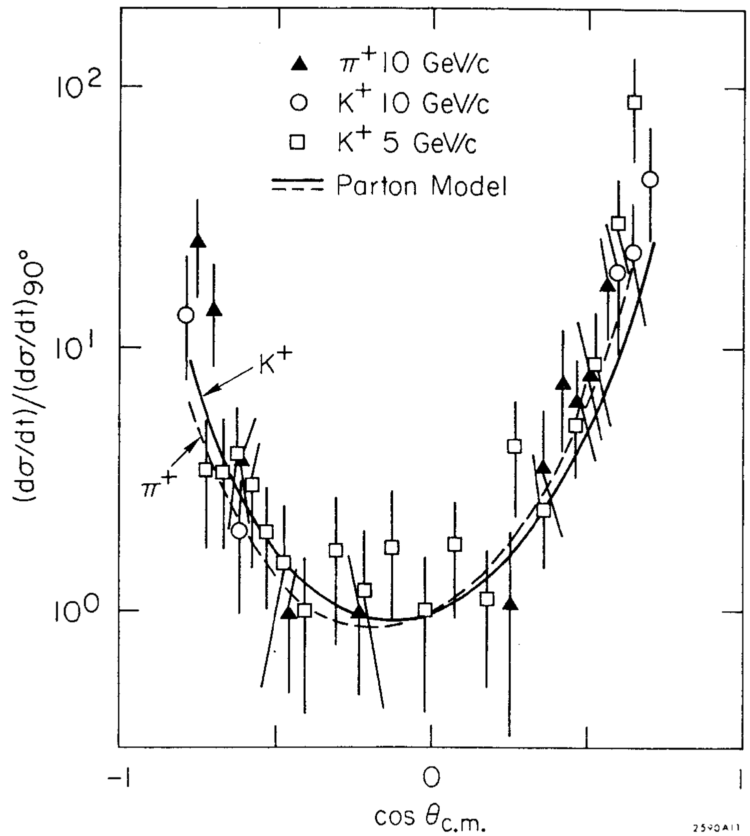

Figure 4

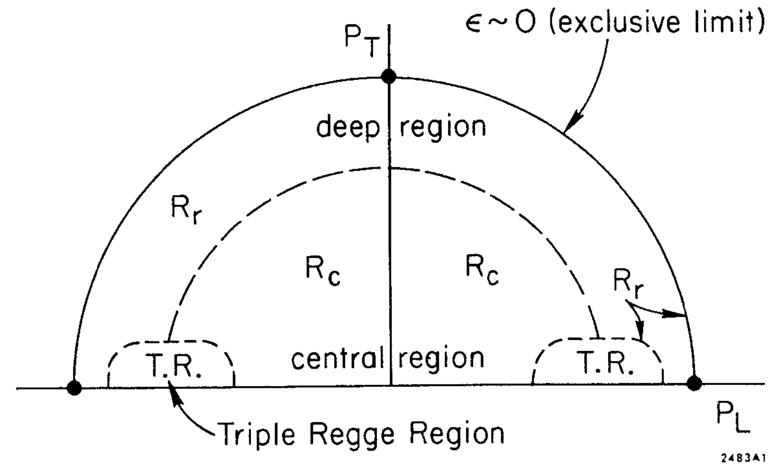

Figure 5

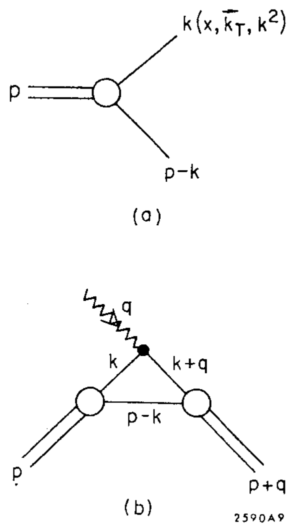

Figure 6

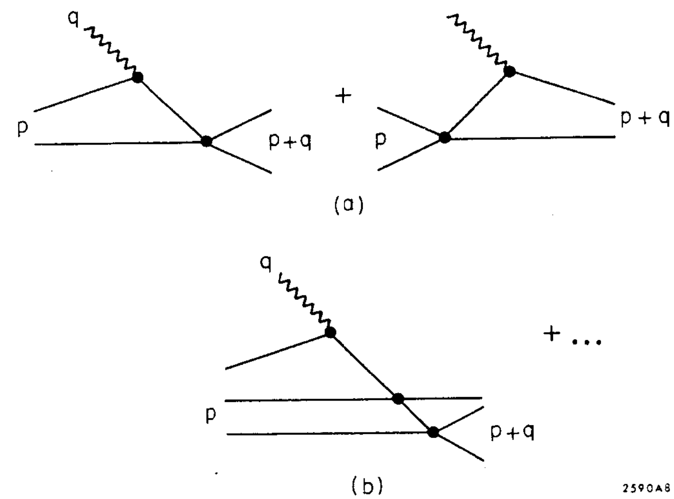

Figure 7

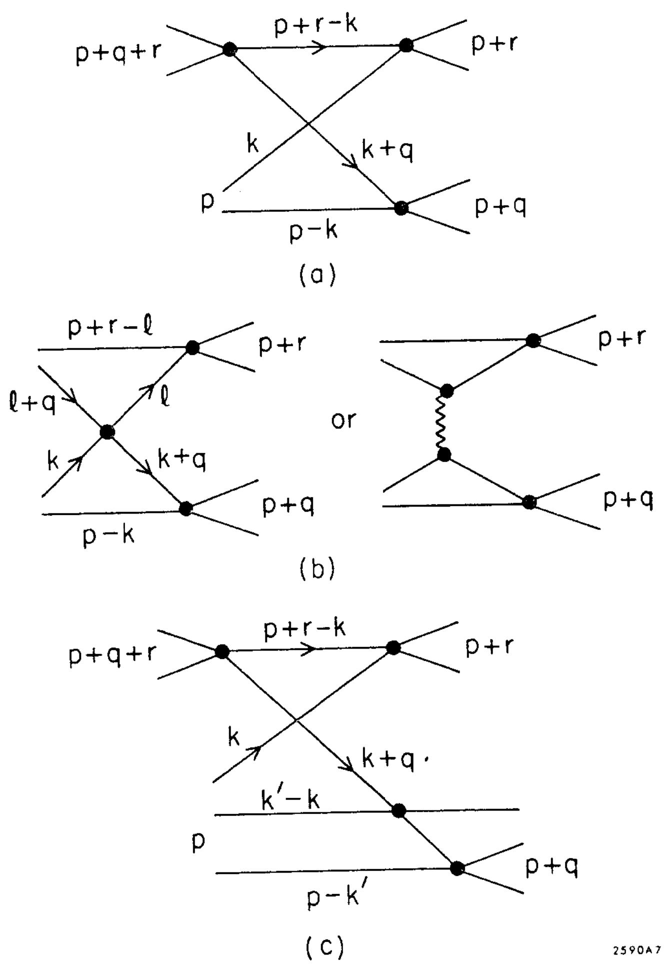

Figure 8

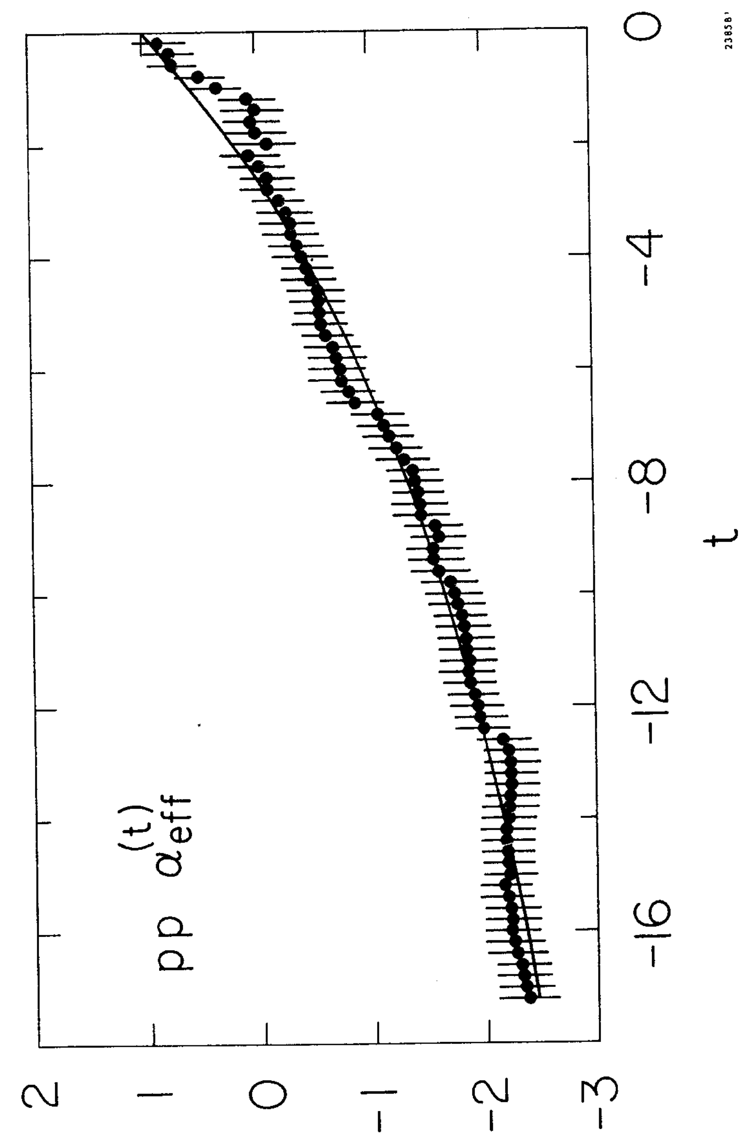

Figure 9

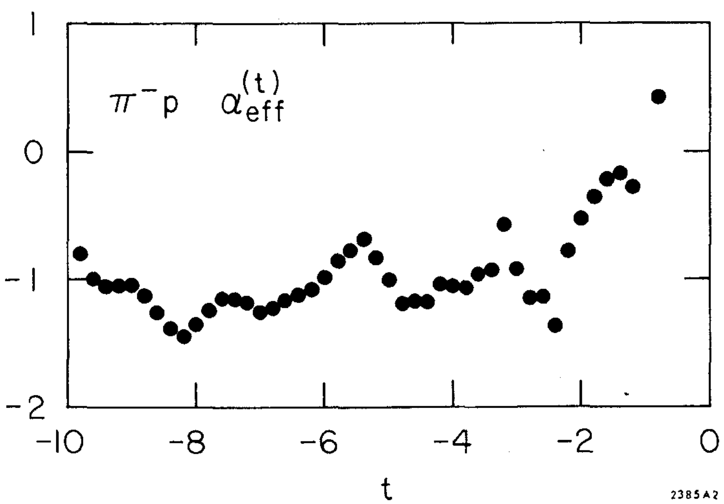

Figure 10

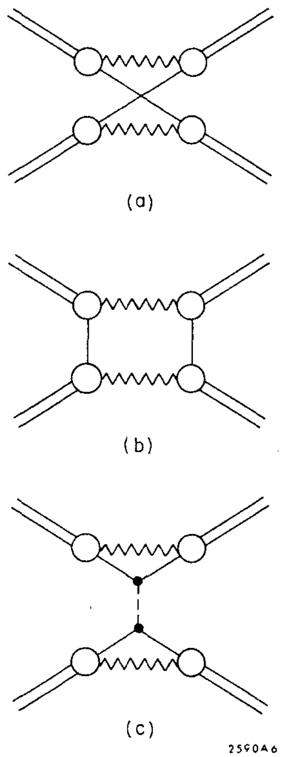

Figure 11

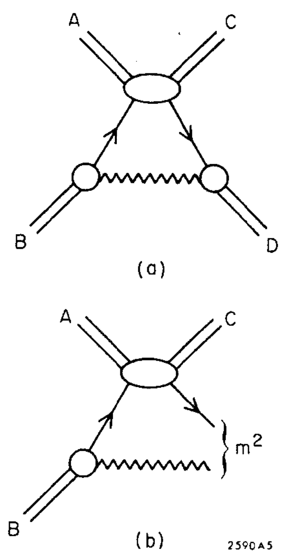

Figure 12

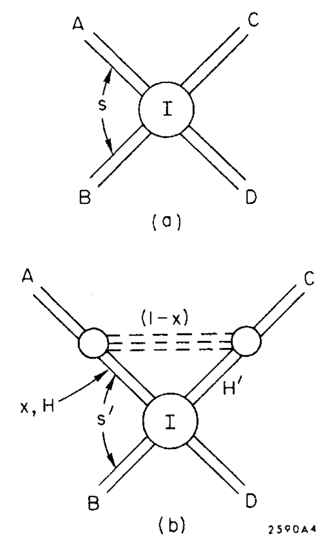

Figure 13

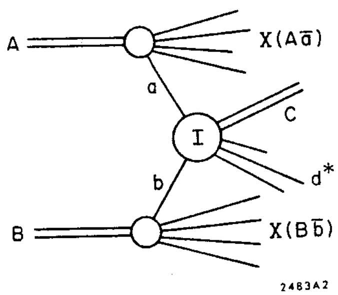

Figure 14

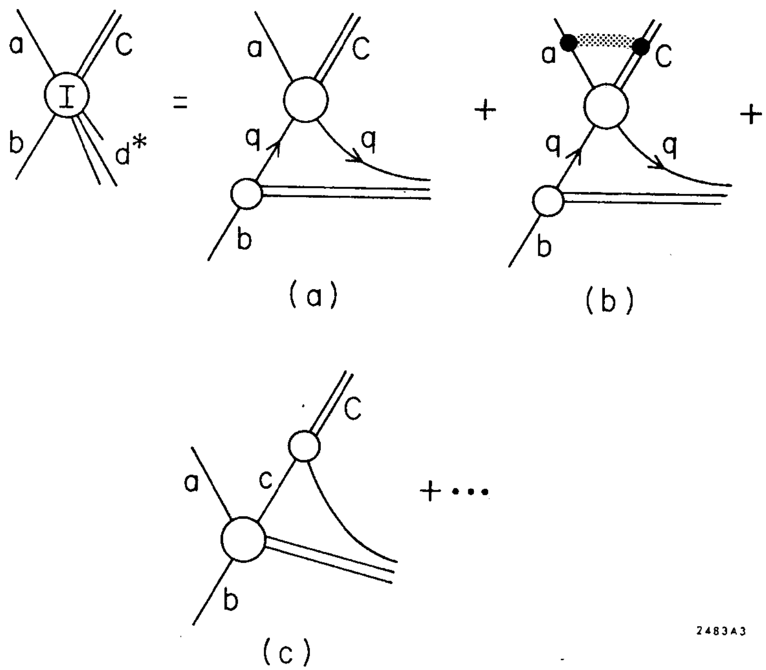

Figure 15

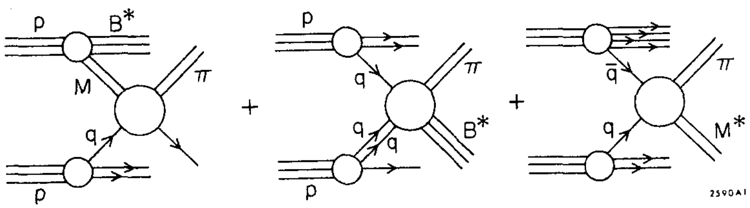

Figure 16

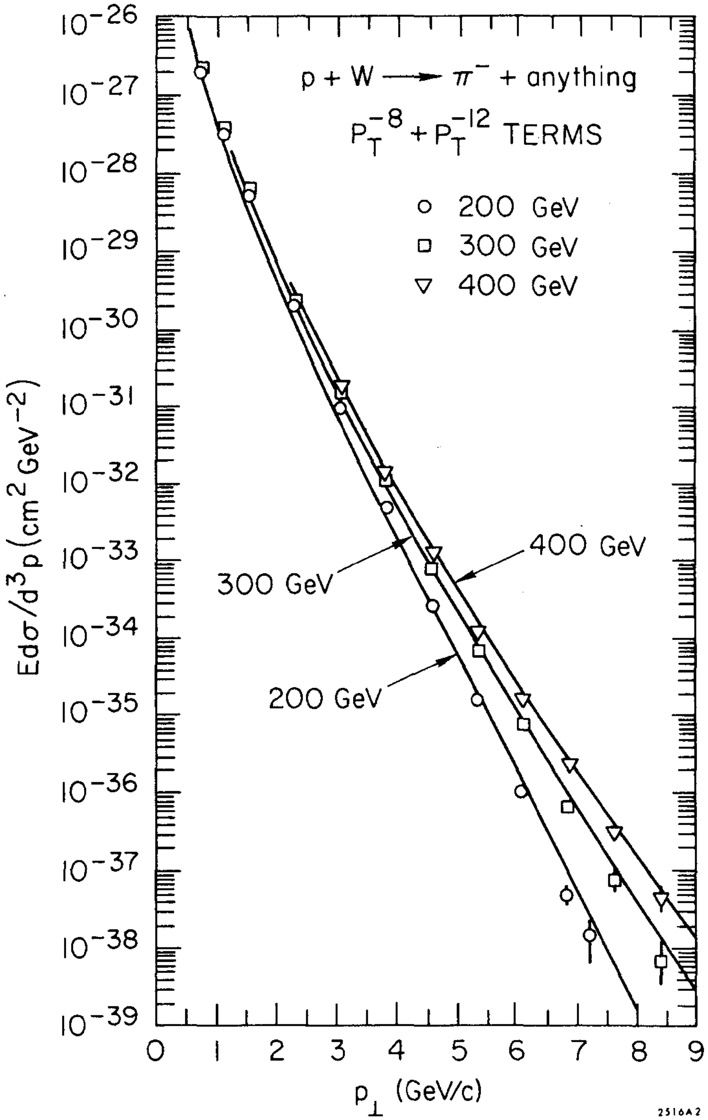

Figure 17

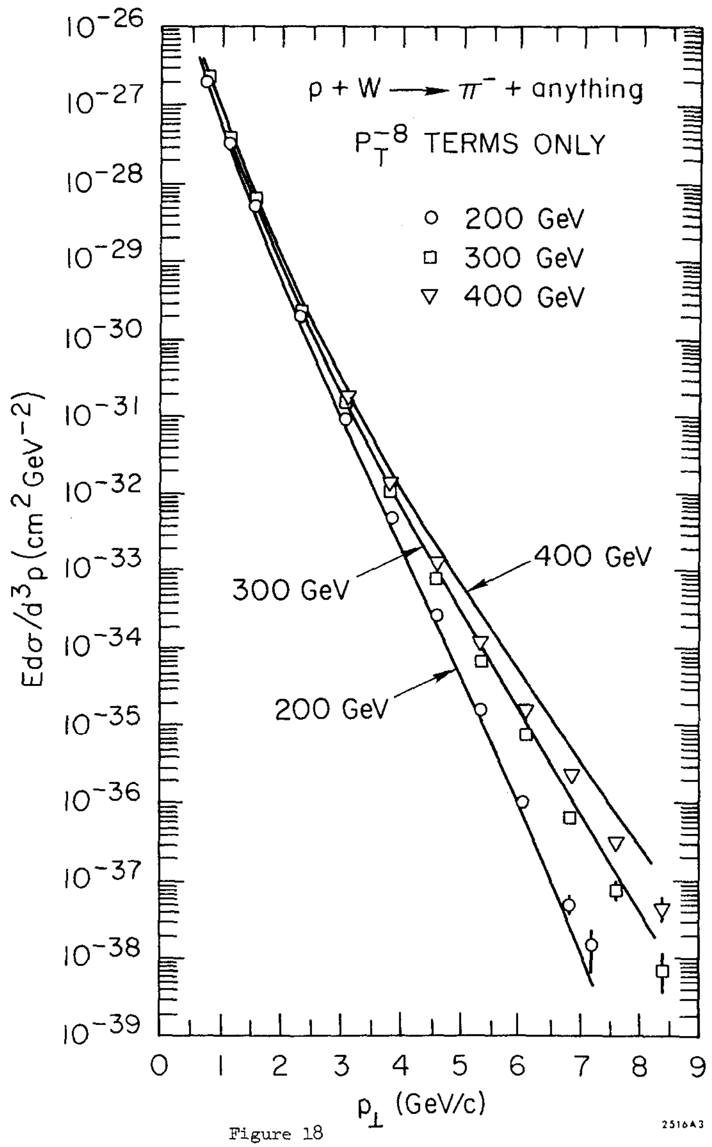

Figure 18

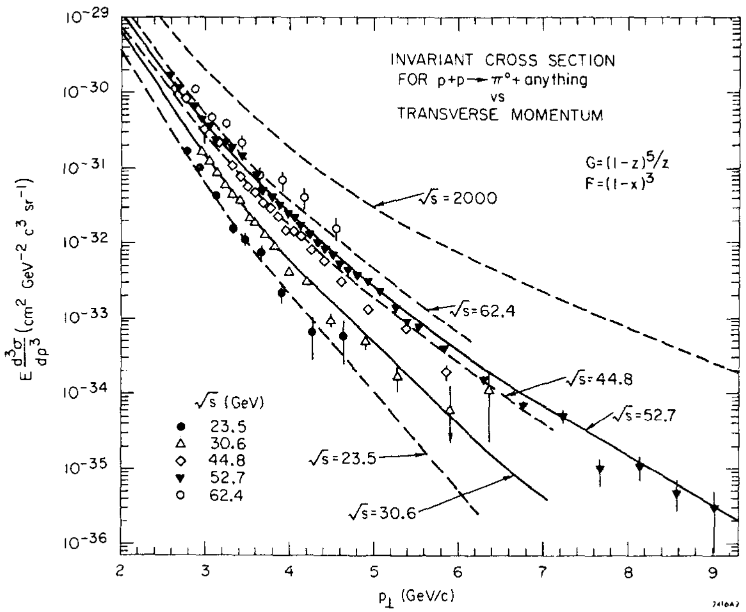

Figure 19

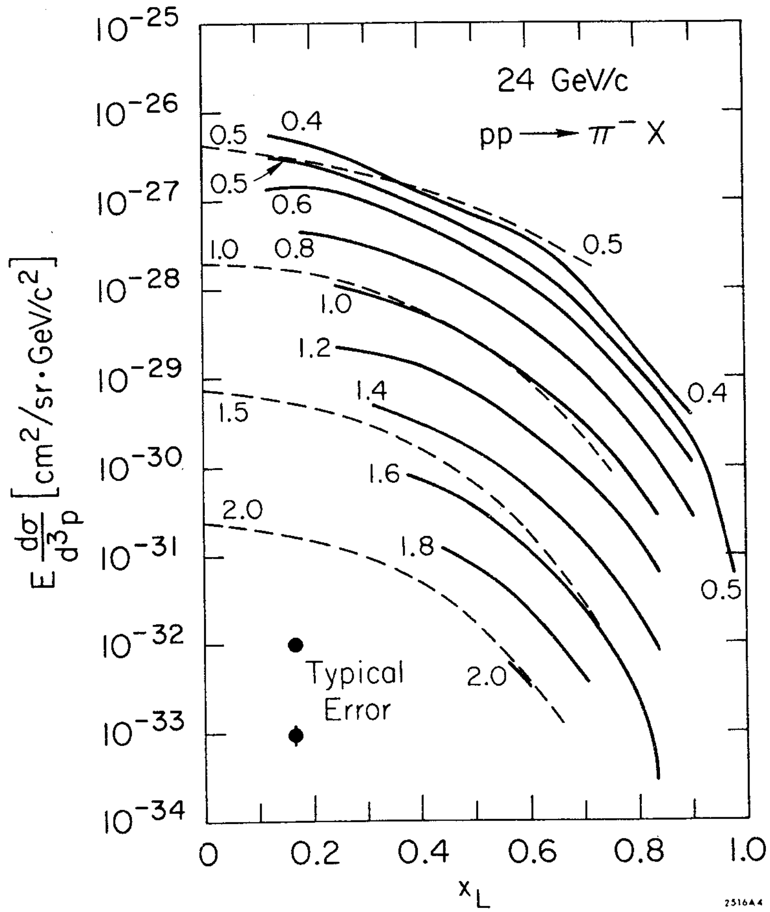

Figure 20

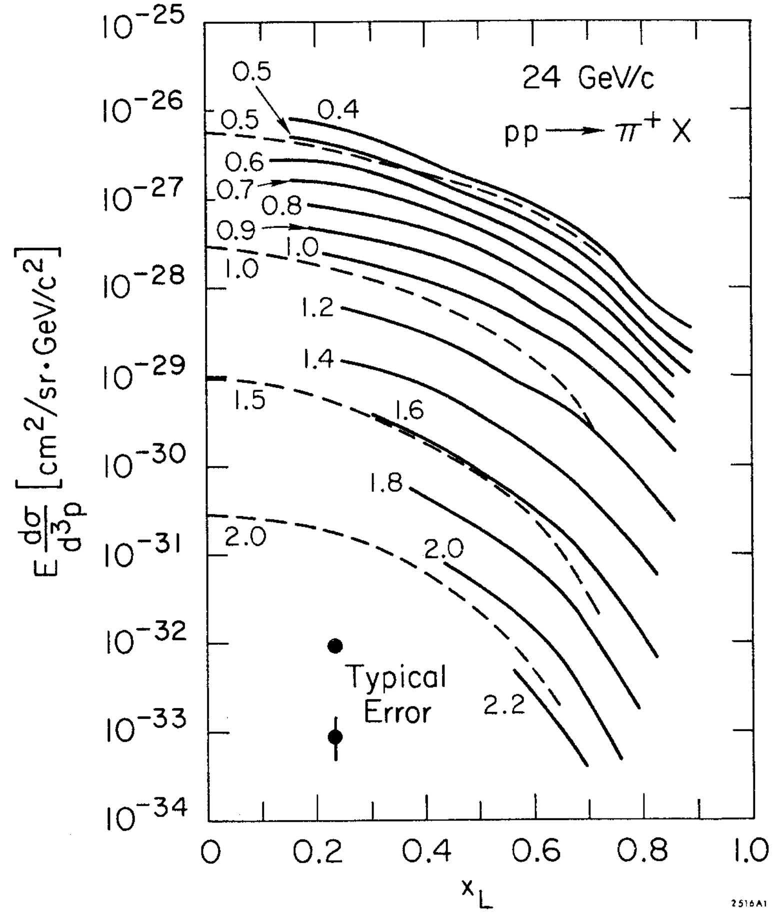

Figure 21

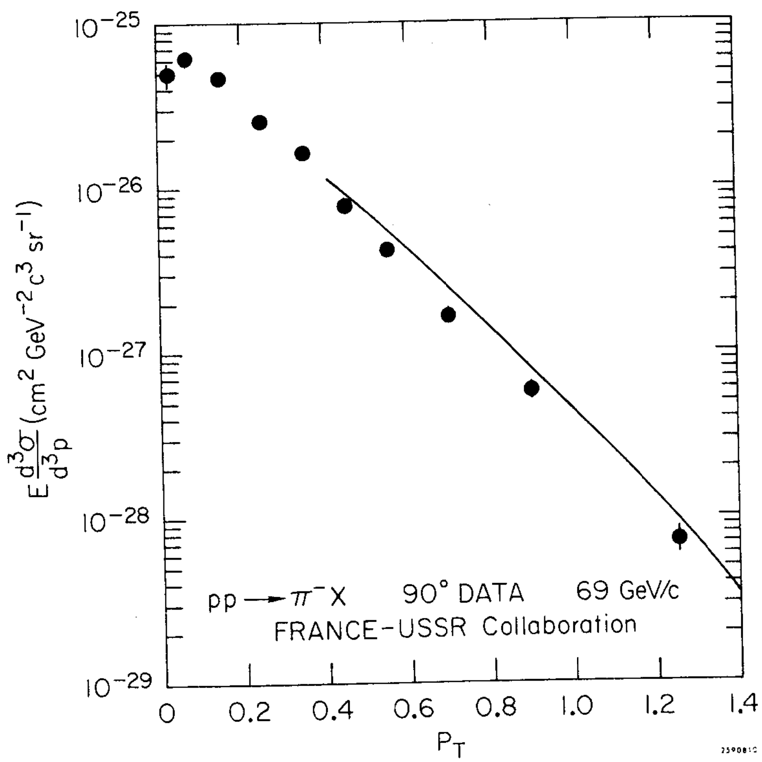

Figure 22

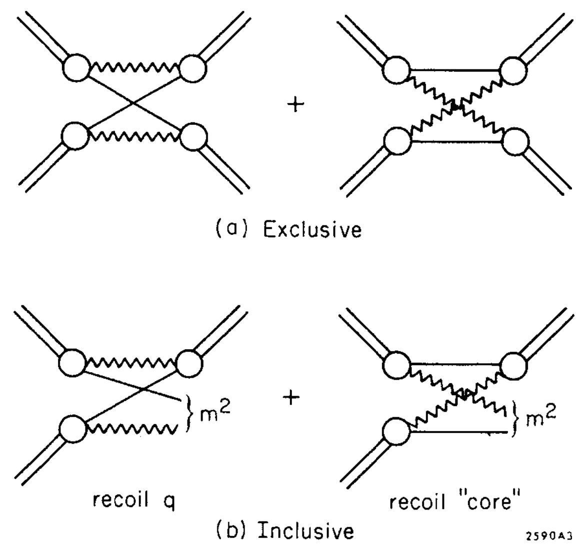

Figure 23

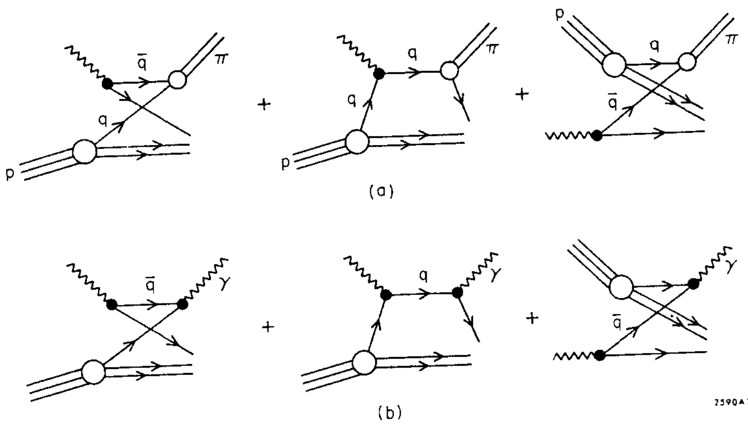

Figure 24

HADRON DYNAMICS*

Henry D.I. Abarbanel

National Accelerator Laboratory
Batavia, Illinois 60510

ABSTRACT

Developments in the dynamics of hadrons and their interactions are presented using the thread of the renormalization group to hold the fabric together. After an introduction to the ideas and equations of the renormalization group we discuss the solution to and usefulness of these equations. Armed with this tool we consider in some depth two seemingly disparate aspects of hadron physics: (1) gauge theories of the strong interactions--in particular, ultraviolet freedom and deep inelastic scattering, models of hadron structure, the use and necessity of charm and color, and so on will be discussed. (2) Diffraction scattering and the Pomeranchuk singularity--in particular, the Reggeon calculus, branch points in the J-plane, decoupling theorems, t-channel discontinuity formula for Reggeons, and so on will be addressed. Some comments will be presented on the relation of these two important subjects.

Throughout the lectures there is an emphasis on pedagogy rather than subtlety. Ideas and elementary examples are stressed and the results of detailed calculations, when presented, are lifted out of the references like magic. This course of lectures should serve as an introduction, then, both to the mainstream of present ideas about hadrons and to the more advanced lectures to be given in the Topical Conference to follow this school.

*Lectures for the SLAC Summer Institute on Particle Physics, 29 July–10 August, 1974.

"We also notice in our audience a bus load of small elderly women from Schnectady, New York. You may stay with us, if you like, but please don't speak out or rustle papers."

A Child's Garden of Grass

J.S. Margolis and R. Clorfene

INTRODUCTION, PHILOSOPHY AND APOLOGY

The subject of these lectures is the most delightful in particle physics: the dynamics and structure of the strong interactions. It is also a field very much in an "open Pandora's box" state:[1] often all one has to go on is hope. On these bare bones there has been a great deal of clever, thoughtful work which attempts to answer some or all of the questions:

1. What is the origin and nature of the J-plane structure, the Pomeranchuk or vacuum singularity, which is responsible for almost constant total cross sections?

2. How can local quantum field theory be consistent with the approximate scaling of deep inelastic structure functions?

3. Are hadrons composites made out of constituents, generically called quarks? How many and what quantum numbers carry these quarks? How is it possible that these presumed constituents have never been seen in the laboratory? Can we make a virtue out of this shyness of quarks?

4. Can we have a Pomeron which gives rise to almost constant cross sections and limiting inclusive cross sections, shows factorization, results in a triple Pomeron coupling, and yet does not decouple from particles?

5. How can one implement unitarity at high energies (direct channel and crossed channel unitarity)? Does this provide the constraints to secure us a solution to the hadron scattering problems?

These are among the major issues of the day. None of them has completely yielded to solution; each of them has been vigorously and imaginatively attacked. The ideas behind this attack are the subject of these lectures. It possible that on finishing a reading of the lectures one may not feel a significant understanding of the deep questions has been achieved. However, I hope that the sense of excitement, which I have, in the feeling that meaningful progress has been accomplished will be transmitted. In many of the concepts we will examine here one can sense a coming to real grips with problems which have remained elusive for years, including most of the questions listed above. If we haven't exactly treed the fox, one cannot help feel that we are hot on the trail.

Enough unsupported, but useful, optimism. Now to a brief outline of the subjects we will cover, how we will do it, and a word or two why. The keystone of these lectures and the work on the questions above is renormalizable local quantum field theory. The use of field theory in electromagnetic interactions needs no defense. In the weak interactions developments over the past several years has raised field theory to the center of the stage again.[2] By establishing that many gauge field theories remain renormalizable when one has a mechanism for giving mass to the gauge bosons,[3] one has renewed the viability of these theories as a framework for building models of weak and electromagnetic processes. The well-known key to the practical use of these field theories is the smallness of the dimensionless coupling constants that appear. Having chosen the fundamental fields (electron, photon, ...) one then perturbs around these excitations. Because of divergences encountered in any non-trivial field theory, the perturbation expansion must be augmented by a set of rules for consistently replacing the divergent quantities by the finite parameters (charges, masses, ...) measured in experiment.[4]

Now all this is quite jolly when one has a small coupling constant in which to expand. Hadronic physics is characterized by the absence of such small couplings. This doesn't mean one cannot write down field theories to describe protons, pions, etc. It only means that having written them down one cannot use perturbation theory to solve them. This impasse led long ago to attempts to study the strong interactions in a more general S-matrix framework[5] which turns away from fundamental fields and focuses on properties one expects the full solution to any field theory to possess: analyticity, unitarity, ... Such an approach has been remarkably successful in underpinning our understanding of many low energy hadronic phenomena. It has provided the tools for a variety of important sum rules when coupled with current algebra. It has significantly enhanced our general outlook on hadron dynamics. It has, I believe, been less valuable in attacking the problems listed above. The reasons are two: (1) the problem of constituents is closely linked with the bound state problem. The bound state problem by its nature requires infinite order perturbation theory in a field theory or equivalently infinite particle intermediate states in S-matrix theory. Because of the plethora of variables in n-particle amplitudes and their extremely complicated analytic properties, these problems are just intractable in an S-matrix framework. (2) High energy scattering involves particle production in an important way (80% of the pp total cross section is inelastic at high energies). Again we have a many body problem.

The achievement of the past couple years in hadronic physics has been the discovery that although the coupling constants of hadrons are not small, there may be regimes of momentum space where <u>the effective coupling is small</u>. After all, the expansion parameter in a field theory is not just the c-number coupling but the product of that and some operator expression of the fields. If the matrix elements of the operator become small, perturbation theory can be called upon once again. The foundation on which these observations rest is the renormalization group.[6] This itself is an expression of the fact that the <u>physical</u> consequences of a renormalizable field theory cannot depend on where in momentum space one chooses to define a set of renormalized parameters. The set of transformations which takes the theory from its realization in terms of parameters defined at one point to its realization in terms of parameters defined at another point gives the so-called renormalization group. (All this will take on a very elementary cast in the next section.) With this in hand the study of field theories for strong interactions has taken an upturn, if not yet a renaissance.

This is the time for apology hard on the heels of the false pride. We are restricted in our studies to renormalizable field theories because we don't know how to compute in any others. Field theories which are non-renormalizable in perturbation theory may, in fact, yield finite Green's functions, but in the absence of a prescription[4] for curing the infinities which arise in the perturbative expansion around a free theory, we join our betters in rejecting their consideration here. The end of the apology is an announcement that none of the problems listed above have been solved in a convincing and lasting sense by the appearance of the renormalization group on the hadronic scene. The framework which it provides is so rich and so tantalizing and so attractive that we may temporarily embrace it with fervor.

The plan of these lectures is to first introduce the renormalization group and study it. We will examine how it is possible that a small effective coupling constant can enter a strong interaction situation. After this we turn to the study of gauge field theories and relate the story of asymptotic freedom.[7] This is the magnificent situation where, the effective coupling is not only small, it is zero!

Next we turn to field theories for Reggeons[8] and formulate the renormalization group properties of such theories.[9] These theories are what, in the language of the angular momentum plane, determine the interaction of poles and branch points relevant near $J = 1$ and $t = 0$ which is the regime that governs diffraction phenomena.

The subject of dual models[10] does not naturally fit into the scheme of these lectures. It is too important to be overlooked, however, so I have artifically extended the period of lectures allowed by our excellent organizers and have asked J. Willemsen to lead some of our afternoon discussion sessions on this topic. His written report will appear as an appendix to these lectures.

Before we start on this adventure let us have a look at the hierarchy of hadron physics indicated in Figure 0. One begins at the most "fundamental" level with the construction of hadrons themselves; presumably out of basic constituents like quarks which may be described by local quantum fermi fields held together by some kind of "glue." Having made hadrons, one may study their interaction at low energies and the processes in which they are produced. This takes us to the second level in our ladder where Reggeons--hadrons whose spin varies with their mass--are made. The bound state problem comes to the fore here. Finally, as far as we know, we reach the last level where Reggeons, in particular the Pomeron (with $\alpha(0) = 1$), begin to interact among themselves. The Reggeon field is to be though of as a "mean" field in the statistical physics sense. The interaction of Pomerons is thus akin to the study of the order parameters in many body physics and the analysis of phase transition phenomena. This analogy will be drawn at some length by A. R. White in his report at the Topical Conference.

> "Therefore, conclusions based on the renormalization group arguments concerning the behavior of the theory summed to all orders are dangerous and must be viewed with due caution.
> So is it with all conclusions from local relativistic field theories."
>
> Relativistic Quantum Fields
>
> J.D. Bjorken and S.D. Drell

THE RENORMALIZATION GROUP

In this lecture we will develop the formalism of the renormalization group[5,9] and see how it provides a structure in which to search for small parameters in hadronic physics. We will carry out our study by examining the simplest example of a renormalizable relativistic field theory: a self-coupled spinless boson with a ϕ^4 interaction.[7] Clearly this field theory is not relevant to hadron physics; we'll get to some which may be. The plan of attack will be to review the renormalization procedure (purists will have to seek proofs elsewhere) and introduce some friendly notation. Then we'll discuss the equations of the renormalization group and how to use them.

The field theory we want to study is given by a Lagrangian density

$$\mathscr{L}(x) = \frac{1}{2}(\partial\mu\ \phi_0(x))^2 - \frac{m_0^2}{2}\phi_0(x)^2 - \frac{\lambda_0}{24}\ \phi_0(x)^4 \qquad (1)$$

for a field with bare mass m_0 interacting with a bare coupling strength λ_0. It is useful to keep thinking of m_0 and λ_0 as just some parameters which characterize the potential energy

$$V = \frac{m_0^2}{2}\phi_0(x)^2 + \frac{\lambda_0}{24}\phi_0(x)^4\ . \qquad (1')$$

To acquire some feeling for this let's digress to consider the Lagrangian (1) in one space and one time dimension. Then we may think of $\phi_0(x,t)$ as the displacement of a string lying along the x-axis where the potential energy is (1'): a simple harmonic Hooke's law force, $(m_0^2\ \phi_0(x)^2)/2$, plus an anharmonic term. If $\lambda_0 = 0$, we have good old simple harmonic motion or equivalently, free field theory. If $m_0^2 > 0$, then the minimum of V is at $\phi_0 = 0$ and the classical string at rest lies with zero displacement. Quantum mechanically this is called the vacuum state. In both cases we solve for oscillations around this ground state.

Since m_0^2 is just a parameter, we may ask what happens when $m_0^2 < 0$. Then V has two minima at $\phi_0 \propto \pm\sqrt{-m_0^2/\lambda_0}$ and the classical string (or quantum vacuum) lies "to the side." For historical reasons this is called spontaneous symmetry breaking. Of course, one still solves for oscillations around these ground states.

Now the object of the game is to solve the equations of motion to find the fully interacting field $\phi(x)$, known as the renormalized field, and all the Green's functions or correlation functions

$$G^{(N)}(x_1,\ \ldots\ ,\ x_N) = \langle 0|T(\phi(x_1),\ \ldots\ ,\ \phi(x_N))|0\rangle\ . \qquad (2)$$

These correlation functions contain all the information about the spectrum of the interacting theory and about the scattering of the ϕ quanta. The determination of the $G^{(N)}$ is usually impossible outside of perturbation theory in λ_0. The formalism for carrying out this evaluation of the $G^{(N)}$ is presented in detail and with clarity in the textbooks of Bjorken and Drell[4] and of Gasiorwicz[11] among others. I do not propose to give here a detailed resumé of those expositions but only to recall some of the salient points.

In doing perturbation theory in λ_0 one encounters divergent integrals all over the place. The renormalization program is a prescription to replace these divergences by a set of finite numbers which then parametrize the fully interacting, or renormalized theory. This procedure relinquishes the actual calculation of the renormalized charges and masses. Instead it introduces them as finite parameters on which all Green's functions must depend. Thus in quantum electrodynamics we depart from the calculation of the electron mass and charge. Instead these are determined from low energy Compton scattering and Coulomb scattering and subsequently appear in all other processes as known parameters. The renormalization program works when the number of parameters one must specify is the same as the number appearing in the unrenormalized Lagrangian and, of course, is finite. To carry out this one proceeds by cutting off or regularizing the Feynman integrals in some manner and then giving a set of rules which yield a finite set of $G^{(N)}$ as the regulator is removed. The usual regularization procedure consists of replacing the good old propagator

$$\frac{1}{p^2 - m_0^2 + i\epsilon} \tag{3}$$

for a boson of momentum p and mass m_0 by

$$\frac{1}{p^2 - m_0^2 + i\epsilon} - \frac{1}{p^2 - m_0^2 - \Lambda^2 + i\epsilon} \tag{4}$$

where Λ is some object with the dimensions of a mass. All work is done with Λ finite, and at the end of time one sends Λ to infinity.

As far as I know there's nothing wrong with this way of going about things. However, there is a much more compact trick around.[12] Alter instead the number of dimensions of space time from 4 to a non-integer number D. Sounds peculiar, doesn't it? To see that it is a clever trick (I emphasize trick since there's no physics in it), let's look at the contribution to $G^{(4)}$ coming from the graph in Fig. 1. This is proportional to

$$\lambda_0^2 \int d^D k \frac{1}{(k^2 - m_0^2 + i\epsilon)} \frac{1}{((P-k)^2 - m_0^2 + i\epsilon)} \tag{5}$$

$$= \lambda_0^2 \int_0^1 dx \int \frac{d^D q}{[q^2 - f(x, P^2, m_0^2)]^2} , \tag{6}$$

by using the usual techniques. f is some easily determined function. Changing variables to

$$\ell = q(f(x, P^2, m_0^2))^{-1/2} , \tag{7}$$

the integral in (6) becomes

$$\lambda_0^2 \int_0^1 dx\, [f(x, P^2, m_0^2)]^{(D/2)-2} \int \frac{d^D \ell}{(\ell^2 - 1)^2} . \tag{8}$$

Now how does one do an integral over D dimensions? Just pretend D is an integer and instead of writing things like $D!$ write $\Gamma(D+1)$ (the standard gamma function). Then (8) becomes

$$i\lambda_0^2 \pi^{D/2} \Gamma(2 - \tfrac{D}{2}) \int_0^1 dx\, [f(x, P^2, m_0^2)]^{(D/2)-2} . \tag{9}$$

If D is not an integer, the Γ function is perfectly well defined. However, when $2 - D/2 = 0, -1, -2, \ldots$ or $D = 4, 6, 8, \ldots$, the Γ function has simple poles! That's where all the divergences of field theory are hiding now. So what one does is to leave D free and then provide a way to eat up the various poles in D at $D = 4$. The real wonders of regularizing the theory in this way are two: (1) D is dimensionless, that is it is just a number, so it introduces no new scales in the problem as does the Λ regularization in Eq. (4). So this trick is sure to respect all the symmetries of the Lagrangian including subtle ones like scale invariance. (2) There are important places in physics where one wants to know the expansion of a theory at $D = 2$ or $D = 3$ around the theory at $D = 4$.[13] This is clearly the way to formulate the answer to such questions.

So now we know how to regularize the theory. How do we renormalize it? It turns out that one need only do this:[7] add to the $\mathscr{L}$ of Eq. (1) the counter Lagrangian

$$\mathscr{L}_c = C_1(\lambda_0, m_0, D)\, \phi_0(x)^2 + C_2(\lambda_0, m_0, D)(\partial\mu\, \phi_0(x))^2 + C_3(\lambda_0, m_0, D)(\phi_0(x))^4, \tag{10}$$

and determine the C_i to cancel the infinities (poles in D) order by order in perturbation theory in λ_0. That's all! The theory is called renormalizable because one only needs to add to $\mathscr{L}$ terms which have the same content in the number of powers of ϕ_0 and not others. The physical meaning of the C_i is straightforward to state: C_1 changes the bare mass m_0 into a new quantity m which will qualify to be called the renormalized mass. C_2 changes the field ϕ_0 into a new field ϕ--the renormalized field. C_3 changes the bare coupling λ_0 into a new coupling λ--the renormalized coupling. The renormalization prescription, which we'll soon launch into, tells us how to replace ϕ_0, m_0, and λ_0 by ϕ, m, and λ. The latter are finite quantities. Further it gives us detailed instructions how we may express all Green's functions $G^{(N)}$ computed to some order in λ_0 by functions of these finite parameters. The parameter m need not have any direct relation to the physical mass M_ϕ of the renormalized ϕ quanta. One discovers M_ϕ by studying the full $G^{(2)}$ and searching for its poles. M_ϕ is some, yet to be learned, function of m and λ. (In gauge theories $G^{(2)}$ is gauge variant. All its poles may not correspond to physical particles.)

One's ability to render the theory finite by the remarkably simple act of adding $\mathscr{L}_c$ to cancel the singularities coming from the use of $\mathscr{L}$ may be given a concrete form as follows: Define the renormalized ϕ, m, and λ as[6]

$$\phi(x) = Z^{-1/2}\,\phi_0(x)\ , \tag{11}$$

$$\lambda = Z^2 Z_\lambda^{-1}\,\lambda_0\ , \tag{12}$$

and

$$m^2 = Z Z_m^{-1}\, m_0^2\ . \tag{13}$$

There is a long tradition of convention going into these definitions. The quantities Z, Z_λ, and Z_m are related to the C_i above. Now we give a set of rules which enable us to determine the Z's. They are divergent quantities at $D = 4$ (poles again).

The procedure we use is to introduce the proper vertex functions $\Gamma^{(N)}(p_j)$ which are the Green's functions in momentum space, $G^{(N)}(p_j)$, ($\Sigma_{j=1}^{N} p_j = 0$, see Figure 2) with the legs amputated:

$$\Gamma^{(N)}(p_1, \dots, p_N) = \prod_{j=1}^{N} [G^{(2)}(p_j^2)]^{-1}\, G^{(N)}(p_1, \dots, p_N)\ . \tag{14}$$

This just saves us constant reference to the singularities of the propagator $G^{(2)}(p^2)$. Note that $\Gamma^{(2)}(p^2) = [G^{(2)}(p^2)]^{-1}$. In lowest order of λ_0 we observe

$$i\Gamma_0^{(2)}(p^2) = p^2 - m_0^2 + i\epsilon \tag{15}$$

and

$$\Gamma_0^{(4)}(p_1, \dots, p_4) = -i\lambda_0/(2\pi)^D\ . \tag{16}$$

We will specify Z, Z_λ, and Z_m by announcing the value of $\Gamma^{(2)}$ and $\Gamma^{(4)}$ at some convenient points in momentum space. This will give us definitions of m and λ.

Let us introduce next a parameter which we call μ. It has the dimensions of momentum and will play the role of setting the scale for the points in momentum space where we choose to normalize our theory and define m and λ.

First, we note that $\Gamma^{(2)}$ is a function of p^2, m, λ, μ and, of course, D. Let us being by requiring that

$$\frac{\partial}{\partial p^2}\, i\Gamma^{(2)}(p^2, m, \lambda, \mu, D)\Bigg|_{\substack{p^2=\mu^2\\ m^2=A\mu^2}} = 1\ , \tag{17}$$

where A is just some number. This clearly is suggested by Eq. (15) for $\Gamma_0^{(2)}$. Since

$$\Gamma^{(N)}(p_j, m, \lambda, \mu, D) = Z^{N/2}\,\Gamma_U^{(N)}(p_j, m_0, \lambda_0, D)\ , \tag{18}$$

where $\Gamma_U^{(N)}$ is the unrenormalized proper vertex computed with the bare parameters--this relation comes directly from Eq. (11), we learn

$$\frac{1}{Z} = \frac{\partial}{\partial p^2}\; i\Gamma_U^{(2)}(p^2, m_0, \lambda_0, D)\Bigg|_{\substack{p^2=\mu^2\\ m_0^2= Z^{-1}Z_m A\mu^2}}\ . \tag{19}$$

We now have one relation for Z and Z_m. Next we ask that

$$i\Gamma^{(2)}(p^2, m, \lambda, \mu, D)\Big|_{\substack{p^2=0 \\ m^2=A\mu^2}} = -A\mu^2 , \tag{20}$$

or

$$i\Gamma_U^{(2)}(p^2, m_0, \lambda_0, D)\Big|_{\substack{p^2=0 \\ m_0^2=Z^{-1}Z_m A\mu^2}} = -A\mu^2/Z , \tag{21}$$

which provides us with a second relation to determine Z and Z_m.

Now we wish to evaluate Z_λ. Mimicking Eq. (16) we require

$$\Gamma^{(4)}(p_1, \ldots , p_4, m, \lambda, \mu, D)\Big|_{\substack{p_i \cdot p_j = \frac{\mu^2}{3}(4\delta_{ij} - 1) \\ m^2 = A\mu^2}} = \frac{-i\lambda}{(2\pi)^D} \tag{22}$$

where we have chosen all momenta p_j to be incoming and selected an especially symmetric point to define λ. (See Fig. 3.) Z_λ now is given by

$$i(2\pi)^{D+1} \frac{\Gamma_U^{(4)}(p_1, \ldots , p_4, m_0, \lambda_0, D)}{\lambda_0}\Bigg|_{\substack{p_i \cdot p_j = \frac{\mu^2}{3}(4\delta_{ij} - 1) \\ m_0^2 = Z^{-1}Z_m A\mu^2}} = Z_\lambda^{-1} . \tag{23}$$

In practice one learns Z,, Z_m, and Z_λ by evaluating $\Gamma_U^{(2)}$ and $\Gamma_U^{(4)}$ to whatever order in perturbation theory in λ_0 one has the fortitude or desire to explore. Then using these normalization conditions one determines Z, Z_m, and Z_λ. From them in turn one evaluates m_0 and λ_0 as functions of m and λ as given by

$$\lambda_0 Z(m_0, \lambda_{0,\mu})^2 Z_\lambda(m_0, \lambda_{0,\mu})^{-1} = \lambda \tag{24}$$

and

$$m_0^2 Z(m_0, \lambda_{0,\mu}) \; Z_m(m_0, \lambda_{0,\mu})^{-1} = m^2 . \tag{25}$$

The renormalization prescription guarantees us that the $\Gamma^{(N)}$ computed by inserting $\lambda_0(m, \lambda, \mu)$ and $m_0(m, \lambda, \mu)$ on the right hand side of

$$\Gamma^{(N)}(p_j, m, \lambda, \mu, D) = Z(m_0, \lambda_{0,\mu})^{N/2}\, \Gamma_U^{(N)}(p_j, m_0, \lambda_0, D) \tag{26}$$

are finite for $D \leq 4$.

A word about the use of the quantity μ. We have introduced it here rather much out of the blue. Its value is unspecified and one suspects it is an artifice that cannot possibly play any role in determining any of the physics in the $\Gamma^{(N)}$: that, of course, is correct. What it has done for us is to provide a common mass scale for p^2 and m^2 at the normalization points which define the theory. The only reason we don't take $\mu = m$ and $A = 1$ straight off is that there is a lot to be learned by requiring that the physics of the $\Gamma^{(N)}$ be independent of μ--indeed, that's precisely where all the action is. Furthermore, it is frequently of enormous physical interest to study a theory with zero renormalized mass. That will correspond to choosing $A = 0$ with AZ_m fixed. A theory with $m = 0$ is full of interesting infrared divergences and normalizing such a theory at $p^2 = 0$ is fraught with danger.[5,14] In such a case a parameter such as μ is a necessity for defining the theory.

So far we have gone through an elaborate exercise to define the theory we are working with. We have not only given no results, but we have also bombarded the reader with seemingly endless definitions and continuous pious statements about renormalizability not a single one of which we proved. I encourage the anxious to have patience since in the words of the trustworthy, late Lyndon B. Johnson, "There is a light at the end of the tunnel."[15] We will indulge in a bit of good old dimensional analysis before we see it though. Ready?

We will indicate the dimensions of a quantity by the powers of momentum it carries, and we'll write [quantity] to mean dimensions. For example, for ordinary space-time,

$$[x] = q^{-1} \; . \tag{27}$$

The Lagrangian has dimensions

$$[\mathscr{L}(x)] = q^{D} \; , \tag{28}$$

to assure the action

$$A = \int d^{D}x \; \mathscr{L}(x) \tag{29}$$

has dimensions

$$[A] = q^{0} \; . \tag{30}$$

It is now straightforward to record the dimensions of the objects in our theory

$$[\phi(x)] = q^{(D-2)/2} \; , \tag{31}$$

and

$$[\lambda] = q^{4-D} \; . \tag{32}$$

The Z's are, of course, dimensionless while m and μ carry dimensions q^{+1}. The Green's functions and proper vertices in momentum space have

$$[G^{(N)}(p_j)] = q^{-N+\frac{D}{2}(2-N)} \; , \tag{33}$$

and

$$[\Gamma^{(N)}(p_j)] = q^{N+\frac{D}{2}(2-N)} \; . \tag{34}$$

We are going to want to do a bit of reasoning on the basis of the dimensions of $\Gamma^{(N)}$ so we will make this easier by trading in our coupling constant λ for the <u>dimensionless coupling</u>

$$g = \lambda\mu^{D-4} \; . \tag{35}$$

Since the Z's are dimensionless and are defined with all momenta and masses proportional to μ, they can depend only on g and things like D. The $\Gamma^{(N)}$ are now to be considered functions of p_j, m, g, μ, and D. Using (34) we learn

$$\Gamma^{(N)}(p_j, m, g, \mu, D) = \mu^{N+\frac{D}{2}(2-N)} \; \psi_N\left(\frac{p_j}{\mu}, \frac{m}{\mu}, g, D\right) \; , \tag{36}$$

where ψ_N is a dimensionless function of its dimensionless arguments. We may employ this to write

$$\Gamma^{(N)}(\xi p_j, m, g, \mu, D)$$

$$= \mu^{N+\frac{D}{2}(2-N)} \; \psi_N\left(\frac{p_j}{\mu/\xi}, \frac{m}{\mu}, g, D\right) \tag{37}$$

$$= \xi^{N+\frac{D}{2}(2-N)} \left(\frac{\mu}{\xi}\right)^{N+\frac{D}{2}(2-N)} \psi_N\left(\frac{p_j}{\mu/\xi}, \frac{m/\xi}{\mu/\xi}, g, D\right) \tag{38}$$

$$= \xi^{N+\frac{D}{2}(2-N)} \; \Gamma^{(N)}(p_j, \frac{m}{\xi}, g, \frac{\mu}{\xi}, D) \; . \tag{39}$$

This elementary result will prove enormously helpful.

After this brief digression we are ready to return to the main stream of our discourse. Namely, how can we guarantee that the physical results of our theory are independent of μ? Clearly we need a constraint equation on the $\Gamma^{(N)}$ which tells us how variations in μ and consequently variations in m and g via the induced variations in the Z's all compensate each other. Such an equation is provided by the observation that the <u>unrenormalized theory</u>

never heard of μ. It only knows about m_0, λ_0 And D and has no possible information about where we choose to define the renormalized parameters. This means

$$\mu \frac{\partial}{\partial\mu} \Gamma_U^{(N)}(p_j, m_0, \lambda_0, D)\Big|_{m_0,\lambda_0 \text{ fixed}} = 0 . \qquad (40)$$

The p_j and D are also fixed during the differentiation, but we'll not keep repeating that.

Remembering that

$$\Gamma^{(N)}(p_j, m, g, \mu, D) = Z(m_0, \lambda_0, \mu, D)^{N/2}\, \Gamma_U^{(N)}(p_j, m_0, \lambda_0, D), \qquad (41)$$

the chain rule informs us

$$\left[\mu \frac{\partial}{\partial\mu} + \beta(g) \frac{\partial}{\partial g} + \eta(g) m \frac{\partial}{\partial m} - \frac{N}{2}\gamma(g)\right] \Gamma^{(N)}(p_j, m, g, \mu, D) = 0 , \qquad (42)$$

with the definitions

$$\beta(g) = \mu \frac{\partial}{\partial\mu} g\Big|_{m_0,\lambda_0 \text{ fixed}} , \qquad (43)$$

$$m\eta(g) = \mu \frac{\partial}{\partial\mu} m\Big|_{m_0,\lambda_0 \text{ fixed}} , \qquad (44)$$

and

$$\gamma(g) = \mu \frac{\partial}{\partial\mu} \log Z\Big|_{m_0,\lambda_0 \text{ fixed}} .$$

This equation is known as the renormalization group equation. (Yes, I am aware that there hasn't been any group activity until this. This little bit of history will be filled in later.[6]) It holds for any value of the momenta p_j. In particular it holds for $\Gamma^{(N)}(\xi p_j, m, g, \mu, D)$. We may now use our dimensional analysis above to change from differentiation with respect to the normalization point μ to differentiation with respect to ξ, the scale of the momenta. Namely, noting that

$$\xi \frac{\partial}{\partial\xi} \Gamma^{(N)}(\xi p_j, m, g, \mu, D)$$

$$= \left\{N + \frac{D}{2}(2 - N) - m\frac{\partial}{\partial m} - \mu \frac{\partial}{\partial\mu}\right\} \Gamma^{(N)}(\xi p_j, m, g, \mu, D) , \qquad (46)$$

using Eq. (39), we write

$$\left\{\xi \frac{\partial}{\partial\xi} - \beta(g)\frac{\partial}{\partial g} + (1 - \eta(g))\, m \frac{\partial}{\partial m} + \frac{N}{2}\gamma(g) - [N + \frac{D}{2}(2 - N)]\right\} \Gamma^{(N)}(\xi p_j, m, g, \mu,$$

$$= 0 \qquad (47)$$

This equation tells us how variations in the momenta of a vertex function must be correlated with variations in the dimensionless renormalized coupling g and the renormalized mass parameter m so that the physical content of the theory is independent of where we choose to define it.

We solve such an equation in the following manner.[7,9] Define a variable $t = \log \xi$ and a two vector $\vec{v}(g) = (-\beta(g), 1 - \eta(g))$. Our equation is

$$\left(\frac{\partial}{\partial t} + \vec{v}(g)\cdot\vec{\nabla}\right) \Gamma^{(N)}(e^t p_j, m, g, \mu, D) = D_N(g)\, \Gamma^{(N)}(e^t p_j, m, g, \mu, D) , \qquad (48)$$

where

$$\vec{\nabla} = \left(\frac{\partial}{\partial g}, m\frac{\partial}{\partial m}\right) , \qquad (49)$$

and

$$D_N(g) = N + \frac{D}{2}(2 - N) - \frac{N}{2}\gamma(g) . \qquad (50)$$

If we introduce some auxiliary quantities $\tilde{g}(t)$ and $\tilde{m}(t)$ which satisfy

$$\frac{d\tilde{g}(t)}{dt} = -\beta(\tilde{g}(t)) , \qquad (51)$$

and

$$\frac{1}{\tilde{m}(t)} \frac{d\tilde{m}(t)}{dt} = 1 - \eta(\tilde{g}(t)) \ , \tag{52}$$

then we may express Eq. (48) as

$$\left[\frac{d}{dt} - D_N(\tilde{g}(t))\right]\Gamma^{(N)}(e^t p_j, \tilde{m}(t), \tilde{g}(t), \mu, D) = 0 \ , \tag{53}$$

whose solution is

$$\Gamma^{(N)}(e^t p_j, \tilde{m}(t), \tilde{g}(t), \mu, D)$$
$$= \Gamma^{(N)}(p_j, m, g, \mu, D) \exp \int_0^t dt' \, D_N(\tilde{g}(t')) \ , \tag{54}$$

when we impose the boundary conditions on $\tilde{g}(t)$ and $\tilde{m}(t)$:

$$\tilde{g}(t = 0) = g \tag{55}$$

$$\tilde{m}(t = 0) = m \ . \tag{56}$$

A significant feature of the equations for $\tilde{g}$ and $\tilde{m}$ is that the right hand side does not depend explicitly on t. Any any "time t" the value of $\tilde{g}(t)$ will depend on the value $\tilde{g}(t_1)$ where we pick the boundary conditions and on the <u>time difference</u> $t - t_1$. Consider now three times: $0, t_1 < t_2$ (Fig. 4). If we determine $\tilde{g}(t_2)$ by giving the boundary condition at $t = 0$, it will be

$$\tilde{g}(t_2) = \tilde{g}(\tilde{g}(t = 0) = g, t_2 - 0) \ . \tag{57}$$

But if we set our boundary conditions at t_1 and evaluate $\tilde{g}(t_2)$ by integrating up to t_2 from t_1, we'll find

$$\tilde{g}(t_2) = \tilde{g}(\tilde{g}(t_1), t_2 - t_1) \ . \tag{58}$$

These must be equal

$$\tilde{g}(g, t_2) = \tilde{g}(\tilde{g}(t_1), t_2 - t_1) \ . \tag{59}$$

In particular choose $t_2 = 0$ and $t_1 = -t$ in (59)

$$\tilde{g}(g, 0) = g = \tilde{g}(\tilde{g}(-t), t) \tag{60}$$

Our Eq. (54) may be written

$$\Gamma^{(N)}(e^t p_j, \tilde{m}(m, g, t), \tilde{g}(g, t), \mu, D)$$
$$= \Gamma^{(N)}(p_j, m, g, \mu, D) \exp \int_0^t dt' \, D_N(\tilde{g}(g, t')) \ . \tag{61}$$

Everywhere you see m in this equation, replace it by $\tilde{m}(-t)$ and everywhere g appears, replace it by $\tilde{g}(-t)$. But according to (60) $\tilde{g}(\tilde{g}(-t), t) = g$, and a similar formula tells us $\tilde{m}(\tilde{m}(-t), \tilde{g}(-t), t) = m$. Furthermore $\tilde{g}(\tilde{g}(-t), t')$ $= \tilde{g}(g, t' - t)$ by Eq. (59). The solution to our renormalization group equation for $\Gamma^{(N)}$ is then $(t = \log \xi)$

$$\Gamma^{(N)}(\xi p_j, m, g, \mu, D)$$
$$= \Gamma^{(N)}(p_j, \tilde{m}(-t), \tilde{g}(-t), \mu, D) \exp \int_{-t}^0 dt' \, D_N(\tilde{g}(t')) \tag{62}$$

where $\tilde{m}(t)$ and $\tilde{g}(t)$ satisfy the auxiliary equations (51) and (52) with the boundary conditions $\tilde{m}(0) = m$, $\tilde{g}(0) = g$.

This result is the <u>key result of the renormalization group</u>. It tells us how the renormalized proper vertex $\Gamma^{(N)}$ varies in momentum space ($\xi = e^t$ varying) in terms of an <u>effective mass parameter</u> $\tilde{m}(t)$ and an <u>effective coupling constant</u> $\tilde{g}(t)$. Let us imagine that for some range of $t = \log \xi$ the solution to Eq. (51) for $\tilde{g}(t)$ is very small (Fig. 5). This means that in a certain range of momentum space one may reliably evaluate $\Gamma^{(N)}(\xi p_j)$ by evaluating $\Gamma^{(N)}(p_j)$ as a perturbation expansion in $\tilde{g} \ll 1$! This is really a remarkable result; namely, in certain regions of momentum space one may evaluate the $\Gamma^{(N)}$ as a perturbation series in an effective coupling no matter how large the renormalized coupling g defined by the renormalization procedure.

Unless there is some reason to point to a special set of values for the $p_i \cdot p_j$ in $\Gamma^{(N)}$, we may expect that it is only in the extreme cases where $\xi \to \infty$, ultraviolet (UV) limit, or $\xi \to 0$, infrared (IR) limit, that $\tilde{g}$ has a chance to be small. It is the UV limit that will be very important for the gauge theories in the next lecture, and it is the IR limit that will prove to be crucial for Reggeon field theories in the lecture after that.

The practical use of the renormalization group equation hinges on our ability to solve the, in general, non-linear equation

$$\frac{d\tilde{g}(t)}{dt} = -\beta(\tilde{g}(t)) .$$

First of all we don't know $\beta(g)$ and even if we did, we might not be better off. In fact in order to know the full $\beta(g)$ we must have already solved the full field theory. In that instance this whole renormalization group story would be an unbelievably dull check on our solution. The best that anybody knows how to do (as of this writing) is (a) evaluate $\beta(g)$ in perturbation theory around $g = 0$, (b) solve the equation for $\tilde{g}(t)$ and look for regimes of t where $\tilde{g}$ is very small, (c) argue, with some force actually, that for such values of t we know $\beta(\tilde{g}(t))$ very accurately from our original perturbative expression so we have achieved a self-consistent solution to the problem.

Before we delve into the results of such calculations, let's examine some of the properties of our equation for $\tilde{g}$. The important item to concentrate on are the zeroes of $\beta(g)$:[6] If $\beta(g)$ has a zero at $g = g_1$, say, then as $\tilde{g}(t)$ gets to the neighborhood of g_1, $d\tilde{g}/dt$ will go to zero and $\tilde{g}$ will remain in that neighborhood.

Let's look at a simple zero first and approximate $\beta(g)$ in the neighborhood of g_1 by

$$\beta(g) = \beta_1(g - g_1) . \tag{63}$$

The quantity entering the solution to the renormalization group equation is $\tilde{g}(-t)$, which is

$$\tilde{g}(-t) = g_1 + (g - g_1)\, e^{\beta_1 t} \tag{64}$$

for our example. If $\beta_1 > 0$ (Fig. 6), then as $t \to -\infty$, namely the IR limit, $\tilde{g}(-t) \to g_1$. If $\beta_1 < 0$, (Fig. 7), then as $t \to \infty$, namely, the UV limit, $\tilde{g}(-t) \to g_1$. This is actually a very general feature: the UV limit is governed by simple zeroes of $\beta(g)$ where $\beta' < 0$, and the IR limit is governed by simple zeroes of $\beta(g)$ where $\beta' > 0$. If the position of the zero at g_1 is such that g_1 is small, then we may use perturbation theory to evaluate the UV or IR limits of the field theory. If g_1 is not small, then in the neighborhood of

$$t = -\frac{1}{\beta_1}\log\left(1 - \frac{g}{g_1}\right) \tag{65}$$

one may use perturbation theory. This last remark is probably a useless one; because unless we know g, it is very doubtful we can pick out the regime of t where $\tilde{g} \approx 0$.

We now know what many theorists are doing late at night. If they are interested in UV behavior of field theory, they are filling their notebooks with $\beta(g)$'s which have zeroes with a negative slope for a small g_1. If they are concerned about the IR behavior of the theory, they are casting about for $\beta(g)$'s which have zeroes with a positive slope for a small g_1. The best "small g_1" is $g_1 = 0$. Indeed, this value is so popular that a theory with

$g_1 = 0$ and $\beta'(0) < 0$ is called UV free, and a theory with $g_1 = 0$ and $\beta'(0) > 0$ is called IR free. No name has been given, yet, to theories with g_1 small but not zero. To fill this gap I will refer to such theories as possessing UV or IR liberty to contrast it with the UV or IR freedom of $g_1 = 0$.

It is worthwhile to study one more simple example in which $\beta(g)$ has a double zero at g_1

$$\beta(g) = \beta_1(g - g_1)^2 . \tag{66}$$

Now $\tilde{g}(-t)$ is

$$\tilde{g}(-t) = g_1 + \frac{g - g_1}{[1 - \beta_1(g - g_1)t]} \tag{67}$$

If $\beta_1(g - g_1) > 0$, then for $t \to -\infty$, the IR limit, $\tilde{g}(-t) \to g_1$, but this time only as a power of t. When $\beta_1(g - g_1) < 0$, then in the UV limit $t \to \infty$, $\tilde{g}(-t) \to g_1$. It is necessary in this case to give both the sign of the coefficient β_1 and the sign of $g - g_1$ in order to determine the IR or UV behavior of the field theory.

We will conclude this already long lecture by showing how the renormalization group equations allow one to go beyond perturbation theory even though we are only able to learn β, η, and γ in perturbation theory. We make a little departure here from the logical development carried out for so long in a ϕ^4 theory and lean on the results from theories with a cubic coupling (ϕ^3 or Yukawa). In such theories each of the Z's has the form,

$$Z^{-1} = 1 + O(\lambda_0^2) \tag{68}$$

so the renormalization group functions are in this order

$$\eta(x) = ax^2 , \tag{69}$$

$$\gamma(x) = cx^2 , \tag{70}$$

and

$$\beta(x) = bx(g_1^2 - x^2) , \tag{71}$$

where the linear term in $\beta(x)$ arises from the μ needed to take λ to g. If the λ, g relation is

$$g = \mu^d \lambda , \tag{72}$$

then

$$d = bg_1^2 , \tag{73}$$

as one can see immediately from Eq. (43). Now look at the equations for β and γ

$$\beta(g) = \mu \frac{\partial}{\partial\mu} g \Big|_{m_0,\lambda_0 \text{ fixed}} \tag{74}$$

and

$$\gamma(g) = \mu \frac{\partial}{\partial\mu} \log Z \Big|_{m_0,\lambda_0 \text{ fixed}} . \tag{75}$$

These together give us an expression for $Z(g)$

$$Z(g) = \exp \int_0^g dx \frac{\gamma(x)}{\beta(x)} , \tag{76}$$

$$= \left(1 - \frac{g^2}{g_1^2}\right)^{-c/2b} \tag{77}$$

using the expressions for β and γ determined in perturbation theory. This statement for Z is definitely an improvement over the lowest order perturbation theory result (68). Similarly one can improve Z_m and Z_λ

$$Z_\lambda(g) = Z(g)^2 \left(1 - \frac{g^2}{g_1^2}\right)^{-1/2} \tag{78}$$

and

$$Z_m(g) = Z(g)\left(1 - \frac{g^2}{g_1^2}\right)^{a/b} . \qquad (79)$$

For the $\Gamma^{(N)}$ we don't find such neat closed results, but instead we find constraints on the functional forms. To see this let's take the very special case where $g = g_1$. (g_1 need not be small.) That is the renormalized coupling is exactly at the zero of $\beta(g)$. In that instance

$$\tilde{g}(-t) = g_1 \qquad (80)$$

for all t, and

$$\tilde{m}(-t) = m\, e^{t(\eta(g_1)-1)} = m\xi^{\eta(g_1)-1} . \qquad (81)$$

The solution to the renormalization group equation becomes

$$\Gamma^{(N)}(\xi p_j, m, g_1, \mu, D)$$
$$= \xi^{N+\frac{D}{2}(2-N)-\frac{N}{2}\gamma(g_1)}\, \Gamma^{(N)}(p_j, m\xi^{\eta(g_1)-1}, g_1, \mu, D) . \qquad (82)$$

The power of ξ on the right-hand side here is the ordinary dimension of $\Gamma^{(N)}$; namely, $N + \frac{D}{2}(2-N)$ plus an amount proportional to $\gamma(g_1)$. This "extra" amount is called the anomalous dimension. Since $\gamma(0) = 0$, it arises because of the interaction. Now we use ordinary dimensional analysis as given in Eq. (36) to express our result in terms of ψ_N

$$\psi_N\left(\frac{\xi p_j}{\mu}, \frac{m}{\mu}, g_1, D\right) = \xi^{N+\frac{D}{2}(2-N)-\frac{N}{2}\gamma(g_1)}\, \psi_N\left(\frac{p_j}{\mu}, \frac{m\xi^{\eta(g_1)-1}}{\mu}, g_1, D\right) . \qquad (83)$$

How can a function of ξp_j, on the left be compatible with the ξ dependence on the right-hand side of this equation?

Well, let's look at it this way. Suppose we have a function $f(Z_1,Z_2)$ which behaves as

$$f(\xi Z_1, Z_2) = \xi^H f(Z_1, Z_2\xi^B) , \qquad (84)$$

for any ξ. In particular suppose $\xi = Z_1^{-1}$, then

$$f(1, Z_2) = Z_1^{-H} f(Z_1, Z_2Z_1^{-B}) . \qquad (85)$$

Now call

$$y_1 = Z_1 , \qquad (86)$$

$$y_2 = Z_2Z_1^{-B} \qquad (87)$$

or

$$Z_2 = y_2y_1^B , \qquad (88)$$

then (85) is telling us

$$f(y_1, y_2) = y_1^H f(1, y_2y_1^B) \qquad (89)$$

$$= y_1^H h(y_2y_1^B) , \qquad (90)$$

that is; the form of a function of two variables is restricted by the scaling law in (84).

For our function ψ_N we may read off

$$\psi_N\left(\frac{p_j}{\mu}, \frac{m}{\mu}, g_1, D\right)$$
$$= \left(\frac{p}{\mu}\right)^{N+\frac{D}{2}(2-N)-\frac{N}{2}\gamma(g_1)} \phi_N\left(\frac{p_j}{p}, \left(\frac{m}{\mu}\right)\left(\frac{p_i\cdot p_j}{\mu^2}\right)^{(-1+\eta(g_1))/2}, g_1, D\right) \qquad (91)$$

where p is some conveniently chosen momentum. For example, choose half of the total number of momenta and let

$$p^2 = \left(\sum_{j=1}^{N/2} p_j\right)^2 . \qquad (92)$$

These scaling laws are not true order by order in perturbation theory. Instead all sorts of logarithms are found lurking around. Those logarithms come from the expansion of (91) for small g_1. What the renormalization group equation has done for us is to reorganize all those logarithms in a masterful way to provide the lovely functional forms in (91). Just how grateful we ought to be for this will depend on what use we can make of this splendor.

This completes the discussion of the renormalization group equations and their solution. There are several small items which I would like to address before we leave this subject. Mostly they are technical, historical or some linear combination. The reader anxious to see why we have done all this stuff ought to pass on to the next section.

1. There is the question of the group. We have normalized our vertex functions at a point μ and thereby defined two quantities $m(\mu)$ and $\lambda(\mu)$. Suppose we had chosen to normalize at another point ν and parametrized the $\Gamma^{(N)}$ by $m(\nu)$ and $\lambda(\nu)$. What is the relation between these two sets of $\Gamma^{(N)}$? Well, they must be related by a finite rescaling of the field

$$\phi(x,\nu) = z^{-1/2}(\nu,\mu)\, \phi(x,\mu) , \qquad (93)$$

where $\phi(x,\mu)$ is the renormalized field we used above when we normalized at μ, and $\phi(x,\nu)$ is the field normalized at ν. With this rescaling of the fields the $\Gamma^{(N)}$ are related by

$$\Gamma^{(N)}(p_j, m(\nu), \lambda(\nu), \nu, D) = z^{N/2}(\nu,\mu)\, \Gamma^{(N)}(p_j, m(\mu), \lambda(\mu), \mu, D) . \qquad (94)$$

Similarly there is a rescaling of the parameters m and λ

$$m(\nu)^2 = z(\nu,\mu)\, z_m^{-1}(\nu,\mu)\, m(\mu)^2 \qquad (95)$$

and

$$\lambda(\nu) = z(\nu,\mu)^2\, z_\lambda(\nu,\mu)^{-1}\, \lambda(\mu) , \qquad (96)$$

where z, z_m, and z_λ are determined as we were able to determine Z, Z_m, and Z_λ. The z's are finite.

If we did rescale again, this time at a point κ, then the product of the rescaling transformations $\mu \to \nu \to \kappa$ must equal the full $\mu \to \kappa$ transformation. We thus have a very non-linear realization of the multiplicative group of real numbers. The differential group equation gotten by considering infinitesimal transformations is none other than our good old renormalization group equation (42).[16]

2. What is special about $D = 4$? True, it is the real number of dimensions of space-time as we know it. But in our considerations above it is the first point where our Feynman integrals for $\Gamma^{(4)}$ become divergent and where the linear term in $\beta(g)$ vanishes. It's significance in the present context is that at $D = 4$ the coupling constant λ becomes dimensionless and the ϕ^4 theory satisfies a naive scaling law.[17] If we had considered a $\lambda_3\phi^3$ theory instead of the ϕ^4 theory, we would have found $D = 6$ singled out instead. This observation will creep into several later remarks.

3. What happens when we have two (or more) coupling constants,[6] call their dimensionless counterparts g and h? Then we have characteristic equations for $\tilde{g}(t)$ and $\tilde{h}(t)$ which are coupled

$$\frac{d\tilde{g}(t)}{dt} = -\beta_g(\tilde{g}(t), \tilde{h}(t)) , \qquad (97)$$

$$\frac{d\tilde{h}(t)}{dt} = -\beta_h(\tilde{g}(t), \tilde{h}(t)) . \qquad (98)$$

The analysis of these coupled equations is somewhat more complicated than our simpler case for the ϕ^4 theory. Not only can one have fixed points g_1 and

h_1, like g_1 above, to which $\tilde{g}$ and $\tilde{h}$ retreat for $t \to \pm\infty$, but also there is the possibility of periodic limiting solutions where $\tilde{g}$ and $\tilde{h}$ go to some closed curve in the $\tilde{g}, \tilde{h}$ plane. These limit cycles and other kinds of solution have not been much discussed or studied in the physics literature but I refer you to the mathematical texts for the catagories of solutions.[18]

"Freedom's just another word for nothin' left to lose.
Nothin', it don't mean nothin', honey, if it ain't free "
Janis Joplin, "Me and Bobby McGee"

GAUGE THEORIES AND STRONG INTERACTIONS

In this lecture we will begin with a review of the ideas of local gauge fields, mention how spontaneous symmetry breaking can provide masses to the gauge vector bosons and proceed on through ultraviolet freedom to a little hadronic model building. Experts in this subject will surely be disappointed at almost every stage with the cavalier treatment most deep ideas receive. I recommend, both to them and the reader, Reference 7 where most of these harder issues are squarely faced.

The importance of gauge theories for the strong interactions is three-fold (at least): (1) if the fields fundamental to hadronic physics are to couple into a renormalizable theory of weak and electromagnetic interactions, then the whole set of interactions will remain renormalizable only if the hadronic physics respects the gauge principle too. It can do that in a trivial or an interesting fashion. (2) If weak and electromagnetic processes are described by gauge theories, then it is certainly unnatural not to expect hadronic physics to do the same. (3) The phenomenon of Bjorken scaling (exact or approximate) means that at small distances hadronic physics behaves nearly as a free field theory. This, in a word, is ultraviolet freedom in operation. Only gauge theories with non-Abelian gauge groups appear to possess this marvelous feature.

The idea of a gauge theory is familiar to us all from childhood:[19] quantum electrodynamics is such a theory. Let's recall that by thinking about matter fields $\psi_a(x)$, where a is some convenient label, coupled to the electromagnetic field $A_\sigma(x)$. If the matter carries charge Q_a, then the Lagrangian density

$$\mathscr{L}(x) = -\frac{1}{4} F_{\sigma\lambda}(x)^2 + \mathscr{L}_M(\psi_a(x), (\partial_\sigma + iQ_a H_\sigma(x))\,\psi_a(x)) \,, \qquad (99)$$

is invariant under the space-time dependent gauge transformation

$$\psi_a(x) \longrightarrow e^{iQ_a\Lambda(x)}\,\psi_a(x) \qquad (100)$$

and

$$H_\sigma(x) \longrightarrow A_\sigma(x) - \partial_\sigma\,\Lambda(x) \,, \qquad (101)$$

if it is invariant under (100) with Λ a constant.

The field strength

$$F_{\lambda\sigma}(x) = \partial_\lambda\, A_\sigma(x) - \partial_\sigma\, A_\lambda(x) \,, \qquad (102)$$

is the standard gauge invariant curl of $A_\sigma(x)$. The important point about this Lagrangian, beyond its well established relevance to physics, is that in the absence of the <u>vector field</u> $A_\sigma(x)$ the matter alone could not sustain an invariance under <u>local gauge transformations</u>.

Two decades ago Yang and Mills[20] asked and answered the question how one might generalize the idea of local gauge invariance for a field interacting via charge to theories with isospin; several years later the generalization of this to more elaborate internal symmetries was discussed by Gell-Mann and Glashow.[21]

Let's being with isospin and consider just an isovector field $\pi_a(x)$ $(a = 1, 2, 3)$. Under isospin transformations generated by the operators I_a we have

$$[I_a, \pi_b(x)] = i\, \epsilon_{abc} \pi_c(x) \ . \tag{103}$$

We want to construct a Lagrangian involving $\pi_a(x)$ which is invariant under the local infinitesimal gauge transformation

$$\pi_a(x) \longrightarrow \pi_a(x) + g\, \epsilon_{abc}\, \Lambda_b(x)\, \pi_c(x) \ . \tag{104}$$

That is, we make an independent isospin rotation at every point in space. As in the case of electromagnetism there is a change suffered by $\partial_\sigma \pi_a(x)$

$$\partial_\sigma \pi_a(x) \longrightarrow \partial_\sigma \pi_a(x) + g\, \epsilon_{abc} (\partial_\sigma \Lambda_b(x))\, \pi_c(x) + g\, \epsilon_{abc}\, \Lambda_b(x)\, \partial_\sigma \pi_c(x) \ , \tag{105}$$

which, because of the second term on the right, would forbid us to construct a gauge invariant theory unless it is canceled. To cure this we introduce three gauge vector bosons, one to cancel each of the $\partial_\sigma \Lambda_b(x)$ terms. Under the transformation characterized by $\Lambda_b(x)$, this field, $B_{a\sigma}(x)$, behaves as

$$B_{a\sigma}(x) \longrightarrow B_{a\sigma}(x) - \partial_\sigma \Lambda_a(x) + g\, \epsilon_{abc}\, \Lambda_b(x)\, B_{c\sigma}(x) \ . \tag{106}$$

When we replace $\partial_\sigma \pi_a(x)$ in any Lagrangian by the gauge covariant derivative

$$D_\sigma \pi_a(x) = \partial_\sigma \pi_a(x) + g\, \epsilon_{abc}\, B_{b\sigma}(x)\, \pi_c(x) \ , \tag{107}$$

then the resulting theory is invariant under the local gauge transformation.

We need a generalization of $F_{\sigma\lambda}(x)$ for the isospin carrying field $B_{a\sigma}(x)$, and here is where the fun begins. The appropriate quantity is

$$G_{a\lambda\sigma}(x) = \partial_\lambda B_{a\sigma}(x) - \partial_\sigma B_{a\lambda}(x) + g\, \epsilon_{abc}\, B_{b\sigma}(x)\, B_{c\lambda}(x) \ , \tag{108}$$

which behaves as

$$G_{a\lambda\sigma}(x) \longrightarrow G_{a\lambda\sigma}(x) + g\, \epsilon_{abc}\, \Lambda_b(x)\, G_{c\lambda\sigma}(x) \ , \tag{109}$$

under the gauge transformation. The most elementary gauge invariant boson field Lagrangian is

$$\mathscr{L}_B(x) = -\tfrac{1}{4}\, G_{a\lambda\sigma}(x)\, G_{a\lambda\sigma}(x) \ . \tag{110}$$

Now this is a non-linear relation among the fields $B_{a\sigma}(x)$ which is not unexpected: we required that $B_{a\sigma}(x)$ cancel the gauging effects on every object that carries isospin. Indeed it must interact with every such field, including, naturally enough, itself. The non-linear terms in $G_{a\lambda\sigma}(x)$ are just the expression of that.

If we add a mass term for the gauge bosons

$$-\frac{m^2}{2}\, B_{a\sigma}(x)\, B_{a\sigma}(x) \ ,$$

then the local gauge invariance is broken. Transformations under a constant gauge parameter Λ_b still leave

$$\mathscr{L} = \mathscr{L}_B + \mathscr{L}_0(\pi_a, D_\sigma \pi_a(x)) - \frac{m^2}{2}\, B_{a\sigma}(x)\, B_{a\sigma}(x) \tag{111}$$

invariant; that is, isospin is globally, but not locally an invariance. This is the reason gauge fields lay dormant for so long. If the gauge bosons have no mass, then the theory is physically unattractive because there is only one known massless vector boson: the photon. (I feel compelled to reveal that it is possible--an attractive possibility--that through interactions the gauge bosons could develop a mass. This is known as dynamical symmetry breaking and does transpose in the soluble case of two dimensional quantum electrodynamics.[22]) If one goes ahead and adds the bare mass term anyway two disasters occur, one logical, one computational: (1) the whole rationale for local gauge invariance goes by the wayside. Having struggled so elegantly to achieve it, should we now toss it aside? (2) With the mass term and the loss of local gauge invariance, we also lose the conservation of a local isospin current. When the current is not conserved, the theory becomes non-renormalizable. Faced with the inability to compute except in a theory which had no apparent connection with physics, the hearty turned to other matters.

That turned out to be a tactical error. The ideas that again opened up the hearts of man to gauge theories were these: (a) in the presence of spontaneous symmetry breaking (soon to be made explicit) the bosons could acquire a mass while (b) the theory retained its renormalizability and full invariance under local gauge transformations.[3,7]

The covariant derivative which involves the product of $B_{a\sigma}(x)$ and $\pi_a(x)$ leads to terms in $\mathscr{L}$ more or less like

$$-\frac{1}{2}\,(B_{a\sigma}(x)\;B_{a\sigma}(x))\;(\pi_b(x)\;\pi_b(x))\;. \tag{112}$$

If there were some reason why $\pi_b(x)$ could take a value

$$\pi_b(x) = v_b \tag{113}$$

constant over space, then it would appear as though $B_{a\sigma}(x)$ had developed a bare mass

$$m_B = \sqrt{\sum_b v_b v_b}\;. \tag{114}$$

Such a pleasant situation might arise if the π field were self-coupled in a way which preserved the local gauge invariance $\{\lambda(\pi_b(x)\;\pi_b(x))^2$ is fine$\}$, and in this self-potential oscillations occurred around $\pi_b(x) = v_b$, instead as we most often imagine around $\pi_b(x) = 0$. Indeed, suppose the π part of the Lagrangian is

$$\mathscr{L}_\pi = \frac{1}{2}\,D_\sigma\,\pi_a(x)\;D_\sigma\,\pi_a(x) - \frac{\mu_0^2}{2}\,\pi_a(x)\;\pi_a(x) - \frac{\lambda_0}{24}\,(\pi_a(x)\;\pi_a(x))^2 \tag{115}$$

$$= \mathscr{L}_\pi(\text{kinetic}) - V(\pi_a(x)\;\pi_a(x))\;. \tag{116}$$

The potential $V(y)$ (Fig. 8) for $\mu_0^2 > 0$ has its minimum at $y = 0$, and our usual notions of describing the theory in a perturbation series in λ_0 with the ground state $\pi_a(x) = 0$ are quite acceptable. If $\mu_0^2 < 0$--when $\lambda_0 \neq 0$ that does not imply space-like particles--then $V(y)$ has its *minima* at

$$y = \pm\sqrt{\frac{-6\mu_0^2}{\lambda_0}}\;. \tag{117}$$

The point $y = 0$ is an unstable position for the field. The ground state is then achieved by $\pi_a(x)$ choosing the value

$$(\pi_a(x))^2 = -\frac{6\mu_0^2}{\lambda_0} > 0, \tag{118}$$

which is precisely the desired happening. Translating the field to the non-symmetric ground state value of $\pi_a(x)$ is commonly referred to as spontaneous symmetry breaking. This is terrible nomenclature since the Lagrangian is still symmetric; the symmetry is hidden. The solutions to the field need not exhibit the symmetry of the Lagrangian--think of $\ell \neq 0$ levels of the hydrogen atom: the hamiltonian is rotationally invariant; the wave function is not. More to the point would be to label the situation we encounter here: shy symmetry. When $\mu_0^2 < 0$, the local gauge invariance of the whole Lagrangian is not broken and, this is the remarkable observation, the theory remains renormalizable. We are invited to further considerations of gauge theories.

A couple of technical points here: the fields which become shy should carry no space-time quantum numbers or the solutions to the field theory will exhibit non-invariance under parity, G-parity, or whatever. It is interesting to consider that the apparent breakdown of parity or CP may be due to such shyness,[23] but for hadron physics we must avoid this. Also, when the gauge bosons acquire mass they pick up an extra degree of polarization (massless vector particles have two degrees of freedom; massive vectors, three). This is purchased at the expense of one of the scalar fields disappearing from the problem; something has to depart since field translation doesn't increase the degrees of freedom of the theory. All this cleverness is exposed in Reference 7.

The generalization of gauge fields to other symmetries than isospin is now straightforward to state. We imagine that there are F matter fields $\psi_a(x)$ which are chosen so the Lagrangian is invariant under a group of G gauge transformations with <u>constant</u> Λ_j

$$\psi_a(x) \longrightarrow \sum_{b=1}^{F} (\exp i \sum_{j=1}^{G} \underset{\sim}{T}_j \Lambda_j)_{ab} \psi_b(x) , \tag{119}$$

where the $\underset{\sim}{T}_j$ are a set of G hermitean matrices in the F-dimensional space spanned by the ψ_a. They are taken to satisfy the commutation relations of some group

$$[T_j, T_k] = i f_{jk\ell} T_\ell , \tag{120}$$

where $f_{jk\ell}$ are the structure constants of the group. For convenience the gauge group with G generators will be taken to be simple for the moment and the $\psi_a(x)$, $a = 1, \ldots , F$ will be considered to transform under at most a finite direct product of irreducible representations of the gauge group. Our example above with isovectors has $a = 1, 2, 3$ and the isospin gauge group has $j = 1, 2, 3$.. Now having $\mathscr{L}_0(\psi_a(x), \partial_\sigma \psi_a(x))$ invariant under the transformation (119) we wish to enlarge this to an invariance under local transformations with $\Lambda_j(x)$ in (119).

To achieve this we add vector gauge fields $B_{j\sigma}(x)$ which undergo the gauge transformation

$$B_{j\sigma}(x) \longrightarrow B_{j\sigma}(x) - \frac{1}{g} \partial_\sigma \Lambda_j(x) + \sum_{k,\ell=1}^{G} f_{jk\ell} \Lambda_k(x) B_{\sigma\ell}(x) , \tag{121}$$

and we change $\partial_\sigma \psi_a(x)$ in $\mathscr{L}_0$ into the gauge covariant derivative

$$D_\sigma \psi_a(x) = \partial_\sigma \psi_a(x) + ig \sum_{j=1}^{G} \sum_{b=1}^{F} (\underset{\sim}{T}_j)_{ab} B_{j\sigma}(x) \psi_b(x) . \tag{122}$$

To the matter Lagrangian $\mathscr{L}_0(\psi_a(x), D_\sigma \psi_a(x))$ we add the B terms

$$\mathscr{L}_B(x) = - \frac{1}{4} \sum_{j=1}^{G} G_{j\lambda\sigma}(x) G_{j\lambda\sigma}(x) , \tag{123}$$

where

$$G_{j\lambda\sigma}(x) = \partial_\lambda B_{j\sigma}(x) - \partial_\sigma B_{j\lambda}(x) + g \sum_{k,\ell=1}^{G} f_{jk\ell} B_{k\sigma}(x) B_{\ell\lambda}(x) . \tag{124}$$

This field tensor transforms as

$$G_{j\lambda\sigma}(x) \longrightarrow G_{j\lambda\sigma}(x) + \sum_{k,\ell=1}^{G} f_{jk\ell} \Lambda_k(x) G_{\ell\lambda\sigma}(x) , \tag{125}$$

under the local gauge transformation.

The total Lagrange density

$$\mathscr{L}(x) = \mathscr{L}_0(\psi_a(x), D_\sigma \psi_a(x)) + \mathscr{L}_B(x) \tag{126}$$

describes F matter fields in interaction with G gauge vector bosons. These bosons are massless as the theory stands. If there is a shy symmetry hiding in $\mathscr{L}_0$, the bosons may acquire a bare mass by eating some of the fields in $\mathscr{L}_0$ with appropriate quantum numbers. If there are several pieces of the gauge group which form via a direct product the full gauge group, there is a separate coupling g for each element of the direct product.

The quantization of locally gauge invariant Lagrangians is not an easy task. The reader will recall (or hurry to the second volume of Bjorken and Drell[4] to remind him or her self), the care which one must employ to quantize even the simplest gauge theory: quantum electodynamics. I happily refer you once again to the lectures of Coleman[7] or for even more detail and care the review paper of Abers and B.W. Lee.[7]

We will turn to a specific example with which we will discuss much physics. Let the matter fields carry two internal indices: one will be an ordinary SU(N) index a which runs from one to three for SU(3) quarks, and also we will endow the field with an index α which describes the transformation under the gauge group which we take to be SU(M). Call the field $q_{a\alpha}(x)$. We will take a to run from one to four and $N = 4$; four quarks will be needed and explained later. We will take $M = 3$ and have an octet of vector gauge bosons. The index α will run from one to three. So the strong symmetry group is to be (see Table 1)

$$\mathscr{G}_{\text{Strong}} = SU(4)_{\substack{\text{Isospin}\\ \text{Hypercharge}\\ \text{Charm}}} \otimes SU(3)_{\substack{\text{Gauge}\\ \text{of Color}}} \quad . \tag{127}$$

I will motivate all of this indexing and name calling (charm, color and all that) later. Right now I ask your patience with this bad pedagogical device. The gauge invariant Lagrangian describing the situation we have set up is

$$\mathscr{L}(x) = i \sum_{\alpha,\beta=1}^{3} \sum_{a=1}^{4} \bar{q}_{a\alpha}(x)\, \gamma_\sigma \left[\partial_\sigma \delta_{\alpha\beta} + i \frac{g_0}{2} \sum_{j=1}^{8} (\lambda_j)_{\alpha\beta}\, B_{j\sigma}(x)\right] q_{a\beta}(x)$$

$$- \frac{1}{4} \sum_{j=1}^{8} G_{j\lambda\sigma}(x)\, G_{j\lambda\sigma}(x) - \sum_{\alpha,\beta=1}^{3} \sum_{a,b=1}^{4} \bar{q}_{a\alpha}(x)\, M_{a\alpha,b\beta}\, q_{b\beta}(x) \ , \tag{128}$$

where the last term is a mass matrix for the quark fields and the λ_j are the usual SU(3) matrices.[24]

What we want to do first is discuss the renormalization group structure of this theory. Our dimensional analysis of the first lecture reveals that in 4 space-time dimensions the coupling g is dimensionless. This means that our crucial function $\beta(g)$ has the power series expansion

$$\beta(g) = \beta_1 g^3 + \beta_2 g^5 + \cdots \ . \tag{129}$$

Suppose only the β_1 term is important, then we must solve the differential equation

$$\frac{d\tilde{g}(t)}{dt} = - \beta_1\, \tilde{g}(t)^3 \ . \tag{130}$$

Subject to the boundary condition $\tilde{g}(0) = g$, one finds

$$\tilde{g}(-t) = g(\ 1 - 2\beta_1 g^2 t)^{-1/2} \ , \tag{131}$$

and for an infrared limit we are interested in $t \to -\infty$, while for an ultraviolet limit we are concerned with $t \to +\infty$. <u>Everything rests on the sign of</u> β_1. And here's the good news, for the gauge theory defined in (128)[25]

$$\beta_1 = - \frac{25}{48\pi^2} \ . \tag{132}$$

Well, I hardly expect you to be turned on by the 25 and the $48\pi^2$, but I certainly trust the minus sign catches your notice. Because $\beta_1 < 0$, the effective coupling in (131) makes sense for the UV limit and

$$\tilde{g}(-t) \underset{t \to \infty}{\sim} \frac{1}{(-2\beta_1)^{1/2}\, t^{1/2}} \ , \tag{133}$$

that is, it goes to zero. <u>In the ultraviolet limit this theory is effectively a free field theory</u>.

This result is not limited to this particular gauge theory.[7,26] It occurs in a wide class of such non-Abelian gauge theories. It is important to remark, however, that it does not occur in electrodynamics or $\lambda\phi^4$ theory or any known renormalizable local field theory which does not involve non-Abelian ($f_{abc} \neq 0$) gauge fields. For all those theories at $D = 4$, $\beta_1 > 0$.[7]

If we recall the solution to our renormalization group equation for the renormalized proper vertex functions Γ_R, we note it reads

$$\Gamma_R(\xi p_j, m, g, \mu, D = 4)$$
$$= \Gamma_R(p_j, \tilde{m}(-\log\xi), \tilde{g}(-\log\xi), \mu, D = 4) \exp \int_{-\log\xi}^{0} \frac{d\xi'}{\xi'} D(\tilde{g}(\log\xi')), \tag{134}$$

dropping the N dependence and noting $t = \log\xi$. The result above for UV free theories

$$\tilde{g}(-\log\xi) \underset{\xi\to\infty}{\sim} \frac{1}{(-2\beta_1)^{1/2}(\log\xi)^{1/2}}, \tag{135}$$

tells us we may evaluate all proper vertices as a power series in $\tilde{g}(-\log\xi)$ as all momenta go to infinity! Also it says that the corrections to free field behavior are likely to be inverse powers of $\log p_i\cdot p_j/\mu^2$ only.

This is first of all a very uninteresting regime from a physical point of view since in no physical process do all momenta go off to infinity--external momenta stay on the mass shell $p_j^2 = m^2$. Second of all it is a trifle disappointing that the correction terms are only down by powers of logarithms. Corrections are, therefore, likely to be large at any present accelerator. Indeed, if the observed Bjorken scaling has any connection with underlying free fields, then its onset at such meagre energies as SLAC provides means the very slow approach to UV freedom possessed by non-Abelian gauge theories is really irrelevant to present day phenomena. By implication unfortunately we have no experimental grounds for conjecturing whether non-Abelian gauge theories having UV freedom are in fact being employed in physics. There is no satisfactory answer to this second matter which is known to me. However, theorists have been clever enough to skirt around the first. Here's how they do it.

In inelastic electron scattering

$$e(k) + P(p) \longrightarrow e(k') + \text{anything} \tag{136}$$

one measures two hadronic structure functions W_1 and W_2 in the double differential cross section

$$\frac{d^2\sigma(e + P \to e' + X)}{d\Omega'\, dE'}$$
$$= \frac{\alpha^2}{4E^2\, m_p \sin^4\frac{\theta}{2}} \left\{\cos^2\frac{\theta}{2}\, W_2(q^2,\nu) + 2\sin^2\frac{\theta}{2}\, W_1(q^2,\nu)\right\}, \tag{137}$$

where E and E' are the initial and final laboratory electron energies, θ is the lab scattering angle of the electrons, and

$$q^2 = (k' - k)^2 \tag{138}$$

$$\nu = q\cdot p/m_p = E - E' .$$

The structure functions are defined by

$$\frac{1}{2}\sum_{\substack{\text{Proton}\\ \text{Spin}}} \int d^4x\, e^{iq\cdot x} \langle P|[J_\lambda^{em}(x), J_\sigma^{em}(0)]|P\rangle$$
$$= \left(-g_{\lambda\sigma} + \frac{q_\lambda q_\sigma}{q^2}\right) W_1(q^2,\nu) + \left(p_\lambda - \frac{(p\cdot q)q_\lambda}{q^2}\right)\left(p_\sigma - \frac{(p\cdot q)q_\sigma}{q^2}\right) \frac{W_2(q^2,\nu)}{m_p^2}. \tag{140}$$

$(-q^2)^{1/2}$ is the mass of the virtual photon. As $q^2 \to -\infty$ with

$$\xi = \frac{-q^2}{2m_p \nu} \tag{141}$$

held fixed (this is the Bjorken limit), then the distance x on the left-hand side of Eq. (140) becomes light like $x^2 \to 0$.[27] In this case one may make an expansion of the time ordered product of the electromagnetic current operators[28]

$$T(J_\lambda(x)\ J_\sigma(0)) = \sum_{n=0}^{\infty} \tilde{C}^{(n)}(x^2)\ A_{\lambda\sigma\alpha_1\cdots\alpha_n}(0)\ x_{\alpha_1}\cdots x_{\alpha_n}$$

$$+ \text{ terms which contribute to } W_1\ , \tag{142}$$

where the $\tilde{C}^{(n)}(x^2)$ are c-<u>number</u> functions and the $A\ldots(0)$ are <u>local</u> operators. This device puts all the dependence on the proton variables into the matrix element of the operator A. The proton momenta stay on the mass shell while the limit $q^2 \to -\infty$, ξ fixed is taken. The importance of all this is that the $\tilde{C}^{(n)}(x^2)$ <u>satisfy renormalization group equations</u>[7,25] with the same $\beta(g)$ and no $\eta(g)$ and a different $\gamma(g)$ as the proper vertices of any theory describing the photon-proton interaction.

How can the $\tilde{C}^{(n)}(x^2)$ satisfy renormalization group equations? Consider the matrix element of Eq. (142) between proton states (dropping tensor indices)

$$\langle p|T(J(x)\ J(0))|p\rangle = \sum_n \tilde{C}^{(n)}(x^2)\ \langle p|A|p\rangle\ x^{(n)}\ .$$

If we apply the renormalization group differential operator

$$D = \mu\frac{\partial}{\partial\mu} + \beta(g)\frac{\partial}{\partial g} + m\eta(g)\frac{\partial}{\partial m}$$

to both sides and note

$$(D - \tilde{\gamma})\ \ \langle p|T(J(x)\ J(0))|p\rangle = 0$$

and

$$(D - \tilde{\gamma}_n)\ \langle p|A|p\rangle = 0\ ,$$

with some anomalous dimensions $\tilde{\gamma}$ and $\tilde{\gamma}_n$ since each matrix element is related to a Green's function of the underlying field theory, then

$$(D - \tilde{\gamma} + \tilde{\gamma}\ )\ \tilde{C}^{(n)}(x^2) = 0\ .$$

Furthermore, the Fourier transforms of the $\tilde{C}_n$ are related to integrals over W_2. More precisely, call

$$C^{(n)}(q^2) = (q^2)^{n+1}\frac{\partial^n}{\partial(q^2)^n}\int d^4x\ e^{iq\cdot x}\ \tilde{C}^{(n)}(x^2)\ , \tag{143}$$

then

$$\int_0^1 d\xi\ \xi^n\left\{\frac{\nu W_2(\nu,\ q^2)}{m_p^2}\right\} = C^{(n)}(q^2)\ . \tag{143}$$

In a free field theory each of the $C^{(n)}(q^2)$ can be computed and each is a constant, c_n, for large $-q^2$. What is the implication of this; namely,

$$\lim_{-q^2\to\infty}\int_0^1 d\xi\ \xi^n\left\{\frac{\nu W_2(\xi,q^2)}{m_p^2}\right\} = c_n \quad ? \tag{144}$$

Inverting the Laplace transform we find

$$\lim_{-q^2\to\infty}\frac{\nu W_2(\xi,q^2)}{m_p^2} = \int_{\delta-i\infty}^{\delta+i\infty}\frac{dn}{2\pi i}\ \xi^{-(n+1)}\ c_n \tag{145}$$

$$= F_2(\xi)\ , \tag{146}$$

that is, the theory exhibits Bjorken scaling.[29] This elementary remark is at the heart of the parton model, and from dimensional analysis alone it is almost obvious because in a free field theory all quantities retain their ordinary engineering dimensions. Since $\nu W_2(\xi, q^2)/m_p^2$ is dimensionless, it can only depend on ξ, a dimensionless variable, in the limit $q^2 \to -\infty$.

What happens in our UV free gauge field theory? Well, each of the $C^{(n)}$ is a dimensionless function of q^2, g--the dimensionless renormalized coupling, and μ--the normalization mass. It cannot depend on, say, the proton mass since that's all buried in the matrix element of the coefficient operator $A\ldots(0)$. So $C^{(n)}$ is

$$C^{(n)}(-q^2/\mu^2, g) . \tag{147}$$

Each $C^{(n)}$ obeys a renormalization group equation similar to (47) above

$$\left[\xi \frac{\partial}{\partial \xi} - \beta(g) \frac{\partial}{\partial g} + \gamma_n(g)\right] C^{(n)}(\xi, g) = 0 \tag{148}$$

with $\xi^2 = -q^2/\mu^2$. The solution to this is

$$C^{(n)}\left(-\frac{q^2}{\mu^2}, g\right) = C^{(n)}(0, \tilde{g}(-t)) \exp \int_{-t}^{0} dt' \, \gamma_n(\tilde{g}(t')) , \tag{149}$$

where

$$t = \frac{1}{2} \log \frac{-q^2}{\mu^2} . \tag{150}$$

In perturbation theory each γ is quadratic in g

$$\gamma_n(g) = a_n g^2 + \cdots \tag{151}$$

and $a_n \geq 0$. Using our expression for $\tilde{g}(t)$ from Eq. (131) we find

$$C^{(n)}\left(\frac{-q^2}{\mu^2}, g\right) = C^{(n)}\left(0, \frac{g}{(1 - \beta_1 g^2 \log(-q^2/\mu^2))}\right) \left(1 + (-\beta_1 g^2) \log\left(\frac{-q^2}{\mu^2}\right)\right)^{-a_n/2\beta_1} . \tag{152}$$

Since $\beta_1 < 0$ and since $C^{(n)}$ is a constant for a free field theory, for large $-q^2$ we have

$$C^{(n)}\left(\frac{-q^2}{\mu^2}, g\right) \underset{-q^2 \to \infty}{\sim} \frac{C_n}{\left(-\beta_1 g^2 \log \frac{-q^2}{\mu^2}\right)^{-a_n/2\beta_1}} , \tag{153}$$

so each moment with $a_n > 0$ of $\nu W_2(\xi, q^2)$ slowly goes to zero as q^2 becomes large.

There is one contribution to the light cone expansion that gives a $n = 0$ term with $a_0 = 0$, indeed $\gamma_0 = 0$. This comes from the presence of a conserved energy-momentum tensor in any quantum field theory. This means that the zero moment of νW_2 remains constant, although all others eventually vanish. The area under the curve for $F_2(\xi)$, thus remains constant while each moment eventually vanishes. Although it occurs very slowly, the eventual configuration for $F_2(\xi)$ is almost $A\delta(\xi)$ where A is the constant area under the curve. In any case, $F_2(\xi)$ ought to become slowly more and more peaked near $\xi = 0$ (Fig. 9).

Applying this same clever reasoning to the annihilation cross section $e^+e^- \to$ hadrons yields for $\sigma_T(s)$, $s = (p_{e^+} + p_{e^-})^2$,

$$\sigma_T(s) = \frac{\text{const}}{s} \left(1 + \frac{b}{\log s} + \cdots \right) \tag{154}$$

and $b > 0$.[30]

This very elegant prediction is at gross variance with the observed annihilation data taken here at SPEAR.[31] It may well be that this kills theories with UV freedom, but it is cautious, certainly not bold, to hold one's judgment for the moment. If it is true that the SPEAR results maintain themselves at higher s, then UV free gauge theories are either not yet formulated properly or may just not be the mechanism particles picked on.

It is now our task to return to the gauge theory and explain why we chose four quarks and an octet of SU(3) gauge vector mesons. Ultraviolet freedom is certainly not the reason. Let's begin with the four quarks.

Nothing in purely strong interaction physics compells us to enlarge the number of quarks from the classical three. However, when one wishes to discuss the semi-leptonic decays of hadrons there are some severe restrictions that are placed on the quark content of hadrons.[32] If we wish to add leptons to the quark and gluon picture we have outlined above, then we must do so by means of some gauge theory so that the net theory remain renormalizable. The most economical way to do this is to organize the three observed electron-type leptons: right-handed electron, left-handed electron, left-handed neutrino into a singlet

$$R = \frac{1}{2}(1 + \gamma_5)\psi_e \tag{155}$$

and a doublet

$$L = \frac{1}{2}(1 - \gamma_5)\begin{pmatrix} \psi_{\nu_e} \\ \psi_e \end{pmatrix} \tag{156}$$

transforming as such under an SU(2) gauge group.[33] The electromagnetic current can be incorporated into this scheme by noting

$$\bar{\psi}_e\gamma_\sigma\psi_e = -\frac{1}{2}\bar{L}\gamma_\sigma\tau_3 L + \bar{R}\gamma_\sigma R + \frac{1}{2}\bar{L}\gamma_\sigma L . \tag{157}$$

The first part of this is the neutral component of the triplet of currents coupling to the three SU(2) gauge bosons. The SU(2) algebra formed by the equal time commutators of the currents

$$J_{a\mu}(x) = \bar{L}(x)\,\gamma_\mu\,\frac{\tau_a}{2}\,L(x) \tag{158}$$

guarantees the renormalizability of the theory. The full weak gauge symmetry of the theory is

$$\mathscr{G}_W = SU(2) \otimes U(1) , \tag{159}$$

where the extra, Abelian, U(1) is associated with the neutral current

$$K_\mu(x) = \bar{R}(x)\,\gamma_\mu\,R(x) + \frac{1}{2}\bar{L}(x)\,\gamma_\mu\,L(x) , \tag{160}$$

which enters because the electromagnetic current is included, and its associated gauge vector boson. This model is known as the Weinberg-Salam model; it unites weak and electromagnetic interactions in a most pleasant and elegant fashion. There are two coupling constants in the model, one for the SU(2) part of $\mathscr{G}_W$ and another for the U(1) part.

We may write the Lagrangian density for this model as

$$\begin{aligned}\mathscr{L}(x) &= \bar{L}\gamma_\sigma\left(i\partial_\sigma + g\sum_{i=1}^{3}\frac{\tau_i}{2}B_{i\sigma} + \frac{g'}{2}D_\sigma\right)L + \bar{R}\gamma_\sigma(i\partial_\sigma + g'D_\sigma)R \\ &\quad - \frac{1}{4}\sum_{i=1}^{3}G_{i\lambda\sigma}G_{i\lambda\sigma} - \frac{1}{4}H_{\lambda\sigma}H_{\lambda\sigma} ,\end{aligned} \tag{161}$$

where the SU(2) gauge bosons $B_{i\sigma}$ couple with g and the U(1) gauge bosons D_σ couple with g'. $G_{i\lambda\sigma}$ and $H_{\lambda\sigma}$ are the appropriate SU(2) and U(1) curls. It is instructive to reorganize the interaction terms in $\mathscr{L}$ to display the electromagnetic current

$$\mathscr{L}_I(x) = \frac{gg'}{\sqrt{g^2+g'^2}} (\bar\psi_e \gamma_\sigma \psi_e) A_\sigma - \frac{g}{\sqrt{2}} \left[\bar\psi_{\nu e} \gamma_\sigma \frac{(1-\gamma_5)}{2} \psi_e W_{+\sigma} + \text{hermitean conjugate} \right]$$

$$- \frac{\sqrt{g^2+g'^2}}{2} W_{3\sigma} \left[\bar\psi_{\nu e} \gamma_\sigma \psi_{\nu e} - \bar\psi_e \gamma_\sigma \frac{(1-\gamma_5)}{2} \psi_e + \frac{2g'^2}{g^2+g'^2} \bar\psi_e \gamma_\sigma \psi_e \right], \tag{162}$$

with

$$A_\mu = \frac{gD_\mu + g'B_{3\mu}}{\sqrt{g^2+g'^2}}, \tag{163}$$

the ordinary vector potential, and

$$W_{3\mu} = \frac{gB_{3\mu} - g'D_\mu}{\sqrt{g^2+g'^2}}, \tag{164}$$

and

$$W_{\pm\mu} = \frac{B_{1\mu} \pm iB_{2\mu}}{2}, \tag{165}$$

a triplet of vector bosons. This tempts us to identify as the electric charge the combination of g and g'

$$e = gg'(g^2+g'^2)^{-1/2}, \tag{168}$$

and to define the angle θ by

$$\tan\theta = \frac{g'}{g} \tag{166}$$

The currents in the model are then

$$J_{-\mu} = \frac{e}{\sqrt{2}\sin\theta} \bar\psi_{\nu e} \gamma_\sigma \frac{(1-\gamma_5)}{2} \psi_e, \tag{167}$$

$$J_{3\mu} = \frac{e}{\sin 2\theta} \left\{ \bar\psi_{\nu e} \gamma_\sigma \psi_{\nu e} - \bar\psi_e \gamma_\sigma \frac{(1-\gamma_5)}{2} \psi_e - 2\sin^2\theta \, J_\sigma^{em} \right\}. \tag{168}$$

The phenomenology of this model is not appropriate for this set of lectures; it is lucidly treated in the references.[34]

What we wish to do here is imitate this construction and incorporate the hadrons, called quarks, into this SU(2) $\otimes$ U(1) gauge model. If the weak gauge group is this, then the organization of quarks must be such that its $\mathscr{L}$ is invariant under this group. Otherwise the gauge symmetry of the full $\mathscr{L} = \mathscr{L}_{\text{Strong}} + \mathscr{L}_{\text{em and weak}}$ is broken and the theory is not renormalizable. We now guarantee this by asking that all the generators of $\mathscr{G}_S$, Eq. (127), commute with those of $\mathscr{G}_W$, Eq. (156). We must still announce the transformation properties of the quarks under the weak gauge group.

If we have only three quarks, called n, p, and λ with the traditional quantum numbers, then the direct imitation of the lepton exercise would be to form a left handed doublet[35]

$$L_h = \frac{1}{2}(1-\gamma_5) \begin{pmatrix} \psi_p \\ \psi_n \cos\vartheta_c + \psi_\lambda \sin\vartheta_c \end{pmatrix} \tag{169}$$

and the associated SU(2) currents

$$J^h_{a\sigma}(x) = \bar L_h(x) \gamma_\sigma \frac{\tau_i}{2} L_h(x). \tag{170}$$

ϑ_c is the Cabbibo angle. There is also a U(1) current, $K^h_\sigma(x)$, which commutes with the $J^h_{a\sigma}(x)$ at equal times. The neutral SU(2) current $J^h_{3\sigma}(x)$ has a term

$$-\frac{1}{2}\sin\vartheta_c\cos\vartheta_c \left\{ \bar\psi_n \gamma_\sigma \frac{(1-\gamma_5)}{2} \psi_\lambda + \bar\psi_\lambda \gamma_\sigma \frac{(1-\gamma_5)}{2} \psi_n \right\} \tag{171}$$

which is a $\Delta S = 1$ neutral current. If this remains in the theory then the rates for decays like $K_L^0 \to \bar{\mu}\mu$ and $K^+ \to \pi^+ \bar{\nu} \nu$ would be comparable to the $\Delta S = 1$, charged transition $K \to \mu\nu$. The experimental facts are that these $\Delta S = 1$, $\Delta Q = 0$ decays are fantastically suppressed with respect to the $\Delta S = 1$, $\Delta Q = 1$ decays.[32] Indeed, $\Gamma(K \to \mu\bar{\mu}) \sim 10^{-9}\ \Gamma(K \to \mu\nu)$.

The easiest solution to this problem[36] is to invent a new quark called p' which has electric charge 2/3 and just a tad of a new quantum number called charm. A second left-handed hadron doublet is constructed

$$L_h'(x) = \frac{1}{2}(1 - \gamma_5) \begin{pmatrix} \psi_{p'} \\ -\psi_n \sin \vartheta_c + \psi \cos \vartheta_c \end{pmatrix} \tag{172}$$

just so the $\Delta S = 1$, $\Delta Q = 0$ neutral currents are eaten up. At first sight this seems not only ad hoc, but silly. One learns to live with ad hoc things, but the initial silliness fades away as model after model dies under the very severe constraints established by the tiny allowed rates for $\Delta S = 1$, $\Delta Q = 0$ transitions. Four quarks would seem to be a real minimum, then.

After carrying out the exercise done for the lepton $SU(2) \otimes U(1)$ model one arrives at the hadronic weak currents

$$J_\sigma^{em} = \frac{2}{3} \bar{\psi}_{p'} \gamma_\sigma \psi_{p'} + \frac{2}{3} \bar{\psi}_p \gamma_\sigma \psi_p - \frac{1}{3} \bar{\psi}_n \gamma_\sigma \psi_n - \frac{1}{3} \bar{\psi}_\lambda \gamma_\sigma \psi_\lambda , \tag{173}$$

which couples to electromagnetism,

$$J_{-\sigma}(x) = \frac{e}{\sqrt{2} \sin \theta} \left[\bar{\psi}_p \gamma_\sigma \frac{(1-\gamma_5)}{2} \left\{ \cos \vartheta_c \psi_n + \sin \vartheta_c \psi_\lambda \right. \right.$$
$$\left. \left. + \bar{\psi}_{p'} \gamma_\sigma \frac{(1-\gamma_5)}{2} \cos \vartheta_c \psi_\lambda - \sin \vartheta_c \psi_n \right\} \right] , \tag{174}$$

which couples to the charged gauge boson, and

$$J_{3\sigma} = \frac{e}{\sin 2\theta} \left[\bar{\psi}_p \gamma_\sigma \frac{(1-\gamma_5)}{2} \psi_p - \bar{\psi}_n \gamma_\sigma \frac{(1-\gamma_5)}{2} \psi_n + \bar{\psi}_{p'} \gamma_\sigma \frac{(1-\gamma_5)}{2} \psi_{p'} \right.$$
$$\left. - \bar{\psi}_\lambda \gamma_\sigma \frac{(1-\gamma_5)}{2} \psi_\lambda - 2 \sin^2 \theta\, J_\sigma^{em} \right] , \tag{175}$$

which couples to the neutral gauge boson. All $\Delta S = 1$, $\Delta Q = 0$ neutral currents are charmingly absent.

Finally we want to discuss the gauge group $SU(3)_{Color}$ chosen for the strong interactions. The history of an extra degree of freedom for quarks is very colorful. Long ago many of our friendc tried to construct quark models for the baryons by building each of them out of three of the classical p, n, and λ. Things worked out pretty well except that the total wave function for the baryon had to be symmetric. This didn't sit well with the Pauli principle, so a new quantum number, with a very colorless name like parastatistics or such, was announced.[37] This allowed the overall wave function to respect Fermi statistics. Only later when it was learned that more than three quarks were necessary to understand how the the $\pi^0 \to 2\gamma$ decay rate could be attributed to the famous triangle anomaly of electrodynamics did the idea receive better publicity.[38] The precise number of quarks suggested by the π^0 decay rate was 3p quarks, 3n quarks, and 3λ quarks. The group structure of such a set of 9 quarks could be as large as SU(9), but if the gauge bosons are taken to commute with the SU(3) of hypercharge and isospin yet couple to the SU(3) that mixes the 3p quarks among themselves, the 3n quarks among themselves, and the 3λ quarks among themselves, then the symmetry would be

$$SU(3)_{\substack{\text{Isospin}\\ \text{Hypercharge}}} \otimes SU(3)_{\substack{\text{Gauge}\\ \text{of color}}} . \tag{176}$$

The name color now is given to the labels on the $2p$'s, $3n$'s, and 3λ's. If the colors are red, white, and blue, then there is a red p quark, a blue p quark, a white p quark, etc.

There is another cute consequence of the color scheme where the interaction among quarks is via an octet of gauge bosons which are neutral with respect to I and Y, but couple to the color index. In such a scheme, only color singlet states have an attractive potential (Fourier transform of the Born approximation) for the interacting quarks, while colorful collections of quarks have a repulsive force acting on them. This argument has been elaborated on in a very vivid and clear fashion by Lipkin at the Topical Conference following last year's SLAC Summer School.[39] If, by the way, one has four plain old quarks--the p, n, λ, and p' of above, then each of them is tripled in number--becomes in red, white, and blue--when the SU(3) color gauge is imposed on strong interactions. This finishes our reasoning behind the choice of Lagrangian way back at Eq. (128).

This completes the topics to be covered by me in this part of the lectures on non-Abelian gauge groups in hadronic physics. Let me assure you that there is no shortage of more complicated models of hadronic physics. Each of them incorporates the ideas I have presented here; each of them faces with more or less equanimity the severe constraints of $\Delta S = 1$, $\Delta Q = 0$ non-leptonic decays. Some are very ambitious and try to unify strong, electromagnetic, and weak interactions.[40] Various of these will be discussed by the practitioners at the Topical Conference after this school.

I would like to add a word of outlook before departing from gauge theories. Once one had established that non-Abelian gauge theories with a shy symmetry were renormalizable, it became clear that an overabundance of models could be built which shared only these properties.[41] Bringing to the problem the desire to have ultraviolet freedom, so approximate Bjorken scaling occurs, is the kind of attractive constraint that is needed to restrict the enormous liberty one otherwise enjoys. Hints from rare K decays, baryon spectroscopy, and any other source is important to further restrict model building. Something like the four colored quark model we wrote down is one of the simplest that still passes all these obstacles. It also has sufficient simplicity to suggest a variety of experiments to further probe its viability. If it turns out to be wrong in detail, I would not be at all surprised if something quite similar to it does survive. (This unabashed subjective opinion is brought to you by the Friends of Charm and Color, NAL branch.[42])

> "I'm no good at being noble, but it doesn't take much to see that the problems of three little Pomerons don't amount to a hill of beans in this crazy world. Some day you'll understand that. Now now. Here's looking at you, kid."
>
> With apologies to
>
> Humphrey Bogart, Casablanca

REGGEON CALCULUS AND THE POMERON

This is the most far reaching lecture of the series. First of all I want to briefly review some of the phenomenological features of diffraction scattering and the Pomeron ($\underset{\sim}{P}$). Next I wish to describe the motivation for two dimensional field theories[8] to describe the interaction and propagation of $\underset{\sim}{P}$'s and discuss how the behavior of partial wave amplitudes near $J = 1$, $t = 0$ can be studied via the renormalization group[9] applied to these field theories. Finally, I will discuss the consequences of a simple application of these ideas.

A serious experimental review of diffraction phenomena will be given as part of this school by Leith.[43] The salient facts are[44]

a. A whole grab bag of cross sections which are at most logarithmically dependent on s, the square of the center-of-mass energy. This includes elastic processes, diffraction dissociation, and inclusive cross sections $(A + B \to 1 + 2 + \cdots + N + \text{anything})$.

b. An amplitude which is mainly pure imaginary.

c. Amplitudes which factorize. For example, the total cross section for $A + B \to$ anything would be (up to $\log s$ factors)

$$\sigma_T^{AB}(s) \underset{s \to \infty}{\sim} \gamma_A \gamma_B + \text{corrections} \tag{177}$$

d. Crossed channel (t-channel) exchange mechanism characterized by the quantum numbers of the vacuum. $I = S = B = 0;\ P = C = G = 1.$

There is no model famine associated with the study of these processes. A short review may be found in the talks by Low and Gribov[45] at the Batavia Conference or a more recent, more biased, talk by myself at the Leipzig Conference.[46] I am not aware of a full blown careful review of all theories of diffraction scattering. Perhaps the Physics Report by Zachariasen[47] of several years ago comes closest to such a scholarly presentation. This is one of those exciting fields where almost no one completely agrees with anyone else (collaborators included). The reason, fortunately, is not sociological but is physics. Once one agrees that total cross sections, for example, are not power behaved in s but only logarithmic, then experiments which concentrate on s dependence are relatively blunt instruments[48] for cutting out the correct theory.

Perhaps a concrete example is in order. As we all know the experiments on the proton-proton total cross section at the CERN Intersecting Storage Rings (ISR) show a 10% rise in σ_T^{pp} over an equivalent laboratory momentum range of approximately[49]

$$500\ \text{GeV/c} \le p_{lab} \le 1500\ \text{GeV/c}. \tag{178}$$

Jacob[50] has given two "casual" fits to this data. The first reflects the school of thought that the observed cross section increase is a portent of things to come and that we are witnessing a saturation of the Froissart bound

$$\sigma_T(s) \le (\log s)^2 . \tag{179}$$

This fit is $(s \approx 2m_p\, p_{lab})$

$$\sigma_T(p_{lab}) = 38\ \text{mb} + 0.68\ \text{mb}[\log(p_{lab}/100\ \text{GeV/c})]^2 . \tag{180}$$

At $p_{lab} = 10^3$ GeV/c, the energy of the proposed NAL energy doubler or the middle of the ISR range, this yields $\sigma_T = 42$ mb.

The second fit reflects the point of view that eventually the cross section will become a constant as the secondary terms die away. This is expressed in

$$\sigma_T(p_{lab}) = 60\ \text{mb}\left(1 - \frac{3}{3 + \log(p_{lab}/1\ \text{GeV/c})}\right) \tag{181}$$

At $p_{lab} = 10^3$, this cross section is also 42 mb! To distinguish the two ideas expressed here by s dependence alone one must build a machine like the ISABELLE colliding beams proposed by Brookhaven. At that facility 200 GeV/c protons intersect giving an equivalent $p_{lab} \approx 8 \times 10^4$ GeV/c. At these energies the $\log^2 p_{lab}$ formula bounds up to 68 mb, while the very-slow-rise-to-a-constant-school reaches only 48 mb. A difference of 20 mb ought to be visible, even if a clumsy theorist takes the data![51]

There are other schools of diffraction practice. Some have cross sections rising only as $\log p_{lab}$,[52] some have σ_T falling as a tiny power of s, and some have σ_T oscillating before having the initiative to decide its asymptotic fate.[53]

It is clear that one must either make a choice among these theories in order to proceed or give a dab of each.[54] I leave the latter course to the reviews mentioned. Here I will discuss the view from the angular momentum plane which is, to be sure, general enough to encompass any of those alternatives. Yet I will adopt a more restricted outlook. First of all, I will only tolerate cross sections which do not fall in s, even as a small power. Secondly, I will concentrate on a t-channel rather an s-channel description of the diffraction mechanism called $\underset{\sim}{P}$.[55] This will lead to a preference for $\sigma_T(s)$ which slowly rises to either a constant or to an asymptote which grows as a very small power of $\log s$. My prejudice exposed, let me proceed.

It is sensible to establish some conventions at the outset. When discussing elastic scattering $A(p_A) + B(p_B) \to A(p_A') + B(p_B')$, I will designate the invariant amplitude as $T_{AB}(s,t)$ which is a function of the standard scalars.

$$s = (p_A + p_B)^2 , \tag{182}$$

and

$$t = (p_A' - p_A)^2 . \tag{183}$$

We will deal with spinless objects of equal mass m. The elastic cross section is

$$\frac{d\sigma_{AB}(s,t)}{dt} = \frac{1}{16\pi\, s(s - 4m^2)} \left|T_{AB}(s,t)\right|^2 , \tag{184}$$

and the total cross section $\sigma_T^{AB}(s)$ is given via the optical theorem as

$$\sigma_T^{AB}(s) = \frac{1}{s(s - 4m^2)} \; \mathrm{Im}\, T_{AB}(s,0) . \tag{185}$$

We will not need to delve into the vagaries of thresholds, signature and such[56,57] (the references are riddled with such complications), but will define the t-channel partial wave amplitude $F(J,t)$ for even signature (physical particles at $J = 0, 2, 4, \ldots$) as

$$F(J,t) = \int_1^\infty ds \; s^{-J-1} \; \mathrm{Im}\, T_{AB}(s,t) , \tag{186}$$

whose Mellin inversion is

$$\mathrm{Im}\, T_{AB}(s,t) = \int_{c-i\infty}^{c+i\infty} \frac{dJ}{2\pi i} \, s^J \, F(J,t) , \tag{187}$$

where $\mathrm{Re}\, c$ lies to the right of all singularities in $F(J,t)$. This is the partial wave amplitude analytically continued in J and t (from $t \geq 4m^2$ to $t \leq 0$) which contains the vacuum singularity: $\underset{\sim}{P}$.

Now what is all this stuff? Well, what we have done via the integral transform (186) is go over from a description of the scattering amplitude in s and t to a description in t and the conjugate variable to $\log s$, called J. Let's rewrite (186) calling $Y = \log s$ (yes, Virginia, it's the rapidity)

$$F(J,t) = \int_0^\infty dY \; e^{-JY} \; \mathrm{Im}\, T_{AB}(Y,t) . \tag{188}$$

It will turn out to be more graphic and eventually simpler to discuss $F(J,t)$ than $\mathrm{Im}\, T_{AB}(s,t)$. We can always recover the latter by doing the integral in (187).

To acquire a feeling where we're at, and where we might go, let's consider an $\mathrm{Im}\, T_{AB}(s,t)$ of the form

$$\mathrm{Im}\, T_{AB}(s,t) = s^{\alpha(t)} (\log s)^{\beta(t)} \tag{189}$$

$$= e^{Y\alpha(t)} \, Y^{\beta(t)} , \tag{190}$$

which is very much like the experimental situation outlined above if $\alpha(0) = 1$. Indeed the Froissart bound tells us

$$\alpha(0) \leq 1, \tag{191}$$

$$\beta(0) \leq 2, \quad \text{when} \quad \alpha(0) = 1. \tag{192}$$

The $F(J,t)$ from this ansatz is

$$F(J,t) = \frac{\Gamma(1 + \beta(t))}{(J - \alpha(t))^{1+\beta(t)}} . \tag{193}$$

This is a branch point in the J plane at $\alpha(t)$ unless $\beta(t) = 0, 1,$ or 2 (or any integer, but never mind). When $\beta(t) = 0$, the singularity in J is a simple pole at $\alpha(t)$, and the cross section

$$\sigma_T^{AB}(s) \underset{s \to \infty}{\sim} s^{\alpha(0)-1} . \tag{194}$$

So we want $\alpha(0) = 1$ to have a more or less constant cross section. When $\beta(0) \neq 0$, $\alpha(0) = 1$,

$$\sigma_T^{AB}(s) \underset{s \to \infty}{\sim} (\log s)^{\beta(0)}. \tag{195}$$

With no further information on the scale of s in the logarithm one would conjecture it was a typical hadron mass or threshold $\approx 1\ \mathrm{GeV}/c^2$. So we will do.

To incorporate feature (a) of the "salient facts" then, we choose $\alpha(0) = 1$ and after that $\beta(t)$ and the form of $\alpha(t)$ away from $t = 0$ become the subject of theoretical discussion. Enter here the "blunt instrument" of experiment. To incorporate feature (b) we ought to treat signature properly. We won't. However, we don't do a terrible injustice when we write

$$\mathrm{Re}\ T_{AB}(s,t) = 0 \tag{196}$$

or

$$T_{AB}(s,t) = i\ \mathrm{Im}\ T_{AB}(s,t) . \tag{197}$$

Finally we can incoprorate feature (c), factorization, by writing

$$T_{AB}(s,t) = i\gamma_A(t)\, \gamma_B(t)\, s^{\alpha(t)}(\log s)^{\beta(t)} , \tag{198}$$

$$\alpha(0) = 1 , \tag{199}$$

to be our improved ansatz.

Some things are known or suspected about the vertex functions $\gamma(t)$.[44] They seem to conserve s-channel helicity (sometimes) and in diffraction dissociation $A + B \to A^* + B$ they seem to relate the parity and spin of A and A^* by

$$P_A = P_{A^*}(-1)^{J_A - J_{A^*}} . \tag{200}$$

We will have nothing to say about these amusing features.

Our first task is to recall what the $\underset{\sim}{P}$ (characterized by $\alpha(t)$ and $\beta(t)$) cannot be. A simple guess for α and β would be

$$\alpha(t) = 1 , \tag{201}$$

$$\beta(t) = 0; \tag{202}$$

namely, a simple fixed (not moving with t) pole in J. This is kind of an "optical model" (whatever that is) result:

$$T_{AB}(s,\ t) = is\ f(t) . \tag{203}$$

Over a decade ago[58] Gribov showed that this is in conflict with unitarity in the t-channel. So our elders turned to the next simplest guess

$$\alpha(t) = 1 + \alpha' t , \tag{203}$$

$$\beta(t) = 0 ; \tag{204}$$

namely, a simple moving pole in J. There were hints over a long period of time that this also was in conflict with unitarity.[59] It took some time to show that with the conjecture (203) and (204) one was forced to conclude that $\gamma(0) = 0!$[60] So $\underset{\sim}{P}$, invented to account for $\sigma_T \approx$ constant, decoupled from σ_T. Clearly, $\underset{\sim}{P}$ <u>cannot be a simple moving pole with</u> $\alpha(0) = 1$ <u>and</u> α' <u>finite</u>.

Enough said about what $\underset{\sim}{P}$ cannot be. The rest of this lecture is devoted to a study of a framework, called Reggeon field theories, to discover what the $\underset{\sim}{P}$ can be and some discussion, within this framework, of models which give us hints as to what $\underset{\sim}{P}$ is.

The first derivation or motivation for Reggeon field theories comes from the work of Gribov.[8] His procedure was to study sets of "hybrid" Feynman graphs for $T_{AB}(s,t)$ when $s \to \infty$ and t was fixed. He used the language of perturbation theory for a $\lambda_3\phi^3$ quantum field theory but didn't really sum order by order in λ_3. Instead he made partial summations to acquire four point amplitudes which were presumed to have Regge or power behavior in subenergies. These modified four leg amplitudes were then substituted into further Feynman graphs of the theory and the interaction of the Regge singularities was studied. He abstracted from his study of very large sets of graphs a set of rules (the Reggeon calculus) for writing down directly the Reggeon interactions he discovered. He then conjectured (1) any field theory, not just ϕ^3, would give rise to essentially the same set of rules. (Small and inessential modifications would be expected, and we'll come to them later.) (2) If one were able to sum all the graphs of the Reggeon field theory, then the resulting partial wave amplitude would correctly represent diffraction phenomena near $t = 0$ and up to order $(1/s)$. I have no intention here of going through any or all of the steps followed by Gribov. The dedicated are referred to Reference 8 for the classical point of view and Reference 55 for a pedagogical treatment. Our procedure here will be to study the t-channel discontinuity formulae[61] for Reggeons as an heuristic way to motivate the Reggeon field theories.

Let's consider the two Reggeon exchange contribution to the elastic amplitude $T_{AB}(s,t)$ as shown in Fig. 10. The partial wave projection (ignoring signature momentarily) leads to a two dimensional integral over the "masses" of the Reggeons, both with trajectory $\alpha(t)$:

$$F_{2\ \text{Reggeon}}(J,t)$$
$$= \int \frac{dt_1\, dt_2}{\sqrt{-\Delta(t,t_1,t_2)}}\, \theta(-\Delta(t,t_1,t_2))\, \frac{N_2^A(J,t,t_1,t_2)\, N_2^B(J,t,t_1,t_2)}{J - \alpha(t_1) - \alpha(t_2) + 1}\,, \qquad (205)$$

where

$$\Delta(x,y,z) = (x + y - z)^2 - 4xy\ . \qquad (206)$$

The functions N_2 are to be interpreted as the amplitude for transition of two particles into a Reggeon of $(\text{mass})^2 = t_1$, spin $\alpha(t_1)$ and a Reggeon of $(\text{mass})^2 = t_2$, spin $\alpha(t_2)$. The factor $(-\Delta(t,t_1,t_2))^{-1/2}$ is a kinematic convention which will be useful in a moment.

Why is the integration two-dimensional? Well, we have a loop integral in four dimensional space-time to begin with--a loop of Reggeons, but that's all right. Now we make a partial wave projection via a $Y_\ell^m(\theta,\phi)$ function and integrate over θ, a polar angle, and ϕ, an azimuthal angle. That leaves a two-dimensional integral. In the hybrid Feynman graph procedure one writes down some diagram then takes the infinite momentum limit, say $p_3 \to \infty$. Since the particles are on the mass shell, if $\vec{p} = (p_1,p_2)$ is held fixed, then $p_0 \to \infty$ also. The remaining two degrees of freedom in the transverse direction are precisely the ones integrated over in (205). This isolation of a two-dimensional space for the discussion of dynamics is familiar from the eikonal approximation, relativistic or non-relativistic. There the elastic amplitude for large s, fixed t is[62]

$$T_{AB}(s,t) = is \int d^2b\ e^{i\vec{q}\cdot\vec{b}}\, [e^{i\chi(x,\vec{b})} - 1] \qquad (207)$$

where

$$t = -|\vec{q}|^2 , \tag{208}$$

and $\vec{b}$ is the two dimensional impact parameter conjugate to the two momentum $\vec{q}$. The dynamics resides in the eikonal phase factor $\chi(s,\vec{b})$. In any case, the two dimensional integral is not coming from an approximation.[63]

The integral in (205) is the explicit representation of a branch point in the J-plane arising from the exchange of two Reggeons $\alpha(t)$. It was first found by Amati, Stanghellini, and Fubini[64] and Mandelstam.[65] Its properties were further studied by Gribov, Pomeranchuk, and Ter-Martirosyan.[61] The branch point due to two Reggeon exchange occurs at $\alpha^{(2)}(t)$ given by

$$\alpha^{(2)}(t) - 1 = 2\left\{\alpha\left(\frac{t}{2^2}\right) - 1\right\}. \tag{209}$$

If two Reggeons can be exchanged, then, consistent with t-channel quantum numbers, any number may be exchanged. (In a sentence, that is unitarity.) From n Reggeons a branch point at

$$\alpha^{(n)}(t) - 1 = n\left\{\alpha\left(\frac{t}{n^2}\right) - 1\right\} \tag{210}$$

arises. Beyond the positions of these branch points, some information is known about the discontinuities across the branch lines.[61,66]

Now here comes the action. Suppose $\alpha(0) = 1$ for the Reggeon; that is, suppose it is the $\underset{\sim}{P}$ of song and saga. Then we are informed for every n

$$\alpha^{(n)}(0) = 1 \qquad \text{if} \quad \alpha(0) = 1 . \tag{211}$$

<u>So all</u> $\underset{\sim}{P}$ <u>branch points lie at</u> $J = 1$ <u>at</u> $t = 0$, <u>when</u> $\alpha(0) = 1$. That is what has made the $\underset{\sim}{P}$ so remarkably difficult to get a theoretical handle on. Right here, however, we see why the $\underset{\sim}{P}$ decoupling result for an $\alpha(t) = 1 + \alpha' t$ trajectory is not much to worry about. The collision of all those branch points at $t = 0$ most likely gives rise to a complicated singularity and no rule known to man requires $\alpha(t)$ to remain analytic at $t = 0$.

Before I launch into the marvels of Reggeon calculus arithmetic, I want to develop an analogy which will give us some useful hints how we are to go about resolving the cut-pole collision problem. Let's think about the radiative corrections in quantum electrodynamics to a charged boson propagator of momentum p. With no photon corrections the propagator is

$$(m_0^2 - p^2)^{-1} \tag{212}$$

where m_0 is the bare mass. To order e^2 (Fig. 11), the propagator develops a branch point at $p^2 = m^2$ (m is the new, renormalized mass at this order of e^2). If the photon had a mass m_γ, then this branch point would occur at $p^2 = (m + m_\gamma)^2$. The <u>massless</u> photon, then, is responsible for the coincidence of the pole and branch point. To order e^4 there arises a second branch point at $p^2 = (m + 2m_\gamma)^2 = m^2$, since $m_\gamma = 0$. Get the picture? There are an infinite number of branch points at $p^2 = m^2$, because the photon is massless. This is known as the infrared problem. In electricity theory one has learned by one technique or another to sum up all the photon corrections.[67] The aspects of the result relevant here are that $(m_0^2 - p^2)^{-1}$ changes into

$$(m^2 - p^2)^{-1-\gamma(e^2)} \tag{213}$$

where $\gamma(e^2)$ is known as a power series in e^2 beginning with e^2. (Now it turns out that in electrodynamics, γ is gauge dependent and actually vanishes in one gauge. For the purposes of motivation being pursued here, that is an irrelevancy.) One can see directly from (213) the series of branch points of $p^2 = m^2$ arising from expansion in e^2

$$(m^2 - p^2)^{-1-\gamma(e^2)} = (m^2 - p^2)^{-1}\sum_{n=0}^{\infty} \frac{[\log(m^2 - p^2)]^n}{n!} (-\gamma(e^2))^n . \tag{214}$$

k soever we may now anticipate the results

s.suming we can find a way to express $\alpha(0) = 1$

ss: particle (we will in a moment), then all

prator (Regge pole)

$$\alpha(t))^{-1} \tag{215}$$

$$(\alpha(t))^{-1-\beta} \ . \tag{216}$$

e er who recalls Eq. (193). So all we have

ngiables in our formula for the two Reggeon

or two dimensional lore. Associate a two-

t $\vec{q}_i$ with t_i; $t = -|\vec{q}|^2$

$$, \quad i = 1, 2, \tag{217}$$

$$\vec{q}_1 + \vec{q}_2 \ . \tag{218}$$

$$- \frac{N_2^A(J,\vec{q},\vec{q}_1,\vec{q}_2)\ N_2^B(J,\vec{q},\vec{q}_1,\vec{q}_2)}{1-J-(1-\alpha(\vec{q}_1)) - (1-\alpha(\vec{q}_2))} \tag{219}$$

drded. Now we want to take the discontinuity

c Remebering that the two particle-two

at, one finds

$$\mathrm{disc}_E\, F_{2\ \mathrm{Reggeon}}(E,\vec{q})$$

$$= \int d^2q_1\, d^2q_2\, \delta^2(\vec{q}-\vec{q}_1-\vec{q}_2)\, \delta(E-E_1-E_2)\, N_2^A(E + i\epsilon,\vec{q},\vec{q}_1,\vec{q}_2)\, N_2^B(E - i\epsilon,\vec{q},\vec{q}_1,\vec{q}_2) \ , \tag{220}$$

where we have written

$$E = 1 - J \tag{221}$$

and

$$E_i = 1 - \alpha(\vec{q}_i) \tag{222}$$

This result generalizes in the obvious way to the n-Reggeon cut discontinuity (Fig. 12)

$$\mathrm{disc}_E\, F_{n\ \mathrm{Reggeon}}(E,\vec{q})$$

$$= \int \prod_{j=1}^{n} d^2q_j\, \delta^2(\vec{q} - \sum_{k=1}^{n} \vec{q}_k)\, \delta(W - \sum_{k=1}^{n} E_k)\, N_n^A(E + i\epsilon,\ \vec{q},\vec{q}_1,\ldots,\vec{q}_n) \times N_n^B(E - i\epsilon,\ \vec{q},\vec{q}_1,\ldots,\vec{q}_2) \ . \tag{223}$$

These discontinuity relations are true in the multiperipheral model, in hybrid Feynman graph theories, in dual models, and have been "proved" in S-matrix theory.[51] One suspects they are correct. A proper signature analysis leads to the conclusion that the sign associated with the $n\underline{P}$ cut at $t = 0$ is $(-1)^{n-1}$. This is incorporated rather easily by writing a factor $(i)^{n-1}$ in front of each N_n.

The set of discontinuity relations has a pleasant interpretation. They are to be regarded as the unitarity formulae for quasi-particles (Reggeons) carrying two momentum $\vec{q}$ and, in the unitarity sum where they are "on shell," an energy $E(\vec{q}) = 1 - \alpha(\vec{q})$. When $\alpha(0) = 1$, then when $\vec{q} = 0$, the energy is zero. This the energy momentum relation of a massless particle! So all the ingredients are present for our formulation of an infrared problem. I can reveal the strategy at this juncture: we will write a field theory to describe the propagation and interaction of these quasi-particles and employ the renormalization group to solve this field theory in the infrared limit: $E \to 0$, $\vec{q} \to 0$ ($J \to 1$, $t \to 0$).

The next logical step is to note that just as one can define the two particle--n-Reggeon amplitudes N_n, one can, by considering the Reggeon discontinuity formulae for the N_n, find pure Reggeon amplitudes M_n. These satisfy discontinuity formulae among themselves. This point allows us to continue the discussion with consideration of Reggeons alone. Particles will enter later (see Fig. 13).

So we wish to describe a field theory in two space dimensions $\vec{x}$, conjugate to $\vec{q}$, and one time τ, conjugate to E. Of course, $\vec{x}$ is just the impact parameter $\vec{b}$ that enters the eikonal formula, Eq. (207). τ is i times the rapidity. We'll denote the field which gives the excitations of the theory as $\phi(\vec{x},\tau)$. As usual the objects of interest will be the Green's functions for n Reggeons incoming and m Reggeons outgoing:

$$G^{(n,m)}(\vec{x}_1, \tau_{x1}, \ldots , \vec{x}_n, \tau_{xn}; \vec{y}_1, \tau_{y1}, \ldots , \vec{y}_m, \tau_{ym})$$
$$= \langle 0|T(\phi^+(\vec{y}_1, \tau_{y1}) \cdots \phi^+(\vec{y}_m, \tau_{ym}) \phi(\vec{x}_1, \tau_{x1}) \cdots \phi(\vec{x}_n, \tau_{xn}))|0\rangle \ . \quad (224)$$

Whatever field theory we construct will consist of a free theory $\mathscr{L}_{\mathrm{Free}}$ and an interaction characterized by a bare coupling λ_B. To whatever order in λ_B we solve for $G^{(n,m)}$, we are guaranteed, if we take all graphs to a given order, to satisfy the Reggeon unitarity relations. If we are able to solve to all orders, so much the better. Even a solution which is an asymptotic formula in some regime of momentum space satisfies the unitarity relations. A Reggeon field theory then may be viewed as a trick for satisfying t-channel unitarity. This is clearly independent of $\alpha(0) = 1$.

To proceed we need a field theory. I will describe one at great length although I trust you will see that most of my remarks apply to a vast set of Reggeon field theories.[55] Most of the sophisticated developments will be described by White at the Topical Conference.

We'll start with a bare linear trajectory

$$\alpha_B(t) = \alpha_0 + \alpha_0' t \quad (225)$$

which gives the E, $\vec{q}$ relation

$$E(\vec{q}) = \alpha_0' \vec{q}^{\,2} + (1 - \alpha_0) \ . \quad (226)$$

This is the energy-momentum relation of a non-relativistic quasi-particle with

$$\alpha_0' = 1/2m \quad (227)$$

and "mass gap"

$$\Delta_0 = 1 - \alpha_0, \quad (228)$$

to steal a little language from our many-body friends. The free Lagrangian which describes this is

$$\mathscr{L}_{\mathrm{Free}}(\vec{x},\tau)$$
$$= \frac{i}{2} \phi_0^+(\vec{x},\tau) \overleftrightarrow{\partial_\tau} \phi_0(\vec{x},\tau) - \alpha_0' \nabla\phi_0^+(\vec{x},\tau)\cdot\nabla\phi_0(\vec{x},\tau)$$
$$- (1 - \alpha_0) \phi_0^+(\vec{x},\tau) \phi_0(\vec{x},\tau) \ . \quad (229)$$

Varying the action

$$A_{\mathrm{Free}} = \int d^2x \, d\tau \, \mathscr{L}_{\mathrm{Free}}(\vec{x},\tau) \quad (230)$$

gives the Schrödinger equation

$$i \frac{\partial}{\partial\tau} \phi_0(\vec{x},\tau) = -\alpha_0'\nabla^2 \phi_0(\vec{x},\tau) + \Delta_0 \phi(\vec{x},\tau) , \quad (231)$$

which is, of course, just the configuration space version of the original energy momentum relation.

Now for an interaction. In hybrid Feynman graphology or the multi-peripheral model or whatever there appear ϕ^N couplings.[8] In two space dimensions only ϕ^3 and ϕ^4 are renormalizable. So following our continuing prejudice, we will ignore any couplings in $\mathscr{L}$ higher than ϕ^4.[68] To begin with actually we are going to ignore the ϕ^4 coupling as well. The heuristic argument for this is that these couplings always involve the emission of more Reggeons at a vertex than do ϕ^3 coupling. In the infrared regime $(E \sim 0, \vec{q} \sim 0)$ plain old phase space will make ϕ^4 less important than ϕ^3. This is born out by detailed calculations.[69] Furthermore, a cubic coupling holds to a triple $\underset{\sim}{P}$ vertex which is of prime physical interest.

So we choose

$$\mathscr{L}_I(\vec{x},\tau) = -\frac{ir_0}{2}\ [\phi^+(\vec{x},\tau)^2\ \phi(\vec{x},\tau) + \phi^+(\vec{x},\tau)\ \phi(\vec{x},\tau)^2]\ , \tag{232}$$

for our bare triple $\underset{\sim}{P}$ coupling. The i is dictated by signature, r_0 is real. The theory defined by $\mathscr{L} = \mathscr{L}_{Free} + \mathscr{L}_I$ has three constants in it α_0', $\Delta_0 = 1 - \alpha_0$, and r_0. These will be renormalized to α', $\Delta = 1 - \alpha(0) = 0$, and r respectively. Different underlying theories: multiperipheral model, dual models, gauge field theories with four quarks, charm, and SU(3) color--all these differ here in the value of α_0', Δ_0, and r_0. They will give, when solved to all orders, different α' and r, but if they have anything to do with total cross sections as we know them, each will yield $\alpha(0) = 1$, $\Delta = 0$. What the renormalization program does is to leave to the future the determination of α' and r from some remarkably majestic solution of a non-linear quantum field theory. Now it simply uses them as parameters, eventually phenomenological, for the Green's functions or proper vertex functions. This is an intellectual retreat from the more grandiose ambitions one may harbor to really compute the parameters of the theory. It is very much akin to procedure followed in many-body physics of expressing the physics in appropriate temperature or frequency domains in terms of "lump" parameters describing some quasi-particle-plasmon, magnon, Cooper pair, or whatever.[70] Then the effective or mean field theory of those quasi-particles yields up the physics. This classifying of lump parameters for the Reggeons is a new departure in hadronic physics. For those wishing to predict all parameters it must be regarded as a convenient intermediate level theory.[71] If our experience with electrodynamics is at all applicable, a certain pessimism is in order about going further than the lumpen program. (I don't share this pessimism, but I thought I'd throw it in for the cynical among us.)

Now in the spirit of renormalization we seek a solution to the theory we have established with parameters α', r, and $\Delta = 0$. Since this is a theory with zero renormalized mass, the infrared problems are serious.[14] We will choose a renormalization point in the E, $\vec{q}$ phase space which is just like the parameter μ of the first lecture. To do this we first remark that E and $\vec{q}$ play very separate roles in Reggeon field theories. So we may choose separate E, and $\vec{q}^2$ normalizations. The only sure symmetry of $\mathscr{L}$ is a rotational symmetry in two dimensions. We will normalize away from the branch points of perturbation theory at

$$E^{(n)} \equiv \frac{\alpha_0'\vec{q}^2}{n} + n(1 - \alpha_0) \tag{233}$$

by choosing the E_i of the appropriate vertex functions

$$E_i\alpha - E_N, \qquad E_N > 0\ , \tag{234}$$

and $\vec{q}_i = 0$.

To guarantee that the renormalized mass gap be zero we require the proper vertex function for one $\underset{\sim}{P}$ in--one $\underset{\sim}{P}$ out to vanish at $E = 0$, $\vec{q}^2 = 0$

$$\left.{}^{(1,1)}(E, \vec{q}^{\,2}, \alpha', r, E_N)\right|_{\substack{E=0 \\ \vec{q}^{\,2}=0}} = 0 . \tag{234}$$

; tlthe propagator

$$G^{(1,1)}(E, \vec{q}^{\,2}) = \{\Gamma^{(1,1)}(E, \vec{q}^{\,2})\}^{-1} \tag{235}$$

ılar at $J = 1$, $t = 0$. It does not require that this singu-

ɔle Next we must specify the wave function renormalization

h ts the unrenormalized field ϕ_0 to ϕ

$$\phi(\vec{x},\tau) = Z^{-1/2}\,\phi_0(\vec{x},\tau) . \tag{236}$$

$$\left.\frac{\partial}{\partial E}\, i\Gamma^{(1,1)}(E, \vec{q}^{\,2}, \alpha', r, E_N)\right|_{\substack{E=-E_N \\ \vec{q}^{\,2}=0}} = 1 . \tag{237}$$

$${}_i, \alpha', r, E_N) = Z^{(n+m)/2}\,\Gamma_U^{(n,m)}(E_i, \vec{q}_i, \alpha_0', r_0, \Delta_0) \tag{238}$$

nremalized vertex Γ_U to the renormalized Γ, we have as in,

$$\left.\frac{\partial}{\partial E}\, i\Gamma_U^{(1,1)}(E, \vec{q}^{\,2}, \alpha_0', r_0, \Delta_0)\right|_{\substack{E=-E_N \\ \vec{q}^{\,2}=0}} . \tag{239}$$

· cis defined by

$$\left.\frac{\partial}{\partial \vec{q}}\Gamma^{(1,1)}(E, \vec{q}^{\,2}, \alpha', r, E_N)\right|_{\substack{E=-E_N \\ \vec{q}^{\,2}=0}} = -\alpha'(E_N) , \tag{240}$$

and in D space dimensions (still one time)

$$\left.\Gamma^{(1,2)}(E_1, \vec{q}_1; E_2, \vec{q}_2, E_3, \vec{q}_3)\right|_{\substack{E_1=-E_N=2E_2=2E_3 \\ \vec{q}_i=0}} = \frac{r(E_N)}{(2\pi)^{(D+1)/2}} \tag{241}$$

Before we write down the renormalization group equations by a swift appeal to the first lecture, it is useful to identify the dimensionless coupling constant g. In this theory E and $\vec{q}$ have separate dimensions

$$[E] = E^1 , \tag{242}$$

$$[\vec{q}] = q^1 , \tag{243}$$

$$[\tau] = E^{-1} , \tag{244}$$

and

$$[\vec{x}] = q^{-1} . \tag{245}$$

Requiring the action to have

$$[A = \int d^Dx\, d\tau\, \mathscr{L}(x,\tau)] = E^0 q^0 , \tag{246}$$

gives

$$[\alpha'] = Eq^{-2} , \tag{247}$$

and

$$[r] = Eq^{-D/2} . \tag{248}$$

So

$$g(E_N) = \frac{r(E_N)}{(\alpha'(E_N))^{D/4}}\, E_N^{D/4-1} \tag{249}$$

is a dimensionless coupling. Note that in the physical number of dimensions $D = 2$, the g, r relation involves E_N so that the renormalization group function $\beta(g)$ will have a term linear in g.

The dimensions of $\Gamma^{(n,m)}$ are

$$[\Gamma^{(n,m)}] = E\, q^{D/2^{(2-n-m)}} , \tag{250}$$

so

$$\Gamma^{(n,m)}(E_i, \vec{q}_i, \alpha', g, E_N)$$
$$= E_N \left(\frac{E_N}{\alpha'} \right)^{(D/4)(2-n-m)} \psi_{n,m} \left(\frac{E_i}{E_N} , \frac{\alpha' \vec{q}_i \cdot \vec{q}_j}{E_N} , g \right), \tag{251}$$

where $\psi_{n,m}$ is dimensionless. Finally this says

$$\Gamma^{(n,m)}(\xi E_i, \vec{q}_i, \alpha', g, E_N) = \xi \Gamma^{(n,m)} \left(E_i, \vec{q}_i, \frac{\alpha'}{\xi}, g, \frac{E_N}{\xi} \right) . \tag{252}$$

The renormalization group equations follow as usual from

$$E_N \frac{\partial}{\partial E_N} \Gamma_U^{(n,m)} = 0 , \tag{253}$$

and read, using (252) ,

$$\left\{ \xi \frac{\partial}{\partial \xi} - \beta(g) \frac{\partial}{\partial g} + z(g)\, \alpha' \frac{\partial}{\partial \alpha'} + \left(\frac{n+m}{2} \gamma(g) - 1\right) \right\} \Gamma^{(n,m)}(\xi E_i, q_i, \alpha', g, E_N)$$
$$= 0 , \tag{254}$$

where $\beta(g)$ and $\gamma(g)$ are as usual, while

$$z(g) = 1 - \frac{1}{\alpha'} E_N \left. \frac{\partial \alpha'(E_N)}{\partial E_N} \right|_{\alpha_0', \Gamma_0, \Delta_0 \text{ fixed}} . \tag{255}$$

Once again we turn to perturbation theory to find the properties of β, γ, and z. The crucial result is that[9]

$$\beta(g) = - \frac{(4 - D)}{4} g + K(D)\, g^3 , \tag{256}$$

where $K(D)$ is positive for $2 \leq D \leq 4$ at least. So $\beta(g)$ has an infrared stable zero at

$$g_1 = \left(\frac{4 - D}{4K(D)} \right)^{1/2} . \tag{257}$$

Only at $D = 4$ do we have $g_1 = 0$, and <u>IR freedom</u> but if one can argue that the value in (257) of g_1 is small enough, then we have <u>IR liberty</u>. That argument has been made more or less successfully. I defer to White and others in the topical conference to defend or malign the smallness of g_1.[72]

Here let us understand the lesson of perturbation theory to be that $\beta(g)$ does have a zero at g_1, with $d\beta/dg\big|_{g=g_1} > 0$. Supposing $g = g_1$, let's look at the implications of the scaling laws. One finds

$$\Gamma^{(n,m)}(E_i, \vec{q}_i, \alpha', g_1, E_N)$$
$$= E_N \left(\frac{E_N}{\alpha'} \right)^{(D/4)(2-n-m)} \left(\frac{-E}{E_N} \right)^{1-(n+m)/2 \cdot \gamma(g_1) + z(g_1)(D/4)(2-n-m)}$$
$$\times\, \phi_{n,m} \left(\frac{E_i}{E} , \left(\frac{-E}{E_N} \right)^{-z(g_1)} \frac{\vec{q}_i \cdot \vec{q}_j}{E_N} \alpha', g_1 \right) , \tag{258}$$

with $E = \Sigma_{i=1}^{n} E_i$. Looking at $\Gamma^{(1,1)}$, this means that, if there is to be a <u>moving singularity</u> it must have the form for $t < 0$.

$$\alpha(t) = 1 + E_N \left(\frac{-\alpha' t}{E_N} \right)^{1/z(g_1)} f(g_1) , \tag{259}$$

where $f(g_1)$ is some dimensionless function of g_1. Except at $g_1 = 0$, $z(g_1)^{-1}$ is not in general an integer; there $z(g_1 = 0) = 1$. So, indeed, <u>in general the $\underline{P}$ trajector is non-analytic at</u> $t = 0$. If one believes the IR liberty formula,

$$z(g_1) > 1 ,$$

so the trajectory has infinite slope at $t = 0$. In a <u>rough</u> sense the inverse propagator is

$$i\Gamma^{(1,1)}(E, \vec{q}^{\,2}, \alpha', g_1, E_N) \approx E_N\left(\frac{-E}{E_N}\right)^{1-\gamma(g_1)}\left\{1 - \frac{\alpha'\vec{q}^{\,2}}{E_N}\left(\frac{E_N}{-E}\right)^{z(g_1)}\right\}. \quad (261)$$

This analytic structure is enough to avoid decoupling results, so the $\underset{\sim}{P}$ can again be held accountable for the structure of $\sigma_T(s)$.

Finally one couples particles back into the theory by the following device. We announce there is a coupling constant which takes two particles into n Reggeons. Then a hierarchy of contributions to $T_{AB}(s,t)$ for large s near $t = 0$ emerges (Fig. 14)

$$\begin{aligned} T_{AB}(s,t) &= s(\log s)^{-\gamma(g_1)} F_{11}^{AB}(t(\log s)^{z(g_1)}) + s(\log s)^{-1} F_{12}^{AB}(t(\log s)^{z(g_1)}) \\ &\quad + s(\log s)^{-2+\gamma(g_1)} F_{22}^{AB}(t(\log s)^{z(g_1)}) + \cdots , \end{aligned} \quad (262)$$

where the F_{nm}^{AB} are undetermined. We can be sure, however, that

$$F_{11}^{AB} = \gamma_A\gamma_B f_{11}(t(\log s)^{z(g_1)}) , \quad (263)$$

so the leading term <u>factorizes</u>. In perturbation theory $\gamma(g_1)$ is a small negative number and $z(g_1) \approx 1$. We have for $\sigma_T^{AB}(s)$

$$\sigma_T^{AB}(s) \underset{s\to\infty}{\sim} (\log s)^{-\gamma(g_1)} \gamma_A\gamma_B - f_{12}^{AB}/(\log s) \cdots , \quad (264)$$

where the <u>sign</u> arises from the signature argument given long ago.

Now we will stop and assess our accomplishments to this juncture; after that I'll toss out a few conjectures and speculations and then stop and toss the ball to the Topical Conference and the audience.

First of all within the context of a specific model we found that the renormalization group coupled with Reggeon field theories is a good tool for investigating the nature of the J-plane near $J = 1$ when t is small. Unfortunately there is some ambiguity in the formulation of the input or free $\underset{\sim}{P}$ theory and less, but residual, ambiguity in choosing the interaction. The natural course of action in such an instance is to seek a principle outside of the narrow framework of the Reggeon field theories alone. One such principle called the renormalization group bootstrap,[73] essentially selects out theories which are IR free. This avoids most of the computational uncertainties associated with IR liberty. For example, among the set of theories suggested by s-channel unitarity with

$$T_{AB}(s,t) = is(\log s)^{\nu} \frac{J_\nu(a\sqrt{-t}\log s)}{(a\sqrt{-t})^{\nu}} \quad (265)$$

as the input, only $\nu = 0$ is permitted by this hypothesis, leading to[74]

$$\sigma_T^{AB}(s) = \gamma_A\gamma_B - f_{AB}/(\log s)(\log\log s)^{1/2} + \cdots \quad (266)$$

essentially the second "casual" fit of Jacob given earlier. There may be other principles which help restrict these Reggeon theories, but they haven't been promulgated yet.

There are a host of other applications for Reggeon field theories besides the elastic amplitudes which we have concentrated on here. The formulation and administration of rules for production amplitudes and inclusive processes is somewhat complicated by signature but can be treated.[75] The heuristic treatment by the Soviet authors in Reference 9 is probably acceptable.

A more demanding question is "When are these theories applicable? What range of s do we need?" The answer to that is quite likely "Right now." First, one has explicit correction terms to the leading behavior $\sigma_T(s) \sim (\log s)^{-\gamma}$, $-\gamma$ small, as given in (264). With these correction terms one can well imagine describing data through the ISR range. But why should that be meaningful, since to get any of these results one sums an infinite number of $\underset{\sim}{P}$ insertions and that would seem to require an infinite number of large subenergies. If the $\underset{\sim}{P}$ insertions were only in absorptive parts, where there are thresholds then this might be correct. Even then our experience with multiperipheral models tells us that the asymptotic formula (s^{α} for that model) may be a smooth envelope of various rising and falling n particle cross sections. So it may also be here where only a finite number of $\underset{\sim}{P}$ links is being smoothly represented by the full sum.[76] Actually the $\underset{\sim}{P}$'s enter in Feynman integrals whose variables are integrated over all of phase space (no threshold step functions as in absorptive parts). Near overall $J \approx 1$, $t \approx 0$, the leading behavior comes from a small region of the multiple integration phase space. The renormalization group sums up those leading behaviors. (See the quote from Bjorken and Drell before the renormalization group lecture.)

Perhaps a closing note on the $\underset{\sim}{P}$ decoupling theorems is in order.[57,60] These theorems were predicated on the simple $\underset{\sim}{P}$: $\alpha(t) = 1 + \alpha' t$, which we know to be unreliable. Almost kinematic arguments led to the vanishing of the triple $\underset{\sim}{P}$ in inclusive reactions and from there down the primrose path to the decoupling of $\underset{\sim}{P}$ from elastic amplitudes at $t = 0$. In the absence of just a simple ansatz for $\underset{\sim}{P}$, the vanishing or not of the triple $\underset{\sim}{P}$ vertex becomes a dynamical issue, since, for sure, the bare triple $\underset{\sim}{P}$ vertex does not vanish. It turns out that in each of the models examined so far, the triple $\underset{\sim}{P}$ vertex vanishes slowly and non-analytically near $t = 0$. Whether this has any immediate bearing on inclusive measurements in diffraction dissociation in the triple Regge region at small t, I leave to the lectures of my colleagues, the discussion sessions, and the famed Topical Conference.

ACKNOWLEDGMENTS

I have learned most of the material herein in extensive conversation and collaborations with J.B. Bronzan, J. Bartels, J. Dash, M.B. Einhorn, B.W. Lee, R. Savit, R.L. Sugar, A.R. White and F. Zachariasen. S. Coleman has been a "secret" instructor through the medium of Reference 7. My debt to L.M. Saunders in all this is more subtle, but very deep.

References

It wasn't until I began writing these lectures out that I realized how impossibly ambitious a task I had been assigned by the conscientious organizers of this school. A finite bibliography simply cannot properly acknowledge all those whose thoughts I have represented and perhaps misrepresented. I've tried to make a more or less complete list of references I've leaned on; my apologies to authors I have left out from ignorance.

1. Hesiod, The Works and Days, Lines 50-105. Trans. By R. Lattimore, Univ. of Mich. Press (1959), pp. 23-31. This reference is courtesy of S. Traweek, Antelope Freeway.
2. T. Appelquist and J. Primack, lectures at the 1973 SLAC Summer Institute on Particle Physics, SLAC-167, Volume II; E.S. Abers and B.W. Lee, Physics Reports 9C, 1 (1973); S. Weinberg, report to the Aix-en-Provence Conference on Elementary Particle Physics, 1973, and Reviews of Modern Physics, to be published; and, of course, all the references in these papers.
3. G. 't Hooft, Nuc. Phys. B33, 173 (1971); B.W. Lee, Phys. Rev. D5, 823 (1972); B.W. Lee and J. Zinn-Justin, Phys. Rev. D5, 3121, 3137, and 3155 (1972); G. 't Hooft and M. Veltman, Nuc. Phys. B44, 189 (1972).
4. J.D. Bjorken and S.D. Drell, Relativistic Quantum Fields (McGraw Hill Book Company, New York, 1965), Chapter 19.
5. G.F. Chew, S-Matrix Theory of Strong Interactions (W.A. Benjamin, Inc., New York, 1962).
6. E.C.G. Stueckelberg and A. Petermann, Helv. Phys. Acta. 26, 499 (1953); M. Gell-Mann and F.E. Low, Phys. Rev. 95, 1300 (1954); N.N. Bogoliubov and D.V. Shirkov, Introduction to the Theory of Quantized Fields (Interscience New York, 1959), Chapter 8; K.G. Wilson, Phys. Rev. D3, 1818 (1971); lectures by J. Zinn-Justin at the 1973 Cargèse Summer School, Saclay Preprint, DPhT/73-79, to be published; J.C. Collins and A.J. Macfarlane, DAMTP Preprints

73/34 and 73/35; S.Y. Lee, UCSD Preprint UCSD-10P10-140; Loh-ping Yu, Rutgers Preprint, April, 1974.

7. My standard references on this will be the splendid lectures "Secret Symmetry: An Introduction to Spontaneous Symmetry Breakdown and Gauge Fields" given by S. Coleman at the 1973 International Summer School of Physics Ettore Majorana and the Physics Reports by Abers and Lee, Ref. 2.
8. V.N. Gribov, Zh. Eksp. Teor. Fiz. 53, 654 (1967) [Sov. Phys.-JETP 26, 414 (1968)].
9. A.A. Migdal, A.M. Polyakov, and K.A. Ter-Martirosyan, ITEP (Moscow) Preprint No. 102, to be published in JETP; H.D.I. Abarbanel and J.B. Bronzan, Phys. Rev. D9, 2397 (1974).
10. J.H. Schwarz, Physics Reports 8C, 269 (1973); G. Veneziano, Physics Reports 9C, 199 (1973).
11. S. Gasiorwicz, Elementary Particle Physics (John Wiley and Sons, New York, 1966).
12. G.M. Cicuta and E. Montaldi, Lett. Nuovo Cim. 4, 329 (1972) and 't Hooft and Veltman, Ref. 3.
13. K.G. Wilson and M.E. Fisher, Phys. Rev. Lett. 28, 240 (1972) and Ref. 9.
14. K. Symanzik, DESY Preprint 73/58, to be published in the Proceedings of the 1973 Cargèse Summer School. R.L. Sugar and A. White, NAL Preprint, June 1974, to be published.
15. Collected Quotes of L.B.J. 1965-1968; R. Blankenbecler, private communicati
16. K.G. Wilson, Phys. Rev. D7, 2911 (1973); Ref. 9.
17. J. Iliopolous, C. Itzykson, and A. Martin, Saclay Preprint DPhT/73-18, to be published in Reviews of Modern Physics; K.G. Wilson, Ref. 6.
18. A.A. Andronow and C.E. Chaikin, Theory of Oscillations (Princeton University Press, 1949), Chapters 5 and 6.
19. Late childhood for some.
20. C.N. Yang and R. Mills, Phys. Rev. 96, 191 (1954). In Ref. 21 it is noted that "R. Shaw (unpublished)" was also responsible for this construction. Needless to say I haven't been able to trace this reference.
21. S. Glashow and M. Gell-Mann, Ann. Phys. (N.Y.) 15, 437 (1961).
22. J. Schwinger, Phys. Rev. 128, 2425 (1962); Theoretical Physics, Trieste Lectures (1962), p. 89 (I.A.E.A., Vienna, 1963); L.S. Brown, Nuovo Cimento 29, 617 (1963); C.M. Sommerfield, Ann. Phys. (N.Y.) 26, 1 (1963); J. H. Lowenstein and J.A. Swieca, Ann. Phys. (N.Y.) 68, 172 (1971); R.J. Crewther, S.-S. Shei, and T.-M. Yan, Phys. Rev. D8, 1730 (1973).
23. This idea is reviewed by T.D. Lee, Physics Reports 9C, 143 (1974).
24. M. Gell-Mann and Y. Ne'eman, The Eightfold Way (W.A. Benjamin, Inc., New York, 1964), p. 49.
25. M.K. Gaillard and B.W. Lee, NAL Preprint 74/34 THY, March, 1974.
26. See the report by K. Symanzik, Proceedings of the Aix-en-Provence Conference on Elementary Particle Physics, p. 117.
27. For a review of these ideas, see the paper by Y. Frishman, Proceedings of the XVI-th International Conference on High Energy Physics, Ed. J.D. Jackson and A. Roberts (NAL, Batavia, 1973), Vol. 4, p. 119.
28. K.G.Wilson, Phys. Rev. 179, 1499 (1969) and Y. Frishman, Phys. Rev. Lett. 25, 966 (1970).
29. J.D. Bjorken, Phys. Rev. 179, 1547 (1969).
30. See the review talk by S. L. Adler, NAL Mini-Conference on Neutrino Physics, NAL Preprint 74/39-THY.
31. B. Richter, report at the 1973 Irvine Conference, December, 1973 and W. Chinowsky, Report at the IV-th International Conference on Experimental Meson Spectroscopy, April, 1974.
32. A full survey has been given by M.K. Gaillard and B.W. Lee, NAL Preprint 74/21-THY, January, 1974.

33. S. Weinberg, Phys. Rev. Lett. 19, 1264 (1967); A. Salam in Elementary Particle Theory, N. Svartholm, ed. (Almquist and Forlag, Stockholm, 1968), p. 367.

34. Abers and Lee, Ref. 2; Reference 30.

35. S. Weinberg, Phys. Rev. D5, 1412 (1972).

36. J.D. Bjorken and S.L. Glashow, Phys. Lett. 11, 255 (1964); S.L. Glashow, J. Ilioupoulos, and L. Maiani, Phys. Rev. D2, 1285 (1970).

37. O.W. Greenberg, Phys. Rev. Lett. 13, 122 (1964); O.W. Greenberg and M. Resnikoff, Phys. Rev. 163, 1844 (1967).

38. M. Gell-Mann, Acta Physica Austriaca, Suppl: IX 733 (1972); W.A. Bardeen, H. Fritzsch, and M. Gell-Mann, CERN Preprint TH-1538, 1972; S.D. Drell, SLAC Preprint 1158, 1972.

39. H.J. Lipkin, Proceedings of the 1973 SLAC Summer Instititue on Particle Physics, SLAC-167, Vol. 1, p. 239.

40. I. Bars, M. Halpern, and M. Yoshimura, Phys. Rev. D7, 1233 (1973); H. Georgi and S.L. Glashow, Phys. Rev. Lett. 32, 438 (1974).

41. See the review by J.D. Bjorken, Proceedings of the XVI-th International Conference on High Energy Physics, Ed. J.D. Jackson and A. Roberts, (NAL, Batavia, 1973), Vol. 2, p. 299.

42. I am, honesty forces me to admit, rather much of an honorary member of this happy club. You see, I haven't really paid my dues lately.

43. D.W.G.S. Leith, Proceedings of the Summer Institute.

44. D.W.G.S. Leith, Proceedings of XVI-th International Conference on High Energy Physics, Ed. J.D. Jackson and A. Roberts, Vol. 3, p. 321; also Proceedings of the 1973 Meeting of the Division of Particle and Fields of the APS, Berkeley, California, Ed. H.H. Bingham, M. Davier, G.R. Lynch, AIP Conference Proceedings, Number 14, (American Institute of Physics, New York, 1973), p. 326.

45. F.E. Low and V.N. Gribov, Proceedings of XVI-th International Conference on High Energy Physics, Ed. J.D. Jackson and A. Roberts (NAL, Batavia, 1973), Vol. 3, p. 459 and p. 491.

46. H.D.I. Abarbanel, Proceedings of the VI-th International Symposium on Many Particle Hadrodynamics, Eisenach-Leipzig, to be published.

47. F. Zachariasen, Physics Reports 2C, 1 (1971).

48. I am indebted to S.C. Frautschi for such a concise statement of this plight.

49. U. Amaldi, et al., Physics Letters 44B, 112 (1973); S.R. Amendolia, et al. Physics Letters 44B, 119 (1973).

50. M. Jacob, CERN Preprint TH-1683.

51. Preliminary data from NAL on $\pi^{\pm}$, $K^{\pm}$, and $p^{\pm}$ cross sections confirm these trends in rising σ_T. W.F. Baker, NAL seminar, May, 1974.

52. J.S. Ball and F. Zachariasen, Cal Tech Preprint 68-431, February, 1974 and collected works.

53. The Berkeley group lead by G.F. Chew is the most articulate representative of these ideas. I understand that at the Topical Conference following this school some discussion will center around these concepts.

54. Or go back and frolic among the gauge theories.

55. My friends tell me that there is a full blown review of this subject forthcoming in a Physics Report by H.D.I. Abarbanel, J.B. Bronzan, and A.R. White. The latter will be present at the Topical Conference here.

56. S.C. Frautschi, Regge Poles and S-Matrix Theory (W.A. Benjamin, New York, 1963); R. Omnes and M. Froissart, Mandelstam Theory and Regge Poles (W.A. Benjamin, New York, 1963); R.J. Eden, High Energy Collisions of Elementary Particles (Cambridge University Press, 1967), Chapter 5.

57. R.C. Brower, C.E. de Tar, and J.H. Weis, "Regge Theory for Multiparticle Amplitudes," CERN Preprint TH 1817, to be published in Physics Reports.

58. V.N. Gribov, Zh. Eks. Teor. Fiz. 41, 1961 (1962)[Soveit Physics-JETP 14, 1395 (1962)].

59. J. Finkelstein and K. Kajantie, Phys. Letters B26, 305 (1968); Nuovo Cimento 56A, 659 (1968).

60. L.M. Saunders, et al., Phys. Rev. Lett. 26, 937 (1971); C.E. Jones et al., Phys. Rev. D6, 1033 (1972); R.C. Brower and J.H. Weis, Phys. Lett. 41B, 631 (1972). The subject is carefully reviewed in Reference 57.

61. V.N. Gribov, I. Ya. Pomeranchuk, and K.A. Ter-Martirosyan, Yad. Fiz. 2, 361 (1965) [Sov. J. Nuc. Phys. 2, 258 (1966)]; H.D.I. Abarbanel, Phys. Rev. D6, 2788 (1972); A.R. White, Nuc. Phys. B50, 130 (1972).

62. H.D.I. Abarbanel, Lecture Notes in Physics: Strong Interaction Physics, Vol. 17 Ed. W. Ruhl and A. Vancura (Springer-Verlag, Berlin, 1973), p. 146.

63. See also L.M. Saunders and H.D.I. Abarbanel, Phys. Rev. D2, 711 (1970).

64. D. Amati, A. Stanghellini, and S. Fubini, Nuovo Cimento 26, 896 (1962).

65. S. Mandelstam, Nuovo Cimento 30, 1127 and 1148 (1962).

66. J.B. Bronzan and C.E. Jones, Phys. Rev. 160, 1494 (1967).

67. T.W.B. Kibble, Phys. Rev. 173, 1527 (1968).

68. The formulation of Reggeon field theories logically allows a cutoff in E on the order of 1. A preliminary exploration of the effect of this on the infrared behavior has been made in Reference 9; it appears inessential. Further work has been done by J.B. Bronzan, private communication.

69. H.D.I. Abarbanel and J.B. Bronzan, Phys. Rev. D9, June 15, 1974.

70. P.W. Anderson, Concepts in Solids (W.A. Benjamin, New York, 1963); D. Pines, The Many Body Problem (W.A. Benjamin, New York, 1961).

71. Or possibly a running away from fundamentals.

72. See also the work of M. Baker, ITEP (Moscow) Preprints, May, 1974; J.B. Bronzan and J.W. Dash, to be published.

73. H.D.I. Abarbanel, NAL Preprint THY 74/42.

74. H.D.I. Abarbanel, J. Bartels and J.W. Dash, NAL Preprint THY 74/36.

75. J. Bartels, Private communication and to be published.

76. J.B. Bronzan, Private communication.

	I	I_3	S	Q	Y	B	C
p	$\frac{1}{2}$	$\frac{1}{2}$	0	$\frac{2}{3}$	$\frac{1}{3}$	$\frac{1}{3}$	0
n	$\frac{1}{2}$	$-\frac{1}{2}$	0	$-\frac{1}{3}$	$\frac{1}{3}$	$\frac{1}{3}$	0
λ	0	0	-1	$-\frac{1}{3}$	$-\frac{2}{3}$	$\frac{1}{3}$	0
p'	0	0	0	$\frac{2}{3}$	0	$\frac{1}{3}$	1

$$Q = I_3 + \frac{Y + C}{2}$$

TABLE 1. The quantum number assignments for the four quarks in a model with "charm." To these numbers may be added a gauge label. When the gauge group is SU(3), each of the quarks comes in three varieties or colors.

Figure Captions

Figure 1. A contribution to $G^{(4)}$ in a $\lambda_0\phi_0^4$ field theory. The integral for this contribution contains a factor $\Gamma(2 - D/2)$ in D space-time dimensions. The pole at $D = 4$ of this gamma function are where the infinities of the local quantum field theory are hiding in the dimensional regularization technique.

Figure 2. The N field Green's function or correlation function.

Figure 3. The definition of the renormalized coupling parameter in terms of the four point proper vertex function at a symmetric momentum point.

Figure 4. The determination of the effective coupling constant $\tilde{g}(t)$ from from integrating $d\tilde{g}(t)/dt = -\beta(\tilde{g}(t))$. The value of $\tilde{g}(t)$ at t_2 must be the same whether we begin integrating at $t = 0$ or begin at $t = t_1 > 0$.

Figure 5. A possible behavior of the effective coupling constant $\tilde{g}(t)$ as the scale ξ of momenta, $\xi = e^t$, varies. Whenever $\tilde{g}(t)$ is small, $\tilde{g}(t) << 1$, one may determine the proper vertex functions of a field theory by a perturbation expansion in this small parameter.

Figure 6. The shape of $\beta(g)$ near a simple zero determining the infrared behavior of a field theory.

Figure 7. The shape of $\beta(g)$ near a simple zero determining the ultraviolet behavior of a field theory.

Figure 8. The shape of the potential $V(y)$ for $\mu_0^2 > 0$ and for $\mu_0^2 < 0$. In the latter case the minimum of the potential and thus the ground state (or vacuum) shifts to $y = \pm(-6\mu_0^2/\lambda_0)^{1/2}$. The vacuum no longer explicitly exhibits the full symmetry of the Lagrangian.

Figure 9. The behavior of $\nu W_2(\xi,q^2)$ in UV free field theories. As $-q^2$ increases, it looks more and more concentrated near $\xi = 0$.

Figure 10. The two Reggeon contribution to the t-channel partial wave amplitude.

Figure 11. Radiative corrections to a propagator due to massless photons. The first term has a pole at $p^2 = m^2$; every other term has a branch point at $p^2 = m^2$.

Figure 12. The n-Reggeon contribution to the discontinuity of the t-channel partial wave amplitude. The crosses on the Reggeon lines indicate that the Reggeons are "on shell:" $J_i = \alpha(t_i)$ or $E_i(\vec{q}_i) = 1 - \alpha(\vec{q}_i)$. This is like a unitarity formula in ordinary field theories.

Figure 13. The two Reggeon cut discontinuity in the four Reggeon amplitude. Reggeon unitarity relations like these allow us to discuss Reggeon interactions separate from particles; they are tacked on later.

Figure 14. The hierarchy of Reggeon contributions to $\sigma_T^{AB}(s)$ arising in the renormalization group treatment of Reggeon field theories.

HIERARCHY OF HADRON PHYSICS

Building Hadrons

Quarks in Bags
Charm and Color
Static Properties:
Masses, Magnetic,
Moments, ...

Giant Grand
Synthesis
(Not available
in time for this
school)

Building Reggeons

Hadron Bound States
s-channel unitarity
Production processes
Correlations in in-
clusive processes
Clusters ...
Dual Models--MP models

Interacting Reggeons

Making the Pomeron
Reggeon "Calculus"
t-channel unitarity
Absorption
Cross sections $\log s \to \infty$

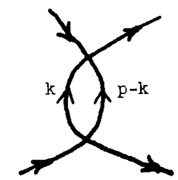

Figure 1

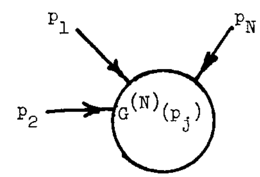

$$\sum_{j=1}^{N} p_j = 0$$

Figure 2

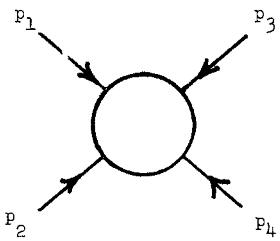

$$= \frac{-i\lambda(\mu)}{(2\pi)^{D+1}}\ , \qquad p_i \cdot p_j = \frac{\mu^2}{3}(4\delta_{ij} - 1)$$

$$m^2 = A\mu^2$$

Figure 3

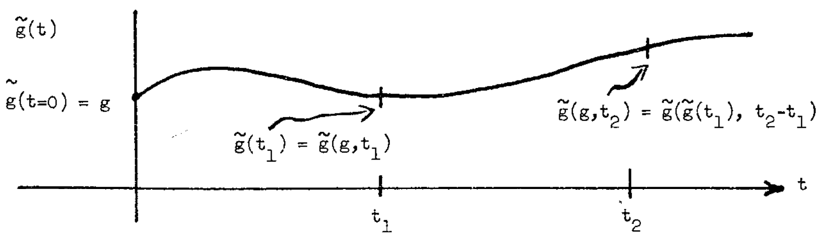

Figure 4

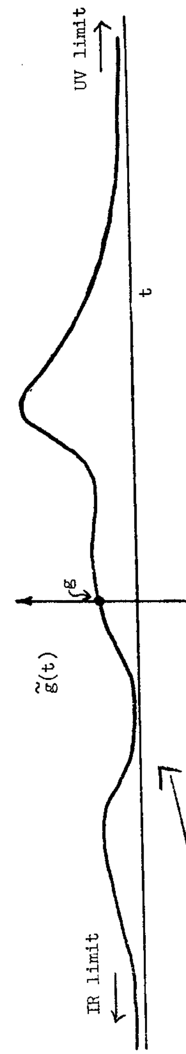

Possible region of small effective coupling: $\tilde{g} \ll 1$

Figure 5

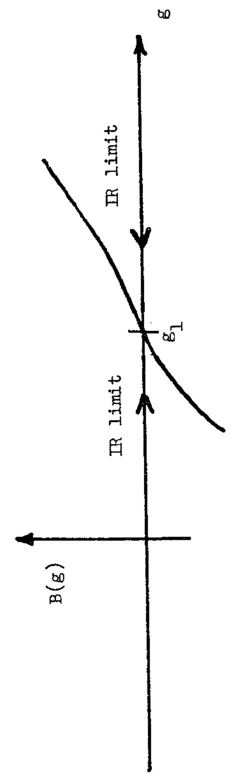

$\beta(g) \approx \beta_1(g-g_1)$, $\beta_1 > 0$. IR stable point. $\tilde{g}(-t) \xrightarrow[t\to-\infty]{} g_1$. g_1 small; IR liberty.

$g_1 = 0$; IR freedom.

Figure 6

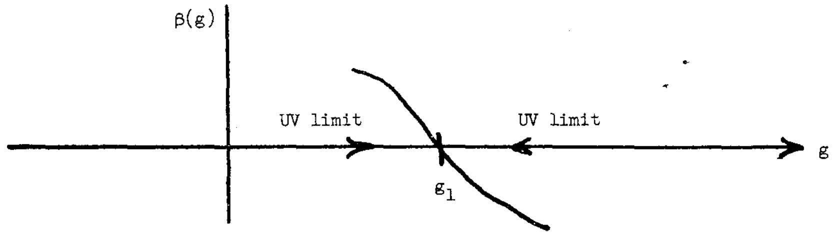

$\beta(g) \approx \beta_1(g-g_1)$, $\beta_1 < 0$. UV stable point. $\tilde{g}(-t) \xrightarrow[t \to +\infty]{} g_1$. g_1 small; UV liberty. $g_1 = 0$; UV freedom.

Figure 7

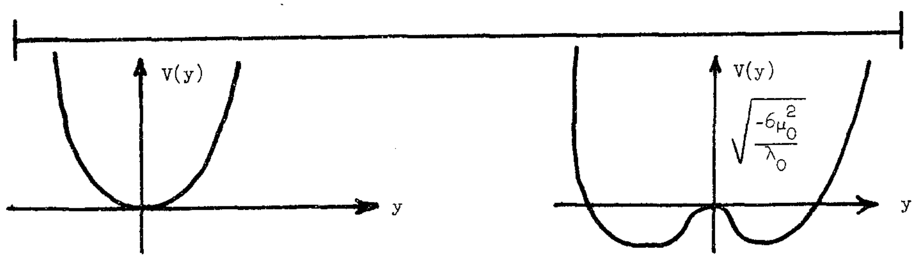

$\mu_0^2 > 0$ $\mu_0^2 < 0$

$$V(y) = \frac{\mu_0^2}{2} y^2 + \frac{\lambda_0}{4!} y^4$$

Figure 8

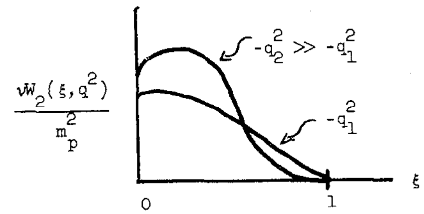

Figure 9

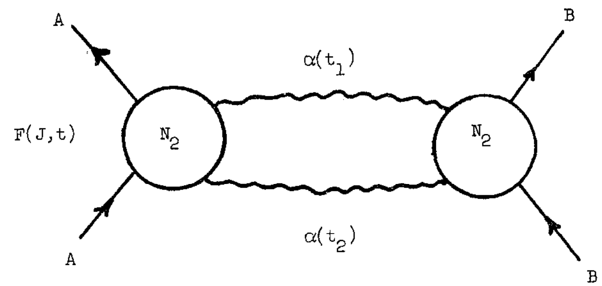

Figure 10

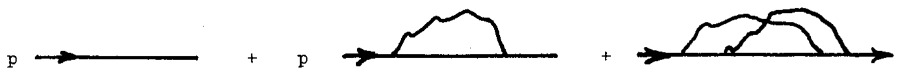

Figure 11

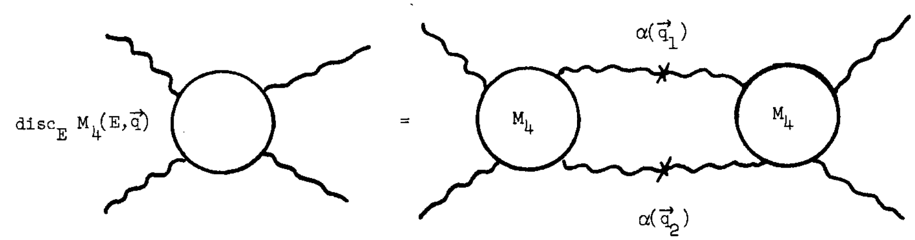

Figure 13

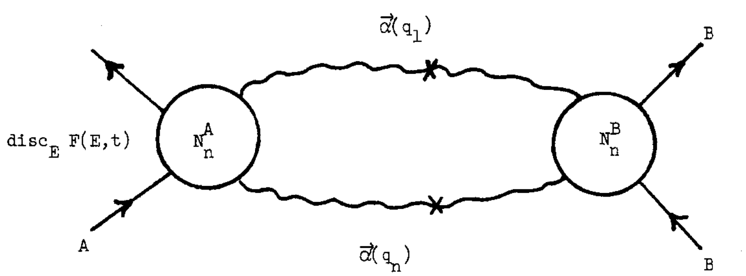

Figure 12

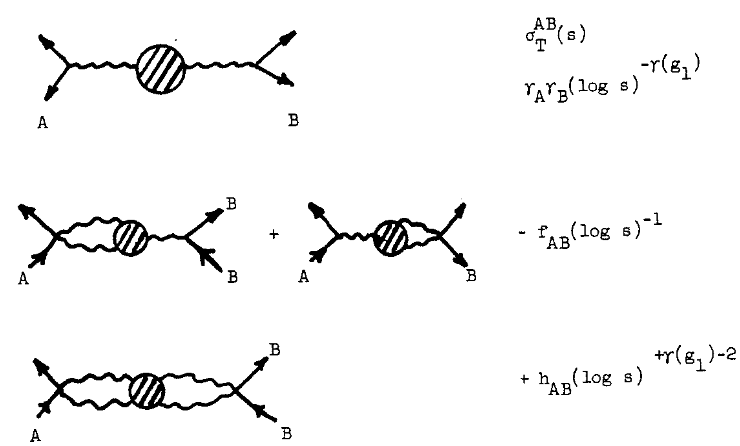

Figure 14

SLAC-PUB-1460
(T)
July 1974

The Beginner's String*

Jorge F. Willemsen

Stanford Linear Accelerator Center
Stanford University, Stanford, Ca., 94305

Preface

Professor Abarbanel has asked me to prepare a set of notes on the string model to supplement the material being presented in his lectures. As a working hypothesis it was assumed that the participants know a modicum about this field. Combining this premise, the extensiveness of the work done on the model, and the constraint of space limitation, it seems to me a "survey" format is appropriate for these notes: no pretenses to completeness are maintained, and the notes are in no way a review. Rather, they are designed to introduce the vocabulary of the field, to provide a source of references to genuine reviews, and to the original literature only where reviews are not available.

(To be presented at the Summer Institute on Particle Physics, Stanford Linear Accelerator Center, Stanford, Ca., July 29 - August 10, 1974)

*Work supported by the U. S. Atomic Energy Commission.

A. What is the String Model?

The string model is basically an attempt to understand what physical structures can underlie scattering amplitudes of the type originally written by Veneziano.[1] The hope is that by understanding the physics of these amplitudes, one may learn something about the structure of hadrons. This, in turn, should lead to a variety of new predictions.

An example of a Veneziano amplitude, for 2 to 2 scattering, is

$$(1)\quad A_4(s,t,u) = g\left[B(1-\alpha_s, 1-\alpha_t) + (s \leftrightarrow u) + (t \leftrightarrow u)\right];$$
$$B(x,y) = \Gamma(x)\Gamma(y)/\Gamma(x+y) = \int_0^1 dz\, z^{x-1}(1-z)^{y-1}.$$

Veneziano proposed this simple expression for the amplitude because it incorporates many desirable features such an an amplitude should have: Regge asymptotic behaviour, crossing symmetry in the case of linearly rising trajectories, daughters with residues in fixed ratios, saturation of superconvergence relations, and duality between Regge poles and resonances. We will discuss other properties of Veneziano amplitudes later.

For now we want to focus on a different feature of Eq. (1), namely, that it is easily generalized to have an arbitrary number of external particles, and that the generalized amplitudes share the good features of the original amplitude. A very concise way to write a term in such an amplitude is the following:[2]

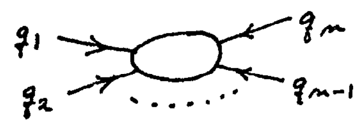

(all q in units of slope $\alpha' \sim (1\ \mathrm{GeV}^2)^{-1}$.)

Figure 1

$$(2)\quad A_n = \langle 0 | V_2 \Delta_{12} V_3 \Delta_{13} \ldots\ldots V_{n-1} | 0 \rangle ,$$

where the "propagators" are

$$\Delta_{ij} = [s_{ij} + R + \alpha(0)]^{-1} = \int_0^1 dx \; x^{s_{ij} + R + \alpha(0) - 1} ,$$

with

$$s_{ij} = (q_i + q_{i+1} + \ldots\ldots + q_j)^2 \quad ;$$

$$(3)\qquad R \equiv \Sigma_{n=1}^{\infty} \, n \, a^{\dagger}_{n\mu} a_n^{\mu} \quad ;$$

and the "vertices" are

$$(4)\quad V_j = \left[\exp \, i \, \Sigma_n \frac{q_{j\mu} a_n^{\dagger\mu}}{\sqrt{n/2}}\right]\left[\exp \, i \, \Sigma_n \frac{q_{j\mu} a_n^{\mu}}{\sqrt{n/2}}\right] .$$

In these equations, a_n^{μ} and $a_n^{\mu\dagger}$ are simple harmonic oscillator creation and annihilation operators,

$$[a_{n\mu}, a^{\dagger}_{m\nu}] = -\delta_{nm} g_{\mu\nu} .$$

The "ground state" $|0\rangle$ is annihilated by the a_n^{μ} : $a_n^{\mu} \, |0\rangle = 0$. Using simple properties of these operators, and the integral representation for the propagators, one can easily calculate an integral representation for A_n analogous to the integral representation for A_4 given in Eq. (1). The properties of the amplitude can then be studies from the integral representation. Historically, the integral representation for the amplitude was proposed first,[3] and then it was discovered that the factorized "operator" form Eq. (2) was possible. This factorization property was a major step forward in arriving at an interpretation of the physics of the model.

To see why, examine what the vertex creates from the ground state (which is interpreted as the initial, unexcited external particle):

$$(5)\quad V|0\rangle = |0\rangle + i \, \Sigma_n \frac{q a_n^{\dagger}}{\sqrt{n/2}} |0\rangle + \frac{i^2}{2!} \Sigma_{n,m} \frac{2}{\sqrt{nm}} (q a_n^{\dagger})(q a_m^{\dagger}) |0\rangle + \ldots\ldots$$

A general term in this power series expansion of the exponential looks like:

$$(6)\quad \frac{i^n}{n!} q_{\mu_1} q_{\mu_2} \cdots q_{\mu_n} \left\{ \begin{array}{l} a^{\dagger}_{1,\mu_1} a^{\dagger}_{1,\mu_2} \ldots\ldots a^{\dagger}_{1,\mu_n} \\ a^{\dagger}_{2,\mu_1} (\qquad '' \qquad) \\ \ldots\ldots\ldots\ldots\ldots\ldots \\ a^{\dagger}_{\alpha,\mu_1} a^{\dagger}_{\beta,\mu_2} \ldots a^{\dagger}_{\omega,\mu_n} \end{array} \right\} |0\rangle$$

Any state in the bracket is an eigenstate of the "mass operator" R, with a definite eigenvalue, and we see that for a given tensor structure of n indices as above, there are an infinite number of such eigenstates. Furthermore, the index "n" also runs to infinity, and so V creates states of all possible spin from the ground state, i.e., excites the initial hadron into all possible Regge recurrences and daughters.

However, the propagators Δ only have poles for a single value of R, namely $R = s + \alpha(0)$, for fixed s. Let us suppose, for example, that $(s+\alpha(0)) = 2$. Eigenstates of R can be

$$a^{\dagger}_{1,\mu_1} a^{\dagger}_{1,\mu_2} |0\rangle \qquad \& \qquad a^{\dagger}_{2,\mu_1} |0\rangle$$

The first, doubly occupied, state has two tensor indices, and so maximum spin 2. The singly occupied state has spin 1. However, there is a second spin one state which is obtained by appropriately anti-symmetrizing the tensor indices μ_1 and μ_2. And so on.

Generalizing, we can readily see that at a pole, there will be a single state with maximum spin $M = \alpha(0) + s$ and a large number of states of lower spin, making up the daughters. The degeneracy of the daughter levels is very large. In fact, asymptotically one finds that the total number of states at a given pole grows exponentially (Hagedorn degeneracy.)

This is the famous requirement that dual amplitudes will be dual only if the direct channel spectrum is very rich. Most of the degeneracy of the model could be removed if we used only a single harmonic oscillator operator a_μ, instead of an infinite number of oscillators $a_{\mu n}$. In fact, one early attempt was made to construct dual amplitudes using only a single harmonic oscillator. The resulting amplitude was not dual.

But what physical system has just the spectrum of R? It is clearly the violin string, that is, the continuum limit of an infinite number of mass points experiencing harmonic forces between them. Eq. (2) can now be pictured as an unexcited string coming in, having momentum dumped in by a series of external potentials, and finally re-emerging as an unexcited string (see Fig. 2)

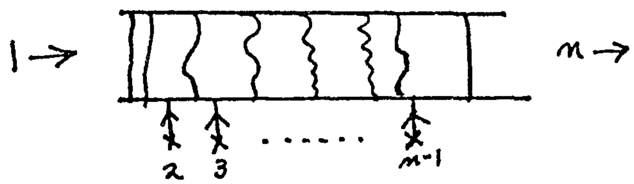

Figure 2

This is clearly a very unsymmetrical way to view a reaction whose amplitude is supposed to be crossing symmetric and dual. In the process of trying to check the crossing and duality properties of dual models directly in the operator formalism, a very interesting discovery was made.[4] It was that when the amplitude was written in one way, less intermediate states appeared than when the amplitude was written in another way. In other words, some of the states created by the vertices were spurious. (See Fig. 3)

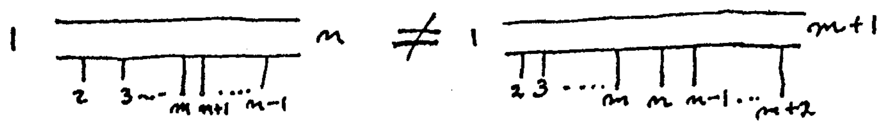

Figure 3

Now, this was very interesting indeed, because many of the states of the type exhibited in (6) are unphysical. If a timelike oscillator creates a state, that state has negative norm. This will show up in certain scattering amplitudes by having negative residues where only positive residues are allowed. Probability will not be conserved.[5]

A lot of work has gone into showing that the spurious states that were discovered are "ghosts" of this type, or else states of zero norm, and can be eliminated consistently from the theory. All of this "ghost elimination" occurs for a price, however, and we will come to that.[6]

Once one gets accustomed to the idea that the Veneziano amplitude is telling us a hadron is behaving like a string, it is natural to ask whether a formalism to deal with this physical picture exists, so that the rules for writing amplitudes can be derived. Elimination of unphysical states of excitation should also follow naturally from the formalism, as in quantum electrodynamics. In a striking generalization from the action principle describing the motion of a classical free point particle, Nambu proposed that the motion of a classical string be described by an action principle based on[7]

$$(7) \quad I = \iint d^2\xi \sqrt{-g}$$

As indicated in Fig. 2, a string propagating in space-time sweeps out a world sheet. In Eq. (7), ξ are the coordinates of the sheet, and g is the determinant of the metric tensor on this two-dimensional manifold. The string is actually propagating in the full four-dimensional Minkowski space, however, so the invariant interval on the sheet is

$$(8) \quad \begin{aligned} ds^2 &= -g^{\alpha\beta}\, d\xi_\alpha\, d\xi_\beta \\ &= -g^{\mu\nu}\, d\chi_\mu\, d\chi_\nu \end{aligned}$$

where

$$g^{\mu\nu} = \begin{pmatrix} 1 & \\ & -\underset{\sim}{1} \end{pmatrix}.$$

These expressions are only compatible if

$$g^{\alpha\beta} \equiv \partial^\alpha \chi_\mu \partial^\beta \chi^\mu .$$

Given this expression for the action, one must try to proceed canonically to obtain the equations of motion of the system, any constraints that may have to be satisfied, and attempt quantization. After all the dust has settled, it turns out that the spectrum of excitations implied by (7) is indeed that of the string; to show this explicitly, it is necessary to impose certain conditions of constraint on the states of the system.[8] These conditions turn out to be just the "ghost elimination" conditions that we mentioned before.

However, we should recall that in electrodynamics the "ghost eliminating" condition $[\partial_\mu A^\mu]^{(+)}|\psi_{ph}\rangle = 0$ is necessary only if we work in the Lorentz gauge, which is expressed classically by $(\partial A) = 0$. If we work in the radiation gauge, we can solve for one spurious photon degree of freedom explicitly, and not have to impose conditions on states. Analogous choices of gauge can be made in the string model, and the results we just mentioned are applicable in the analogue of the Lorentz gauge.

A different choice of gauge is possible.[9] We can motivate it by observing that one of the sheet coordinates, $\xi_0 \equiv \tau$ is like a "proper-time" variable; clearly one of the Minkowski variables, X_0, is a time variable in some frame, and so we expect things can be simplified if we identify these two to be the <u>same.</u> Working in a gauge of this type, it was found that the theory is not Lorentz invariant if the Minkowski space has only four dimensions. For the Lorentz algebra to close, it is necessary to have a 26 dimensional space-time. What is more, the ground state has to be a tachyon, $(m^2 = -1)$! (Actually, these catastrophes can be dug out of the manifestly covariant gauge as well, but we won't go into that here.)[6]

We have, then, a well-defined action and a perfectly well-behaved classical theory. Somewhere in the canonical quantization of the theory, something goes wrong, and no one quite knows what it is. I will mention some recent attempts to deal with this question as we go along.

B. <u>How Can A Hadron Look Like a String, Anyway?</u>

Hadrons, as opposed to leptons, are not point objects. We think they are <u>composed</u> of point objects, maybe quarks and gluons, which, dancing to some unknown ryhthm, give the hadron a spatial extent that can be measured experimentally. In short, we are used to visualizing a hadron as a little clump of matter - but a <u>string</u>?

To gain some insight into how a hadron can look like a string,[10] just remember the Feynman-Wilson interpretation of the inclusive distribution in a plot of rapidity vs. $p_\perp$. For moderate values of $p_\perp$, say $p_\perp \lesssim 400$ MeV, the "central region" is supposed to look like this:

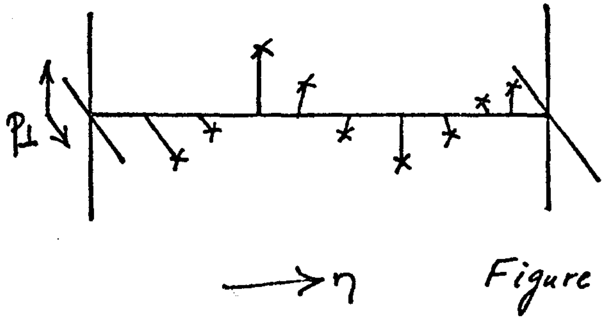

Figure 3

This figure is supposed to represent a "snapshot" of the typical, universal, interior hadronic matter distribution in terms of partons.

Imagine that at energies so large that we can see very many partons, it turns out that we can better and better interpolate between the parton-points on this plot by a smooth curve. In this case, our "snapshot" of the hadron would look like a string! If we keep the longitudinal momentum fractions as the "length" axis, and Fourier transform from $p_\perp$ -space to $x_\perp$ - space, we get just the interpretation that follows from the GGRT formulation of the string model. It is because of this precise matching of the string formalism with the parton language that we will develop the parton language to gain physical insight.

Now, what can it mean to have this kind of smooth distribution of partons? Again, recall that the Feynman-Wilson picture of scattering in the Regge region has the dominant contribution to the amplitude arising from the following steps: 1) The hadrons convert virtually into large numbers of partons, including a "wee sea" of partons with infinitesimally small fraction of the parent's longitudinal momentum; 2) the wee partons forget which hadron they belong to because all the hadrons' wee seas look pretty much alike; 3) recombination into hadrons occurs.

The probability for these things to happen can be estimated,[10] and depends on the distribution function for wee partons in the hadron. If this goes like $x^{-\alpha}dx$, α is the Regge intercept for the Regge behaved amplitude that results. Well, this is just multiperipheralism, and by looking at graphs in simple theories, one can see these dominant contributions occur when the cascade from the parents into the wee sea proceeds sequentially in the longitudinal momentum fraction x.

Multiperipheral ladder graphs, however, do not look very dual, so we must make some changes in this scheme:

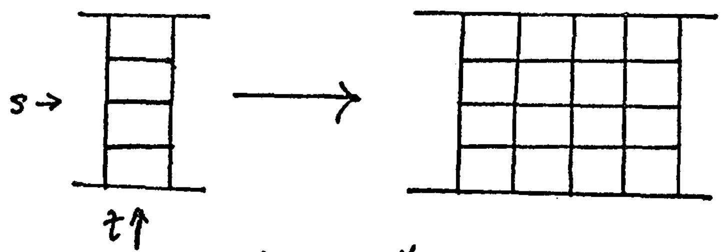

Figure 4

The first attempt to derive dual models from conventional field theory proceeded by calculating graphs of the type Fig. (6) in varying degrees of sophistication.[11] This is the "fishnet diagram" approach you may have heard of.

Another very pretty way to motivate in terms of graphs the verbal description we have been giving is due to Bjorken.[12] If we actually calculate the graph

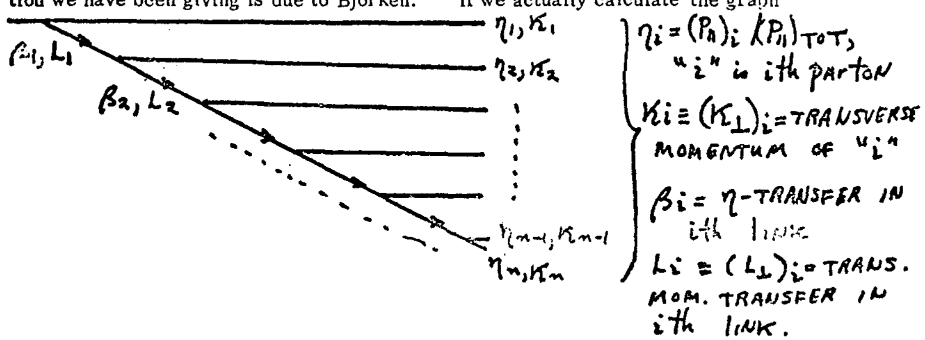

Figure 5

in the infinite momentum frame using old-fashioned perturbation theory, with the assumption that in the cascade the η - transfers are ordered ($\beta_n \to \eta_{n+1} + \beta_{n+1}$, with $\beta_{n+1} \ll \eta_{n+1}$, just as in the dominant multiperipheral scattering graphs, a very interesting qualitative picture emerges - near neighbor partons in rapidity are also close together in transverse configuration space. (It is an open question how much of this result survives in theories with vertices less trivial than ϕ^3. See Section F.)

If we want to examine rescattering corrections to this basic parton model picture of the hadron's wavefunction, it is plausible to consider that these corrections involve repeated soft interactions between near neighbors in rapidity, with the basic dynamical variables involved being the distances in transverse configuration space between the interacting partons. (This is why the string picture starts off as a first quantized theory.)

One then attempts to describe the behaviour of the wee parton sea by means of an effective Hamiltonian, which is a function of the partons' relative transverse momenta, labeled by an ordered parameter corresponding to the parton's longitudinal momentum fraction. The simplest dynamical hypothesis is that the near neighbor forces are harmonic. If, in addition, the density of partons along the longitudinal fraction axis is chosen to be constant, the string Hamiltonian is obtained in the continuum limit:

$$(9)\quad (H_{eff})_{\infty p_z} \sim \sum_{i=1}^{n} p_{i,\perp}^2 + (x_{i,\perp} - x_{i+1,\perp})^2/2\eta_i$$

$$\to \int d\theta\, \rho^{-1}(\theta)\left[\rho^2(\theta)\,\dot{x}_\perp^2 + (\partial x_\perp/\partial\theta)^2\right]$$

$$\to \int d\theta\, \left[\dot{x}_\perp^2 + x_\perp'^2\right]$$

$$\text{iff.}\quad \rho(\theta) \equiv d\eta(\theta)/d\theta = \text{const.}$$

Here θ labels the parton, $(\theta/\pi) \sim (P_\parallel)_{TOT}^{-1} \int_0^\theta d\theta' P_\parallel(\theta')$, and $x_\perp(\theta)$ is the transverse coordinate of the parton labelled by θ. (Actually, instead of working in the $\infty\, P_z$ frame, we can do our quantum theory off planes tangent to the light cone. Then $P_\parallel$ is replaced by $P^+ = P^0 + P^z$, but P^z is not necessarily approaching infinity.) The choices of relevant dynamical variables, and the interpretation of the θ label in terms of longitudinal fraction, match exactly with what emerges mathematically from the string model in the GGRT gauge.

To reiterate, physical insight into how a hadron can look like a string is gained by looking at the planar graphs in a ϕ^3 theory; observing that in a sequential ordering approximation the longitudinal and transverse dynamics decouple (see Bj's paper for details), with the longitudinal fraction serving only as a label; assuming a soft, near-neighbor residual parton-parton interaction; and finally, assuming the parts of the wavefunction with the number of partons $\to \infty$ are the most important, in some sense, so there is no $\Sigma_n P(n)$ in Eq. (9).

All of these assumptions are subject to questioning. We will see later that dual models fail to predict certain qualitative behaviours that we expect from hadrons. In most such instances of failure, we will be able to point to some suspicious assumption from among the above as the one that is likely at fault.

A reasonable way to proceed would be to always keep in mind that the string picture of hadrons can make sense as an approximation to some complex dynamical situation occurring within each hadron. One of the things the string model contributes to our requirements on a theory of hadrons is that it should correlate properties of the spectrum with the "soft" physics of the Regge region. However, this requirement of duality does not seem to force any of our assumptions to be strictly valid.[13]

Finally, I should mention that it is not at all clear from $H_{eff}(p^+; x_\perp)$ that the theory can be relativistically covariant. With the string action principle, the covariance can be shown using canonical methods, albeit with the troubles that have been mentioned. However, with the strict factorization of longitudinal and transverse dynamics that occur in H_{eff}, alternate methods of analysis exist. The expressions for the Lorentz generators could have been "guessed" in advance of the string action principle if one had been clever enough. This is important for future model-building, and we will say more about it in the next section.

C. What if the Partons Have Spin?

So far we have argued the amplitudes of oscillation of the string are the transverse coordinates of the partons, and we are working in first-quantization. Experiments suggest that the valence partons have spin 1/2, and it is reasonable to assume the wee parton sea will have many spin 1/2 partons as well. We now wish to expand on Bjorken's ϕ^3 theory arguments, and suppose that, in addition to $X_\perp(\theta)$, it is legitimate to include the spin variables among the possible dynamical variables upon which near-neighbor parton scatterings can depend.

Working in complete analogy with the $X_\perp(\theta)$ arguments, we can suppose the first quantized Pauli spin matrices $\sigma_\perp(\theta)$ are the relevant dynamical spin variables. (Actually, Bjorken, Kogut, and Soper have shown that in the light-cone quantization of the free Dirac theory,[15] these 2 x 2 Pauli matrices are really the spin variables of the second quantized theory, even taking anti-particles into account.) As good fortune would have it, a reasonable, simple guess for the H_{eff} depending on near-neighbor spin-spin couplings,[16]

$$(H_{eff})_{SPIN} = g' \sum_i \sigma_\perp(\theta_i) \cdot \sigma_\perp(\theta_{i+1})$$

is exactly solvable in the continuum limit! It becomes just the Hamiltonian of the free, massless Dirac theory in two dimensions.[10]

Now, depending on the boundary conditions one chooses, which amounts in this case to selecting whether the string has an even or odd number of spin 1/2 partons, one obtains either the Neveu-Schwarz (NS) model[17] or the Ramond model,[18] respectively. The N-S model was originally proposed as a model for the $(\rho\pi)$ trajectory system, as we will see. The Ramond model, because of its odd number of fermion constituents, is a candidate for a fermi particle and its recurrences and their daughters. This could be a nucleon, or perhaps even a quark itself. The $q\bar{q}$ amplitude in this model has poles at bosons with the same structure as the bosons of the N-S model, and in fact the emission vertices are just those of the N-S model.[19] However, let me just concentrate on the features of the N-S model, so as to get the general ideas across.

In momentum space, if $b^\dagger$ creates a fermion and $c^\dagger$ creates an anti-fermion, the H_{eff} of the N-S model is

$$[H_{eff}]_{TOT} = R + \sum_{n=1}^{\infty} (n - 1/2)(b_n^\dagger b_n + c_n^\dagger c_n).$$

Here R is just the "orbital" contribution to the energy discussed earlier. The new piece is due to the spin-spin interaction, and has a spectrum of eigenvalues of 1/2, 3/2, 5/2, ...

In the quark model we expect the ρ and π to be $q\bar{q}$ bound states in s waves, in triplet and singlet spin states respectively. Since the spin in the only difference between the ρ and π states, the only thing that can account for the mass difference between them is the spin-spin interaction. Just as we needed more than one oscillator for duality, however, we now are forced to have an infinite number of spins. We get higher and higher energy states depending upon how many of these spins are deviated from the ground state configuration (which is like the ground state of an anti-ferromagnet). On top of any one of these "spin-deviate" states we can pile on orbital excitations, with the energy spectrum given by R.

The resulting trajectory structure is

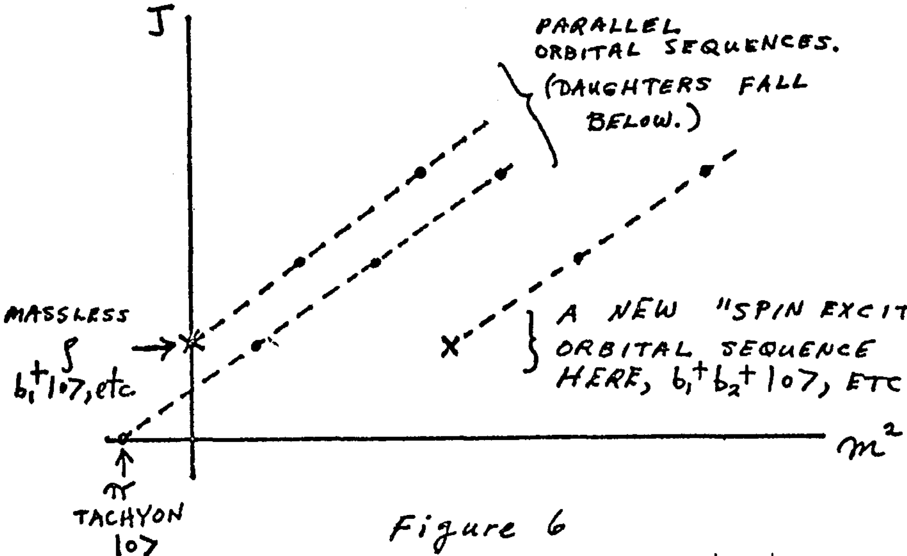

Figure 6

The reader should not be misled into believing that b^+ or c^+ are creating quarks or anti-quarks. They are creating spin deviation excitations as described above. When a spin is flipped at one point, H_{eff} moves that spin flip down the chain. A spin flip means helicity 1/2 (say) is going to helicity (-1/2) for a net helicity flip magnitude 1. That is why this system describes bosons. But at any given point there can be at most one fermion to be flipped - that, in a nutshell, is why we need operators satisfying Fermi-Dirac statistics. The helicity of an excitation is just the "charge" $Q = \sum_n (b_n^+ b_n - c_n^+ c_n)$.

Actually, the fact the interesting excitations of the system are bosons can be brought out more clearly using the Fourier decomposition of the current $j_\mu = \bar{\Psi}\gamma_\mu \Psi$. (Remember $\mu = 0,\ 1$ in 2 dimension, and Ψ are 2-component spinors.) It is a peculiarty of two dimensions that the Fourier coefficients

$$\rho_n \equiv 1/\pi \int_0^\pi d\theta \, [j_0 \cos n\theta + i j_1 \sin n\theta]$$

satisfy Bose statistics exactly,[20] $[\rho_n, \rho_m^\dagger] = \delta_{nm}$. These are, of course, "composite" operators built out of the b^+ and c^+, and one can show that[21b]

$$(H_{eff})_{TOT} = R + \frac{Q^2}{2} + \sum_{n=1}^{\infty} n \, \rho_n^\dagger \rho_n .$$

We could as well write $[a_{n\perp}^\dagger a_{n\perp} + \rho_n^\dagger \rho_n]$ as $\sum_{j=1}^{3} a_{nj}^\dagger a_{nj}$, where $a_{n3} \equiv \rho_n$. If this system is to have any hope of being Lorentz invariant in four-dimensions, we might expect a transformation from a transverse direction to a longitudinal direction to take $a_{n\perp}$ into ρ_n. The generator that does this would have the form

$$i \sum_n f(n) \, [a_{n\perp}^\dagger \rho_n - \rho_n^\dagger a_{n\perp}]$$

where f(n) can be fixed by dimensional arguments.[21a] In fact, Iwasaki and Kikkawa (IK) have discovered that the Lorentz generators indeed have terms of just this form.[22]

Unfortunately, however, there is more to the Lorentz generators than this. Remember that for the orbital part of the model, we had originally $X_\mu(\theta)$ with $\mu = 0, 1, 2, 3$. We argued $X_0 \sim \tau$, and kept $X_\perp$ as the dynamical variables. What-ever happened to X_3? Remember $\theta \sim P_\parallel$, so that is not it. Actually, X_3 (or X_- to be precise) could be solved for in terms of $X_\perp$, and that is why it has not been heard from. But there will be Lorentz generators of the form $\int d\theta \, [X_3 \dot{X}_\perp - X_\perp P_\parallel]$ which in momentum space looks like[9] $i \sum_n g(n) \, [L_n^\dagger a_{n\perp} - a_{n\perp}^\dagger L_n]$, where $L_n \sim \sum_{m=-\infty}^{\infty} C_{nm} : a_{n-m} a_m :$, $a_{-m} \equiv a_m^\dagger \ (m>0)$.
These Virasoro operators[4] are also composite operators as indicated, but they do not satisfy the algebra of simple harmonic oscillators. These satisfy instead

$$[L_n, L_m] = (n-m) L_{m+n} + \frac{d_\perp}{12} m (m^2-1) \delta_{m,-n}$$

Technically it is because of the algebraic properties of these L_n that we need tachyons and 26 dimensions in the orbital model.[23]

Now, there are a priori two ways to combine these two kinds of contributions to the Lorentz generators. The string formalism, properly generalized by I and K in Ref. 22 to handle the spin, *seems to give naturally the result*

$$M_{j+} \sim i \Sigma_n [f(n) \rho_n \epsilon_{jk} a^+_{nk} + g(n) a^+_{nj} L_n] + h.c.,$$

where $\epsilon_{12} = 1$, $\epsilon_{21} = -1$.

This turns out to be much worse for Lorentz invariance than it was before, with just the orbital part. Basically what happens is that a transverse excitation doesn't make up its mind properly whether it wants to go to an L_n or a ρ_n. To patch things up, we have to abandon our nice interpretation of the ρ_n as "longitudinal" bosons, and replace the ($a^+_n \rho_n$) generators with other objects containing 2 fermions and one boson:

$$i \Sigma_n \rho^+_n a_{n\perp} + h.c. \rightarrow \Sigma_n (b^+_n \pm i c^+_n) G_n (a,b,c) + h.c$$

$$G_n \equiv \Sigma_m : a^{\perp}_{n-m} b^{\perp}_m :$$

The G_n are the famous "super-gauge" operators which have come into their own recently, independent from the string or dual models.[24]

The advantage, for our purposes, of these supergauges is that for $d_\perp > 2$ the Lorentz algebra can be made to close once again. The fermions and the orbital operators a_i are assigned the <u>same</u> transverse dimensionality, and for d = 10 the theory is Lorentz invariant. The supergauge construction allows this generalization for the fermions, while the ρ_n construction is wedded to $d_\perp = 2$.[25] (Of course, we also need a tachyon at $m^2 = -1/2$, as indicated in Fig. 7)

Alternately, we might have tried to put by hand

$$M_{j-} = i \Sigma_n a^+_{nj} [f(n) \rho_n + g(n) L_n] + h.c.$$

This type of expression has been suggested by Fairlie, and discussed by Chodos and Thorn.[26] The net result is that you still have a tachyon but you do <u>not</u> need extra spatial dimensions. This sounds wonderful at the outset, but unfortunately, in the context of the NS model, it turns out that "Q" does not measure the helicity properly anymore. If we give up the fermions altogether and stick to ρ_n as bosons, we lose the two-trajectory structure that was so attractive.

Let me try to summarize. Partons with spin allow us to get fermionic physical particles, and a quark-model-like structure for the vector and pseudoscalar meson families. There exist reasonable physical motivations for including the effects of spin by choosing H_{eff} to be of Heisenberg type. Unfortunately, when we check Lorentz invariance, the pretty physical picture evaporates completely. I have tried to give a bit of the flavor of how the Lorentz business works so this point can be properly appreciated.

What could be some flaws in the argument?

- Why only $\sigma_\perp(i) \cdot \sigma_\perp(i+1)$? Why not put in σ_z as well? Since $2i\sigma_z = [\sigma_x, \sigma_y]$, if $\sigma_\perp \rightarrow \psi$ (fermi field, by a Klein transformation), we might try a Thirring model as a generalization[27]. What happens in the end is that the "charge = helicity" Q gets renormalized, and not much else. Nothing is gained except the useless information that in ($0 < \theta < \pi$) the coupling constant is quantized.
- If we have a Nambu-Goldstone pion, how do we reconcile it with the quark picture ? In principle the string-with-spin model should be capable of shedding new light on this old question. The reason is that each individual hadron has all the complications of many-body theory. The net quantum numbers have to be given by the quark model, but we have a fermion sea to play with. The pion occupies a special position because it is the ground state meson. Bardacki has been working on this kind of approach.[28]
- How about spin-orbit couplings? This has also been studied by Bardacki, and Halpern.[29] Not much has been done to study the relativistic properties of these models. Also, they suffer from a much larger degeneracy than the uncoupled theories. A more modern approach would be to Melosh transform the N-S model.[30]
- Perhaps the whole picture of how spin is to be incorporated is totally wrong.

See Section F for a concrete way this could be so.

D. What good is the String Model?

The string model is only as good as the amplitudes it predicts. These are, unfortunately, not well-suited for phenomenological analysis at all. In recent years, dual phenomenologists seeking to fit data have turned increasingly to non-Veneziano, non-factorizable dual amplitudes that have nothing to do with strings.[31]

Nevertheless, generalized Veneziano amplitudes do maintain the qualitative features we mentioned at the outset that motivated Veneziano in the first place. This makes them valuable tods, satisfying many desirable prerequisites on hadronic amplitudes, for studying questions of consistency among the assumptions. They are, in other words, a valuable theoretical laboratory. Extensive references to studies into high energy limits of dual amplitudes and their discontinuities, relating to multiparticle production, inclusive reactions, and the role of the Pomeron, can be found in Veneziano's review paper, Ref. 5.

We mustn't try to get off the hook that easily, though. The string model, and the possible "variations on a string" models, do consistently come up with features that must be dealt with as predictions, even if they are unpleasant. It is, for the time being, excusable if the spectrum is not fully correct; it is a serious defect that we have a persistent tachyon. It is satisfying to have a mathematical realization of Muellerism; but immensely disturbing that "deep scattering"[32] cannot be dealt with even qualitatively.[1] It is stated one needs a Hagedorn spectrum to accomodate duality; but I know of only one unpublished paper (by Koba) where the decay patterns of high mass, high spin resonances of dual models are analyzed, to give experimentalists an idea of what to look for.

Let me say a bit more about the "deep scattering" qualitative failure of the Veneziano model. For both s and t large, where the CM scattering angle is held fixed, the elastic ($2 \to 2$) amplitude Eq. (1) behaves[1] like $\exp(-s \ln 2)$ at 90°, as opposed to the power-law behaviour observed experimentally. This is interesting, because (apart from an overall ∞ !) a straight forward calculation of the elastic form factor[33] of the ground state hadron also behaves as $\exp(-q^2 \ln 2)$. The origin of the factor ($\ln 2$) in the latter case is that the mean-square distance in transverse configuration space between the partons at opposite ends of the string is

$$\left[\langle(x_\perp(\pi) - x_\perp(0))^2\rangle - \langle x_\perp^2(\pi)\rangle - \langle x_\perp^2(0)\rangle\right]$$

$\sim \ln 2$. We see the obscene constant ($\ln 2$) is something like the size of the hadron, and even in deep-scattering the hadron behaves according to this characteristic size.[34]

This is important, because current theoretical explanations for power-law fall-offs in these kinds of experiments invariably start from the assumption it is the behaviour of the pointlike constituents that is responsible. In the string picture, the extreme view is taken that the important part of the hadron wavefunction is the one that is maximally occupied by partons. We tend to lose touch of the "valence" partons, of the part of the wavefunction measured by extremely short wavelength probes.

Another interesting physical point should be noted. Dual models tend to give form factors[33] (forgetting the $2-q^2$ for now) that look like

$$F_{elastic}(q^2) \sim \int d\theta \, (\sin\theta)^{\alpha - q^2}.$$

Ideally, one would like to get form factors like $\int d\theta \, (\sin\theta)^{\alpha - q^2} \cos^\beta\theta$ which fit data well,[35] but this does not emerge naturally from any model. (Remember that θ is the longitudinal momentum fraction of the parton with coordinate $X_\perp(\theta)$).

Now, BBG also get formulae for how form factors behave asymptotically, from a more direct parton approach. They find $F(q^2) \sim (q^2)^{-n} I$, where I is a definite integral over the longitudinal fraction.[32] The significant point to note is that the string model result cannot be written in this form. The asymptotic behaviours in the two models are coming from different regions of phase space.

These brief discussions are intended to illustrate significant ways in which the assumptions that go into the string model can be inadequate. A straight forward look at how deep-inelastic e p scattering works for strings supports these views as to how the string model fails: the partons never behave point-like;[36] and probably it would be helpful to relax the strict adherence to a one-dimensionally extended object.[37]

It is possible that more recent developments in the string model can overcome the second of these problems. Let's see what these developments are.

E. Are Strings Alive and Well?

There are several directions in which recent progress has been made. One of these directions is in addressing the nagging problems of dimensions, and of tachyons. Recent approaches to these problems share a belief that there is no strict requirement that "canonical quantization" has to give a consistent quantum theory. In one view, the string picture is not required to make sense except in the large occupation number limit. The low lying levels of the spectrum can be totally different, and in fact the ground state particle is not anymore a simple mechanical object.[14]

This is important because suppose (classically) the "ground state" is simply a collection of particles moving together at the speed of light in the z-direction. Going over to a quantum picture, the "springs" between these particles cannot simply be at equilibrium, but rather there must be ground state random oscillations. The string cannot be well-localized, but must have a spread. But if a portion of the string is spending time moving in a transverse direction while neighboring portions are proceeding in the z-direction, the string will not hold together and move at V = C - unless the transverse moving portion exceeds the speed of light. While this argument is incomplete, it suggests we really do not want the ground state to be a mechanical object. Anyway, a simple model has been constructed which illustrates a non-mechanical ground state.[14]

Other interesting ways to deal with the problem of dimension which have been proposed rely on giving the operators in the theory a "color" index. In one method, new colorful gluons are required,[38] and the interesting result is obtained that (d = dim. of space-time) $d = 10 - 2N$, where SU(N) is the color symmetry group. In another approach, basic ambiguities inherent in the canonical quantization prescription are exploited to introduce a "color" - like index in a very natural fashion, without requiring extra fields.[39] (There are still tachyons in these models.) These developments are technical because the questions they are trying to answer arise from technical points, and I will not be able to supply any details. It should be realized, however, that the modifications in Refs. 38, 39 are not merely relabellings of the redundant transverse degrees of freedom.

By and large, the most interesting recent progress achieved has been in completing the formal theory of the interacting string. So far, after all, we have been talking about free strings, while the great virtue of the whole approach was that scattering amplitudes exist. How do we derive the rules for obtaining Eq. (2)?

To eliminate the asymmetry already noted in Fig. 2, it would be nice to say that two strings come together, fuse into a single string, and then other strings split off.

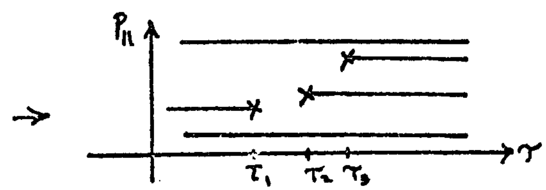

(The τ_i are the "times" at which string fusions and fissions occur.) Mandelstam succeeded in inventing the clever tricks needed to make this plausible picture into a mathematical reality.[40a] To do it, he first re-drew the Rosner-Harari structure in the figure as indicated. Recognizing that in terms of these drawings the length of the string should represent its longitudinal momentum, rather than its spatial "size" (which, recall, had nothing to do with $0 < \theta < \pi$), is a very important point. The constant width of the strip is simply an expression of $P_{\parallel}$ momentum conservation.

The mathematical problem of calculating the amplitude is complicated, but only once. As in the Feynman-Dyson theory, once the rules for calculation are justified, we can forget the derivation if we like, and use the rules with ease. Also as in Feynman-Dyson theory, the underlying physical picture is as elegant as the rules are simple. The Feynman particle path integral is the relevant formal tool, and one has

$$A_n = \int \cdots \int dz_2 \ldots dz_{n-2}\, H(z_1, \ldots ; z_n) \;;$$

$$H = V(z_1 \ldots z_n) \prod_{r=1}^{m} \prod_{n,i} dp^{i}_{n,r}\, \psi_r(p^{i}_{n,r})\, W(p^{i}_{n,r}, P_r^{TOT}).$$

One must ask for the probability that n strings can come in, merge, and become m strings, over all possible things they were and could be. Here the z_i are the "times" associated with points on the graph where splittings or recombinations occur, indicated by X's on the graph. The integrand H contains a normalization V; the products of the wavefunctions associated with the N interacting strings (r labels the string), $\psi_r(p^{i}_{n,r})$; and a weight factor W. The $(p^{i}_{n,r})$ are the momenta in the i th transverse direction carried in the normal mode of excitation n of the r th string. W is a complicated factor containing three pieces of information: a) A Fourier transform to relate this path integral to the standard one in configuration space; b) the statistical weight exp $i \iint d\sigma d\tau\, \mathcal{L}^{eff}$ where $\mathcal{L}^{eff}$ is the string Lagrangian, $(\dot{x}^2 + x'^2)$; and c) (Neumann) functions that assert, essentially, that one is interested in an amplitude with a given topology, such as that of the figure. This picture has been extended to include fermions, and allows calculation of fermion-fermion and meson-fermion couplings,[40b] as discussed earlier.

Now among the things that could happen, if we are really to count them all, is the following possibility:

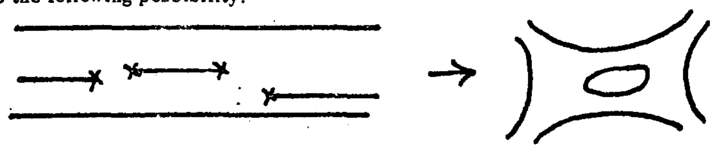

The string decides it isn't time to split yet, so it recombines for awhile. You can see in the drawing how that would look as a Harari-Rosner diagram. If we had point particles instead of strings, this diagram would be a radiative correction to a Feynman graph:

We can have, then, virtual string states, strings off-shell.

The desire to describe these processes using conventional second quantization techniques rather than particle path integrals has recently led Kaku and Kikkawa to develop a field theory of strings.[41] The bookkeeping for the various possibilities is generally simpler this way, and these authors have enumerated the basic vertices of the theory, the possible ways strings interact. They have found that the triple coupling used in the above drawings must be supplemented by a direct four-string interaction.

The new interaction that must be included from the outset in the theory has the graphical form

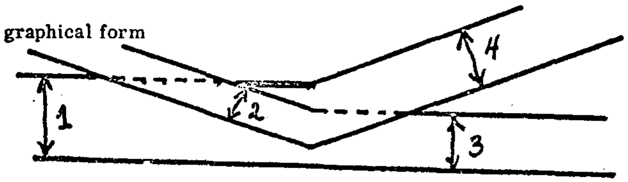

I want to stress that this observation is not merely a curiosity, but is intimately connected with the possibility of resolving some of the basic qualitative problems the model has had up to now. For example, I have not harped on the point that the resonances of the Veneziano model have zero width. This is alright in Born approximation, provided "Born approximation" has meaning within a complete theory. The field theory of strings accomodates this approximation, and justifies formally the hope perturbative unitarity may be implemented. Note that this field theory is a field theory of a totally new kind, involving multilocal rather than local dynamical variables. Many questions regarding whether such a theory satisfies general requirements that locality insures in ordinary field theories are discussed in Ref. 41, but many problems remain that require investigation. There are other potentialities in the field theory, and this brings us to our final topic.

F. What do Strings Have to do with Anything Else?

So far we have tried to motivate why the string model is interesting, and to explain in what ways it might succeed, in what ways it might fail. We now want to try to view this model in a broader context, asking its relation to other recent developments in strong interaction physics, and, in aswering this question, attempt to assess its remaining potentialities.

The string model is actually one of a class of models which try to recognize at the outset that hadrons are composite objects, although perhaps of a very different kind than other bound states such as atoms or nuclei. It has long been suspected that string models are "infinite component wave equation" (ICWE) models, for example, although only with the recent formulation of the field theory of strings could this connection be firmly established. I mention this because, even though I have stressed the "parton" school's views about the meaning of the string, there is no logical necessity for this point of view. Any approach which succeeds by whatever means to incorporate relativity, quantum mechanics, and reality as revealed by experiment into a consistent synthesis is surely logically acceptable. String models in light-cone quantization and in noncovariant gauges bring to ICWE a fresh approach, unencumbered by manifest covariance or manifest locality. This can perhaps help in evading the premises of no-go theorems that plague the ICWE approach, and its cousin, saturation of the current algebra.

Even in the conventional field theory, however, there has been a recent resurgence of interest in obtaining non-conventional solutions. One possible way to view a composite hadron is as a three-dimensionally extended volume in which fields are contained. To actually do this, however, the boundary of the domain aquires the status of an independent entity - the bag.[42] But other possibilities exist. Approximate solutions to the classical Yang-Mills isospin theory in the static approximation exist, e.g., that tend to be localized in a finite region of space.[43] The fields just sit there and feed on each other. In addition, field theories of fermions coupled to scalar mesons have been discussed using various methods to display at least approximate "confinement" of the fermions.[44] And what is of interest to us, solutions exist to the electrodynamics of scalar mesons that in the strong coupling limit, tend to look like strings.[45]

This last result is exceedingly important if we want to know whether some of the features mentioned in the parton interpretation of the string model are due only to the simplicity of the ϕ^3 theory used to discuss them, or whether they can be present in a large class of field theories. The derivation of stringlike solutions from a gauge invariant theory (which are like vortex circulations about trapped magnetic fields in Type II superconductors) encourages the belief that the relevant features may be quite general.[46]

Additional support for this point of view comes from calculations in Yang-Mills gauge theories utilizing a new kind of approximation scheme. Assume, for example, that there are not just three colors for the quarks, but N, where N is very large. In the limit where N is infinte, all the possible Feynman graphs of the theory collapse into a small subset of graphs.[47] In the case that an external colorless source current creates a $q\bar{q}$ pair and subsequently another current annihilates it, e.g., the surviving graphs are those with a single quark loop on the periphery, and with vector gluons filling in the loop, but only in planar configurations. If N is not infinite, say N = 3, other graphs survive, but are suppressed by powers of 1/N:

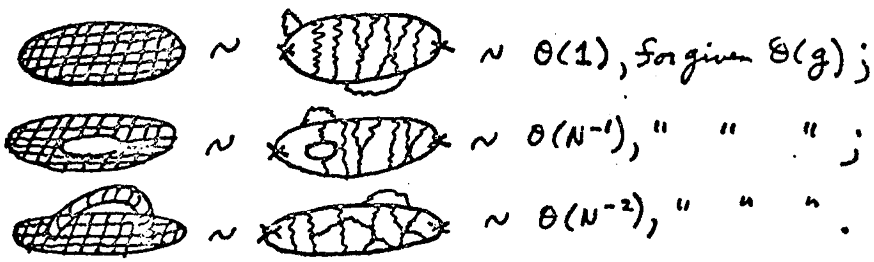

In this application, therefore, the 1/N expansion is a topology-selecting expansion.[48] There are three points I want to discuss regarding this:

1) Perturbation expansion of string model is similar.

Kaku and Kikkawa have gone on to study higher order effects in their field theory of strings. "Hole" and "wormhole" graphs of the kind drawn in the figure have long been proposed as candidates for radiative corrections to the basic string amplitudes,[5] and this come out systematically in the string field theory approach. There are other, more exotic, topologies possible in both the string and the Yang-Mills gauge theories which I have not written down. I am not trying to argue that there is an exact matching, graph for graph, between these theories. (Indeed, so far we have said nothing about isospin, SU(3), color, etc., in the K and K theory.)

What I am trying to suggest is that since the Yang-Mills theory has dynamics in all three spatial directions, but can be made to look like a planar theory in a well-defined approximation, the inverse process may be possible for string models. There, the "two-dimensional" structure was constructed first, but by calculating higher order corrections, latent higher-dimensional dynamical structure may emerge (i.e., the longitudinal and transverse variables may no longer decouple as they did in Bj's illustrative model.) Some support for this point of view already exists: more sensible results for amplitudes involving currents are found if the currents are "tubelike" probes.[33b]

The idea, then, is to perturb away from the planar approximation. A natural question is whether this perturbation expansion converges rapidly enough to be useful. It is important to do calculations in higher orders to see whether any of the gross qualitative failures of the string picture get rectified by this procedure, in manageable orders of the perturbation.[49]

2) But there are big differences !

The analogy between the second quantized string perturbation theory and the 1/N expansion for gauge fields should not be taken too literally. One simple difference, e.g., is that in the latter case, the $q\bar{q}$ loop is filled with gluons, and there is no fermi sea. If the physical arguments we gave really have anything to do with the Neveu-Schwarz and Ramond models, the fermi sea should be present in the hadron wavefunction to "leading order." On the other hand, the Yang-Mills approach readily picks out valence particles for us.

Another important point has been discussed in detail by 't Hooft.[41] It is that while the 1/N perturbation procedure selects out planar graphs as the leading order, there is no reason to conclude from this fact that the "effective" theory obtained in this approximation looks anything at all like the string theory.[50] Recall that to say that the planar ϕ^3 theory could look like a string, it was necessary to assume more than just that the relevant graphs were planar. Assumptions had to be made as to how momentum flows through the graphs. It is important to study what sensible approximations to the momentum flow problem will lead to in gauge theories. There is no reason to expect they will be identical to what happens in φ^3 (but see point 3 below.)

One should not get the impression, however, that it is necessary to "derive" the string theory in full from conventional field theories. The string theory may well prove to be a new and fully consistent approach to hadron physics which is not equivalent to conventional field theory. Still, it is necessary to understand the general features the string theory may share with other theories, since the string theory is incomplete.

3) Other Surprising Similarities.

I will conclude by mentioning two further points of similarity between the string theory and Yang-Mills gauge theories that are surprising and tantalizing.

The first has to do with a remarkable property of Neveu-Schwarz amplitudes in the limit that the slope of the Regge trajectories goes to zero.

Each amplitude is assigned an isospin factor in such a manner that correct SU(2) values are assigned to graphs, and such that amplitudes with poles in exotic channels (such as $\pi^+ + \pi^+$) receive coefficient zero.[51] It is then found that the tree graphs of the theory have the coupling structure of the analogous SU(2) Yang-Mills theory with vectors and pseudoscalars.[52] However, in the usual NS model, there are only trilinear couplings of strings, and care is required in taking the $\alpha' \to 0$ limit to pick up all the required terms. (Recall that in YM theory, there are also quadrilinear couplings of the gauge fields.)

In the K and K field theory, a number of simplification occur.[41] One does not have to put the isospin factors by hand, but can assign quantum numbers directly to the string field variables. Also, the new four-string interaction leads to just the isospin and helicity structure of the four field interaction in the Yang-Mills theory in an appropriate gauge. One may conjecture from this that the connection between strings and Yang-Mills theory is deep-seated.

Finally, I want to mention a different kind of calculation that has been done recently. In the study of phase transitions in bulk matter, it seems to be the case that detailed knowledge of the microscopic interaction in the particular species of matter is totally irrelevant to understanding certain features of the phase transition. An atomistic point of view is not relevant for a study of these systems-rather than seeking what differences arise in systems as we probe deeper into them, the relevant question is something like "what is it the deeper 'layers' share in common in their response to certain kinds of probes?"[53] K. Wilson has developed a theoretical formalism to deal with this kind of question.[54] One of the features of this formalism is the sensible point that if the microscopic details are really irrelevant, we are better off if we "integrate" these details out at the outset.

This kind of procedure may be reasonable for the study of the planar graphs of the YM theory. If we want to study those graphs in which momentum flows more or less uniformly throughout, we might do it by first lumping subgraphs in which "hot" lines occur into new effective vertices among soft lines.

In any case, K. Wilson himself has recently studied spinor electrodynamics in a spatial lattice, and in the strong coupling limit.[55] The first device cuts off the magnitudes of the momenta that can flow. The strong coupling requirement intuitively suggests dominance of graphs rich in vertices. The result of his calculation is that, unlike weak coupled electrodynamics, the current-current correlation function in this theory can be described using an effective action which is proportional to the area of a fermion loop. It is difficult to pin down precisely what the connection of this result with the Nambu action principle, Eq. (7) actually is.

So, again: Are strings a separate contribution, or are they an extrapolation from existing theories? It is clear that the physical picture itself points to inadequacies, and the string theorist has much to gain by studying how conventional theories deal with these problems. On the other hand, the manner in which string theory actually realizes the underlying physical assumptions can still be viewed as a promising and stimulating approach.[56]

References and Footnotes

(As noted in the preface, this article is not a comprehensive review. References are representative rather than exhaustive, and I apologize for many omissions. The interested reader should, however, be able to trace the relevant literature from this sample. PRT means "plus references therein" that are essential.)

1. G. Veneziano, N.C. 57A, 190 (1968)
   C. Lovelace, Phys. Lett. 28B, 265 (1968)
   J. A. Shapiro, Phys. Rev. 179, 1345 (1969)

2. S. Fubini, P. Gordon, G. Veneziano, Phys. Lett. 29B, 679 (1969).
   S. Mandelstam, Phys. Rev. D1, 1734 (1969), (PRT)
   Y. Nambu, Proc. Intern. Conf. on Symmetries and Quark Models, Wayne University (1969), p. 269 (Gordon and Breach, 1970).
   L. Susskind, Phys. Rev. Lett. 23, 545 (1969)

3. Z. Koba, H. B. Nielsen, Nucl. Phys. B12, 517 (1969), (PRT).

4. M. A. Virasoro, Phys. Rev. D1, 2933 (1970), (PRT)

5. We have little space for calculations. Almost all needed details, as well as different points of view, can be found in one or more of the recent extensive reviews by:
   G. Veneziano, Physics Reports v.9C, No. 4 (1974);
   J. Schwarz, Physics Reports v.8C, No. 4 (1973);
   C. Rebbi CERN-TH-1785, to be published in Physics Reports;
   P.H. Frampton, Syracuse Lectures;
   J. Scherk, NYU-TR3-74.
   S. Mandelstam, Berkeley preprint to be published in Physics Reports, has just appeared.

6. R. C. Brower, Phys. Rev. D6, 1655 (1972)
   P. Goddard and C. B. Thorn, Phys. Lett. 40B, 235 (1972)
   My prejudice is that if unphysical features are required to show ghost elimination at the free theory level, the theory is already sick. An alternate view is that only some gauges are consistent for quantization of the free theory, and these gauges turn out to be disease-free. See, e.g.,
   A. Patrascioiu, C00-2220-23 (1974). The unphysical features may then show up only in scattering amplitudes, so that 26 dim. is no problem at all, since the amplitudes are alright in the physical subspace. The tachyon would be the only real trouble. Those who like puzzles, however, may find relevant comments on quantization in Schwinger functional and Feynman path integral formalisms in, resp.,
   R. Arnowitt and S. Fickler, Phys. Rev. 127, 1821 (1962);
   K. S. Cheng, J. Math. Phys. 13, 1723 (1972).

7. Y. Nambu, Copenhagen Summer Symposium (1970).

8. L. N. Chang and F. Mansouri, Phys. Rev. D5, 2535 (1972)
   T. Goto, Prog. Theor. Phys. 46, 1560 (1971)
   O. Hara, Prog. Theor. Phys. 46, 1549 (1971)
   F. Mansouri and Y. Nambu, Phys. Lett. B39, 375 (1972)

9. P. Goddard, J. Goldstone, C. Rebbi, C. B. Thorn, Nucl. Phys. B56, 109 (1973), hereafter referred to as GGRT.

10. Complete discussions along these lines are in J. Kogut, L. Susskind, Physics Reports v.8C, No. 2 (1973), (PRT).

11. A. B. Kraemmer, H. B. Nielsen, L. Susskind, Nucl. Phys. B28, 34 (1971), (PRT).

12. J. D. Bjorken, Proc. of Intern. Conf. on Duality and Symmetry in Hadron Physics, Tel-Aviv, (1971), ed. by E. Gotsman (Weizmann Science Press, Jerusalem, 1971).

13. H. B. Nielsen, Nucl. Phys. B54, 477 (1973) argued the "softness" of the interparton force led to one-dimensionally extended hadrons.
    J. Dethlefsen, H. B. Nielsen, and H. C. Tze, Phys. Lett. B48, 48 (1974), (PRT) maintain that the Hagedorn spectrum is independent of the dimensionality in a "jelly" of n-dimensions.
    A. Kraemmer, H. B. Nielsen, and H. C. Tze, NBI-HE-74-10 more recently advocate the notion of a "dynamical dimensionality" for hadronic matter, i.e., what we see depends on how we look. This is our point of view as well.

14. A reasonably complete set of Refs. may be found in C. E. Carlson, L. N. Chang, F. Mansouri, and J. F. Willemsen, SLAC-PUB 1418 (to be publ. in Phys. Rev. D.)

15. J. D. Bjorken, J. Kogut, and D. Soper, Phys. Rev. D3, 1382 (1971), (PRT).

16. Y. Aharonov, A. Casher, L. Susskind, Phys. Rev. D5, 988 (1972), (PRT).

17. A. Neveu, J. Schwarz, Nucl. Phys. B31, 86 (1971),
    A. Neveu, J. Schwarz, C. B. Thorn, Phys. Lett. 35B, 529 (1971).

18. P. Ramond, Phys. Rev. D3, 2415 (1972).

19. S. Mandelstam, Nucl. Phys. B69, 77 (1974)

20. D. Mattis, E. Lieb, J. Math. Phys. 6, 304 (1965) See also Ref. 14.

21. a. J. F. Willemsen, Phys. Rev. D9, 507 (1974)
    b. J. F. Willemsen, Phys. Rev. D, to be published (SLAC-PUB-1397), (PRT).

22. Y. Iwasaki, K. Kikkawa, Phys. Rev. D8, 440 (1973), (PRT).

23. If the "$a_{\perp,n}$" operators have ($d_\perp$) transverse dimensions, one finds that the (null-plane quantization) "boosts" M_{i+} (see Ref. 14, 15) do not commute as they should, but rather give in the orbital model

$$[M_{i+}, M_{j+}] \propto \sum_n \Big\{ \big[n\,(1 - d_\perp/24) + n^{-1}\Big(\frac{d_\perp}{24} - \alpha_0\Big) \big] \big[a^i_{-n} a^j_n - a^j_{-n} a^i_n \big] \Big\}$$

The operators on the right-hand side have coefficient zero term by term if $d_\perp = 24$, and if the Regge intercept is $\alpha_0 = 1$, implying the presence of a tachyon. Notice this is a purely quantum effect.

24. A recent contribution with earlier reference is S. Ferrara, J. Wess, B. Zumino, CERN-TH 1863 (1974).

25. Historically, supergauges were invented in the first paper of Ref. 17, and were incorporated into the Lorentz algebra in Ref. 22. However, the particular combination of fermions and supergauge operators that appears in the Lorentz generators collapse to the orbital operator and "plasmon" (ρ_n) form when $d_\perp = 2$.

26. A. Chodos, C. B. Thorn, MIT-CTP-389, (1973), submitted to Nucl. Phys. B. These authors also discuss a modification of the basic action, so the string is massive.

27. I. Andric, J. L. Gervais, Nucl. Phys. B42, 240 (1972)
K. Kikkawa, Prog. Theor. Phys. 48, 625 (1972)
(R. Pettorino and I studied whether fermi fields of the forms given in these papers (PRT) can actually be solutions of the equations of motion. With some minor modifications, this turns out to be so provided the coupling constant is quantized.) One reason the Thirring model was appealing was the belief the Regge intercept depended upon the field theoretic dimension of the dynamical variables. In Thirring model this dimension depends upon the strength of the coupling. However, the dimensions of the currents do not change, and it is these that ultimately affect the value of the intercept. A very different use of the Thirring model has been proposed by H. Tye, MIT-CTP-383, to be published in Phys. Rev.

28. K. Bardakci, Nucl. Phys. B68, 331 (1974).

29. K. Bardakci, M. Halpern, Phys. Rev. D3, 2493 (1971).
L.N. Chang and F. Mansouri, Proc. of Johns Hopkins Workshop on Current Problems in High Energy Particle Theory (1974).

30. H. J. Melosh, Phys. Rev. D.9, 1095 (1974)
Comments relevant in the present context may be found in R. Dashen, M. Gell-Mann, Coral Gables Conf. on Symm. Principles at High Energy, (1966); E. Eichten, F. Feinberg, J. F. Willemsen, Phys. Rev. D8, 1204 (1973); A. Casher, L. Susskind, Phys. Rev. D9, 436 (1974) ; (PRT).

31. Examples: G. Schierholz, M. Schmidt, Phys. Lett. B48, 341 (1974); L. Gonzales Mestres, R. Hong-Tuan, Orsay preprints (1973, 1974); G. Cohen-Tannoudji, F. Henyey, G. L. Kane, W. J. Zakrzewski, Phys. Rev. Lett. 26, 112 (1971); P. Olesen, Nucl. Phys. B32, 609 (1971). See also Veneziano's review, Ref. 5.

32. J. Gunion, S. J. Brodsky, R. Blankenbecler, Phys. Rev. D8, 287 (1973), (PRT). (hereafter referred to as BBG.)

33. Elastic and Inelastic form factors in dual models have an extensive literature of their own. There are no real reviews on this subject. Samples:

a. Strings
Y. Nambu and A. Hacinliyan, EFI-70-67 (1970) unpublished
Y. Nambu, Phys. Rev. D4, 1193 (1971)
I. T. Drummond, Nucl. Phys. B35, 269 (1971)
Kraemmer et al, Ref. 11
A. Hacinliyan, Nuovo Cim. 8A, 541 (1972)
K. Kikkawa, B. Sakita, Phys. Rev. D6, 1734 (1972)
R. C. Brower, L. Susskind, Phys. Rev. D7, 1032 (1973)
C. Rebbi, Lett. Nuovo Cim. 1, 967 (1971)
H. C. Tze, Phys. Rev. D7, 1675 (1973)
L. Susskind, A. Casher, J. Kogut, Phys. Rev. D8, 4449 (1974)
J. F. Willemsen, ibid., p. 4457.

b. Non-planar Approaches:
A. Neveu, J. Scherk, Nucl. Phys. B41, 365 (1972)
E. Cremmer, J. Scherk, Nucl. Phys. B48, 29 (1972)
J. Schwarz, Nucl. Phys. B65, 131 (1973), and CALT-68-419, 424.

34. Actually, $\langle (x_\perp(\pi) - x_\perp(0))^2 \rangle \to \infty$.
This may be viewed as a statement that the hadron fills all $\perp$ space. As an exercise, the reader may wish to calculate at what harmonic the string should be cut off to give a size of 1 fermi. The result is physically indistinguishable from ∞, even considering ultraviolet scales such as those associated with gravitation.

35. P. H. Frampton, Phys. Rev. D1, 3141 (1970)

36. This may not be bad after all: M. Chanowitz, S. D. Drell, Phys. Rev. D9, 2078 (1974).

37. In addition to Ref. 13, See F. Mansouri, Phys. Rev. D8, 1159 (1973)

38. J. Schwarz, Nucl. Phys. B68, 221 (1974)

39. F. Ardalan, F. Mansouri, Yale 3075-72 (1974), (PRT).

40. S. Mandelstam, a) Nucl. Phys. B64, 205 (1973), b) Ref. 19.

41. M. Kaku, K. Kikkawa, CC of the CUNY preprints (1973, 1974)

42. A. Chodos, R. Jaffe, K. Johnson, C. Thorn, V. Weisskopf, to be publ. in Phys. Rev. D. (See also M. Creuz, BNL 18789 (1974)).

43. C. N. Yang, T. T. Wu, "Properties of Matter under unusual Conditions", ed. Fernbach and Mark, p. 349.

44. E. P. Solodovnikova, A. N. Tavkhelidze, O. A. Khrustalev, Theo. and Math. Phys. 10, 162 (1972) (a lot of physics is already in this non-relativistic model.)
T. D. Lee and G. C. Wick, Phys. Ref. D9, 2291 (1974)
W. Bardeen, M. Chanowitz, S. Drell, M. Weinstein, T. M. Yan, to be publ.

45. H. B. Nielsen, P. Olesen, Nucl. Phys. B61, 45 (1973)

46. Strings appear elsewhere in mathematical physics, associated with the theory magnetic poles. P. A. M. Dirac, Phys. Rev. 74, 817 (1948); J. Schwinger,

Phys. Rev. 144, 1087 (1966). Since a trapped magnetic field is required in Ref. 45, an open string should have magnetic poles at the ends. The possible relevance of magnetic poles to the string model has been discussed previously in Ref. 7, and Mansouri and Nambu, Ref. 8, e.g. More recent physical discussions, with Ref. 45 in mind, have been given by Y. Nambu, Proc. of the Johns Hopkins Workshop on Current Problems in High Energy Particle Theory (1974);
P. Olesen, H. C. Tze, Niels Bohr Inst. preprint (1974);(PRT);
G. Parisi, CO-2271-29 (1974).

47. Case of O(N): G. 't Hooft, CERN-TH-1786; SU(N): G. Canning, Niels Bohr Inst. preprint (1974).

48. References to (N^{-1}) expansion in other applications are given in S. Ma, Rev. Mod. Phys. 45, 589 (1973). Recent in particle physics: H. Schnitzer, Brandeis preprint; S. Coleman, R. Jackiw, H. Politzer, MIT-CTP-413, (PRT).

49. D. Amati, V. A. Alessandrini, Nuovo Cim. 4A, 793 (1971). With one loop, these authors obtain a negative result for deep scattering. An interesting physical discussion is in P. G. O. Freund, S. Nandi, EFI-74/33 (1974).

50. G. 't Hooft constructs an "effective Hamiltonian" for ϕ^3 that generates the planar graphs, and discusses the problem of having the eigenvalues of H_{eff} "crystallize" from a continuous to a discrete spectrum. This may occur as a function of the coupling constant - see Ref. 44.

51. H. M. Chan, J. E. Paton, Nucl. Phys. B10, 516 (1969).

52. J. Scherk, Nucl. Phys. B31, 222 (1971)
A. Neveu, J. Scherk, Nucl. Phys. B36, 155 (1972).

53. Kadanoff's hypothesis, Physics 2, 263 (1966), is that in a spin system, as $T \rightarrow T_c$, small clusters of spins start to act as though they were a single big spin; next, these clusters form larger ones which behave as a unit, etc., until finally the entire sample is correlated. See also J. Kogut, L. Susskind, Phys. Rev. D9, 697 (1974).

54. J. Kogut, K. Wilson, Physics Reports (to be published).

55. K. Wilson, preprint CLNS-262 (1974). A special feature of Wilson's methods is that gauge invariance (though not Lorentz invariance) is maintained. The values of planar graphs in the N^{-1} method, Ref. 47, on the other hand, depend on the choice of gauge.

56. In the field theory of strings, Ref. 41, the master field is a functional of the configuration space coordinates $X_\mu(\theta, \tau)$, $\Psi = \Psi(X(\theta, \tau))$. These X_μ in turn may be viewed as fields on the manifold (θ, τ). A generalization could be $\Psi = \Psi(\phi(X))$, where $\phi(X)$ are quantum fields in the four-dimensional Minkowski manifold.